Hahn-Meitner-Institut Berlin
in der Helmholtz-Gemeinschaft

Berlin Neutron Scattering Center

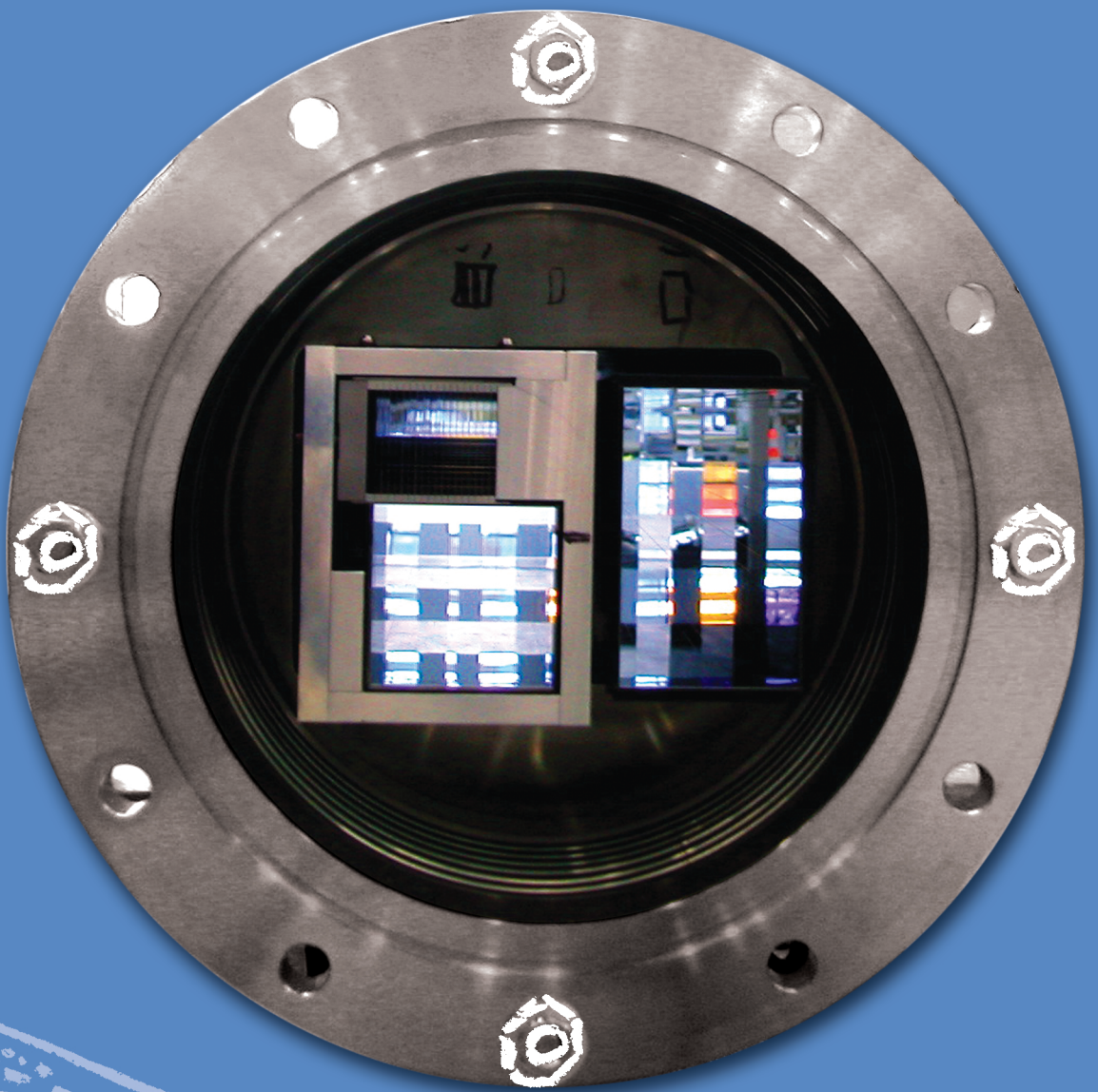

BENSC EXPERIMENTAL REPORTS 2006

BENSC
EXPERIMENTAL REPORTS
2006

edited by

U. Stahnke, A. Brandt
and H.A. Graf

Berlin Neutron Scattering Center
Hahn-Meitner-Institut Berlin
in der Helmholtz Gemeinschaft

April 2007

Berichte des Hahn-Meitner-Instituts Berlin

HMI – B 612

ISSN 0936 - 0891

The front-cover picture represents a „multispectral“ outlook to the coloured windows at the south wall of the neutron guide hall II seen through the first part of the new guide system for this hall. Three guides can be distinguished within the metal tube: The guide on the right hand side transports cold and thermal neutrons from the novel multi-spectral beam extraction device installed at the cold source of the reactor to the extreme-environment diffractometer EXED. The guide on the left hand side is split into an upper part leading to the VSANS instrument and a lower part providing neutrons for the spin-echo spectrometer SPAN.

The back cover picture displays the 2D hexagonal scattering pattern of colloidal dispersions of magnetite nanoparticles in a magnetic field as measured by time-resolved stroboscopic SANS. Further details are given in the experimental report PHY-04-1387on page 182.

The cover was designed by *screenworks*, Leibnizstraße 59, 10629 Berlin, www.screenworks.de

---

Editorial:

The *Berlin Neutron Scattering Center* (BENSC) is a department of *the Hahn-Meitner-Institut Berlin* GmbH. BENSC develops and runs the Neutron Scattering Instruments at the Berlin Research Reactor BER II and is responsible for the service to external users.
The *Hahn-Meitner-Institut Berlin in der Helmholtz-Gemeinschaft* (HMI) is a national research institution financed by the Federal Republic of Germany and the City State of Berlin.

Address:

Berlin Neutron Scattering Center
BENSC
The Scientific Secretary
Dr. Hans-Anton Graf
Hahn-Meitner-Institut
in der Helmholtz-Gemeinschaft
Glienicker Strasse 100
D – 14109 Berlin

Phone: +49-30-8062 2778, -2304, -3153

FAX: +49-30-8062 2523

Email: bensc@hmi.de

Net: http://www.hmi.de/bensc

CONTENTS

Introduction

The present volume of the Experimental Reports gives an overview on the research performed with neutrons at BENSC during the year 2006. In addition, a selection of reports on experiments performed with synchrotron radiation at the five HMI-BENSC instruments at the Berlin Synchrotron Radiation Source BESSY has also been incorporated. The 16 synchrotron reports included represent only a small part of the experiments performed. A complete coverage is intended for the near future, when the administrative structures for incorporating the user service at these five instruments into BENSC will be fully developed.

The neutron experiments performed at BENSC are described by 216 reports - 129 from external users and 87 from BENSC scientists. In 2006, the reactor was running on 221 days. Eleven instruments - including the reflectometer E6 on the new guide system - were fully scheduled for external user operation, two instruments only about 1/3 of the time: the flat-cone diffractometer E2 and the focussing diffractometer E6. E2 was shut down in April for the long-planned refurbishment of the detector system. It will become operational again in spring 2007. E6 had a severe detector problem which has meanwhile been resolved.

BENSC User Service

BENSC is open to the national and international scientific community. About 70% of the beam time is available to external users, 30% to in-house researchers. A fraction of the beam time for external users (up to 20% of the total beam time of an instrument) can be assigned to long term collaborating groups from German universities and other research institutions, the rest (at least 50% of the total beam time) is allocated to short term projects via a peer-review selection process.

An up-to-date description of the BENSC neutron scattering instrumentation can be found on the BENSC webpages:

http://www.hmi.de/bensc/instrumentation/instrumentation_en.html

A new instrument brochure is available on request. It replaces the brochure HMI-B 577 from March 2001.

BENSC has an outstanding tradition in providing sample environment for extreme conditions. A special emphasis is put on high magnetic fields and low and ultra low temperatures. Sample environment for high pressures and high temperatures is equally available and presently an advanced and highly specialised instrumentation for adsorption experiments is being built up. A detailed technical handbook describing the existent equipment has been published by the BENSC sample environment group. The handbook is being updated continuously and available on the internet under

http://www.hmi.de/bensc/sample-env/index_en.html

Scientific Selection Panel

The beam-time allocation for the short-term projects is decided by the Scientific Selection Panel of BENSC which meets twice a year, in May and in November. In 2006 the Selection panel consisted of the following ten external and two in-house members:

External members:

Dr. G. Auffermann
MPI CPfS Dresden, Germany

Dr. K. Clausen
Paul-Scherrer-Institute, Switzerland

Prof. Dr. J. Lu
UMIST, Manchester, U.K.

Prof. Dr. K. McEwen
University College of London, U.K.

Dr. M. Prager
FZ Jülich, Germany

Prof. Dr. D.K. Ross
Salford University, Greater Manchester, U.K.

Dr. O. Stockert
MPI CPfS Dresden, Germany

Prof. Dr. J. Texeira
CEA/CNRS/LLB Saclay, France

Prof. Dr. R. Triolo
University of Palermo, Italy

Prof. Dr. R. von Klitzing
TU Berlin, Germany

Internal members:

Prof. Dr. F. Mezei,
HMI Berlin

Prof. Dr. A. Tennant
HMI Berlin

Support for European Access to BENSC from the European Commission

Right from the beginning of the BENSC user programme in 1993, the access of European research groups to BENSC was generously supported by the EU under framework programmes FP3, FP4 and FP5 of the European Commission with funds for the BENSC access programme increasing from contract to contract. This programme turned out to be extremely successful and had a great impact in making BENSC a facility of truly European importance.

This successful European Access programme is presently continued under the 6th EU Framework Programme (FP6), however, with a slightly modified contractual situation: BENSC is now a partner in the ***Integrated Infrastructure Initiative for Neutron Scattering and Muon Spectroscopy (NMI3).*** NMI3 brings together 23 partners from 14 countries, including 10 research infrastructures, together with other interested organisations. The most important branch of NMI3 includes 12 different Access Activities offering European users approximately 5000 beam days of access to more than 150 instruments at different facilities with support for travel and subsistence. Under NMI3, BENSC has committed to provide a minimum of 1040 instrument days for European users, distributed over four and a half years.

In 2006, the third year under NMI3, 68 projects of European user groups have been completed. BENSC delivered 377 instrument days. A total of 129 users from 60 different groups from 15 countries were involved. A list of the respective experimental reports included in this volume can be found on page XIII.

Since the start of NMI3, BENSC has now already delivered more than 1200 days for the European user community.

Meetings and Workshops

The annual HMI neutron tutorial has a long tradition. In February 2006 it was the 27th time that this tutorial was held. 31 participants, 21 of them coming from foreign countries, 10 from German institutions visited the HMI to attend lectures on neutron scattering and to perform experiments at selected BENSC instruments.

In September 2006 the international conference on Polarised Neutrons in Condensed Matter Investigations (PNCMI 2006) took place in Berlin organised by BENSC. With nearly 150 scientists from all over the world it was the largest PNCMI conference so far. This underlines the increasing importance of polarised neutrons in condensed matter research, but also the attractiveness and international reputation of BENSC. A school allowing hands-on experiments with polarised neutrons at BENSC instruments and a workshop on inelastic neutron spectroscopy (WINS) accompanied the conference.

The three German national committees for research with synchrotron radiation, neutrons and ion beams have organised the SNI2006 as a joint national conference for users of these three probes. The conference took place in Hamburg in October 2006 with more than 500 participants from over 120 institutions. The particular strength of BENSC in high-field and low temperature sample environment was once again demonstrated by the fact that more than 30% of all contributions on magnetism were based on experiments performed at BENSC.

New Neutron Guide Hall

Between 2004 and 2005 the building of the new neutron guide hall II was completed and the first part of the new guide system together with a novel multispectral-beam extraction system installed at the cold source. In 2006 the focus was on completing the neutron guides for the three instruments VSANS, SPAN and EXED in the new guide hall and on continuing with the instrumentation. The installation of the wide-angle

spin-echo spectrometer SPAN which had been shifted from the old neutron guide hall to the new one could be finished end of 2006. SPAN will resume user operation in March 2007 after a short commissioning phase. First measurements demonstrate an excellent performance of its new polarising guide system. The commissioning of the high resolution SANS-instrument VSANS and of the extreme-environment diffractometer EXED is expected for end of 2007 / beginning of 2008. The design work for the new high-field magnet of 25 T (first stage – later upgrade to 35 T) to be used with EXED is going on.

HMI instruments at BESSY

To promote the complementary use of neutrons and synchrotron radiation, HMI has initiated the development and installation of two new insertion devices at the Berlin 3rd generation synchrotron source BESSY: the undulator UE46 providing soft X-rays with worldwide highest brightness and flux density and the 7T wiggler 7T-MPW shifting the photon energies to the hard X-ray regime. HMI-BENSC has built and operates 3 beamlines with four instruments S1 – S4 at these devices and a further instrument, the X-ray tomography station S5, at a none-HMI beamline. Access to these instruments is organised via the BESSY proposal system,

http://www.bessy.de/boat/www/

while the user service is performed by HMI-BENSC personnel.

The instrument S1 at the undulator beamline is in routine user operation since 2003. In 2005 a second experimental station in addition to the spectroscopy chamber has been commissioned: a reflectometer with a magnet providing a field of 7T at the sample position. This high-field end station opens up exciting new possibilities, in particular for investigating thin magnetic films and nanostructures.

Two beamlines are installed at the 7T wiggler: a monochromatic beamline providing photons with energies between 4 keV and 40 keV for the instruments S2 and S3 and a white beamline providing photons of energies up to 150 keV for the materials science instrument S4. The instrument S2 is specialised on resonant magnetic scattering and high resolution diffractometry, the instrument S3 on anomalous small-angle scattering (ASAXS) and grazing incidence scattering (GISAXS). S2 and S3 are operated alternatively at the monochromatic beamline. The instrument S4 at the white beamline is dedicated to materials science and engineering investigations, in particular to stress analysis using energy dispersive methods. All three wiggler instruments have been commissioned in 2005. S2 and S3 are in full user operation since April 2005, S4 since beginning of 2006.

The X-ray tomography instrument S5 operated by HMI-BENSC at the 7T wavelength-shifter beamline of the Bundesanstalt für Materialprüfung (BAMline) at BESSY is in full user operation since 2004.

A detailed description of these five instruments is given in the new instrument brochure of BENSC which can be found on the BENSC web pages. A printed version is available on request.

Short user statistics for HMI-BENSC instruments at BESSY in 2006

	Main instrument characteristics	External projects	External beam time	In-house projects	In-house beam time
S1 at UE46	Spectroscopy / reflectometry	18	26 weeks	8	13 weeks
S2 at 7T-MPW	Res. magn. scatt. / high-resol. diffract.	9	11 weeks	7	8 weeks
S3 at 7T-MPW	ASAXS/GISAXS (commissioning)	7	7 weeks	6	7 weeks
S4 at 7T-MPW	Materials Science / stress analysis	7	10 weeks	11	20 weeks
S5 at BAMline	Tomography	9	20 days	5	12 days

List of BENSC-Photons Instruments

Instruments at HMI-BESSY

No.	Instrument	Instrument Scientists	Phone	Room
S1	UE46-PGM	Detlef Schmitz	(Adlershof) 6392-5689 6392-4717 (Wannsee) 8062-2025	AHB 6317 A 225
		Hermann Rossner	(Adlershof) 6392-5762 6392-4717 (Wannsee) 8062-2914	AHB 6316 KH 203
		Nora Daroski	(Adlershof) 6392-5756 (Wannsee) 8062-2400	AHB 6415 P122
		Enrico Schirle	(Adlershof) 6392-5689	AHB 6317
S2	MagS	Ralf Feyerherm	(Adlershof) 6392-5750 6392-3163 (Wannsee) 8062-3082	AHB 6319 LR 139
		Esther Dudzik	(Adlershof) 6392-5687 (Wannsee) 8062-2925	AHB 6319 A 224
S3	ASAXS / GISAXS	Armin Hoell	(Adlershof) 6392-4678 (Wannsee) 8062-2925	AHB 6414
S4	EDDI	Christoph Genzel	(Adlershof) 6392-5751 (Wannsee) 8062-3097	AHB 6318 A 136
		Jens Gibmeier	(Adlershof) 6392-5686	AHB 6315
		Ingwer Denks	(Adlershof) 6392-5751 (Wannsee) 8062-3097	AHB 6318 A 136
		Manuela Klaus	(Adlershof) 6392-5751 (Wannsee) 8062-3097	AHB 6318 A 136
S5	Tomography@BAMline	Simon Zabler	(Adlershof) 6392-3159 6392-5760 (Wannsee) 8062-2822	AHB 6411 LR 240

List of BENSC-Neutrons Instruments

Instruments in the BER2 Experiment Hall (Thermal Neutrons)

No.	Instrument	ext.	Tube	Instruments Scientists	ext.	room
E1	3-Axis Spectrometer with Polarisation Analysis	3101	D 1N	Vadim Sikolenko Roland Schedler	2847 2793	LR 135 LR 129
E2	Flat-Cone Single Crystal and Powder Diffractometer (/E2 a: Neutrons Photography)	3102	R 1	Jens Hoffmann Uwe Amann	2185 2708	A 241 A 239
E3	Residual Stress Analysis and Texture Diffractometer	3103	T 2	Rainer Schneider Tobias Poeste	3096 3237	A 132 A 131
E4	2-Axis-Diffractometer (E4b: Position for Single Crystal Orientation)	3104	R 2	Karel Prokes Andrei Podlesnyak	2804 2768	LR 138 LR 144
E5	4-Circle Diffractometer	3104	R 3	Manfred Reehuis	2692	A 343
E6	Focusing Single Crystal Diffractometer (Due to technical problems E6 is not on schedule at the moment.)	3105	R 3	Norbert Stüßer Anthony Arulraj Alexandra Buchsteiner	3171 2793 2686	LR 142 LR 129 LR 143
E7	Residual Stress Analysis Diffractometer	3107	D 1S	Rainer Schneider	3096	A 132
E9	Fine Resolution Powder Diffractometer (FIREPOD)	3106	T 5	Dimitri Argyriou Oleksandr Prokhnenko Michael Tovar Nadir Aliouane	3016 2847 2768 3079	LR 137 LR 135 LR 144 LR 141
E10	HELINE, ^{3}He-Diffractometer	3106	D 1S	Konrad Siemensmeyer	2757	LS 132

Instruments in the BER2 Cold Neutron Guide Halls

No.	Instrument	ext.	Tube	Instruments Scientists	ext.	room
V1	Membrane Diffractometer	3121	NL 1A	Thomas Hauß Silvia Dante	2071 2071	LS 333 LS 333
V2	I: 3-Axis Spectrometer (FLEX) II: FLEX with NRSE opt.	3122	NL 1B	Klaus Habicht Kirrily Rule	2807 3067	A 333 A 331
V3	Time-of-Flight Spectrometer (NEAT)	3133	NL 2^{0}	Margaritta Russina Zunbeltz Izaola Ewout Kemner	3159 3179 3073	A 351 A 349 A 348
V4	Small Angle Scattering Instrument (SANS)	3124	NL 3A	Albrecht Wiedenmann Uwe Keiderling Astrid Brandt Sylvain Prévost Oliver Perroud	2283 2339 2169 2339 2340	LR 211 LR 209 LS 233 LR 209 LR 213
V5	Spin-Echo Spectrometer with ToF Option (SPAN)	3125	NL 4B	Catherine Pappas Phillip Bentley Evgney Moskvin	2046 3174 --	A 346 A 335 --
V6	Reflectometer	2806	NL 4B	Roland Steitz Ralf Köhler Anke Teichert	2149 -- 2044	A 221 -- A 230
V7	Cold Neutron Tomography and Radiography (CONRAD)	--	NL 1B$_{U}$	Nikolay Kardjilov Andre Hilger	2298 2490	A 317 A 316
B8	Neutron-Autoradiography	3121	NL 1A	Birgit Schröder-Smeibidl	2337	GE 145
V12a	Bent-crystal Diffractometer (USANS) / Tomography	3131	NL 3B	Wolfgang Treimer Markus Strobl	2221 2490	A 319 A 316
V12b	I: Double-crystal Diff. / Tomo. II: Tomography option	3131	NL 3B	Wolfgang Treimer Markus Strobl	2221 2490	A 319 A 316
V13	Fundamental Physics Beam Position	--	NL 3B	Margaritta Russina	3159	A 351
V14	Mirror Test Device	--	NL 1B^{O}	Thomas Krist	2045	A 233
V15	Extreme Environment Diffractometer (EXED) (under construction)		NL 4A	Hans-Jürgen Bleif	2758	A 235
V16	Very Small Angle Neutron Scattering (VSANS) (under construction)	--	NL 4C	Daniel Clemens	2280	V 131

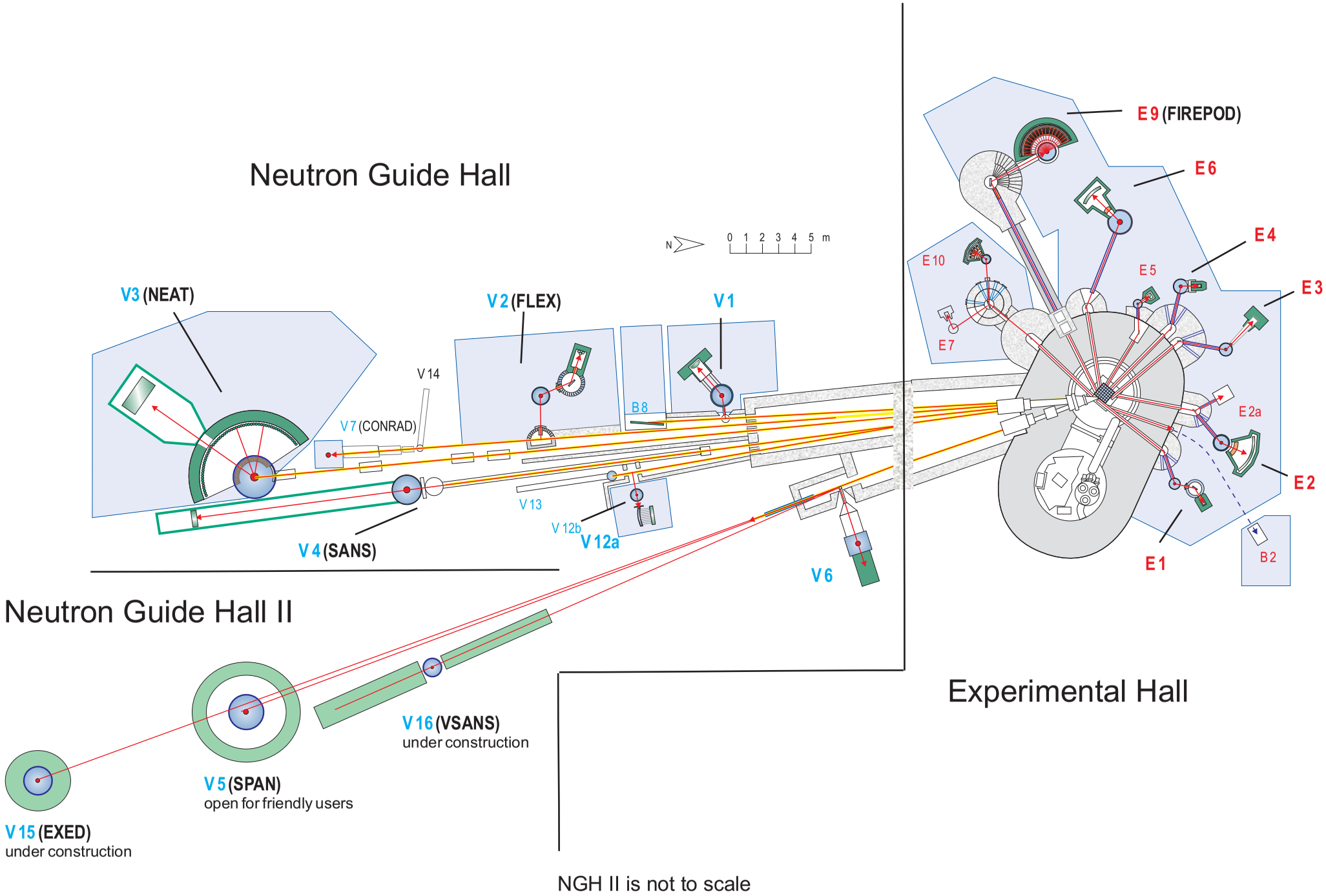
Neutron Guide Hall
N
0 1 2 3 4 5 m
V3 (NEAT)
V2 (FLEX)
V1
V14
V7 (CONRAD)
B8
V13
V12b
V12a
V4 (SANS)
V6
E9 (FIREPOD)
E6
E4
E3
E10
E5
E7
E2a
E2
E1
B2
Neutron Guide Hall II
V16 (VSANS)
under construction
V5 (SPAN)
open for friendly users
V15 (EXED)
under construction
Experimental Hall
NGH II is not to scale

The Wide Angle Neutron Spin Echo Spectrometer SPAN in NLH2

C. Pappas, F. Mezei, Ph. Bentley, E. Moskvin, R. Kischnik, P. Granz, L.A. Mertens SF1

The Wide Angle Neutron Spin Echo SPAN provides a broad dynamic range for inelastic scattering studies and optimal intensity conditions for polarization analysis in both diffuse and inelastic scattering. The instrument was shutdown end of September 2004 and after a passage between the old and new guide halls was opened, it was totally dismounted and moved into the new guide Hall. This relocation of SPAN was a particularly delicate operation due to the complexity of the instrument and to the large dimensions and weight of some components like the magnetic coils with diameters as large as 4.8 m and 3 m.

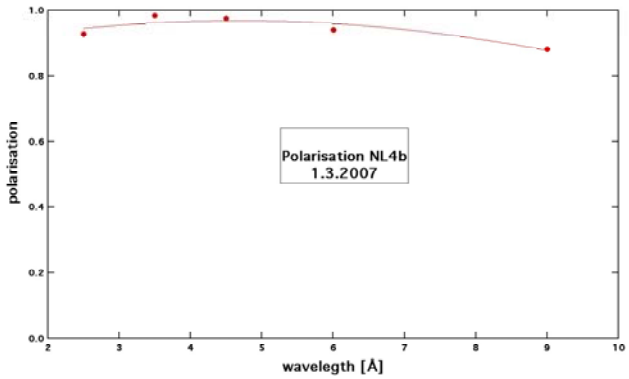

Fig. 2: *Polarization of the polarizing cavity of SPAN as a function of the wavelength.*

The reconstruction of SPAN at the new position started late 2005, when the mounting of the novel multispectral guide system was advanced enough to determine the sample position with the required accuracy. The smooth mounting of the spectrometer was followed by the mounting of the guide system and of the polarizing cavity, with FeSi m=2.5 supermirrors in transmission. The shielding components for the guide were installed end of 2006 and the instrument got its first neutrons on January 4rth 2007. After a commissioning period of two months the first “real” Neutron Spin Echo experiment was scheduled on SPAN to investigate phasons in quasicrystals with Richard Brand of the University of Duisburg.

SPAN was reconstructed at the new positions with some important modifications: the mounting and adjustment possibilities of the precession coils were improved, a new highly efficient polarizing cavity was installed as a part of the beam delivery system and the spectrometer is now using CARESS to communicate with the hardware (detectors, motors etc) but it operates with a software, compatible with the majority of the NSE spectrometers worldwide.

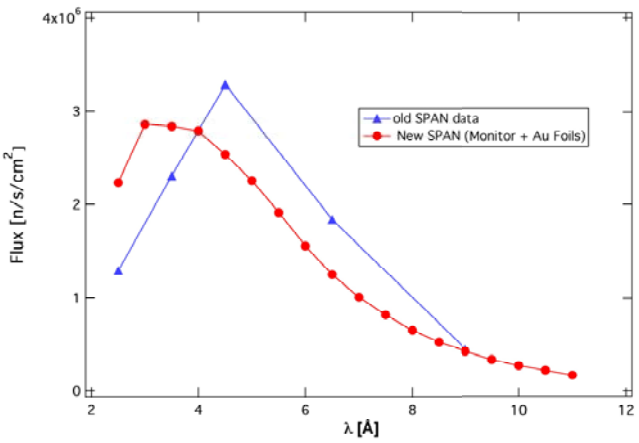

Fig. 1: *Polarized neutron flux at the sample position of SPAN: new position (circles) and previous position (triangles).*

One of the first measurements on SPAN were dedicated to the determination of the beam characteristics: flux and polarization. The flux (fig.1) is compatible with that at the previous position and with the results of the simulations, by taking the spectral distribution of the new guide into account. The polarization (fig. 2) is excellent, close to 95% in most of the wavelength range. Both the flux at the sample of SPAN and the polarization, especially at high wavelengths, will be slightly improved in the future, by further optimising the magnetic field configuration of the polarizing cavity. The first NSE measurements showed an improved resolution function, due to the non-magnetic environment of the new position.

News about the Instrumentation in the Neutron Guide Hall-II

In 2006 the project “Neutron Guide Hall II (NGH-II)” has to a large extent left the phase of planning and entered the phase of final constructions and installations.
The neutron guide system is almost finished. Its design and installation was technologically as well as logistically very challenging. Only the installation of the 7.5 m long last section of the EXED (V15) guide needed to be postponed to 2007. This elliptic guide end piece is capable of focusing the beam down to sample volumes of 20 H 20 mm . Gold foil activation measurements prove that the concept of the new guide system and its realization can be regarded as a big success. It is intended to periodically repeat these tests in order to monitor possible aging processes.

In February 2006, the operation of the reflectometer V6 could be resumed. V6 has been built up at its old place in the first neutron guide hall (NGH-I), but is now provided with neutrons by one of the new guides leading to NGH-II. A new detector test station (V17) has also been built up at this new guide and the mirror test station (V14) will be shifted to it, as well. End of 2006, the wide-angle spin-echo spectrometer SPAN (V5) was successfully re-installed in the NGH-II. SPAN will take up user operation in 2007 after a short commissioning period.

The completion of V15 (EXED) suffered from delays in the development of new position sensitive detectors, a project undertaken jointly with the Indiana University. The concept could successfully be tested, however, by measurements performed with a prototype. The performance of the prototype exceeded the specifications for the new detector. The development of special sample environment to be used with the future high field magnet (25 T in the first stage) on EXED has been started.
On VSANS the large detector vacuum chamber and a corresponding pumping system were installed and tested. The high-resolution detector of VSANS passed the commissioning tests. As a second detector for VSANS, a system based on a further development of the EXED-type detector is foreseen. The last large component to be installed for completing VSANS is the collimator exchange chamber. Its delivery is expected for the second half of 2007.

Fig. 1: *View to the new neutron guide hall II showing the progress in instrumentation. The photograph was taken end of 2006.*

<u>From the right to the left one can see:</u>

- *the partly shielded neutron guide leading to the sample position (not to be seen) of the Extreme Environment Diffractometer EXED (V15), which is located between the platform covering the spin-echo spectrometer SPAN and the coloured windows;*
- *the completely shielded neutron guide leading to SPAN (V5) which is already fully built up;*
- *the detector chamber for the new Very Small Angle Neutron Scattering instrument VSANS (V16) with the large box on its left hand side containing the pumping system*

By D. Clemens, SF1, HMI, Berlin

How to Apply for BENSC-Neutrons Beam Time

BENSC is open to both the national and the international user community with up to 70% of the beam time available to external users. The main portion of this beam time is foreseen for short term research proposals. Applications for short term beam time will be examined by an international scientific selection committee twice each year,

deadlines for submission of proposals are 15 March and 15 September.

The instrument responsibles of BENSC are asked to comment on the technical feasibility of the proposed experiments and have access to the submitted proposals for this purpose.

Requests for urgent or confidential experiments (Director's discretionary time) and for industrial use may be submitted at any time.

Applications for BENSC-Neutrons beam time should be made by using the BENSC Online Proposal Submission (OPS) system, which is available at the **BENSC VISITORS CLUB**

http://www.hmi.de/pubbin/bensc_club.pl

Further information on BENSC-Neutrons instrumentation can be obtained from the internet via

http://www.hmi.de/bensc/instrumentation/instrumentation_en.html

or

Hahn-Meitner-Institute Berlin
BENSC Guest office
Glienicker Str. 100
D - 14109 Berlin (Wannsee)
Germany
Phone +49 - 30 - 8062 2304
Fax: +49 - 30 - 8062 2523
Email: **bensc@hmi.de**

The BENSC Experimental Reports are intended as interim summaries. In view of the short time available between the termination of certain experiments and the deadline for this report, the results presented here have to be considered as preliminary. The inclusion of reports in this volume does not constitute a publication in the usual sense. Final results will be submitted for publication in regular scientific journals.

Acknowledgement for Support by the European Commission

The access of BENSC users from European Community Member States and Associated States to BENSC has been substantially supported by the European Community under the Framework Programme FP5, FP6.

FP5: Access to Research Infrastructure Action of the Improving Human Potential Programme (IHP) second BENSC contract, effective 11/2001 – 02/2004, with contract number **HPRI-CT-2001-00138**

FP6: BENSC is a partner in the EU supported network of European neutron facilities – the **Neutron and Muon Integrated Infrastructure Initiative (NMI3)**, an action within the EU FP6 activity 'Structuring the European Research Area: Research 11 research infrastructures.
The BENSC Access contract under NMI3 is effective for 4 years, from 01/2004 until 12/2007, the relevant EU contract number (NMI3I for acknowledgements is **RII3-CT-2003-505925.**

Results of EU supported groups are contained in 67 reports of this volume.

IHP-n°.	***p.***	***authors***	***affiliation***
305	95	Saint Grégoire et al.	Univ. Toulon, F

NMI3-n°.	***p.***	***authors***	***affiliation***
1043	56	Köbler et al.	FZ, Jülich
1120	191	De La Prida et al.	Univ. Oviedo, E
1122	61	Yusuf et al.	Univ. Zaragoz, ICMA, E
1130	127	Garab et al.	HAS BRC Szeged, H
1135	145	Miloto et al.	Univ. Palermo, I
1138	39	van Dijk et al.	TU Delft, NL
1144	77	Temst et al.	KU Leuven, B
1146	79	Hansen et al.	ETHZ & PSI, CH
1147	21	Šaroun et al.	ASCR NPI Rez, CZ
1148	35	Miliyanchuk et al.	CU Prague, CZ
1150	206	Morales-Flórez et al.	Univ. Cadiz, E
1152	143	Zanotti et al.	LLB-CEA/CNRS Saclay, F
1153	141	Brüning et al.	ILL Grenoble, F. + Uni Göttingen
1154	108	Bordallo et al.	ILL, Grenoble, F
1155	157	Zeghal et al.	Univ. Paris XI, F
1156	150	Montes et al.	UPMC – ESPCI, Paris, F
1157	151	Perzynski et al.	UPMC LI2C, F
1158	179	Bastie et al.	CNRS St. Martin d'Heres, F
1160	109	Wood et al.	Univ. of Cambridge, UK
1161	192	Lee et al.	Univ. Liverpool, UK
1162	201	Nikbin et al.	ICL, UK
1163	80	McEwen et al.	UCL, UK
1164	82	Rüegg et al.	UCL, UK
1165	139	Panayiotou et al.	AU Thessaloniki, GR
1166	212	Fiori et al.	UPM Ancona, I
1167	193	Baglioni et al.	Univ. Firenze, I
1168	100	Purans et al.	Univ. Povo, IT
1169	26	Purans et al.	Univ. Povo, IT
1173	202	Ohms et al.	EC-JRC-IE Petten, NL
1174	64	Gondek et al.	AGH-UST, Kraków, PL
1175	164	Kolasińska et al.	PAS Kraków, PL
1176	147	Rajexska, et al.	IAE Otwock, PL
1177	66	Khalyavin et al.	Univ. Aveiro, P
1178	174	Smrcok et al.	SAS Bratislava, SK
1179	180	Zrník et al.	TU Kosice, SK
1180	97	Werner et al.	TU, Wien, A
1181	78	Temst et al.	KU Leuven, B
1182	84	Kenzelmann et al.	ETHZ & PSI, CH
1183	189	Ryukhtin et al.	ASCR NPI Rez, CZ

1184	190	Strunz et al.	ASCR NPI Rez, CZ
1189	85	Chatterji et al.	ILL Grenoble, F
1190	104	Chatterji et al.	ILL Grenoble, F
1191	130	Bellissent-Funel et al.	LLB-CEA/CNRS Saclay, F
1196	120	Bradshaw et al.	Univ. Edinburgh, UK
1197	203	Nikbin et al.	ICL, UK
1198	73	Fennell et al.	UCL, UK
1199	176	Cosgrove et al.	Univ. Bristol, UK
1201	125	Berti et al.	Univ. Firenze, I
1202	204	Manescu et al.	UPM Ancona, I
1203	205	Giuliani et al.	UPM Ancona, I
1204	131	Venturoli et al.	Univ. Bologna, I
1207	134	Berti et al.	Univ. Firenze, I
1208	148	Triolo et al.	CNR IPCF, Messina, I
1210	207	Manescu et al.	UPM Ancona, I
1211	196	Renghini et al.	UPM Ancona, I
1212	172	Paduano et al.	Univ. Napoli, I
1213	209	Fiori et al.	UPM Ancona, I
1214	210	Triolo et al.	CNR IPCF Messina, I
1215	67	Bormanis et al.	Univ. of Latvia, Riga, LV
1216	29	Bormanis et al.	Univ. of Latvia, Riga, LV
1217	68	Gondek et al.	AGH-UST, Kraków, PL
1218	60	Nowicki et al.	AMU Poznań, Poland
1219	98	Salak et al.	Univ. Aveiro, P
1220	69	Mihalik et al.	IEP SAS, Košice
1254	182	Erné et al.	Univ. Utrecht, NL
1876	43	Ronnow et al.	LNS, ETHZ & PSI

Notice:

The quality of figures in the electronic versions, CD and WEB (http://www.hmi.de/bensc) – especially in colour presentation – is remarkably higher than in the print version

List of Contributed Experimental Reports

Development of Instruments and Methods

PAGE	TITLE	TEAM			PROPOSAL
2	**Test of the new E4 area detector**	K. Prokeš[1] A. Podlesnyak[1] T. Wilpert[1]	[1]HMI, Berlin	E4	**OTH-01-1831-EF**
3	**Polarization option at E4**	K. Prokeš [1] A. Podlesnyak[1]	[1]HMI, Berlin	E4	**OTH-01-2003-EF**
4	**A new detection system for the E6 experiment**	T. Wilpert[1] N. Stüßer[1] A. Arulraj[1] A. Buchsteiner[1] B. Gebauer[1] C. Schulz[1] F.V. Levchanovsky[2] E.I. Litvinenko[2] A.S. Nikiferov[2] V.I. Prikhodko[2]	[1]HMI, Berlin [2]FLNP JINR, Dubna, RU	E6	**Inst. Dev.**
6	**Test of high pressure CuBe Cell HMI-6 at E9**	O. Prokhnenko[1] J. Kamarad[2]	[1]HMI, Berlin [2]ASCR IP Prague, CZ	E9	**PHY-01-1913**
7	**Larmor phase topology with NRSE**	K. Habicht[1]	[1]HMI, Berlin	V2	**PHY-02-0543-EF**
8	**The TISANE technique applied to field-induced ordering in a ferrofluid**	Wiedenmann[1] R. Gähler[2] K. Habicht[1] U. Keiderling[1] M. Russina[1] P. Granz[1]	[1]HMI, Berlin [2]ILL Grenoble, F	V3	**PHY-03-0443-EF**
9	**Benchmarking of the SANS instrument V4**	M. Kammel[1] A. Wiedenmann[1]	[1]HMI, Berlin	V4	**Inst.Dev.**
10	**Tests of ^{3}He filled spin filter cells for polarization analysis**	U. Keiderling[1] A. Wiedenmann[1] A. Rupp[1] W. Heil[2] J. Klenke[2] M. Meißner[1]	[1]HMI, Berlin [2]Uni Mainz	V4	**PHY-04-1242-EF**
11	**Polarization analysis of SANS data**	U. Keiderling[1] A. Wiedenmann[1] A. Rupp[1] W. Heil[2] J. Klenke[2]	[1]HMI, Berlin [2]Uni Mainz	V4	**PHY-04-1246-EF**
12	**New Sample Environment for Experiments under Controlled Gas Atmospheres I: Low Temperatures, Low Pressures**	A. Brandt[1] D. Wallacher[1] M. Meißner[1]	[1]HMI, Berlin	V4	**PHY-04-1340-EF**
14	**Closed-cycle refrigerator for SANS measurements in ac and dc magnetic fields**	A. Wiedenmann[1] D. Wallacher[1] R. Gähler[2] U. Keiderling[1] P. Granz[1] K. Thillosen[3]	[1]HMI, Berlin [2]ILL Grenoble, F [3]Gonit, St. Egreve, F	V4	**PHY-04-1342-EF**
15	**Diffuse scattering from Si-Fe multilayers**	A. Teichert[1] R. Steitz[1] T. Krist[1]	[1]HMI, Berlin	V6	**Inst. time**

List of Contributed Experimental Reports

Magnetic Structure and Phase Transitions

List of Contributed Experimental Reports

List of Contributed Experimental Reports

List of Contributed Experimental Reports

List of Contributed Experimental Reports

Magnetic Excitations

List of Contributed Experimental Reports

PAGE	TITLE	TEAM			PROPOSAL
Chemical Structure					
91	**Investigation of giant linear superelasticity phenomenon in Ni-Mn-Ga single crystal martensite**	I. Glavatskyy[1] J.-U. Hoffmann[2]	[1]NAS IMP Kiev, UA [2]HMI, Berlin	E2	**MAT-01-1855**
92	**Patterning of Sodium Ions and the Control of Electrons in Sodium Cobaltate**	D.A. Tennant[1] J. Goff[2] J. Morris[2] J.-U. Hoffmann[1]	[1]HMI, Berlin [2]Univ. Liverpool, UK	E2	**PHY-01-1811-EF**
93	**Crystal structure of $Ca_{0.01}Y_{0.99}VO_3$ and $Ca_{0.05}Y_{0.95}VO_3$**	M. Reehuis[1] C. Ulrich[1] B. Keimer[1]	[1]MPI, Stuttgart	E5	**PHY-01-1724-LT**
94	**Crystal structure of CaV_2O_4**	B. Lake[1] M. Reehuis[2] J.-Q. Yan[3] A. Niazi[3] D.C. Johnston[3]	[1]HMI, Berlin [2]MPI Stuttgart [3]Iowa State Univ., USA	E5	**PHY-01-2008-EF**
95	**Understanding the mechanism of the phase Instrument E6-E9 transition and the nature of the chemical disorder in SBT: a neutron diffraction study**	P. Saint Grégoire[1] Y. Gagou[1] M.A. Frémy[1] D. Többens[2]	[1]Univ. Toulon, F [2]HMI, Berlin	E6 E9	**MAT-01-1104 (1147)**
96	**Determination of Light Elements via Neutron Diffraction**	G. Auffermann[1] P. Höhn[1] R. Niewa[1] N. Aliouane[2] D. Argyriou[2]	[1]MPI CPfS Dresden [2]HMI, Berlin	E9	**CHE-01-1859**
97	**Structural study of $Pr_{9.33}(SiO_4)_6O_2$, $Pr_9Li(SiO_4)_6O_2$ and $Pr_8M(II)_2(SiO_4)_6O_2$ (M(II)=Mg, Ca, Sr, Ba, Zn, Cu)**	F. Werner[1] M. Tovar[2]	[1]TU Wien, A [2]HMI, Berlin	E9	**CHE-01-1960**
98	**Temperature-induced structure transformations in perovskite lanthanum magnesium titanate**	A.N. Salak[1] V.M. Ferreira[1] O. Prokhnenko[2]	[1]Univ. Aveiro, P [2]HMI, Berlin	E9	**MAT-01-1966**
99	**Is Deuteration really Chaning the Crystal Structure of the Simpler Amino-acid l-alanine?**	H. N. Bordallo[1] D. N. Argyriou[1] D. Többens[1]	[1]HMI, Berlin	E9	**PHY-01-1411-EF**
100	**Neutron diffraction study of the atomic and magnetic structure in the $La_{0.7}Sr_{0.3}Co_{1-x}Nb_xO_3$ and $La_{0.3}Sr_{0.7}Co_{1-x}Nb_xO_3$ ($x = 0.0 \div 0.35$)**	J. Purans[1] A. Kuzmenko[2] V.Efimov[3] V. Sikolenko[4]	[1]Univ. Povo, IT [2]Univ. Genf, CH [3]JINR Dubna, RU [4]HMI, Berlin	E9	**PHY-01-1863**
101	**Neutron diffraction structural investigation of natural kesterite**	S. Schorr[1] M. Tovar[1]	[1]HMI, Berlin	E9	**PHY-01-1957**
Structural Excitations					
102	**Lattice dynamics of strongly doped GaAs**	A. Naberezhnov[1] V. Sikolenko[2] S. Borisov[1]	[1]PTI St. Petersbg., RU [2]HMI, Berlin	E1	**PHY-02-0524**
103	**NRSE investigation of the electron-phonon interaction in the BCS superconductor Nb**	K. Habicht[1] F. Mezei[1] T. Keller[2] P. Aynajian[3] B. Keimer[3]	[1]HMI, Berlin [2]MPI Stuttgart + TUM [3]MPI FKF Stuttgart	V2	**PHY-02-0511-LT (0569-EF)**
104	**Short range charge ordering in Fe_3O_4**	T. Chatterji[1] K. Habicht[2]	[1]ILL Grenoble, F [2]HMI, Berlin	V2	**PHY-02-0559**

List of Contributed Experimental Reports

Geology

Biology

List of Contributed Experimental Reports

List of Contributed Experimental Reports

Soft Matter

List of Contributed Experimental Reports

List of Contributed Experimental Reports

Structures and Phases

List of Contributed Experimental Reports

Nanostructures

List of Contributed Experimental Reports

Strain & Stress

List of Contributed Experimental Reports

List of Contributed Experimental Reports

List of Contributed Experimental Reports

Development of Instruments and Methods

	EXPERIMENTAL REPORT Test of the new E4 area detector	Proposal N° OTH-01-1831-EF Instrument **E4** Local Contact K. Prokeš, A. Podlesnyak
Principal Proposer: Experimental Team:	K. Prokeš – HMI, Berlin K. Prokeš – HMI, Berlin A. Podlesnyak – HMI, Berlin T. Wilpert – HMI, Berlin	Date(s) of Experiment 31.10. – 12.11.2006

Date of Report: 29.12.2006

Good news: the new area detector made by Mirrotron Ltd has been finally delivered and after joint tests performed by Mirrotron Ltd., detector group of HMI and the E4 instrument responsibles accepted by HMI.

The detector has physical active-area dimensions of 200mm x 200mm and efficiency at 2.4 Å of about 80%. It is attached to a dedicated PC and controlled by software developed by E.I. Litvinenko from JINR Dubna. Although it is, in principle possible to use any resolution (number of cannels in x or y direction), the spatial resolution of the detector is about ±1mm in both directions limiting the practical number of channels to up to 256x256. At present, we run the detector mostly in 128x128 channel mode.

Communication with CARESS that provides start and stop signals and download of the measured histograms is done via direct computer-computer link and independent on the network.

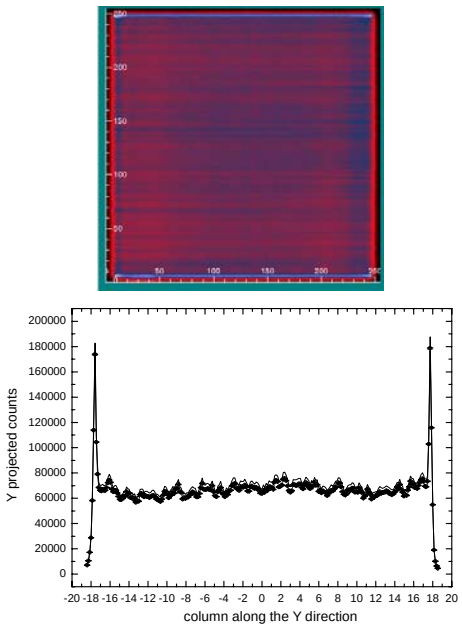

Fig. 1: *The 2D pattern from vanadium rod (top). Projection onto the y-axis (bottom).*

Due to a large variety of sample environment conditions used for different experiments at E4 it is necessary to optimize the distance (and hence also the resolution) of the detector from the sample (magnet). The closest distance presently used for OS, OM and VM3 is 600 mm. Consequently, the detector covers about 19 degrees in this position. The largest distance used for e.g. HM1 and VM1 is 870 mm and coverage is reduced to about 13 degrees. Unpleasant consequence of the not-fixed sample-detector distance is a difficulty with collimation that needs to be adjusted for each individual distance. At present is this problem not solved yet.

Another sensitive point is that one should determine efficiency of each individual pixel. For that, uniform irradiation of the detector is needed. This appeared to be rather difficult. In Fig 1. we show the diffraction pattern resulting from 1 hour counting of a thin vanadium rod at 90 deg. scattering angle in the 256x256 channel resolution. Apart from some obvious horizontal lines one can discerns also weak vertical and diagonal lines. All these lines are, however of rather minor importance as the difference in intensity is few percents. This, however, does not apply for two strong horizontal lines near the upper and lower edge of the figure. These areas are to be excluded from the use during the experiments. By combining patterns taken for 12 hours for 128x128 and 256x256 channel binning we have obtain efficiency file yielding the systematic statistical error of about 0.9%.

In Fig 2. we show as the first example of a real measurement the angular dependence of the integrated intensity of the twelve equivalent (210)

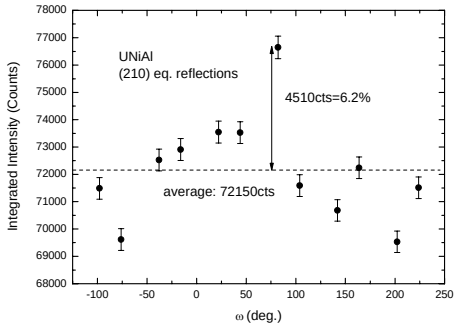

Fig. 2: *The angular dependence of the twelve equivalent (210) structural reflections of UNiAl.*

reflections of UNiAl measured at RT. The intensities differ from the average intensity by not more than 6.2%. Such a differences are often due to absorption/extinction of the sample.

We are confident that the new detector makes the E4 instrument more competitive and leads to new scientific possibilities.

BENSC	**EXPERIMENTAL REPORT** **Polarization option at E4**	Proposal N° OTH-01-2003-EF Instrument **E4** Local Contact K. Prokeš, A. Podlesnyak
Principal Proposer: Experimental Team:	K. Prokeš – HMI, Berlin K. Prokeš – HMI, Berlin A. Podlesnyak – HMI, Berlin	Date(s) of Experiment 28.02. – 03.03.2006 07.08. – 16.08.2006

Date of Report: 05.01.2007

Recently we have identified the space region responsible for the depolarization of the originally polarized neutron beam on E4. In the Part I, in order to test the improved set-up we have performed extended mapping of the influence of the compensation and flipping currents onto the flipping ratio measured in the direction of the attenuated direct beam.

For the tests we have removed the shielding block after the polarizing bender in the front of the cryomagnet and introduced an analyzing bender and guide field sections one of them containing π-flipper together with compensating coil. The sketch of the experimental set-up for the first part is shown in Fig.1.

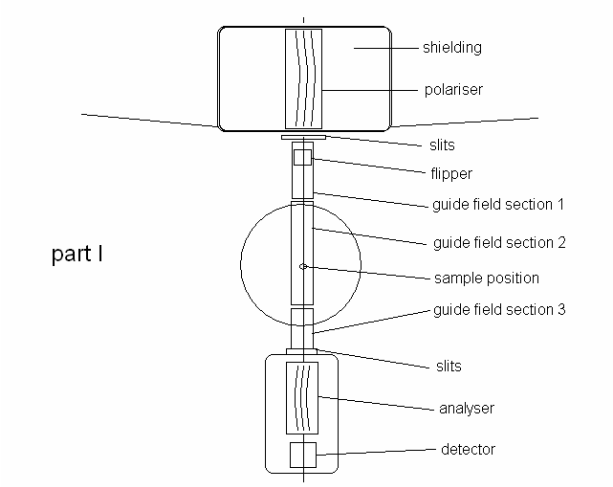

Fig. 1: *Layout for the first part of the experiment.*

It appeared that we can achieve the flipping ratio defined as a ratio of counting rates with flipper off and on as high as 25. However, the intensity at the sample position amounts in this case merely to about 0.1 10^6 n/cm^{2}s. Typical 2θ dependence of the polarization degree defined as $P = N^+/(N^+ + N^-)$ across the direct beam is shown in Fig. 2. Correction for the dead-time of about 12 μs is necessary in this case because of partial saturation of the detector.

In the second part we have used as a testing sample Heusler crystal inserted into the magnetic field of up to 5T generated by asymmetric VM2 cryomagnet. We have followed the flipping and compensating current dependences of the detected neutrons and determined the polarization degree and the values of currents for each value of applied magnetic field. The field dependences of the resulting flipping and compensating currents giving the best flipping values (always around 14, slightly improving with increasing field) is shown in Fig. 3

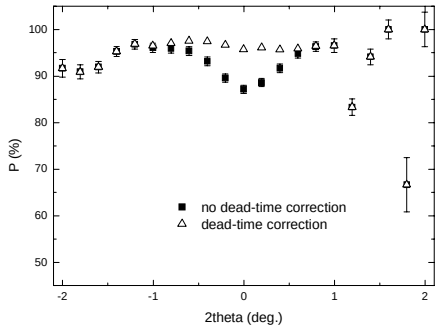

Fig. 2: *Typical 2θ dependence of the polarization degree across the direct beam*

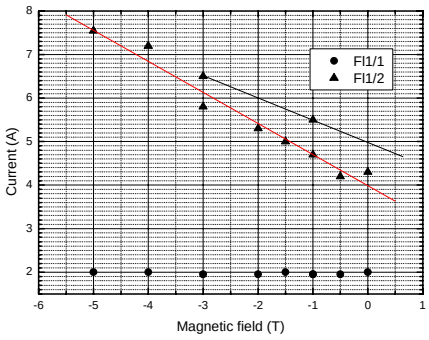

Fig. 3: *The field dependence of the flipping FLl/1 and compensating FL1/2currents at which the best flipping ratio using the Heusler crystal has been observed. The two lines for FLl/1values correspond to the best fit to data obtained for two positions of the flipper.*

Although is the flipper placed inside an iron joke there is still a non-negligible interference between the stray field of the cryomagnet and the guide field which add together resulting in necessity to use higher compensating current.

In conclusion, we have proved that polarization experiments are at E4 possible. However, rather serious modifications to the shielding just in the front of the cryomagnet (removal of the shielding block) are necessary.

	EXPERIMENTAL REPORT A new detection system for the E6 experiment	Proposal N° Inst. Dev. Instrument **E6** Local Contact Norbert Stüßer
Principal Proposer: Experimental Team:	T. Wilpert – HMI, Berlin N. Stüßer, A. Arulraj, A. Buchsteiner – HMI Berlin B. Gebauer, C. Schulz – HMI, Berlin F.V. Levchanovsky, E.I. Litvinenko, A.S. Nikiferov, V.I. Prikhodko – FLNP JINR, Dubna, RU	Date(s) of Experiment 2006

Date of Report: 12.01.2007

Introduction:

The BENSC experiment E6 was recently equipped with a modern 300 x 300 mm² position-sensitive detector (300TN, *DENEX*) with delay-line position encoding. The detector is filled with 4.8 bar ^{3}He and 1.2 bar CF_4 as stopping gas and has a detection gap of 20 mm while the entrance window has a thickness of only 9 mm aluminum. The neutron absorption efficiency is thus 80% for a wavelength of 2.44 Å and the position resolution is about 2 mm for the X- and 3 mm for the Y-coordinate. These values could be verified during test measurements. The detector is connected to HMI's preamplifiers IV112 (anode, gain 20 dB) and IV110 (cathodes, gain 20 dB), respectively, and each preamplifier to the main amplifier IV111 (gain 23–53 dB), which can be used with filters of different shaping times. This electronics developed at HMI is characterized by superior low noise performance (1.7 dB noise figure for IV110 and IV112), impedance adaptable cathode preamplifiers matching the true delay line impedance, a large band width of up to 300 MHz and very high gain of up to 73 dB. For the discrimination of the fast timing signals a constant-fraction discriminator (CF8000, *Ortec*) is used.

For read-out of such delay-line encoded position sensitive detectors a specialized data-acquisition board with PCI adapter (Fig. 1) was developed by HMI (SF7 and BENSC) in collaboration with Frank Laboratory of Neutron Physics, Joint Institute for Nuclear Research in Dubna, Russia. The PCI board is provided with a deadtime-less 8-channel multihit TDC of the F1 type (*acam*) with 120 ps LSB, a 40 MHz flash ADC, a FPGA, a FIFO and a 0.9 GFLOP DSP chip TMS320C6711. The X and Y positions of a detected neutron are determined via the time difference of the prompt anode signal (T_{Start}) of the detector and the position-dependent delayed signals of either end of the

Fig. 1: *Front side of the data acquisition board DeLiDAQ, provided with a TDC (1), a FPGA (2), a DSP (3) and a large histogramming memory (4) as main components.*

X- and Y-delay line ($X_{L\text{-}Stop}$, $X_{R\text{-}Stop}$, $Y_{U\text{-}Stop}$, $Y_{D\text{-}Stop}$). By online filtering in the FPGA with rates of up to 2.5 MHz. and by employing the multihit capability of the TDC, two events occurring at different positions within the delay line time length T_{DL} of e.g. 300 ns can be correctly measured utilizing the filter functions $|X_{L\text{-}Stop} + X_{R\text{-}Stop} - 2T_{Start} - T_{DL}| < \varepsilon_{DL}$ and $|Y_{U\text{-}Stop} + Y_{D\text{-}Stop} - 2T_{Start} - T_{DL}| < \varepsilon_{DL}$, where ε_{DL} is chosen according to the time resolution achieved in the measurement. Moreover, the PCI board performs time-of-flight measurements in reference to a pulsed beam or chopper with ≥25 ns bin size for TOF ranges of up to ~420 ms (not used at E6). The on-board DSP can be used for accumulating and buffering 1D, 2D and 3D histograms of any combination of parameters with selectable resolution in an external 512 kB SBSRAM or in 256 MB SDRAM memory. Optionally the data can be transferred in list-mode (i.e. event-wise data recording) to the hosting PC. The DSP is also responsible for the communication with the controlling PC program DeLiDAQ [1]. The PC program can work either in stand-alone mode (simple start and stop) or can be controlled by the experimental control program *CARESS* via the *CORBA* interface. For precise timing of

measurements a logical TTL signal vetoing the FPGA has to be provided. A more detailed description of the hardware can be found elsewhere [2].

Results:

After few months experience with the new detection system and adaptation of the data processing programs, the results are very promising and exemplified by measurements of an yttrium iron garnet powder within a cylindrical vanadium container with a diameter of 8 mm and an effective height <40 mm.

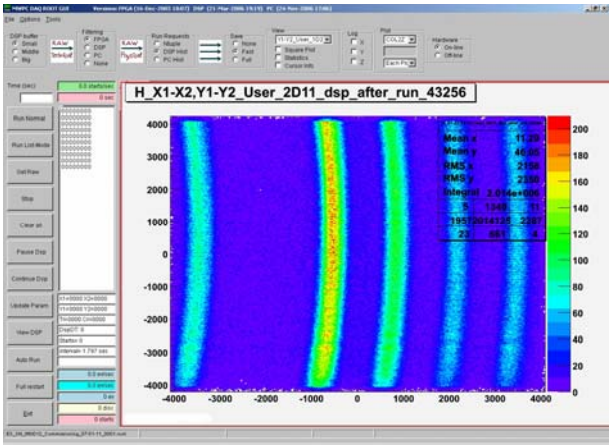

Fig. 2: *On-line display of the controlling software DeLi-DAQ showing Debye Scherrer lines of an yttrium iron garnet powder.*

Fig. 2 shows the on-line visualization of Debye Scherrer lines of a single measurement of a 2θ angular scan, while the complete 2θ scan consists of 20 measurements. The used wavelength was 2.44 Å obtained from a pyrolythic graphite monochromator. An in-pile fan collimator was used so that the angular resolution was only weakly dependent on the diffraction angle. With the help of the program *Bean* data of all 20 measurements were converted and merged with appropriate normalizations to a diagram showing intensity vs. scattering angle (Fig 3). A profile matching procedure was applied by using the program *Fullprof*, and the fit result is shown together with the difference plot in Fig. 4. A simple Gaussian profile is sufficient to obtain very good agreement between the measurements and calculations.

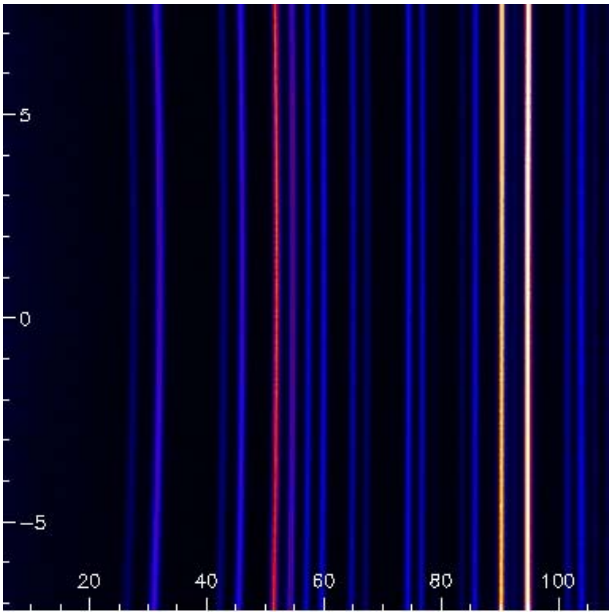

Fig. 3: *Debye Scherrer lines of an yttrium iron garnet powder of a complete 2θ scan after normalizing and merging 20 individual measurements.*

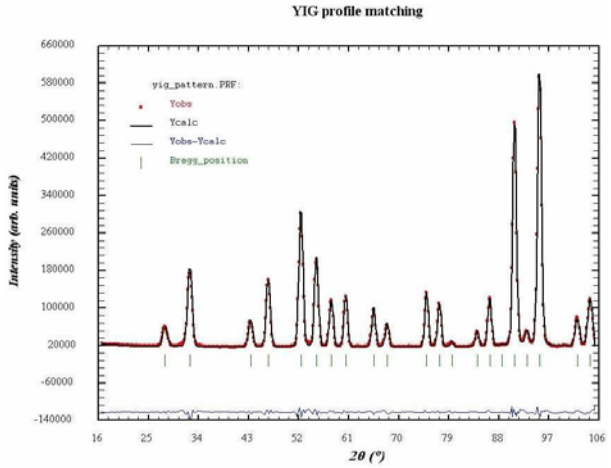

Fig. 4: *Result of a refinement using Fullprof showing the measured data, fit result, and difference spectrum in the lower part.*

References:

[1]. Levchanovsky, et al., Nucl. Instr. and Meth. A **569** (2006) 900–904

[2]. Levchanovsky, et al., Nucl. Instr. and Meth. A **529** (2004) 413-416

	EXPERIMENTAL REPORT **Test of high pressure CuBe Cell HMI-6 at E9**	Proposal N° PHY-01-1913-EF Instrument **E9** Local Contact Oleksandr Prokhnenko
Principal Proposer: Experimental Team:	O. Prokhnenko – HMI, Berlin J. Kamarad – ASCR IP Prague, CZ	Date(s) of Experiment 22.05. – 29.05.2006

Date of Report: 30.11.2006

Neutron diffraction measurements at extreme conditions (low temperatures, high magnetic fields, and high pressures) become more and more used nowadays. In modern science we need to be able to perform either or all types of these measurements. The proposed experiment has been carried out to test a high pressure CuBe Cell HMI-6 at E9 in order to evaluate its capabilities and E9's performance. A set of measurements including different samples (NaCl for pressure calibration and Lu_2Fe_{17} for crystal and magnetic structure refinement), different pressure transmitting media (mixtures of mineral oils and Fluorinetr FC70 / FC77) and different pressures and temperatures revealed the following features of using HMI-6 high pressure cell at E9 diffractometer:

(i) Maximum pressure of 9.5 ± 0.5 kbar was reached at room temperature. Maximum sample volume corresponds to ~ 700 mm^3 (height ~ 25 mm and 6 mm). Pressure value was determined from the known pressure dependence of the lattice parameters of NaCl.

(ii) CuBe pressure cell produces a number of strong parasitic peaks that significantly restrict the available 2theta range (Fig. 1). In addition to high background level (produced by incoherent scattering from the pressure cell and pressure transmitting media) and small sample (volume=)signal, this means that one can hardly refine the (crystal / magnetic) structure under pressure using present setup. In the best case, a pressure dependence of the lattice or strong low angle magnetic peaks can be investigated.

(iii) In contrast to successful use of mineral oils mixture as a pressure transmitting media in similar type of high pressure cell at single crystal E4 diffractometer, we found that it is impossible to use the same mixture in powder diffraction experiment. It leads to significant increase of the background caused most probably by the incoherent scattering coming from the hydrogen containing mineral oils. Fluorinetr FC70 / FC77 1:1 mixture gives much lower background providing a proper pressure transmitting media that can be used in powder diffraction experiments under pressure.

(iv) Cooling the pressure cell down to 20 K leads to the decrease of pressure from 9 down to 6.7 kbar (dP = - 2.3 kbar) for mixture Fluorinetr FC70 / FC77.

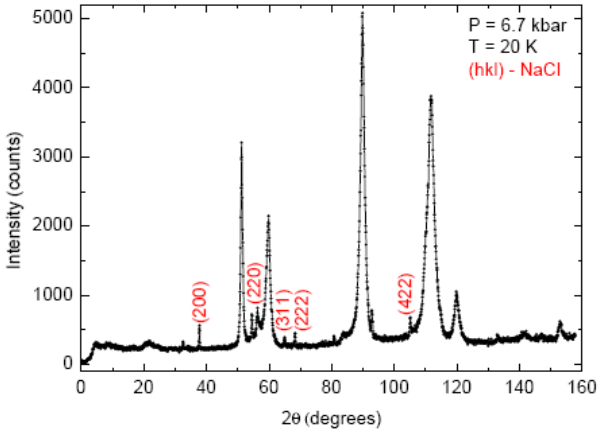

Fig. 1: *Neutron diffraction pattern of NaCl in CuBe cell under pressure of 6.7 kbar at 20 K.*

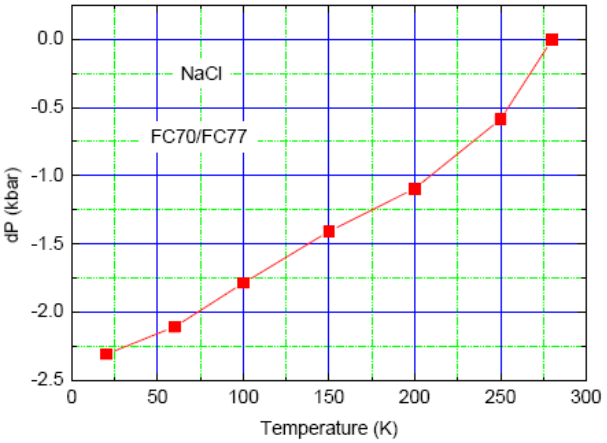

Fig. 2: *Decrease of pressure in CuBe cell with changing temperature.*

	EXPERIMENTAL REPORT Larmor phase topology with NRSE	Proposal N° PHY-02-0543-EF Instrument **V2-NRSE** Local Contact Klaus Habicht
Principal Proposer: Experimental Team:	K. Habicht – HMI, Berlin K. Habicht – HMI, Berlin	Date(s) of Experiment 12.12. – 17.12.2006

Date of Report: 03.01.2007

As part of the NMI3-JRA-PNT project this research task is focussed on manipulating the Larmor phase topology within the resolution volume of an NRSE-equipped triple-axis spectrometer. Ultimately, additional Larmor precession, provided by a set of correction elements, should yield tuneable, curved surfaces of constant Larmor phase, which are matched to the dispersion surfaces of elementary excitations.

Previous experiments carried out at V2 in direct beam geometry have shown that a combination of current sheets (constant current density) and π-flippers, all inserted between the two (untilted) bootstrap coils of the first NRSE arm, can be used to provide an effective tilt angle. The present experiments focussed on mapping the Larmor phase topology using the (200) Bragg peak of a high-quality Nb single crystal (mosaicity ~ 8.9 arcmin) to probe the phase of the spin-echo within the resolution volume.

V2/FLEX was operated in a configuration with scattering senses (SM=-1, SS=-1, SA=+1) at fixed $k_i = k_f = 2.4\ ^{-1}$ where second-order contamination is substantially suppressed by the curved neutron guide. No additional collimators were used besides bender polarizers after the PG monochromator and after the PG analyzer. The NRSE option was operated in bootstrap-mode with an effective frequency f_{eff} = 1 MHz. Data sets have been collected (1) under the normal Larmor diffraction conditions, i.e. with tilt angles of the RF-coils set to θ_1= +37.9° and θ_2= -37.9°, and (2) with tilt angles of the coils set to θ_1= +29.8° and θ_2= -46°. The topology of the Larmor phase inside the resolution ellipsoid of the TAS was then measured by TAS-scanning the Bragg peak along the longitudinal and transverse directions in Q-space keeping the NRSE parameters fixed. As expected, the Bragg peaks appear intensity modulated along the longitudinal direction in Q-space for configuration (1), while for configuration (2) the modulation appears to be tilted in Q-space.

Four current sheets (vertical direction) and 3 π-flippers (single flat coils with horizontal field direction) were introduced in between the tilted RF-flippers of the first NRSE arm. Although the echo polarization is lost if the current sheets are operational, it can well be recovered if the 3 flippers provide π-flips and in addition all bootstrap coils downstream the insert have reversed polarity. Fig. 1 shows the intensity modulated Bragg peak for these experimental conditions. Another set of measurements has been performed for non-linear current distributions which have been realized by simply reversing the polarity of half of the current sheets. It was found that the polarization was reduced to 80% of its original value. An example is shown in the contour plot of Fig. 2 which shows that the linear modulation still dominates and a substantial second order modification towards curved Larmor surfaces is not evident.

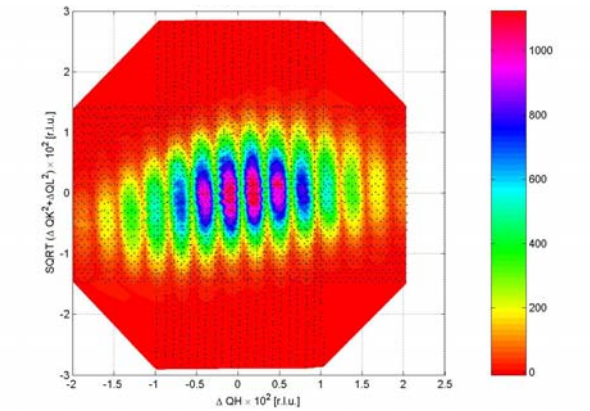

Fig. 1: *Larmor phase map measured with configuration (1) (see text), current sheets with constant lateral current distribution and flippers in first NRSE arm.*

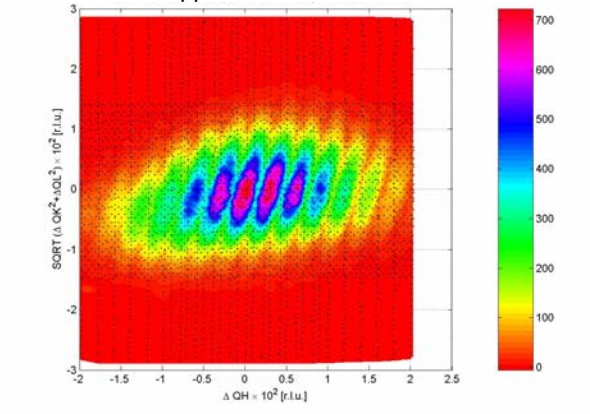

Fig. 2: *Larmor phase map measured with configuration (2) (see text), current sheets with non-linear lateral current distribution and flippers in first NRSE arm.*

This research project has been supported by the European Commission under the 6th Framework Programme through the Key Action: Strengthening the European Research Area, Research Infrastructures. Contract n°: RII3-CT-2003-505925.

BENSC	**EXPERIMENTAL REPORT** **The TISANE technique applied to field-induced ordering in a ferrofluid**	Proposal N° PHY-03-0443- EF Instrument **V3** Local Contact Margarita Russina
Principal Proposer: Experimental Team:	A. Wiedenmann – HMI Berlin R. Gähler – ILL Grenoble K. Habicht, A. Wiedenmann – HMI, Berlin U. Keiderling, M. Russina, P. Granz – HMI Berlin	Date(s) of Experiment 20.06.-29.06.2006

Date of Report: 09.01.2007

TISANE is a time-resolved SANS technique based on the frame-overlap TOF (FOTOF) principle combined with a periodically modulated sample property. The main advantage is that it allows extending the time scale accessible with neutron scattering into the sub-millisecond range. Previously we have applied the technique to investigate the dynamics of field-induced ordering effects in a magnetic colloid of Co nanoparticles and demonstrated that the technique is superior to stroboscopic SANS with a continuous neutron beam [1]. Here we report on detailed measurements of (de-)tuning curves to find the optimum frequencies by an experimental approach.

In the TISANE configuration realized at V3/NEAT, we used a single fast chopper with variable frequencies up to ν_C = 666 Hz at a distance L_1= 10.9 m from the sample. A periodic sine-wave modulation of the external magnetic field at the sample is produced by the output signal of a high-precision function generator fed into an RF amplifier which drives the same solenoid device as in [1]. With this device amplitudes up to 26 mT and frequencies up to 3 kHz are accessible. The data acquisition of the 2-D SANS-detector (with distance sample-detector L_2 = 4.1 m) was triggered by another function generator operated with frequency ν_D. For fixed L_1, L_2 and a particular sample frequency ν_S, the chopper frequency ν_C and the detector frequency ν_D must be chosen to satisfy the TISANE conditions

$$\nu_D = \nu_S - \nu_C \quad \text{and} \quad \frac{\nu_S - \nu_C}{\nu_C} = \frac{L_1}{L_2}. \qquad (1)$$

As opposed to the previous TISANE experiment, the frequencies ν_S and ν_D were phase-locked to the master clock of the NEAT chopper system which was transformed into a 10 MHz signal by a dedicated PLL circuit to provide the proper external reference signal for the function generators.

Tuning curves have been measured close to a nominal sample frequency ν_S = 1kHz by recording the TISANE signal for (1) small variations in the sample frequency ν_S at fixed detector and chopper frequencies ν_D and ν_C respectively and for (2) small variations in the detector frequency ν_D at fixed sample and chopper frequencies ν_S and ν_C respectively. The data is integrated over the whole detector area and fit to a simple sinusoidal function (Fig. 1) which allows extracting the contrast of the TISANE signal. In each case two subsequent data sets have been recorded under identical conditions (see Fig.1) which in addition allows to extract the phase shift during the time between two measurements. As seen from Fig. 2, the tuning curves have a FWHM corresponding to a relative accuracy $\Delta\nu/\nu \sim 10^{-6}$. Note that this quantity depends of course on the absolute measurement time. Larger variations in sample frequency and detector frequency can be accepted if both frequencies change by the same amount. This has been confirmed by changing these frequencies in a ~1% interval without noticeable loss of contrast keeping ν_D-ν_S=const..

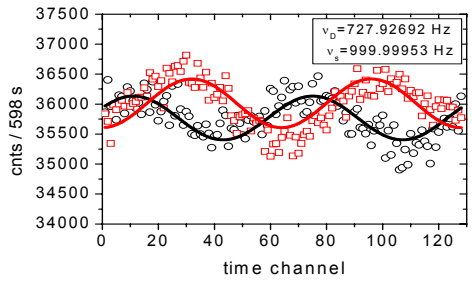

Fig. 1: *Time dependence of the TISANE signal integrated over the detector area for two subsequent measurements. One time channel corresponds to 7.81 μs.*

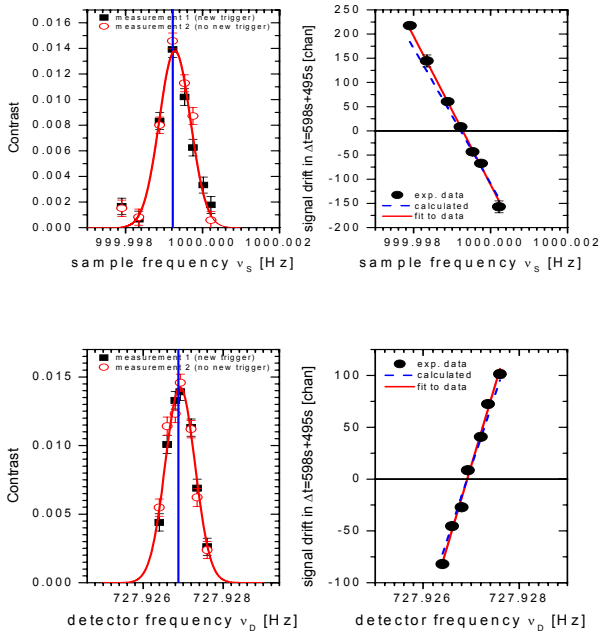

Fig. 2: *Contrast variation (left panels) and phase shift (right panels) for detuning the sample frequency (top panels) or the detector frequency (bottom panels).*

Reference:

[1]. A. Wiedenmann , U. Keiderling, K. Habicht, M. Russina, R. Gähler, PRL **97**, 057202 (2006).

	EXPERIMENTAL REPORT **Benchmarking of the SANS instrument V4**	Proposal N° Inst.Dev. Instrument **V4** Local Contact Martin Kammel
Principal Proposer: Experimental Team:	M. Kammel – HMI, Berlin A. Wiedenmann – HMI, Berlin M. Kammel – HMI, Berlin	Date(s) of Experiment 06.01. – 08.01.2006 01.02. – 04.02.2006

Date of Report: 17.01.2007

The Helmholtz Association intended a bench-marking between their Small Angle Scattering (SAS) instruments. For this purpose several round-robin samples have been selected and measured on the instrument V4.
Table 1 gives an overview of the samples investigated under different instrumental conditions such as wavelength resolution $\Delta\lambda/\lambda$, collimation length and sample to detector distance.
The advantage of a contrast variation with contrast matching of the solvent was shown on sample containing PB10-PS10 block copolymer micelles. This copolymer was solved in thee different H/D ratios of the solvent to match with the scattering length density the core, the shell and with an average contrast. Additionally the pure solvent was measured for a correction of the incoherent scattering of the solvent.
In a second series a Polystyrene–block–Poly-isoprene–block-Polystyrene (later denoted as PS-PI-PS) copolymer thermoplastic was measured under different conditions. The aim was to show the influence on the smearing of the scattering by changing the wavelength distribution as a result of a different tilting angle of the velocity selector. Additionally the samples was measured with the same collimation – sample and sample - detector distance(later denoted as symmetric measurement) resulting in a high flux as well as an improved collimation (none symmetric measurements). The results of the PS-Pi-PS samples are partly shown in figure 1. There is no significant smearing effect visible over a broad range so that the highest flux condition is in case of similar samples satisfactory.
For the comparison of the conditions with polarised neutrons we investigated a FeCu-alloy.

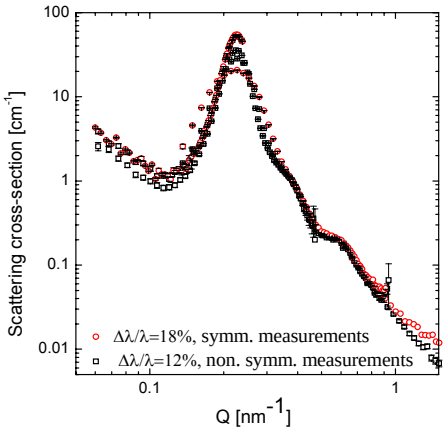

Fig. 1: *The PS-Pi-PS thermoplast measured with A) highest neutron flux(symmetric condition and tilting the detector) marked with red points and with B) better instrument resolution(none symmetric condition and no tilting of the detector) marked with black points*

Table 1: *Samples measured in the framework SAS-Benchmarking*

wavelength resolution	11%							17%				
Collimation [m]	2	4		8	12	16		2	4	8	12	16
sample detector distance [m]	0.98	4			12	8	16	0.98	4		12	16
none polarised neutrons												
PB-PS Diblockcopolymere solutions (different contrasts)	x	x	x	x				x	x	x	x	
solvents of PB-PS Diblockcopolymere solutions								x	x			
PS-PI-PS Diblockcopolymere (solid)	x	x	x	x		x	x		x	x		x
silica spheres	x		x				x	x	x			x
polarised neutrons												
FeCu-alloy	x		x		x							

	EXPERIMENTAL REPORT **Tests of ^{3}He filled spin filter cells for polarization analysis**	Proposal N° PHY-04-1242-EF Instrument **V4** Local Contact Uwe Keiderling
Principal Proposer: Experimental Team:	A. Wiedenmann, U. Keiderling – HMI, Berlin A. Rupp, U. Keiderling – HMI, Berlin W. Heil, J. Klenke – Univ. Mainz	Date(s) of Experiment 03.04. – 06.04.2006 10.07. – 14.07.2006 20.11. – 23.11.2006

Date of Report: 19.01.2007

The V4 SANS instrument has recently been equipped with a ^{3}He spin filter setup to enhance the SANSPOL option with a tool for polarization analysis. The main part of this setup is a ^{3}He filled spin filter cell which is placed in the homogeneous field of the sample magnet, immediately behind the sample. Since the ^{3}He polarization permanently decays, the setup also includes a refilling device which allows the exchange of the polarized ^{3}He gas by pumping off the decayed gas filling from the cell and refilling fresh polarized gas from an external reservoir. This gas exchange is a discontinuous process and cannot be performed during data acquisition. It is therefore desirable to have filter cells with a long lifetime of polarization, in order to maximize the usable uninterrupted period of beamtime between two refillings.

To determine the lifetime of polarization, transmission measurements of the filter cell (without sample) were performed with alternating Flipper "ON" and "OFF" settings. From the flipping ratio, the ^{3}He polarization P(t) was calculated as a function of time, and fitted with an exponential decay

$$P(t) = P_0 \exp\left[-\frac{t}{\tau}\right]$$

to obtain the decay time τ as a quantitative measure for the quality of the cell and the general setup. Each decay series was started immediately after refilling the cell, and ran between approximately 2 and 5 hours.

In the beginning, the homogeneity of the magnetic field within the space between the two pole shoes was measured using a Hall sensor and a PC-controlled 3D scanning system. At a ^{3}He pressure p = 1 bar and a typical field B_0 = 0.6 T, this yielded a relative field gradient $\frac{dB(r)/dr}{B_0} < 7*10^{-4}$ cm^{-1}, which according to the theory should allow a maximum τ in the order of 120 h. However, the first measured τ were only in the order of 1 h. To determine the reason of this discrepancy, different cells, valves, magnetic fields and gas pressures were attempted, and environmental conditions at the location of the filter cell were modified. This research program involved design modifications of the cell and the surrounding parts, and was therefore spread over different beam time periods. The main results are:

(1) The decay time strongly depends on the individual cell. From a larger manufacturing series of "GE 180" glass cells, only 2 usable cells were identified in a first NMR test (B_0 = 8...20 Gs) at university Mainz. Even under identical experimental conditions on the V4 instrument, both cells still revealed a noticeable difference in τ.

(2) The decay time was not influenced by magnetic interferences from outside the sample magnet. Neither a modification of the constant collimator guide field close to the sample position, nor a HF shielding of the cell with two isolated layers of aluminium foil gave rise to a systematic change in τ.

(3) The magnetisation of the cell itself turned out to be a serious problem. In a NMR test in Mainz (B_0 = 20 Gs), the decay time of the best cell with Titanium valve dropped from τ = 8.5 h (de-magnetized) to τ = 2.5 h (after magnetization). This result was confirmed by a measurement at the very strong NMR device (15000 Gs) at the medical center of University Mainz, and by the neutron measurements.

(4) A valve made of Titanium turned out to be superior to a valve made of Vitronit. The best results were obtained with a Duran glass valve driven by compressed air.

(5) Small technical details turned out to have a significant influence on the decay time, like the adhesive used to connect the GE 180 glass cell and the Duran glass valve, or the covering of this adhesive binding with grease.

At present, the best decay time achieved with neutrons was approximately 7800 s ± 650 s (2.2 h), which is still far away from the expected decay time in the order of 100 h. It must be concluded that the design of the cell and the adjacent valve has not been systematically understood yet.

	EXPERIMENTAL REPORT **Polarization analysis of SANS data**	Proposal N° PHY-04-1246-EF Instrument **V4** Local Contact Uwe Keiderling
Principal Proposer: Experimental Team:	U. Keiderling, A. Wiedenmann – HMI, Berlin U. Keiderling, A. Wiedenmann – HMI, Berlin A. Rupp – HMI, Berlin W. Heil, J. Klenke – Uni Mainz	Date(s) of Experiment 20.11. – 23.11.2006

Date of Report: 19.01.2007

In a different report of this volume, we described tests with ^{3}He based spin filter cells that were tested in the electromagnet of the V4 instrument. The disadvantage of this type of spin filter is the permanent decay of the ^{3}He polarization which continuously changes the transmissions of the filter T(+) and T(-) for nuclear spin polarizations parallel (+) and anti-parallel (-) to the guide field of the electromagnet. In the given experiment, the best available filter cell featured a decay time (to e^{-1} of the original polarization) of approximately (7800 ± 650)s. This is too short to consider the transmission as being "time-independent" for more than a few minutes. Even with a stable filter cell, an additional second spin flipper placed between the sample and the filter would have been necessary to properly separate the flip and non-flip components for (+) and (-) polarization directions, but was not available. To overcome these issues, we developed an alternative way to perform the experiment and process the scattering data, which even takes advantage of the insufficient stability of the filter.

In the experiment a concentrated Co-ferrofluid sample "MFT3N" was placed in the sample position in the homogeneous field of the electromagnet, immediately in front of the filter cell. With the normal POLARIS setup, two sample intensities

(1) $I(+) = T(+)I(++) + T(-)I(+-)$ (Flipper OFF)

and

(2) $I(-) = T(+)I(-+) + T(-)I(--)$ (Flipper ON)

were measured alternately, into 5-minute files, over a period of 5 hours. Between these measurements, in regular intervals the sample was removed from the beam position by the automatic sample changer, and replaced with an empty slit to measure the transmission of the filter cell, into 1-minute files. We thus obtained two separated but time-linked sets of data: the sample scattering and the transmission of the filter cell both as a function of measurement time. From the transmission data sub-set, we approximated the time dependence of the transmissions T(+) (falling from approximately 0.26 to 0.14 within 5 hours) and T(-) (rising from approximately 0.08 to 0.12) with appropriate fit functions. Using these time dependencies, we then performed linear regressions of the sample scattering data, to extract the flip I(+-) and non-flip I(++) components from Eq.(1), and the flip I(-+) and non-flip I(--) components from Eq.(2).

An example for the scattering data and results of Eq.(2) is given in the figures. Fig.1 shows the change in the raw data during the experiment time due to the filter cell transmission change caused by the ^{3}He polarization decay. Fig.2 shows the flip component I(-+) extracted from the raw data set consisting of the starting and ending spectra shown in Fig.1 and the intermediate stages between them. The absolute intensity of this first result has not yet been scaled properly to the input data intensity and corrected for background. However, the typical "butterfly" pattern of the flip component caused by the $(\sin\alpha*\cos\alpha)^2$ dependence of the intensity (α is the between the scattering vector Q and the magnetic field B) is obvious.

This analyzing procedure has been included in the "BerSANS" data processing software of HMI Berlin. Further improvements of the procedure are under way.

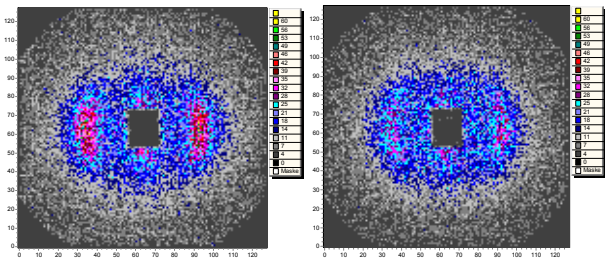

Fig.1: *Raw data at t = 0 and t ≈ 5h.*

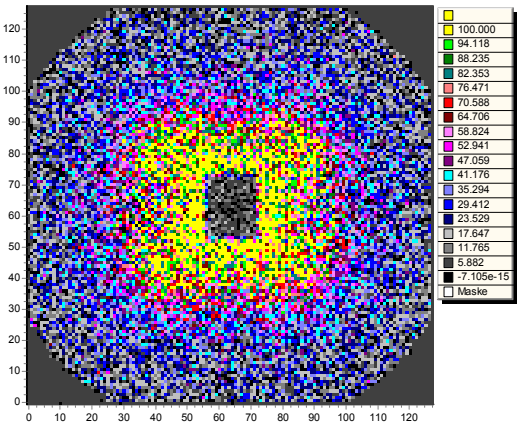

Fig.2: *Flip component I(-+).*

Reference for "BerSANS" program:

[1]. U.Keiderling, Appl. Phys. A **74** [Suppl.] (2002) S1455-S1457.

	EXPERIMENTAL REPORT **New Sample Environment for Experiments under Controlled Gas Atmospheres I: Low Temperatures, Low Pressures**	Proposal N° PHY-04-1340-EF Instrument **V4** Local Contact Dirk Wallacher
Principal Proposer: Experimental Team:	A. Brandt – HMI, Berlin D. Wallacher – HMI, Berlin M. Meißner – HMI, Berlin	Date(s) of Experiment Mai – September 2006

Date of Report: 18.01.2007

In consideration of the increasing relevance and request of complementary in-situ investigation methods at BENSC, a supplementation of the exiting temperature sample environment is projected, which will allow controlled gas atmospheres (CGA) at the sample position. The goal is to provide several modular devices for neutron scattering experiments under gas and vapour atmospheres in the pressure range from 10^{-8} bar to 10^{4} bars, and at temperatures from 2K to 1500K. In 2006 several components have been developed to cover the demands of the CGA-project in the low temperature (4K < T < 320K) and low pressure (P < 1.3 bar) regime. In some cases these setups can also be used for somewhat higher temperatures and pressures up to about 400K and 50bars.

In principle for all these sample conditions the gas of interest is supplied to the sample by a gas manifold, which is connected via a thin capillary with a vacuum sealed and temperature regulated sample compartment.

The gas manifold in fig.1 for pressure applications P < 50bars is equipped with high accuracy (< 0.2% of reading) capacitive pressure transducers (type Baratron, MKS-Instruments) with full ranges of 10torr, 100torr, 1000torr. The system is designed for isothermal gas adsorption measurements by the volumetric method [1]. The size of the dosing volume can be adapted by several calibrated gas tanks in the range of 50cm^3 to 10.000cm^3. This has the advantage, that even for the controlled filling of the sample cell with large amounts of gas, only a few gas dosing steps are necessary.

All pressures during a measurement can be displayed and recorded by data acquisition software. For the calculation of the total amount of gas dosed into the sample cell, a sophisticated EXEL-application is provided, which contains all necessary calibration data of the system. A fully atomized version of this manifold is under construction and scheduled for the proposal round 2007/II.

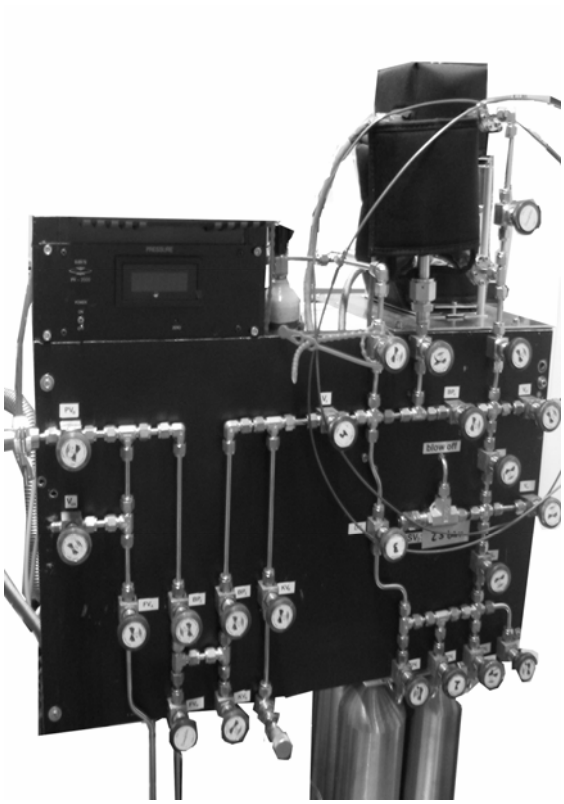

Fig. 1: *Manifold with gas inlets, supply tanks, dosing volumes, and temperature stabilized pressure gages.*

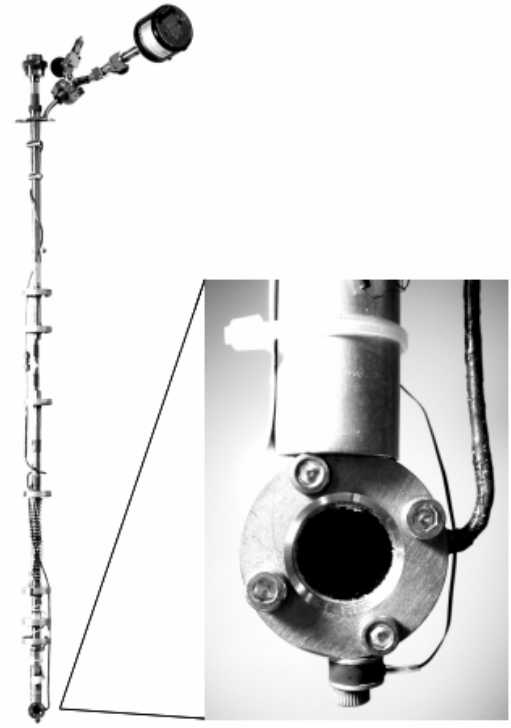

Fig. 2: *CGA-OS sample stick for in-situ gas adsorption measurements in a standard orange cryostat (left). Sample cell for SANS and USANS investigations (right).*

The CGA-OS sample stick (fig.2) can be used for adsorption measurements in the standard orange cryostat from 2K to 300K (OS) and in the cryo-furnace (OF) from 4K to 400K. Thereby the temperature is limited by the use of Indium seals for the sample cells. For special requirements CGA-OM stick, fitting in the sample tube of an orange maxi cryostat (OM), can also be provided. The sample sticks can be used together with a couple of sample cells of different size and shape, see fig.3. Thereby the cell is thermally coupled to the VTI-temperature of the OS by a small amount of ^{4}He exchange gas. The gas supply capillary can be heated among the whole length of the stick to ensure that the sample cell is the coldest point of the adsorption parts. This is important to avoid the condensation of solid or liquid plugs in the capillary.
The CGA-OS sample stick has successfully been used in a first N_2-adsorption experiment at 77K combined with USANS. The results are published elsewhere in this report.

Fig.3: *Photograph of available sample containers with different shapes for CGA-OS and CGA-OM.*

For in-situ adsorption experiments in the temperature range from 55K to 320K the closed cycle pulse tube cooler CGA-PTR (TransMIT) can be used instead of the orange cryostat. The whole pulse tube setup (including the He-compressor) is 320 x 300 x 200 mm in size, only. This system provides an easy access to the sample cell by removing simply the outer vacuum can.
Driven by a 130W/50Hz power supply, the thermal load of 200g can be cooled down from 295K to the base temperature of 55K in about 45 minutes, as can been seen from the cooling curve in fig.5. The temperature can be stabilized by an Lakeshore 340 temperature controller in between 10mK. The installation has successfully been used with SANS-studies on hierarchical mesopores combined with N_2-adsorption; see B. Smarsly et al. in this report.

Reference:

[1]. Characterization of Porous Solids and Powders: Surface Area, Porosity and Density, S. Lowell, J. Shields, M.A. Thomas & M. Thommes, Springer, (2004)

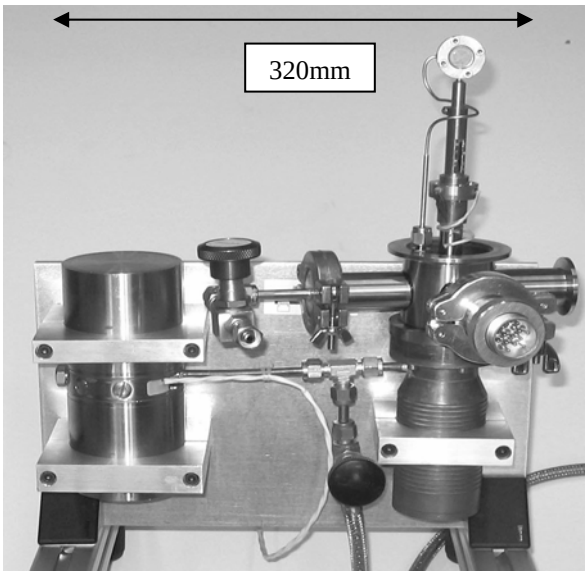

Fig.4: *Mini pulse tube refrigerator (CGA-PTR) with the SANS gas adsorption cell. The outer vacuum can is not shown here.*

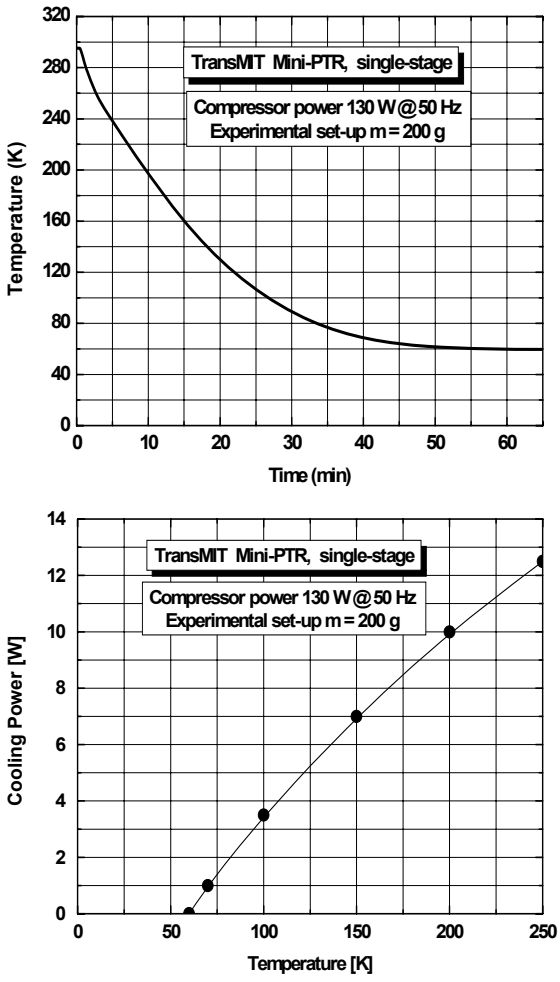

Fig.5: *Recorded cooling curve (top) and power diagram (bottom) of the new CGA-PTR device.*

	EXPERIMENTAL REPORT Close-cycle refrigerator for SANS measurements in ac and dc magnetic fields	Proposal N° PHY-04-1342-EF Instrument **V4** Local Contact Albrecht Wiedenmann
Principal Proposer: Experimental Team:	A. Wiedenmann, D. Wallacher – HMI, Berlin M. Meißner – HMI, Berlin R. Gähler – ILL Grenoble, F A. Wiedenmann, U. Keiderling – HMI, Berlin D. Wallacher, P. Granz – HMI, Berlin K. Thillosen – Gonit, St. Egreve, F	Date(s) of Experiment 07.09. – 12.09.2006 22.10. – 24.10.2006

Date of Report: 17.01.2007

Precisely defined static and oscillating magnetic fields have to be applied at variable temperatures for time-resolved SANS and SANSPOL investigations of magnetic relaxation processes in nanomaterials [1,2].

We have set up a special device adapted to the V4 instrument which should fulfil these requirements in a broad range of parameters. A special power coil was built around a core of soft magnetic material and equipped with a high-stability frequency generator and power supply. Periodic sine-wave modulations of the magnetic field up to amplitudes of B_{max}=40 mT and frequencies between ν_s = 50 Hz and 3000 Hz can be applied to the sample. The pole gap of 30 mm allows placing standard Hellma cuvettes in the homogeneous part of the horizontal magnetic field. Using a special impedance adjustment device it is possible to superimpose a static magnetic field up to B_{dc}=40 mT. The resulting magnetic field is of well defined sinusoidal shape. In addition, the dc- field can be cycled between ±40 mT without or with offset in a frequency range above 10^{-3} Hz which allows measuring even very slow relaxation processes onto equilibrium.

A mini closed cycle cooling system has been built for the thermalization of the sample and inserted in the pole gap of the magnetic core, see inset of fig.1. The temperature regulation system, based on a Stirling refrigerator (TransMIT) which is driven by a small He-compressor (50W/50Hz), provides a temperature stability of 10mK in the range from 35K to 320K. Fig.1 shows the cooling curve of the mini-cryostat: Cooling down to 45K from room temperature is achieved typically within one hour.

All parameters defining the magnetic field such as shape, amplitude, frequency and dc-offset as well as the temperature can be set remote controlled by CARESS.

First measurements on magnetic colloids [3,4] showed the long term stability of the device which is easy to handle and allows very fast sample changes.

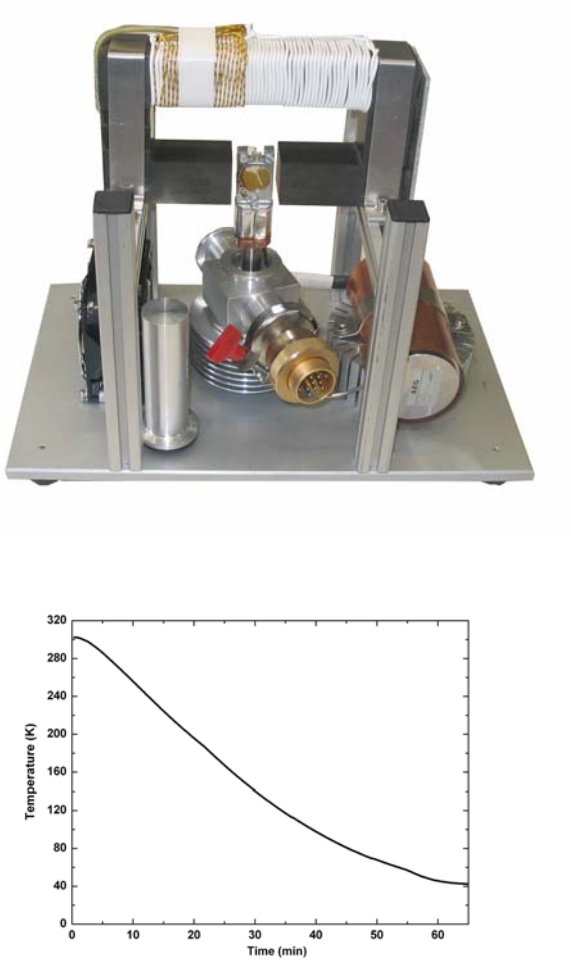

Fig. 1 top: *Photograph of Mini-Stirling refrigerator with the yoke and the coil for the oscillating magnetic field with dc offset. Two pickup coils are used for controle and to produce a trigger signal for time-resolved measurements. Bottom: Cooling curve.*

References:

[1]. A. Wiedenmann, U. Keiderling', K. Habicht, M. Russina, R. Gähler,PR L **97**, 057202 (2006)

[2]. K. Habicht, A. Wiedenmann, R. Gähler, U. Keiderling, BENSC report 2006

[3]. A. Wiedenmann, U. Keiderling, S. Prévost , D. Wallacher, M. Meissner, BENSC report 2006

[4]. B. Erné, M. Klokkenburg, S. Prévost, A. Wiedenmann, U. Keiderling , BENSC report 2006

	EXPERIMENTAL REPORT **Diffuse scattering from Si-Fe multilayers**	Proposal N° Inst. time Instrument **V6** Local Contact Anke Teichert
Principal Proposer: Experimental Team:	A. Teichert – HMI, Berlin A. Teichert – HMI, Berlin R. Steitz – HMI, Berlin T. Krist – HMI, Berlin	Date(s) of Experiment 02.11. – 07.11.2006

Date of Report: 16.01.2007

Si-Fe multilayers are frequently used as neutron optical elements, such as polarizers. Optimum performance requires low roughness, minimal interface layer thickness and low stress in the layers. Here, we report an investigation of the specular and off-specular (diffuse) neutron scattering from two selected Si-Fe multilayers.

The samples were prepared in a triode sputter device. The argon pressure and sputter power were 6.8×10^{-4} mbar and 240 W, respectively. This way, supermirrors with m=2.6 were built on both sides of Si wafers with dimensions of 84 mm × 126 mm × 0.5 mm. "m" denotes the ratio of the critical angle of the supermirror to the critical angle of natural nickel. Bending measurements on a profilometer, DEKTAK 3030, yielded radii *R* of 316±10 m for sample A and 7.8±2 m for sample B.

At first we performed polarized neutron reflectometry (PNR) measurements at V14 (BENSC, HMI) at a wavelength of 4.8 Å. In those experiments both samples showed a reflectivity of 92% at the critical angle and an average flipping ratio of 62.5 between 0.4° and 1.2° in transmission.

After the specular scattering measurements at V14 we recorded the diffuse neutron scattering at V6 at a wavelength of 4.66 Å and a divergence of the incident beam of 0.02°. For these measurements were used a positive sensitive detector (PSD). The distance between the sample and detector was 1.57 m, thus giving to a divergence of 0.02° also on the exit side. The supermirror samples worked simultaneously as analysers in our experimental set up.

Fig.1 and Fig.2 display the 2D maps of diffuse scattering recorded from sample A at magnetic fields of 203 and 1570 Gauss, respectively. The PSD was moved with the exit angle during the measurements. Thus, the reflected beam shows up as straight bright line at constant y-pix, independent of the sample angle, while the transmitted beam varies with sample angle. The diffuse scattering, which is the bright area surrounding reflected and transmitted beam, decreases at higher magnetic field by more than two orders of magnitude.

Magnetic field scans from 300 and 3757 Gauss at fixed incident angle of 0.8° and different detector (exit) angles between 0.3° and 0.9° revealed that at all angles the strong diffuse scattering vanished at a critical magnetic field of 1560 Gauss.

Sample B, however, did show a different behaviour (see Fig. 3). In that case the strong diffuse scattering did not depend on the applied magnetic field. We hold the larger bending of that wafer responsible for this effect.

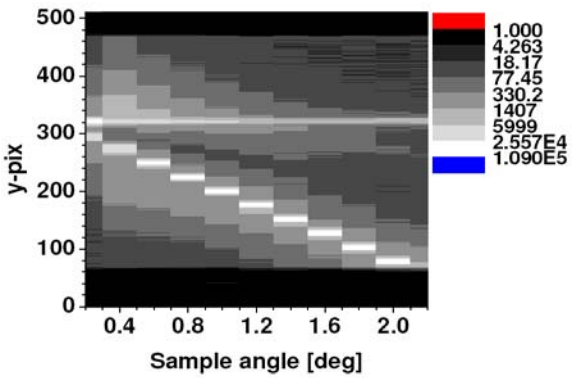

Fig.1: *Scattered intensity from sample A at 203 Gauss with incident spin down neutrons (R=316 m).*

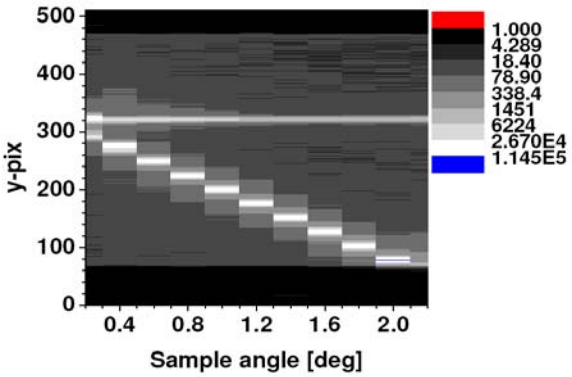

Fig.2: *Scattered intensity from sample A at 1570 Gauss with incident spin down neutrons (R=316 m).*

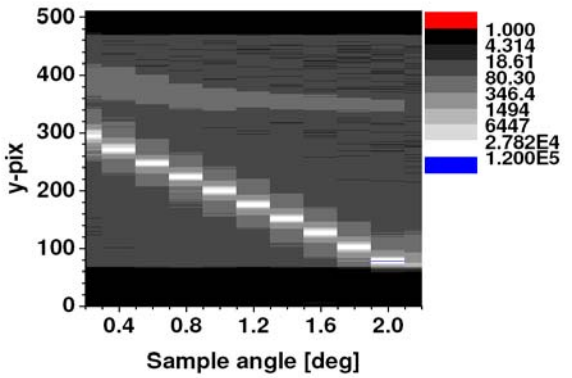

Fig.3: *Scattered intensity from sample B at 1570 Gauss with incident spin down neutrons (R=7.8 m).*

	EXPERIMENTAL REPORT V12a instrument development	Proposal N° OTH-04-1352-EF Instrument **V12a** Local Contact M. Strobl, W. Treimer
Principal Proposer: Experimental Team:	M. Strobl – HMI, Berlin + TFH Berlin K. Staack – HMI, Berlin + TFH Berlin W. Treimer – HMI, Berlin + TFH Berlin	Date(s) of Experiment Feb. + Nov. 2006

Date of Report: 06.01.2007

The new V12a instrument is settled on a new optical bench independent of the V12b instrument [1]. Due to the new construction the housing of the instrument is not available anymore and the instrument is more exposed to temperature fluctuations and background in the guide hall. Additional background has been caused by the new guides passing very close to the V12 instrument. These facts introduced the need for a new shielding concept for the double crystal diffractometer which needs, due to its high resolution (arcsec), on one hand high angular i.e. high mechanical stability that is influenced by temperature changes and it needs a low background due to the low available flux densities in such instruments. Therefore new walls of 10 cm thick PE pieces with a height of 50 cm were built around the instrument parts starting from the walls of the guide shielding which also houses the monochromator of the DCD. An additional wall between the sample position and the analyser with a hole only for the neutron beam establishes together with a roof plate a complete housing for the sensitive analyser and detector group. The walls as well as the ceiling (Al) are covered by 5 mm Boroncarbide (B4C) on the inside. Measurements concerning background and stability demonstrate the success of these measures (Fig. 1 and 2). The background at opened shutters for the new guides is improved by more than a factor of 2 (Fig.1, black) compared to the same situation with an improvised shielding before (Fig. 1, green) and even better than compared to closed shutters with the old shielding (red). Also the stability measured by the stability of the peak position over several days (Fig. 2) could be improved clearly. The peak is stable within the errors of the position determination which is less exact for the actual situation (Fig. 2, black) as the values had to be taken from long term user measurements with lower resolution, while before (red) the day cycle superposed by a general shift is clearly visible. Additional improvements are a new, implemented slit construction and an independent construction for the use of standard sample environment.

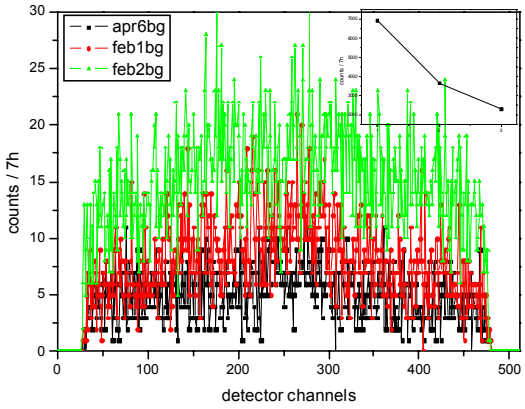

Fig. 1: *Different background measurements*

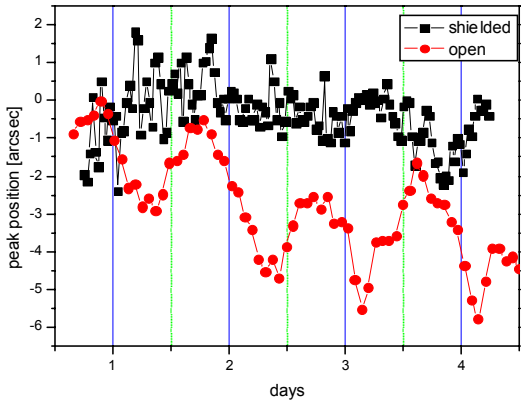

Fig. 2: *Long term behaviour of peak position*

References:

[1]. BENSC reports 2005, p. 165

	EXPERIMENTAL REPORT V12a & V12b USANS test and calibration measurements	Proposal N° OTH-04-1352-EF Instrument **V12a, V12b** Local Contact M. Strobl, W. Treimer
Principal Proposer: Experimental Team:	Strobl – HMI, Berlin + TFH, Berlin Strobl – HMI, Berlin + TFH, Berlin W. Treimer - HMI, Berlin + TFH, Berlin	Date(s) of Experiment March + August 2006

Date of Report: 06.01.2007

Samples with well known size distributions have been used to test the new set-ups of the V12a and V12b double crystal diffractometers.
Special interest was put on the lower resolution limit at the V12a instrument in order to demonstrate the ability to overlap with the resolvable range of SANS measurements and the upper limit at the V12b instrument for its high resolution.
SiO2 particles with known diameters of app. 60 nm and 260 nm in D2O have been used as reference samples for the V12a diffractometer. The results of three measurements are represented in Fig. 1. Two samples contain either 60 nm or 280 nm particles while both sizes of particles are present in the third sample. The particle sizes (mean radii) could be determined for all samples with an accurateness of a few percent from the measurements by fitting the treated data with corresponding mono-disperse respectively di-disperse structural models using SASProFit software [1]. The volume fractions on the other hand could not be verified and were clearly higher than given by the provider of the samples (Frauenhofer Institute Silicatforschung). This might be due to deposition effects of the particles with two time the density of D2O. Although the absolute lowest limit for resolvable structure sizes is app. 50 nm the 60 nm particles could be determined despite of noisy data in this region without problems.
The V12b diffractometer was tested with porous Hydroxyapatite-Caseinate samples [2] that have been measured before at the V12a instrument. The result represented in Fig. 2 is for a sample that has been rendered porous with templates of three different droplet sizes. The smaller sizes could be identified by measurements at the V12a DCD as well. However, the biggest pores of app 20 µm diameter could only be determined with the high resolution V12b DCD.

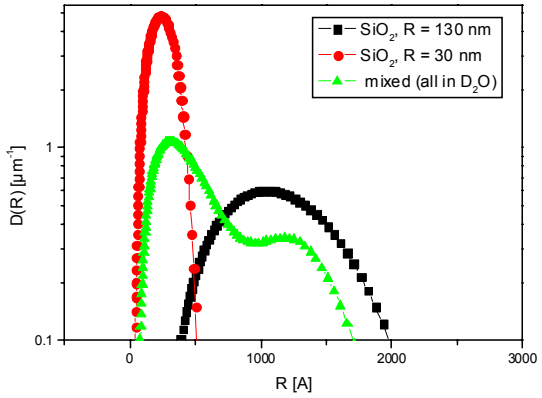

Fig. 1: *Size distributions determined from V12a USANS data for SiO2 particles of defined diameters in D2O*

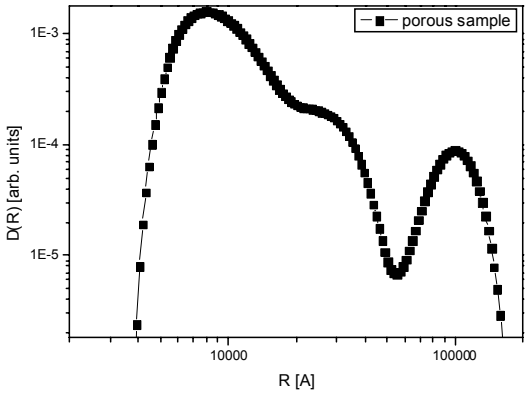

Fig. 2: *Pore size distribution in porous Hydroxyapatite-Caseinate samples determined from V12b USANS measurements*

References:
[1]. http://omega.ujf.cas.cz/SAS
[2]. BENSC reports 2005, p. 99

BENSC	**EXPERIMENTAL REPORT** **Test of solid state polarising benders**	Proposal N° OTH-04-1352-EF Instrument **V12c** Local Contact M. Strobl, W. Treimer
Principal Proposer: Experimental Team:	W. Treimer – HMI, Berlin + TFH, Berlin M. Strobl – HMI, Berlin + TFH, Berlin T. Krist – HMI, Berlin	Date(s) of Experiment February + March 2006

Date of Report: 06.01.2007

A solid state polarising bender [1] built and constructed at HMI has been tested at the V12b double crystal diffractometer and the V12c monochromatic imaging set-up. The bender consists of bent Si wafers with supermirror layers on one side and absorbing Gd layers on the other (Fig. 1). A magnetic field is applied by two permanent magnets. Due to the geometry only neutrons of a certain spin orientation and of the wavelength of a few Angstrom - depending on the angular alignment - are reflected by the supermirror layers and hence can pass the polarising bender.

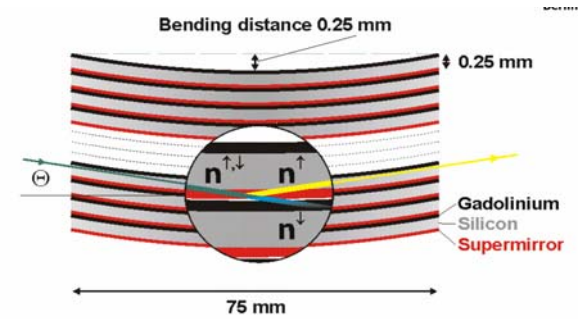

Fig. 1: *Schematic drawing of solid state polarising bender*

The active area of the polarising benders was app. 4 x 1.5 cm^2. One polarising bender was aligned between the V12b instrument shutter and the V12b monochromator. The neutron wavelength was 5.2 Å. This way the polarised beam could be used in the V12b DCD as well as in the V12c set-up, where the second bender was installed right in front of the scintillator-CCD camera detector serving as a polarisation analyser. Fig. 2 represents the image taken with the V12c set-up. It clearly shows in-homogeneities over the cross section of the bender. The transmission of the first polarising bender could be evaluated with a mean value of 15 %. 50% of neutrons transmitted by the first bender were also transmitted by the second bender which was located app. 1.5 m down-stream without any guide field. In the V12b DCD a rocking curve has been recorded and has been compared to another one recorded afterwards, when the first polarising bender has been aligned between the instrument monochromator and analyser crystal (Fig. 3). The instrumental resolution function did not change significantly in none of these cases. Hence the solid state polarising benders are suited components for polarised USANS as well as for imaging.

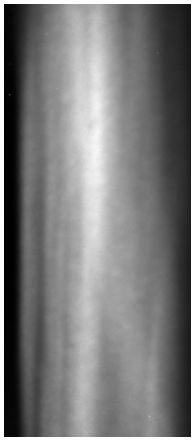

Fig. 2: *beam cross section as recorded in the V12c monochromatic imaging set-up behind a solid state polarising bender and a polarisation analysing bender with a distance of 1.5 m between them; image size: 1.5 cm x 4 cm*

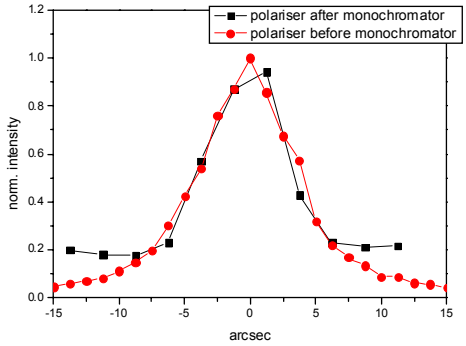

Fig. 3: *V12b rocking curves with a solid state polarising bender in front of the instrument monochromator (red) and with a polarising bender between monochromator and analyser crystal (black)*

Reference:

[1]. T. Krist, et al., Physica B **241-243**, 82-85, (1998)

	EXPERIMENTAL REPORT V12b & V12c instrument development	Proposal N° OTH-04-1352-EF Instrument **V12b** Local Contact M Strobl, W. Treimer
Principal Proposer: Experimental Team:	M. Strobl – HMI, Berlin + TFH, Berlin Y. Gau – HMI, Berlin + TFH, Berlin W. Treimer – HMI, Berlin + TFH, Berlin	Date(s) of Experiment Nov. + Dec. 2006 Jan. 2007

Date of Report: 06.01.2007

Various progress has been achieved in the instrument development of the new V12b (double crystal diffractometer) and V12c (monochromatic tomography) set-ups. Due to new constructed PE and B4C shielding the background produced by the tomography set-up V12c as well as the background contaminating the V12b high resolution DCD data could be reduced significantly. Additionally the installation of an instrument shutter between V12b and V12c i.e. behind the V12b high resolution monochromator enables a more independent use of both instruments. The shielding around the V12b monochromator and analyser crystals also provides better thermal stability. An optical bench installed in the V12c housing has been aligned accurately in order to install flexible neutron optical equipment for imaging experiments.

A special feature of the V12b high resolution double crystal diffractometer is the opportunity to install refractive wedges in the monochromator and analyser in order to tune the resolution function of the instrument to the highest available values i.e. 10^{-5} nm^{-1}. This value equals an instrumental curve width of down to 1 arcsec. However, up to now the angular resolution of the analyser rotation stage was limited to 1 arcsec. Therefore it was necessary to employ a new rotation table which was installed on top of the conventional rotation stage. The new high resolution rotation is driven by a piezo which provides an angular resolution of 0.156 arcsec on a range of approximately 2.5 arcmin (PI M-036 tangent arm rotation stage). To extend this range the other table is still connected and available in the instrument control. Test measurements could demonstrate the efficiency of this hybrid set-up especially when a new crystal had to be aligned (rough step on big range) and the very narrow reflection profiles had to be examined (accurate fine steps). In Fig. 1 two rocking curves of the same crystal geometry are represented scanned with the old set-up (black curve) with its highest resolution of 1 arcsec and with the new rotation stage (red) with a medium resolution of 0.45 arcsec. Fig.2 displays a similar rocking curve recorded using the highest angular resolution of the new stage of 0.156 arcsec (1.7 x 10^{-6} µrad).

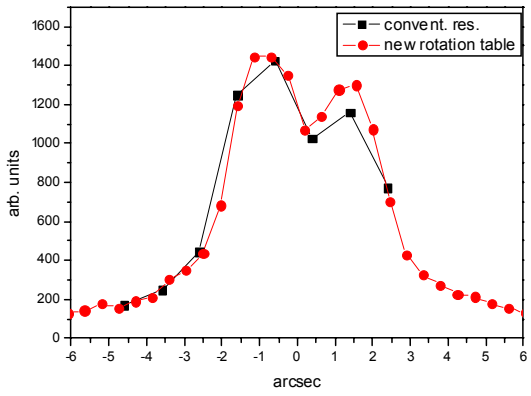

Fig. 1: *Rocking curves measured with highest angular sampling of old rotation stage (black) and medium sampling of new stage (red)*

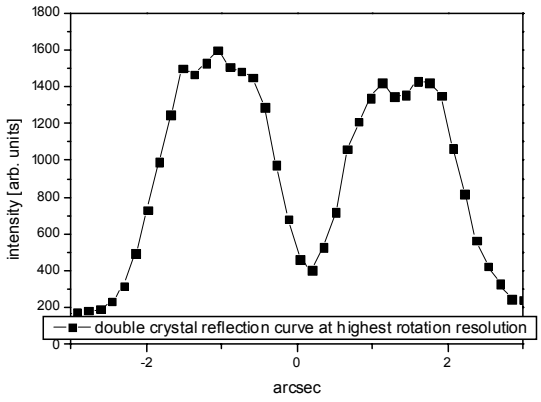

Fig. 2: *Rocking curve sampled with highest angular resolution*

	EXPERIMENTAL REPORT **Fast quantitative refraction contrast tomography**	Proposal N° OTH-04-1352-EF Instrument **V12a** Local Contact M. Strobl, W. Treimer
Principal Proposer: Experimental Team:	M. Strobl – HMI, Berlin + TFH, Berlin K. Staack – HMI, Berlin + TFH, Berlin M. Strobl – HMI, Berlin + TFH, Berlin W. Treimer – HMI, Berlin + TFH, Berlin	Date(s) of Experiment Jan.;Jun.;Jul.;Oct.;Dec. 2006

Date of Report: 06.01.2007

The flux density in the new V12a set-up is clearly increased compared to the old set-up [1]. This enables tomographic scan measurements with at least a factor of 5 shorter exposure times. Several measurements have been performed on different time scales in order to compare the quality of the reconstruction results. On the other hand an effort has been made to investigate the potential for quantitative analyses. New data treatment and reconstruction programs have been developed with respect to the refraction and USANS contrast signals [1]. The raw data is corrected and the parameters for attenuation, refraction and USANS reconstructions are extracted on the basis of a correct physical description of the measurements. Thus, e.g. in the case of refraction, where the measured refraction angles are extracted and converted to a phase map for every projection by integration with respect to the given dimensions the resulting images represent the refractive index distribution of the sample cross section.

Samples with well known refractive indices have been used in order to test the accuracy of the results and a good agreement with theoretical values could be found. The example presented here consists of three rectangular profiles made of Cu, Al and brass with cross sections of app 3.3 x 3.3 mm^2 respectively 4 x 4 mm^2 in the case of Al. The measurement has been taken within one day using a slit of 200 µm scanning the sample in 53 steps of 200 µm for 60 projection angles on a range of 360°. The exposure time was app. 28 seconds per step.

In table 1 the theoretical values of the real part of the refractive indices $\delta = n - 1$ of the corresponding materials are compared to the measured respectively reconstructed values. The values extracted from the measurements are mean values of the reconstructed cross section of the corresponding material. Figure 1 is an image of the reconstructed cross section.

	theory	measured
Al	7.5050E-06	7.0268E-06
Brass	1.8997E-05	1.9372E-05
Cu	2.2816E-05	2.1786E-05

Tab. 1: *comparison of theoretical and measured (respectively reconstructed) values of the real part of the refractive index δ = n – 1of the present sample materials*

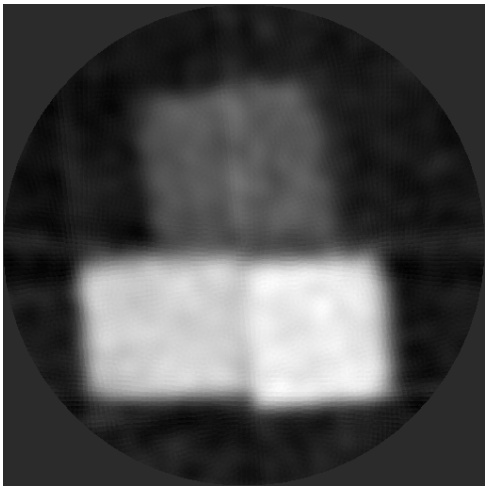

Fig. 1: *reconstructed cross section in terms of refractive indices of a sample consisting of three rectangular profiles made of Cu, brass and Al*

References:

[1]. M. Strobl et al., Physica B **385-386** (2006) 1388-1391

	EXPERIMENTAL REPORT **Round-robin test of DC-SANS diffractometers**	Proposal N° PHY-04-1215 Instrument **V12a** Local Contact Markus Strobl
Principal Proposer: Experimental Team:	J. Šaroun – ASCR NPI Rez, CZ M. Strobl – HMI, Berlin	Date(s) of Experiment 29.05. – 02.06.2006

Date of Report: 02.01.2007

This experiment was carried out with the aim to provide data for intercomparison of two doublecrystal (DC) SANS instruments: V12a at the HMI Berlin and DN-2 at the NPI Rež. Main difference of the DN-2 instrument with respect to V12a is the use of different monochromator setup (bent silicon single crystal), beamstop for the primary beam and thermal neutron wavelength (λ= 0.21 nm). This intercomparison involved measurements of well defined standard samples on both the instruments, raw data treatment and data fitting using the same structural model and software (SASProFit, http://omega.ujf.cas.cz/SAS). Polystyrene microspheres (NIST Traceable Particle Size Standards) dispersed in H_2O were diluted by D_2O in order to achieve lower volume fraction and higher scattering contrast. Two monodisperse and one bidisperse samples were thus prepared with parameters summarized in Table 1. SANS measurements were carried out in a single Q-range with mean neutron wavelength λ=0.467 nm. Raw data were corrected for transmission, detector homogeneity and absorption in the analyzer crystal. Absolute calibration of scattering cross-sections was done by normalizing on measured integral intensity of the beam transmitted through reference sample (cell with D_2O+H_2O mixture). Resulting scattering crosssections are plotted in Fig.1 together with model scattering curves calculated from nominal parameters and smeared by measured instrumental curve (water cell). Experimental data were further fitted to a model of monodisperse or bidisperse system of spheres with radii and volume fractions taken as free parameters. Scattering contrasts were fixed at the nominal values from Table 1. Resulting values of radii and volume fractions and standard errors determined from counting statistics (in brackets) are compared with those obtained from complementary measurements at the DN-2 instrument at the NPI Rež, which was carried out three weeks later (see Table 2 and 3) on the same samples. Very good agreement between the two experiments was obtained in determination of mean radii, where the differences fall within standard deviation limits. Small systematic underestimation of mean radii (< 5 %) with respect to their nominal values was observed. The differences are larger (< 10 %) for volume fractions, where problems with spatial inhomogeneity of detector efficiency contribute to larger systematic errors in absolute calibration of scattering cross-sections.

Table 1: *Nominal parameters of the standard samples*

sample	Radius [nm]	Volume [%]	$\lvert\Delta\rho\rvert$ [10^{10}cm^{-2}]
monodisperse 1	495	0.209	3.445
monodisperse 2	99	0.208	3.453
bidisperse	495 99	0.108 0.101	3.45

Table 2: *Measured mean radii in nm.*

sample	DN-2	**V12a**
monodisperse 1	482(8)	**482(6)**
monodisperse 2	96(2)	**93(2)**
bidisperse	484(9) 96(3)	**475(7)** **96(4)**

Table 3: *Measured volume fractions.*

sample	DN-2	**V12a**
monodisperse 1	0.209(6)	**0.187(3)**
monodisperse 2	0.224(5)	**0.222(4)**
bidisperse	0.117(5) 0.098(4)	**0.106(4)** **0.107(3)**

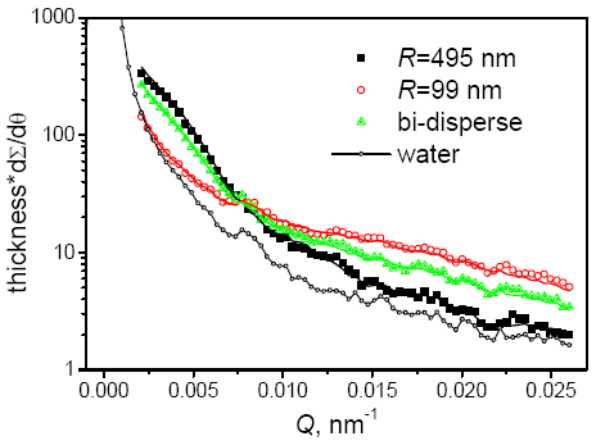

Fig.1: *Scattering cross-sections measured at the V12a instrument, including instrumental smearing and background. Solid lines represent model curves calculated from the nominal parameters (see Table 1) and measured instrumental response. All curves are shown on absolute scale without any adjustable scaling parameter.*

	EXPERIMENTAL REPORT **A novel Bragg prism analyzer for SUSANS studies**	Proposal N° PHY-04-1305 Instrument **V12b** Local Contact Wolfgang Treimer
Principal Proposer: Experimental Team:	A. G. Wagh – BARC, IN S. Abbas – BARC, IN M. Strobl – HMI, Berlin W. Treimer – HMI, Berlin	Date(s) of Experiment 04.12. – 17.12.2006

Date of Report: 15.01.2007

An understanding of dynamical neutron diffraction through a single crystal prism in the vicinity of a Bragg reflection [1,2] leads to the design of a pair of prisms in opposite asymmetric Bragg configurations, serving as a monochromator and an analyser respectively. For 5.24 Å neutrons and {111} silicon reflections, the analyser prism should accept only an ~ 0.21 arcsec wide pair of peaks in incidence angle separated by ~ 2.2 arcsec (Fig.1). Convolution of this acceptance curve with the beam emerging from the monochromator prism increases each peak width to ~ 0.475 arcsec (triangles in Fig.3), opening up a possibility of probing Q ~ 10^{-6} $Å^{-1}$ in a SUSANS (Super UltraSmall Angle Neutron Scattering) instrument.

The optimally designed monochromator and analyser silicon prisms were cut and ground at the Centre for Design and Manufacture, BARC. The prism surfaces were polished and given a long and slow etch to relieve all strains.

The analyser prism was mounted on a piezocrystal-driven high precision rotation stage capable of scanning angular ranges upto 140 arcsec in 0.16 arcsec steps (specially acquired by HMI for the present experiment), on the analyser goniometer assembly. With an asymmetric Bragg reflecting monochromator, the analyser rocking curve displayed a well resolved pair of ~ 1.7 arcsec wide peaks, in good agreement with theory (Fig.2). The rocking curve, as well as marked pendellösung oscillations modulating it, was extremely sensitive to the analyser tilt, which had hence to be adjusted to within 9 arcsec. Each rocking curve took nearly a day to stabilise due to angular drifts within the setup. The analyser thus performs as per the design.

With the optimal Bragg prism monochromator however, the observed pair of peaks in the rocking curve was much wider than the theoretically predicted sub-arcsec peaks (Fig.3), even after all possibilities of any contamination with the direct Bragg reflected beam from the monochromator were eliminated.

Furter experiments are needed to understand and overcome this failure of the monochromator prism to operate to its specifications.

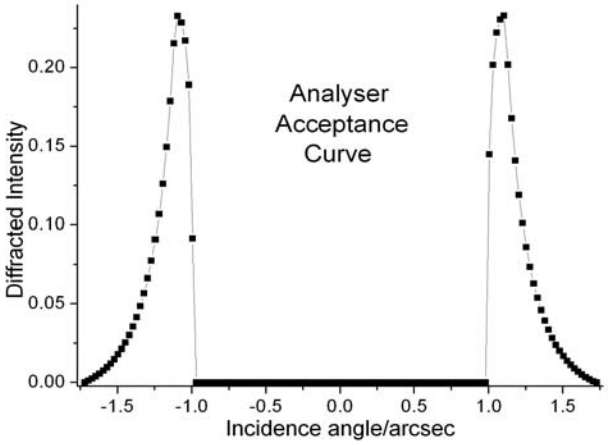

Fig.1: *Calculated acceptance curve of the asymmetric Bragg prism.*

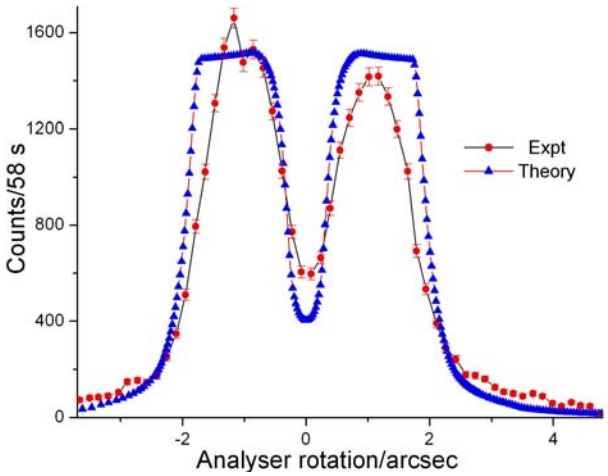

Fig.2*: Analyser curve with asymmetric Bragg reflecting monochromator*

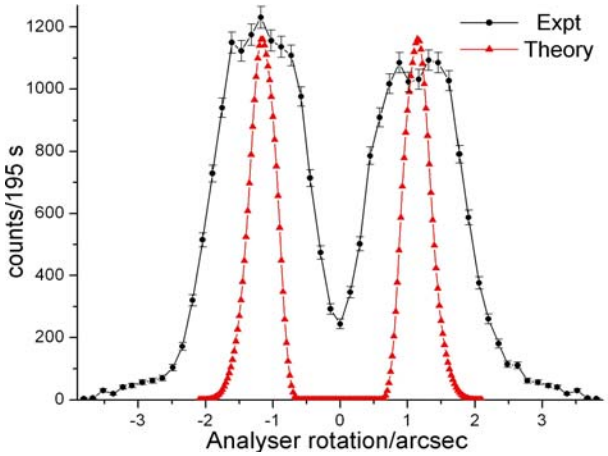

Fig.3: *Analyser curve with asymmetric Bragg prism monochromator.*

References:

[1]. A.G. Wagh and S. Abbas, Sol. St. Phys. (India) **51**, 353 (2006).

[2]. A.G. Wagh, Phys. Lett. A **121**, 45 (1987); **123**, 499

	EXPERIMENTAL REPORT **Development of a wavelength filter**	Proposal N° Inst.time Instrument **V14** Local Contact Thomas Krist
Principal Proposer: Experimental Team:	A. Teichert – HMI, Berlin A. Teichert – HMI, Berlin T. Krist – HMI, Berlin J.-E. Hoffmann – HMI, Berlin	Date(s) of Experiment 21.09. – 20.10.2006

Date of Report: 16.01.2007

A prototype of a wavelength filter was developed, built and tested. Into a collimator with absorbing walls coated wafers are inserted, which reflect up to their critical angle and transmit above. Thus it simultaneously works as a filter for large wavelengths and at each wavelength for large angles.
Depending on how the reflecting and absorbing layers are arranged one gets a triangular or rectangular transmission profile.
Fig.1 shows the construction. The filter has a total length *L* of 400 mm, a width of 50 mm and tilting angles β of to 1.125°, 1.25° and 1.5°.
For the collimator Si wafers with dimensions of 51 mm high × 100 mm long × 0.5 mm thick were coated on both sides with Si-Fe supermirrors with m=2.15. The reflectivity was 94% at the critical angle θ_c=1.025°±0.025° (FWHM) for the wavelength of 4.8 Å. The given uncertainty is spread given by the production process.
In the wavelength filter neutrons are transmitted up to an incident angle given by β-θ_c. The substrates (SS) are arranged in a X-shape at different angles α=2β thus transmitting halfwidths of 0.2°, 0.45° and 0.95°, all ±0.05. The neutrons are reflected on the Si-Fe multilayers (SR) and absorbed on the inner wall (SA) above the critical angle of the coating.

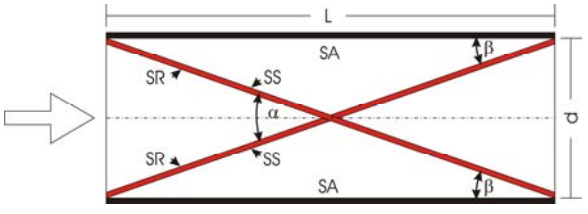

Fig.1: *Construction of the wavelength filter.*

Measurements are performed at the BENSC reflectometer V14 with a wavelength of 4.8 Å. The distance between the collimator and the ^{3}He detector with a slit of 8 mm width was 1.2 m. The divergence in front of the filter was 0.035°. Furthermore, a 300 Gauss magnetic field was applied to saturate the supermirror.
Fig.2 shows the transmission of the spin up component for the wafers at an angle of α=3°.

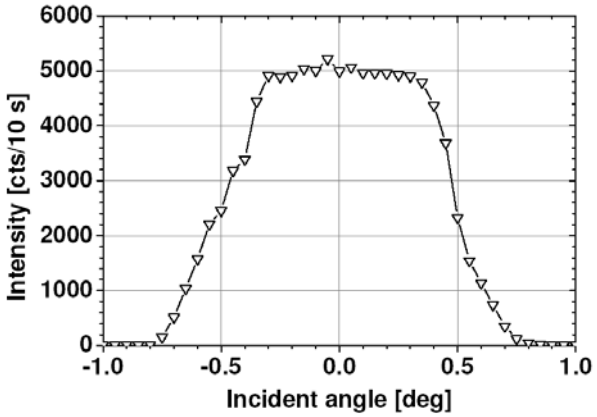

Fig.2: *Transmitted neutron intensity through the filter at an angle α = 3°.*

The neutrons are transmitted between -0.5° and 0.5°. The rather large width of about 0.3° for the decay from 80% to 20% is determined by the reflectivity curve of the supermirrors and the bending of the wafers.
The result of another measurement performed for an angle of α=2.25° is displayed in Fig.3. The FWHM is 0.4°, showing that the device performs as expected.

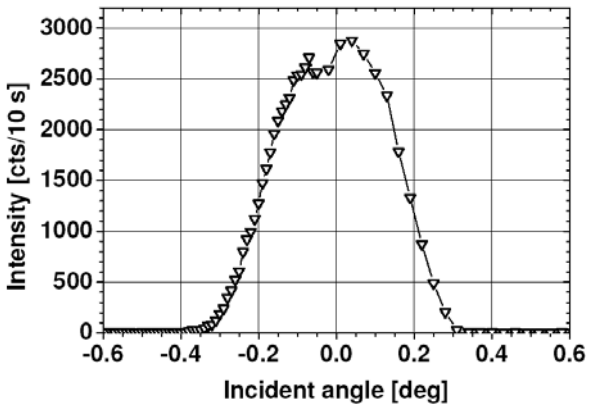

Fig.3: *Transmitted neutron intensity through the filter at an angle α of 2.25°.*

	EXPERIMENTAL REPORT **New polarizers for SPAN and FLEX**	Proposal N° Inst.time Instrument **V14** Local Contact Thomas Krist
Principal Proposer: Experimental Team:	T. Krist – HMI, Berlin A. Teichert – HMI, Berlin T. Krist – HMI, Berlin J.-E. Hoffmann – HMI, Berlin	Date(s) of Experiment 05.01. – 25.09.2006

Date of Report: 16.01.2007

The relocation of the Spin-Echo instrument SPAN to the new guide hall required a new polarizer system. The old beam splitter made from FeCo-Si supermirrors with m=2 could not be used again due to its high activation. Therefore it was decided to use Fe-Si supermirrors. According to the requirements of SPAN the lower wavelength limit was set to 2.5Å while the old analyser polarized down to 4Å.
A 9m long polarizing cavity with a cross section of 60mm x 100mm was set up with Si wafers coated on both sides with Fe-Si polarizing supermirrors This amounts to a total supermirror area of 2m^2. The angle of the wafers to the walls is 0.38°.

In addition, a new polarizer for FLEX was built designed to work above 2Å. It also replaces a ten years old system with FeCo-Si supermirrors with m=2. Here a multiple cavity with a cross section of 25mm x 124mm was built with similar wafers and a total supermirror area of 1.6m^2. It was designed to fit into the monochromator shielding to reduce the radiation yield.

The requirements for the wafers were for both systems:

- a critical angle of the supermirrors of above m=2.5 (this are 1.2° for a neutron wavelength of 4.8Å),
- a flip ratio in transmission above 20 at m=2.5,
- a bending radius of the coated wafer larger than 7m (which corresponds to a stress of 400 MPa).

We report here on the results of the wafer tests. Neutron measurements were performed at the BENSC reflectometer V14 with a wavelength of 4.8Å. The bending measurements were performed on a profilometer DEKTAK 3030.
Fig.1. shows a profilometer measurement for a wafer with a concave surface having a radius of 325 ±4m which corresponds to a tensile stress of 3 MPa.
All the wafers for SPAN had radii between 8m (350 MPa) and 3260m (<1 MPa) and for FLEX between 10m and 750m. They all met or exceeded the standards given above.

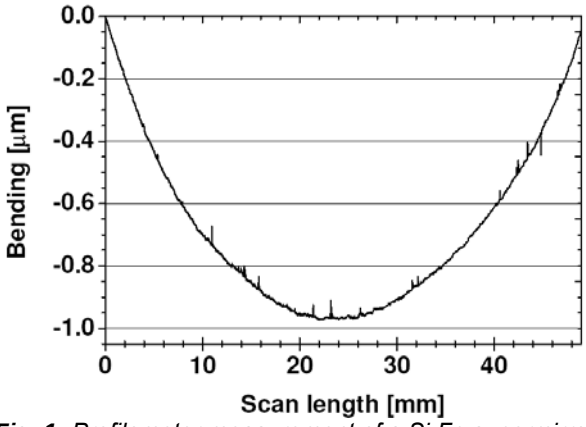

Fig. 1: *Profilometer measurement of a Si-Fe supermirror.*

Fig.2 shows the curves for the transmitted intensity of the two spin states of neutrons through a typical wafer, which has a radius of 11m. The wafer shows an average polarization of 96%, which corresponds to a flip ratio of 50.

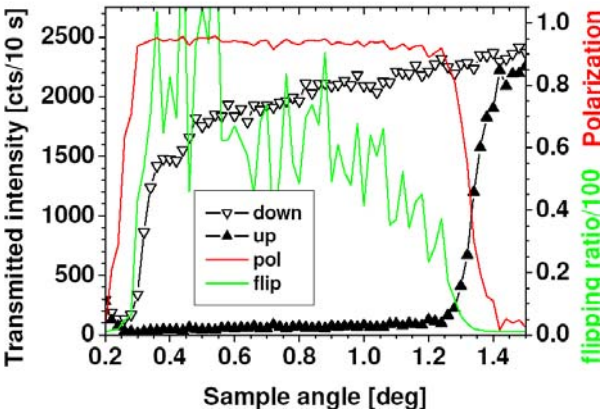

Fig. 2: *Transmitted neutron intensity of a Si-Fe supermirror for both spin components together with flip ratio and polarization.*

The results of the neutron reflection measurements of the coatings for the wafers for FLEX were similar.
Presently the first tests of the complete systems have started.

Magnetism

	EXPERIMENTAL REPORT	Proposal N° PHY-02-0520
BENSC	**Magnetic structure in the $La_{0.7}Sr_{0.3}Co_{1-x}Nb_xO_3$ and $La_{0.3}Sr_{0.7}Co_{1-x}Nb_xO_3$ (x = 0.0 ÷ 0.35)**	Instrument **E1** Local Contact Vadim Sikolenko
Principal Proposer: Experimental Team:	J. Purans – Univ. Povo, IT A. Kuzmenko – Univ. Genf, CH V. Efimov – JINR Dubna, RU V. Sikolenko – HMI, Berlin	Date(s) of Experiment 29.03. – 07.04.2006

Date of Report: 03.06.2006

The discovery of the "colossal" magnetoresistance (CMR) in the manganites with perovskite structure [1] has stimulated the research of the compounds exhibiting large magnetoresistance. The magnetic and transport properties of $La_{1-x}Sr_xCoO_3$ cobaltites with perovskite structure and manganites such as $La_{1-x}Sr_xMnO_3$ have common features [2]. In both systems the substitution of La with divalent ion Sr creates paramagnetic (x < 0.15) to ferromagnetic (x > 0.3) transition as the dopant concentration is increased. The Sr^{2+} ionic radius is significantly greater than that of the La^{3+} ion, so it is possible to expect stabilization of the intermediate spin state of cobalt ions by substituting Sr^{2+} ions for La^{3+} ones. However, at such heterovalent substitution Co^{4+} ions appear, leading to the ferromagnetic metallic ground state [3]. The origin of the ferromagnetic state in metallic cobaltites and manganites has been a subject of discussion for a long time [4]. To prevent the Co^{4+} ion appearance, it is possible to introduce simultaneously Nb ions, which at the presence of Co^{3+} ions will be in oxidizing state 5+. By simultaneously introducing Sr^{2+} and Nb^{5+} the cobalt ions keep their valence state and the electro conductivity of $La_{1-x}Sr_xCo_{1-x/2}Nb_{x/2}O_3$ solid solutions decreases with dopant concentration enhancement. Thus, the different nature of ferromagnetic interactions formation in the given systems is obvious.

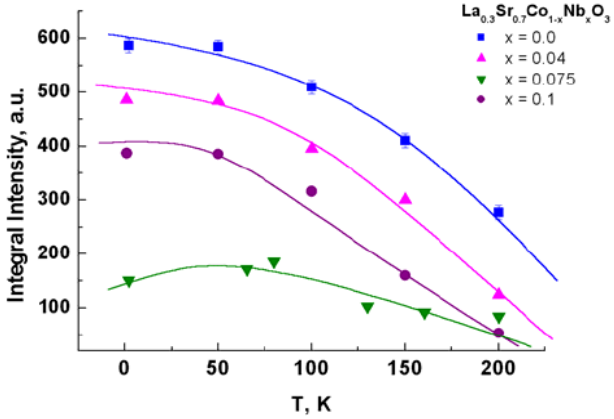

Fig.1: *Rietveld refinement pattern of the $La_{0.7}Sr_{0.3}Co_{0.925}Nb_{0.075}O_3$ powder at the 2 K.*

In this work the atomic and magnetic structu-changes effects induced in $La_{0.7}Sr_{0.3}Co_{1-x}Nb_xO_3$ (x = 0.0; 0.04; 0.075; 0.1 and 0.15) and $La_{0.3}Sr_{0.7}Co_{1-x}Nb_xO_3$ (x = 0.0; 0.04; 0.075; 0.15 and 0.35) powder were studied on the diffractometer E9 with incident neutron wavelength λ = 1.79 Å at the BER-II in Hahn-Meitner Institute.

Fig.1 shows a neutron Powder diffraction pattern and Rietveld refinement of $La_{0.7}Sr_{0.3}Co_{0.925}Nb_{0.075}O_3$ powder at the 2 K.

We have found that the increase of the Nb concentration in the $La_{0.7}Sr_{0.3}Co_{1-x}Nb_xO_3$ and $La_{0.3}Sr_{0.7Co1-x}Nb_xO_3$ leads to the gradual increase of the lattice volume and significant decease of the magnetic moment (table 1a,b). It should be noted that no essential change of the rhombohedral distortions with increase Nb in the $La_{0.7}Sr_{0.3}Co_{1-x}Nb_xO_3$ are observed (table 1 a).

These results were confirmed by X-ray absorption fine structure (EXAFS) and X-ray absorption near edge structure (XANES) at the cobalt K-edge measurements [3].

Table 1: *Structural parameters for (a) $La_{0.7}Sr_{0.3}Co_{1-x}Nb_xO_3$ (x = 0.0-0.15) and (b) $La_{0.3}Sr_{0.7}Co_{1-x}Nb_xO_3$ (x = 0.0-0.35) powder at the 2 K.*

a)

x	0.0	0.04	0.075	0.1	0.15
Sp.gr.	R-3c	R-3c	R-3c	R-3c	R-3c
a (Å)	5.4351	5.4359	5.4367	5.4375	5.4389
b (Å)	5.4351	5.4359	5.4367	5.4375	5.4389
c (Å)	5.4351	5.4359	5.4367	5.4375	5.4389
α	60.410	60.411	60.412	60.410	60.413
V (Å^3)	**113.067**	**113.078**	**113.091**	**113.104**	**113.119**
μ(μ_B)	**2.2**	**1.7**	**0.8**	**-**	**-**
R_{wp}	4.02	5.26	4.81	4.34	5.05

b)

x	0.0	0.04	0.075	0.15	0.35
Sp.gr.	Pm3m	Pm3m	Pm3m	Pm3m	Pm3m
a (Å)	3.8327	3.8331	3.8339	3.8352	3.8363
b (Å)	3.8327	3.8331	3.8329	3.8352	3.8363
c (Å)	3.8327	3.8331	3.8329	3.8352	3.8363
V (Å^3)	**56.3007**	**56.3184**	**56.3536**	**56.4110**	**56.4595**
μ(μ_B)	**2.6**	**1.9**	**1.0**	**-**	**-**
R_{wp}	4.39	5.17	4.49	5.24	5.71

References:

[1]. J.B. Goodenough, Phys. Rev. 155, 932 (1967).
[2]. G. Briceno et.al. Science 270, 273 (1995).
[3]. M.A. Senaris-Rodriguez and J.B. Goodenough, J.Solid State Chem. 118(2), 323 (1995).
[4]. I.O. Troynchuk, J.Exp. Theor.Phys. 75(1), 132 (1992).
[5]. V. Sikolenko, I.O. Troynchuk, A. Kuzmin, V. Efimov, E. Efimova, S. Khasanov, D.I.Kochubey V. Kriventsov, A. Shmakov, S.I. Tiutiunnikov, //Surface investigation X-ray, Synchrotron and Neutron Techniqucs **6**, 23-29 (2006).

	EXPERIMENTAL REPORT **Impurity- and Field-Induced Magnetic Ordering in the Doped Spin Dimer System $TlCu_{1-x}Mg_xCl_3$**	Proposal N° PHY-02-0523 Instrument **E1** Local Contact Hans Anton Graf
Principal Proposer: Experimental Team:	H. Tanaka – TIT, JP T. Ono, F. Yamada – TIT, JP V.Silkolenko, H.A.Graf, K.Kiefer – HMI, Berlin S. Gerischer, M. Meißner – HMI, Berlin	Date(s) of Experiment 22.06. – 02.07.2006

Date of Report: 25.10.2006

$TlCuCl_3$ is a 3D coupled spin dimer system with an excitation gap of Δ/k_B=7.5 K [1]. When nonmagnetic ions are substituted for magnetic ions, unpaired spins are produced. The unpaired spins interact through effective exchange interactions mediated by intact dimers, which leads to the 3D long-range order. Magnetization measurements and neutron scattering experiment [2,3] revealed that $TlCuCl_3$ doped with nonmagnetic Mg^{2+} undergoes the impurity-induced magnetic ordering. In order to investigate both impurity- and field-induced phase transitions in $TlCu_{1-x}Mg_xCl_3$, we performed specific heat measurements in various magnetic fields, and found that there is no boundary separating impurity- and field-induced ordered phases. This implies that the impurity- and field-induced ordered phases are identical. To confirm this observation and to clarify the impurity- and field-induced phase transitions in $TlCu_{1-x}Mg_xCl_3$, we performed neutron elastic scattering in magnetic fields.

Experiment was carried out at E1 spectrometer installed in the experimental hall with the vertical field cryomagnet VM1. The incident neutron energy was fixed at E_i=13.9 meV, and the horizontal collimation sequence was chosen as 40'-80'-40'. Single crystal for x=0.012 with a volume of approximately 0.3 cm^3 was used. The sample was mounted in the cryostat with its cleavage (0,1,0) plane parallel to the scattering plane, so that the reflections in the a^*-c^*-plane were investigated. The external magnetic field up to 12 T was applied along the b-axis. Temperature of the sample was lowered to 0.4 K using ^{3}He cryostat.

The magnetic peaks were observed at $\boldsymbol{Q}$=(h,0,l) with integer h and odd l. These reciprocal points are the same as those for the magnetic Bragg peaks of the field-induced magnetic ordering in $TlCuCl_3$. For zero field, magnetic phase transition was observed at T_N=2.8 K. With increasing magnetic field at T=0.4 K, the intensities of two Bragg reflections at $\boldsymbol{Q}$=(0,0,1) and (1,0,-3) decrease up to 3.5 T and then increase rapidly. However, no anomaly indicative of field-induced phase transition was observed. This field dependence of the Bragg intensities is due not to the change in the spin direction, but to the change in the magnitude of the ordered moment. This unusual field dependence of the order parameter results from the competition between effective interactions and triplet gap in intact dimers, the latter of which acts to separate the impurity- and field-induced phases, as discussed by Mikeska *et al*. [4]. Figure 1 shows the experimental phase diagram for magnetic field vs temperature. Squares and circles are transition points determined by temperature and field scans, respectively. This phase diagram is consistent with that obtained by specific heat measurements. The present result confirms that the impurity- and field-induced ordered phases are the same phase. A part of the present study was published in Ref. [5].

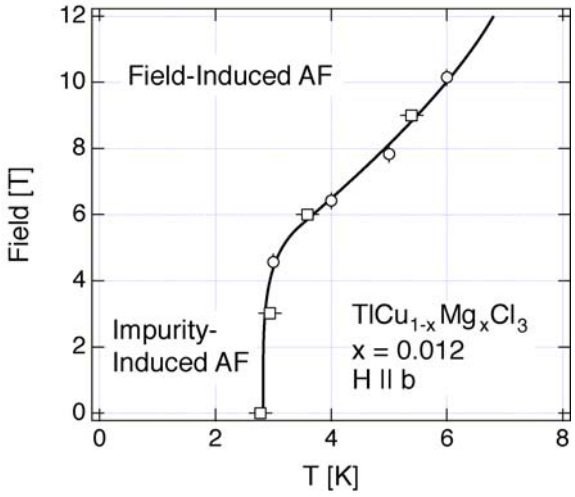

Fig. 1: *Phase diagram for magnetic field vs temperature in $TlCu_{1-x}Mg_xCl_3$ with x=0.012. The magnetic field is parallel to the b-axis.*

References:

[1]. A. Oosawa, M. Ishii and H. Tanaka: J. Phys.: Condens. Matter **11** (1999) 265.

[2]. A. Oosawa, T. Ono and H. Tanaka: Phys. Rev. B **66** (2002) 020405.

[3]. A. Oosawa, M. Fujisawa, K. Kakurai and H. Tanaka: Phys. Rev. B **67** (2003) 184424.

[4]. H.-J. Mikeska, A. Ghosh and A. K. Kolezhuk: Phys. Rev. Lett. **93** (2004) 217204.

[5]. M. Fujisawa, T. Ono, H. Fujiwara, H. Tanaka, V. Sikolenko, M. Meissner, P. Smeibidl, S. Gerischer and H. A. Graf: J. Phys. Soc. Jpn. **75** (2006) 033702.

	EXPERIMENTAL REPORT **Magnetic properties of the $La_{1-x}Ba_xCoO_3$ system**	Proposal N° PHY-02-0550 Instrument **E1** Local Contact Vadim Sikolenko
Principal Proposer: Experimental Team:	A. P. Sazonov – RWTH Aachen @ FRM2 A. P. Sazonov – RWTH Aachen @ FRM2 V. V. Sikolenko – HMI, Berlin	Date(s) of Experiment 08.08. – 19.08.2006

Date of Report: 19.01.2007

$La_{1-x}M_xCoO_3$ (M Ï alkaline-earth metal) systems attract much attention due to the possibility of practical application (cathode material, catalysts, etc.) and because of its unusual properties (appearance of both ferromagnetism and metallicity by doping or increasing temperature, spin state transition of the Co ions, etc).

With temperature increase both in Ca- (T ~ 400 K; orthorhombic-rhombohedral) and in Sr-doped (T ~ 600 K; rhombohedral-cubic) systems the phase transition to a higher symmetry is observed for x near the magnetic percolation threshold (x ~ 0.2). It is expected that such transition will take place in Ba-doped system at lower temperature. However, there are few experimental data for $La_{1-x}Ba_xCoO_3$.

It is worth noting that we have already performed the neutron powder diffraction measurements of the $La_{1-x}Ba_xCoO_3$ (x = 0.2 and 0.3) compounds. These experiments were carried out on the E9 instrument in the angular range of $10° < 2\mathit{И} < 150°$ at several temperatures.

However, to observe an evolution of the Co magnetic moment value (M_{Co}) and to determine precisely the transition temperature into the magnetically ordered state the additional experiments are necessary. Therefore we have continued our study of $La_{1-x}Ba_xCoO_3$ [The compositions with x = 0.2 and 0.3 were synthesized by the conventional ceramic method at T = 1200 °C]. We have measured the (012) and (110) reflections with the most intensive magnetic contribution by using E1 instrument with incident neutrons of wavelength $л$ = 2.42 E. Data were collected on warming from 4 to 250 K. In addition, the magnetization measurements on the SQUID magnetometer were done. The neutron diffraction data were analyzed with the Rietveld method [1] using the FullProf program [2].

Our preliminary results are resented in the figures below.

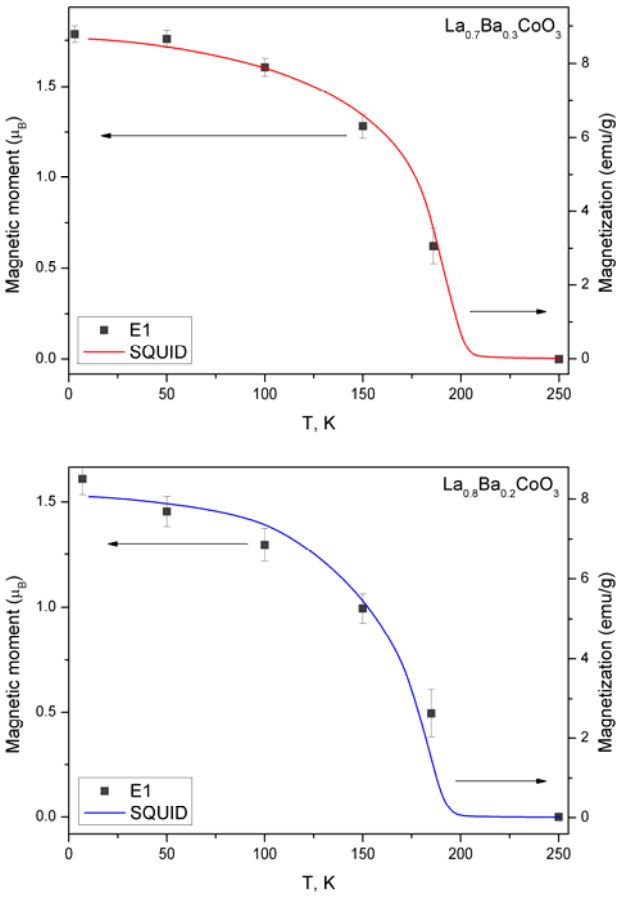

Temperature dependencies of the Co magnetic moment value and the magnetization for $La_{1-x}Ba_xCoO_3$ (x = 0.2 and 0.3) according to the measurements on E1 instrument and SQUID magnetometer respectively.

The experimental M_{Co} values for the x=0.2 and 0.3 compounds are in a good agreement with the following model of the valence and spin state of Co. The Co^{3+} ions are in the intermediate spin state ($t_{2g}^5e_g^1$, S = 1) and the Co^{4+} ions are in the low spin state (t_{2g}^5, S = 1/2) predominantly.

References:

[1]. H. M. Rietveld, J. Appl. Crystallogr. **2**, 65 (1969).
[2]. J. L. Rodrнguez-Carvajal, Physica B **55**, 192 (1992).

	EXPERIMENTAL REPORT **Neutron diffraction study of the magnetic structure of the $La_{0.5}Sr_{0.5}CoO_{3-d}$ and $La_{0.5}Ba_{0.5}CoO_{3-d}$ (d = 0.0; 0.25 and 0.5)**	Proposal N° PHY-02-0551 Instrument **E1** Local Contact Vadim Sikolenko
Principal Proposer: Experimental Team:	K. Bormanis – Univ. of Latvia, Riga, LV K. Stanislav – ASCR IP Prague, CZ V. Efimov – JINR Dubna, RU V. Sikolenko – HMI, Berlin	Date(s) of Experiment 05.09 – 15.09.2006

Date of Report: 12.10.2006

Cobaltites oxides with perosvskite-like structure attract a considerable interest of many researchers because of their specific properties making them promising materials in SOFC, chemical reactors catalysis, gas separation membranes and many other applications [1,2]. The magnetic properties of these compounds are of particular interest [3]. An especially interesting feature observed for these materials is an ordering of oxygen vacancies which can drastically change the physical properties of such compounds in comparison with stoichiometric ones.

The main goal of this proposal was to study the magnetic and nuclear structural transformation effects induced in the layered cobaltites $La_{0.5}Sr_{0.5}CoO_{3-d}$ and $La_{0.5}Ba_{0.5}CoO_{3-d}$ (d = 0.0; 0.25 and 0.5) with equal oxygen deficit content assuming that for the former compounds there are no evidences for La and Sr ions arrangement.

The temperature dependence if the (0 1 2) magnetic peak in $La_{0.5}Sr_{0.5}CoO_{3-d}$ and $La_{0.5}Ba_{0.5}CoO_{3-d}$ (d = 0.0; 0.25 and 0.5) was studied on the diffractometer E1 with incident neutron wavelength λ = 2.24 Å at the BER-II in Hahn-Meitner Institute.

Fig. 1: shows the temperature dependence of the magnetic moment behaviour for the $La_{0.5}Sr_{0.5}CoO_{3-d}$ at the d = 0.0; 0.25 and 0.5. We have found that the increase of the d oxygen deficit content in $La_{0.5}Sr_{0.5}CoO_{3-d}$ leads to the gradual increase of the lattice volume, to the growth of the rhombohedral distortions and to an essential decease of the magnetic moment (table 1).

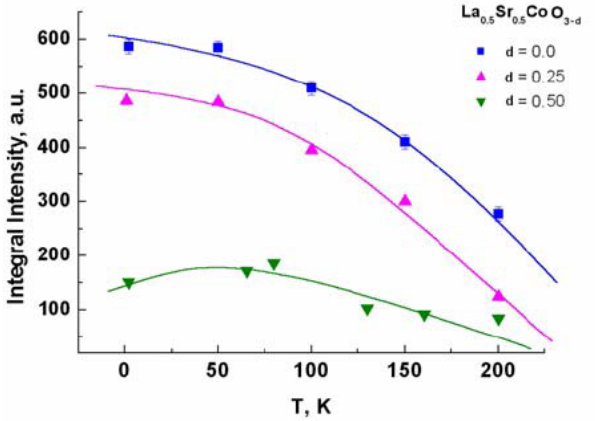

***Fig. 1**: The temperature dependence of the magnetic moment behavior for the $La_{0.5}Sr_{0.5}CoO_{3-d}$ at the **d** = 0.0; 0.25 and 0.5.*

These results were confirmed by X-ray absorption fine structure (EXAFS) and X-ray absorption near edge structure (XANES) at the cobalt K-edge measurements [4,5] and correlated well with SQUID measurements [3].

***Table 1:** Structural parameters for $La_{0.5}Sr_{0.5}CoO_{3-d}$ and $La_{0.5}Ba_{0.5}CoO_{3-d}$ (d = 0.0; 0.25; 0.5) at the 2 K.*

d	0.0	0.25	0.50	0.0	0.25	0.50
	$La_{0.5}Sr_{0.5}CoO_{3-d}$			$La_{0.5}Ba_{0.5}CoO_{3-d}$		
Sp.gr.	R-3c	R-3c	R-3c	R-3c	R-3c	R-3c
a (Å)	5.4351	5.4453	5.4697	5.4575	5.4712	5.4989
α	60.410	60.621	60.782	60.470	60.542	60.413
V (Å^3)	**113.067**	**113.098**	**113.14**	**113.104**	**113.147**	**113.171**
μ(μ_B)	**2.2**	**1.7**	**0.8**	**2.0**	**1.4**	**0.5**
R_{wp}	4.02	5.26	4.81	4.34	5.79	5.05

References:

[1]. I.O. Troyanchuk, N. Kasper, D. Khalyavin,R. Szymczak, Phys. Rev. Lett. **80**, 3380 (1998).

[2]. A. Maignan, C. Martin, D. Pelloquin, N. Nguyen, B. Raveau. J. Solid State Chem. **142**, 247 (1999).

[3]. V. Sikolenko, D. Tobbens, U. Zimmermann, E. Pomjakushina, J.Phys.:Cond.Mat. **16**, 7313 (2004).

[4]. V. Sikolenko, I. Troynchuk, V. Efimov, Surface investigation X-ray, Synchrotron and Neutron Techniqucs **6**, 23-29 (2006).

[5]. V. Sikolenko, V. Efimov, A. Kuzmin, Journal of Physics and Chemistry of Solids **67** 2007 (2006).

	EXPERIMENTAL REPORT **The measurement of the antiferromagnetism induced in $HoFeO_3$ by external magnetic field**	Proposal N° PHY-02-0552 Instrument **E1** Local Contact Vadim Sikolenko
Principal Proposer: Experimental Team:	V. Nietz – JINR Dubna, RU V. Sikolenko – HMI, Berlin R. Schedler – HMI, Berlin	Date(s) of Experiment 03.11. – 13.11.2006

Date of Report: 28.01.2007

Each elementary cell of this compound contains four magnetic ions of Fe^{3+} and four magnetic ions of Ho^{3+}. In principle, the next vectors of magnetism are possible:

$\mathbf{F}=\mathbf{M_1}+\mathbf{M_2}+\mathbf{M_3}+\mathbf{M_4}, \mathbf{G}=\mathbf{M_1}-\mathbf{M_2}+\mathbf{M_3}-\mathbf{M_4},$

$\mathbf{C}=\mathbf{M_1}+\mathbf{M_2}-\mathbf{M_3}-\mathbf{M_4}, \quad \mathbf{A}=\mathbf{M_1}-\mathbf{M_2}-\mathbf{M_3}+\mathbf{M_4}$

for Fe^{3+} ions and

$\mathbf{f}=\mathbf{M_5}+\mathbf{M_6}+\mathbf{M_7}+\mathbf{M_8}, \quad \mathbf{g}=\mathbf{M_5}-\mathbf{M_6}+\mathbf{M_7}-\mathbf{M_8},$

$\mathbf{c}=\mathbf{M_5}+\mathbf{M_6}-\mathbf{M_7}-\mathbf{M_8}, \quad \mathbf{a}=\mathbf{M_5}-\mathbf{M_6}-\mathbf{M_7}+\mathbf{M_8}$

for Ho^{3+} ions.

Exchange interaction in this compound corresponds to Γ_4-type antiferromagnetic ordering when the **G** vector is large and directed along x-axis ($G_x \neq 0$), and there are the very small components A_y and F_x. The Ho sublattices retain the paramagnetic state down to the liquid helium temperature range. The magnetic field H_y induces the addition of Γ_3-type antiferromagnetism when $C_x \neq 0, F_y \neq 0, A_z \neq 0, c_x \neq 0, f_y \neq 0$. The degree of such ordering is proportional to the H_y magnitude, and for Fe^{3+} ions it is determined mainly by the antisymmetric exchange Fe-Fe interaction, while for Ho^{3+} ions by the antisymmetric and anisotropic-symmetric exchange Ho-Fe interactions.

The experimental investigation of antiferromagnetic ordering induced by external magnetic field applied along the y-axis, enables the determination of the corresponding exchange constants, which is of essential importance in research on rare-earth compounds.

At the first the effect of inducement by magnetic field of antiferromagnetism was observed on the SNIM-2 spectrometer at the IBR-2 reactor using the time of flight method and pulsed magnetic field [1].

Present diffraction measurements were carried out with $HoFeO_3$ single crystal on the E1 spectrometer. Three reflections sensitive to the above-mentioned components of the mixed phase of states Γ_4 and Γ_3 were measured: (102), (302) and (201). (102) and (302) reflections are connected mainly with C_x and c_x components, but the (201) reflection is connected with c_x. Several results of the measurements are presented in Fig.1 and Fig.2. Here Sqrt(I) is square root of the reflection intensity.

Scattering amplitudes related to one pair of iron and holmium ions and expressed in terms of spin units are the next:

$$F_{(102)} = f_{Fe(102)} \cdot S_{Fe,x} + f_{Ho(102)} \cdot \cos(2\pi \cdot \delta x) \cdot S_{Ho,x}$$

$$F_{(302)} = f_{Fe(302)} \cdot S_{Fe,x} + f_{Ho(102)} \cdot \cos(6\pi \cdot \delta x) \cdot S_{Ho,x}$$

$$F_{(201)} = f_{Ho(201)} \cdot \sin(4\pi \cdot \delta x) \cdot S_{Ho,x}$$

where f_{Fe} and f_{Ho} are the magnetic form factors for the given reflection, $S_{Fe,x}$ and $S_{Ho,x}$ are the effective spin components induced along the the x-axis.

The C_x magnitude does not depend of temperature in broad temperature range, and the combined measurements of indicated reflections permit to determinate the C_x magnitude and temperature dependence of c_x magnitude, i.e. of Ho^{3+} antiferromagnetic ordering value.

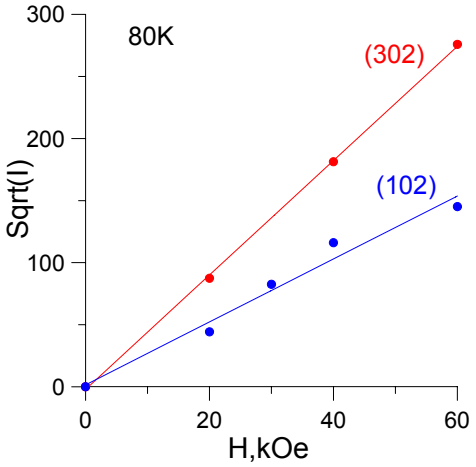

Fig.1

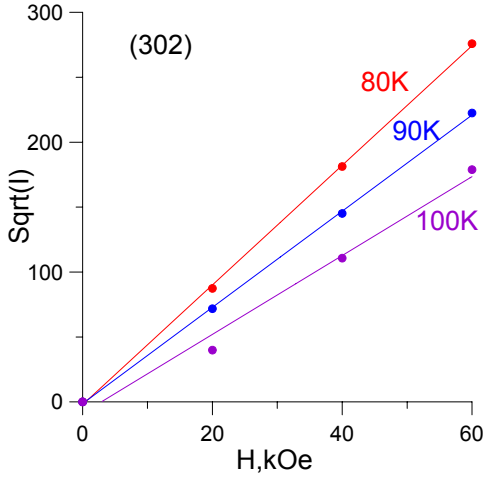

Fig.2

Reference:

[1]. S.Bujko, D.Georgiev, K.Krezhov, V.Nietz, G.Passagev, Journ. Phys.:Condens Matter, **vol.7**, 8099, 1995

	EXPERIMENTAL REPORT Elastic neutron scattering of $Sr_3Ru_2O_7$	Proposal N° PHY-02-0567-EF PHY-02-0506-EF Instrument **E1** Local Contact Alan Tennant
Principal Proposer: Experimental Team:	S. A. Grigera – Univ. St. Andrews. UK S. L. Lee, S. Lister – Univ. St. Andrews. UK K. Prokeš , V. Sikolenko – HMI, Berlin D. A. Tennant – HMI, Berlin	Date(s) of Experiment 12.01. – 19.01.2006 15.05. – 22.05.2006 08.12. – 16.12.2006

Date of Report: 03.01.2007

We conducted a series of neutron scattering experiments investigating the magnetostriction and magnetic structure of the itinerant metamagnet $Sr_3Ru_2O_7$. Using the information from these experiments, in addition to thermodynamic and transport properties measured in St Andrews, we have been able to show the existence of a nematic electronic fluid in the vicinity of the quantum critical point in $Sr_3Ru_2O_7$.

The magnetic phase diagram of clean $Sr_3Ru_2O_7$ contains a metamagnetic quantum critical point (QCP) which can be accessed by the application of a magnetic field of approximately 7.8 T parallel to the crystalline *c* axis[1]. As the purity is increased, new first-order phase transitions appear as the QCP is approached [2-4], and measurements of five thermodynamic and transport properties contain features whose loci enclose a well-defined region of the phase diagram in the vicinity of the QCP. The angle of the applied magnetic field to the *ab* plane of the crystal is a known tuning parameter in $Sr_3Ru_2O_7$ [5]. In close proximity to metamagnetic quantum critical points, the electron fluid in $Sr_3Ru_2O_7$ develops a strong resistive anisotropy, whose 'hard' and 'easy' axes can be interchanged by the application of modest in-plane magnetic fields.

Pronounced in-plane resistive anisotropy can, in principle, have a number of origins. There is known to be a strong magneto-structural coupling in $Sr_3Ru_2O_7$, so one possibility is a symmetry-lowering structural phase transition giving the resistive anisotropy due to a corresponding anisotropy in the hopping integrals. To check for a large spontaneous lattice parameter anisotropy, we performed elastic neutron scattering measurements at temperatures of app. 80 mK and for magnetic fields ranging from 0 to 12 tesla in the three axis spectrometer E1. Within our experimental resolution of 4 x 10^{-5} Å, we saw no evidence of any difference in lattice parameters *a* and *b* in the anomalous region.

The combination of these results allowed us to show that the many-electron fluid that forms in the close vicinity of a metamagnetic quantum critical point in $Sr_3Ru_2O_7$ has the key features of an electronic nematic. This result leads to the publication [7].

In addition to these results, there are two different aspects of these experiments that are still work in progress: i) a more complete and detailed study of the magnetostriction of $Sr_3Ru_2O_7$ at different temperatures: So far we have measured the *a* and *c* lattice parameters for fields along the *c*-axis and the *ab*-plane and temperatures of approximately 80 mK. We have found a clear correlation with the field in the c-axis between the metamagnetic jump in the magnetisation and a highly hysteretic change in the ab-plane lattice parameters. It would be desirable to measure the temperature dependence of this phenomenon, and to investigate the possible build up of tensions in this transition. ii) determination of possible inhomogeneous phases: there are some theoretical suggestions which link the existence of an anisotropic transport phase with the existence of anomalous scattering with transverse components in the magnetisation [6]. In this picture, details in the electronic density of states of the material lead to the existence of magnetic textures (*e.g.* spirals) in restricted parts of the magnetic phase diagram. If this prediction were true, it would be possible to see additional scattering peaks as a result of the inhomogeneous magnetic phase. We have started to investigate this possibility, doing preliminary line scans in regions of the phase diagrams where anomalies in transport or magnetisation have been measured.

References:

[1]. S.A. Grigera *et al*, Science **294**, 329 (2001).
[2]. R.S. Perry *et al.*, Phys. Rev. Lett. **92**, 166602 (2004).
[3]. S.A. Grigera *et al*,, Science **306**, 1155 (2004).
[4]. A.G. Green *et al*, Phys. Rev. Lett. **95**, 086402 (2005).
[5]. S.A. Grigera *et al*,, Phys. Rev. B **67**, 214427 (2003).
[6]. A. Berridge, A. Green, S. A. Grigera and B. D. Simons, in preparation.
[7]. *Formation of a nematic fluid at high fields in $Sr_3Ru_2O_7$* R. A. Borzi, S. A. Grigera, J. Farrell, R. S. Perry, S. Lister , S. L. Lee, D. A. Tennant, Y. Maeno, and A. P. Mackenzie, Science 2006, [DOI:10.1126 /science.1134796]

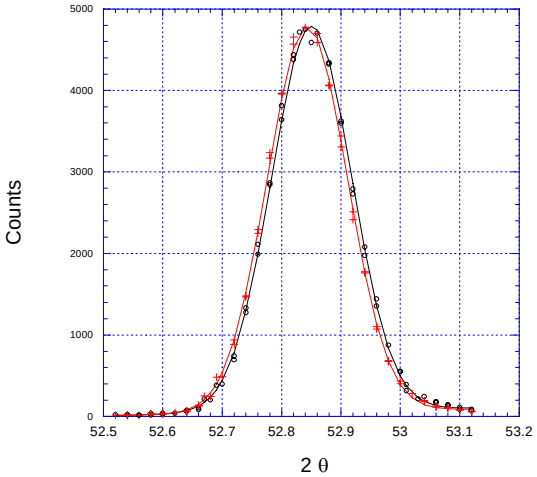

Fig. 1: *Elastic neutron scattering peak from the 020 reflection of a high quality single crystal of $Sr_3Ru_2O_7$ in zero applied magnetic field (black) and a field of 8 tesla applied parallel to c (red).*

	EXPERIMENTAL REPORT **Magnetic order in the frustrated compound $HoInCu_4$**	Proposal N° PHY-01-1746 Instrument **E2** Local Contact Uwe Amann
Principal Proposer: Experimental Team:	O. Stockert – MPI CPfS Dresden V. Fritsch – Uni Karlsruhe U. Amann – HMI, Berlin	Date(s) of Experiment 13.02. – 18.02.2006

Date of Report: 06.12.2006

The ternary rare-earth compounds $REInCu_4$ (RE = Gd, Dy, Ho and Er) show strong indications of frustration. The crystal structure, in which the rare-earth ions occupy a face-centered cubic lattice, suggests the presence of geometrical frustration. $HoInCu_4$ exhibits magnetic order below $T_N = 0.75K$ as evidenced by heat capacity measurements [1]. Therefore we investigated the magnetic order of $HoInCu_4$ by powder neutron diffraction on the diffractometer E2 in order to gain a better understanding of the magnetically frustrated ground-state in this compound. Measurements were performed at temperatures between $T = 65mK$ and 50K with a neutron wavelength $\lambda = 2.39Å$

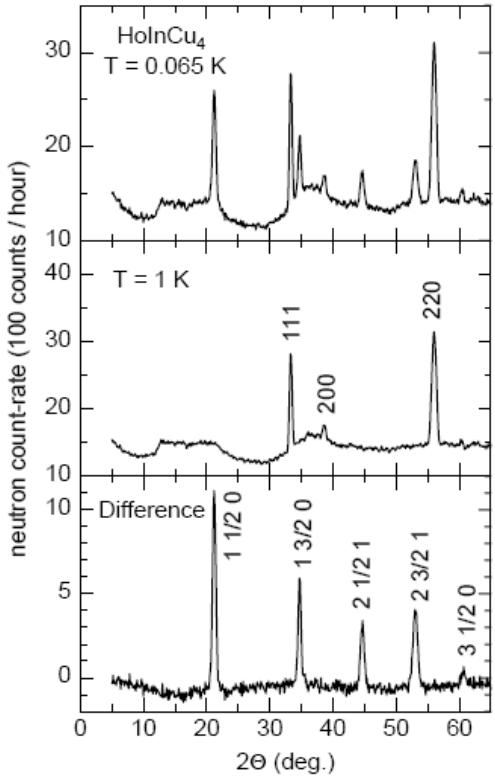

Fig. 1: *Neutron count-rate versus scattering angle 2Θ of $HoInCu_4$ powder for T = 0.065K (top) and T = 1K (middle). The bottom panel shows the difference diffraction pattern.*

Fig. 1 displays diffraction pattern taken at lowest temperature $T = 65mK$ and at $T = 1\ K$, i.e., well below and slightly above T_N. The cubic crystal structure is confirmed by the measurements. At lowest temperature additional peaks are visible. To receive just the magnetic part of the scattering, the 1K data were subtracted from the low T data. All magnetic peaks seen in Fig. 1 bottom can be unambiguously indexed. The magnetic structure is commensurate with a propagation vector $\tau = (1\ 1/2\ 0)$. Surprisingly, the magnetic intensity does not completely vanish at the Néel temperature, instead a considerable amount persists into the paramagnetic state (at T_N about 30% of the maximum intensity is present). However, the peak width clearly increases at T_N (not shown) indicating the breakdown of long-range order. To further study the evolution of the magnetic correlation above TN diffraction pattern were taken up to T = 50K. Fig. 2 shows the difference pattern between 1K and 50K indicating the strong magnetic correlations in the paramagnetic state of $HoInCu_4$. Such short-range correlations with a transition into the long-range magnetically ordered state at quite low T are expected in systems with strong frustration.

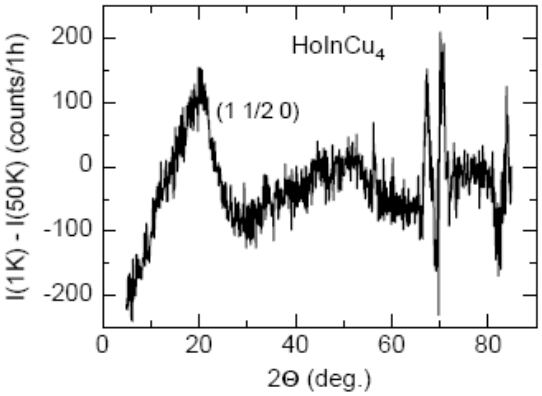

Fig. 2: *Difference diffraction pattern of $HoInCu_4$ between T = 1K and 50K.*

Reference:

[1]. V. Fritsch, J. D. Thompson, J. L. Sarrao, Phys. Rev. B **71**, 132401 (2005).

	EXPERIMENTAL REPORT **Magnetic short range correlations in multiferroic $BaMnF_4$**	Proposal N° PHY-01-1810-EF Instrument **E2** Local Contact Uwe Amann
Principal Proposer: Experimental Team:	J. R. Veira – HMI, Berliln D. N. Argyriou, H. N. Bordallo – HMI, Berlin K. Kiefer, J.-U. Hoffmann – HMI, Berlin U. Amann – HMI, Berlin R. Almairac – Univ. Montpellier, F	Date(s) of Experiment 21.11. – 26.11.2005

Date of Report: 14.12.2006

Multiferroics, materials exhibiting magnetism and ferroelectricity in a single phase, have attracted a lot of attention in recent years, due to their strong magnetoelectric coupling [1]. In this context, $BaMnF_4$ is often named as an example for a multiferroic with a spontaneous magnetoelectric effect [2]. $BaMnF_4$ has an orthorhombic crystal structure at room temperature and is ferroelectric up to the melting point. It undergoes a structural ferroelastic phase transition at T_{IC}=253 K to an incommensurate low temperature phase. At T_N=26.3 K the materials orders antiferromagnetically with easy axis along the crystallographic *b*-axis. At about T=50 K a maximum is found in the magnetic susceptibility, that has been associated with a magnetic short range ordering [3].

In the past especially the ferroelectric properties and the incommensurate phase transition of $BaMnF_4$ have been studied intensively [3], but no detailed investigations of the magnetic short range ordering exist. In the context of the risen interest in multiferroics and with the purpose of a deeper understanding of the multiferroic magnetoelectric coupling in $BaMnF_4$ a complete and detailed understanding of the magnetic properties of the material is needed, including the short range ordering.

The experiments were performed on a single crystal sample of dimensions 8 mm x 4.5 mm x 5 mm. Measurements were perfomed in the reciprocal space (h k k) plane. With initial measurements at several temperatures between 300 K and 2 K the commensurate and incommensurate crystal structure and the magnetic long range ordering have been confirmed. At T=2 K peaks arising from the commensurate magnetic structure as well as from the incommensurate magnetic superstructure have been found. Above the Neel temperature T_N broad diffuse scattering features have been found at the position of the magnet peaks. Detailed measurements were performed for T=45 K. The resulting diffuse scattering is shown in Figure 1. It is possible to fit the diffuse magnetic scattering according to a mean field model, as described in [4]. For that purpose the software packet TVtueb has been used. A model taking only magnetic interactions between nearest neighbour Mn^{2+} ions into account led to the best fitting results. With this model the magnetic short range ordering is described as 2D like within the *ac*-sheets of the structure. The fitting result is shown in Figure 1.

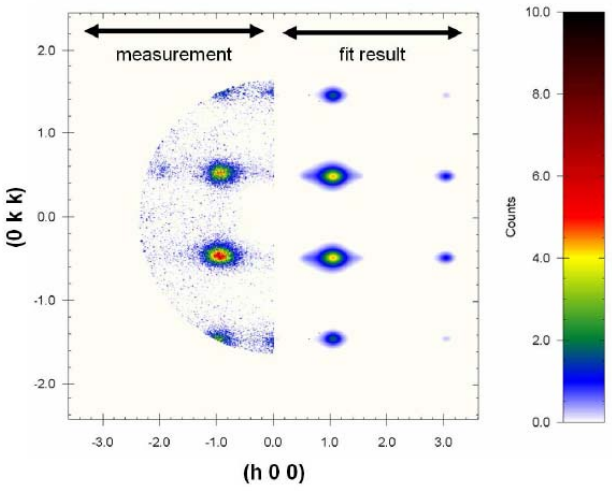

Fig. 1: *Diffuse magnetic neutron scattering from $BaMnF_4$ in the reciprocal (h k k) plane arising from magnetic short range correlations for T = 45 K. On the left side the measured diffraction pattern is shown and on the right side the fitting result according to a 2D short range ordering with only nearest neighbour interactions present is shown. A good agreement between model and measurement is found.*

References:

[1]. M. Fiebig, J. Phys. **D 38, R123** (2005).
[2]. W. Eerenstein, N. Mathur, and J.F. Scott, Nature **442**, 759 (2006).
[3]. J.F. Scott, Rep. Prog. Phys. **12**, 1055 (1979).
[4]. D. Hohlwein, J.-U. Hoffmann, R. Schneider, Phys. Rev. B **68**, S. 140408–1–4 (2003).

	EXPERIMENTAL REPORT **Magnetic structure of Tm_2PdSi_3**	Proposal N° PHY-01-1846 Instrument **E2** Local Contact Jens-Uwe Hoffmann
Principal Proposer: Experimental Team:	M. Frontzek, A. Kreyssig – IFP, TU Dresden S. Raasch – IFP, TU Dresden J.-U. Hoffmann – HMI, Berlin U. Amann – HMI, Berlin	Date(s) of Experiment 06.02. - 13.02.2006

Date of Report: 06.06.2006

In a recent neutron scattering experiment in September 2005 on the E2 diffractometer the focus was the magnetic structure of Er_2PdSi_3 (T_N = 7.0 K) and Tm_2PdSi_3 (T_N = 1.8 K) [1]. During this experiment it became obvious that the vertical resolution was insufficient for the correct determination of the magnetic structure of Tm_2PdSi_3. Magnetic intensity had been found on positions (1/8 1/8 *n*/16), (3/16 3/16 *n*/16), (5/16 5/16 *n*/16) and (3/8 3/8 *n*/16) with *n* equal an odd integer. With the vertical focused PG monochromator the vertical resolution is about 3 degrees while the flat cone angle between neighbouring magnetic reflections from different reciprocal planes is only 2.1 degrees. As a result, the indexing of the magnetic reflections is based only on a hypothesis. For the detailed discussion see the related report [1].

The conceptual formulation for the experiment was to investigate the magnetic structure of Tm_2PdSi_3 with maximised resolution e. g. a non-focussed PG monochromator and 15' collimation. However, the Tm_2PdSi_3 single crystal was misaligned in both configurations, thus reflections from higher reciprocal planes could still be observed. The flat-cone technique of the E2 allowed us to map the reciprocal space by measuring (*H K n*/16) and (*H*+*n*/16 *H*-*n*/16 *L*) planes with *n* = 0,…,7. The HS-1 insert in a standard-orange cryostat was used to reach temperatures well below T_N.

Figure 1 shows a comparison between the reciprocal (*HHL*)- and the (*H*+1/16 *H*-1/16 *L*)-plane at *T* = 0.4 K. In the (*HHL*) plane additional reflections can be observed. These reflections can be either attributed to a crystallographic superstructure or magnetic intensity from the (*H*+1/16 *H*-1/16 *L*)-plane. In the (*H*+1/16 *H*-1/16 *L*)-plane no additional reflections are observed. The reason is that in the (*H*+2/16 *H*-2/16 *L*)-plane no magnetic intensity is observed. The first order of magnetic reflections can be found in the (*HHL*)-plane at (1/8 1/8 *n*/16) positions. The next magnetic satellites in this plane are of third order (3/8 3/8 *n*/16). In the (*H*+1/16 *H*-1/16 *L*)-plane magnetic intensity is found on positions (3/16 3/16 *n*/16) and (5/16 5/16 *n*/16). In reciprocal space these positions then are (2/8 1/8 *n*/16) and (3/8 2/8 *n*/16).

A careful analysis of all measured reciprocal planes will result in a proposal for the magnetic structure of Tm_2PdSi_3.

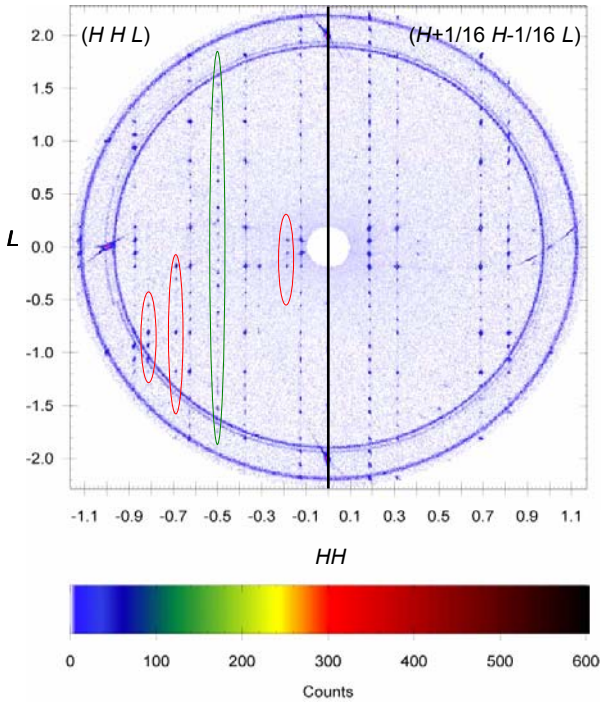

Fig. 1: *Reciprocal (HHL)- and (H+1/16 H- 1/16 L)-plane of Tm2PdSi3 at T = 0.4 K. In the (HHL)-plane additional reflections are marked: crystallographic superstructure (green) and magnetic intensity from the (H+1/16 H-1/16 L)- plane (red) due to crystal misalignment.*

We gratefully acknowledge the financial and technical support from the HMI, Berlin.

References:

[1]. M. Frontzek, A. Kreyssig, E. Faulhaber, J.-U. Hoffmann, HMI Exp. Report PHY-01-1747 (2005)

	EXPERIMENTAL REPORT **Crystal structure and magnetic structure studies on new uranium-based deuterides**	Proposal N° PHY-01-1849 Instrument **E2** Local Contact Karel Prokeš
Principal Proposer: Experimental Team:	K. Miliyanchuk – CU Prague, CZ L. Havela – CU Prague, CZ K. Prokeš – HMI, Berlin	Date(s) of Experiment 10.03. - 14.03.2006

Date of Report: 30.05.2006

U_2Ni_2Sn belongs to large group of isostructural compounds with U_2T_2X composition (T – transition metal, X – p-element), which are characterized by wide range of magnetic properties from weak Pauli paramagnetism to antiferromagnetism. It was found that hydrogenation has strong impact on the magnetic properties of these compounds. In all cases it leads to stronger magnetic interactions, increase of the ordering temperatures or even to the formation of magnetic order in non-magnetic compounds. U_2Ni_2Sn absorbs 1.8 H/ f.u. and the Néel temperature of U_2Ni_2Sn increases from 26 K to 87 K in $U_2Ni_2SnH_{1.8}$ [2].

Both $U_2Ni_2SnH_{1.8}$ and $U_2Ni_2SnD_{1.8}$ crystallize in the tetragonal Mo_2FeB_2 structure type (space group P4/mbm) similar to the initial compound. The lattice and crystal structure parameters are listed in Table 1. The positions of deuterium atoms were determined as (8k) site inside the [U_3Ni] tetrahedra, which are coupled by sharing a face. Two neighbouring tetrahedra can not be occupied simulteneously, due to the proximity of the interstitials. The stoichiometry of the deuteride ($U_2Ni_2SnD_{1.79(2)}$) corresponds well with the value, obtained by the volumetric method ($U_2Ni_2SnD_{1.8(1)}$).

Table 1: *Lattice parameters a and c, unit cell volume V of $U_2Ni_2SnH_{1.8}$ and $U_2Ni_2SnD_{1.8}$ measured at room temperature, and atomic parameters, and the coefficients of the site occupancy n, obtained from neutron diffraction of $U_2Ni_2SnD_{1.8}$ at 120 K (R_B = 4.22 %).*

U_2Ni_2Sn		a = 7.263(1) Å	c = 3.695(1) Å	V = 194.9(1) Å^3	
$U_2Ni_2SnH_{1.8}$		a = 7.445(1) Å	c = 3.764(1) Å	V = 208.6(1) Å^3	
$U_2Ni_2SnD_{1.8}$		a = 7.435(1) Å	c = 3.762(1) Å	V = 207.9(1) Å^3	
Atom	Site	x	y	z	n
U	(4h)	0.1788(6)	0.6788(6)	0.5	1
Ni	(4g)	0.3747(5)	0.8747(5)	0	1
Sn	(2a)	0	0	0	1
D	(8k)	0.3859(10)	0.8859(10)	0.5338(63)	0.448(6)

Unlike pure U_2Ni_2Sn, which exhibited additional magnetic reflection (1/2, 1/2, 1/2) in neutron diffraction pattern collected in the ordered state [*3*], no additional reflections were observed on for $U_2Ni_2SnD_{1.8}$ at T = 1.8 K (Fig. 1). Thus the unit cell doubling along c, indicated at U_2Ni_2Sn, is lost in the deuteride.

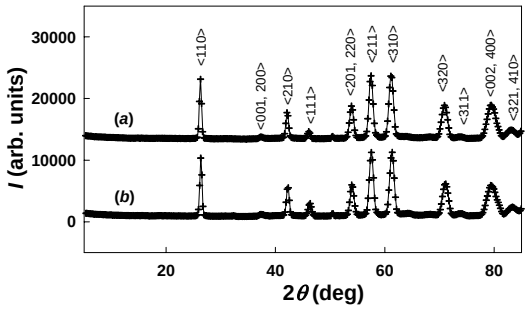

Fig. 1*: Neutron powder diffraction patterns of $U_2Ni_2SnD_{1.8}$ at T = 120 K (a) and 1.8 K (b).*

The best fit was found for the model having non-collinear uranium moments of 0.8(3) μ_B within the basal plane, similar to the situation found in U_2Pd_2In [4].

Deuterides of two more compounds, UCoSn and URuSn, crystallizing in hexagonal ZrNiAl structure type, were chosen for the structure studies. The deuterium positions in $UCoSnD_x$ were determined as 3g (0.467, 0, 0.5), 4h (1/3, 2/3, 0.447) and 3f (0.564, 0, 0). However, total calculated occupancy yields x = 0.6 only, what is considerably smaller, than the value obtained volumetrically for the hydride. Therefore the volumetric determination of x for the deuterides is still required. The structural model described above does not work for the $URuSnD_x$, what was to be proved, however more precise structure data have to be collected.

References:

[1]. L. Havela, V. Sechovsky, P. Svoboda et al, J.Magn.Magn.Mater. **140-144** (1995) 1367.

[2]. K. Miliyanchuk, L. Havela, A. V. Kolomiets et al, Physica B, in press.

[3]. F. Bourée, B. Chevalier, L. Fournès, et al, J. Magn. Magn. Mater., **138** (1994) 307.

[4]. A. Purwanto, R. A. Robinson, L. Havela, et. al, Phys. Rev. B, **50** (1994) 6792

	EXPERIMENTAL REPORT **CDW transition and magnetic ordering in Fe intercalated compound $Fe_{0.5}TiSe_2$**	Proposal N° PHY-01-1854 Instrument **E2** Local Contact Uwe Amann
Principal Proposer: Experimental Team:	N. Baranov – USU Ekaterinburg, RU N. Selezneva – USU Ekaterinburg, RU A. Podlesnyak, U. Amann – HMI, Berlin V. Maksimov – USU Ekaterinburg, RU	Date(s) of Experiment 31.03. - 03.04.2006

Date of Report: 15.11.2006

The titanium dichalcogenide TiX_2 (X = S, Se, Te) compounds are of special interest since their hexagonal crystal structure of the CdI_2 type allows to intercalate the various guest ions into van der Waals (vdW) gap between triple X-Ti-X layers [1]. Within the TiX_2 family the compound $TiSe_2$ is one of the best known material due to the existence of a structural phase-transition induced by a charge density wave (CDW) below $T_t \sim 200$ K [1,2]. Depending on the nature of the guest M-ions and their concentration the intercalated M_xTiX_2 compounds reveal a rich variety of different physical properties. The existence of different magnetic states ranging from spin-glass like behavior up to states with three-dimensional magnetic order was established in M_xTiS_2 and M_xTiSe_2 intercalated by 3d-transition metals [2,3]. According to previous X-ray and neutron diffraction studies the $Fe_{0.50}TiSe_2$ compound exhibits an antiferromagnetic order below $T_N \sim 130$ K [2]. Our recent electrical resistivity studies imply the reappearance of the CDW state in M_xTiSe_2 at a high content of intercalated M atoms.

In the present project we have performed the powder neutron diffraction (PND) study of the $Fe_{0.50}TiSe_2$ compound in a temperature range 2 – 300 K using a wave-length $\lambda = 1.215$ Å. The PND patterns obtained at selected temperatures are displayed in Fig. 1. The program FullProf was used for refinement of the crystal and magnetic structures. At room temperature, the crystal structure can be described according to the monoclinic unit cell ($I2/m1$ space group) with parameters $a=a_0\sqrt{3}$, $b=a_0$, $c= 2c_0$ (a_0 and c_0 are hexagonal cell parameters) which are presented in Table 1. The superstructure is caused by an ordering of Fe atoms inserted into vdW gaps along the b axis. Our room temperature data for $Fe_{0.50}TiSe_2$ are in a good agreement with Ref. 3. The new reflections (shown by arrows) were observed on NPD patterns with decreasing temperature below 135 K. The appearance of these reflections may be associated with both antiferromagnetic ordering and change of the crystal structure. In order to separate the magnetic and structural phase transition in $Fe_{0.50}TiSe_2$ with decreasing temperature the additional X-ray diffraction are needed. The magnetic structure which appeared below ~ 135 K may be described by the wave vector $\boldsymbol{k}$ = (½, 0, ½).

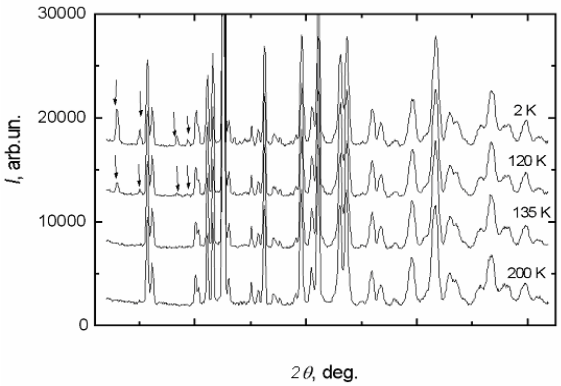

Fig. 1: *Powder neutron diffraction patterns for the $Fe_{0.50}TiSe_2$ compound at selected temperatures. Additional reflections appear with decreasing temperature are indicated by arrows.*

			x	y	z
a(Å)	6.2732(1)	Fe	0	0	0
b(Å)	3.5949(1)	Ti	0.0250	0	0.2493
c(Å)	11.9529(2)	Se1	0.1686	0.5	-
β(°)	89.647(1)	Se2	0.3374	0	0.1286
R(%)	1.596				0.1160

Table 1: *Structural refined parameters of $Fe_{0.5}TiSe_2$ at room temperature.*

The present work was supported by the Russian Foundation for Basic Research (Grant No 05-03-32772)

References:

[1]. A. R Beal, *Intercalated Layered Materials*, F.A. Levy, ed. (D. Reidel Publishing Company) 1979, p.251.
[2]. F. J. Di Salvo et al., 1976 *Phys. Rev. B* **14** 4321
[3]. G. Calvarin et al., 1987 *Revue Phys. Appl.* **22** 1131

	EXPERIMENTAL REPORT **Modulated quadrupole ordering structures in $PrPb_3$**	Proposal N° MAT-01-1976 Instrument **E4** Local Contact Karel Prokeš
Principal Proposer: Experimental Team:	T. Onimaru – Univ. Tokyo, ISSP, JP N. Aso – Univ. Tokyo, ISSP, JP T.J. Sato – Univ. Tokyo, ISSP, JP K. Prokeš – HMI, Berlin	Date(s) of Experiment 17.07. – 31.07.2006

Date of Report: 19.01.2007

Antiferroquadrupolar (AFQ) ordering in the intermetallic *f* electron compounds has been attracting much attention in these years. $PrPb_3$ crystallizes in a simple $AuCu_3$-type cubic structure, and it has a Γ_3 non-Kramers doublet in the crystalline-electrical-field (CEF) ground state. There is a second order transition at 0.4 K with a lambda type anomaly in the specific heat.[1)] From various macroscopic experiments, it is considered that an AFQ ordering of Γ_3 type quadrupolar moments, such as $O_2^0 = (2\boldsymbol{J}_z^2 - \boldsymbol{J}_x^2 - \boldsymbol{J}_z^2)/2$ and/or $O_2^2 = \sqrt{3}(\boldsymbol{J}_x^2 - \boldsymbol{J}_y^2)/2$, should occur. Very recently, we have firstly observed the quadrupole ordered state on the material by neutron diffraction technique in magnetic field. To our surprise, the quadrupole are aligned with modulated structures, although quadrupoles are distributed alternatively in the other AFQ materials.[2)]

In the present work, we used a 5x5x5mm^3 single crystal grown by the Bridgman method with using a Molybdenum crucible. Neutron diffraction measurements were performed using the two-axis spectrometer E4 installed at the research reactor in the Hahn Meitner Institut. The wave length of neutrons was 2.44 Å and a 40'-40'-(sample)-40' collimation was used. We chose the (*hk*0) scattering plane, and the magnetic field was applied along the [001] direction which is perpendicular to the scattering plane. The sample was attached on a copper holder, and mounted on a mixing chamber of a ^{3}He-^{4}He dilution refrigerator. Magnetic field up to 14.5 T was applied by a superconductor magnet vertically along the [001] direction.

Fig. 1 shows the results of ***Q***-scans along the line with ***Q***=(*h* 1/2 0) at the temperature of *T*=50 mK and in various magnetic fields up to *H*=14.5 T. In zero field (*T*=2 K), there is no superlattice reflection other than the nuclear reflections. Once field was applied, field induced magnetic reflections were observed at $\boldsymbol{Q}_1$= (1/2 3/8 0) and $\boldsymbol{Q}_2$=(3/8 1/2 0). In addition, above 5 T, we observed magnetic reflections at $\boldsymbol{Q}_1$=(3/8 1/2 0) and $\boldsymbol{Q}_1$'= (1/8 1/2 0). The reflections at $\boldsymbol{Q}_1$ and $\boldsymbol{Q}_2$ disappeared above 8 T. On the other hand, we found a new reflection at $\boldsymbol{Q}_3$=(0 1/2 0) and $\boldsymbol{Q}_4$=(1/2 0 0) between 6 T and 8 T. Above 8 T, we could not observe any superlattice reflections. The behaviour is very consistent with the *H-T* phase diagram determined by magnetization measurements.

In the field applied along the [110] direction, we have determined field induced magnetic structure and the order parameter (OP) to be the O22-type quadrupole. On the other hand, in the case of the field of [001], the OP should be the O_2^0-type quadrupole since the direction of the field induced antiferromagnetic components were parallel to the magnetic field. Therefore, it should be noted that the OP should be switched from O_2^2 to O_2^0 by changing the field direction above 6 T.

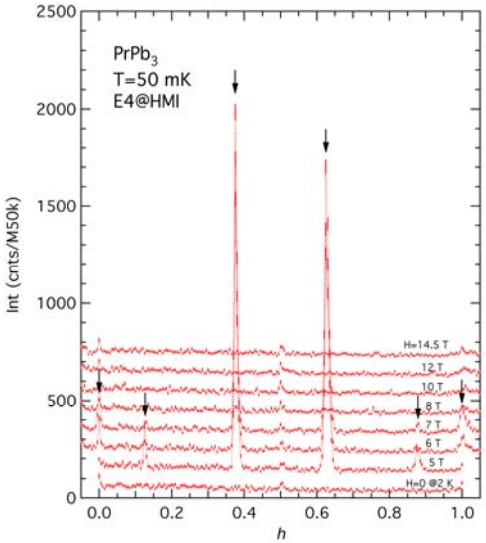

Fig. 1: ***Q****-scan along (h k 0) at the temperature of T=50 mK and in the magnetic fields up to 14.5 T which was applied along [001].*

References :

[1]. E. Bucher *et al*., J. Low Temp. **2** (1972) 322.
[2]. Onimaru *et al*., Phys. Rev. Lett. **94** (2005) 197201.
[3]. Onimaru *et al*., in preparation.

	EXPERIMENTAL REPORT UIrGe in high magnetic fields	Proposal N° PHY-01-1414-EF Instrument **E4** Local Contact Karel Prokeš
Principal Proposer: Experimental Team:	K. Prokeš – HMI, Berlin K. Prokeš – HMI, Berlin E. Bruck, F.R. de Boer – Univ. Amsterdam,NL V. Sechovsky – CU Prague, CZ	Date(s) of Experiment 07.02. – 14.02.2006

Date of Report: 29.12.2006

UIrGe crystallizes in the orthorhombic TiNiSi-type of structure (space group *P*nma). It belongs to the large family of UTX compounds (T = transition metal and X = Si or Ge). UIrGe orders antiferromagnetically (AF) below T_N = 16-18 K [1]. Magnetic measurements on single crystals of UIrGe reveal a large magnetic anisotropy with the hard magnetization direction along the *a* axis. For magnetic fields applied along the *b* and the *c* axis, metamagnetic transitions exist [2].

The magnetic structure of UIrGe is non-collinear and commensurate with the crystallographic unit cell [3]. The ordered U magnetic moment is strongly reduced (0.36 μ_B/U at 1.8 K) compared with U^{3+} or U^{4+} single ions. However, it appears that bulk magnetic properties are rather sensitive to the preparation details. Therefore, new crystal has been prepared with the aim to confirm the magnetic structure.

A single crystal of UIrGe was grown in a tri-arc furnace by the Czochralski method from a stoichiometric mixture of the pure elements (99.9% U, 99.99% Ir and 99.999% Ge) which according to Laue pictures is of better quality than previously grown crystals. Neutron diffraction experiments were performed in the double-axis diffractometer E4, with either the *a*- or the *c*- axis aligned along the rotational axis of the diffractometer that was parallel to the applied field of 14.5 T. The incident-neutron wavelength was 2.44 Å.

We have collected for the two orientations three sets of data consisting of total 29 inequivalent reflections: at 25 K in zero field; at 2K in zero field and at 2 K in 14.5 T. The magnetic signal has been obtained by subtracting the paramagnetic set obtained at 25 K and fitted to all allowed models described in Ref. 3. The magnetic structure of the crystal was clearly in accord with the magnetic structure reported in Ref. 3. Slightly different magnetic-moment components were, however, determined. The AF *a*- and the *c*- axis components amount to 0.18(8) μ_B and 0.27(2) μ_B respectively, with χ^2 = 5.2. Compared with the results found in Ref. 3, we have found for the present crystal a much smaller *a*-axis component and a larger *c*-axis component. The total magnetic moment in the present sample amounts to 0.32(5) μ_B/U.

The found components along the *a*- and *c*-axis are seemingly in contradiction with the equivalent magnetization behavior found along the *b*- and *c*-axis. This apparent inconsistency is not yet understood and will be subject of further study.

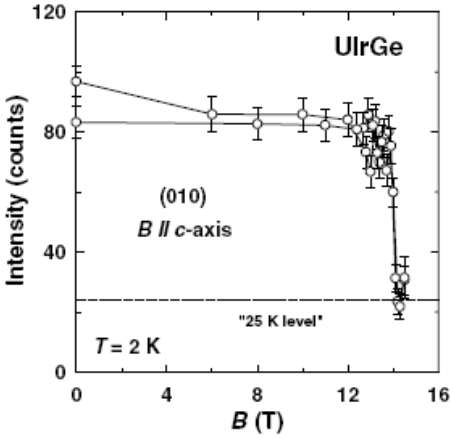

Fig. 1: *Field dependence of the integrated intensity of the AF (010) reflection. The small intensity above the transition is due to $\lambda/2$ contamination from the (020) reflection.*

While there is, in agreement with the magnetization data, no effect on the AF structure of UIrGe of 14.5 T applied along the *a*-axis, application of a field along the *c*-axis causes a metamagnetic transition to a field-induced ferromagnetic state. Above the transition, the ferromagnetic *c*-axis component amounts to 0.45(9) μ_B, in agreement with the magnetization data. Whether the AF *a*-axis component prevails in the field-induced ferromagnetic state, as it is in the case of the isostructural compound UNiGe [4], is still unclear at present and needs further study.

References:

[1]. V. Sechovský and L. Havela, in *Handbook of Magnetic Materials*, ed. K.H.J. Buschow (North Holland, Amsterdam, 1998), Vol. **11**, p. 1

[2]. S. Chang, et al. *Int. J. Modern Phys. B* **16** (2002) 3041

[3]. K. Prokeš, et al., *Physica B* **350** (2004) E199

[4]. K. Prokeš, et al., *Phys. Rev. B* **65** (2002) 144429

	EXPERIMENTAL REPORT **Determination of the magnetic structure in the ferromagnetic superconductor UIr**	Proposal N° PHY-01-1786 Instrument **E4** Local Contact Karel Prokeš
Principal Proposer: Experimental Team:	N.H. van Dijk – TU Delft, NL S. Sakarya – TU Delft, NL K. Prokeš – HMI, Berlin	Date(s) of Experiment 10.01. – 22.01.2006

Date of Report: 12.01.2007

Recently, UIr was found to show a coexistence of ferromagnetic order and superconductivity at applied pressures of 26-27 kbar [1]. This coexistence originates from a proximity to a quantum-critical point. UIr is the only system of this class where the crystal structure lacks inversion symmetry.

UIr crystallises in the monoclinic PbBi-type structure (space group $P2_1$) without inversion symmetry. The unit cell, with dimensions a = 5.62 Å, b = 10.59 Å, and c = 5.60 Å ($\alpha = 90^o$, $\beta = 98.9^o$, $\gamma = 90^o$), contains 8 formula units with 4 inequivalent U and Ir sites [2]. UIr is an itinerant ferromagnet with a Curie temperature of T_C = 46 K at ambient pressure. Magnetisation measurements on a single crystal [3] revealed that the easy axis is parallel to [10-1], whereas the anisotropy with the hard axes [101] and [010] is large. Along the easy direction, the average saturated moment is equal to 0.5 μ_B/U-atom. The coefficient of the linear electronic specific heat c/T = 50 mJ/molK^2 indicates a moderate enhancement of the electron correlations at ambient pressure.

Magnetisation under pressure [1] showed that the ferromagnetic structure collapses at a pressure of 17 kbar and transforms into a new ferromagnetic structure. For a simple ferromagnetic structure it is difficult to imagine why the phase transition observed at a pressure of about 17 kbar would occur. This suggests that the magnetic structure is more complicated, possibly involving canted moments or a difference in ordered moment at the 4 inequivalent U sites. We therefore studied the magnetic structure of UIr at ambient pressure.

So far, only a single neutron powder diffraction measurement has been performed by Dommann et al. [2], which revealed a weak magnetic contribution to the [111] and [12-1] Bragg peaks. No sizeable new magnetic Bragg peaks, in addition to the nuclear Bragg peaks, were reported. The average spin orientation of the ordered moment was deduced from magnetisation measurements on a single crystal [3].

We have performed neutron diffraction measurements on a spherical single crystalline sample with a diameter of 2 mm (mass 0.2 g) on diffractometer E4. At a fixed neutron wavelength of λ = 2.4396 Å neutron diffraction experiments were performed at temperatures of 55 K ($T > T_C$) and 2 K ($T << T_C$). The sample was mounted in two orientations with [10-1] and [101] perpendicular to the scattering plane. Along the easy axis applied magnetic fields up to 5 T were applied.

Due to the relatively large absorption of iridium relatively long counting times were needed. The obtained results for our single crystal are consistent with those obtained by Dommann et al. [2] for a powder. Systematic **Q**-scans at low temperature revealed no additional magnetic Bragg peaks indicating that the magnetic structure has the same lattice as the nuclear structure (**k** = **0**). All the accessible Bragg peaks were monitored above and below the ferromagnetic transition to deduce the magnetic contribution. A limited number of finite magnetic Bragg peaks could be resolved within the statistical accuracy. The results are compatible with a simple ferromagnetic structure with equal moments, oriented along [10-1]. In order to resolve the magnetic structure in more detail additional experiments at a shorter wave length would be desirable.

References:

[1]. T. Akazawa et al., J. Phys.: Condens. Matter 16 (2004) L29.

[2]. A. Dommann et al., J. Magn. Magn. Mater. 67 (1987) 323.

[3]. A. Galatanu et al., J. Phys. Soc. Japan 73 (2004) 766.

	EXPERIMENTAL REPORT **Coupling of magnetic and structural properties in multiferroic $BaMnF_4$**	Proposal N° PHY-01-1827-EF Instrument **E4** Local Contact Karel Prokeš
Principal Proposer: Experimental Team:	J.R. Veira – HMI, Berlin D. N. Argyriou , H.N. Bordallo – HMI, Berlin K. Kiefer, K. Prokeš – HMI Berlin R. Almairac – Univ. Montpellier, F	Date(s) of Experiment 05.12. – 09.12.2005

Date of Report: 14.12.2006

Multiferroics, materials exhibiting magnetism and ferroelectricity in a single phase, have attracted a lot of attention in recent years, due to their strong magnetoelectric coupling [1]. In this context, $BaMnF_4$ is often named as an example for a multiferroic with a spontaneous magnetoelectric effect [2]. $BaMnF_4$ has an orthorhombic crystal structure at room temperature and is ferroelectric up to the melting point. The material undergoes a structural phase transition at T_{IC}=253 K to an incommensurate low temperature phase. At T_N=26.3 K it orders antiferromagnetically with easy axis along the crystallographic *b*-axis. In the dielectric constant slope changes are found at T_N and about twice T_N that have been associated with the existence of a spontaneous magnetoelectric effect [3].

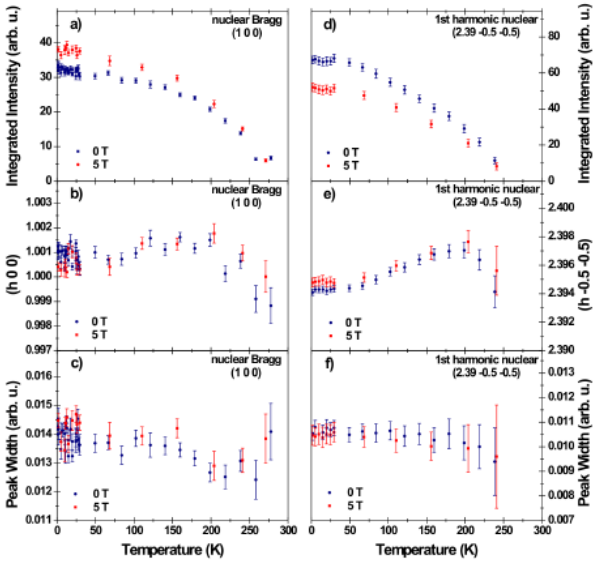

Fig. 1: *Temperature and field dependence of nuclear peaks arising from the orthorhombic crystal structure (a-c) and the incommensurate superstructure (d-f).*

Albeit $BaMnF_4$ is well know, no detailed investigations of the coupling between the magnetic and structural properties have been performed in the past. In the context of the risen interest in multiferroics and with the purpose of a deeper understanding of the magnetoelectric effect in $BaMnF_4$ an invest-igation of this coupling is of imminent need.

Experiments were performed on a single crystal sample (8 mm x 4.5 mm x 5 mm), mounted within the vertical magnet VM-3 (maximum field B=5 T). For peaks arising from both, the nuclear and the magnetic structure, measurements have been performed temperature dependent (see Fig 1 and 2). The application of a magnetic field (see Fig. 1 a,d and 2 a,d) slightly effected both the nuclear and the magnetic structure. This weak coupling is in agreement with measurements of the dielectric constant showing no signs of a strong coupling in $BaMnF_4$ but a weak magnetostrictive coupling (data not shown here). The results show $BaMnF_4$ as a material with a weak magnetostrictive coupling, but show no signs of the spontaneous magnetoelectric coupling proposed by [3].

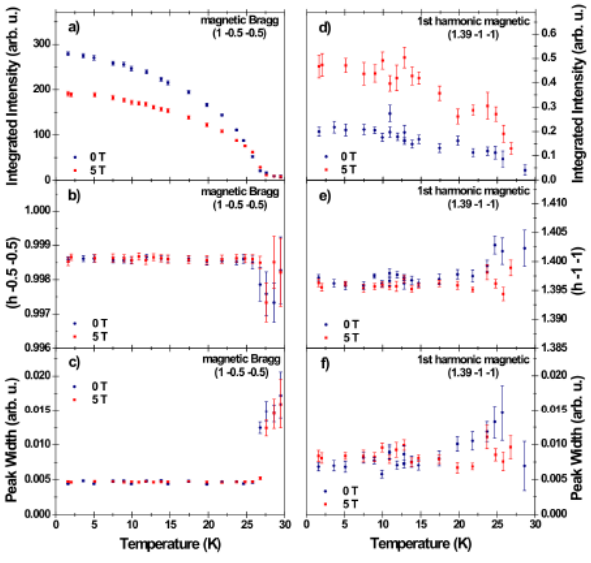

Fig. 2: *Temperature and field dependence of magnetic peaks arising from the orthorhombic structure (a-c) and the incommensurate superstructure (d-f).*

References:

[1]. [M. Fiebig, J. Phys. D **38**, R123 (2005).
[2]. W. Eerenstein, at. al, Nature **442**, 759 (2006).
[3]. J.F. Scott, Rep. Prog. Phys. **12**, 1055 (1979).

BENSC	**EXPERIMENTAL REPORT** **Examination of the magnetic field dependency of the (0kl)-reflections of cobalt vanadate ($Co_3V_2O_8$) in the ferro- and antiferromagnetic phase by neutron single crystal diffraction**	Proposal N° PHY-01-1874 Instrument **E4** Local Contact Karel Prokeš
Principal Proposer: Experimental Team:	N. Qureshi – TU Darmstadt N. Qureshi – TU Darmstadt K. Prokeš – HMI, Berlin	Date(s) of Experiment 15.05. – 24.05.2006

Date of Report: 03.01.2007

The aim of the performed experiment has been the investigation of the crystal structure as well of the multiple magnetic structures of $Co_3V_2O_8$. Therefore, various measurements have been performed at different temperatures in order to extract information of every respective phase. Integrated intensities have been collected of as many reflexions as possible. Unfortunately, the measured intensities turned out to be useless due to some unclear reasons. Possibly, the single crystal was not perfectly aligned, so that the peaks were cut off and not the maximum intensity was detected, which lead to wrong structure factors. Therefore, no structure refinement could be carried out. Nevertheless, quantitative measurements have been performed, which were very interesting. By following the k-component of the (020)± reflection in reciprocal space the temperature dependence of the propagation vector modulating the magnetic structures of $Co_3V_2O_8$ could be deduced (figure below). This result was part of a publication concerning the 'Magnetic properties of the Kagomé mixed compounds $(Co_xNi_{1-x})_3V_2O_8$', which has recently been published in Physical Review B (Phys. Rev. B **74** (2006) 212407).

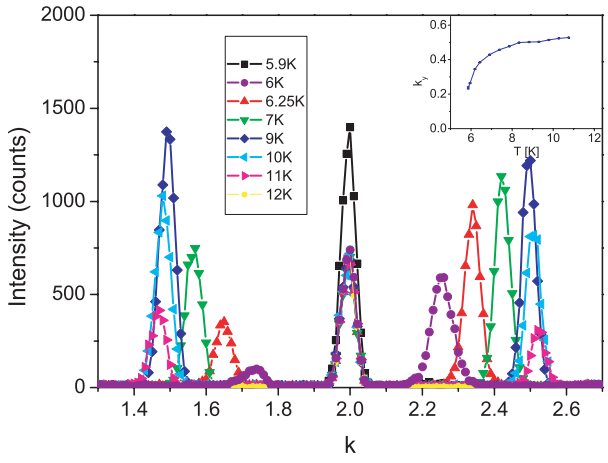

	EXPERIMENTAL REPORT **Short range correlations and spin fluctuations in the f-d electron subsystems of Tb_3Co.**	Proposal N° PHY-01-1875 Instrument **E4** Local Contact Andrei Podlesnyak
Principal Proposer: Experimental Team:	A. Podlesnyak – HMI, Berlin N. Baranov – USU Ekaterinburg, RU A. Gubkin – USU Ekaterinburg, RU	Date(s) of Experiment 14.03. – 19.03.2006

Date of Report: 09.10.2006

According to previous powder neutron diffraction studies the Tb_3Co compound has complex non-coplanar magnetic structure which can be described at low temperatures by the wave vector $\boldsymbol{k}$=0 [1]. However, the results of bulk magnetization and magnetoresistance measurements performed on single crystalline samples [2] imply a more complicated magnetic structure in Tb_3Co. Moreover, the properties of Tb_3Co were suggested to be influenced by short-range correlations above T_N =82 K. In the present project, the neutron diffraction measurements on a single crystal of Tb_3Co have been performed in the temperature range 1.5 – 170 K. The *c*-axis of the single crystal was oriented vertically. The scans were made along the directions [h00], [0k0], [hk0] at various temperatures. We have observed magnetic satellites around the integer-valued peaks and high intensity satellite $(000)^+$ which appear at the T>65 K and disappears at $T_N \approx 82$ K (fig. 1). These satellite may be described by the wave vector $\boldsymbol{k}=\mu\boldsymbol{b}_1$, $0.154<\mu<0.164$, $\boldsymbol{b}_1=2\pi/a(\mathbf{1}00)$. The scans along the direction [hh0] have revealed the magnetic satellites around the integer-valued peaks which exist in the temperature range below 75 K.

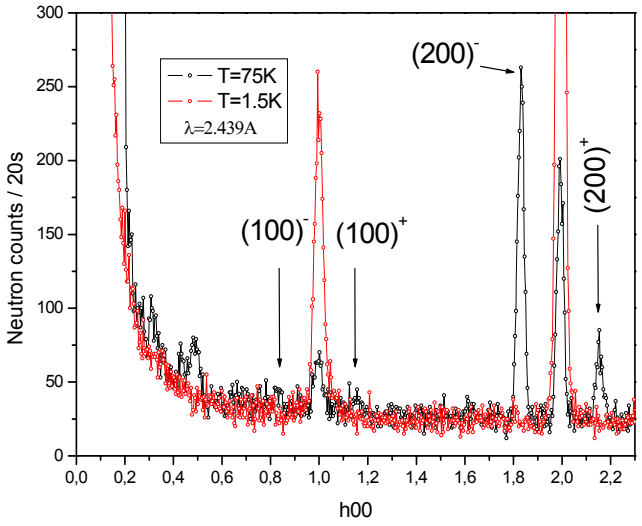

Fig. 1: *Scan along the [h00] direction at temperatures T=1.5 K and T=75 K.*

The intensity of these satellites decreases with increasing temperature up to T~75 K. These observations are indicative of incommensurability of the magnetic structure of Tb_3Co at low temperatures. The satellites observed may be described by wave vector $\boldsymbol{k}=\mu\boldsymbol{b}_1+\mu\boldsymbol{b}_2$, μ~0.33, $\boldsymbol{b}_1=2\pi/a(\mathbf{1}00)$, $\boldsymbol{b}_2=2\pi/b(0\mathbf{1}0)$ (fig. 2).

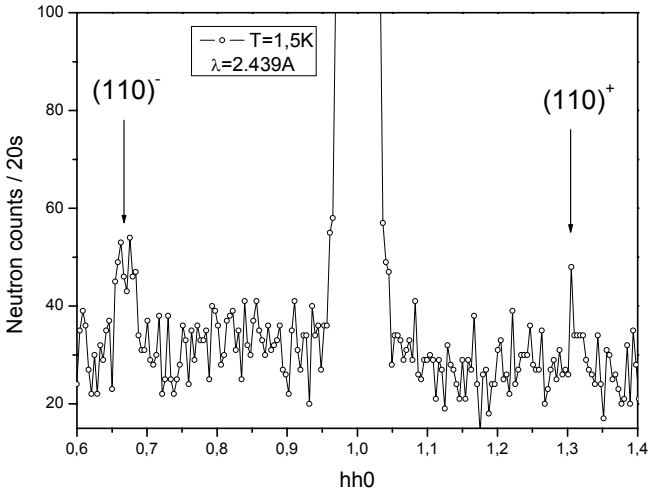

Fig. 2: *Scan along the [hh0] direction at T=1.5 K.*

The obtained results allow us to conclude that the magnetic structure of Tb_3Co is incommensurate at low temperatures. At low temperatures ($T<T_t\approx$ 72 K), the magnetic structure is described by a combination of the wave vectors $\boldsymbol{k}$=0 and $\boldsymbol{k}=\mu\boldsymbol{b}_1+\mu\boldsymbol{b}_2$, while within temperature range $T_t<T<T_N$ the magnetic structure is described by a wave vector $\boldsymbol{k}=\mu\boldsymbol{b}_1$. The magnetic phase transition at T_t is classified as of the first order type. In the present project, we have not revealed clear evidences of the short-range magnetic order well above T_N.

References:

[1]. D. Gignoux et al., Solid State Com. Vol. **44**, No. 5, pp 695-700, 1982.
[2]. N.V. Baranov et al., JMMM, **177-181** (1998) 1133.
[3]. N.V. Baranov et al., JMMM, **272-276** (2004) 637

	EXPERIMENTAL REPORT **Quantum phase transitions of $LiRe_xY_{1-x}F_4$ Re=(Ho,Er)**	Proposal N° PHY-01-1876 Instrument **E4** Local Contacts Karel Prokeš
Principal Proposer: Experimental Team:	H. Ronnow, C. Kraemer – LNS, ETHZ & PSI C. Gannarelli – LCN UCL, UK K. Prokeš, A. Podlesnyak – HMI, Berlin S. Gerischer, K. Kiefer – HMI, Berlin	Date(s) of Experiment 23.05 – 04.06.2006 12.06 – 16.06.2006

Date of Report: 14.09.06

The $LiReF_4$ (Re=rare-earth) series form a promising host for studies of various interesting phenomena close to zero temperature. The majority of experimental work to date has focused on the Re=Ho and Tb members, with several interesting observations from susceptibility measurements upon Y-dilution in the Ho case.

One initial goal of this experiment was to investigate the phase diagram of the dilution series $LiHo_xY_{1-x}F_4$ using neutron diffraction. Unfortunately, problems with these samples arose prior to the experiment. Therefore, to most valuably use the beamtime, emphasis was put on two other important goals:

1) It had been suggested that random distribution of Li-isotopes might influence the phase diagram in $LiHoF_4$. To answer this question, an isotopically pure $^7LiHoF_4$ crystal was prepared and investigated.
2) Due to the complementary crystal field properties between Ho and Er, the compound $LiErF_4$ could provide a similar fertile model system realisation with *planar anisotropy* – in contrast to the *Ising* class of $LiHoF_4$. However, very few experimental results existed on $LiErF_4$ to date, and our main goal was to determine the phase diagram and magnetic structures of $LiErF_4$.

1) The experiment to determine the influence of ^7Li isotopes suffered from several problems with the He^3 Cryostat for the $LiHoF_4$ measurement. It did not stabilize by any set temperature and therefore we changed to a Dilution refrigerator.

Nevertheless, we successfully were able to determine the critical temperature of 1.53+-0.02 K, which is within error identical to the non-isotopic case. Hence, on the basis of this experiment we can rule out that Li-isotopes influence the transition temperatures.

2) Using a high quality $LiErF_4$ single crystal, we were able to determine the phase diagram as a function of temperature and magnetic field along both the crystallographic c-axis and a-axis. We observed a thermal phase transition at 375 mK and at base temperature we found a quantum phase transition about 4 kOe in the case of magnetic field along the c-axis. In the case of a field along the a-axis we found for different Bragg peaks different field dependences. We interpret this as a Spin-Flop Transition at 0.5 kOe. The phase transition to the high field phase was observed at 2 kOe. We also determined the magnetic structure by zero field and by nonzero field, and could confirm the antiferromagnetic ordering we had predicted from mien-field modelling. For the high field phase the expected a ferromagnetic ordering is only qualitatively reproduced, most likely due to large extinction effects in the perfect single crystal and partial relief thereof due to magnetostriction. The measurements took more time than planed, because the thermalisation of our sample was very slow.

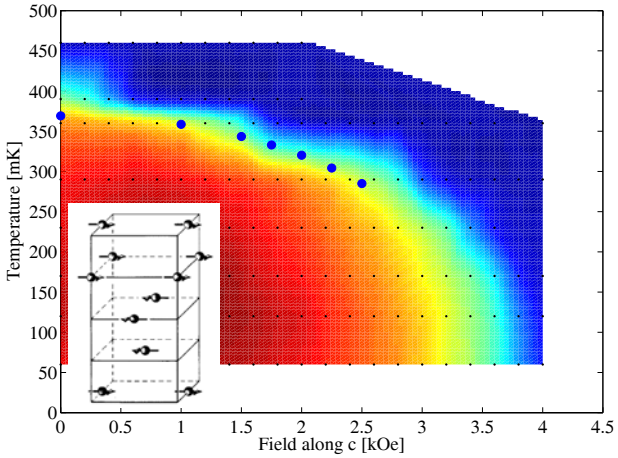

Fig. 1: *Phase diagram as function of temperature and field along the c-axis, from neutron diffraction studies (colour-scale is 010 peak intensity) and specific heat (blue circles). Inset: Obtained structure of the antiferromagnetic ordered Phase*

BENSC	**EXPERIMENTAL REPORT** **Field Induced Ferroelectric State in Frustrated Heisenberg Magnet $CuFe_{1-x}Al_xO_2$**	Proposal N° PHY-01-1878 Instrument **E4** Local Contact Karel Prokeš
Principal Proposer: Experimental Team:	S. Mitsuda – Tokyo US, JP T. Nakajima, S. Kanetsuki – Tokyo US, JP S. Mitsuda – Tokyo US, JP K. Prokeš, G. Andrew – HMI, Berlin	Date(s) of Experiment 29.03. – 13.04.2006

Date of Report: 27.05.2006

Geometrical spin frustration effect on magnetic phase transition and critical phenomena in triangular lattice antiferromagnet (TLA) have been extensively investigated experimentally and theoretically. As one of the model materials of TLA, delafossite-type compound $CuFeO_2$ has been extensively investigated. Owing to the competing interactions, several magnetization plateaus and linear magnetization-slopes appear in the magnetization process of $CuFeO_2$ where the second field-induced state (13T<H<21T) from 4-sublattice ground state was successfully identified as 5-sublattice commensurate magnetic state [1]. The first field-induced state (1st-FIS: 7T<H<12T), however, remains to be unidentified, because accessible magnetic reflections of 1st-FIS in (HK0) zone under vertical magnetic field along the c axis is not fundamental reflection, but only second harmonic reflection. Recently, we performed magnetization measurements on $CuFe_{1-x}Al_xO_2$, and found that the transition field from 4-sublattice state to 1st-FIS decreases with increasing x, suggesting that the 1st-FIS continuously connects with zero-field impurity-induced state that is ground state for $0.014<x<0.030$, as shown in Fig. 1(a). We confirmed this scenario through the H-T phase diagram of x=0.012 [2]. The magnetic structure of the impurity-induced state (at x=0.0155) at zero field has been identified as the Orthogonal Double Sinusoidal (ODS) magnetic structure that consists of two sinusoidal spin modulations (PD-modulation with c axis-parallel spin component and LT-modulation with c axis-perpendicular spin component)[3]. The typical profile of ODS state characterized 4-magnetic reflections (q_{LT}, q_{PD}, 1/2-q_{LT}, 1/2-q_{PD}- reflection) is shown in Fig. 1(d). These previous results imply that the ODS magnetic structure should be found in 1st-FIS.

In present experiments, we performed neutron diffraction measurements on $CuFe_{1-x}Al_xO_2$(x=0.012, 0.0155) to investigate 1st-FIS in (HHL) zone under magnetic field up to 6.0[T] along the c axis using Horizontal Magnet HM-1 at two-axis neutron diffractometer E4. (Note that the direction of external field is canted by ∽14 degrees from c axis to provide access to the magnetic reflections at (q, q, 3/2). Thus, effective maximum field along c axis is ∽5.8[T].) The wavelength of incident neutron is 2.44Å, and collimation '40-'40-'40 was employed. For x=0.012 sample whose ground state is 4-sublattice state, we performed magnetic field scan at T=5.0[K], and found that the magnetic Bragg reflection corresponding to the magnetic ordering of 4-sublattice state ($q_{4\text{-sub}}$∽0.25) rapidly decreases around transition field H_c=4.5[T], at the same time, the magnetic Bragg reflections corresponding to magnetic ordering in 1st-FIS appear at q and 1/2-q (q∽0.206). As clearly seen in Fig. 1(c), the diffraction profile in 1st-FIS are different from that of ODS state, and the wave number of 1st-FIS is close to q_{LT}(∽0.207) seen in the profile of x=0.0155 at zero field. We also performed magnetic field scan at T=6.0[K] for the sample with x=0.0155 whose zero-field ground state has been identified as ODS state. With increasing magnetic field, the intensities of q_{PD} and 1/2-q_{PD} (q_{PD}∽0.213) reflections gradually decreases, and instead, the intensities of q_{LT} and 1/2-q_{LT} (q_{LT}∽0.207) reflections are enhanced, as shown in inset of Fig. 1(d). Finally, only the q_{LT} and 1/2-q_{LT} reflections remains at H=5.8[T]. These results clearly show that the magnetic structure in 1st-FIS is characterized only by q and 1/2-q reflecctions (q∽0.206), indicating that the picture of ODS structure is incorrect and two magnetic ordering, the magnetic ordering of 1st-FIS and that of thermally induced Partially Disordered (PD) state, coexist in zero-field for $0.014<x<0.030$. Quite Recently, spontaneous electric polarization was found in 1st-FIS of $CuFeO_2$ [4]. Thus, $CuFeO_2$ is expected to be a good candidate to inspect the recently presented "spin current theory" that predicts magnetoelectric effect in spiral spin structure [5]. To determine the magnetic structure in the 1-FIS, additional neutron diffraction measurements are strongly desired.

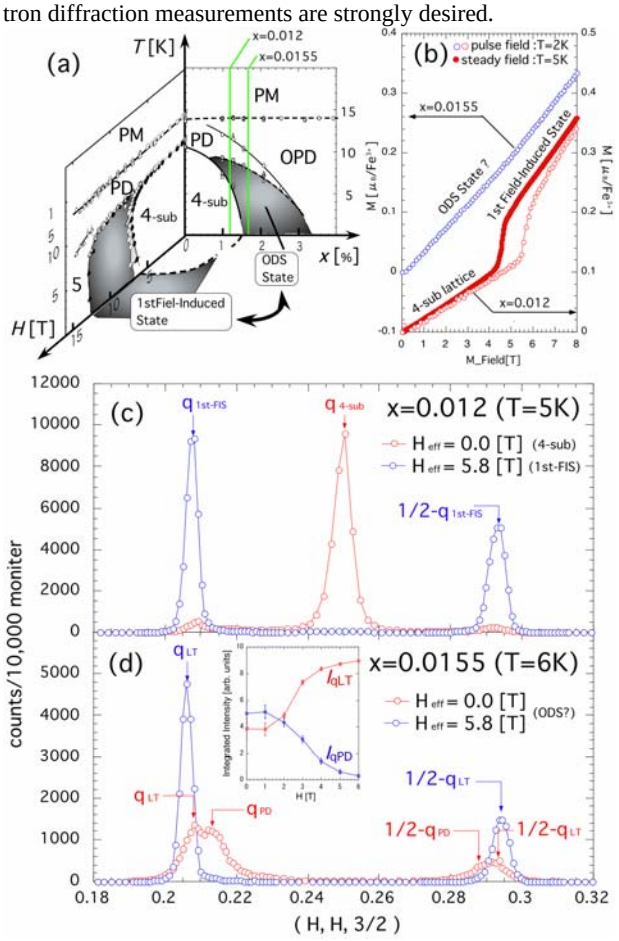

Fig. 1: *(a) Schematic drawing of H-T-x phase diagram. (b) Magnetization process for x=0.012, 0.0155. Typical profiles at H=0, 5.8[T] for (c) x=0.012, (d) x=0.0155.*

References:

[1]. S. Mitsuda *et al*, J. Phys. Soc. Jpn **69** 3513 (2000)
[2]. S. Kanetsuki *et al*, submitted to proceedings for FM2006.
[3]. N. Terada *et al*, Phys. Rev. B **73** 014419 (2006)
[4]. T.Kimura *et al*, cond-mat. 0510701 (2005)
[5]. H. Katsura *et al*, Phys. Rev. Lett **95,** 057205(2005)

BENSC	**EXPERIMENTAL REPORT** **Magnetic and crystalline structures of the Ni_2MnGe Heusler alloy at low temperatures**	Proposal N° PHY-01-1879 Instrument **E4** Local Contact Karel Prokeš
Principal Proposer: Experimental Team:	Y.V. Kudryavtsev – NAS IMP Kiev, UA Y.V. Kudryavtsev – NAS IMP Kiev, UA V.O. Oksenenko – NAS IMP Kiev, UA K. Prokeš – HMI, Berlin	Date(s) of Experiment 19.06. – 26.06.2006

Date of Report: 21.11.2006

Introduction: According to our previous results [1] and SQUID-measurements at HMI, bulk Ni_2MnGe Heusler alloy exhibits some peculiarities on the dependencies of the magnetic susceptibility, $\chi(T)$, and magnetic moment, $\mu(T)$ below 293 K (Fig. 1). In the present work, we have performed elastic neutron scattering experiments aiming to determine the nature of magnetic peculiarities in the Ni_2MnGe alloy.

Experiments: Measurements have been performed at the two-axes diffractometer E4, by using the cryomagnet HM2. We have collected some sets of scans at different temperatures ($2 < T < 258$ K) at which the peculiarities in the $\mu(T)$ dependence have been observed. Additionally, the temperature as well as magnetic field dependences of the magnetic reflection have been measured.

Results: According to the neutron diffraction measurements, in addition to parent Ni_2MnGe phase, some amount of $Ni_5Mn_4Ge_3$ phase has been found. The structural transformations at 2 - 258 K have not been observed. Therefore, it can be suggested, that peculiarities in the $\mu(T)$ dependence may be a consequence of some changes in magnetic structure of alloy.

On Fig. 2 the neutron diffraction pattern, collected at 2 K is shown. At $2\theta = 27.5^{o}$ and 45.4^{o} one can see the antiferromagnetic reflections, which disappear at $T > 130$ K and are suppressed by magnetic field. The temperature dependence of the antiferromagnetic peak intensity at 27.5^{o} was nicely fitted by the phenomenological expression: $I(T) = C\left(1-(T/T_N)^d\right)^e$ [2], with d = 1.75 and e = 0.227. The Néel temperature was determined to be T_N = 132.5 K, that coincides with the transition 1 on the $\mu(T)$ dependence (Fig. 1). The $\chi(T)$ dependence for another sample without $Ni_5Mn_4Ge_3$ phase have not manifested the peculiarity at this temperature. Therefore, we suggest that the antiferromagnetic ordering takes place in the additional $Ni_5Mn_4Ge_3$ phase. Further increase of the temperature leads to the relative decrease of the ferromagnetic addition to the main structural peaks. This addition disappears at about T_C = 260 K and coincide with the transition 3 on the $\mu(T)$ dependence. The nature of the transition 2 needs additional investigation.

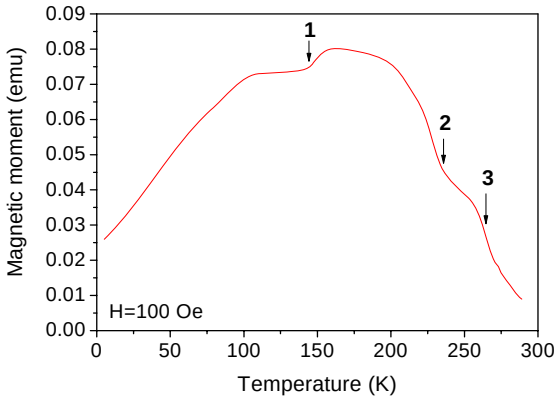

Fig. 1: *Temperature dependence of the dc-magnetization for the investigated Ni_2MnGe alloy.*

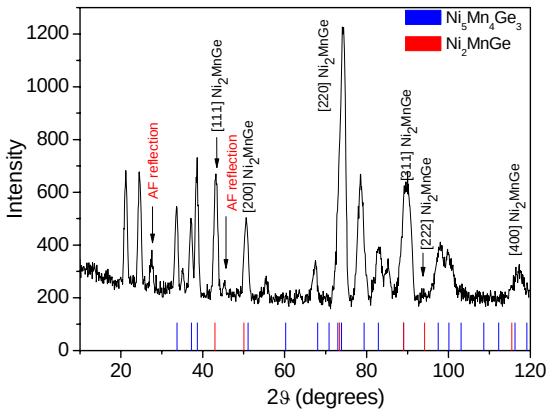

Fig. 2: *Neutron diffraction pattern of the Ni_2MnGe alloy at 2 K (the strokes relate to the positions of modeled diffraction peaks).*

References:

[1]. V. A. Oksenenko, L. N. Trofimova, Yu. N. Petrov, Y. V. Kudryavtsev, J. Dubowik, and Y. P. Lee, J. Appl. Phys **99,** 063902 (2006).

[2]. K. Hagdorn *et. al.*, Eur. Phys. J. **B 11**, p.243 (1999).

	EXPERIMENTAL REPORT **Determination of Magnetic structure of CaV_2O_4**	Proposal N° PHY-01-1918-EF Instrument **E4** Local Contact Karel Prokeš
Principal Proposer: Experimental Team:	B. Lake – HMI, Berlin A. Daoud-Aladine – RAL ISIS, UK O. Pieper – HMI, Berlin K. Prokeš – HMI, Berlin	Date(s) of Experiment 24.10. – 31.10.2006

Date of Report: 05.12.2006

CaV_2O_4 becomes magnetically ordered below T_N=71 K with a magnetic propagation vector (0, ±½, ½). The aim of this measurement was to determine the magnetic structure by measuring the intensity of the magnetic Bragg peaks. For the experiment we used a (0.2×0.3×0.3) cm^3 sized single crystal and measurements took place at T=1.5 K. From previous measurements we know, that the crystal passes through an orthorhombic to monoclinic phase transition at T~150 K, which means that we have to deal with two monoclinic domains at low temperatures. Since the magnetic propagation vector is (0, ½, ½) and since the monoclinic angle occurs between the **b** and **c** direction of the crystal, we decided to align its **b-c**-plane horizontal with respect to the incoming neutron beam. In this (0 k l)-configuration we were able to collect a substantial data set of magnetic and structural peaks (within the geometric limits of the instrument). Because there are two equally populated monoclinic domains all the measured peaks show a twin structure (except along the common **b**-axis) (see Fig.1). It is possible to assign each peak to its domain and therefore gain twice the information. The peaks were fitted to determine their intensity as displayed in Fig. 2.

We chose the strong (0, ½, ½) reflection to investigate the temperature dependence of the magnetic order parameter and observed a antiferromagnetic to paramagnetic phase transition at T_N=71 K (Fig.3), which is in good agreement with susceptibility measurements [1].

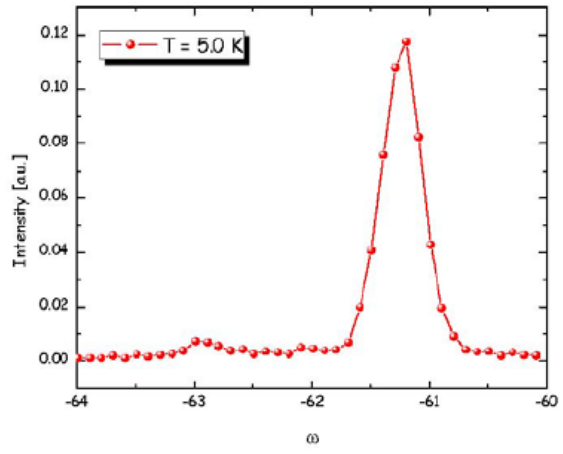

Fig. 1: *Intensity vs. ω for the magnetic* (0, ½, ½) *reflection. One can see the twinning caused by the monoclinic structure of the system. The right handed peak is much stronger.*

Finally, to complete our data, we reorient the crystal and measured another set of reflections within the (h, k, h/2)-plane. Here the crystal mosaic resulted in a complicated pattern of several peaks at each reciprocal lattice point. Analysis is ongoing to extract these intensities and fit them to a model of the magnetic structure.

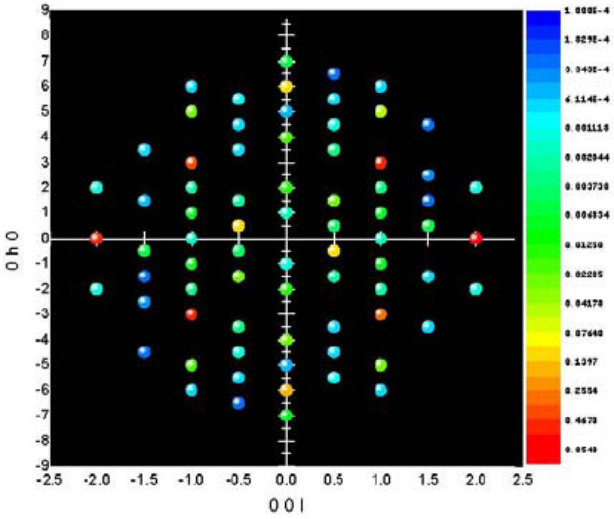

Fig. 2: *Intensity map of all the measured reflections in the (0 k l) plane. To improve the statistic we used the following symmetry relations: [1.] (0, k, l) = (0, -k, -l) and [2.] (0, k, l)-Domain 1 = (0, -k, l)-Domain 2. The magnetic reflections are at the half positions.*

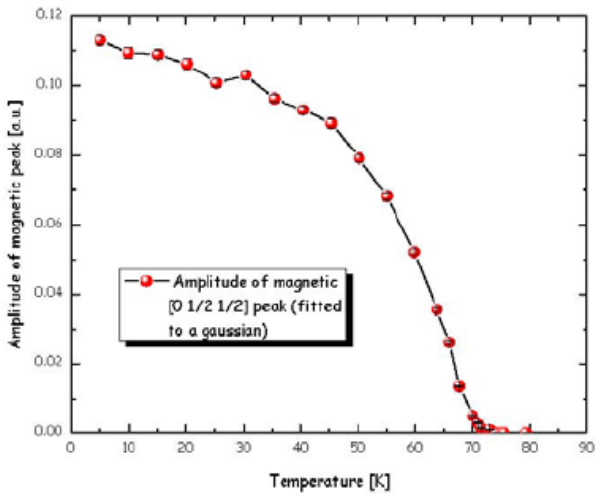

Fig. 1: *Amplitude of the magnetic* (0, ½, ½) *reflection vs. temperature. The phase transition occurs at T_N=71 K.*

Reference:

[1]. D.C. Johnston, private communication

	EXPERIMENTAL REPORT Collapse of Ce moments in heavy-fermion CePdAl under pressure	Proposal N° PHY-01-1921-EF PHY-01-1829-EF Instrument **E4** Local Contact Karel Proke
Principal Proposer: Experimental Team:	K. Proke – HMI, Berlin K. Proke – HMI, Berlin P. Manuel – RAL ISIS, UK D. T. Adroja – RAL ISIS, UK	Date(s) of Experiment 31.01. – 06.02.2006

Date of Report: 29.12.2006

CePdAl is reported to order antiferromagnetically below 2.7 K with a propagation vector $\boldsymbol{q}$=(0.5 0 τ), τ ≅ 0.35. Two, of the three Ce atoms (Ce1 at x 0 0, with x=0.58 and Ce3 at –x –x 0) in the hexagonal unit cell cary magnetic moment of about 1.6 μ_B while the remaining one at 0 x 0 seems to be paramagnetic [1]. There are three metamagnetic-like transitions in fields applied along the c axis [2].

Small single crystal with approximate dimensions 1.5x1.3x2mm^3 extracted from a larger crystal prepared in Toyama university by a Czochralski method was mounted inside a clamp-type CuBe pressure cell with a maximum pressure at room temperature of 1.0 GPa. We have oriented the crystal with its *a-c* plane in the scattering plane. The pressure cell was placed into either a ^{3}He insert (base temperature 0.35K) or a dilution stick (base temperature 0.03 K) that were inserted in the 4T or 6T horizontal-field magnet. The magnetic field has been applied along the c axis.

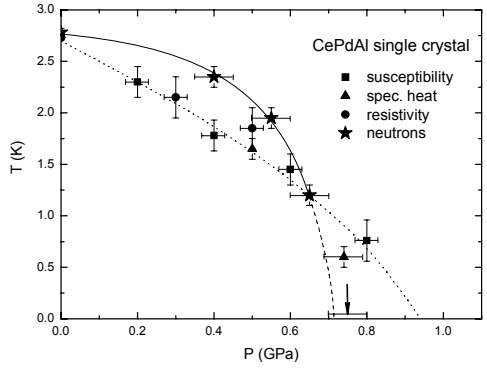

Fig. 1: *The P-T phase diagram of CePdAl constructed from our neutron data compared with the literature phase diagram after [3]. The lines are guides for an eye. The arrow and the horizontal line near 0.75 GPa indicate the limit of the neutron experiment to which the CePdAl has been found paramagnetic.*

Due to complicated sample environment we were restricted to a very few observable reflections of the *(h0l)* type. Nevertheless, we can rule out robust structural distortions. In the course of diffraction experiments it became clear that the propagation vector *q = (0.5 0 τ)* remains preserved at all applied pressures that are lower than a critical value. The value of τ is nearly temperature independent in the whole range, similar to ambient-pressure dependence below 1.9 K [2]. However, its value is little bit smaller and amounts to 0.349 (2).

At each pressure, we have collected typically six to ten nuclear Bragg reflections (each for about 30 minutes), which were used to determine the scaling factor that was in turn used in the magnetic moment determination. Normally, six magnetic reflections which appeared to have non-zero intensity were recorded for about 180 minutes each. The fitting procedure led to conclusion that the best agreement is still found for the antiferromagnetic structure having magnetic moments on the Ce1 and Ce3 equal and that on Ce2 atom zero moment. Also other main features of the magnetic structure in CePdAl under pressure remain similar to those found at ambient pressure.

In Fig. 1 we show the P-T phase diagram constructed from the presented neutron experiments compared with diagram resulting from previous magnetic bulk measurements (after ref. 3). Although the agreement is relatively good, the neutron data differs. Apart from a different pressure dependence, which leads to higher transition temperatures at lower pressures for neutron experiments, it suggests the critical value above which the CePdAl remains paramagnetic to be smaller than originally suggested. The field dependence of the integrated intensities of nuclear reflections at 0.035K does not show any signatures of metamagnetic-like transitions (at ambient pressure there are three transition at 3.2, 3.4 and 4T with field along the c axis, respectively [2]) seen at lower pressures. It is therefore very tempting to conclude that 0.75 (5) GPa CePdAl is indeed paramagnetic.

References:

[1]. A. Dönni, G. Ehlers, H. Maletta, P. Fischer, H. Kitazawa, M. Zolliker, J. Phys.: Condens. Matter **8** (1996) p. 11213.

[2]. K. Prokes et al., Physica B (2006) in press.

[3]. T. Goto, S. Hane, K. Umeo, T. Takabatake, Y. Isikawa, J. Phys. Chem. of Solids **63** (2002) 1159.

	EXPERIMENTAL REPORT **Magnetic structure of Er_3Co single crystal**	Proposal N° PHY-01-1977 Instrument **E4** Local Contact Andrei Podlesnyak
Principal Proposer: Experimental Team:	N. Baranov – USU Ekaterinburg, RU A. Gubkin – USU Ekaterinburg, RU A. Podlesnyak – HMI, Berlin	Date(s) of Experiment 20.11. - 04.12.2006

Date of Report: 29.12.2006

The series R_3M with R = rare earth and M = Ni, Co, Rh exhibit the largest R content among R compounds and crystallize in the Fe_3C type of structure (space group: Pnma) [1]. The magnetic moments of R atoms in R_3M form complex non-collinear antiferromagnetic (AF) or ferromagnetic (F) structures which result from competition between RKKY exchange interaction and influence of the low symmetry crystal electric fields. Since rare earth atoms occupy two non equivalent crystallographic positions 4c and 8d, each of them can be described by its own local direction of magnetic moment. The M atoms were found do not have ordered magnetic moments. Because of the complex magnetic structures the magnetization process in the ordered state of R_3M reveals a rich variety of field-induced phase transitions [2-3]. According to previous powder neutron diffraction study [4] Er_3Co exhibits a noncollinear magnetic structure with strong ferromagnetic component along the *b*-axis below $T_C = 13$ K. The magnetization process along main directions is suggested to involve the spin-flip processes and rotation of magnetic moments as well as the motion of domain walls [5].

In the present work single-crystal neutron diffraction was employed to study the magnetic transition in Er_3Co compound under external magnetic fields up to 6.5 T. Note, that this was the very first experiment with the use of the new 2D position sensitive detector (PSD), recently installed at the E4 diffractometer. The phase transition into an AF ordered state has been verified and the Néel temperature T_N turned out to be ~13 K in excellent agreement with the data measured on polycrystalline material [5]. The field induced magnetic transition, as measured by neutron diffraction, was found at surprisingly low magnetic field < 1 T (see Fig. 1). The symmetry of the ordered state is currently analyzed. We have found that the translational symmetry of the magnetic structure is commensurate in contrast to the Ho_3Co case [6]. We plan to combine powder and single crystal fit to determine complex magnetic structure of Er_3Co compound.

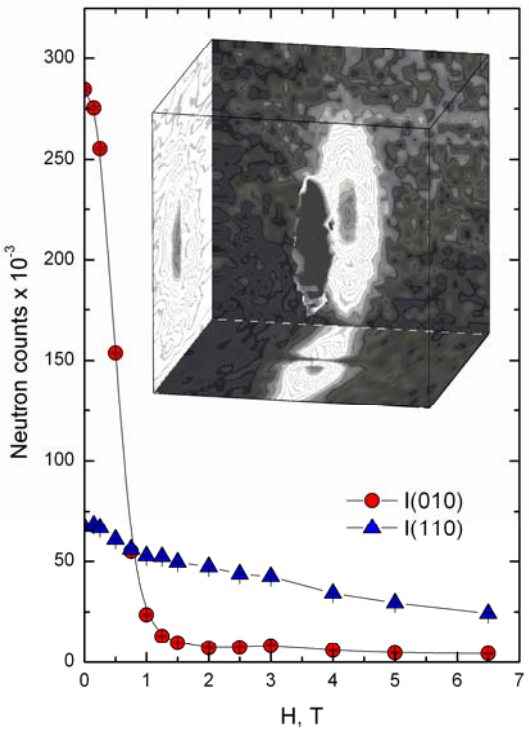

Fig. 1: *Integrated intensities of the [010] (circles) and [110] (triangles) Bragg peaks as a function of magnetic field at T = 2 K. The external field is parallel to the c-axis. The insert shows three-dimensional pattern of the typical omega scan measured on E4 using the new PSD detector.*

The present work was supported by the Russian Foundation for Basic Research (Grant No 04-02-96060) and by Swiss National Science Foundation (SCOPES 2005-2008, Project No IB7420-110849).

References:

[1]. K.H.J. Buschow and A.S. van der Goot, J. Less-Common Metals, **18** (1969) 309.
[2]. N.V. Baranov, *et al*., Eur. Phys. J. B, **16** (2000) 67.
[3]. N. V. Baranov, *et al.*, J. Phys.: Condens. Matter, **17** (2005) 3445–3462.
[4]. J.L. Feron, *et al.*, Elements Ter. Rar., **2** (1970) 75.
[5].N.V. Baranov, *et al.*, Physica B, **324** (2002) 179.
[6].A. Podlesnyak, *et al.*, JMMM 272-276 (2004) 565.

	EXPERIMENTAL REPORT **Spin Noncollinearlity in Multiferroic phase of Triangular Lattice Antiferromagnet $CuFe_{1-x}Al_xO_2$**	Proposal N° PHY-01-1978-DT Instrument **E4** Local Contact Karel Prokeš
Principal Proposer: Experimental Team:	S. Mitsuda – Tokyo US, JP T. Nakajima, S. Mitsuda – Tokyo US, JP K. Prokeš, A. Podlesnyak – HMI, Berlin	Date(s) of Experiment 17.10. – 23.10.2006

Date of Report: 29.12.2006

Delafossite compound $CuFeO_2$ has been extensively studied as a model material of geometrically frustrated spin systems for last fifteen years. Recently, Kimura and co-workers discovered a spontaneous electric polarization in the field-induced low temperature phase of $CuFeO_2$, and showed that $CuFeO_2$ provides an opportunity to study a new class of multiferroics. To investigate the microscopic mechanism of the multiferroic behavior, determination of detailed magnetic structure is indispensable. However, the magnetic structure in the field-induced ferroelectric phase was not elucidated. The previous neutron diffraction measurements revealed only that the wave number of the magnetic structure is incommensurate and magnetic field dependent, because the accessible magnetic reflections in the previous measurements with a vertical field cryomagnet were restricted to the higher-harmonic 2*q*-reflections in (*hk*0) zone.[2] [Hereafter, we refer to this phase as the ferroelectric incommensurate (FEIC) phase.] To provide access the fundamental magnetic reflections in the FEIC phase of $CuFeO_2$, the horizontal field beyond H~7.3T is indispensable, although such a cryomagnet has not been available for neutron diffraction measurements. The recent neutron diffraction and magnetization measurements[3], however, revealed that the only 1.2% dilution of Fe^{3+} sites with nonmagnetic Al^{3+} ions reduces the transition field from the ground state 4-sublattice phase to the FEIC phase down to ~5[T] and the FEIC phase can be realized even in H~4T by field cooling. In present experiments, we thus performed neutron diffraction measurements using the single-crystal $CuFe_{1-x}Al_xO_2$ sample with x = 0.012 and a horizontal field cryomagnet HM-2 installed at HMI, which has quite small blind angle and horizontal field up to H = 4T, and determined the magnetic structure of the FEIC phase.

The neutron diffraction measurement was carried out at the two-axis neutron diffractometer E4. The wavelength of incident neutron is 2.44Å and collimation `40-`40-`40 was employed. The sample was mounted in the cryostat with (*hhl*) scattering plane, whose slight misalignment was corrected at zero magnetic field by the intensities of magnetic Bragg reflections in well-studied partially disordered phase [4]. An external field was applied along [001] axis.

For the magnetic structure analysis for the FEIC state, we collected the integrated intensities of 20 fundamental magnetic Bragg reflections at T=1.7K, in H=4T, by ω-scans and ω-2θ scans. Since a slope of magnetization curve in the FEIC phase implies that the magnetic structure is a kind of noncollinear structure, we performed the model-fitting analysis with three models illustrated in Figs. 1(a)-(c). As discussed in Ref [4], for a helical structure, the factor $|F_{obs}|^2/f(\kappa)^2$, where $|F_{obs}|$ is observed structure factor and $f(\kappa)$ is the magnetic form factor of Fe^{3+}, is proportional to the Spin Orientation Factor (SOF). We thus check the proportionality between the l-variation of $|F_{obs}|^2/f(\kappa)^2$ and that of the SOFs calculated for three models. (Note that the extinction effect on these magnetic Bragg reflections is quite small and therefore neglected.) As shown in Fig. 1(e), the l-variation of $|F_{obs}|^2/f(\kappa)^2$ is apparently well explained by the proper helical model (solid line). In addition, the repetition of the diffraction pattern in the FEIC phase implies that magnetic modulations on the d = 1 and d = 2 sites in the unit cell shown in Fig. 1(d) should be coupled with the finite phase shift δ ($0 < \delta < \pi$). By the least-square analysis with this proper helical model for the $|F_{obs}|$ data, the δ is determined to be δ ~ 76[degrees]. This is indicative of the *ferromagnetic* coupling between the d = 1 and d = 2 sites, ($2\pi q_{FEIC}$-δ ~ 0).

→

The previous works on the sample with x=0.012[3] also revealed that the FEIC phase of $CuFeO_2$ continuously connects with the impurity-induced low temperature phase of $CuFe_{1-x}Al_xO_2$ ($0.014 < x < 0.03$), where a spontaneous electric polarization has been found for the sample with $x = 0.02$ under zero-field. We thus performed the neutron diffraction measurements for the sample with x=0.0155 in the same manner as for the sample with x=0.012, and found that the magnetic structure in the impurity-induced FEIC phase in the sample with x=0.0155 is also the proper helical structure with $\delta \sim 2\pi q_{FEIC}$.

The induction of electric polarization by the proper helical magnetic ordering in the FEIC phase, however, was not explained by the recently developed theory for the ferroelectricty in noncollinear magnets [5]; a naive application of this theory to the proper helical magnetic ordering does not lead to a finite uniform electric polarization. Nevertheless, the fact that the proper helical structure appears only in the FEIC phase among various magnetically ordered phases of $CuFe_{1-x}Al_xO_2$ strongly suggests that the spin noncollinearlity is relevant to the multiferroic nature in $CuFe_{1-x}Al_xO_2$.

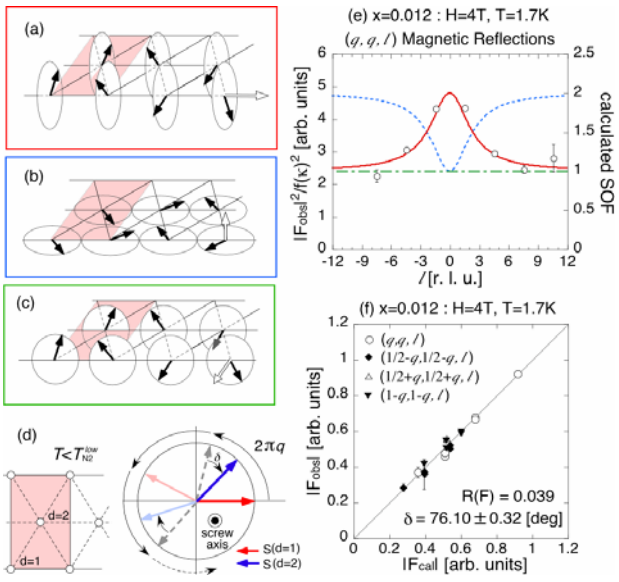

Fig. 1: *Schematic drawing of (a) proper helical model, (b) cycloidal-model-I and (c) cycloidal model-II. (d) The magnetic unit cell in c-plane in the FEIC phase (left) and definition of phase shift δ (right). (e) Typical index l-dependence of the $|F_{obs}|^2/f(\kappa)^2$ and SOFs for x=0.012. The open circles denote the $|F_{obs}|^2/f(\kappa)^2$ data, and the solid, dotted and dashed lines correspond to the SOFs for the models of peoper helical model, cycloydal model-I and cycloydal model-II, respectively.*

References:

[1]. T. Kimura *et al*: Phys. Rev. B **73** 220401R (2006)
[2]. S. Mitsuda *et al*.: J. Phys. Soc. Jpn. **69** 3513(2000)
[3]. S. Kanetsuki *et al*.: J. Pbys.: Condensed Matter (in press)
[4]. N. Terada *et al*.: J. Phys. Soc. Jpn. **74** 1561(2005)
[5]. H. Katsura *et al*.: Phys. Rev. Lett. **95** 057205(2005)

	EXPERIMENTAL REPORT	Proposal N° PHY-01-1724-LT
BENSC	**Spin structure of the insulating vanadates $La_{0.85}Sr_{0.15}VO_3$ and $La_{0.90}Sr_{0.10}VO_3$**	Instrument **E5** Local Contact Manfred Reehuis
Principal Proposer: M.Reehuis, C.Ulrich, B.Keimer – MPI Stuttgart Experimental Team: M. Reehuis – MPI Stuttgart		Date(s) of Experiment 22.06. – 29.05.2006 12.06. – 22.06.2006

Date of Report: 03.01.2007

The description of the interplay between spin and orbital degrees of freedom in insulating vanadates is an excellent basis for an investigation of the influence of mobile charge carriers. These compounds undergo insulator-metal transitions when doped by substituting divalent for trivalent cations [1]. The insulator $LaVO_3$ undergoes two successive transitions, a Néel transition into an antiferro-magnetically ordered state at 143 K and a structural transition at 145 K [2]. The latter transition has been interpreted as evidence of orbital ordering. The interpretation is consistent with our neutron scattering study, which shows that the measured magnon dispersions are highly anisotropic. This is in contrast to our observations in YVO_3 [3]. Here the Néel transition sets in at 116 K and the structural one at 200 K [3, 4]. Here it was interesting to see that the yttrium compound shows an additional *G*-type component along the *c*-axis, whereas the order in $LaVO_3$ are purely *C*-type. The same type could be observed for the Sr-doped vanadates [5]. In the case of $La_{0.90}Sr_{0.10}VO_3$ an untwinned single crystal was available. This allowed us to determine the spin direction of the V-sublattice. Here the moments were found to be aligned in the *ab*-plane. This alignment is identical to that one observed in YVO_3. So it is likely that $LaVO_3$ and $La_{0.85}Sr_{0.15}VO_3$ also show a *C*-type ordering in the *ab*-plane.

In our present study we tried to find out, whether an additional *G*-type component occurs in Sr-doped vanadates as observed for YVO_3. Therefore a single-crystal neutron diffraction study of the insulators $La_{0.90}Sr_{0.10}VO_3$ and $La_{0.85}Sr_{0.15}VO_3$ was carried out on the four-circle diffractometer E5 (PG: λ = 2.36 Á). First we investigated the almost detwinned single crystal of $La_{0.90}Sr_{0.10}VO_3$. In the case of the presence of *G*-type ordering along *c* magnetic intensity should appear on the positions of the reflections 101 and 011, respectively. Here the magnetic intensities of both reflections are expected to be almost the same. In Fig. 1 it can be seen that the intensity of 011 is spontaneously decreasing at 110 K. This can be ascribe either to the magnetic or the structural that phase transition, which sets in practically at the same temperature. But due to the fact the intensity of the 101 is spontaneously increasing, it can be claimed that this transition purely can be ascribed to the structural change from the orthorhombic (*Pbnm*) to the monoclinic structure ($P2_1/b$). Further, the thermal variation of 101 and 011 is similar to that of 022, where a magnetic contribution is absent. Here it can be seen, that the intensity does not change significantly up to 105 K followed by a spontaneous change of intensity at 110 K. In contrast the pure magnetic peak 100 (Fig. 1) is continuously decreasing with increasing temperature. Here we can conclude that it is possible for these materials to distinguish magnetic and structural phase transitions from the thermal variation of particular Bragg reflections.

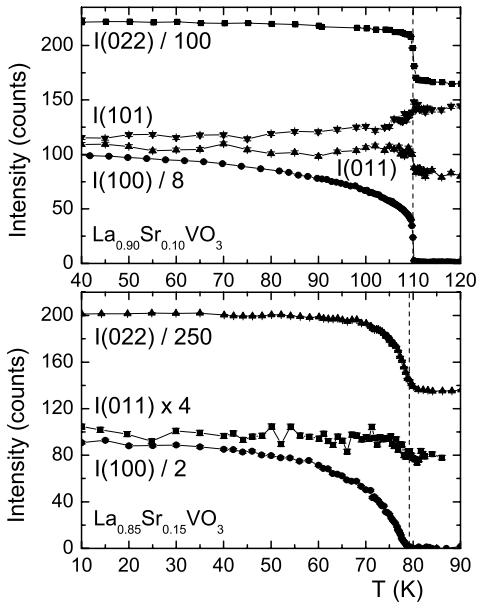

Fig. 1: *Temperature dependence of the intensity of the Bragg reflections 100, 011 (101) and 022 for $La_{0.85}Sr_{0.15}VO_3$ and $La_{0.90}Sr_{0.10}VO_3$.*

References:

[1]. S. Miyasaka, T. Okuda, Y. Tokura, Phys. Rev. Lett. **85** (2000) 5388.

[2]. C. Ulrich, B. Keimer, M. Reehuis, BENSC Experimental Report 2003, p. 36.

[3]. C. Ulrich, G. Khaliullin, J. Sirker, M. Reehuis, M. Ohl, S. Miyasaka, Y. Tokura, B. Keimer, Phys. Rev. Letters **91** (2003) 257202.

[4]. M. Reehuis, C. Ulrich, P. Pattison, B. Ouladdiaf, M.C. Rheinstädter, M. Ohl, L.P. Regnault, M. Miyasaka, Y. Tokura, B. Keimer, Phys. Rev. B. **73** (2006) 094440.

[5]. M. Reehuis, C. Ulrich, B. Keimer, BENSC Experimental Report 2005, p. 25.

	EXPERIMENTAL REPORT	Proposal N° PHY-01-1724-LT
BENSC	**Magnetic structure of the hole-doped vanadates $Ca_{0.02}Y_{0.98}VO_3$ and $Ca_{0.05}Y_{0.95}VO_3$**	Instrument **E5** Local Contact Manfred Reehuis
Principal Proposer: M.Reehuis, C.Ulrich, B.Keimer – MPI, Stuttgart Experimental Team: M. Reehuis – MPI, Stuttgart		Date(s) of Experiment 10.08. – 16.08.2006 20.11. – 22.11.2006 12.12. – 17.12.2006

Date of Report: 03.01.2007

Our neutron scattering investigations on insulating YVO_3 has led to the discovery of unusual magnetic ground states and excitations due to the interplay of spin and orbital degrees of freedom [1, 2]. YVO_3 exhibits two magnetic phases, a *C*-type phase between 116 K and 77 K and a *G*-type phase below 77 K. While the magnetic properties of the *G*-type phase are in accordance with standard theoretical descriptions, the *C*-type phase shows highly unusual static and dynamic spin correlations. The V-moment is strongly reduced and the spin structure is highly non-collinear. This can be ascribed to the presence of an additional *G*-type component in the so-called *C*-type phase.

In the present study we give an account on the magnetic properties of the hole-doped oxides $Ca_{0.02}Y_{0.98}VO_3$ and $Ca_{0.05}Y_{0.95}VO_3$. The *T*-dependence of the specific heat and magnetization for $Ca_xY_{1-x}VO_3$ showed that the second magnetic transition from the *C*-type in to the *G*-type phase disappears with $x(Ca) \geq 0.02$ [3]. This could be confirmed by our neutron diffraction experiments carried out on the four-circle diffractometer E5 using the wavelength $\lambda = 2.36$ Å. In Figs. 1 and 2 it can be seen that the reflections 100 and 010 are continuously increasing down to 10 K, indicating a collinear *C*-type ordering in the *ab*-plane. The observation of the magnetic reflection 011 finally suggests the presence of the additional component G_z, resulting finally in a noncollinear spin structure. Thus the magnetic structure of the Ca-doped vanadates is identical to that of YVO_3 observed above 77 K. It can be seen that the total magnetic moment μ_{exp} of the vanadium in $Ca_{0.02}Y_{0.98}VO_3$ is at 85 K slightly larger than that of YVO_3 (Table 1). Due to the reduced T_N of $Ca_{0.05}Y_{0.95}VO_3$ the moment value is again reduced at 85 K. In contrast, the vanadium moment of $Ca_{0.05}Y_{0.95}VO_3$ at 10 K was found to be slightly larger than that of $Ca_{0.02}Y_{0.98}VO_3$.

***Table 1**: Magnetic moments of the V-atoms in $Ca_xY_{1-x}VO_3$.*

	$x = 0$	$x = 0.02$	$x = 0.05$	T (K)
$\mu(C_x)$ (μ_B)	0	0.92(4)	0.92(4)	10
$\mu(C_y)$ (μ_B)	0	1.17(3)	1.35(3)	
$\mu(G_z)$ (μ_B)	1.72 (5)	0.09(3)	0.09(3)	
μ_{exp} (μ_B)	1.72 (5)	1.49(3)	1.64(3)	
$\mu(C_x)$ (μ_B)	0.49(3)	0.65(3)	0.28(3)	85
$\mu(C_y)$ (μ_B)	0.89(2)	0.98(2)	0.84(2)	
$\mu(G_z)$ (μ_B)	0.30(4)	0.30(3)	0.18(3)	
μ_{exp} (μ_B)	1.05(3)	1.21(3)	0.90(3)	
T_S (K)	200	184	162	
T_N (K)	116	114	103	

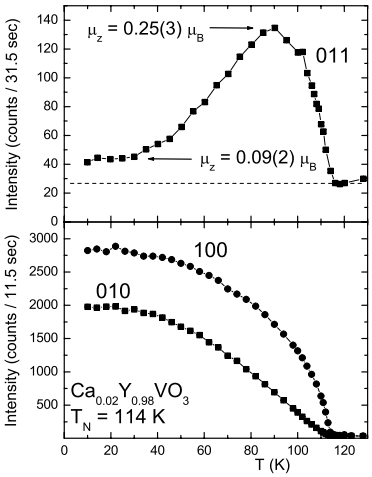

***Fig. 1:** Temperature dependence of the intensity of the Bragg reflections 100, 010 and 011 for $Ca_{0.02}Y_{0.98}VO_3$.*

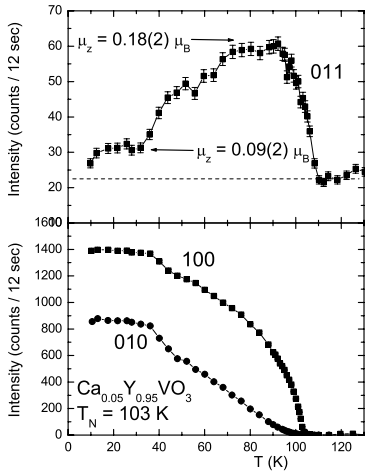

***Fig. 2:** Temperature dependence of the intensity of the Bragg reflections 100, 010 and 011 for $Ca_{0.05}Y_{0.95}VO_3$.*

References:

[1]. C. Ulrich, G. Khaliullin, J. Sirker, M. Reehuis, M. Ohl, S. Miyasaka, Y. Tokura, B. Keimer, Phys. Rev. Letters **91** (2003) 257202.

[2]. M. Reehuis, C. Ulrich, P. Pattison, B. Ouladdiaf, M.C. Rheinstädter, M. Ohl, L.P. Regnault, M. Miyasaka, Y. Tokura, B. Keimer, Phys. Rev. B. **73** (2006) 094440.

[3]. J. Fujioka, S. Miyasaka, Y. Tokura, Phys. Rev. B **72** (2005) 024460.

	EXPERIMENTAL REPORT	Proposal N° PHY-01-1724-LT
BENSC	**Metastable *C*-type ordering in the hole-doped vanadate $Ca_{0.01}Y_{0.99}VO_3$**	Instrument **E5** Local Contact Manfred Reehuis
Principal Proposer: M.Reehuis, C.Ulrich, B.Keimer – MPI, Stuttgart Experimental Team: M. Reehuis – MPI, Stuttgart		Date(s) of Experiment 17.08. – 27.08.2006

Date of Report: 03.01.2007

YVO_3 has proven to be an interesting material, since it undergoes a series of temperature induced reversals in the magnetization [1]. We have used single-crystal neutron diffraction to carry out a comprehensive investigation of the crystal structures and magnetic ground states of YVO_3 [2, 3]. This vanadate shows a structural phase transition at 200 K from an orthorhombic structure (*Pbnm*) to a monoclinic one ($P2_1/b$). A so-called *C*-type ordering in the *ab*-plane sets in at the Néel temperature T_N = 116 K. For this magnetic phase we finally could observe an additional G_z-component, resulting in a noncollinear spin structure. A further structural phase transition back to the orthorhombic space group *Pbnm* is observed upon cooling below 77 K. Only recently it could be shown, that a minimal Ca-doping as low as x = 0.02 causes a melting of the *G*-type spin ordering [4]. In the present study we have investigated the magnetic order of the hole-doped vanadate $Ca_{0.01}Y_{0.99}VO_3$, where the *G*-type ordering is still observable. Single-crystal neutron diffraction experiments were carried out on the four-circle diffractometer E5 (λ = 2.36 Å). The presence of the reflections 100 and 011 (Fig. 1) indicates the *C*-type ordering in the *ab*-plane and the *G*-type ordering along the *c*-axis, respectively. It was interesting to see that a fast cooling of the sample, starting from 290 K, could completely freeze the *C*-type ordering down to 10 K. A change from the *C*-type into the *G*-type occurs by heating up to 40 K. After cooling again this phase remains unchanged down to 10 K. So it was possible to collect data sets of two different magnetic phases at 10 K. It could be clearly evidenced, that the vanadium moment in the *G*-type phase of $Ca_{0.01}Y_{0.99}VO_3$ is strongly reduced (Table 1). With increasing temperature this *G*-type

Table 1: *Magnetic moments of the V-atoms in YVO_3 and $Ca_{0.01}Y_{0.99}VO_3$.*

	YVO_3		$Ca_{0.01}Y_{0.99}VO_3$		
T (K)	10, *G*	85, *C*	10, *G*	10, *C*	85, *C*
$\mu(C_x)$ (μ_B)	0	0.49(3)	0	0.82(4)	0.60(4)
$\mu(C_y)$ (μ_B)	0	0.89(2)	0	1.28(3)	0.99(3)
$\mu(G_z)$ (μ_B)	1.72 (5)	0.30(4)	1.22(3)	0.10(3)	0.31(3)
μ_{exp} (μ_B)	1.72 (5)	1.05(2)	1.22(3)	1.53(3)	1.20(3)
T_S (K)	200			189	
T_N (K)	116			114	
T_2	77			48 – 62	

changes at 62 K in to the *C*-type, but with decreasing temperature the transition back to the *G*-type is observed at 48 K indicating the presence of hysteresis effects. In Figs. 1 and 2 different hysteresis loops are presented for particular reflections. For the magnetic reflections 100 and 011 a hysteresis is observed at the second phase transition (48 K – 62 K). For the nuclear and magnetic reflection 101 as well as for the pure nuclear one 202 a hysteresis is additionally observable up to the first phase transition at 189 K.

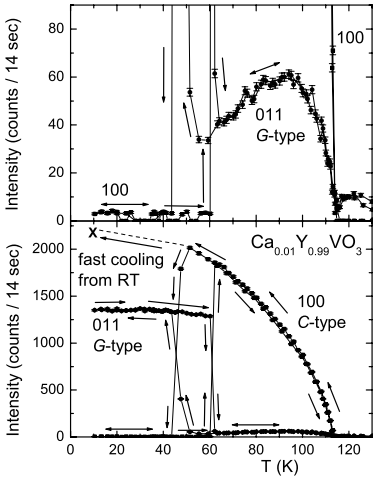

Fig. 1: *Temperature dependence of the intensity of the Bragg reflections 100 and 011 for $Ca_{0.01}Y_{0.99}VO_3$.*

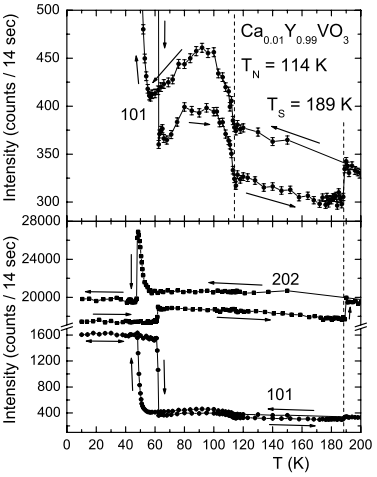

Fig. 2: *Temperature dependence of the intensity of the Bragg reflections 101 and 202 for $Ca_{0.01}Y_{0.99}VO_3$.*

References:

[1]. Y. Ren, T.T.M. Palstra, D.I. Khomskii, E. Pellegrin, A.A. Nugroho, A.A. Menovsky, G.A. Sawatzky, Nature **396** (1998) 441.

[2]. C. Ulrich, G. Khaliullin, J. Sirker, M. Reehuis, M. Ohl, S. Miyasaka, Y. Tokura, B. Keimer, Phys. Rev. Letters **91** (2003) 257202.

[3]. M. Reehuis, C. Ulrich, P. Pattison, B. Ouladdiaf, M.C. Rheinstädter, M. Ohl, L.P. Regnault, M. Miyasaka, Y. Tokura, B. Keimer, Phys. Rev. B. **73** (2006) 094440.

[4]. J. Fujioka, S. Miyasaka, Y. Tokura, Phys. Rev. B **72** (2005) 024460.

	EXPERIMENTAL REPORT **Single-crystal neutron diffraction study of $TbMnO_3$**	Proposal N° PHY-01-1923-EF Instrument **E5** Local Contact Manfred Reehuis
Principal Proposer: Experimental Team:	O. Prokhnenko – HMI, Berlin M. Reehuis – HMI, Berlin N. Aliouane – HMI, Berlin D.N. Argyriou – HMI, Berlin	Date(s) of Experiment 27.02. – 13.03.2006

Date of Report: 30.11.2006

$TbMnO_3$ has been attracting a lot of attention in the last years because of its strong coupling between ferroelectricity and magnetism [1-3]. However, difficulties in magnetic structure determination and last experiments on single crystals showed that crystal structure of ferroelectric $TbMnO_3$ compound could be different from the orthorhombic *Pbnm*. We measured a set of nuclear reflections (including the forbidden ones for *Pbnm*) at room temperature in order to clarify the crystal structure of $TbMnO_3$, a set of nuclear reflection at 90 K (above T_N) to see whether the crystal structure changes before the compound becomes magnetically ordered, and a set of nuclear and magnetic reflections at 30 K and 15 K in magnetically ordered state as well as temperature scan of selected reflections. The crystal structure refinements were done by Xtal software.

In order to check the crystal structure of $TbMnO_3$, a data set of about 150 structural factors has been collected at room temperature. Here we used the Cu monochromator selecting the neutron wavelength $\lambda 1 = 0.889$ Å. Our data analysis showed no violation of the symmetry of the orthorhombic space group *Pbnm*. Some of the forbidden reflections observed with the second wavelength $\lambda 2 = 2.36$ Å (PG monochromator) originate from multiple scattering (as can detected by ψ-scans around scattering vector) and $\lambda_2/2$. Finally, we successfully refined the crystal structure $TbMnO_3$ in *Pbnm*. The results are summarized in Table 1.

Table 1: *Crystal structure parameters of $TbMnO_3$ at room temperature.*

Pbnm	*x*	*y*	*z*	*U* (100 Å^2)
Tb	-0.0156	0.0814	¼	0.34
Mn	½	0	0	0.43
O1	0.1069	0.4668	¼	0.47
O2	0.7038	0.3273	0.0514	0.54

$R_F = 0.078$

$a = 5.320(6)$ Å, $b = 5.883(5)$ Å, $c = 7.414(6)$ Å

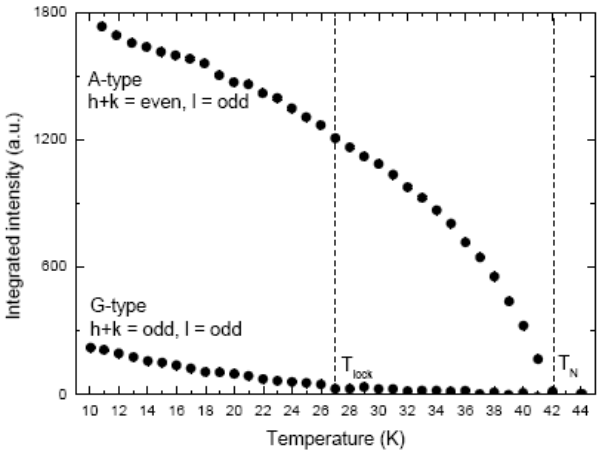

Fig. 1: *Temperature dependence of selected characteristic A- and G-type reflections.*

Refinement of the neutron diffraction data at 90 K, however, gives much worse results ($R_F \sim 0.2$) and at this stage we cannot judge whether this is real or caused by some experimental problems. In order to solve these problems further investigations will be performed in the next future.

Further, magnetic superlattice reflections were observed below $T_N \sim 40$ K. This is in agreement with already published data [2]. The Mn-spins show an incommensurate order with a propagation vector $\boldsymbol{k}$ = (0, ~ 0.27, 0). Here the spins of the four different Mn-atoms in the unit cell are aligned in the modulated *A*-type structure (condition for the observed (*hkl*): *h + k = even, l = odd*). Below $T_{lock} \sim 27$ K magnetic reflections appear with the conditions *h + k* = odd and *l = odd*. This suggests the presence of a *G*-type order up in a temperature region where a spontaneous polarization is observed [1-2]. The temperature dependence of both the *A*- and *G*-type characteristic magnetic reflections is shown in Fig. 1.

References:

[1]. T. Kimura et al, Nature **426**, 55 (2003).

[2]. M. Kenzelmann et al., Phys. Rev. Lett. **95**, 087206 (2005).

[3]. M. Mostovoy, Phys. Rev. Lett. **96**, 067601 (2006).

	EXPERIMENTAL REPORT **NiO - a one dimensional bulk antiferromagnet**	Proposal N° PHY-01-1470 Instrument **E6** Local Contact Norbert Stüßer
Principal Proposer: Experimental Team:	U. Köbler – FZ Jülich U. Köbler – FZ Jülich A. Hoser – RWTH Aachen + FZ Jülich N. Stüßer – HMI, Berlin	Date(s) of Experiment 11.09. – 15.09.2006

Date of Report: 19.12.2006

The 3d transition metal monoxides MnO, FeO, CoO and NiO are cubic in the paramagnetic phase but undergo axial lattice distortions at the Néel temperature [1]. NiO with T_N=519 K is rhombohedral in the ordered state [2]. Associated with this lattice distortion is a reduction of the dimensionality of the magnetic interactions. We have identified NiO together with a number of other antiferromagnets with axial lattice symmetry as systems with three-dimensional spin and one-dimensional (1D) interactions (see Fig. 1).

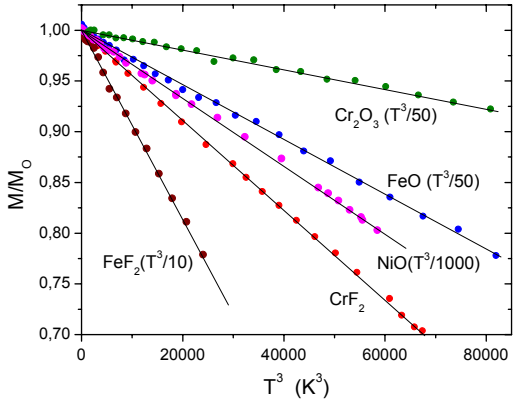

Fig. 1

Typical for magnets with 1D and 2D interactions is a magnetic excitation gap. Classically 1D and 2D magnets should show no long range order [3]. Opening of a gap at T_N can be considered as a spontaneous self-stabilization of the long range order. Moreover, gap and sublattice magnetization are components of a two-component order parameter. This can be concluded from the identical temperature dependence of gap and sublattice magnetization. Our neutron scattering results on NiO powder are consistent with this view. Fig.2 shows normalized data for gap and sublattice magnetization vs. reduced temperature to the third power. The fitted exponents are ε=2.99±0.22 and ε=2.94±0.03, respectively. These values are consistent with ε=3.

The universality class of 1D magnets with integer spin is represented by T^3 function [4]. Fig.1 demonstrates that universal T^3 function

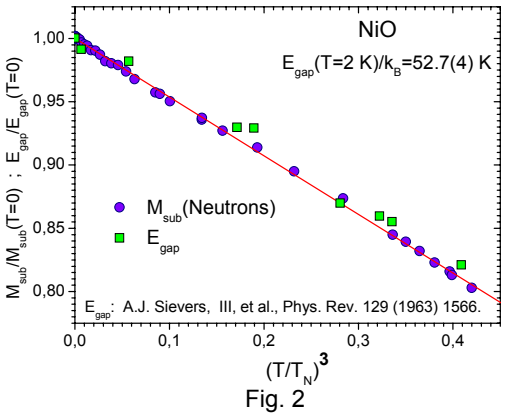

Fig. 2

holds for many axial antiferromagnets with different chemical composition and lattice symmetry. Universality, i.e. independence of the exponent of atomistic details can be explained only by a continuum theory of magnetism. Such a continuum theory is missing. In particular, the magnetic excitation spectra evaluated by inelastic neutron scattering exhibit no universal features but are material specific. As a conclusion, these interactions are on atomistic length scale and are not the relevant long range interactions for the dynamics. On the other hand, the observed gap could, in principle, be interpreted as long range interactions. The absolute gap value is, however, much too large.

References:

[1]. W.L. Roth, Phys. Rev. 110 (1958) 1333.
[2]. L.C. Bartel, B. Morosin, Phys. Rev. B **3** (1971) 1039.
[3]. N.D. Mermin, H. Wagner, Phys. Rev. Lett. **17** (1966) 1133.
[4]. U. Köbler, A. Hoser, Physica B **362** (2005) 295.

	EXPERIMENTAL REPORT **Shrinking transverse coherence upon magnetic polarization in bcc Fe**	Proposal N° PHY-01-1590 Instrument **E6** Local Contact Norbert Stüßer
Principal Proposer: Experimental Team:	U. Köbler – FZ Jülich U. Köbler – FZ Jülich A. Hoser – RWTH Aachen + FZ Jülich N. Stüßer – HMI, Berlin	Date(s) of Experiment 28.10. – 29.10.2006

Date of Report: 19.12.2006

The ground state of an isotropic ferromagnet such as bcc iron is characterized by an equal orientation of domains along all three space directions. As a consequence, in magnetic neutron scattering only 2/3 of all moments are sampled. On the other hand, in the magnetically saturated state with all moments oriented perpendicular to the scattering plane all moments are sampled. Therefore, upon application of the demagnetization field the magnetic scattering intensities should increase by a factor of 1.5.

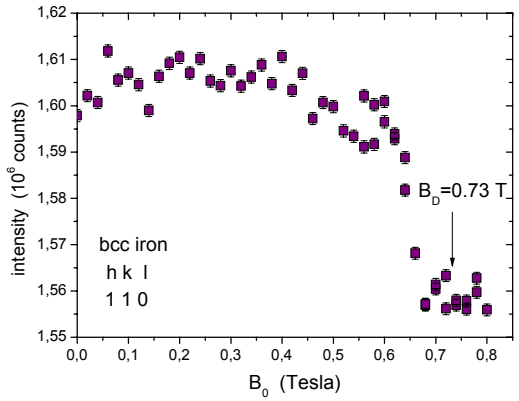

Fig. 1

This is not observed for the itinerant ferromagnets bcc iron and hcp cobalt. Fig.1 shows the (110) neutron scattering intensity measured on a spherical Fe single crystal as a function of a vertical magnetic field. Instead of increasing, the scattering intensities are rather constant and show a small drop just before the demagnetization field that is B_D=0.73 T for the iron sphere.

This field dependence is in sharp contrast to the macroscopic spontaneous magnetization that increases linearly with field and saturates sharply at B_D. In order to explain this discrepancy we have to consider that the macroscopic magnetization samples the time average of the field parallel spin component. Neutron scattering is a probe that is much faster than the Larmor precession of the spin. For λ_n=0.24 nm the dwell time of the neutron at an atom is 10^{-14} s while the Larmor precession time in small fields is 10^{-8} s. Therefore magnetic neutron scattering relies on a phase coherent Larmor precession in the scattering plane. As a conclusion, the coherence length in the scattering plane must be very short.
This effect is dramatic in hcp cobalt (cf. our previous experiment on E1, PHY-02-0490).

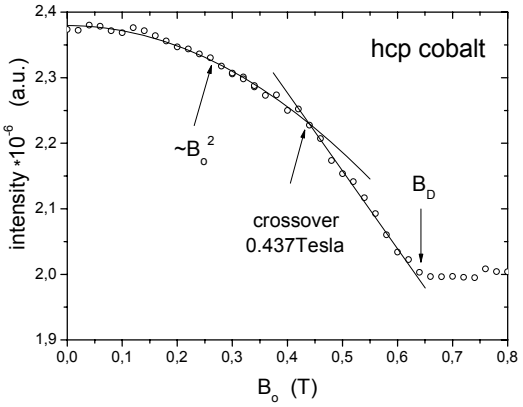

Fig. 2

The scattering intensities decrease substantially as a function of the vertical field, i.e. the coherence length shrinks. The decreasing transverse coherence length is consistent with the observation that Co is 1D in the magnetically saturated state but 3D anisotropic at field zero. This universality change should be associated with a crossover. In fact, we identify the observed anomaly at B_o=0.437 T as crossover from 3D anisotropic to 1D. On the other hand, iron remains 3D isotropic also in the polarized state [1,2] meaning that the transverse coherence length remains above the threshold for the crossover to 1D universality class.

References:

[1]. U. Köbler, J. Englich, O. Hupe, J. Hesse, Physica B 339 (2003) 156.
[2]. U. Köbler, A. Hoser, Physica B 362 (2005) 295

	EXPERIMENTAL REPORT **Neutron diffraction study of $NaFe(WO_4)_2$**	Proposal N° PHY-01-1793 Instrument **E6** Local Contact Norbert Stüßer
Principal Proposer: Experimental Team:	H. Ehrenberg – TU, DA S. Sangaa, L. Nyam-Ochir - NUM Ulanbator,MN H. Fuess – TU, DA N. Stüßer – HMI, Berlin	Date(s) of Experiment 06.09. – 08.09.2006

Date of Report: 05.01.2007

Introduction:

The structure of sodium iron tungstate, $NaFe(WO_4)_2$, is similar to the structure of wolframite-type $FeWO_4$ with the same space group P2/c, but with doubled a parameter [1,2]. Therefore, less magnetic coupling paths between FeO_6-octahedra exist in $NaFe(WO_4)_2$ than in binary iron oxides, because of additional diamagnetic units in the structure. This system provides a suitable test for the proposed dominance of supersuperexchange couplings Fe-O-O-Fe, with Fe-O-O and O-O-Fe angles close to 180° and both bridging oxygens belonging to the same coordination polyhedra of a diamagnetic ion [3].

Experiment:

Powder sample of $NaFe(WO_4)_2$ was measured at temperature between 1,5K and 10K in order to study magnetic structure.

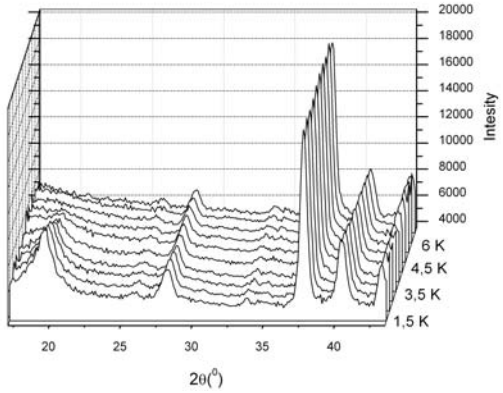

Fig. 1: *Diffraction patterns of $NaFe(WO_4)_2$ at temperature from 1,5K to 10 K.*

Diffraction data were measured in range from 17^0 to 43^0 of 2Θ. Under ~4,5K temperature were observed magnetic Bragg peaks.

For the refinement were measured data in range 7^0 to 90^0 of 2Θ, at 1,5K and 10K for paramagnetic and antiferromagnetic phase, respectively.

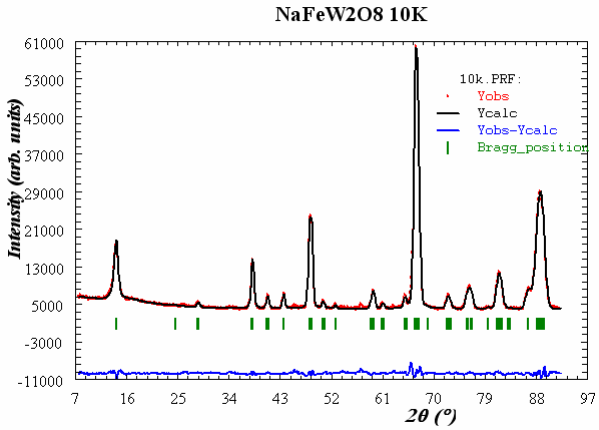

Fig. 2: *Observed and calculated profiles together with difference curve for the experiment at 10K.*

In 1,5K temperature measured data used for magnetic structure determination with propagation vector k = (0;0;1/2). The diffraction data don't agree with spin order models from group theory [4]. Refinement of magnetic structure is in progress.

References:

[1]. P.V. Klevtsov and R.F. Klevtsova, Journal of Solid State Chemistry **2**, 278-282 (1970)

[2]. R.F. Klevtsova and N.V.Belov, Soviet Physics-Crystallography Vol.15, No.1 July-Aug., 1970

[3]. H. Ehrenberg, K.G. Bramnik, E. Muessig, T. Buhrmester, H. Weitzel, C. Ritter, J. Magn. Magn. Mater. **261**, 353-359 (2003).

[4]. E.F. Bertaut, Acta Cryst. (1968). **A24**, 217-231

	EXPERIMENTAL REPORT **Diffuse magnetic scattering, spin waves, and Magnetic structure under pressure in $CsCuCl_3$**	Proposal N° PHY-01-1835-EF Instrument **E6** Local Contact Vadim Sikolenko
Principal Proposer: Experimental Team:	N. Stüßer – HMI, Berlin A. Hoser – RWTH Aachen + FZ Jülich R. Sadykov – RAS IHPP Troitsk, RU V. Sikolenko – HMI, Berlin	Date(s) of Experiment 23.05. – 30.05.2006

Date of Report: 11.01.2007

$CsCuCl_3$ belongs to the family of frustrated magnetic systems with a triangular lattice of antiferromagnetically coupled S = 1/2 spins of Cu^{2+}-ion in the *ab*-plane ("120° structure"); the dominating magnetic interaction along the *c*-axis is ferromagnetic and there is an additional antisymmetric interaction favouring a state with adjacent spins perpendicular to each other. The competition of both leads to an incommensurate long wavelength magnetic spiral along *c*. The magnetic structure forming below 10.6 K has a propagation vector (1/3 1/3 0.085).

Aim of the experiments was to look to the pressure dependence of the magnetic structure up to 3 GPa a value we did not achieved in the experiment one year ago where the piston was broken.

For the experiments we used a clamp cell made of a NiCrAl alloy in the inner part and of Al in the outer part. The cell was loaded with a single crystal of $CsCuCl_3$.

Fluorinert was used as pressurizing medium. The experiments this time were successful until a pressure of about 2.3 GPa. It was not possible to get a larger pressure to the cell due to some malfunction.

At this value the magnetic propagation vector was determined to be (0.343 0.32 0.147). The determined elongation of the spiral along c is within the errors consistent with the result of a former experiment. For the first time we realized now a deviation in the triangular structure from (1/3 1/3 q). This new feature needs for further investigations in order to rule out sample quality effects or deviations from hydrostatic conditions for the pressurizing medium.

	EXPERIMENTAL REPORT **Investigation of the critical chiral exponents on the one dimensional frustrated binary compound $CuCl_2$**	Proposal N° PHY-01-1883 Instrument **E6** Local Contact Norbert Stüßer
Principal Proposer: Experimental Team:	M. Banks – MPI FKF Stuttgart R. Kremer – MPI FKF Stuttgart N. Stüßer – HMI, Berlin	Date(s) of Experiment 16.05. – 22.05.2006

Date of Report: 17.12.2006

We aimed to measure the critical scattering exponents on the strongest magnetic reflection of the binary compound $CuCl_2$. $CuCl_2$ is a quasi - one dimensional Heisenberg antiferromagnetic spin chai n compound, with a small inter-chain coupling which gives rise to 3D order at T_N = 24 K. Recently, we have successfully obtained the magnetic structure of $CuCl_2$ from a single crystal four circle experiment. The magnetic structure can be described by a propagation vector of τ = (0.5, 0.224, 0) being incommensurate, and implying a helicoidal spin ordering along the chain direction. We aimed on E6 at HMI to advance in greater detail our investigation by measuring the critical exponents on a strong magnetic reflection and measuring the field dependence of the propagation vector.

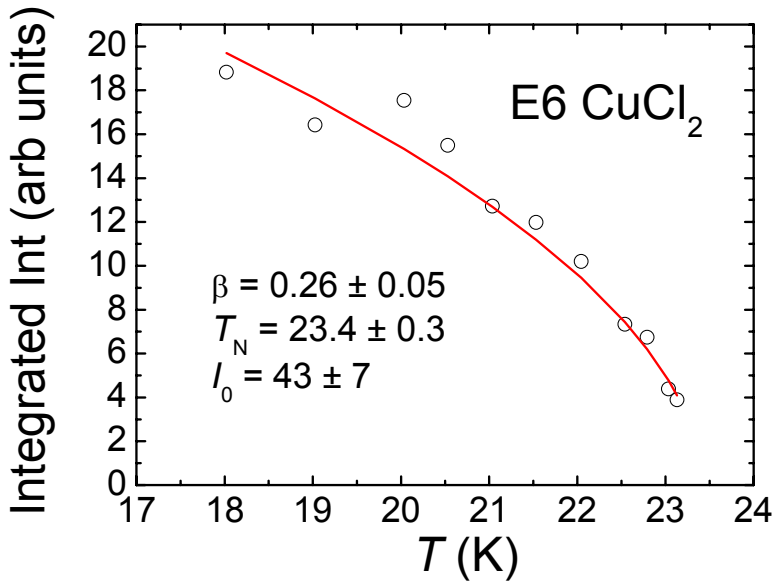

Fig. 1: *shows the temperature dependence of the (0.5 -0.224 -1) magnetic reflection in $CuCl_2$ near the long range ordering temperature. Fitting the experimental data (open circles) to a critical exponent (solid line in fig 1) revealed a Neel temperature of 23.4 ± 0.3 K in excellent agreement with a priori bulk measurements and a critical exponent, β, of 0.26 ± 0.05.*

Fig 1.: *Integrated intensity of a strong magnetic reflection for $CuCl_2$, (0.5 -0.224 -1) as a function of temperature.*

Due to the crystal size and the small moment, time restrictions meant only preliminary experiments could be performed under the influence of a magnetic field. We aimed to investigate the nature of the propagation vector when the magnetic field is applied along the crystallographic *b* direction. At $H \sim 4$ T, $CuCl_2$ undergoes a spin flop transition which should include a spin re-orientation in the *ab* plane. However, we did not detect any change of the incommensurate propagation vector which indicates that the transition, as seen clearly in magnetisation measurements, only involves a spin re-orientation. Further measurements are needed in applied field to understand the magnetic structure in this phase.

BENSC	**EXPERIMENTAL REPORT** **Crystallographic and magnetic structure of the ferrimagnetic spinel oxides**	Proposal N° CHE-01-1968 Instrument **E9** Local Contact M.Tovar,O.Prokhnenko
Principal Proposer: Experimental Team:	W. Nowicki – AMU Poznań, Poland W. Nowicki, J.Darul – AMU, Poznań O. Prokhnenko, M. Tovar – HMI, Berlin	Date(s) of Experiment 11.09. - 18.09.2006

Date of Report: 23.10.2006

A series of compounds $Li_xMn_{3-x-y}Fe_yO_4$, have been investigated by neutron powder diffraction [1,2]. We report new results obtained for the single phase spinel solid solution, with Fe/(Fe+Mn)= 0.5 of composition $Li_{0.53}Mn_{1.235}Fe_{1.235}O_4$ and compare to our previous experiment of the compound $Li_{0.63}Mn_{1.422}Fe_{0.948}O_4$ (n_{Fe}=0.4).

The experiment was performed at HMI, on the high-resolution neutron powder diffractometer E9 (FIREPOD), using Ge monochromator, plane (511). The incident neutron wavelength was 1.79740Å, and standard cryostat/furnace has been used to measurements.

The intensity measurements of magnetic reflection *111* enabled to separate the nuclear and magnetic scattering effect.

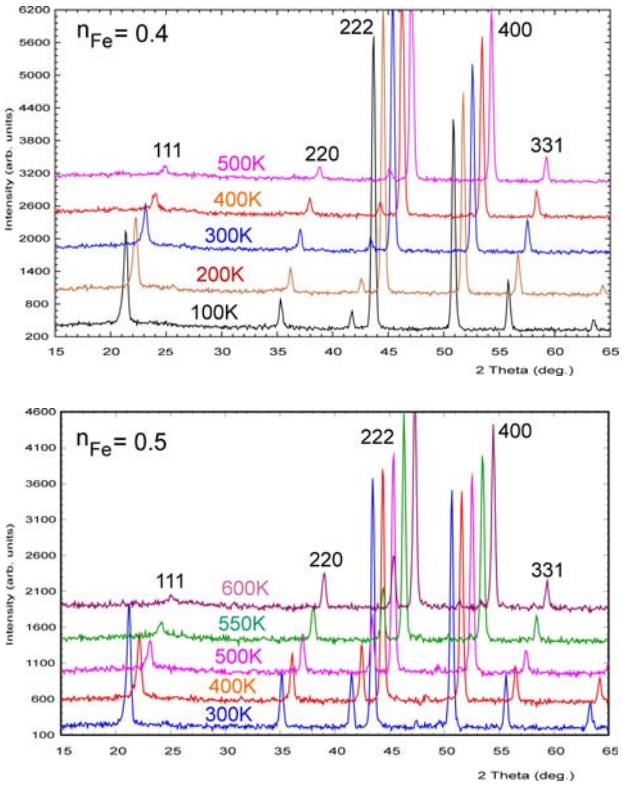

Fig.1: *Neutron powder diffraction patterns of the $Li_{0.63}Mn_{1.422}Fe_{0.948}O_4$ (n_{Fe}=0.4) and $Li_{0.53}Mn_{1.235}Fe_{1.235}O_4$ (n_{Fe}=0.5) spinel solid solution.*

The samples $Li_{0.63}Mn_{1.422}Fe_{0.948}O_4$ and $Li_{0.53}Mn_{1.235}Fe_{1.235}O_4$ reveal different magnetic properties, i.e. they are ferrimagnetic. The gradual decrease of intensity of the reflection *111,* for both compounds, shows that the temperature of magnetic order-disorder transition (Curie temperature) clearly increases of about 100 K, with the increase of n_{Fe} ratio (*Fig.1*). The refinement of spinel structure could be performed on the basis of neutron diffraction patterns recorded at the temperature above Curie point.

An example of the Rietveld profile matching the $Li_{0.63}Mn_{1.422}Fe_{1.948}O_4$ pattern from 500K is presented in *Fig.2*. From the structural point of view this spinel oxide contains the lithium, manganese and iron ions in the tetrahedral as well as in octahedral positions [3,4].

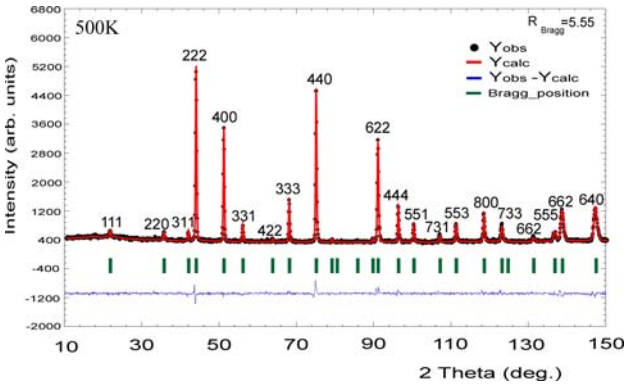

Fig.2: *Observed, calculated and difference profile resulting from the Rietveld analysis of neutron powder diffraction. Data collected on $Li_{0.63}Mn_{1.422}Fe_{0.948}O_4$ (n_{Fe}=0.4).*

References:

[1]. E. Wolska, M. Tovar, B. Andrzejewski, W. Nowicki, J. Darul, P. Piszora, Solid State Sciences **8** (2006) 31.

[2]. Experimental Report:CHE-01-1773.

[3]. E. Wolska, W. Nowicki, J. Darul, M. Tovar, O. Prokhnenko, P. Piszora, Proc. EPDIC-10 (to be published).

[4]. E.Wolska, J. Darul, W. Nowicki, P.Piszora, M. Tovar, O.Prokhnenko, C Baehtz, M. Knapp, Acta Cryst. A**62** (2006) 198.

	EXPERIMENTAL REPORT **Magnetic and Structural Study of $Tb_{0.5}Ba_{0.5}CoO_3$ in *H-T* Plane using Neutron Diffraction**	Proposal N° PHY-01-1771 Instrument **E9** Local Contact Dimitri Argyriou
Principal Proposer: Experimental Team:	S. M. Yusuf – Univ. Zaragoza, ICMA, E S. M. Yusuf – Univ. Zaragoza, ICMA, E D. Argyriou – HMI, Berlin	Date(s) of Experiment 09.02. – 13.02.2006

Date of Report: 19.01.2007

Manganites and cobaltates have been an area of intense research for decades due to their intriguing physical properties and promising performances for technological applications. However, the physics, controlling these properties, is not well understood yet, especially in the case of rare earth cobaltates of the type $R_{0.5}Ba_{0.5}CoO_3$ (R = rare earth). These compounds show ferromagnetism when R = La (T_C = 190 K) and Nd (T_C = 130K). For R = Gd and Tb, the compounds show unusual magnetic and electrical properties. In our dc magnetization study (Fig. 1) as a function of temperature for the titled compound $Tb_{0.5}Ba_{0.5}CoO_3$, a paramagnetic to an weak ferromagnetic-like transition was found around 282.9 K. Following this, an antiferromagnetic-like transition around 248 K was also observed. Below ~50 K, a sharp rise in magnetization was also found under higher magnetic field.

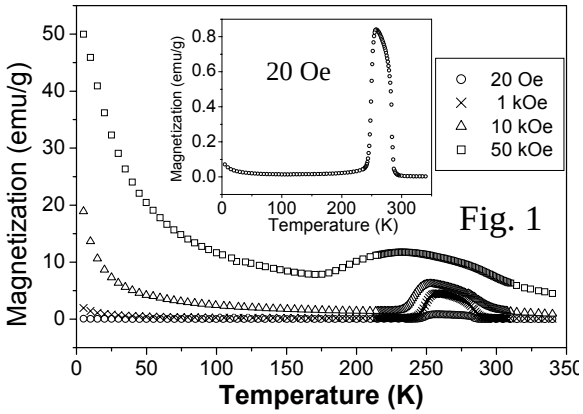

The Rietveld refinement of the room temperature neutron diffraction pattern (Fig. 2) showed that the sample is in single phase (space group *Pmmm* (z = 2) with a = 3.8672(2), b = 7.8159(3), and c = 7.5155(4) Å. Figure 3 shows the neutron diffraction patterns over lower angular region recorded at 1.6, 210, 266, and 301 K (from top to bottom). With decreasing temperature there is an appearance of few additional Bragg peaks. Figure 4 shows the neutron diffraction patterns at 1.6 and 210 K under zero and 50 kOe applied field. At 1.6 K, an enhancement of the peak intensities under applied field is evident.

The refinement of the neutron diffraction patterns for determination of magnetic structure is underway.

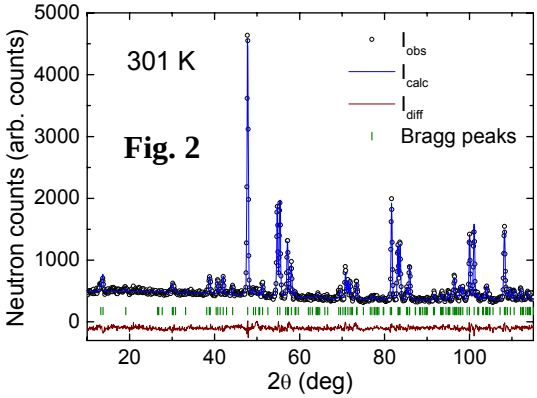

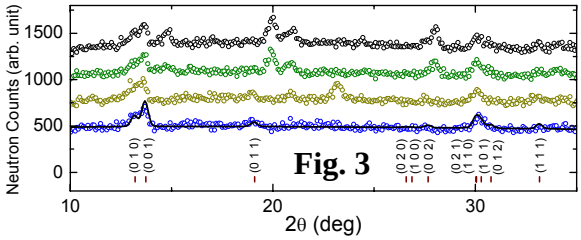

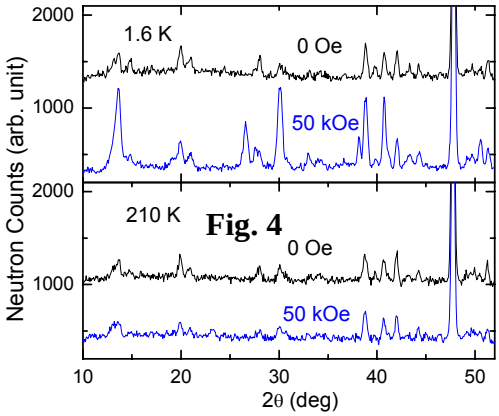

	EXPERIMENTAL REPORT **Magnetic and Structural Phase Transitions in $La_{1-x}Ba_xCoO_3$ System**	Proposal N° PHY-01-1772 Instrument **E9** Local Contact Vadim Sikolenko
Principal Proposer: Experimental Team:	H. Gamari-Seale – NCSR Demokritos, Athens, GR A. P. Sazonov, I. O. Troyanchuk – NAS Minsk, BY K. L. Stefanopoulos – NCSR Demokritos, GR V. Sikolenko – HMI, Berlin	Date(s) of Experiment 12.01. – 16.01.2006

Date of Report: 17.01.2007

$La_{1-x}M_xCoO_3$ (M — alkaline-earth metal) systems attract much attention due to the possibility of practical application (cathode material, catalysts, etc.) and because of its unusual properties (appearance of both ferromagnetism and metallicity by doping or increasing temperature, spin state transition of the Co ions, etc).

With temperature increase both in Ca- ($T \sim 400$ K; orthorhombic-rhombohedral) and in Sr-doped ($T \sim 600$ K; rhombohedral-cubic) systems the phase transition to higher symmetry is observed for x near magnetic percolation threshold ($x \sim 0.2$). It is expected that such transition will take place in Ba-doped system at lower temperature. However, there are few experimental data for $La_{1-x}Ba_xCoO_3$.

The $La_{0.8}Ba_{0.2}CoO_3$ composition was synthesized by the conventional ceramic method at $T = 1200$ °C. The neutron powder-diffraction experiments were carried out on FIREPOD (E9) with incident neutrons of wavelength $\lambda = 1.7973$ Å. Data were collected on warming from 4 to 550 K. The neutron diffraction data were analyzed with the Rietveld method [1] using the FullProf program [2]. It was found that less then 3% of CoO was present in the sample. It was taken into account in the final calculations.

The results of our preliminary refinement for the $La_{0.8}Ba_{0.2}CoO_3$ compound are resented in figures.

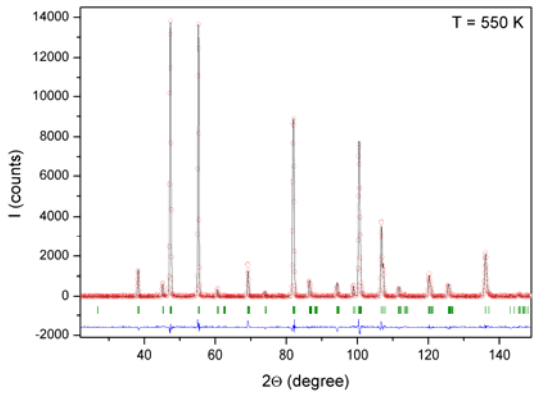

Fig. 1: *The ticks show the predicted 2Θ positions for the Bragg peaks.*

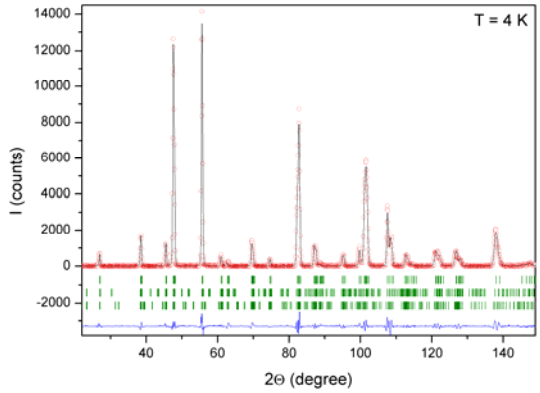

Fig. 2: *The ticks show the predicted 2Θ positions for the Bragg peaks of the rhombohedral crystal phase (upper row), orthorhombic phase (middle row) and the magnetic phase (lower row).*

Structural parameters as determined by the Rietveld refinement as well as the magnetic moment of the Co sublattice (M_{Co}) and the reliability factors are listed in table.

T, K	**550**	**300**	**150**	**4**	
Sp.Gr.	R-3c	R-3c	R-3c	R-3c	Pbnm
	100%	100%	100%	48%	52%
a	5.4881(1)	5.4706(1)	5.4620(1)	5.4599(1)	5.4723(2)
b	5.4881(1)	5.4706(1)	5.4620(1)	5.4599(1)	5.4292(2)
c	13.3939(2)	13.3147(3)	13.2767(2)	13.2662(4)	7.6791(3)
$\mathbf{x_{La/Ba}}$	0	0	0	0	0.00073(77)
$\mathbf{y_{La/Ba}}$	0	0	0	0	0.00492(236)
$\mathbf{z_{La/Ba}}$	0.25	0.25	0.25	0.25	0.25
$\mathbf{x_{Co}}$	0	0	0	0	0.5
$\mathbf{y_{Co}}$	0	0	0	0	0
$\mathbf{z_{Co}}$	0	0	0	0	0
$\mathbf{x_{O1}}$	0	0	0	0	0.04259(136)
$\mathbf{y_{O1}}$	0.47553(21)	0.46992(27)	0.46792(13)	0.46892(60)	0.50038(347)
$\mathbf{z_{O1}}$	0.75	0.75	0.75	0.75	0.25
$\mathbf{x_{O2}}$	-	-	-	-	0.74550(259)
$\mathbf{y_{O2}}$	-	-	-	-	0.25629(202)
$\mathbf{z_{O2}}$	-	-	-	-	0.02277(46)
$\mathbf{M_{Co}, \mu_B}$	-	-	1.057(52)	2.315(78)	
$\mathbf{R_B}$, %	3.46	3.49	2.74	3.12	4.03

References:

[1]. H. M. Rietveld, J. Appl. Crystallogr. **2**, 65 (1969).
[2]. J. L. Rodríguez-Carvajal, Physica B **55**, 192 (1992).

	EXPERIMENTAL REPORT **Inhomogeneous magnetic states in Fe and Cr substituted $LaMnO_3$**	Proposal N° PHY-01-1862 Instrument **E9** Local Contact Vadim Sikolenko
Principal Proposer: Experimental Team:	H. Gamari-Seale - NCSR Demokritos, Athens, GR D.V. Karpinsky – JISSSP NAS, Minsk, Belarus L.S. Labanovsky – JISSSP NAS, Minsk, Belarus V. Sikolenko – HMI, Berlin	Date(s) of Experiment 09.01. – 12.01.2006

Date of Report: 05.01.2007

Magnetization and neutron diffraction measurements have been performed on $LaMn_{0.5}Fe_{0.5}O_{3+d}$ and $LaMn_{0.5}Cr_{0.5}O_{3+d}$ perovskites. Neutron diffraction study revealed a G-type antiferromagnetic component as well as a ferromagnetic one for both stoichiometric compounds. Magnetic structure refinement for the $LaMn_{0.5}Fe_{0.5}O_3$ compound was performed on the basis of the three different models: noncollinear, multiphasic and ferrimagnetic. There liability factors obtained for the Fe doped $LaMnO_3$ nearly coincide for the mentioned models and there are certain difficulties in preferring one of them. The magnetic moments calculated for these compounds have smaller values than the theoretically estimated ones, which can be explained by a magnetically frustrated phase within the samples. Magnetic properties can be well described using a superexchange mechanism. This model supposes Mn^{3+}–O–Mn^{3+} ferromagnetic interactions when static Jahn–Teller distortions are removed, whereas Cr^{3+}–O–Cr^{3+} and Fe^{3+}–O–Fe^{3+} interactions are strongly antiferromagnetic. The magnetic properties of both compounds have been interpreted in terms of the 'two-phase' model supposing certain segregation into ferromagnetic and antiferromagnetic regions (figure). Some arguments in favour of the phase separation scenario have been proposed.

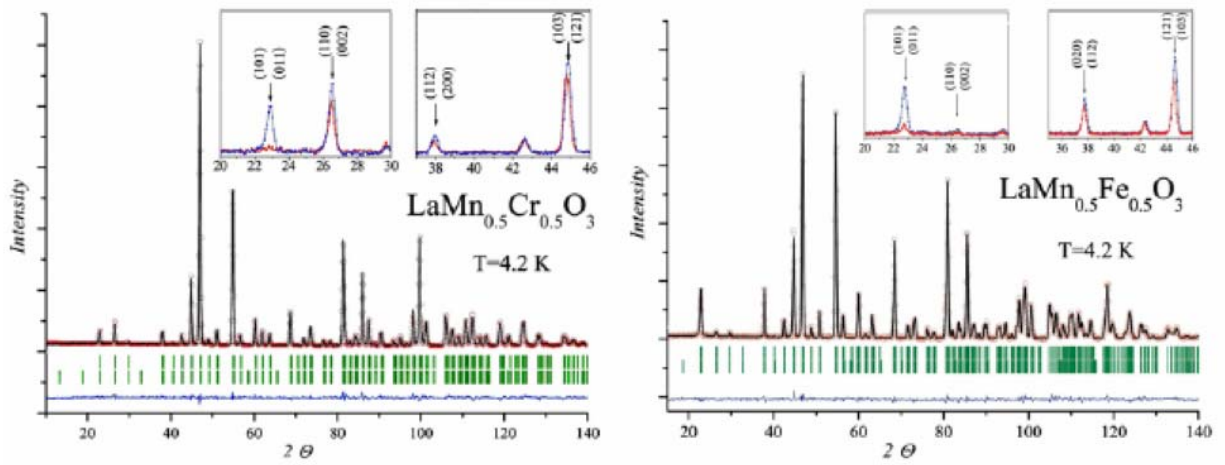

Fig. 1: *NPD refined patterns for the $LaMn_{0.5}Cr_{0.5}O_3$ (left) and $LaMn_{0.5}Fe_{0.5}O_3$ (right) samples recorded at 4.2 K. The observed intensities are shown by red circles and the calculated ones by a solid line. The positions of the Bragg reflections are shown by the small vertical lines below the patterns (the upper lines denote crystal structure and the lower ones magnetic). The line at the bottom indicates the intensity difference between the experimental and the refined patterns. The comparison for the most informative peaks recorded at 300 and 4.2 K is shown on the insets.*

	EXPERIMENTAL REPORT **Multiple magnetic transitions in $Ho_3Cu_4Sn_4$ compound.**	Proposal N° PHY-01-1865 Instrument **E9** Local Contact Oleksandr Prokhnenko
Principal Proposer: Experimental Team:	Ł. Gondek – AGH-UST, Krakow, PL Ł. Gondek – AGH-UST, Krakow, PL O. Prokhnenko – HMI, Berlin	Date(s) of Experiment 13.02. – 19.02.2006

Date of Report: 14.03.2006

The $Ho_3Cu_4Sn_4$ compound belongs to the novel family of compounds, where the rare earth ions occupy two different crystallographic positions: 2d and 4e. The Néel temperature was found to be 7.6 K and below this temperature a complex magnetic phase diagram was observed. The 2d and 4e rare earth sublattices orders independently at 7.6 K and 3.3 K respectively. Neutron diffraction patterns were recorded at temperatures of 1.7 K, 3 K, 4 K, 5 K, 6 K, 7 K and 11 K. The analysis of the collected data reveals existence of five different magnetic phases.

At 1.7 K both 2d and 4e magnetic sublattices are described by propagation vectors $\boldsymbol{k_{2d}}$=(0;0.5;0) and $\boldsymbol{k_{4e}}$=(0.3712;0.5;0.5) for 2d and 4e sublattices respectively. The 2d sublattice is ordered along the b-axis and the 4e sublattice is ordered along the a-axis. The analysis of pattern recorded at 3 K reveal a change of propagation vector in 4e sublattice. Now $\boldsymbol{k_{4e}}$=(0.5;0.5;0.4694). Above 3.3 K the 4e sublattice is no longer ordered. At 4 K the propagation vector $\boldsymbol{k_{2d}}$ describing the 2d sublattice is commensurate (0;0.5;0), however a change of Ho magnetic moments orientation was observed. Ho moments lie now in the *b*-*c* plane. At 5 K the 2d magnetic moments lie along the *b*-axis again. Just below the Néel point, at 6 K a change of propagation vector from commensurate into incommensurate one is visible. The new propagation vector is $\boldsymbol{k_{2d}}$=(0.0695;0.4821;0). At 11 K magnetic moments of Ho do not exhibit long-range order.

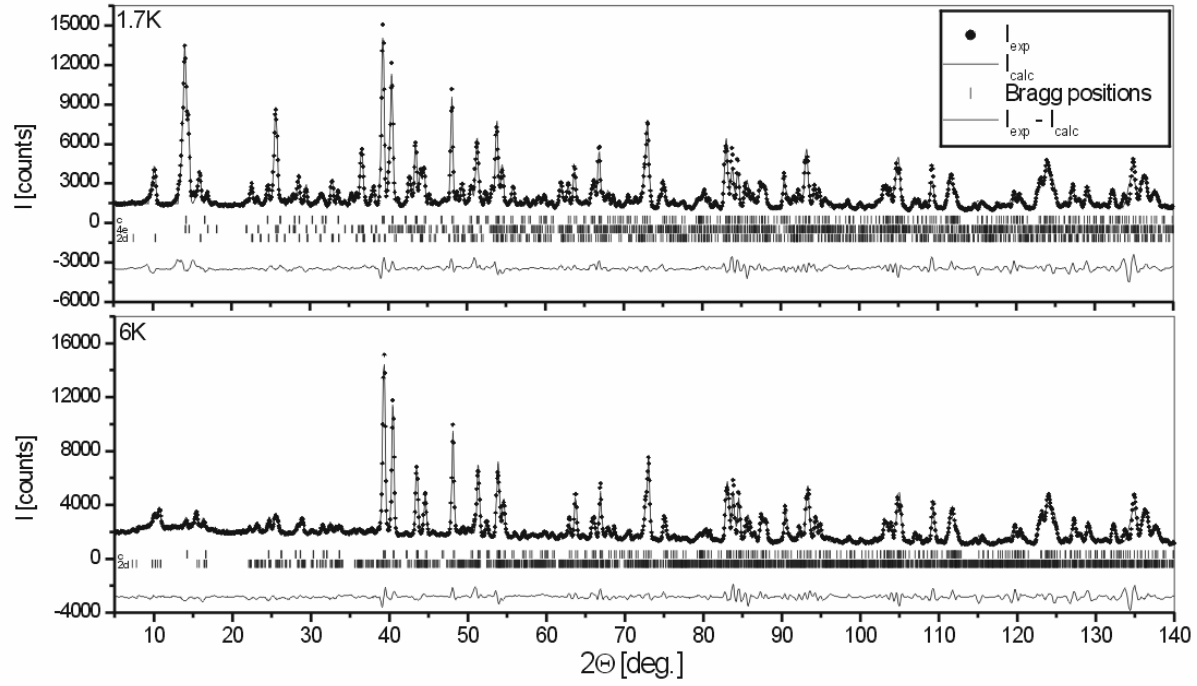

Fig. 1: *Neutron diffraction patterns collected at 1.7 and 6 K in the magnetically ordered state.*

	EXPERIMENTAL REPORT **Phase Transformations in $Pr_{0.5}Sr_{0.5}CoO_3$**	Proposal N° PHY-01-1867 Instrument **E9** Local Contact D.Argyriou, N.Aliouane
Principal Proposer: Experimental Team:	H. Szymczak – PAS IP Warsaw, PL D.V. Karpinsky – JISSSP NAS, Minsk, Belarus D. Argyriou – HMI, Berlin N. Aliouane – HMI, Berlin	Date(s) of Experiment 03.04. – 07.04.2006

Date of Report: 05.01.2007

The elastic properties and crystal structure of the $Pr_{0.5}Sr_{0.5}CoO_3$ have been studied. Two types of crystal structure transitions have been found. The structure of the sample was refined from neutron diffraction data obtained at temperatures of 318, 290, 150, and 4.2 K. An analysis of the obtained neutron diffraction patterns indicates that a structural phase transition occurs above room temperature, which confirms the results of studying the elastic properties of the sample. It is found that the best reliability factors for the unit cell parameters refined at T = 318 K are obtained in the model that suggests a twophase crystal structure of the sample. This structure is characterized by the coexistence of the monoclinic (space group P21/n) and rhombohedral (space group R-3c) phases, whose fractions in the sample are in a ratio of 72: 28. At a temperature of 290 K, the presence of the rhombohedral phase can be neglected, and the sample is characterized by only monoclinic distortions of the unit cell. As the temperature decreases to 150 K, the angle â characterizing the monoclinic distortions becomes close to 90° while changes in the remaining lattice parameters are insignificant. At this temperature, magnetic neutron scattering makes a substantial contribution to the peak intensities of the neutron diffraction pattern, which is caused by the transition of the sample to a magnetically ordered state. A significant increase in intensity is observed for the (110), (002), (112), and (200) reflections, which indicates that the sample has a ferromagnetic structure. The calculated magnetic moment 1.1 μ_B per cobalt ion is predominantly aligned with the c axis of the unit cell. With a further decrease in the temperature to 4.2 K, no significant changes are observed in the crystal and magnetic structures of the sample. As a result of refining the magnetic structure of the sample at T = 4.2 K (figure) it was found that the magnetic moment per cobalt ion equals 1.8 μ_B and is predominantly aligned with the y axis of the unit cell. The obtained magnetic moment is in good agreement with the suggestion that Pr ions make no significant contribution to the magnetic structure of the sample. It is suggested that the high-temperature transition is caused by the dimensional effect, while the low-temperature transition is associated with the presence of praseodymium ions actively involved in chemical bonding. Authors assume that the active participation of praseodymium ions in the formation of chemical bonds is the most probable cause of the lowtemperature phase transformation.

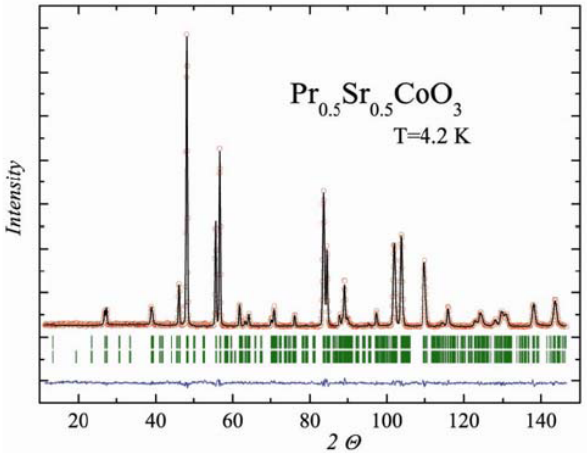

Fig.: *Crystal and magnetic structures of $Pr_{0.5}Sr_{0.5}CoO_3$ refined by a neutron diffraction pattern measured at T =4.2 K: (circles) experimental data, (solid line) calculated curve, and their (lower solid line) difference; vertical line segments mark the calculated positions of reflections; the upper row of reflections corresponds to the crystalline monoclinic phase, and the lower row corresponds to the ferromagnetic structure.*

BENSC	**EXPERIMENTAL REPORT** **Magnetic Ground State of $YBaCo_2O_{5.5/5.44}$ Cobalt Oxides**	Proposal N° PHY-01-1869 PHY-01-1852 Instrument **E9, E2** Local Contact D. Argyriou, U. Aman
Principal Proposer: Experimental Team:	D. Khalyavin – Univ. Aveiro, P A. Yaremchenko - Univ. Aveiro, P D. Argyriou – HMI, Berlin U. Amann – HMI, Berlin	Date(s) of Experiment 19.01. – 22.01.2006 (E9) 14.03. – 17.03.2006 (E2)

Date of Report: 18.10.2006

The aim of the experiment was to study the antifferromagnetic - ferromagnteic phase transition in $YBaCo_2O_{5.5}$ and $YBaCo_2O_{5.44}$ compositions with different types of oxygen ions ordering in [$YO_{0.5}$/$_{0.44}$] layers by neutron powder diffraction. The transition occurs at T_i ~ 260K and 160 K for the compositions with the different oxygen content, respectively.

The samples were prepared by a solid state reaction in oxygen flow with appropriate cooling conditions. Two diffractometers have been used, the fine-resolution powder diffractometer (E9) and the high-intensity flat-cone- and powder diffractometer (E2). The former with incident neutrons of wavelength λ = 1.7974 Å and resolution $\Delta d/d \sim 2*10^{-3}$ was used for the crystal structure refinement. The latter (λ = 2.39 Å) equipped with a position sensitive detector providing a very high intensity is efficient in the magnetic structure investigations.

Using magnetic symmetry arguments in combination with group-theoretical analysis, the crystal and magnetic structures above and below a temperature of the phase transformation, T_i, have been determined and successfully refined (Figs.1, 2). In both the cases, the proposed models involve a spin-state ordering between diamagnetic ($t_{2g}^6e_g^0$, $S = 0$) and paramagnetic ($t_{2g}^4e_g^2$, $S = 2$) Co^{3+} ions with octahedral coordination. The electronic ordering results in a nonzero spontaneous magnetic moment in the high temperature magnetic phase with isotropic negative exchange interactions. In the case of $YBaCo_2O_{5.5}$, the phases transformation does not change *Pmma* ($2a_p \times 2a_p \times 2a_p$) symmetry of the crystal structure. The wave vectors of the magnetic structures above and below T_i are $\boldsymbol{k} = 0$ and $\boldsymbol{k} = \boldsymbol{c}^*/2$, respectively. In the case of $YBaCo_2O_{5.44}$ a crossover *P4/nmm* ($3\sqrt{2}a_p \times 3\sqrt{2}a_p \times 2a_p$) ↔ *I4/mmm* ($3\sqrt{2}a_p \times 3\sqrt{2}a_p \times 4a_p$) was involved to solve the low temperature magnetic structure. The wave vectors in both the high temperature and the low temperature magnetic phases are $\boldsymbol{k} = 0$.

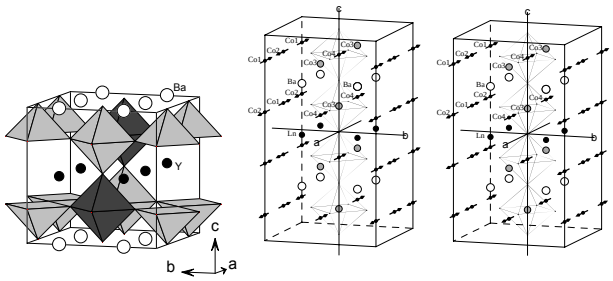

Fig.1: A polyhedral representation of the crystal structure of $YBaCo_2O_{5.5}$ (*Pmma*, $2a_p \times 2a_p \times 2a_p$) (a). Non-equivalent octahedral Co positions are presented by the light and dark grey polyhedra, respectively. A schematic representation of the magnetic structure above T_i (b) and below T_i (c) (Co1, Co2 and Co3, Co4 - pyramidal and octahedral positions, respectively). Diamagnetic low-spin state Co ions are denoted by grey circles.

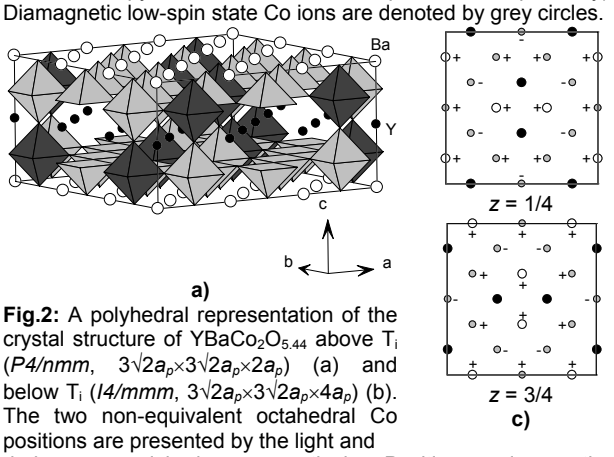

Fig.2: A polyhedral representation of the crystal structure of $YBaCo_2O_{5.44}$ above T_i (*P4/nmm*, $3\sqrt{2}a_p \times 3\sqrt{2}a_p \times 2a_p$) (a) and below T_i (*I4/mmm*, $3\sqrt{2}a_p \times 3\sqrt{2}a_p \times 4a_p$) (b). The two non-equivalent octahedral Co positions are presented by the light and dark grey polyhedra, respectively. Positive and negative directions of the magnetic moments on paramagnetic Co ions in the neighbour (*ab*) planes containing Co ions in octahedral (large circles) and pyramidal (small grey circles) coordination in the corresponding $3\sqrt{2}a_p \times 3\sqrt{2}a_p \times 2a_p$ (c) and $3\sqrt{2}a_p \times 3\sqrt{2}a_p \times 4a_p$ (d) unit cells. The magnetic moments llie in the (*ab*) plains. The diamagnetic sixfold coordinated Co ions are shown by the black circles.

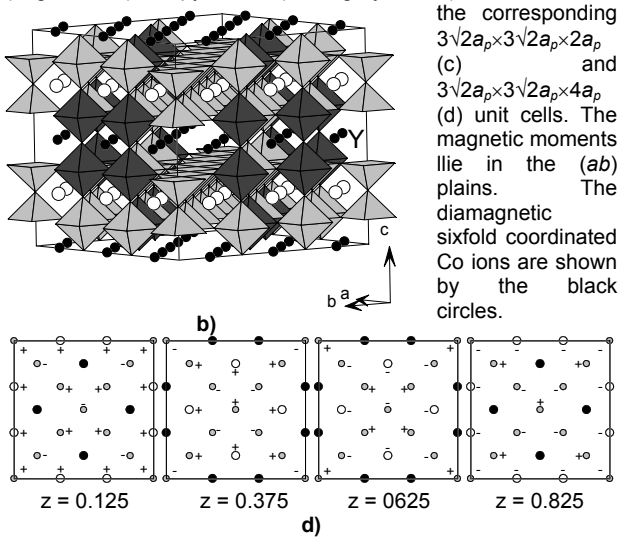

BENSC	**EXPERIMENTAL REPORT** **Neutron diffraction study of the atomic and magnetic structure of the La $_{0.5}$ $Sr_{0.5}CoO_{3-d}$and $Re_{0.5}Ba_{0.5}CoO_{3-d}$ (d= 0.0; 0.25 and 0.5)**	Proposal N° PHY-01-1965 Instrument **E9** Local Contact Vadim Sikolenko
Principal Proposer: Experimental Team:	K. Bormanis – Univ. of Latvia, Riga, LV K. Stanislav – ASCR IP Prague, CZ A. Kuzmenko – Univ. Genf, CH V. Efimov – JINR Dubna, RU V. Sikolenko – HMI, Berlin	Date(s) of Experiment 06.09. – 11.09.2006

Date of Report: 09.10.2006

Cobaltites oxides with perosvskite-like structure attract a considerable interest of many researchers because of their specific properties making them promising materials in SOFC, chemical reactors catalysis, gas separation membranes and many other applications [1,2]. The magnetic properties of these compounds are of particular interest [3]. An especially interesting feature observed for these materials is an ordering of oxygen vacancies which can drastically change the physical properties of such compounds in comparison with stoichiometric ones.

The main goal of this proposal was to study the magnetic and nuclear structural transformation effects induced in the layered cobaltites $La_{0.5}Sr_{0.5}CoO_{3-d}$ and $La_{0.5}Ba_{0.5}CoO_{3-d}$ (d = 0.0; 0.25 and 0.5) with equal oxygen deficit content assuming that for the former compounds there are no evidences for La and Sr ions arrangement.

The applicants of the project planned to study a magnetic and crystal structure of the $La_{0.5}Sr_{0.5}CoO_{3-d}$ and $La_{0.5}Ba_{0.5}CoO_{3-d}$ (d = 0.0; 0.25 and 0.5) powder by means of neutron powder diffraction using E9 instrument at 2 K, 150 K and 290 K. In summary 18 measurements: 6 spectra at 2 K, 150 K and 290 K.

The atomic and magnetic structure changes effects induced in $La_{0.5}Sr_{0.5}CoO_{3-d}$ and $La_{0.5}Ba_{0.5}CoO_{3-d}$ (d = 0.0; 0.25 and 0.5) powder were studied on the diffractometer E9 with incident neutron wavelength λ = 1.79 Å at the BER-II in Hahn-Meitner Institute.

Fig.1 shows a neutron Powder diffraction pattern and Rietveld refinement of $La_{0.5}Sr_{0.5}CoO_{2.75}$ powder at the 2 K.

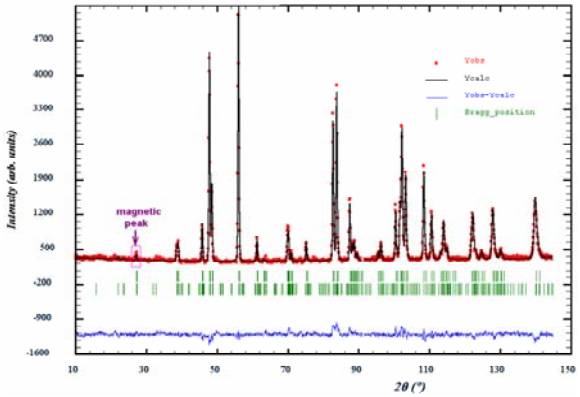

Fig.1. *Rietveld refinement pattern of the $La_{0.5}Sr_{0.5}CoO_{2.75}$ powder at the 2 K.*

We have found that the increase of the **d** oxygen deficit content in the $La_{0.5}Sr_{0.5}CoO_{3-d}$ leads to the gradual increase of the lattice volume, to the significant decease of the magnetic moment and to the growth of the rhombohedral distortions (table 1). These results were confirmed by X-ray absorption fine structure (EXAFS) and X-ray absorption near edge structure (XANES) at the cobalt *K*-edge measurements [4,5].

Table 1. *Structural parameters for $La_{0.5}Sr_{0.5}CoO_{3-d}$ (d = 0.0; 0.25 and 0.5) powder at the 2 and 290 K.*

d	**0.0**	**0.25**	**0.5**	**0.0**	**0.25**	**0.5**
T, K		**T = 2 K**			**T = 290 K**	
Sp.gr.	R-3c	R-3c	R-3c	R-3c	R-3c	R-3c
a (Å)	5.4351	5.4359	5.4367	5.4375	5.4399	5.4421
α	60.410	60.621	60.782	60.380	60.493	60.627
V (Å^3)	**113.067**	**113.078**	**113.091**	**113.104**	**113.139**	**113.119**
μ(μ_B)	**2.2**	**1.7**	**0.8**	-	-	-
R_{wp}	4.02	5.26	4.81	4.34	5.05	5.29

Unfortunately due to unscheduled breakdown of the BER-II reactor we could not fulfill all planned experiment. We hope to finish our measurement next year.

References:

[1]. I.O. Troyanchuk, N. Kasper, D. Khalyavin, R. Szymczak, Phys. Rev. Lett. **80**, 3380 (1998).

[2]. A. Maignan, C. Martin, D. Pelloquin, N. Nguyen, B. Raveau. J. Solid State Chem. **142**, 247 (1999).

[3]. V. Sikolenko, D. Többens, U. Zimmermann, I. Troyanchuk, E. Pomjakushina, J.Phys.:Cond.Mat**. 16**, 7313 (2004).

[4]. V. Sikolenko, I. Troynchuk, V. Efimov, Surface investigation X-ray, Synchrotron and Neutron Techniqucs **6**, 23-29 (2006).

[5]. V. Sikolenko, V. Efimov, K. Iakoubovskii, A. Kuzmin, Journal of Physics and Chemistry of Solids **67** 2007 (2006).

	EXPERIMENTAL REPORT **Magnetic phase transitions in $Ho_3Cu_4Si_4$ compound.**	Proposal N° PHY-01-1967 Instrument **E9** Local Contact Oleksandr Prokhnenko
Principal Proposer: Experimental Team:	Ł. Gondek – AGH-UST, Kraków, PL Ł. Gondek – AGH-UST, Kraków, PL O. Prokhnenko – HMI, Berlin	Date(s) of Experiment 18.09. - 23.09.2006

Date of Report: 26.10.2006

The $Ho_3Cu_4Si_4$ compound belongs to the novel 3-4-4 family of compounds, where the rare earth ions occupy two different crystallographic positions: 2d and 4e. Systematic studies of such compounds are carried out in order to find the origin of peculiar magnetic properties. According to our results many of $R_3Cu_4X_4$ compounds exhibit independent ordering of both sublattices resulting with different ordering temperatures (eg. [1,2]) and/or independent changes of propagation vectors at each sublattice. For the 2d magnetic sublattice a propagation vector (0;1/2;0) is very common whereas the 4e sublattice exhibits many different propagation vectors, often incommensurate.

The former neutron diffraction data taken using E6 diffractometer turned out to be not satisfactory, thus proposed model of magnetic ordering did not index all magnetic peaks. The current experiment was carried out at E9 instrument. Keeping in mind very complex magnetic structure the experiment was performed using high wavelength of 2.816 Å, which together with high resolution of E9 apparatus let us to observe splitting of some magnetic reflections. The neutron diffraction patterns were taken at following temperatures: 1.7 K, 4.2 K, 7.2 K, 13.4 K, 18 K and 24 K. The above temperatures were chosen according to specific heat data, which are indicating multiple magnetic transitions at 2 K, 5.5 K, 11.5 K, 17 K and 20 K.

The neutron diffraction patterns (see figure) revealed that the $Ho_3Cu_4Si_4$ crystallizes in the orthorhombic $Gd_3Cu_4Ge_4$-type crystal structure. No distortions of the crystal structure were noticed down to 1.7 K. The lattice constants just above the ordering temperature of 20 K are: a=13.5970(4) Å; b=6.5028(2) Å; c=4.1007(1) Å.

According to neutron diffraction data the 4e sublattice disorders at 5.5 K whereas the 2d sublattice remains ordered up to 20 K. The significant changes in comparison to former E6 data can be noticed for pattern taken at 1.7 K. Some of the reflections exhibit a little splitting, moreover some satellites of very low intensity were observed as well. According to preliminary refinements of our data the magnetic ordering of 2d sublattice is described by propagation vector (0; 0.5; 0). Half of magnetic moments of the 4e sublattice seems to be indexed by propagation vector close to (0; 0.5; 0), whereas the rest are forming very complicated incommensurate structure.

References:

[1] E. Wawrzyńska et. al. J. Magn. Magn. Mater. **280** (2004) 234

[2] Ł. Gondek et. al. Intermetallics, accepted for press

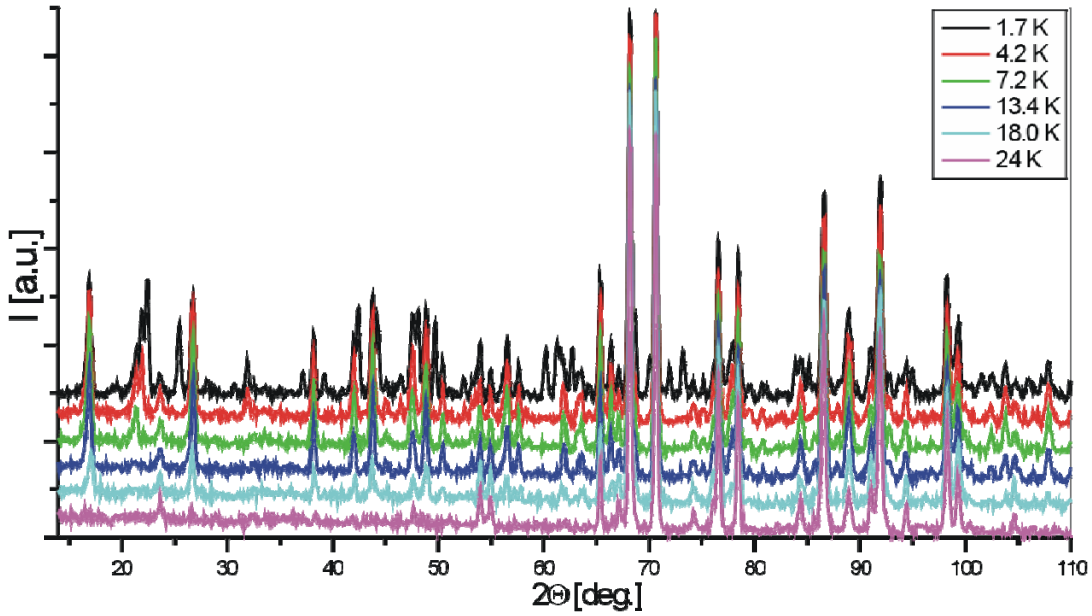

BENSC	**EXPERIMENTAL REPORT** **The neutron response of $TM_3[Cr(CN)_6]_2 \cdot 15D_2O$, TM = Mn, Ni, system**	Proposal N° PHY-01-1969 Instrument **E9** Local Contact Oleksandr Prokhnenko
Principal Proposer: Experimental Team:	M. Mihalik – SAS Košice, SK S. Mat'aš, V. Kavečanský – SAS Kosice, SK M. Zentková – SAS Košice, SK O. Prokhnenko – HMI, Berlin	Date(s) of Experiment 18.10. – 23.10.2006

Date of Report: 05.01.2007

Neutron diffraction data were taken from $TM_3[Cr(CN)_6]_2x15D_2O$ powders (TM = Mn, Ni, at T = 100 K (above the Curie temperature) and at T = 2 K (below magnetic phase transition). The hydrogen atoms were replaced with deuterium in the process of samples preparation, however the high value of background observed on both samples indicates that D_2O molecules are substituted by H_2O molecules during the aging of the samples and incoherent scattering from hydrogen contributes to background (see Fig.1.). The incoherent scattering can be reduced if the sample is stored in D_2O vapours. The incoherent scattering resulted in extension of the time of measurement but finally good statistic was obtained and preliminary results indicate that the crystal structure, including D-sites, will be fully described (see Fig.1., Fig.2. and Table 1.). The magnetic contribution was observed on $Mn_3[Cr(CN)_6]_2x15D_2O$ at 2K (see Fig.3.) and appeared only on allowed nuclear reflections – no additional reflections were observed on forbidden nuclear reflections. On the other hand, no magnetic contribution was observed on $Ni_3[Cr(CN)_6]_2x15D_2O$ at 2 K. Additional magnetization measurements of $M(T)$ in zero magnetic field revealed a maximum at about 60 K and low value of M at T = 2 K. Neutron diffraction measurements performed in magnetic field or at 60 K can reveal magnetic contribution on this sample.

Table.1. Refined values of positional parameters for $Mn_3[Cr(CN)_6]_2x15D_2O$; fcc crystal structure, the space group $Fm\text{-}3m$, a=10.7297(3) Å, V=1235.27(6) Å^3 at 100 K.

Atom	Wyck.	Site	S.O.F.	x / a	y / b	z / c
Mn	4a	m-3m		0	0	0
Cr	4b	m-3m	0.67019	1/2	1/2	1/2
C	24e	4m.m	0.67011	0.3092(9)	0	0
N	24e	4m.m	0.536	0.1875(13)	0	0
O1	24e	4m.m	0.464	0.2140(9)	0	0
O2	32f	.3m	0.052	0.35000	0.35000	0.35000
O3	96k	..m	0.006	0.26890	0.26890	0.30000
D21	192l	1	0.0086	0.33180	0.38910	0.41400
D31	192l	1	0.003	0.21680	0.31610	0.27510

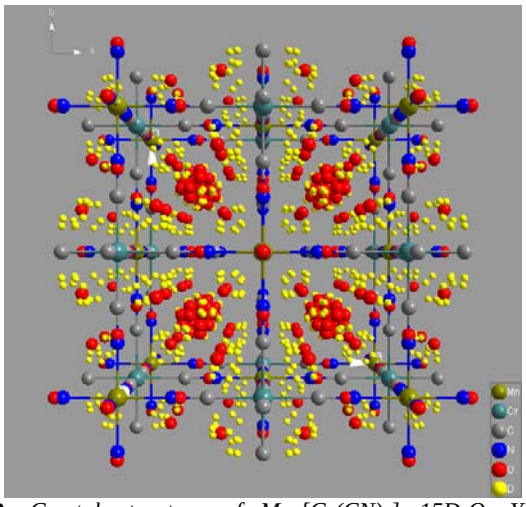

Fig.2: *Crystal structure of $Mn_3[Cr(CN)_6]_2x15D_2O$. Yellow circles indicate sites of D atoms in the zeolite water characterized by oxygen in two sites 32f and 96k.*

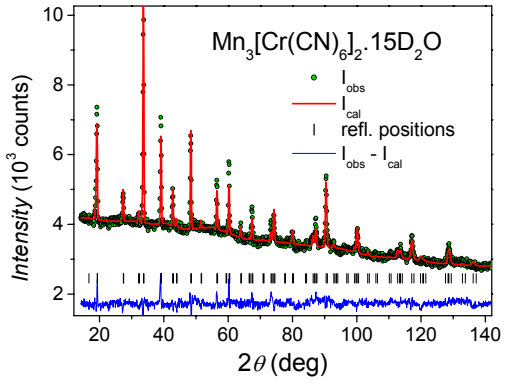

Fig.1: *Rietveld refinement of $Mn_3[Cr(CN)_6]_2x15D_2O$; neutron diffraction data were taken at 100K.*

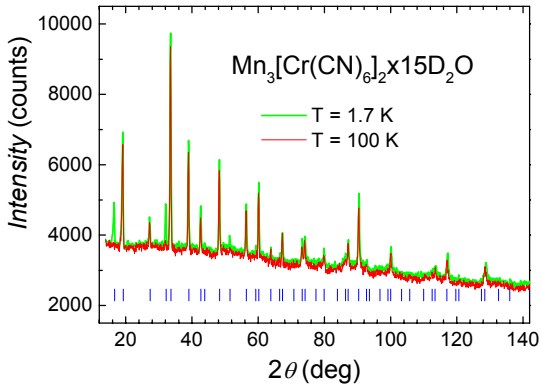

Fig.3: *Magnetic contribution appears only on nuclear reflections and is pronounced on very weak nuclear reflections.*

	EXPERIMENTAL REPORT **Structural and magnetic properties of Sr_2CrTaO_6, Sr_2MnTaO_6, and Sr_2FeTaO_6**	Proposal N° PHY-01-2013-EF Instrument **E9** Local Contact Michael Tovar
Principal Proposer: Experimental Team:	Y.Krockenberger – MPI FKF Stuttgart M. Reehuis, M. Tovar – HMI, Berlin L. Alff – TU, Darmstadt Y.Krockenberger – MPI FKF Stuttgart	Date(s) of Experiment 23.06. – 29.06.20069

Date of Report: 03.01.2007

The crystal structure symmetry of $A_2BB'O_6$-type perovskites strongly depends on the size of the *A*- and *B*-site cations. If cations *B* and *B'* are sufficiently different in charge and/or size, a *B*-site ordering occurs (ordered double perovskite). On the other hand it simply leads to a solid solution $AB_{0.5}B'_{0.5}O_3$, where a cation *B* substitutes for *B'*. In the case of Sr_2YTaO_6 the double perovskite was found to be fully ordered, and it crystallizes in the monoclinic space group $P2_1/n$ [1]. A fully ordered double perovskite could also be found recently for the chromium compound Sr_2CrOsO_6 [2]. In contrast, the tantalum containing compound Sr_2CrTaO_6 was found to be partially disordered at the *B*-sites [3].

In the present study we give an account on the structural and magnetic properties of tantalum perovskites containing Cr, Mn, and Fe. Neutron powder diffraction experiments have been carried out on the instrument E9 using the neutron wavelength λ = 1.7971 Å. Powder patterns of the tantalum perovskites were collected at 2 K and room temperature. For the compound Sr_2CrTaO_6 we could show the presence of a partial disordering at the *B*-site (in 2*a*): *occ*(Cr)/*occ*(Ta) = 0.74(5)/0.26(5). This ratio is similar to the value reported earlier [3]. But in contrast to Ref. 3 we could determine a crystal structure with a lower symmetry than the cubic one with the space group *Fm*–3*m*. The best refinement we could obtain by the use of the monoclinic space group *I*4/*m*. The same tetragonal space group was found at 2 K for Sr_2MnTaO_6. The refinements showed that the *B*-sites are nearly disordered. Here we found the ratio *occ*(Cr)/*occ*(Ta) = 0.472(8)/0.528(8). The crystal refinements of Sr_2FeTaO_6 finally lead to a solid solution $AB_{0.5}B'_{0.5}O_3$. For the data set collected at 2 K the crystal structure could be refined in the orthorhombic structure with the space group *Pnma* ($GdFeO_3$-type). The results of the structure refinements are summarized in Tables 1 to 3. From our SQUID-measurements the susceptibility data of Sr_2CrTaO_6 and Sr_2FeTaO_6 show maxima at 6 K and 17 K, respectively. However, for all the investigated compounds no magnetic Bragg reflections could be detected at low temperature in the neutron powder patterns. This indicates the presence of spin-glass behaviour.

***Table 1**: Crystal structure parameters of Sr_2CrTaO_6 at 2 K.*

*I*4/*m*	site	*x*	*y*	*z*	*B* (Å^2)
Sr	4*d*	0			0.52(3)
Cr(Ta)	2*a*	0	0	0	0.10(3)
Ta(Cr)	2*b*	0	0		0.10(3)
O1	4*e*	0	0	0.252(4)	0.40(3)
O2	8*h*	0.272(2)	0.229(2)	0	0.40(3)

a = *b* = 5.5562(1) Å, *c* = 7.8721(3) Å

***Table 2:** Crystal structure parameters of Sr_2MnTaO_6 at 2 K.*

*I*4/*m*	site	*x*	*y*	*z*	*B* (Å^2)
Sr	4*d*	0			1.20(6)
Mn(Ta)	2*a*	0	0	0	0.69(20)
Ta(Mn)	2*b*	0	0		0.69(20)
O1	4*e*	0	0	0.252(4)	1.33(4)
O2	8*h*	0.272(2)	0.229(2)	0	1.33(4)

a = *b* = 5.5920(2) Å, *c* = 7.9299(5) Å

***Table 3:** Crystal structure parameters of Sr_2FeTaO_6 at 2 K.*

Pnma	site	*x*	*y*	*z*	*B* (Å^2)
Sr	4*c*	0.0041(12)		0.9994(8)	0.54(3)
Fe,Ta	4*a*		0	0	0.06(2)
O1	4*c*	0.4958(15)		0.0425(6)	0.21(6)
O2	8*d*	0.2607(8)	0.0239(3)	0.7395(8)	0.57(4)

a = 5.6015(1) Å, *b* = 7.9116(2) Å, *c* = 5.6153(1) Å

References:

[1]. C.J. Howard, P.W. Barnes, B.J. Kennedy, P.M. Woodward, Acta Cryst. B**61**, 258, 2005.

[2]. Y. Krockenberger, M. Reehuis, M. Tovar, K. Mogare, M. Jansen, L. Alff, J. Magn. Magn. Mater., in print

[3]. J.-H. Choy, J.-H. Park, S.-T. Hong, and D.-K. Kim, J. Solid State Chem. **111**, 370, 1994.

	EXPERIMENTAL REPORT **Field-induced magnetism in pressure tuned $CeRhIn_5$**	Proposal N° PHY-02-0527 Instrument **V2** Local Contact K. Habicht, N. Stüßer
Principal Proposer: Experimental Team:	M. Nicklas – MPI-CPfS, Dresden O. Stockert – MPI-CPfS, Dresden T. Park – LANL, USA K. Habicht, N. Stüßer – HMI, Berlin	Date(s) of Experiment 07.04. – 13.04.2006 05.09. – 06.09.2006 30.10. – 06.11.2006

Date of Report: *

At atmospheric pressure the heavy fermion antiferromagnet (AF) $CeRhIn_5$ orders below T_N=3.8K [1] in an incommensurate structure with propagation vector Q= (1/2,1/2, 0.297) and an ordered moment μ_0=0.84 μ_B [2]. On applying pressure $CeRhIn_5$ can be tuned from a purely antiferromagnetic (AF) ground state to coexisting superconductivity (SC) with AF. Above a critical pressure $p_1 \approx 1.9$ GPa only SC is reported in zero-magnetic field. However, in applied magnetic field a field-induced magnetic phase has been reported to coexist with the SC phase [3,4].

The aim of this neutron diffraction experiment was to elucidate the nature of the field-induced, supposedly magnetic, phase appearing above p_1. In order to generate pressures up to 2.5 GPa we used a double-wall piston-cylinder-type pressure cell consisting of an inner cylinder made of NiCrAl and a outer body of CuBe. Fluorinert served as pressure transmitting medium. The pressure inside the cell was determined in a separate experiment by the inductively measured shift of the superconducting transition temperature (T_c) of a Pb sample inside the pressure cell close to the $CeRhIn_5$ sample compared with T_c of a piece mounted outside.

The elastic neutron diffraction experiment was carried out on V2 using the vertical magnet VM3 and a dilution stick in order to reach fields up to 5 T and temperatures down to 50 mK. Neutrons with an incident wave vector k_I = 2.3 $Å^{-1}$ were used to optimize the intensity. To reduce the background and to improve the signal-to-background ratio the energy analysis of the TAS V2 was inevitable.

The $CeRhIn_5$ sample was mounted with the (110) axis parallel to the axis of the pressure cell and, respectively parallel to the direction of the magnetic field fixing the scattering plane to (110). We carried out experiments at two different pressures, first at 2.14 GPa and, after releasing part of the pressure, at 1.86 GPa. The first pressure was chosen to be in the in the purely SC state at zero magnetic field, where a presumably magnetic phase is reported for B>4 T. The second pressure point is close to the critical pressure where the AF phase disappears and only SC remains in B=0, but presumably on the side where the AF ground state is supposed to coexist with the SC state at zero magnetic field.

We verified the orientation of the sample by measuring selected nuclear peaks. The signal to background ratio was optimized at the (003) and (220) reflection, respectively, in order to reduce the large incoherent scattering contribution due to the pressure cell. At both pressure we looked carefully for magnetic peaks. We mainly concentrated on a propagation vector in the (1/2,1/2, l) direction, where AF order has been reported previously at Q= (1/2,1/2, 0.297) at pressures up to 1.6 GPa at 1.8 K in zero magnetic field. In addition, we looked at all principal direction. Whereas we focused on measurements in 5 T, the highest accessible field, where the existence of magnetic order inside the SC phase was suggested by specific heat experiments, we also measured carefully at 0 T at the same positions in reciprocal space. Despite a very careful investigation and long counting times we could not detect any magnetic intensity neither at 2.14 GPa nor at 1.86 GPa, although the resolution of our experiment was comparable to previous measurements at lower pressures and higher temperatures [2] finding incommensurate AF order in the purely magnetic state.

References:

[1]. H. Hegger et al., Phys. Rev. Lett. 84, 4986 (2000).
[2]. A. Llobet et al., Phys. Rev. B 69, 024403 (2004); W. Bao, et al., Rev. B 62, R14621 (2000).
[3]. T. Park et al., Nature 440, 65 (2006).
[4]. G. Knebel et al., Phys. Rev. B 74, 020501(R) (2006).

	EXPERIMENTAL REPORT **Magnetic Ordering of Charge Ordered Manganites**	Proposal N° PHY-02-0528 Instrument **V2** Local Contact Klaus Habicht
Principal Proposer: Experimental Team:	D. Senff – Uni Köln M. Braden – Uni Köln O. Schumann – Uni Köln K. Habicht – HMI, Berlin	Date(s) of Experiment 31.01. – 14.02.2006

Date of Report: 10.12.2006

Charge ordering is today in the center of interest in the physics of CMR-manganites; the metal-insulator transition seems to result from a close competition between FM metallic and these charge ordered insulating states.

In our recent work we focused on the charge ordered states in single layered manganites $La_{1-x}Sr_{1+x}MnO_4$ around half doping and analysed the static and dynamic spin correlations in a series of neutron scattering experiments [1]. At the FLEX-spectrometer we proposed to extend these studies of the two compounds with doping x=0.5 and 0.4 (i) to polarized neutrons, and (ii) to the influence of strong magnetic fields.

At the beginning of the experiment the FLEX-spectrometer was equipped with the polarization devices yielding typical flipping ratios on structural Bragg-reflections as good as I^{++}/I^{+-}~15. In the second half, we operated the spectrometer in the classical TAS set-up with the 14.5T magnet mounted on the sample table. In this report, we will restrict ourselves to a brief discussion of the results obtained in this second part of the experiment. All scans were performed with the energy of the neutrons fixed to 8.3meV. Two samples of the x=0.4-compound were studied, one with the [001]- and the other with the [110]-direction aligned parallel to the external field.

In $La_{0.6}Sr_{1.4}MnO_4$, the combined charge, orbital and spin ordering of the CE-type is considerably disturbed. Elastic diffuse magnetic scattering suggests a scenario, in which the typical FM zig-zag chains of the CE-type pattern are formed, but the correlations between the chains are significantly disturbed. In Fig. 1 we summarize the field-response of this complex ordered state. Macroscopic magnetisation reveals an instability towards ferromagnetic ordering, as e.g. a magnetic field of 14T induces a large magnetic moment of ~1.5μ_B. On FLEX, we could easily detect this large induced moment, and the field-dependence of the (002)-Bragg reflection scales nicely with the macroscopic data (see Fig. 1). Moreover, the data acquired on FLEX allow us to determine the microscopic origin of the magnetic response: the raw data scans presented in Fig. 2 prove that the applied field suppresses the diffuse magnetic scattering while the quarter-indexed CE-reflexes remain unaffected.

We think this behaviour has to be interpreted in a picture where well-aligned CE-type phases coexist with somehow disordered regions which both exhibit a different response to the applied magnetic field. However, further studies using e.g. small angle scattering are needed to strengthen this interpretation.

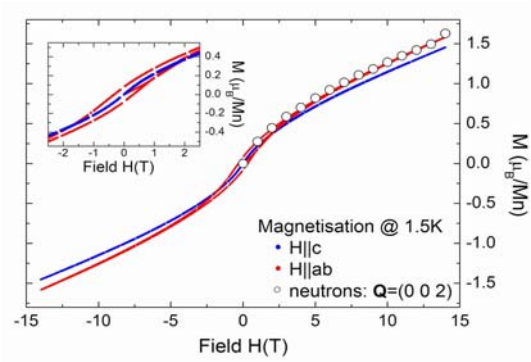

Fig 1.: *Macroscopic magnetisation of $La_{0.6}Sr_{1.4}MnO_4$ at low temperatures and field response of the (002)-reflex measured at FLEX.*

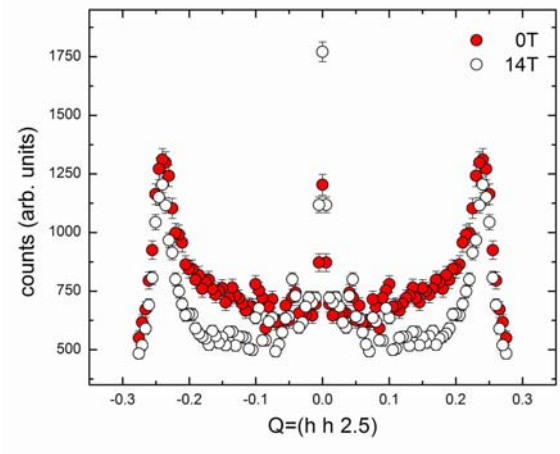

Fig 2.: *Raw-data scans aiming at the field dependence of the CE-type and the diffuse magnetic scattering. The strong magnetic field suppresses the diffuse scattering, while the quarter reflexes are unaffected.*

Reference:

[1]. D. Senff *et al.*, Phys. Rev. Lett. **96**, 257201 (20

	EXPERIMENTAL REPORT **Magnetic smectic phase in spin ice?**	Proposal N° PHY-02-0557 Instrument **V2** Local Contact Kirrily Rule
Principal Proposer: Experimental Team:	T. Fennell – UCL, UK T. Fennell – UCL, UK D. McMorrow – UCL, UK S. Bramwell – UCL, UK K. Rule – HMI, Berlin	Date(s) of Experiment 14.08. – 21.08.2006

Date of Report: 19.10.2006

$Ho_2Ti_2O_7$ is a spin ice: a frustrated magnet on the pyrochlore lattice in which the extensively degenerate manifold of ground state spin configurations maps onto the manifold of proton configurations in ice. Strong anisotropy means that the properties of spin ice materials in applied magnetic field are strongly direction dependent. When the field is applied along the [111] direction it is parallel to one of the spins on each tetrahedron and at an angle of 35° to the other three. These three spins are part of a kagome lattice (corner sharing triangles), perpendicular to the field. In intermediate fields the exchange energy competes with the Zeeman energy to maintain the ice rule resulting in a magnetization plateau, in which the system is named kagome ice. The pinning of the interstitial sublattice reduces the dimensionality of the system from 2-d to 3-d, as the kagome layers are decoupled. The reduction of dimensionality allows the mapping of the remaining degrees of freedom to a dimer model on a honeycomb lattice leading to a detailed description that includes the dynamics of the plateau phase and its termination. Neutron scattering studies have shown a strange critical point which we believe to be a manifestation of the Kasteleyn transition, a unique property of the honeycomb dimer model which is due to the manipulation of dimer activities. The transition can be realized in spin ice by tilting the field away from [111] and since we already have data in a slightly tilted field, we aimed to carry out a similar study in zero tilt using V2.

In fact, we were unable to achieve zero tilt, the field being applied at approximately 0.5° to [111] (about half the tilt used in our previous experiments). Again we observed the critical-like scattering at -1,-1,2 which we have subsequently shown is definitely due to the tilt of the field. Evidently kagome ice is extremely sensitive to this field tilt. The scattering at -1,-1,2 feature should show two maxima in the kagome ice phase which drift together as the field (or tilt) is increased toward the Kasteleyn transition. Our observations of this splitting and its field dependence were very unclear.

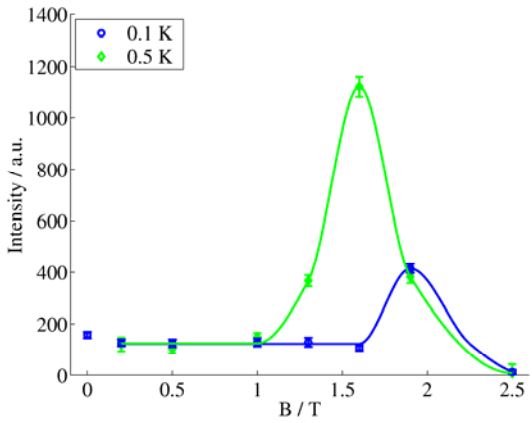

Fig. 1: *Intensity of the critical-like scattering at -1,-1, 2. This is consistent with our other data which suggests that the critical temperature (here probably somewhere between these measurements) depends on the tilt and that the critical point is the intersection of a line of Kasteleyn transitions with the always-existing/zero tilt plateau termination process.*

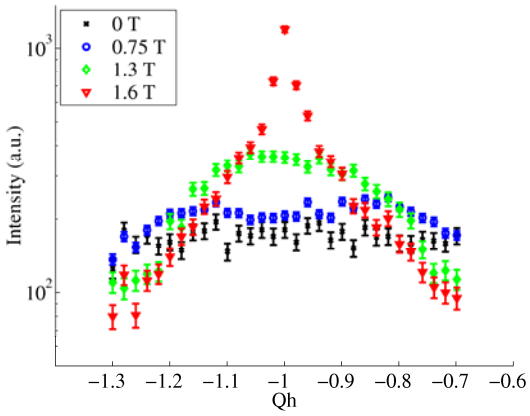

Fig. 2: *Transverse lineshape of the -1,-1,2 scattering as a function of field at 0.5 K. The splitting supposed to be characteristic of kagome ice (blue) is barely discernible.*

	EXPERIMENTAL REPORT **Larmor diffraction measurement of relative changes in lattice-spacing of MnF_2**	Proposal N° PHY-02-0598-EF Instrument **V2** Local Contact Klaus Habicht
Principal Proposer: Experimental Team:	K. Habicht – HMI, Berlin K. Habicht – HMI, Berlin K. Rule – HMI, Berlin	Date(s) of Experiment 01.06. – 04.06.2006 21.09. – 23.09.2006

Date of Report: 10.01.2007

Originally intended to serve as a demonstration experiment for training purposes in the frame of the PNCMI School 2006, an NRSE experiment was performed aimed at measuring changes in lattice spacing in the classical antiferromagnet MnF_2. In view of the recent discovery of anomalous displacement of magnetic Bragg peaks in the presence of short range order observed by resonant x-ray scattering [1], it is interesting to complement such measurements with neutron diffraction data. In principle this requires to measure an incommensurate shift of a magnetic Bragg peak relative to the underlying lattice. During the limited beam time at V2/FLEX we were able to test the sensitivity of the method on the nuclear (101) Bragg peak in Larmor diffraction geometry (see e.g. [2]) and perform spin-echo scans on the magnetic (100) Bragg peak in standard spin-echo mode. Due to restrictions in incident wavevector k_I imposed by the V2 transmission polarizers which are suitable for wavevectors $k \leq 1.7$ $^{-1}$ only, Larmor diffraction geometry could not be realized for a purely magnetic Bragg peak.

V2/FLEX was operated in a configuration with scattering senses (SM=-1, SS=+1, SA=-1) at fixed $k_i = k_f = 1.4$ $^{-1}$ or $k_i = k_f = 1.16$ $^{-1}$ for the nuclear (101) reflection and the magnetic (100) reflection respectively. The MnF_2 crystal was aligned in the (h0k) scattering plane. No additional collimators were used besides the transmission polarizers behind the PG monochromator and the PG analyzer. The absence of a PG-filter is in fact leading to a substantial second-order contamination. This effect however appears only as background, i.e. in a reduction of the echo-polarization which was typically P=30-40%. The NRSE option was operated in bootstrap-mode with an effective frequency f_{eff} = 1.2 MHz. For the (101) measurements the tilt angles of the RF-flippers were θ_1= -35.15° and θ_2= 35.15° and the same relative orientation of precession fields, whereas (100) measurements were taken at $\theta_{1,2}$= 0° and opposite relative orientation of precession fields.

Close to the Néel temperature T_N=67.5 K phase-sensitive spin-echo scans have been taken by varying the length of the second precession field region, i.e. by translating the last RF-flipper around two positions (see Fig. 1). The phase-shift as a function of temperature has been converted to a relative change of d-spacing defining Δd(T=56K)=0.

Fig.2 shows that the relative change in d-spacing exhibits substantial hysteresis upon heating or cooling the sample. The phase shift observed at the (100) in spin-echo scans is negligible on the scale of the large changes in d as observed at (101). Above T_N the polarization is lost immediately and no phase information can be extracted from the spin-echo scans.

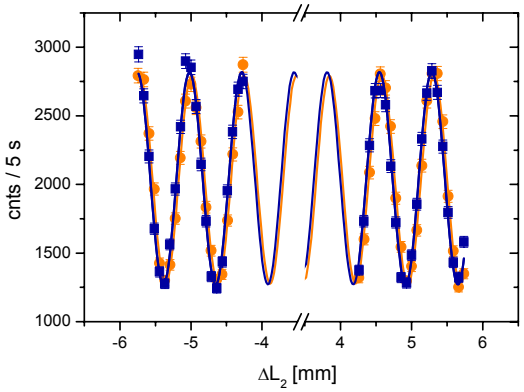

Fig. 1: *Two typical spin-echo scans at temperatures T=63.5 K (circles) and T=64.5K.*

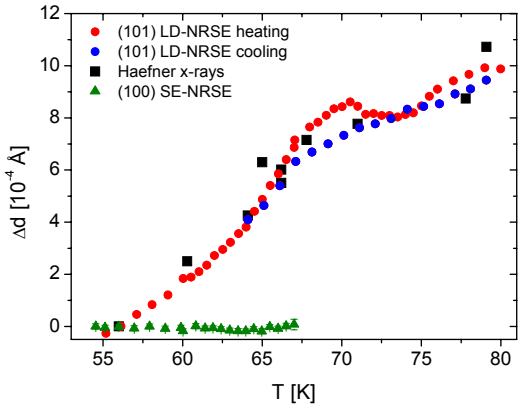

Fig. 2: *Temperature dependence of the variation in lattice spacing Δd as extracted from phase-sensitive NRSE scans (circles). For comparison x-ray data from [3] (squares) and data obtained from spin-echo scans at (100) converted into Δd with the same scaling factor are also shown (triangles).*

I am indepted to W.Jauch for loan of the MnF_2 crystal.

References:

[1]. N. Bernhoeft *et al.*, J. Phys. Cond. Mat. **16**, 3869 (2004)

[2]. M.T. Rekveldt, T. Keller, R. Golub, Europhys. Lett. **54**, 342 (2001)

[3]. K. Haefner, Thesis University of Chicago 1964

BENSC	**EXPERIMENTAL REPORT** **High resolution diffraction and small angle scattering neutron investigations of $LaCo_{0.5}Mn_{0.5}O_{3+\delta}$: effect of oxygen content**	Proposal N° PHY-04-1192 Instrument **V4** Local Contact André Heinemann
Principal Proposer: Experimental Team:	K. Bärner – Uni Göttingen D. V. Karpinsky – JISSSP NAS, Minsk, Belarus A. Heinemann – HMI, Berlin	Date(s) of Experiment 17.01. – 22.01.2006

Date of Report: 05.01.2007

$LaCo_{0.5}Mn_{0.5}O_{3+\delta}$ compounds with different oxygen content have been investigated by means of magnetization, high resolution and small-angle neutron diffraction measurements. Authors have estimated that scattering regions for both of the studied samples (δ=-0.03, 0.05) have nearly spherical shape and temperature dependent size (figure). At low temperature a coalescence of the mentioned clusters begins. But for the as-prepared sample one can observe such a percolation about 100 K whereas for the oxygen deficit sample a coalescence occurs below 20 K only. These clusters start melting with temperature increase and have less than hundred angstrom size near the magnetic transition temperature. At high temperatures the interactions between such formations are almost neglible. From the analysis about valence and spin state of antisite defects and taking into account magnetization measurements one can suppose that mentioned clusters most probably have AF nature (Co^{2+} or Mn^{4+} enriched). That for the oxygen deficit sample clusters coalescence occurs at such a low temperature can be explained by model, according to which Mn^{3+} ions participate in newly generated ferromagnetic interactions with Mn^{4+} ions, thus decreasing AF clusters size. As the as-prepared sample does not contain any noticeable amount of Mn^{3+} ions, they have not such influence on magnetic interactions. Whereas Co^{3+} ions being in the low spin state do not participate actively in the interatomic coupling keeping AF clusters as they formed by synthesis process. The investigations performed incline authors that magnetic structure of the samples assumes spin-glass component within the samples. Parallel with long range magnetic ordering which is undoubtedly exists as seen from magnetization and high resolution neutron study a small spin-glass component play a certain role in magnetic properties of the samples. The most probable scenario explaining magnetic properties of the compounds assumes a coexistence of long-range ferromagnetic matrix with Co^{2+} - Mn^{4+} dominated interactions and clusters with short range antiferromagnetic coupling. Most probably the key role in magnetic properties determination plays a valence state of transition metal ions rather than their ordering. This provides an indication of intricate behavior of the magnetic materials under study what assert a further interest of them to a scientific community.

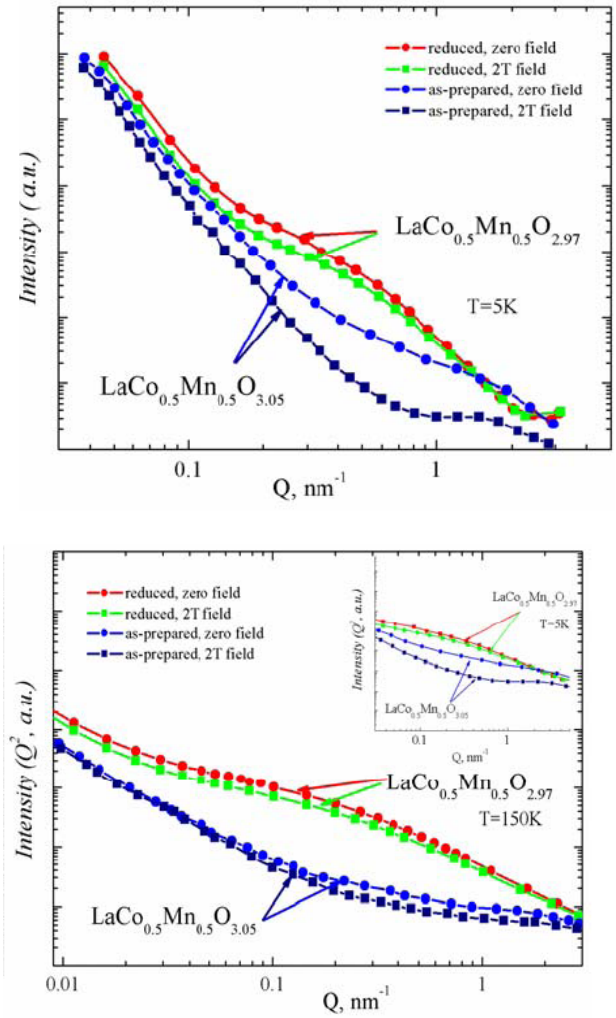

Fig. 1+2: *I(Q) and I(Q2) dependences of the SANS intensity for the oxygen deficit and the prepared compounds.*

	EXPERIMENTAL REPORT **Time-resolved SANS study of superparamagnetic particles in an oscillating magnetic field**	Proposal N° PHY-04-1243-EF Instrument **V4** Local Contact Albrecht Wiedenmann
Principal Proposer: Experimental Team:	A. Wiedenmann – HMI, Berlin J. Kohlbrecher – PSI, CH J. Kohlbrecher – PSI, CH A. Wiedenmann – HMI, Berlin	Date(s) of Experiment 07.04. – 13.04.2006 15.05. – 18.05.2006

Date of Report: 17.01.2007

Dynamical studies of nanoszied inhomogneities by means of SANS have been reported previously on magnetic colloids where the moment reversal was governed by the slow Brownian rotation of superparamagnetic particles [1,2]. The aim of the experiment was to apply this technique to alloy systems where nanosized particles of controlled sizes were embedded in a solid matrix preventing any particle rotation. The samples with the radius of the magnetic precipitates are collected in Table 1. We used a stroboscopic technique with a continuous neutron flux by a applying a periodic sine wave modulation of the magnetic field up to 200 Gs. The dynamics of the reorientation of particle moments could be followed up to about 500Hz, limited by the damping of the oscillations due to the 11% spread of the neutron flight times.

Table 1: *Samples investigated, particle radius*

CuCo (0.8%)	CuCo (0.4%)	CuNiFe-a	CuNiFe b	Finemet
4.7 nm	3.9	4.9	13.2	5.4

The reversal and reordering of magnetic particle moments was expected to be governed by the Neel mechanism where the characteristic time is given by $\tau_N = f_o \exp(K_A V_c / k_B T)$ which strongly depend on the particle size and the aniosotropy constant K_A. For frequencies $\upsilon < 1/\tau_N$ the response of the system is expected to follow the applied external magnetic field i.e. the scattering intensities would oscillate as a function of time following the Langevin dynamics as described in Eqn. 3 of ref [1]. Approaching the critical frequency $1/\tau_N$ an increasing phase shift is expected between the inducing field and the response. For $\upsilon > 1/\tau_N$ the particle moments are expected to be blocked and the oscillations should disappear. We hoped to find a system for which the critical frequency would be inside the experimental window. This was expected for CuCo by using the particle volume and the literature value of K_A for fcc Co. In Fig. 1 we show the scattering intensities for CuCo0.8 in an oscillating field of 0.02 T integrated over angle sectors along and perpendicular to the magnetic field. The solid lines are fits according to Eqn. 3 of ref [1]. It turned out that all curves could be fitted simultaneously with the same parameters as observed for the static magnetic field of the same strength. I.e. up to 500 Hz there is no blocking of the magnetic moments, which shows that either K_A or the magnetic particle volume must be smaller than expected.

The phase shift has been determined individually for all frequencies showing only a small difference with respect to the instrumental phase shift between the trigger signal and magnetic field. Similar behaviours was found for the other samples. We plan to repeat these measurements at low temperatures by which the critical frequency should be exponentially decreased allowing the crossover from oscillating to static behaviour to be monitored.

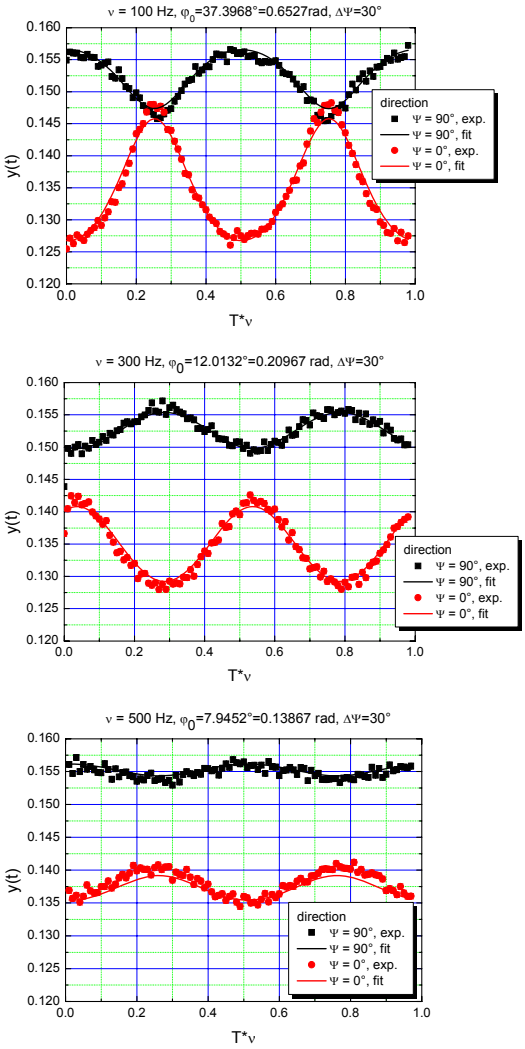

Fig. 1: *SANS intensities of CuCo(0.8%) as a function of time in an oscillating magnetic field for differnet frequencies. Solid line fit to eq 3. ref [1].*

References:

[1]. A. Wiedenmann et al. PRL 97,057202
[2]. A. Wiedenmann et al. BENSC report 2006

	EXPERIMENTAL REPORT **PNR study of the re-entrance of the untrained state in a Co/CoO exchange bias system**	Proposal N° PHY-04-1229 Instrument **V6** Local Contact Roland Steitz
Principal Proposer: Experimental Team:	K. Temst – KU Leuven, B K. Temst, J. Mohanty – KU Leuven, B S. Brems – KU Leuven, B R. Steitz – HMI, Berlin	Date(s) of Experiment 22.06. - 02.07.2006

Date of Report: 10.09.2006

The aim of this proposal was to study in detail so-called training effects in a Co/CoO ferromagnet/antiferromagnet exchange bias system. Exchange bias refers to a strong coupling at the interface between the ferromagnet and the antiferromagnet and manifests itself as an increase in coercivity and a shift of the hysteresis loop along the field axis after field cooling through the Néel temperature of the antiferromagnet. In the Co/CoO system it has been observed that the resulting hysteresis loop is asymmetric, hinting at the occurrence of two different magnetization reversal mechanisms in the two branches of the loop. Furthermore, it has been observed that the loop shape changes after application of subsequent hysteresis loops. The initial loop shape could only be recovered after heating the sample above the Néel temperature and starting the field cooling procedure again. Recently [1] we discovered that the untrained state can, at least partially, be recovered without any heating. Rather, a re-entrance of the untrained state was induced by applying a magnetic field perpendicular to the initial field cooling direction. Apparently the application of the perpendicular field can markedly change the magnetization configuration of the ferromagnet and the antiferromagnet. It was the intention to study, therefore, in detail the magnetic profile while going through this measurement procedure.

The experiments were carried out on the V6 reflectometer, which was first optimized again for the use of polarized neutrons and spin analysis after the refurbishment work performed in the experiment hall. As sample a Co/CoO layer was used with 20 nm Co and 2 nm CoO on top. The sample is prepared by sputtering a Co layer on a Si/SiO_2 wafer and oxidizing it in situ in a reduced oxygen atmosphere. X-ray reflectivity and atomic force microscopy measurements indicated a low-roughness surface. The sample was placed in a cryocooler and a magnetic field can be applied using an electromagnet.

Figure 1 shows the spin-analyzed specular reflectivity measured at 15 K after field cooling in a field of 0.4 T. The untrained reversal is measured in a field of 0.105 T and indicated a reversal by domain wall nucleation and motion. A subsequent measurement in 0.058 T (the trained loop) is characterized by a markedly increased spin-flip contribution, indicating that rotation of the magnetization has become more important.

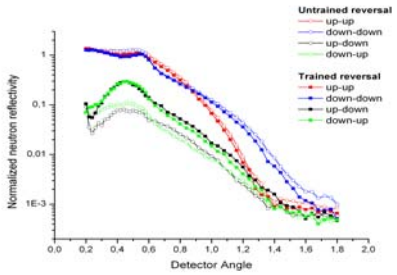

Fig. 1

After this measurement, a hysteresis loop is performed (with a field up to 0.15 T) in the in-plane direction perpendicular to the cooling field. After this perpendicular loop a specular PNR measurement is carried out in a field of 0.083 T. Figure 2 shows these data, for clarity again compared with the trained loop already shown in Fig. 1. It is clear that the spin-flip contribution has decreased again. At present we are trying to fit these specular data in order to analyze the magnetic depth profile.

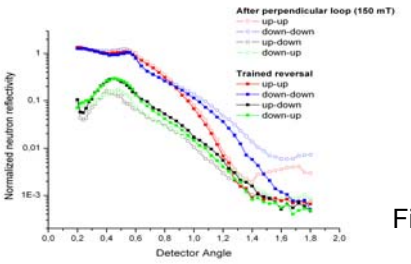

Fig. 2

For future work, we plan to extend these measurements by studying the importance of the magnitude of the maximum field in the perpendicular loop, since recent magnetoresistance measurements suggest a strong influence.

Reference:

[1]. S. Brems et al., Phys. Rev. Lett. **95**, Art. No. 157202 (2005)

	EXPERIMENTAL REPORT PNR study of a Co/CoO film with pattern-induced in-plane anisotropy	Proposal N° PHY-04-1328 Instrument **V6** Local Contact Roland Steitz
Principal Proposer: Experimental Team:	K. Temst – KU Leuven, B K. Temst – KU Leuven, B R. Steitz – HMI, Berlin	Date(s) of Experiment 07.12. – 12.12.2006

Date of Report: 04.01.2007

The aim of this proposal was to study in detail a Co/CoO film in which a lattice of submicrometer-sized holes (defined by electron beam lithography) is present. Earlier work had shown that the presence of such holes in a ferromagnetic Co-film leads to an artificially induced in-plane anisotropy that is defined by the size of the holes and the distance between them. A new element in this work is that the Co layer is covered by a thin CoO layer, turning it into an exchange bias system, when cooled in the presence of a magnetic field.

The sample was produced by evaporation of a 20 nm thick Co layer in a molecular beam epitaxy system, followed by an in situ oxidation process by exposing the sample to areduced oxygen atmosphere. A lift-off step finalized the lithography procedure. The sample was characterized by atomic force microscopy and its magnetic properties were measured by SQUID magnetometry. It was found that at the lowes temperatures (4 K) the unidirectional anisotropy resulting from exchange bias strongly dominates any other anisotropy contribution. The situation is entirely different at higher temperatures, however, especially in the temperature zone (around approx. 130 K) where a 'positive exchange bias' can be observed. SQUID measurements indicate a clear in-plane anisotropy of the exchange bias field in this temperature region.

These PNR experiments therefore had the goal to explore what happens to the magnetization reversal at 130 K. It is well-known that at lower temperatures, Co/COO systems show a clear asymmetric behaviour: the magnetization reversal mechanism is different in both branches of the hysteresis loop. The experiments were carried out on the V6 reflectometer. The sample was placed in a cryocooler and a magnetic field can be applied using an electromagnet.

Figure 1 shows the spin-analyzed specular reflectivity measured at 130 K after field cooling in a field of 0.4 T. The applied field equals -0.012 T. This is at the left hand side of the hysteresis loop, where typically in Co/CoO at low temperatures a reversal by domain wall nucleation and motion is observed. Also in this case, there is only a very limited contribution from spin-flip scattering, suggesting a reversal by domain wall motion.

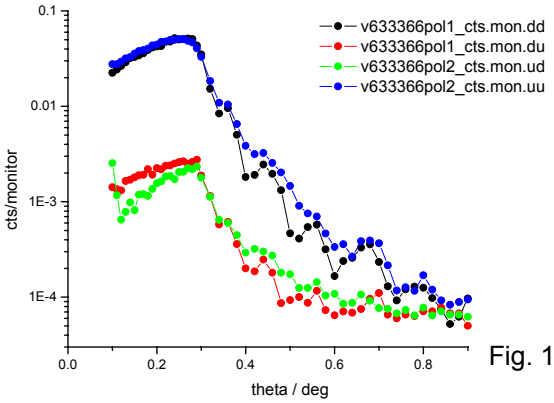

Fig. 1

Figure 2 shows the specular reflectivity at 0.012 K, i.e., at the right hand side of the hysteresis loop. At low temperatures, Co/CoO typically displays a reversal by rotation in this branch of the loop. However, the behaviour at 130 K is much more similar to what happens at the left hand side coercive field, namely a small spin flip signal and a much larger non-spin flip signal, suggesting again domain wall motion. At present we are trying to fit these specular data.

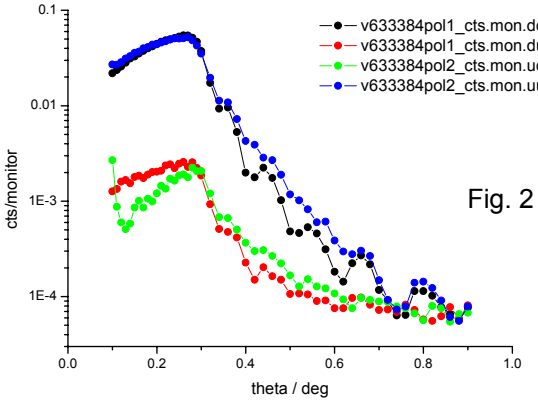

Fig. 2

BENSC	**EXPERIMENTAL REPORT** **Bose-Einstein condensation in a quantum magnet with varying spin-anisotropy**	Proposal N° PHY-02-0529 Instrument **V2** Local Contact Klaus Habicht
Principal Proposer: Experimental Team:	B. R. Hansen – ETHZ & PSI, CH M. Kenzelmann – ETHZ & PSI, CH K. Habicht – HMI, Berlin	Date(s) of Experiment 09.03. – 19.03.2006

Date of Report: 13.04.2006

DTN ($NiCl_2$•$4SC(NH_2)_2$) is a spin-1 quantum magnet with a tetragonally coordinated lattice, where the spins are strongly coupled along the crystallographic c-axis and only weakly between these chains [1]. Due to a uniaxial crystalline field, the S=1 spin triplet is split leaving a singlet ground state and S_z=±1 as excited states. Applying a magnetic field along the tetragonal axis at close to zero temperature causes a quantum phase transition (QPT) as one of the excited doublet states mixes with the ground state singlet. As a result long-range antiferromagnetic order is induced in the system at H_c= 2.1T. Such a field induced magnetic ordering at zero temperature has been shown theoretically to be described as a Bose-Einstein Condensation of magnons [2]. Furthermore, DTN is a rare example of a quantum magnet belonging to the three-dimensional XY universality class as has been shown by a careful measurement of the critical exponent α=1.5 [1].

To elucidate the nature of the quantum phase transition manifested by DTN, we performed inelastic neutron scattering measurements using the triple-axis spectrometer FLEX (V2) utilizing the 6T horizontal field magnet HM1 with a dilution stick insert. Four deuterated single crystals with a combined weight of more than 4g were used.

Selected plots of the experimental data are presented in Fig. 1. Fig. 1a shows that the zero-temperature excitations splits in a magnetic field into two excitations due to its doublet nature, and the gap closes as the field increases. Fig. 1b illustrates the different natures of the magnetic excitations on the zone boundary at the critical field and at the maximum obtainable field of 6T. While the lower excitation on the zone boundary is well-defined at H=2.1T, this is seen not to be the case for an applied field of 6T.

From the scans at higher applied fields one interesting result of the analysis is that the gap appears to reopen at 6T indicating a small symmetry breaking. Further experiments will be needed to understand the origin of this anisotropy, its energy scale and its influence on the QPT.

We also measured the field dependence of the order parameter and a preliminary analysis suggests a critical exponent β=0.5 consistent with both the 3D Ising and XY universality class.

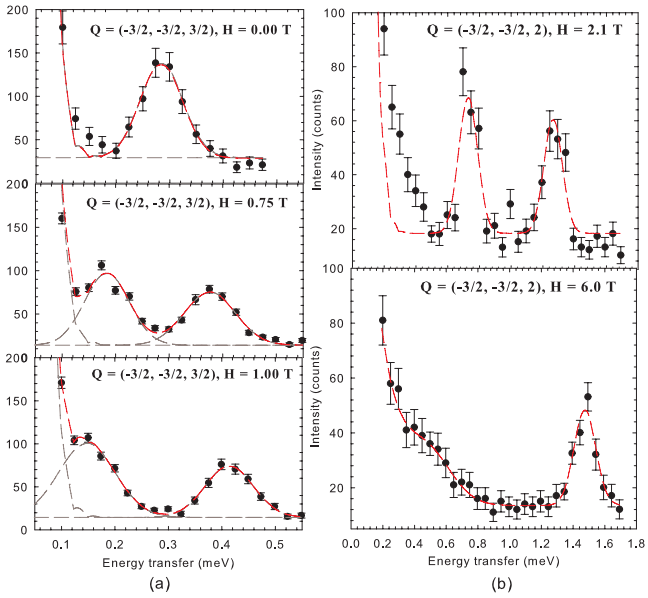

Fig. 1: (a) *Inelastic energy scans at wave vector transfer* ***Q****=(-3/2,-3/2,3/2) at three different applied fields showing the splitting of the excited doublet.* ***(b)*** *Inelastic energy scans on the zone boundary at the critical field* H_c *= 2.1T and H = 6T.*

References:

[1]. V. S. Zapf, D. Zocco, B.R. Hansen *et al.*, Phys. Rev. Lett. **96**, 077204 (2006).

[2]. I. Affleck, Phys. Rev. B **43**, 3215 (1991); E. Sorensen and I. Affleck, Phys. Rev. Lett. **71**, 1633 (1993).

BENSC	**EXPERIMENTAL REPORT** **Spin dynamics of the incommensurate and commensurate phases of PrB_6**	Proposal N° PHY-02-0532 Instrument **V2** Local Contact Kirrily Rule
Principal Proposer: Experimental Team:	K. A. McEwen – UCL, UK J.-G. Park – SKKU Suwon, Korea M. D. Le – UCL, UK K. Rule – HMI, Berlin	Date(s) of Experiment 13.06. – 21.06.2006

Date of Report: 28.07.2006

Praseodymium Hexaboride is a rare-earth metallic compound which exhibits two transitions, at 7K to an incommensurate (IC) antiferromagnetic (AFM) structure and at 4.2K to a commensurate AFM structure, with ordering wave-vector Q = (¼ ¼ ½) [1]. The crystal field (CF) ground state of the Pr^{3+} ion is a Γ_5 triplet, with a first excited Γ_3 doublet at 27meV [2]. Hence the low energy excitations are expected to be due entirely to spin waves from the splitting of the ground state triplet.

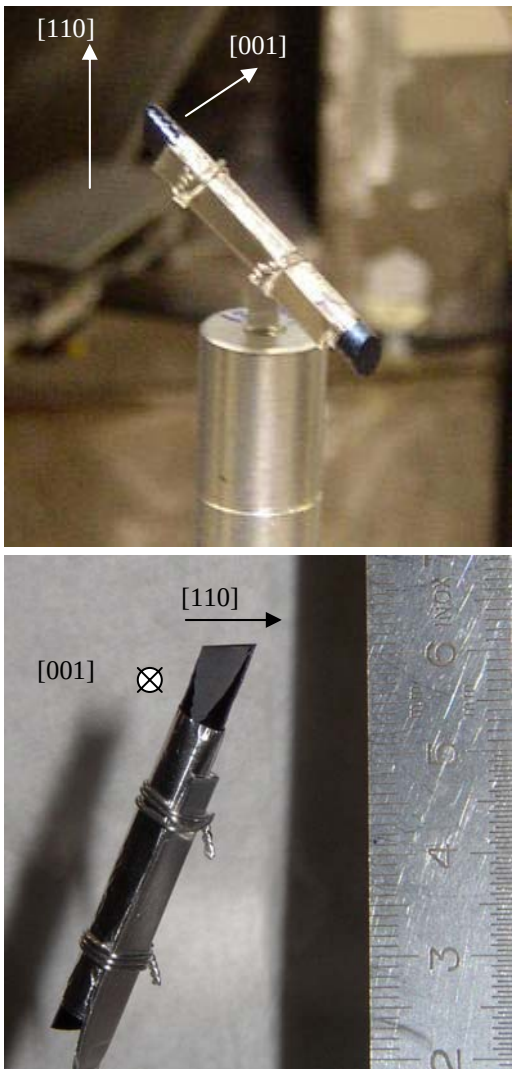

Fig. 1: The PrB_6 single crystal sample as mounted

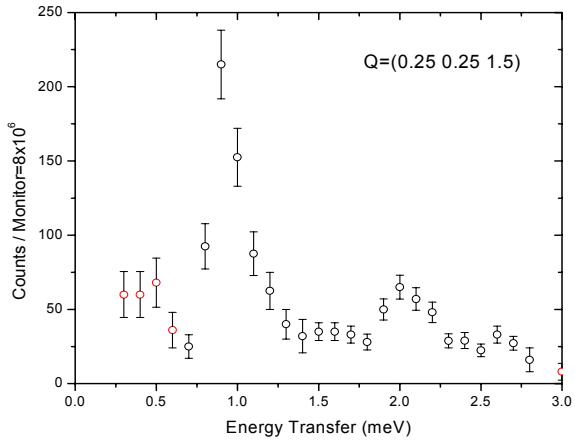

Fig. 2: Scan of the magnetic zone centre at Q = (¼ ¼ 1½). Two modes can be seen at ~1meV and ~2meV energy transfer.

We measured the dispersion of these excitations using the V2 triple axis spectrometer, at 2K, in a -1,-1,+1 configuration with PG(002) monochromator and analyser using 60'-60'-60' collimation. We prepared a large single crystal of PrB_6 using the low absorption isotope ^{11}B (see figure 1) at the University of Hiroshima. Figure 2 shows a typical scan, whilst Figure 3 shows the position of the peaks as a function of energy and momentum transfer.

Two modes can clearly be seen from the data. The modes along the [h h 0] directions show very little dispersion, indicating that there is little exchange coupling in the basal plane. It is known that the IC to commensurate transition has an associated lattice change from cubic to orthorhombic symmetry, and this may be related.

On the other hand, the dispersion for the modes in the [0 0 l] direction may be fitted to a model for spin waves arising from a crystal field splitting [3]:

$$E(q) = [\Delta\{ \Delta - 2n_{01}M_z^2 J_{zz}(q)\}]^{1/2}$$

Where Δ is the CF splitting, n_{01} is the difference in population between the two states, and $M_z^2=|\langle GS|J_z|ES\rangle|^2$ is their matrix element squared. Taking $M_z^2=3.2$ we found that we needed to include at least four nearest neighbours for a good fit, with:

→

Δ	1.67 ± 0.06
J_1	0.12 ± 0.02
J_2	-0.02 ± 0.02
J_3	0.03 ± 0.02
J_4	-0.01 ± 0.01

Table 1: *Values of fitted parameters in meV*

$$J_{zz}(q) = J_1\cos(\mathbf{Q}.[0\ 0\ 1]) + J_2\cos(\mathbf{Q}.[0\ 0\ 2]) + J_3\cos(\mathbf{Q}.[0\ 0\ 3]) + J_4\cos(\mathbf{Q}.[0\ 0\ 4])$$

The fitted parameters are shown in table 1, and the fitted curve in figure 3. The dashed line in figure 3 shows a fit with three nearest neighbours

We were also able to complete some scans in the incommensurate phase between T_{IC}=4.2K and T_N=7K, but because of time constraints were unable to map out how the dispersion changes due to this phase transition. In particular, we observed that the peak at around 1meV energy transfer at the zone centre shifted down in energy by a significant amount in the incommensurate phase, as shown in Figure 4.

Reference:

[1]. P. Burlet et al., J. Phys (Paris) C, **8** (1988) 459

[2]. M. Loewenhaupt and M. Prager, Z. Phys. **62** (1986) 195

[3]. J. Jensen and A. R. Mackintosh, Rare Earth Magnetism, Clarendon Press (1991).

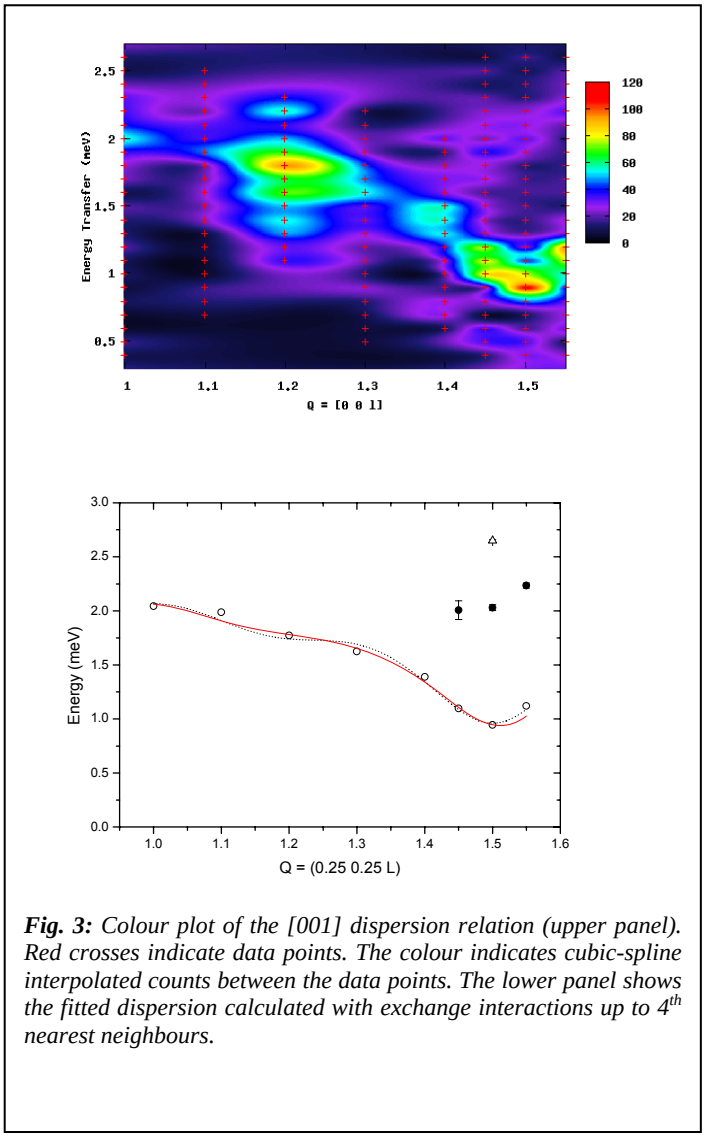

Fig. 3: *Colour plot of the [001] dispersion relation (upper panel). Red crosses indicate data points. The colour indicates cubic-spline interpolated counts between the data points. The lower panel shows the fitted dispersion calculated with exchange interactions up to 4th nearest neighbours.*

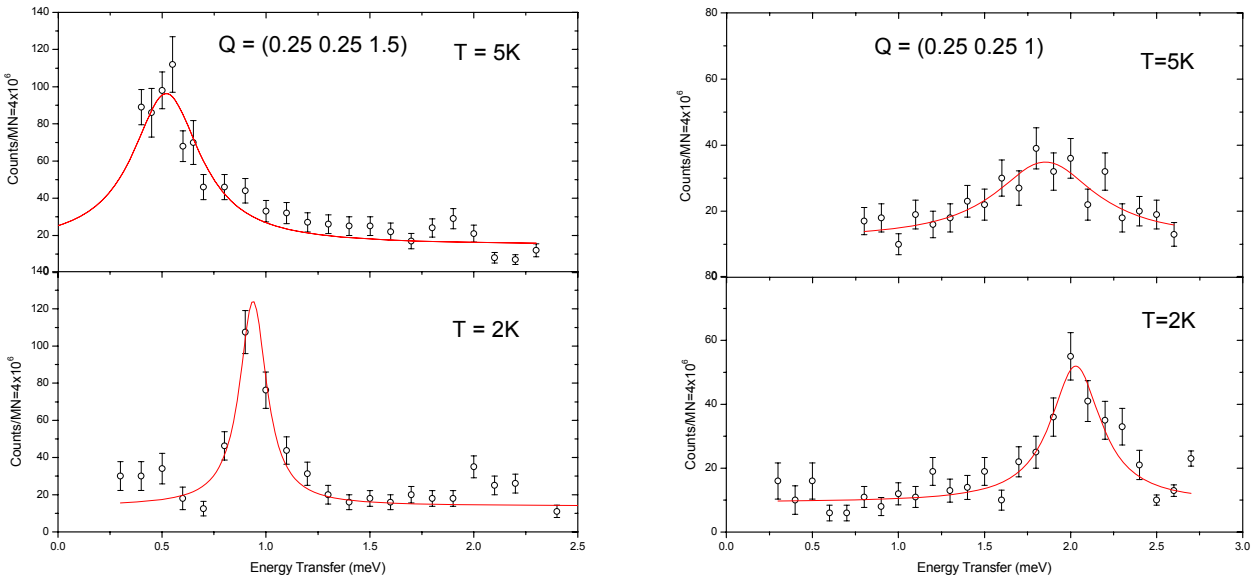

Fig. 4: *Scans at the magnetic Brillouin zone centre (1), left, and zone edge (1), right, in the commensurate (bottom) and incommensurate phase (top). Solid lines are lorentzian fits to the data.*

	EXPERIMENTAL REPORT **Triplet Dispersion and Frustration in the Quasi-2D BEC System $BaCuSi_2O_6$**	Proposal N° PHY-02-0533 Instrument **V2** Local Contact Klaus Habicht
Principal Proposer: Experimental Team:	C. Rüegg – UCL, UK C. Rüegg – UCL, UK A. Walters – RAL ISIS, UK K. Habicht – HMI, Berlin	Date(s) of Experiment 21.06. – 02.07.2006

Date of Report: 08.01.2007

$BaCuSi_2O_6$is a quasi-2D compound comprising layers of spin dimers (S=1/2 Cu2+ ions paired by antiferromagnetic exchange coupling J) arranged vertically on a square lattice [1-5]. In zero magnetic field, each spin dimer has a singlet ground state with three degenerate triplet excited levels. Moderate inter-dimer coupling $J' \approx 0.5$ meV within each layer leads to dispersion of the triplet excitations, see Fig. 1 (a) [1,5] . A magnetic field closes the gap between the singlet level and the lowest triplet excitation (at $k_x = k_y = \pi$) in a critical magnetic field Hc, leading to longrange magnetic order. Hence, a quantum critical point (QCP) at H_c= 23.5 T and T= 0 K separates the quantum paramagnetic regime from the ordered state. Recent experiments on $BaCuSi_2O_6$ probing the critical exponent associated with the QCP indicate that it is possible to describe the phase transition in terms of BEC of triplet states in an extended temperature range close to H_c [4].

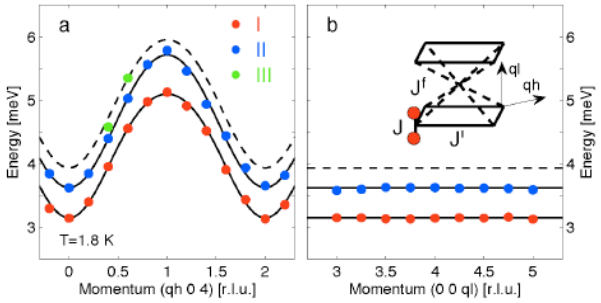

Fig. 1: *Triplet dispersion in* $BaCuSi_2O_6$ *at H=0 T: (a) in the square-lattice plane, (b) perpendicular. From Ref. [5].*

The interlayer antiferromagnetic interaction J_f in $BaCuSi_2O_6$is geometrically frustrated due to the lattice structure, in which square dimmer plaquettes are staggered between consecutive layers (Fig. 1 (b)). The degree of frustration is a crucial parameter to understand a dimensional reduction, which was identified in this material close to the QCP [4]. In earlier INS studies, Ref. [5] and 4F2 (LLB), an upper limit of 0.05 meV was found for the dispersion perpendicular to the square-lattice planes at the relevant points for the QCP. A highresolution and low-temperature INS experiment was performed on FLEX/V2 to further reduce this limit. A compact sample out of 2 big single crystals was used to avoid systematic corrections required by sample geometry. The preliminary results of this experiment are summarised in Fig. 2. The multiple magnon modes [5], related to a structural modulation of the dimer sites, have a maximum bandwidth of the order of 0.02 meV perpendicular to the square-lattice planes. Thanks to the good energy resolution additional information about the geometrical arrangement of the inequivalent sites could be gained via dimer structure factors.

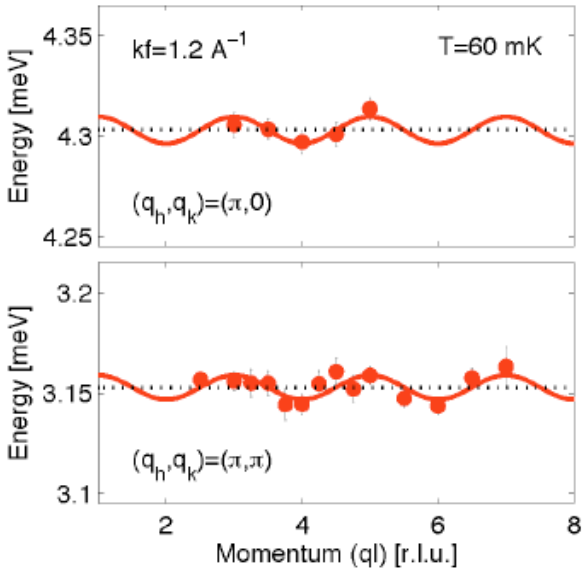

Fig. 2: *Interlayer dispersion in* $BaCuSi_2O_6$ *measured at two in-plane wave vectors with potentially perfect geometrical frustration. FLEX/V2,* k_f*=1.2 Å*$^{-1}$ *and T=60 mK.*

References:

[1]. Y. Sasago et al., Phys. Rev. B **55**, 8357 (1997).
[2]. M. Jaime et al., Phys. Rev. Lett. **93**, 087203 (2004).
[3]. K. Sparta and G. Roth, Acta Cryst. B **60**, 491 (2004).
[4]. S. E. Sebastian et al., Phys. Rev. B **71**, 100404(R) (2005); Nature **441**, 617 (2006).
[5]. Ch. Rüegg et al., Phys. Rev. Lett. **98**, 017202 (2007).

BENSC	**EXPERIMENTAL REPORT** **Field Effect on Spin Fluctuations and Induced Magnetic Order in an N-type Cuprate**	Proposal N° PHY-02-0534 Instrument **V2** Local Contact Klaus Habicht
Principal Proposer: Experimental Team:	S. Wilson – Univ. Tennessee, USA P. Dai – Univ. Tennessee, USA S. Li – Univ. Tennessee, USA K. Habicht – HMI, Berlin	Date(s) of Experiment 11.07. – 24.07.2006

Date of Report: 5.01.2007

The role of magnetism within the underlying mechanism of high-T_c superconductivity remains an issue of considerable debate. In order to investigate the precise interaction of spin dynamics with the superconducting (SC) phase in the high-T_c cuprates, systematic inelastic neutron experiments have been carried out on a variety of cuprate classes over the past two decades. One of the key unanswered questions remains: How does magnetism evolve into the field-suppressed nonsuperconducting (NSC) groundstate of the cuprates? This has proven particularly challenging to answer due to the extremely high magnetic fields required to suppress superconductivity in the hole-doped cuprates (H_{c2}~40-60T). However, electron-doped superconductors have much lower upper critical fields required to suppress superconductivity. Recently, we have shown that the spin fluctuations in the electron-doped cuprates have universal features in the spin spectrum of the cuprates regardless of doped carrier type (holes or electrons) [1,2]. These new neutron studies in N-type cuprates along with the known lower upper critical fields in the n-type cuprates also present the possibility of studying the magnetism in a cuprate system that can now be suppressed into its NSC groundstate.

Our experiments on V2 studied both the static order and low energy spin dynamics in a nearly optimally doped concentration of $Pr_{.88}LaCe_{.12}CuO_{4-\delta}$ (PLCCO T_c = 24K) with a measured $H_{c2}\approx$7T. In this system, we observed field induced static SDW order centred at the Q=(π, π, 0) position. This appears in a PLCCO system with no zero-field SDW order, and the induced order appears only below the zero-field T_c in the field suppressed ground state (under H=H_{c2}). This quantum phase transition from a phase pure SC into a "mixed phase" where both SC and SDW order coexist is similar to that observed in nearly optimally, hole-doped $La_{1.856}Sr_{.144}CuO_4$ [3].

Additionally, quasielastic magnetic scattering, at $\hbar\omega$ < 2meV, was observed to be suppressed under field (Fig. 1). This field induced suppression was observed only below the zero-field T_c of the system (Fig. 1E&F), and the suppression of magnetic intensity at low energies saturated at H~H_{c2} (Fig. 1B). This is highly suggestive that this effect is coupled to the destruction of SC in the sample.

While further experiments are required, we have preliminarily observed the coupling of low energy spin excitations to the suppression of SC in the cuprate PLCCO. This fact along with the observed competition between SDW order and SC suggest a fundamental link between magnetism and the mechanics of the superconducting phase in high-T_c.

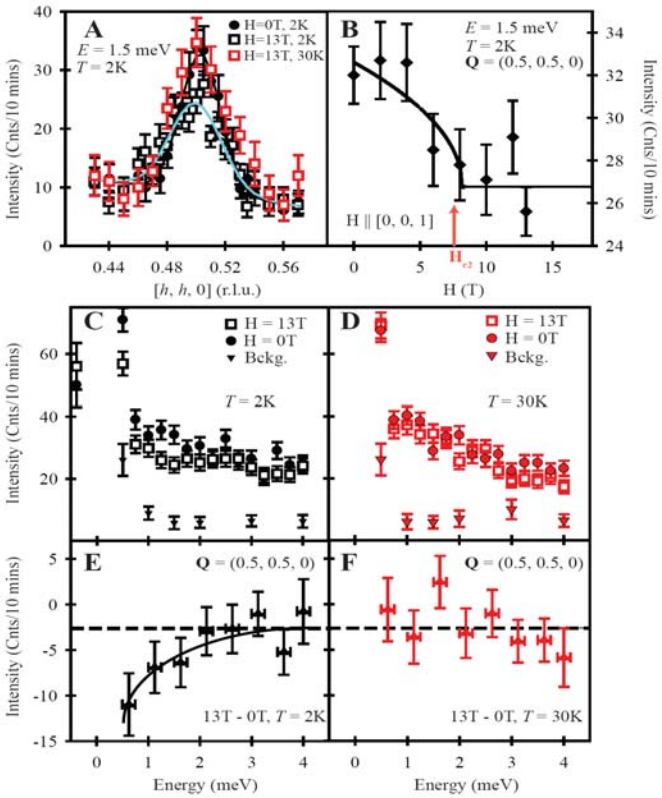

Fig. 1: *Field induced suppression of low energy magnetism in PLCCO. A) 1.5 meV Q-scans showing the reduction in spectral weight under 13T field. B) Field dependence of 1.5 meV excitations. C) 2K E-scans at (π, π, 0) in both 0T and 13T. D) 30K E-scans at (π, π, 0) in both 0T and 13T. E-F) Field subtraction (13T-0T) of E-scans at 2K and 30K respectively.*

References:

[1]. Stephen D. Wilson et al., PRB. **74**, 144514 (2006).
[2]. Stephen D. Wilson et al., Nature **442**, 59 (2006).
[3]. Khaykovich et al., PRB **71**, 200508(R) (2005).

	EXPERIMENTAL REPORT **Critical spin dynamics in NiC_2*4SC(NH_2)$_2$**	Proposal N° PHY-02-0556 Instrument **V2** Local Contact K. Rule, K. Habicht
Principal Proposer: Experimental Team:	M. Kenzelmann – ETHZ & PSI, CH B. Hansen – ETHZ & PSI, CH K. Rule – HMI, Berlin K. Habicht – HMI, Berlin	Date(s) of Experiment 15.10. – 30.10.2006

Date of Report: 17.01.2007

$NiCl_2$•4SC(NH_2)$_2$ is an ideal model quantum magnet to investigate field-induced magnetic phases. The material adopts a singlet ground state at zero field which is separated by an energy gap Δ from upper energy levels [1,2]. The singlet ground state results from a large uniaxial crystalline field which splits the S=1 spin triplet of Ni^{2+} and carries S_z=0, as has been shown with macroscopic and neutron measurements [3]. Our inelastic neutron scattering measurements using V2 from March 2006 gave direct evidence of the splitting of the doublet as a function of field.

We have extended our inelastic cold-neutron scattering experiments to explore the field-induced order in more detail. The measurements were performed for fields up to 6T applied at angles 0-20 degrees to the tetragonal c-axis. At 6T we have clear evidence of a splitting of the lower spin band, as shown in Fig. 1, while no splitting of the lower spin band had been observed in the disordered phase (not to be confused with the splitting of the doublet in the disordered phase). We measured the dispersion of the magnetic excitations at 6T along the c-axis and perpendicular to it. We found that while there is a considerable dispersion along the c-axis, there is no measurable dispersion in he basal plane, as shown in Fig. 2.

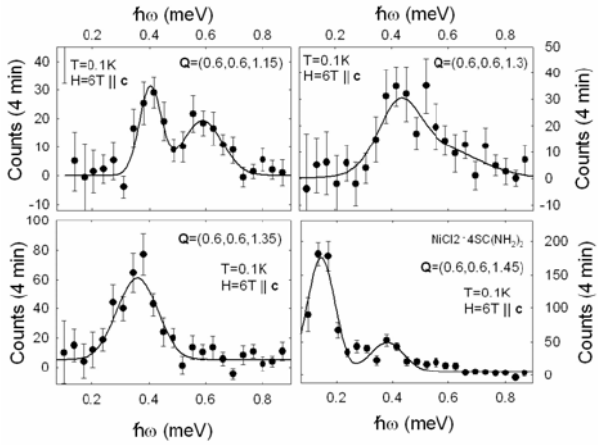

Fig. 1: *The energy spectrum at H=6T || c shows two magnetic excitations, giving evidence for a strong coupling of the magnetism on the two body-centered sublattices.*

The analysis of this data is still in progress. The splitting of the spin band may arise from the presence of interpenetrating tetragonal spin sublattices. For purely antiferromagnetic order, the two sublattices are completely decoupled because the interacting mean field is zero. If however, the sublattices are magnetized due to the presence of an external field, this is no longer the case. The two sublattices interact, and the result is a competition between ferromagnetic and antiferromagnetic spin arrangements between the two sublattices, that may be released by a distortion of the crystal structure. Further experiments of magnetic excitations as a function of field will be needed to directly study the release of this frustration with increasing field.

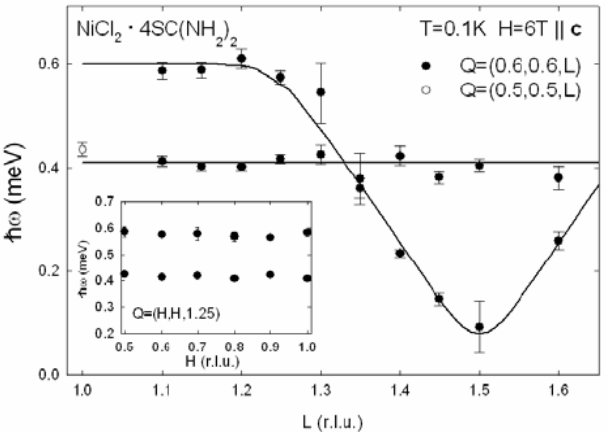

Fig. 2: *The magnetic excitations at H=6T || c show a dispersion along the c-axis, but are dispersionless in the basal plane (see inset). The solid lines are guides to the eye.*

References:

[1]. A. Paduan-Filho, X. Gratens and N. F. Oliveira, Jr., Phys. Rev. B **69**, 020405(R) (2004).

[2]. A. Paduan-Filho, X. Gratens and N. F. Oliveira, Jr., J. Appl. Phys. **95** (11), 7537 (2004).

[3]. V. S. Zapf et al. Phys. Rev. Lett. **96**, 077204 (2006).

BENSC	**EXPERIMENTAL REPORT** **AF fluctuations in bilayer manganite $La_{1.2}Sr_{1.8}Mn_2O_7$**	Proposal N° PHY-02-0558 Instrument **V2** Local Contact Kirrily Rule
Principal Proposer: Experimental Team:	T. Chatterji – ILL Grenoble, F K. Rule – HMI, Berlin	Date(s) of Experiment 07.11. – 12.11.2006

Date of Report: 15.11.2006

We have investigated the magnetic field dependence of the antiferromagnetic fluctuations in the bilayer manganite $La_{1.2}Sr_{1.8}Mn_2O_7$ on the cold triple-axis spectrometer V2 of BENSC. The spectrometer collimation was: guide - PG(002) – 60 – sample – slits - Be filter – open – PG(002) – open – detector. The monochromator PG(002) was vertically curved and the analyser PG(002) was horizontally focused. We used a W spectrometer configuration. The constant-Q scans at Q = (0.5,0,0) were performed at two temperatures T = 133 and 153 K under applied magnetic field parallel to the b-axis of the crystal by keeping $k_f = 1.55$ A^{-1}. Typical scans are shown in Fig. 1 and 2. Quasielastic scattering is observed along with the incoherent elastic peaks. The continuous lines are the results of the fit of the scattered intensity by a Gaussian line shape for the incoherent elastic peak and a Loretzian line shape for the quasielastic scattering due to the AF fluctuations. The quasielastic intensity is drastically reduced by the application of magnetic fields. At H = 4 Tesla the quasielastic peak disappears almost completely. The magnetic field dependence of the quasielastic intensity is more pronounced at T = 133 K which is close to the ferromagnetic Curie temperature T_C = 128 K than that at T = 153 K. The half-width of the Lorentzian quasielastic scattering gave the time correlation of the AF fluctuations. We could not determine the field dependence of the space correlation of the AF fluctuations in the limited beam time available to us.

We have measured the resistivity of the sample in situ along with scattering neutron intensity. The resistivity was found to decrease as a function of the magnetic field in a very similar way as that of the quasielastic intensity due to the AF fluctuations. However, a quantitative determination of the resistivity was not possible due to the presence of the aluminium foils and wires used to fix the ferromagnetic sample in a magnetic field.

We wish to continue this experiment in near future with better contacts for the resistivity measurements and determine both time and space correlations of the AF fluctuations at several more magnetic field values than was achieved during the present experiment.

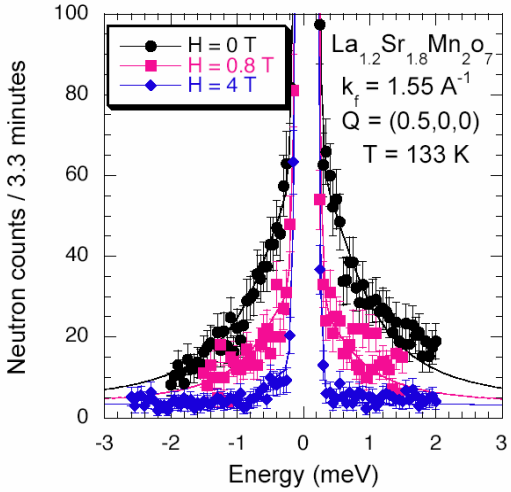

Fig. 1: *Magnetic field dependence of the quasielastic scattering due to AF fluctuations in the bilayer manganite $La_{1.2}Sr_{1.8}Mn_2O_7$ at T = 133 K.*

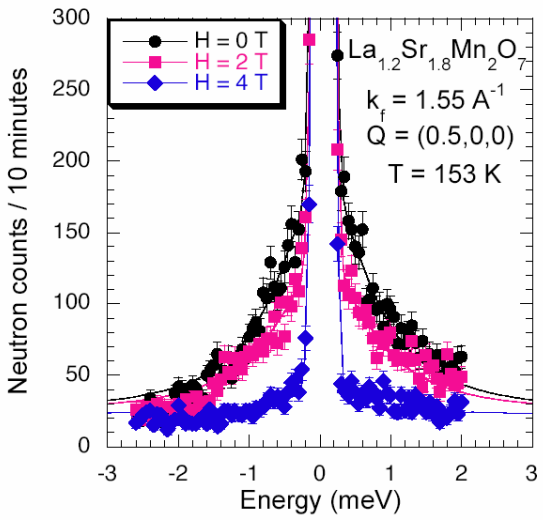

Fig. 2: *Magnetic field dependence of the quasielastic scattering due to AF fluctuations in the bilayer manganite $La_{1.2}Sr_{1.8}Mn_2O_7$ at T = 153 K.*

	EXPERIMENTAL REPORT **Investigations of crystal field levels in the frustrated pyrochlore $Tb_2Sn_2O_7$**	Proposal N° PHY-02-0596-EF Instrument **V2** Local Contact Kirrily Rule
Principal Proposer: Experimental Team:	K. Rule – HMI, Berlin P. Bentley – HMI, Berlin	Date(s) of Experiment 07.08. – 14.08.2006

Date of Report: 20.12.2006

V2, the triple axis spectrometer was used to investigate the crystal electric field (CEF) levels of a polycrystalline sample of $Tb_2Sn_2O_7$. Both the ground state doublet and first excited state doublet of this geometrically frustrated material are separated by a small energy gap of about ~1.2meV.

About 30g of $Tb_2Sn_2O_7$ was loaded into a Cu sample can within a dilution cryostat. The final wave vector was fixed at 1.55 $Å^{-1}$ and a Be filter was placed in the scattered beam to reduce λ/2 reflections. The energy resolution of the instrument was 0.14 meV full width half maximum. The spectrometer was arranged with a -1,-1,+1 configuration with collimation set to 60'-open-open. PG (002) was used for both the monochromator and analyzer, which were focused vertically and horizontally, respectively, to increase the scattered intensity.

Figure 1: Elastic neutron scattering of $Tb_2Sn_2O_7$ as a function of temperature

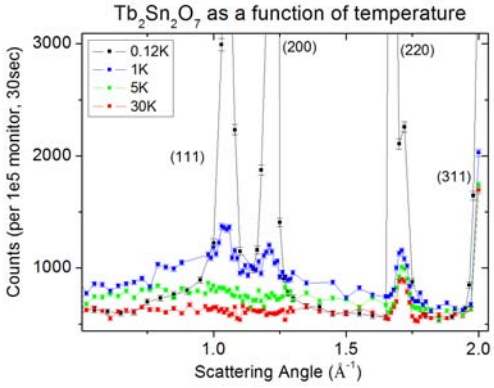

Magnetic ordering was confirmed by taking Q-scans at the elastic position. These can be seen in Figure 1, clearly indicating the onset of ferromagnetic correlations below ~1K. Sharp, intense Bragg peaks were observed at 0.12K similar to earlier studies[1].

Constant-Q, energy-scans were taken at temperatures below 30K. The position of the excited state doublet was plotted as a function of |Q| and temperature and can be seen in Figure 2.

At temperatures below 30K, the first excited CEF level softened towards the first magnetic zone centre at a scattering angle of ~1.1 $Å^{-1}$. This softening is believed to be related to the increasing strength of the short ranged magnetic correlations.

Figure 2: Softening of the 1st excited CEF

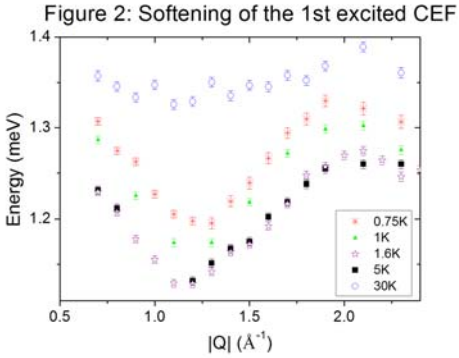

Below ~1K the mode appeared to "harden" again as can be seen in Figure 3. This hardening occurred around the same temperature at which the ferromagnetic correlations were observed.

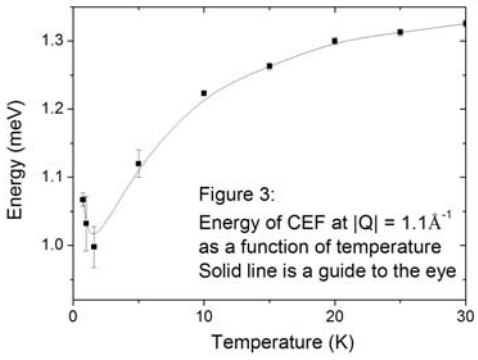

Figure 3:
Energy of CEF at |Q| = 1.1Å⁻¹
as a function of temperature
Solid line is a guide to the eye

It is believed that the onset of magnetic order observed in the elastic neutron scans may contribute to the observed changes in the dispersive crystal electric field levels. Further investigations are required to confirm this. A continuation of this experiment is planned to perform more detailed temperature scans below ~ 1K.

Reference:

[1]. [1]I. Mirebeau, A. Apetrei, J. Rodriguez-Carvajal, P. Bonville, A. Forget, D. Colson, V. Glazkov, J. P. Sanchez, O. Isnard, and E. Suard, *Physical Review Letters* **94**, 246402 (2005).

BENSC	**EXPERIMENTAL REPORT** **Crystal field interaction for the intermetallic series RNiAl4 (R = rare earth)**	Proposal N° PHY-03-0430 Instrument **V3** Local Contact Alexandra Buchsteiner
Principal Proposer: Experimental Team:	G. A. Stewart – UNSW@ADFA, Australia P. C. M. Gubbens – TU Delft, NL A. Buchsteiner – HMI, Berlin	Date(s) of Experiment 10.07. - 20.07.2006

Date of Report: 02.11.206

The orthorhombic, intermetallic series $RNiAl_4$ (R = rare earth) exhibits intriguing magneto-crystalline anisotropy and metamagnetic behaviour that is expected to be strongly influenced by the crystal electric field interaction. For this reason, the crystal field (CF) scheme for Er^{3+} in $ErNiAl_4$ has been determined using inelastic neutron scattering (INS) measurements conducted on the NEAT time of flight spectrometer. The 7 g mass of finely ground $ErNiAl_4$ was loaded (65 % packing density) into the 50 mm diameter x 1 mm cavity of a rigid, aluminium holder.

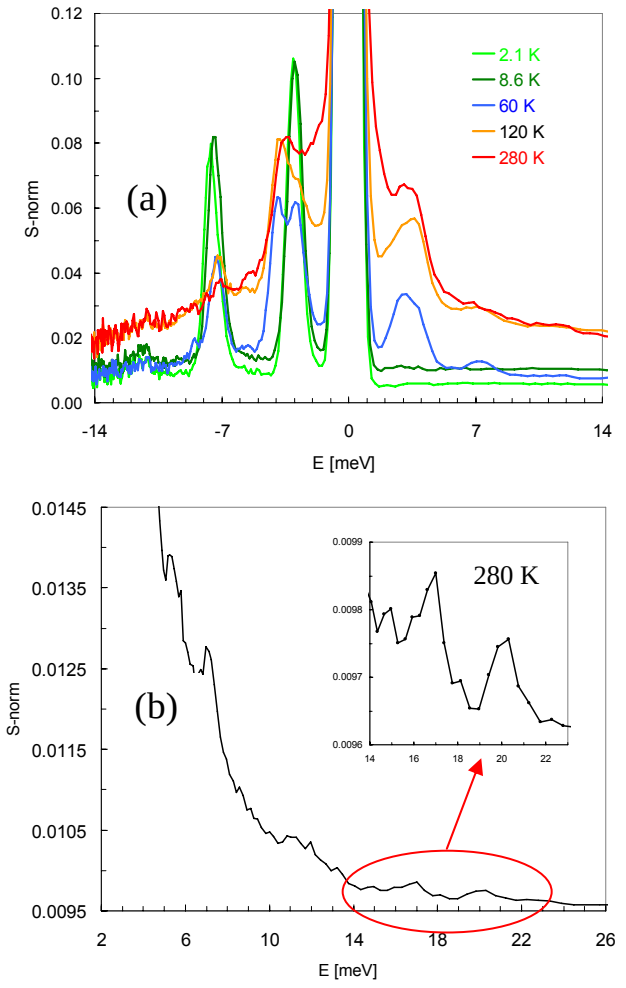

***Fig. 1**: INS spectra for $ErNiAl_4$ (a) E_i = 20.5 meV (b)E_i = 3.2 meV (energy gain)*

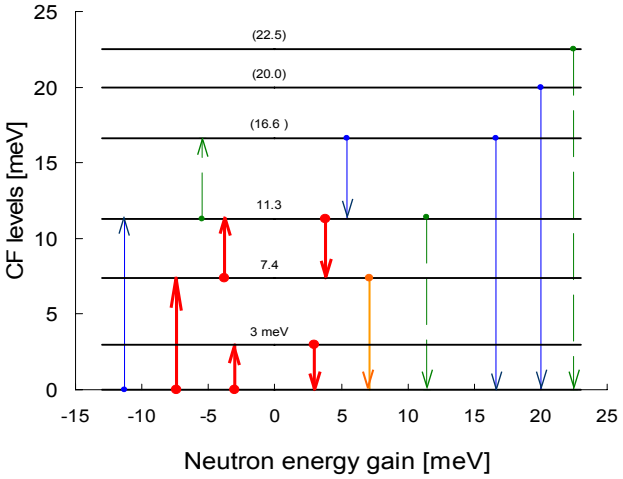

***Fig. 2**: Proposed CF scheme for Er^{3+} in $ErNiAl_4$, indicating strong, medium, weak and faint experimental transitions.*

INS spectra were recorded for $ErNiAl_4$ with E_i = 20.5 meV over a range of temperatures (**Fig. 1a**) and with E_i = 3.2 meV at 280 K (**Fig. 1b**). Additional spectra were recorded for an $YNiAl_4$ reference sample and for the empty cell to estimate the phonon and background contributions. A vanadium standard sample (1 mm thick) was employed for the calibration of detector efficiency and for the determination of the experimental resolution function. Based on these results, the CF scheme for Er^{3+} is deduced to be as shown in **Fig. 2**. Only one of the eight Kramers doublet levels could not be identified. A full CF analysis of the INS spectra is currently underway using this proposed CF scheme as a starting point. The local rare earth site symmetry is orthorhombic, mm (C_{2v}) and requires 9 CF parameters. However, the number of CF parameters needed to be fitted is reduced by computation of within-rank CF parameter ratios and the conversion of existing ^{155}Gd-Mössbauer spectroscopy data (for isostructural $GdNiAl_4$) to three possible sets of rank 2 CF parameters.

Banchachit Saensunon is acknowledged for his preparation of the specimen material.

	EXPERIMENTAL REPORT **Magnetic excitations of the molecular magnet Mn_6**	Proposal N° PHY-03-0452 Instrument **V3** Local Contact Schnegg/ Russina
Principal Proposer: Experimental Team:	J.v. Slageren – Uni, Stuttgart O. Pieper – HMI, Berlin B. Lake – HMI, Berlin A. Schnegg, M. Russina – HMI, Berlin	Date(s) of Experiment 21.07. – 28.07.2006

Date of Report: 10.09.2006

We measured the magnetic excitation spectrum of the molecular magnet Mn_6 (full formula $[Mn_6O_2(O_2CMe)_2(salox)_6(EtOH)_4]\cdot 4EtOH$) using inelastic neutron scattering at the time-of-flight machine V3 NEAT. In Mn_6 the six Mn(III) ions (S = 2) form two antiferromagnetic coupled triangles, which are ferromagnetically coupled to each other. This leads to a predicted S = 4 ground state [1]. The expected single ion anisotropy $\sim DS_z^2$ splits the levels and the ground state would be $S^z=\pm 4$. Starting from that state (T = 2 K) and considering the neutron selection rules, various transitions were expected. One transition is the $|M_s=\pm 4> \rightarrow |M_s=\pm 3>$ transition within the ground state multiplet in addition other transitions are expected between multiplets with different total spin S. By heating the sample up to T = 20 K we could populate the lower lying energy levels and cause also transitions to other levels. See figures 1 and 2. We measured with incident wavelengths of 5, 4.6 and 3.2 Å. The positions of the magnetic peaks at higher temperatures (fig. 1b and 2) could not all be explained within the anisotropy model mentioned above, which means that we have to expand the model by including higher order anisotropy terms.

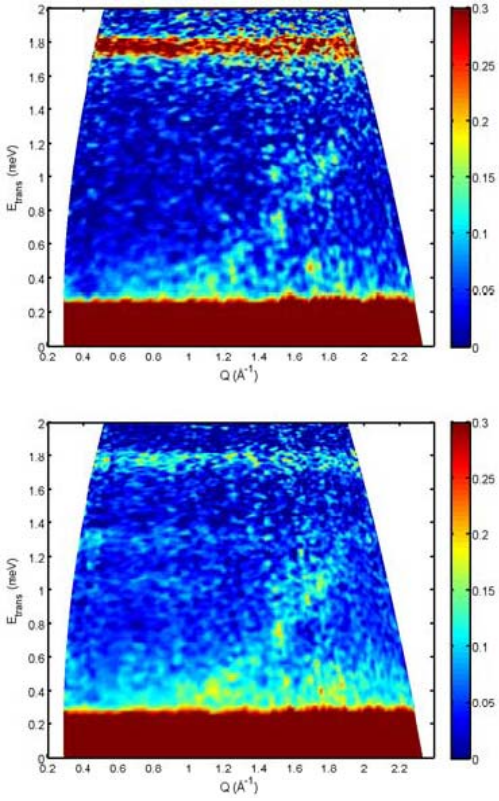

Fig. 1: *Background subtracted intensity as a function of wavevector vs. energy transfer measured with an incident wavelength of* λ=5.0Å at (a) T=2.32K and (b) T=20.0K. *The colour bar shows the relative intensity. The diagonal line on the lower right site can not originate from magnetic excitations, because of its |Q|-dependence.*

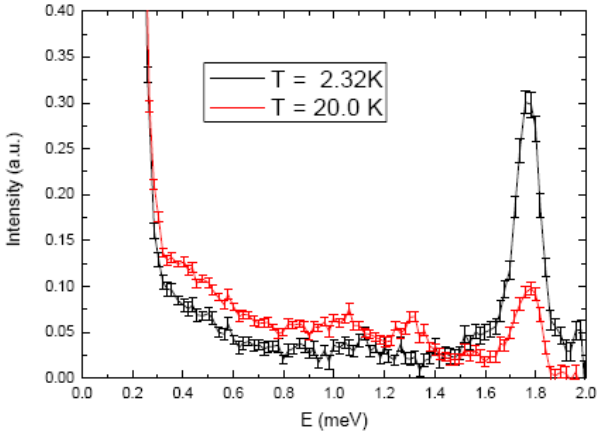

Fig.2: *Energy transfer vs. Intensity for* λ=5.0Å *at the two different temperatures. At T=2.32 K there is only one peak at 1.76 meV, resulting from the* the $|M_s=\pm 4>\rightarrow |M_s=\pm 3>$ *transition. At higher temperature the intensity of this peak decreases and additional peaks occur.*

λ (Å)	T (K)	Peak Position (meV)	S Transition	M_S Transition
5.0	2.32	1.77±0.02	-	±4→±3
5.0	20.0	0.858±0.008	-	?
		1.040±0.006	-	?
		1.295±0.006	-	±3→±2
		1.765±0.004	-	±4→±3
4.6	2.33	1.760±0.003	-	±4→±3
		2.482±0.006	4→?	-
4.6	20.0	0.976±0.005	?	-
		1.310±0.005	-	±3→±2
		1.757±0.003	-	±4→±3
		2.13±0.02	?	?
		2.483±0.009	4→?	-
3.2	2.30	1.79±0.02	-	±4→±3
		2.54±0.02	4→?	-
		4.01±0.04	?	?
		5.28±0.02	?	?

Table 1: *Positions of all measured peaks due to inelastic neutron scattering and there interpretation. The position and error values are estimated by fitting the data to Lorentzian functions.*

Reference:

[1]. J. Milios et al. Angew. Chem. Int. Ed. **43** (2004) 210-212.

	EXPERIMENTAL REPORT **Magnetic excitations in a high spin (S=12) Mn_6-(Et-saoH_2) Single Molecule Magnet**	Proposal N° PHY–03–0475–EF Instrument **V3** Local Contact Buchsteiner/ Russina
Principal Proposer: Experimental Team:	T. Guidi – HMI, Berlin O. Pieper – HMI, Berlin B. Lake – HMI, Berlin A. Buchsteiner, M. Russina – HMI, Berlin	Date(s) of Experiment 23.10. - 02.11.2006

Date of Report: 28.12.2006

We measured the magnetic excitation spectrum of the molecular magnet Mn_6-(Et-saoH_2) (full formula $[Mn_6O_2$(Et-sao$)_6$ $(EtOH)_4(O_2CPh)_2(H_2O)_2]\cdot 2(EtOH)$) [1] using inelastic neutron scattering with the time-of-flight spectrometer V3 NEAT. In Mn_6-(Et-saoH_2) the six Mn^{3+}-ions have spin state s=2 and are all ferromagnetically coupled leading to an S=12 ground state [1]. The degeneracy of the ground state is lifted by the single ion anisotropy and the 'real' ground state has $S_z=\pm 12$.
We focused on the low energy region of the spectrum and used incident neutron wavelengths of 4.6, 5 and 7 Å. At lowest temperature (T=2K) only the ground state is populated and due to the neutron selection rules only transitions with $\Delta S=0, \pm 1$ and $\Delta M=0, \pm 1$ could be detected. With an incident wavelength of 7 Å we observed a sharp peak at 1.12 meV energy transfer corresponding to the $|M_s=\pm 12\rangle \rightarrow |M_s=\pm 11\rangle$ transition within the ground state multiplet. By heating up the sample to T=10 K higher energy levels can be populated and transitions originating from these levels were detected. With 4.6 Å incident wavelength and T=2 K further excitations from the ground state were observed at higher energy transfer, associated to transitions towards different S=11 spin multiplets.

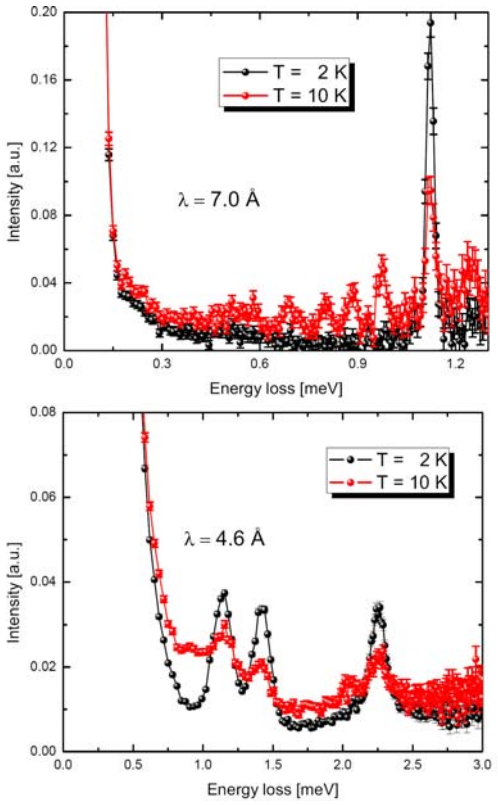

Fig.1: *Intensity vs. energy transfer for two different neutron wavelength and two temperatures.* ***a****.) λ=7.0 Å, at T=2 K only the $|M_s=\pm 12\rangle \rightarrow |M_s=\pm 11\rangle$ transition is detectable. At T=10 K the low lying levels are thermally populated and transitions to higher levels occur.* ***b****.) λ=4.6 Å, in addition to a. two other excitations were observed at T=2K. These excitations are associated to transitions from the ground state to excited states with total spin S=11.*

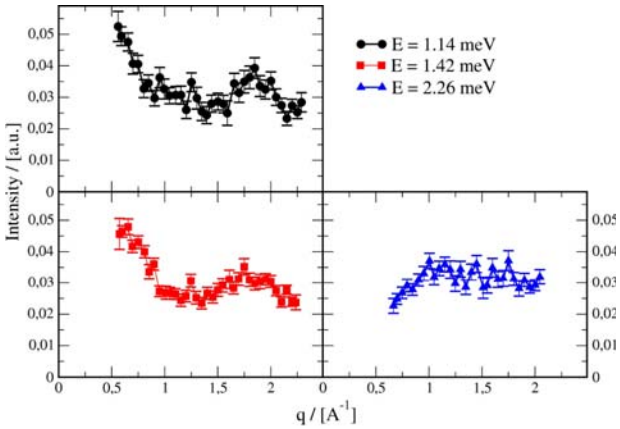

Fig.2: *q-dependence of the three magnetic peaks measured at λ=4.6 Å and T=2 K (see Fig.1b). From the q-dependence of the observed excitations it will be possible to gain further information on the nature of the transition and on the symmetry of the spin wave functions.*

Table 1: *Positions of all measured peaks. The position and error values are estimated by fitting the data to Lorentzian functions.*

λ (Å)	T (K)	Peak Position (meV)
7.0	2.0	1.122±0.001
7.0	5.0	1.122±0.001
		1.253±0.005
7.0	10.0	0.559±0.005
		0.690±0.003
		0.812±0.006
		0.885±0.005
		0.977±0.003
		1.125±0.001
		1.249±0.006
4.6	2.0	1.14±0.01
		1.42±0.01
		2.26±0.01
4.6	10.0	1.157±0.005
		1.415±0.004
		2.03±0.01
		2.257±0.003

Reference:

[1]. C.J. Milios *et al.*, J. Am. Chem. Soc. *in press*

Structure

	EXPERIMENTAL REPORT **Investigation of giant linear superelasticity phenomenon in Ni-Mn-Ga single crystal martensite**	Proposal N° MAT-01-1855 Instrument **E2** Local Contact Jens-Uwe Hoffmann
Principal Proposer: Experimental Team:	I. Glavatskyy – NAS IMP Kiev, UA J.-U. Hoffmann – HMI, Berlin	Date(s) of Experiment 03.04. – 10.04.2006

Date of Report: 27.11.2006

Present investigation concerns neutron diffraction studies of the structural mechanisms of giant linear elasticity in the martensite phase of near–stoichiometric Ni_2MnGa and $Ni_2MnGaCu$ single crystals under compressive tests at room temperature. Studied specimens having 10M, 14M and T-martensites have temperatures of martensite transformation T_M=322K, 365K and 470K correspondingly, with Curie point $T_c \sim 370$K.

Experiment: The 0.239nm wavelength was used for the experiments. Investigations were performed at T=295K. The single crystalline specimens were aligned to have $[010]_{fct}$ as zone axis for 10M and 14M and $[001]_{fct}$ for T-martensite crystals. Zone axis was also the direction of the compressive stress application. For the neutron diffraction studies under compressive stress, a special uniaxial pressure cell was constructed.

Results: The unit cell of the 10M martensite in the single crystal discussed below was approximated as face-centered tetragonal with a=0.557 nm, c=0.657 nm at 295K. The single crystal is twinned as described in [1], thus the $[010]_{fct}$ direction, being the "hard magnetization" axis of the martensite, is conserved. Fig.1. gives an example of the stress-strain behavior for the martensite phase of the discussed single crystal.

Fig.2 shows an example of the diffraction pattern evolution with compressive stress application for 0 MPa and 100MPa. With 100MPa stress along $[010]_{fct}$ the redistribution of the twin variants in the $(010)_{fct}$ plane is neglectible, instead the strong diffuse scattering and peak broadening appears especially fr high order reflections. This marks the strong lattice distortion and strong increase of the stacking faults density. Though, with unloading back to 0 MPa the initial pattern is completely recovered (not shown for a lack of space) presenting a completely elastic behavior with loading-unloading cycling.

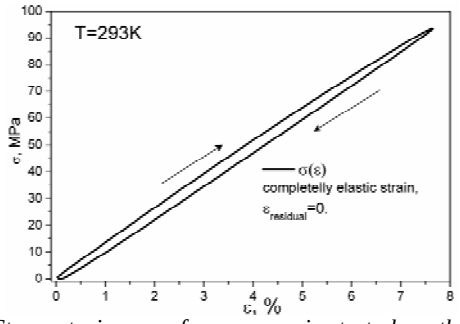

Fig.1: *Stress-strain curve for compressive test along the* $[010]_{fct}$.

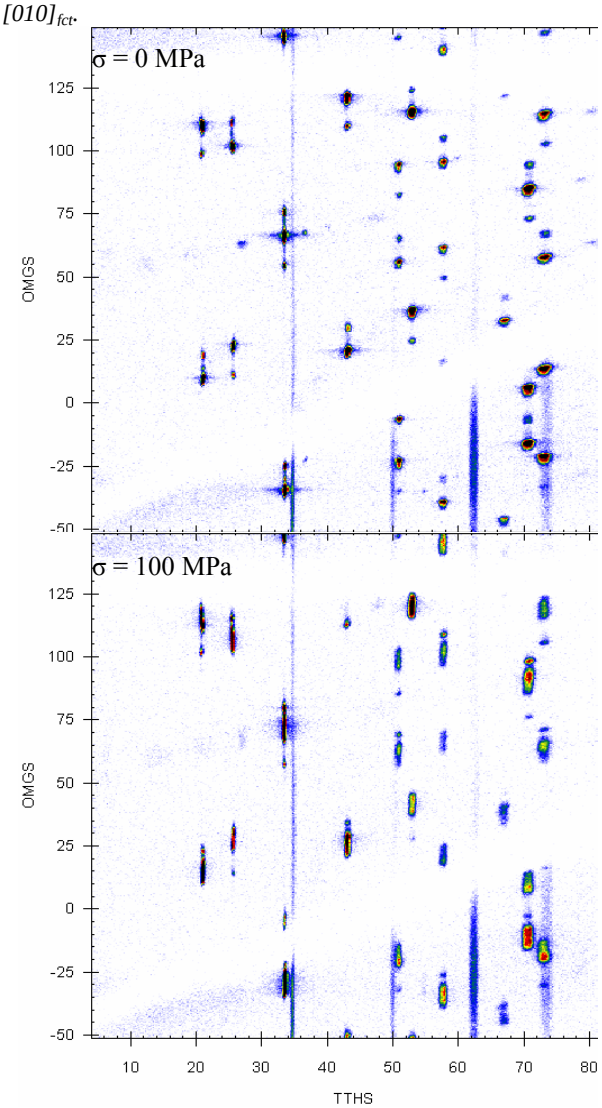

Fig.2: *Diffraction patterns for the free single crystal and under compressive stress ~100MPa along* $[010]_{fct}$*, coinciding with zone axis.*

References:

[1]. G. Mogylnyy, I. Glavatskyy, N. Glavatska, O. Söderberg, Y. Ge, V.K. Lindroos, Scripta Materialia **48** (2003) 1427–1432.

[2]. I. Glavatskyy, N. Glavatska, ISPMA-10 conference, Prague (2005).

	EXPERIMENTAL REPORT **Patterning of Sodium Ions and the Control of Electrons in Sodium Cobaltate**	Proposal N° PHY-01-1811-EF Instrument **E2** Local Contact Jens-Uwe Hoffmann
Principal Proposer: Experimental Team:	D. A. Tennant – HMI, Berlin J. Goff – Univ. Liverpool, UK J. Morris – Univ. Liverpool, UK J.-U. Hoffmann – HMI, Berlin	Date(s) of Experiment 09.01. – 14.01.2006

Date of Report: 23.01.2007

Na_xCoO_2 has emerged as a material of exceptional scientific interest due to the potential for thermoelectric applications[1,2], and because the strong interplay between the magnetic and superconducting properties has led to close comparisons with the physics of the high-T_c cuprates[3]. The density, x, of the sodium in the intercalation layers can be altered electrochemically, directly changing the number of conduction electrons on triangular Co layers[4]. Recent electron diffraction measurements reveal a kaleidoscope of Na^+ ion patterns as a function of concentration[5].

We used single-crystal neutron diffraction on E2 to determine the long-range three dimensional sodium superstructures of single crystal sodium cobaltate. Measurements were performed using a variable-temperature cryostat down to a base temperature of 1.5 K and the temperature dependence was determined through the sodium ordering phase transition. Other small samples from the same rods were examined by synchrotron x-ray diffraction using the MAGS beamline at BESSY in Berlin, and electrical transport and magnetometry measurements were performed to assess their quality

We find that the sodium ordering and its associated distortion field are governed by pure electrostatics, and the organizational principle is the stabilization of charge droplets that order long range at some simple fractional fillings.

The results of this experiment are published in ref [6].

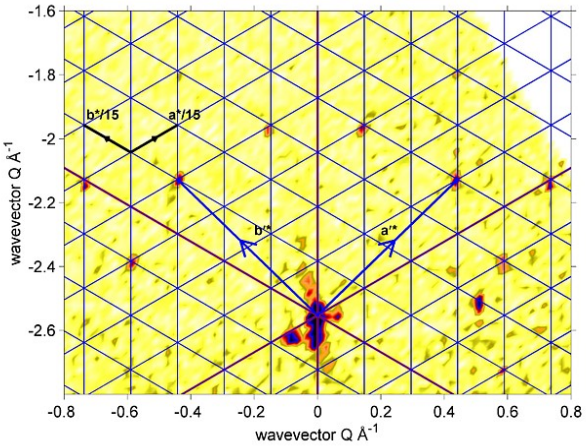

Fig 1: High wave-vector transfer resolution neutron scattering data observed on the E2 spectrometer from x=0.75 for (H,K,0) at T=1.5K. *These data show conclusively that the modulation wave vector is commensurate and can be indexed on a lattice* ***a'*** *=* ***a*** *+ 3****b*** *and* ***b'*** *= 4****a*** *- 3****b****, where* ***a*** *and* ***b*** *are the underlying hexagonal lattice vectors. All peaks lie on the grid except for the peak at* ***Q****~(0.5,-2.5) which is the main hexagonal reflection from another much smaller crystallite.*

References:

[1]. I. Terasaki, Y. Sasago, K. Uchinokura Large thermoelectric power in $NaCo_2O_4$ single crystals. *Phys. Rev. B* **56**, R12685 (1997).

[2]. M. Lee *et al*. Large enhancement of the thermopower in Na_xCoO_2 at high Na doping. *Nature. Mater.* **5**, 537-540 (2006).

[3]. K. Takada *et al*. Superconductivity in two-dimensional CoO_2 layers. *Nature* **422**, 53-55 (2003).

[4]. C. Delmas *et al*. Electrochemical intercalation of sodium in Na_xCoO_2 bronzes. *Solid State Ionics* **3-4** 165-169 (1981).

[5]. H.W. Zandbergen *et al.* Sodium ion ordering in Na_xCoO_2: Electron diffraction study. *Phys. Rev. B* **70** 024101 (2004).

[6]. M.Roger, D.J.P. Morris, D.A. Tennant, M.J.Gutmann, J.P. Goff, J.-U. Hoffmann, R. Feyerherm, E. Dudzik, D.Prabhakaran, N. Shannon, B. Lake and P.P. Deen, accepted *Nature* for publication January (2007).

	EXPERIMENTAL REPORT **Crystal structure of $Ca_{0.01}Y_{0.99}VO_3$ and $Ca_{0.05}Y_{0.95}VO_3$**	Proposal N° PHY-01-1724-LT Instrument **E5** Local Contact Manfred Reehuis
Principal Proposer: Experimental Team:	M.Reehuis, C.Ulrich, B.Keimer – MPI, Stuttgart M. Reehuis – MPI, Stuttgart	Date(s) of Experiment 08.09. – 24.09.2006 20.10. – 02.11.2006 29.11. – 11.12.2006

Date of Report: 02.01.2007

Only recently we gave a detailed description of the crystal structure of YVO_3 [1]. This compound shows a structural phase transition at 200 K from an orthorhombic to a monoclinic phase with the space group *Pbnm* and $P2_1/b$, respectively. A second phase transition back to the orthorhombic space group *Pbnm* is observed upon cooling below 77 K. Below and above this temperature the vanadium moments show a *G*-type and a *C*-type ordering, respectively. In the present work we give an account on the crystal structure of Ca-doped vanadates $Ca_xY_{1-x}VO_3$. It could be seen that a minimal Ca-doping has a strong influence on the structural and magnetic properties of these materials [2, 3]. For the vanadate with x(Ca) = 0.01 the first phase transition sets in at the lower temperature 189 K; the second one sets in between 48 K and 63 K [2]. This transition is absent for the vanadate with $x(\mathrm{Ca}) \geq 0.02$, and *C*-type ordering of the V-sublattice is stable down to 10 K. In order to study the influence of the Ca-doping on the interatomic distances, especially those in the VO_6-octahedra, we carried out neutron diffraction experiments on the four-circle diffractometer E5 (Cu-monochromator: λ = 0.889 Å). For the experiment cylindrical crystals with dimensions d = 3 mm and h = 3 mm were used. At 10 K data sets were collected for the orthorhombic phase of $Ca_{0.01}Y_{0.99}VO_3$ (1378 reflections, 649 unique) and for the monoclinic one of $Ca_{0.05}Y_{0.95}VO_3$ (1755 reflections, 696 unique). Due to the fact that the monoclinic distortions were found to be rather weak [1] the crystal structure of $Ca_{0.05}Y_{0.95}VO_3$ was refined in the orthorhombic space group *Pbnm*. The results of the refinements are presented in Table 1. Here the V-O-bond distances of the vanadates $Ca_xY_{1-x}VO_3$ are compared with the values of undoped YVO_3. It can be seen that the obtained values of the *G*-type ordered $Ca_{0.01}Y_{0.99}VO_3$ show an excellent agreement with those obtained for YVO_3. Due to the presence of *Jahn-Teller* effect the V-O21-bond distance is strongly elongated, while the lengths of other bonds are almost the same. In contrast, for the *C*-type phase of $Ca_{0.05}Y_{0.95}VO_3$ (at 10 K) and YVO_3 (at 85 K) as well as for their paramagnetic phases (at 295 K) the V-O22-bond distance is clearly the largest. In order to study the influence of Ca-doping on the structural parameters further systematic studies will be necessary.

Table 1: *Crystal structure parameters of $Ca_{0.01}Y_{0.99}VO_3$ and $Ca_{0.05}Y_{0.95}VO_3$. The thermal parameters U_{ii} are given in 100 Å^2). The isotropic thermal parameter of the V-atom was fixed. The shortest interatomic distances (in Å) between the V and O-atoms of the Ca-doped vanadates are compared with those of pure YVO_3.*

	$Ca_{0.05}Y_{0.95}VO_3$	$Ca_{0.01}Y_{0.99}VO_3$	
T (K)	10, *C*-type	10, *G*-type	295
a [Å]	5.2770(5)	5.2808(4)	5.2808(5)
b [Å]	5.6044(4)	5.5847(4)	5.6059(5)
c [Å]	7.5395(6)	7.5511(5)	7.5707(7)
V [Å^3]	222.98(3)	222.70(3)	224.12(4)
x (Ca/Y)	–0.01975(8)	–0.02094(7)	–0.01904(6)
y (Ca/Y)	0.06944(7)	0.07013(7)	0.06878(6)
x (O1)	0.10910(11)	0.11185(10)	0.11032(8)
y (O1)	0.46209(10)	0.46155(9)	0.46046(8)
x (O2)	–0.30821(8)	–0.31247(7)	–0.30848(6)
y (O2)	0.30321(7)	0.29964(6)	0.30392(6)
z (O2)	0.05565(5)	0.05666(5)	0.05605(5)
U_{11} (Ca/Y)	0.262(18)	0.274(13)	0.519(12)
U_{22} (Ca/Y)	0.212(14)	0.213(14)	0.499(13)
U_{33} (Ca/Y)	0.307(19)	0.228(14)	0.546(13)
U_{12} (Ca/Y)	0.001(11)	0.004(10)	–0.057(9)
U_{is}(V)	0.20	0.20	0.30
U_{11}(O1)	0.454(23)	0.395(18)	0.592(16)
U_{22}(O1)	0.288(20)	0.400(19)	0.684(17)
U_{33}(O1)	0.392(24)	0.271(17)	0.370(18)
U_{12}(O1)	–0.054(15)	–0.003(14)	–0.098(13)
U_{11}(O2)	0.492(19)	0.390(12)	0.542(11)
U_{22}(O2)	0.288(16)	0.330(14)	0.599(12)
U_{33}(O2)	0.514(18)	0.402(12)	0.687(13)
U_{12}(O2)	–0.011(10)	–0.053(9)	–0.132(9)
U_{13}(O2)	0. 037(10)	0. 044(11)	0. 084(10)
U_{23}(O2)	–0.050(10)	–0.055(10)	–0.121(10)
d(V-O1)	1.9823(2)	1.9897(2)	1.9927(2)
d(V-O21)	2.0094(4)	2.0391(4)	2.0105(3)
d(V-O22)	2.0219(4)	1.9910(4)	2.0262(3)
	YVO_3	YVO_3	
T (K)	85, *C*-type	5, *G*-type	295
d(V-O1)	1.9830(4)	1.9903(5)	1.9941(2)
d(V-O21)	2.0128(12)	2.0412(11)	2.0115(5)
d(V-O22)	2.0268(13)	1.9910(11)	2.0258(5)

Reference:

[1]. M. Reehuis, C. Ulrich, P. Pattison, B. Ouladdiaf, M.C. Rheinstädter, M. Ohl, L. P. Regnault, M. Miyasaka, Y. Tokura, B. Keimer, Phys. Rev. B **73** (2006) 094440.

[2]. M. Reehuis, C. Ulrich, B. Keimer, BENSC Experimental Reports 2006, this volume.

[3]. J. Fujioka, S. Miyasaka, Y. Tokura, Phys. Rev. B **72** (2005) 024460.

	EXPERIMENTAL REPORT **Crystal structure of CaV_2O_4**	Proposal N° PHY-01-2008-EF Instrument **E5** Local Contact Manfred Reehuis
Principal Proposer: Experimental Team:	B. Lake – HMI, Berlin M. Reehuis – MPI, Stuttgart J.-Q. Yan, A. Niazi – Iowa State Univ., USA D. C. Johnston – Iowa State Univ., USA	Date(s) of Experiment 16.01. – 22.01.2006 30.01. – 19.01.2006

Date of Report: 02.01.2007

A neutron diffraction study of CaV_2O_4 was performed on the four-circle diffractometer E5 using a Cu-monochromator selecting the neutron wave-length λ = 0.8869 Å. For the experiment a single crystal of CaV_2O_4 with dimensions 2 × 2 × 3 mm^3 was used. A data set with a total of 1341 (873 unique) reflections could be collected at room temperature. The refinement of the crystal structure was carried out with the program Xtal 3.4. The crystal structure of CaV_2O_4 could be successfully refined in the orthorhombic space group *Pnam*. All the atoms are placed on the Wyckoff position 4*c* (x,y,¼). The refinement of the overall scale factor, the positional and anisotropic thermal parameters resulted in the residual R_F = 0.045 (R_w = 0.050). Due to the weak scattering power of vanadium the atomic parameters could not be determined with a good accuracy from our single-crystal neutron diffraction data. Therefore, these values were determined complementarily by synchrotron powder diffraction. It is interesting to note that the positional parameters presented in Table 1 are similar to those of the isotypic compound $CaFe_2O_4$ [1]. In Fig. 1 it can be seen that the V-atoms are octahedrally coordinated by O-atoms build a three-dimensional network of corner- and edge-sharing VO_6-octahedra. Further it can be seen that the VO_6-octahedra are strongly distorted.

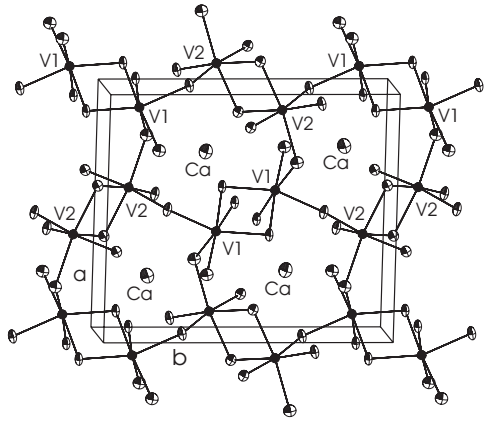

Fig. 1: *Crystal structure of CaV_2O_4.*

In Table 3 the shortest interatomic distances between the V- and O-atoms are listed. These values were determined using the structural parameters given in Table 1.

Table 1: *Results of the single-crystal neutron diffraction study of CaV_2O_4 at 295 K. The lattice constants and the x-, and y-parameters of the V-atoms have been determined by synchrotron powder diffraction.*

	x	*y*	*z*	*occ*
Ca	0.75500(12)	0.65490(14)	¼	1.00
V1	0.4330(3)	0.6113(2)	¼	1.00
V2	0.4215(3)	0.1047(2)	¼	1.00
O1	0.20982(9)	0.16145(7)	¼	1.00
O2	0.11727(8)	0.47564(7)	¼	1.00
O3	0.52133(10)	0.78139(7)	¼	1.00
O4	0.41860(9)	0.42752(7)	¼	1.00

a = 9.2118(2) Å, *b* = 10.6840(2) Å, *c* = 3.0000(1) Å

Table 2: *Thermal parameters U_{ij} (given in 100 Å^2) of CaV_2O_4 at 295 K. They are in the form $exp[-2\pi^2(U_{11}\, h^2a^{*2} + \ldots 2U_{13}\, hla^*c^*)]$. For symmetry reasons the values U_{13} and U_{23} of all the atoms are equal to zero in this structure.*

	U_{11}	U_{22}	U_{33}	U_{12}
Ca	0.80(4)	0.63(4)	1.09(4)	–0.12(3)
V1, V2	0.30			
O1	0.51(3)	0.58(3)	0.53(3)	0.02(2)
O2	0.43(3)	0.38(3)	0.51(3)	–0.07(2)
O3	0.66(3)	0.25(3)	0.55(3)	–0.20(2)
O4	0.58(3)	0.20(3)	0.49(3)	–0.03(2)

Table. 3: *Shortest interatomic distances between the V- and O-atoms.*

	No. of bonds	*d*(V-O) [Å]
V1-O1	2	2.0659(6)
V1-O3	1	1.9911(8)
V1-O4	1	1.9680(7)
V1-O4	2	2.0715(6)
V2-O1	1	2.0421(6)
V2-O2	2	2.0685(8)
V2-O2	1	1.9973(8)
V2-O3	2	2.0021(5)

Reference:

[1]. B. F. Decker and J. S. Kasper, Acta Cryst. **10** (1957) 332.

	EXPERIMENTAL REPORT **Understanding the mechanism of the phase transition and the nature of the chemical disorder in SBT: a neutron diffraction study**	Proposal N° MAT-01-1104 MAT-01-1147 Instrument **E6 – E9** Local Contact Daniel Többens
Principal Proposer: Experimental Team:	P. Saint Grégoire – Univ. Toulon, F Y. Gagou, M.A. Frémy – Univ. Toulon, F D. Többens – HMI, Berlin	Date(s) of Experiment 11.03. – 21.03.2002 21.03. – 28.03.2002

Date of Report: 14.01.2003

Strontium bismuth tantalate $SrBi_2Ta_2O_9$ (SBT) is a member of Bi-layered perovskites and are expected to be the most promising materials in use in non-volatile ferroelectric memories due to its fatigue-free properties. SBT undergoes a ferroelectric transition at the Curie temperature Tc = 608 K with a structural change from tetragonal to orthorhombic systems (1).

We have carried out experiments on this compound SBT in order to get information on the symmetry change at the phase transition and on the mechanism of the transition. No significant change was observed at low resolution, but with the high resolution instrument, noticeable changes as a function of temperature were observed.

We began to perform Rietveld refinements of the data, but till now they were not successful: we could not refine the structure satisfactorily since in the Fourier difference map, we observe excess of electron density in some regions, which could suggest that the admitted symmetry group of this compound is not the correct one.
At present time, attempts to refine the structure are still in progress. (Our results and conclusions are not reliable to write an article). A PhD student will probably soon continue this work which possibly will need complementary neutron diffraction data acquisition, in particular to check the symmetry at room temperature.

References:

[1]. E.C. Subbarao, J. Phys. Chem. Solids **23** 665-676 (1962)

BENSC	**EXPERIMENTAL REPORT** **Determination of Light Elements via Neutron Diffraction**	Proposal N° CHE-01-1859 Instrument **E9** Local Contact Dimitry Argyriou
Principal Proposer: Experimental Team:	G. Auffermann, R. Kniep – MPI CPfS Dresden P. Höhn, R. Niewa – MPI CPfS Dresden G. Auffermann – MPI CPfS Dresden N. Aliouane, D. Argyriou – HMI, Berlin	Date(s) of Experiment 16.05. - 22.05.2006

Date of Report: 15.09.2006

The chemistry of ternary and higher nitrdometalates is a rapidly grown field in inorganic solid state chemistry. In case of nickel, an abundance of compounds with nickel in low oxidation states ≤ +1 was reported. In the system Sr-Ni-N the existence of "$Sr_2[NiN_2]$" has only been reported. However, the crystal structure refinement is questionable [1]. A re-investigation led to the assumption that the correct composition is $Sr_2[Ni(CN)N]$. Chemical analysis and a neutron diffraction experiment confirmed the stoichiometry and led to the complete structure determination [2].

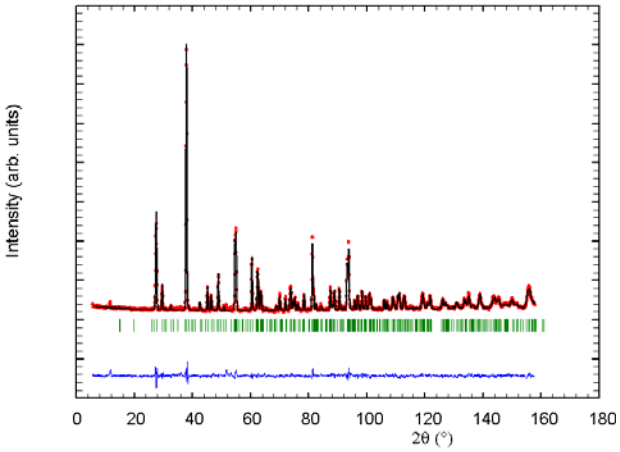

Fig. 1: *Neutron powder diffraction pattern of $Sr_2[Ni(CN)N]$ at 297 K (observed (red), calculated (black) and difference (blue) profiles, green ticks mark the Bragg positions (upper row)).*

Table 1: Structural parameters of $Sr_2[Ni(CN)N]$ from a neutron powder diffraction experiment using E9 (*Pnma*, *a* = 7.8215(3) Å; *b* = 3.8888(1) Å; *c* = 14.0077(5) Å; 347 reflections).

	x	*y*	*z*	B_{iso}(Å^2)
Sr in (4*c*)	0.8549(5)	¼	0.1161(4)	1.1(1)
Sr in (4c)	0.881(1)	¼	0.4090(4)	0.8(1)
Ni in (4*c*)	0.1083(7)	¾	0.2759(5)	1.06(7)
N in (4c)	0.119(1)	¾	0.4031(5)	1.4(1)
C in (4*c*)	0.119(2)	¾	0.1508(5)	0.5(2)
N in (4c)	0.123(1)	¾	0.0670(4)	1.5(1)
R_{Profil}/R_{Bragg}	0.053/0.062			

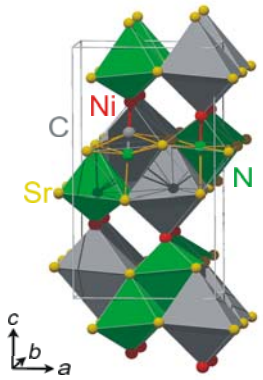

Fig. 2: *Crystal structure of $Sr_2[Ni(CN)N]$. The predominate feature of the crystal structure are isolated $[(NC)NiN]^{4-}$ - units (C-N distance 1.16 Å). Additionally, the octahe-dra NSr_5Ni (green) and $(CN)Sr_5Ni$, which build slabs by edge-sharing, (dark grey) are empha-sized.*

Additional detailed investigations were carried out on the system $(Sr_{3-x}Ba_x)N)Bi$. The mechanism of the transition from cubic perovskite via the various hexagonal stacking variants on increasing barium content was studied with X-ray and neutron diffraction. The homogeneity ranges are as follows:

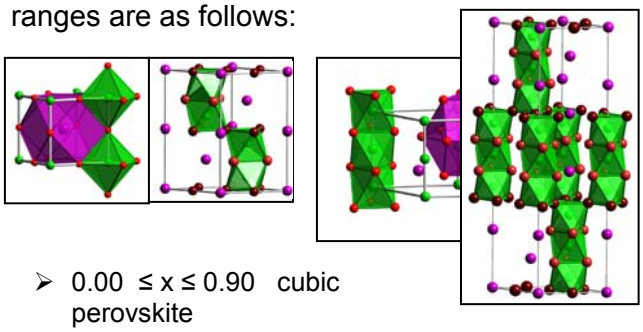

- 0.00 ≤ x ≤ 0.90 cubic perovskite
- 1.55 ≤ x ≤ 2.10 stacking variant 4H
- 2.50 ≤ x ≤ 2.55 stacking variant 9R
- 2.75 ≤ x ≤ 3.00 hexagonal perovskite 2H

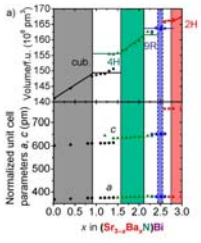

References:

[1]. G.R. Kowach, N.E. Brese, U.M. Bolle C.J Warren, F.J. DiSalvo. J. Solid State Chem. **154** (2000) 542.

[2]. P. Höhn, M. Armbrüster, G. Auffermann, U Burkhardt, F. Haarmann, A. Mehta, R. Kniep. Z. Anorg. Allg. Chem. **632** (2006) 2129.

	EXPERIMENTAL REPORT **Structural study of $Pr_{9.33}(SiO_4)_6O_2$, $Pr_9Li(SiO_4)_6O_2$ and $Pr_8M(II)_2(SiO_4)_6O_2$ (M(II) = Mg, Ca, Sr, Ba)**	Proposal N° CHE-01-1960 Instrument **E9** Local Contact Michael Tovar
Principal Proposer: Experimental Team:	F. Werner – TU Wien, A M. Tovar – HMI, Berlin F. Werner – TU Wien, A	Date(s) of Experiment 31.10. – 03.11.2006

Date of Report: 04.01.2007

The study's aim is to obtain detailed structural information, especially thermal displacement parameters, of the title compounds which constitute potential low temperature oxide ion conductors [1]. The phases were prepared by firing pellets of co-ground Pr_6O_{11}, quartz and the corresponding carbonates at about 1400°C. All products were of light green colour. Powder diffraction measurements were carried out at ambient temperature on the instrument E9 at a wavelength of <λ> = 1.79764 Å with the pulverised samples filled to standard vanadium cans. The powder data were refined with the program GSAS [2]. An example of the structure refinements is shown in Fig. 1.

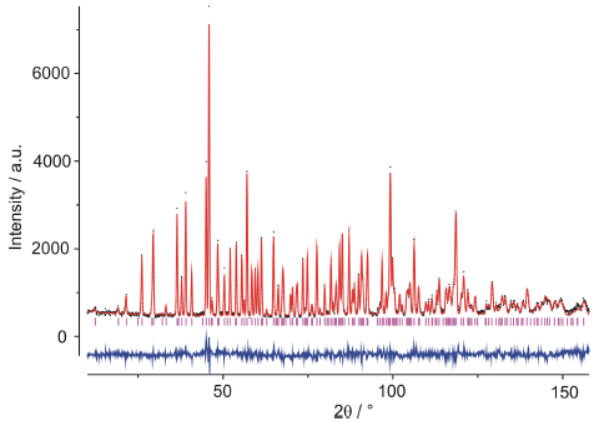

Fig. 1: *Structure refined neutron powder pattern (<λ> = 1.79764 Å) of $Pr_9Li(SiO_4)_6O_2$, R_{wp}=0.061, d^2=2.98, R_{Bragg}=0.060.*

The phases crystallise with the regular apatite structure (SG $P6_3/m$). One of the most interesting structural parameters, the temperature factors of the "free", i.e. nonsilicious oxygens (O4), located in the hexagonal channels were found to be strongly elongated parallel to the c-axis. This is in accordance with the corresponding potassium substituted silicate described earlier [3]. To improve the results simultaneous refinements with X-ray powder data will be undertaken. In addition measurements of the temperature dependent oxide ion conductivity will support to answer the question if there is a relation to the displacement parameters of the oxygen O4.

References:

[1]. Single crystal growth and oxide ion conductivity of apatite-type rare-earth silicates. M. Higuchi, Y. Masubuchi, S. Nakayama, S. Kikkawa, K. Kodaira, Solid State Ionics **174** (2004), pp. 73-80

[2]. A.C. Larson, R.B. Von Dreele, General Structure Analysis System (GSAS), Los Alamos National Laboratory Report LAUR 86-748 (2004)

[3]. Apatite-type Pr9K(SiO4)6O2 - a potential oxide ion conductor. F. Werner, F. Kubel, Mater. Lett. **59** (2005), pp. 3660-3665

Acknowledgement:

This research project has been supported by the European Commission under the 6th Framework Programme through the Key Action: Strengthening the European Research Area, Research Infrastructures. Contract n°: RII3-CT-2003-505925 (NMI3).

BENSC	**EXPERIMENTAL REPORT** **Temperature-induced structure transformations in perovskite lanthanum magnesium titanate**	Proposal N° MAT-01-1966 Instrument **E9** Local Contact Oleksandr Prokhnenko
Principal Proposer: Experimental Team:	A. N. Salak – Univ. Aveiro, P V.M. Ferreira – Univ. Aveiro, P O. Prokhnenko – HMI, Berlin	Date(s) of Experiment 23.10. – 27.10.2006

Date of Report: 05.01.2007

The proposal was aimed to perform a high resolution neutron diffraction experiment on $La(Mg_{1/2}Ti_{1/2})O_3$ at particular temperature ranges to reveal structure transformations associated with oxygen octahedral tilting.
Detailed (short temperature steps) diffraction experiments were performed over two particular temperature ranges: between 60 and 330 K as well as within 1250-1420 K. Intermediate temperature points (700 and 900 K) were also involved in the data collection in order to complete the picture of the temperature evolution of structure parameters.
The collected data were successfully refined with the monoclinic $P2_1/n$ space group (tilt system $a^-b^+a^-$) below 1245 K and rhombohedral $R\bar{3}$ ($a^-a^-a^-$) above 1320 K, respectively (Fig. 1).

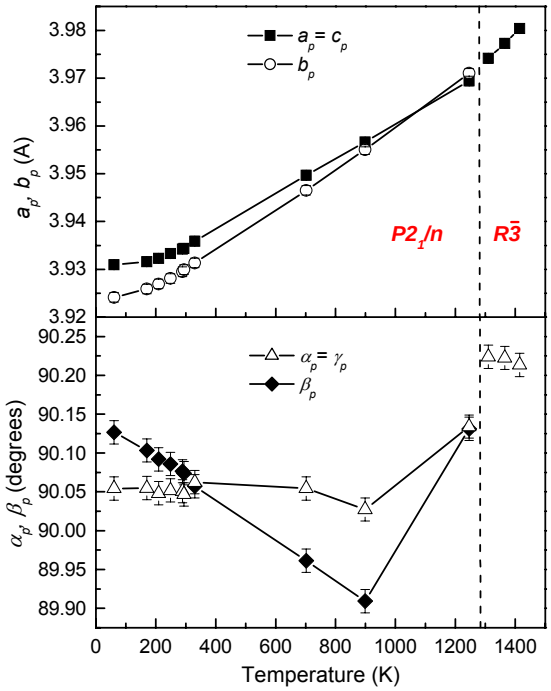

Fig. 1: *Parameters of the primitive perovskite unit cell of LMT (a_p, b_p, c_p and α_p, β_p, γ_p) as a function of temperature. Dash line denotes a range of the phase transition.*

At the same time, the Mg/Ti ordering degree was found to remain unchanged (~96%) over the whole temperature range investigated. Judging from the refined data, the first order phase transition from the monoclinic to the rhombohedral structure occurs without any intermediate phase. Discontinuous character of this structure transformation is also confirmed by the temperature variation of the in-phase tilt angle in the vicinity of the phase transition (see Inset of Fig. 2).

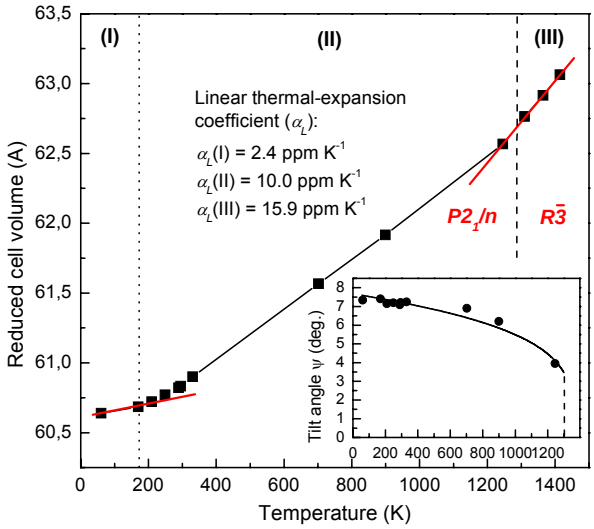

Fig. 2: *Temperature variation of the primitive perovskite unit cell volume of LMT.* ***Inset:*** *the in-phase tilt angle as a function of temperature.*

Since the temperature coefficient of the dielectric permittivity changes a sign at this type of structure transformation, the obtained data on this $P2_1/n$ - $R\bar{3}$ crossover can be useful for a development of the temperature-compensated materials derived from LMT-based perovskite solid solutions.
It has also been revealed that at the lower temperature range the crystal structure of LMT remains monoclinic $P2_1/n$. At the same time, the observed variation of both the structure parameters (Fig. 1) and the value of the linear thermal-expansion coefficient (Fig. 2) suggest some relaxation-like process (stress release) involving the oxygen octahedra in LMT.

Acknowledgement:
This research project has been supported by the European Commission under the 6th Framework Programme through the Key Action: Strengthening the European Research Infrastructures. Contract n°: RII3-CT-2003-505925 (NMI 3).

	EXPERIMENTAL REPORT **Is Deuteration really Changing the Crystal Structure of the Simpler Amino-acid l-alanine?**	Proposal N° PHY-01-1411-EF Instrument **E9** Local Contact Daniel Többens
Principal Proposer: Experimental Team:	H. N. Bordallo – HMI, Berlin D. N. Argyriou – HMI, Berlin D. Többens – HMI, Berlin	Date(s) of Experiment 28.07. – 04.08.2003

Date of Report: 31.10.2006

The origin for the selection of chiral molecules in naturally occurring macromolecules is a fascinating problem for physicists, chemists and biologists not yet fully understood. Protein molecules are composed of L-amino acids while polynucleotides and polysaccharides contain only D-sugars. In spite of the many unanswered questions, it seems nowadays more and more likely that the cause of homochirality of biologically relevant molecules can be assigned to the intrinsic chirality at the elementary particle level. Under these lines the investigation of amino acids serving as building blocks for proteins is of great interest. Considering that the smallest amino-acid, L-alanine, is often used as a model system, we performed accurate powder neutron diffraction study in a broad temperature range in order to complement the available data on possible differences between D- and L-alanine, as well as to analyze questionable structural changes due to deutaration.

L-$C_3D_7NO_2$ was synthesized by Dr. Ehrenstorfer GmbH (Augsburg, Germany). , and the enantiomer was purchased from Cambridge Isotope Laboratories. The samples were quoted with purity greater than 99%, and loaded into their containers in a glove bag flooded with helium.

In agreement with previous work [1], [2],[3] our determination of the structure by the Rietveld method of L- and D-alanine shows no obvious evidence of geometric changes between enantiomers as a function of temperature. However a subtle molecular deformation is clearly revealed by changes in specific bond lengths. One also notes that the $O_2…H_2$ bond distance diverges below 200K, and L-alanine shows a longer $O_2…H_2$ bond distance. On the other hand, while the average N..H bond length as a function of temperature is almost constant in D-alanine, its shows a slight temperature dependence in L-alanine. Consequently our results demonstrate differences in the geometric changes between enantiomers as a function of temperature. This result can be correlated to the fact that in other amino acids the response of the crystal structures of enantiomers is amazingly different to changes of temperature or pressure[4],[5],[6]. In fact we can argue that the compressibility of the H-bonds, or the flexibility of the torsional angles will influence the softness of a structure along a preferred direction. No clear evidence of structural changes due to deutaration could be evidenced.

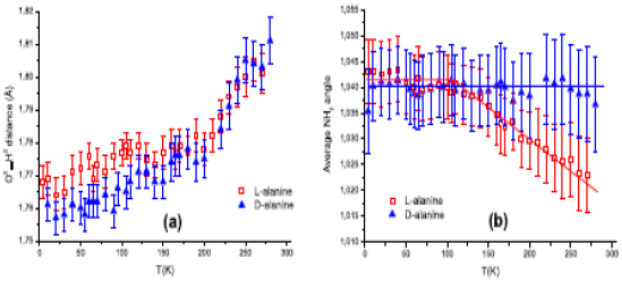

Temperature dependence of the O2 H2 bond distance and (b) average N. H. bond length in Alanine enantiomers. The atoms are labeled as in reference [7].

References:

[1]. R. Sullivan, M. Pyda, J. Pak, B. Wunderlich, J. R.Thompson, R. Pagni, H. Pan, C. Barnes, P. Schwerdtferger, R. Compton J. Phys. Chem. A 2003, **107**, 6674.

[2]. M. S. Lehman, T. F. Koetzle, W. C. Hamilton J. Am. Chem. Soc. 1972, **94**, 2657.

[3]. C. C. Wilson, D. Myles, M. Ghosh, L. N. Johnson, W. Wang, New J. Chem. 2005, **29**, 1318.

[4]. E. V. Boldyreva, S. N. Ivashevckaya, H. Sowa, H. Ahsbahs, H.-P. Weber, H.-P.; Z. Kristallogr. 2005, **220**, 50.

[5]. E. V. Boldyreva, E. N. Kolesnik, T. N. Drebushchak, H. Sowa, H. Ahsbahs, Y. V. Seryotkin, Z. Kristallogr. 2006, **221**, 150.

[6]. S. A. Moggach, D. R. Allan, C. A. Morrison, S. Parsons, L. Sawyer, Acta. Cryst.B 2005, **61**, 58.

[7]. R. Destro, R. E. Marsh, J.; Phys. Chem. 1988, **92**, 966.

BENSC	**EXPERIMENTAL REPORT** **Neutron diffraction study of the atomic and magnetic structure in the $La_{0.7}Sr_{0.3}Co_{1-x}Nb_xO_3$ and $La_{0.3}Sr_{0.7}Co_{1-x}Nb_xO_3$ (x = 0.0 ÷ 0.35)**	Proposal N° PHY-01-1863 Instrument **E9** Local Contact Vadim Sikolenko
Principal Proposer: Experimental Team:	J. Purans – Univ. Povo, IT A. Kuzmenko – Univ. Genf, CH V. Efimov – JINR Dubna, RU V. Sikolenko – HMI, Berlin	Date(s) of Experiment 07.03. – 11.03.2006

Date of Report: 03.06.2006

The discovery of the "colossal" magnetoresistance (CMR) in the manganites with perovskite structure [1] has stimulated the research of the compounds exhibiting large magnetoresistance. The magnetic and transport properties of $La_{1-x}Sr_xCoO_3$ cobaltites with perovskite structure and manganites such as $La_{1-x}Sr_xMnO_3$ have common features [2]. In both systems the substitution of La with divalent ion Sr creates paramagnetic (x < 0.15) to ferromagnetic (x > 0.3) transition as the dopant concentration is increased. The Sr^{2+} ionic radius is significantly greater than that of the La^{3+} ion, so it is possible to expect stabilization of the intermediate spin state of cobalt ions by substituting Sr^{2+} ions for La^{3+} ones. However, at such heterovalent substitution Co^{4+} ions appear, leading to the ferromagnetic metallic ground state [3]. The origin of the ferromagnetic state in metallic cobaltites and manganites has been a subject of discussion for a long time [4]. To prevent the Co^{4+} ion appearance, it is possible to introduce simultaneously Nb ions, which at the presence of Co^{3+} ions will be in oxidizing state 5+. By simultaneously introducing Sr^{2+} and Nb^{5+} the cobalt ions keep their valence state and the electro conductivity of $La_{1-x}Sr_xCo_{1-x/2}Nb_{x/2}O_3$ solid solutions decreases with dopant concentration enhancement. Thus, the different nature of ferromagnetic interactions formation in the given systems is obvious.

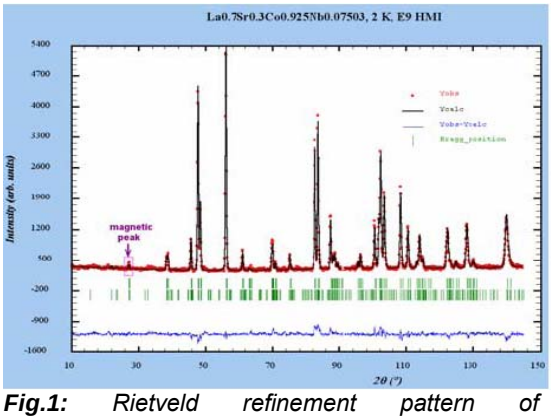

Fig.1: *Rietveld refinement pattern of the $La_{0.7}Sr_{0.3}Co_{0.925}Nb_{0.075}O_3$ powder at the 2 K.*

In this work the atomic and magnetic structu-changes effects induced in $La_{0.7}Sr_{0.3}Co_{1-x}Nb_xO_3$ (x = 0.0; 0.04; 0.075; 0.1 and 0.15) and $La_{0.3}Sr_{0.7}Co_{1-x}Nb_xO_3$ (x = 0.0; 0.04; 0.075; 0.15 and 0.35) powder were studied on the diffractometer E9 with incident neutron wavelength λ = 1.79 Å at the BER-II in Hahn-Meitner Institute.

Fig.1 shows a neutron Powder diffraction pattern and Rietveld refinement of $La_{0.7}Sr_{0.3}Co_{0.925}Nb_{0.075}O_3$ powder at the 2 K.

We have found that the increase of the Nb concentration in the $La_{0.7}Sr_{0.3}Co_{1-x}Nb_xO_3$ and $La_{0.3}Sr_{0.7Co1-x}Nb_xO_3$ leads to the gradual increase of the lattice volume and significant decease of the magnetic moment (table 1a,b). It should be noted that no essential change of the rhombohedral distortions with increase Nb in the $La_{0.7}Sr_{0.3}Co_{1-x}Nb_xO_3$ are observed (table 1 a).

These results were confirmed by X-ray absorption fine structure (EXAFS) and X-ray absorption near edge structure (XANES) at the cobalt K-edge measurements [3].

Table 1: *Structural parameters for (a) $La_{0.7}Sr_{0.3}Co_{1-x}Nb_xO_3$ (x = 0.0-0.15) and (b) $La_{0.3}Sr_{0.7}Co_{1-x}Nb_xO_3$ (x = 0.0-0.35) powder at the 2 K.*

a)

x	0.0	0.04	0.075	0.1	0.15
Sp.gr.	R-3c	R-3c	R-3c	R-3c	R-3c
a (Å)	5.4351	5.4359	5.4367	5.4375	5.4389
b (Å)	5.4351	5.4359	5.4367	5.4375	5.4389
c (Å)	5.4351	5.4359	5.4367	5.4375	5.4389
α	60.410	60.411	60.412	60.410	60.413
V (Å^3)	**113.067**	**113.078**	**113.091**	**113.104**	**113.119**
μ(μ_B)	**2.2**	**1.7**	**0.8**	**-**	**-**
R_{wp}	4.02	5.26	4.81	4.34	5.05

b)

x	0.0	0.04	0.075	0.15	0.35
Sp.gr.	Pm3m	Pm3m	Pm3m	Pm3m	Pm3m
a (Å)	3.8327	3.8331	3.8339	3.8352	3.8363
b (Å)	3.8327	3.8331	3.8329	3.8352	3.8363
c (Å)	3.8327	3.8331	3.8329	3.8352	3.8363
V (Å^3)	**56.3007**	**56.3184**	**56.3536**	**56.4110**	**56.4595**
μ(μ_B)	**2.6**	**1.9**	**1.0**	**-**	**-**
R_{wp}	4.39	5.17	4.49	5.24	5.71

References:

[1]. J.B. Goodenough, Phys. Rev. 155, 932 (1967).
[2]. G. Briceno et.al. Science 270, 273 (1995).
[3]. M.A. Senaris-Rodriguez and J.B. Goodenough, J.Solid State Chem. 118(2), 323 (1995).
[4]. I.O. Troynchuk, J.Exp. Theor.Phys. 75(1), 132 (1992).
[5]. V. Sikolenko, I.O. Troynchuk, A. Kuzmin, V. Efimov, E. Efimova, S. Khasanov, D.I.Kochubey V. Kriventsov, A. Shmakov, S.I. Tiutiunnikov, //Surface investigation X-ray, Synchrotron and Neutron Techniqucs **6**, 23-29 (2006).

	EXPERIMENTAL REPORT **Neutron diffraction structural investigation of natural kesterite**	Proposal N° PHY-01-1957 Instrument **E9** Local Contact Michael Tovar
Principal Proposer: Experimental Team:	S. Schorr – HMI, Berlin S. Schorr – HMI, Berlin M. Tovar – HMI, Berlin	Date(s) of Experiment 22.08. – 24.08.2006

Date of Report: 19.01.2007

The multinary chalcogenide Cu_2ZnSnS_4 (kesterite) has newly attracted attention as possible photovoltaic material [1]. It crystallizes in the kesterite type structure (s.g. *I* 4) which is described in literature [2] as an ordered distribution of the cations Cu^+ and Zn^{2+}. In doing so one Cu occupies the 2a (0,0,0) position, while Zn and the remaining Cu are ordered at 2d (0,¼,¾) and 2c (0,½,¼). Because the elements Cu and Zn are neighbours in the periodic table, the cations Cu^+ and Zn^{2+} have the same number of electrons (28), thus they have equal atomic form factors. Hence both cations are not distinguishable by conventional X-ray diffraction. Neutron powder diffraction is a powerfull method to investingate structures containing electronic similar elements, as the neutron scattering length of Cu and Zn (b_{Cu}=7.718(4) fm, b_{Zn}=5.680(5) fm) is different.
Two natural and one synthetic sample were studied by neutron powder diffraction. The natural kesterites are from different localities. The synthetic sample was prepared by solid state reaction of the elements in a sealed evacuated silica tube at 750°C and finally cooled with 1K/h to room temperature. The chemical composition of all samples was determined by electron microprobe (CAMECA SX100).

Tab. 1: *Chemical composition of the samples.*

no.	chemical composition	locality
1	$Cu_{1.99}(Zn_{0.85}Fe_{0.15})Sn_{1.00}S_4$ and Mushistonite	Xuebaoding, China
2	$Cu_{2.00}(Zn_{0.49}Fe_{0.49})Sn_{1.02}S_4$ and Quartz	Vernérev, Tsch. Rep.
3	$Cu_{1.99}ZnSn_{1.01}S_4$	synthetic

Neutron powder diffraction experiments were performed at the high resolution powder diffractometer E9 (λ=1.79734 Å). Structural parameters and cation site occupancies were obtained by Rietfeld analysis (FullProf) of the data using the kesterite structure as model. The average neutron scattering length of the cation sites 2a, 2c and 2d were determined from the cation site occupanies resulting from the Rietveld analysis. They showed that in the cooled sample (synthetic) a certain degree of cation order is achieved, whereas in the quenched sample Zn and Cu are completely disordered on 2c and 2d [3].

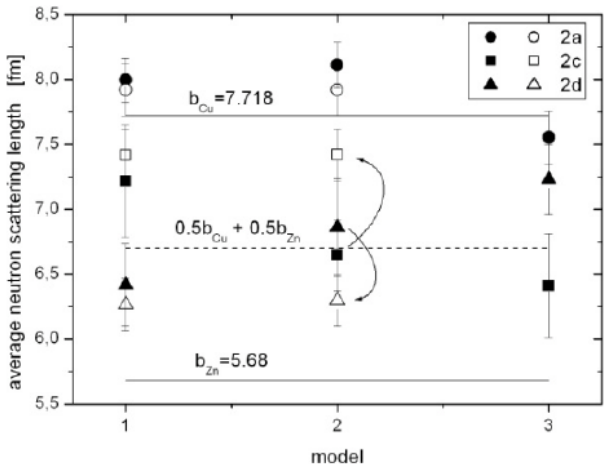

Fig. 1: *Average neutron scattering length of the cation sites 2a, 2c and 2d for the quenched (solid symbols) and controlled cooled (open symbols) synthetic kesterite. In the refinement different cation distribution models (no. 1-3) were used (cf. [3]).*

The natural kesterites contain a second mineral phase, Mushistonite $CuSn(OH)_6$ and Quartz, respectively. For sample no. 2 the average neutron scattering length of the cation sites 2a and 4d (s.g. *I* 42m) show clearly a different cation distribution as a comparable quenched synthetic sample [3] (cf. table 2). A more detailed data analysis is ongoing.

Tab. 2: *Comparison quenched and natural kesterite.*

sample	b_{av}(2a)	b_{av}(4d)
quenched [3]	7.900 (160)	7.675 (162)
no. 2	7.481 (170)	7.282 (170)

Thus the results allow the suggestion that the degree of cation order depends on the thermal history of the kesterite.

References:

[1]. Katagiri, H. Thin Sol. Films **480-481**, 426-432 (2005).
[2]. Hall, S.R. et al., Can. Mineral., **16**, 131 – 137(1978).
[3]. S. Schorr, H.-J. Hoebler, M. Tovar, Europ. J. Min. **19** (2007) in print.

	EXPERIMENTAL REPORT **Lattice dynamics of strongly doped GaAs**	Proposal N° PHY-02-0524 Instrument **E1** Local Contact Vadim Sikolenko
Principal Proposer: Experimental Team:	A. Naberezhnov – PTI St. Petersbg., RU V. Sikolenko – HMI, Berlin S. Borisov – PTI St. Petersbg., RU	Date(s) of Experiment 07.02. – 18.02.2006

Date of Report: 29.10.2006

Earlier it was shown that doping with tellurium (to a carrier concentration $N_e \approx 2\times10^{18}cm^{-3}$) results in the appearance of an additional contribution to neutron scattering on the high-energy side of the TA phonon resonances at values of the reduced wave vector $q < 0.1$ a^*. Below 320 K, the intensity of this additional component rises sharply, and then, below 273 K, the main TA peak and the additional shoulder merge almost completely [1, 2]. It was supposed that this additional scattering is believed to be due to a defect-induced mode, which may be responsible for the observed anomalies in the physical properties such as sound velocity specific heat and IR absorption near the room temperature in this crystal [3].

We have carried out the study of evolution of Δ_{TA} resonance lineshape and temperature evolution of QES at 297, 308, 318, 335, 355 and 375 K at different BZ ((220), (004), (222) and (331)) using strongly doped and pure GaAs single crystals. On Fig. 1 the results of E-constant scan in a vicinity of (220) BZ at E=0.9 THz are presented for both crystals. At high temperature the width of phonon resonance in doped sample (upper figure) corresponds practically the width observed in pure GaAs (bottom figure). Approaching 320 K it increases and additional scattering is observed at smaller q. This result confirms the appearance of defect induced mode at small q located above Δ_{TA} normal resonance as it was supposed in papers [1, 2].

At present time the inelastic and QES data obtained for different BZ in PHY-02-0448 and PHY-02-0524 experiments treat. The preliminary results were presented as poster on 19th Russian National Workshop on Applications of Neutron Scattering in Study of Condensed Matter, 12-15 September 2006, Obninsk

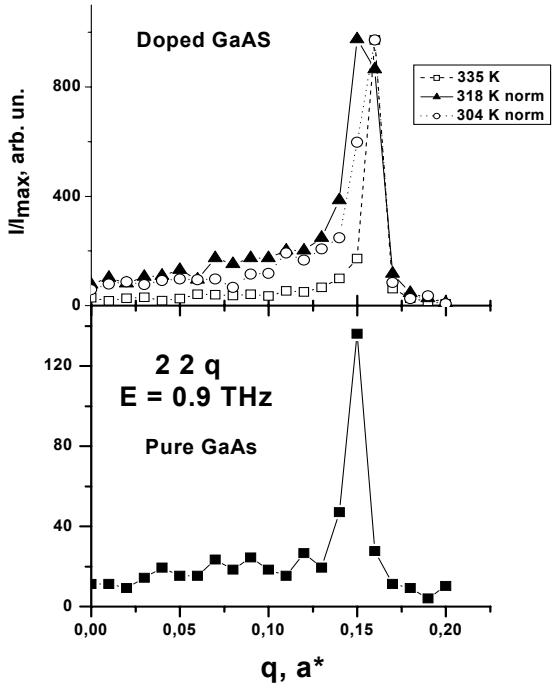

Fig. 1

References:

[1]. S.A. Borisov, S.B.Vakhrushev, A.A. Naberezhnov, N.M. Okuneva Phys. of the Solid State 47(6), 2005, 1060

[2]. A. Naberezhnov, V. Sikolenko, S. Borisov BENSC experimental report PHY-02-0448 (2005), Berlin, Germany

[3]. Balagurova, E.A., Grekov, Yu.B., Kravchenko, A.F., Prudnikov, V.V., Prudnikova, I.A., Semikolenova, N.A., Physics and Technics of Semiconductors, 19, 1985, 1566 (in Russian)

	EXPERIMENTAL REPORT NRSE investigation of the electron-phonon interaction in the BCS superconductor Nb	Proposal N°PHY-02-0511-LT PHY-02-0569-EF Instrument **V2** Local Contact Klaus Habicht
Principal Proposer: Experimental Team:	K. Habicht, F. Mezei – HMI, Berlin T. Keller – MPI Stuttgart +TUM P. Aynajian, B. Keimer – MPI FKF Stuttgart K. Habicht – HMI, Berlin	Date(s) of Experiment 05.01. – 11.01.2006 07.09. – 14.09.2006 23.11. – 11.12.2006

Date of Report: 09.01.2007

The electron-phonon interaction is the well-known underlying mechanism in the BCS theory of superconductivity where it provides the small but attractive potential between electrons responsible for the formation of Cooper-pairs. For metallic, superconducting elements modern *ab-initio* calculations yield accurate predictions for the electron-phonon coupling parameters of every phonon over the Brillouin zone. The experiments performed here are aimed at providing precise experimental data for comparison with such theoretical predictions.

To achieve high resolution the NRSE option has been used on V2/FLEX measuring the electron-phonon contribution to the phonon linewidth of several individual acoustic phonons in Nb in the low-q part of the [ξξ0] T_2 phonon branch where significant changes in the linewidth have been observed by Shapiro *et al.* [1]. Following the approach developed by Axe and Shirane [2], linewidths were measured at two temperatures T=2 K and 12 K, i.e. well below and above T_C=9.2 K. For phonons with energy lower than twice the superconducting gap energy 2Δthe decay channel via electron-phonon interaction is suppressed due to the stability of Cooper-pairs. Above T_C this decay channel opens up such that the electron-phonon contribution to the phonon linewidth is simply given by the difference $\Gamma_{e\text{-}p}$= Γ(12K) - Γ(2K). Fig. 1 displays the temperature dependence observed for the [ξξ0] T_2 phonon with ξ= 0.05 rlu.

FLEX was operated in a configuration with scattering senses (SM=-1, SS=-1, SA=+1) with an experimental transverse Q-resolution of about 0.025 $^{-1}$ FWHM at fixed incident k_i = 2.62 $^{-1}$. No additional collimators were used besides bender polarizers inserted behind the PG monochromator and behind the PG analyzer. Second-order contamination is substantially suppressed by the curved neutron guide. The required tilt angles of the RF-flippers were calculated from linear fits to dispersion data taken during the beginning of the experiment in the present setup, e.g. for the [2 0.06 0.06] T_2 phonon θ_1= -29.2°, θ_2= 25.3° were used. The Nb-crystal was mounted with the [hkk] plane as the scattering plane and T_2 phonons were measured along [2ξξ].

Fig. 2 summarizes the experimental results on the q-dependence of the phonons investigated in the range 0.03 rlu ≤ξ ≤ 0.10 rlu. As expected the high-temperature linewidth exceeds the low-temperature linewidth for all ξexcept for ξ =0.10 rlu where the phonon energy E_{phonon}=3.41 meV exceeds 2Δ at all temperatures. With decreasing ξ≤ 0.07 rlu the measured linewidths increase for both temperatures due to the increasing curvature of the dispersion surface. At ξ =0.03 rlu substantial elastic contamination of the signal is present with the effect of decreasing the uncorrected linewidth again.

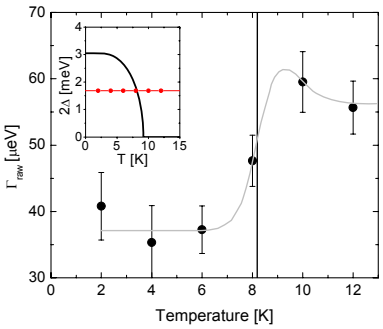

Fig. 1: *Temperature dependence of the linewidth (raw data) for the [ξξ0] T_2 phonon with ξ = 0.05 rlu and E_{phonon} = 1.685 meV. The vertical line indicates the crossover temperature T~8.2K where the phonon energy equals 2 Δ(see also insert).*

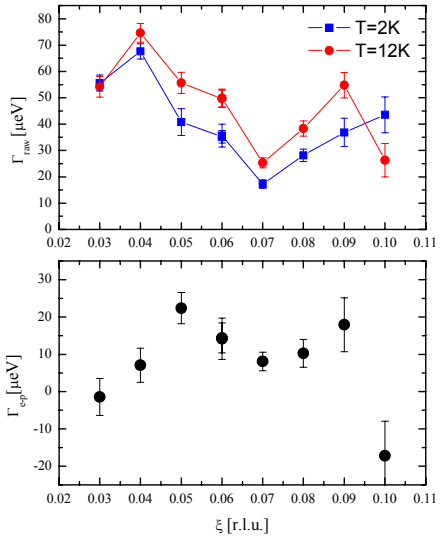

Fig. 2 - top: *Raw data linewidths above and below T_C for the low-q region of the [ξξ0] T_2 phonon; bottom: $\Gamma_{e\text{-}p}$= Γ(12K) - Γ(2K).*

References:

[1]. S.M. Shapiro *et al.,* Phys. Rev. B **12**, 11, 4899 (1975)

[2]. J.D. Axe, G. Shirane, PRL. **30**, 6, 214 (1973).

	EXPERIMENTAL REPORT **Short range charge ordering in Fe_3O_4**	Proposal N° PHY-02-0559 Instrument **V2** Local Contact Klaus Habicht
Principal Proposer: Experimental Team:	T.Chatterji – ILL Grenoble, F T.Chatterji – ILL Grenoble, F K. Habicht – HMI, Berlin	Date(s) of Experiment 21.08. – 27.08.2006

Date of Report: 09.09.2006

The Verwey transition observed in strongly correlated electron systems is caused by the strong Coulomb repulsion leading to electron crystallization. It is characterized by the simultaneous changes in crystal symmetry and electrical conductivity and was first discovered in magnetite Fe_3O_4 near T_V = 120 K. The transition is accompanied by a) a jump in the magnetization, b) a specific heat anomaly, c) a drop in the resistivity (metal-insulator transition) and d) an abrupt thermal expansion of the lattice parameters [1]. To explain these effects Verwey originally proposed a model of charge ordering (Fe^{2+} - Fe^{3+}) within the octahedral Fe sites in the inverse spinel structure of magnetite. The original orthorhombically distorted superstructure proposed by Verwey is, however, only approximate and the actual low temperature structure of magnetite has monoclinic symmetry. In a recent model, charge ordering is described by complex charge density waves accompanied by (small) atomic displacements on a local scale [2]. Short range order has been indeed found in magnetite by neutron diffuse scattering above the Verwey transition and appears to be essential to explain the transport properties of magnetite [3].

Our proposal (PHY-02-0559) had two parts. The first part was to study the diffuse scattering in magnetite in more details and fit the experimental data with some realistic model including strong electron correlations. Previous inelastic neutron scattering experiments [4] have shown that the diffuse scattering in magnetite has different characteristics than the one caused by soft phonons in the immediate vicinity of a structural phase transition and was later interpreted in terms of cooperative motion of molecular polarons [5] where charge density fluctuations at octahedral sites are coupled with transversal phonons [6]. Because of insufficient resolution (thermal neutrons), the energy-width of the quasi-elastic scattering as a function of a function of both temperature and momentum transfer, q could not be studied.

We have done the experiment on the cold triple-axis spectrometer V2 at the Berlin Neutron scattering Center. In the allocated beam time (6.5 days) we could do a few constant-Q scans from Fe_3O_4 at two values of Q, viz. Q = (0.15,0.15,4) and

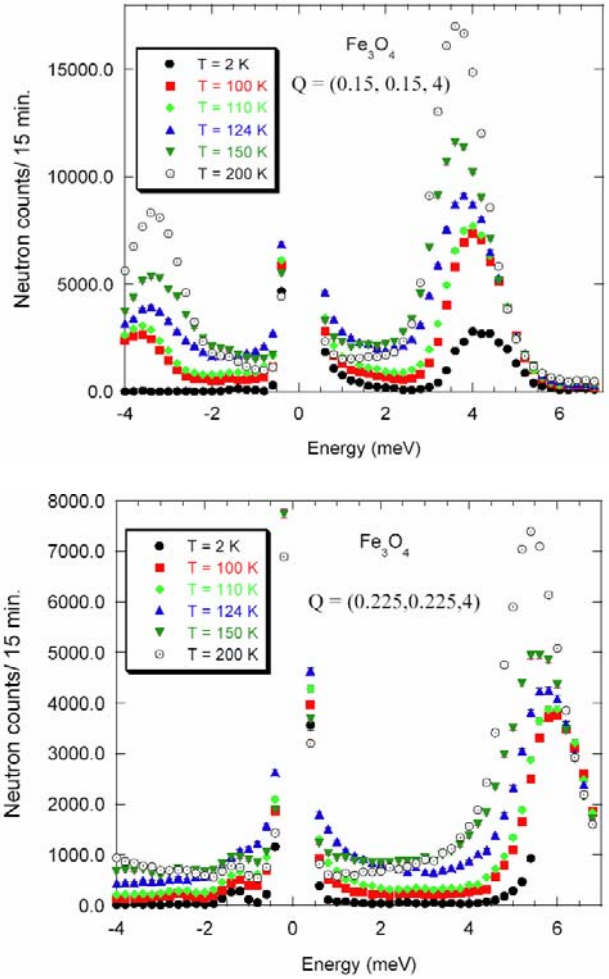

***Fig. 1**: Inelastic neutron spectra of Fe_3O_4 (top) at **Q** = (0.15,0.15,4) and at (bottom) **Q**=(0.225,0.225,4) at T = 2, 100, 110, 124, 150 and 200 K. The transverse acoustic phonons are observed in both energy gain and loss sides for the scan at **Q** = (0.15,0.15,4) whereas for the scan at **Q**=(0.225,0.225,4) the phonon at the energy loss side is outside the scan range. The quasielastic scattering becomes prominent at temperature close to T_V = 120 K.*

→

Q = (0.225,0.225,4) and at six temperatures viz., T = 2, 100, 110, 124, 150 and 200 K. The data were obtained at k_f = 1.97 A^{-1} and colli-

mation guide-open-open-open. We used vertically curved PG(002) monochromator and a horizontally curved PG(002) analyser crystals and also PG(002) filter. The energy resolution was about 0.46 meV. Fig. 1 shows inelastic neutron spectra of Fe_3O_4 (top) at Q = (0.225,0.225,4) and (bottom) at Q = (0.15,0.15,4) at T = 2, 100, 110, 124, 150 and 200 K. To analyse the data we first considered Yamada's model [6]. The same model was applied by Shapiro [4] to analyze his data. Yamada [6] considered acoustic phonons coupled to some variables called 'spins'. The explicit form can be found in Reference [6] and consists essentially in a damped-harmonic oscillator to describe the phonon line-shape and in a Debye-like relaxation function to describe the dynamics
of the pseudo-spins. We found out that this model does not fit the experimental data satisfactorily. At present we are trying to fit the data with a more sophisticated model which includes strong electron correlations involved in the Verwey transition.

The second part of our accepted proposal was to investigate spin wave dispersion of Fe_3O_4 close to the zone center and determine the spin wave gap as a function of temperature. We could not do this part of measurement during the limited beam time allocated to us. We have submitted a continuation proposal for completing this part and requested 7 days of neutron beam time.

References:

[1]. F. Walz, J. Phys.: Condensed Matter **14**, R285 (2002).
[2]. J. P. Wright et al. Phys. Rev. B **66**, 214422 (2002).
[3]. D. Ihle and B. Lorenz, J. Phys. C: Solid State Phys. **19**, 5239(1986).
[4]. S. M. Shapiro et al., Phys. Rev. B **14**, 200 (1976).
[5]. Y. Yamada et al., Phys. Rev. B **21**, 4642 (1980).
[6]. Y. Yamada et al., J. Phys. Soc. Japan **36**, 641 (1874).

	EXPERIMENTAL REPORT **Density of states of the superconductor $Na_{0.3}Ca_{O3}$ * y H_2O**	Proposal N° PHY-03-0307-EF Instrument **V3** Local Contact Jörg Pieper
Principal Proposer: Experimental Team:	H. N. Bordallo – HMI, Berlin N. Aliouane, C. Milne – HMI, Berlin D. Argyriou – HMI, Berlin J. Pieper – HMI, Berlin	Date(s) of Experiment 08.08. – 10.08.2006

Date of Report: 15.06.2006

The tuning of Na content in the alkali layered cobaltate Na_xCoO_2 results in remarkable changes in its physical behaviour, ranging from magneto-thermoelectricity at x=0.75 to charge ordering at x=0.5 and 5 K superconductivity (SC) after intercalation of H_2O for x=0.3 [1]. The crystal structure of this system is complex and has been solved using sophisticated neutron scattering methods. While our inelastic neutron scattering (INS) studies does not provide an insight into the SC itself, it is critical to understand the crystal chemical mechanism of inserting water between Na and CoO_2 sheets. This mechanism is critical as it makes the electron density more 2D like and induces a SC transition at low temperatures. Our INS results provide interesting information about the water vibrational modes, connected to the structure of $Na_{0.3}CoO_2$*yH_2O, which can not be obtained using any coherent scattering.

The generalized density of states (GDOS) of $Na_{0.3}CoO_2$*yH_2O was obtained within the framework of the "incoherent approximation" [2]. The results were obtained using V3, with λ_i= 5.1 Å, ΔE of 98 μeV (FWHM), within an angular range of 13.3°< φ<136.7°. An orientation angle of α= 135° with respect to the incident neutron beam direction was used.

From previous GDOS measurements of bulk water obtained by means of neutron an Raman scattering [3,4], the vibrational motions have been assigned as follows. The peaks around 6 and 20-35meV correspond respectively to the bending of the O-O-O and to the stretching of the O-O units, while a broad vibration around 70meV is related to librational modes. Furthermore a manifestation of the four-coordinated molecules can be observed only at low temperatures at 33meV. In the particular case of $Na_{0.3}CoO_2$1.3H_2O, the local environment of the water consists of 2 nearest neighbours sodium atoms, consequently one expects 2 water/cation stretch modes, that will contain contributions of both water/cation and H-bond stretch. Thus the spectra of $Na_{0.3}CoO_2$1.3H_2O, shown below can be compared with those of water-mixtures, water in zeolites and crystal hydrates [4-6], where the sharpening of the band around 20meV, barely visible in pure water, corroborates with the idea of an enhancement of cation/water correlations. Furthermore, in the dry $Na_{0.3}CoO_2$ compound we observe collective motions below 40 meV and librational motions around 60meV. Thus the band observed in $Na_{0.3}CoO_2$1.3H_2O, in the region 20-40 meV can be assigned to water/cation and H-bond stretch modes. Furthermore it is expected that the frequency of the stretching mode to be dependent on the OH…Na distance [7], so the observed frequencies observed in this study can be directed compared to [8].

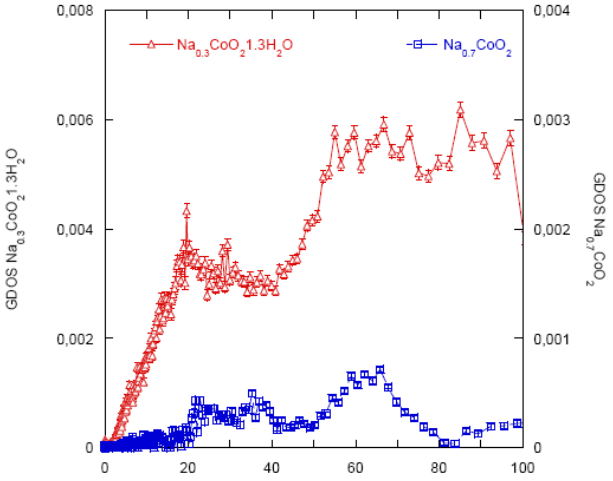

References:

[1]. Takada K., et al., Nature 422, 53 (2003)
[2]. Carpenter, J. M. ; Pelizarri, C. A. Phys. Rev. B 1975, 12, 2391
[3]. M.-C. Bellissent-Fune et al. J. Mol. Struct. 250, 213 (1991)
[4]. V. Venuti et al.l, J. Phys. IV 10 Pr7 (2000)
[5]. H.J. Prask and H. Boutin, J. Chem. Phys. 45, 3284 (1966)
[6]. V. Crupi et al. J. Phys.: Condens. Matter 16, S5297 (2004))
[7]. I.A. Beta et al. Physical Chemistry, Chemical Physics 6 1975 (2004)
[8]. C.M.B. Line and G.J. Kearley, J. Chem. Phys. 112, 9058, (2000)

	EXPERIMENTAL REPORT **Dynamical transition in the amino acid L-alanine**	Proposal N° PHY-03-0364-EF Instrument **V3** Local Contact Alexandra Buchsteiner
Principal Proposer: Experimental Team:	H. N. Bordallo – HMI, Berlin M. Barthès – Univ. Montpellier II, F F. Denoyer – Univ. Paris XI, F C. Fehr, J. Pieper, A. Buchsteiner– HMI Berlin	Date(s) of Experiment 21.09. – 26.09.2004

Date of Report: 21.10.2004

The role of dynamics in enzyme function is a subject of increasing interest. Trying to address such issues at the molecular level, changes in the internal dynamics of proteins as a function of solvent conditions have been examined using several techniques X-ray diffraction, INS, other spectroscopies and simulations have demonstrated the existence of a so-called dynamical transition; i.e. a qualitative change in the nature of internal motions of proteins, generally at about 220 K [1]. Below the transition, the internal motions are thought to be essentially harmonic, while above their unharmonicity contributes and, at physiological temperatures, dominates the internal fluctuations. While it is well accepted that solvent can strongly influence protein structure and dynamics, up to now experiments to test the comportment of isolated amino acids have not been done.

With this in mind we started a series of experiments on alanine, one of the amino acids serving as building blocks for proteins. Here we report on the continuation of a selective deuteration study of the dynamics of each hydrogen group in polycrystalline L-alanine ($C_2H_4(NH_2)COOH$). The experiments were performed using NEAT at HMI from 100 to 300K [2]. Between 100 and 190 K no quasi-elastic component was observed implying a solid like behavior, whereas the development of quasi-elastic signal above 190K suggests the onset of a "liquid like" motion on alanine. Furthermore the observation of a boson peak is a sign of orientation disorder [3,4] what corroborates with our recent diffraction experiments [5].

The figure shows the evolution of the mean-square displacement of each the hydrogen group and the evolution of the $\tau(CO_2)$ group (red line). Since the S(Q) signal arises manly from the incoherent neutron scattering from hydrogen atoms, the elastic intensity follows the expression $\ln[S(Q)=-\langle u_H^2\rangle Q^2$. We can observe that $\langle u_H^2\rangle$ increases steadily with increasing temperature. But near 150K and again near 200K the line breaks indicating the excitation of new degrees of freedom.

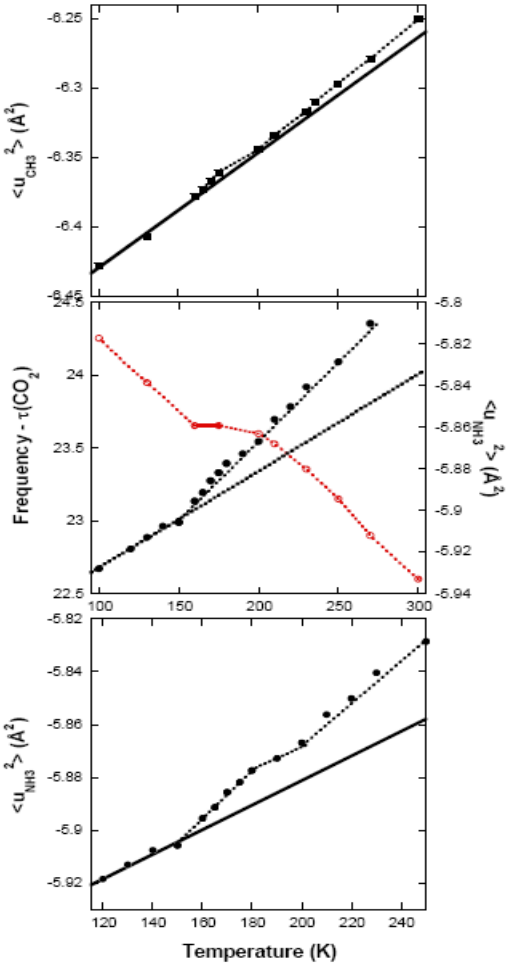

One needs to ask what physical mechanisms are responsible for this new excitation and if they are correlated to the torsional jumps observed in protein. A more detailed analysis is under way, but we would like to point out that both the $\tau(NH_3)$ [6] and $\tau(CO_2)$, as shown here, present discontinuities at the same temperatures where breaks on the evolution of the mean-square displacement were observed.

References:

[1]. See for example W. Doster et al, Nature 337 754 (1999)
[2]. H.N. Bordallo et al, BENSC Report (2003)
[3]. E. Whalley and J.E. Berthe, J. Chem. Phys. 46 1264 (1967)
[4]. H. Leyser et al, PRL **82** 2987 (1999).
[5]. M. Barthes, et al European Phys. J. B **37**, 375 (2004); and experimental report on E9 results.
[6]. M. Barthes et al. J. Chem. Phys. A **106,** 5230 (2002)

	EXPERIMENTAL REPORT **Understanding the dynamics of alpha, beta and gamma polymorphs of glycine**	Proposal N° CHE-03-0423 Instrument **V3** Local Contact Alexandra Buchsteiner
Principal Proposer: Experimental Team:	H. N. Bordallo – ILL, Grenoble E. Boldyreva – RAS SB+NSU, Novosibirsk,RU S. Landsgesell – HMI, Berlin A. Buchsteiner – HMI, Berlin	Date(s) of Experiment 16.05. – 23.05.2006

Date of Report: 15.06.2006

Here we used dynamic neutron scattering to investigate the 3 polymorphs (α - $P2_1/n$, β- $P2_1$, γ- $P3_1$ ($P3_2$)) of glycine [1]. In the α-polymorph zwitter-ions are linked by hydrogen bonds in double antiparallel layers, the interactions between these double layers being purely Van-der-Waals. In the β-polymorph individual parallel layers are linked by H-bonds in a 3D network. And in the γ-polymorph zwitter-ions form helixes linked with each other in a 3D network. Our interest in glycine is two fold. First it is smallest amino-acid, and like so it can serve as a model for studying important interactions in biological systems, as well as factors determining the changes in the secondary structure of biopolymers. Moreover insight in the strength of the intermolecular hydrogen bonds that link the zwitter-ions in the crystal can shed light on the origin of polymorphism in glycine and in extension in the polymorphism of drugs. To perform our experiment we benefited of two points: (i) our ability to get reproducibly pure β-glycine without admixtures of α and γ-forms in quantities of grams, following the original method described in reference 2; and (ii) as the £\-polymorph does not show any structural anomalies on cooling, so its QE and INS results can be used as a very good reference point when compared to those for β and γ-forms.

Time-of-flight spectra were measured using V3, with incident wavelength of 5.1 Å, corresponding to elastic energy resolution ΔE of 98 μeV (FWHM) within an angular range of $13.3° \leq \varphi \leq 136.7°$. An orientation angle of φ= 135° with respect to the incident neutron beam direction was used for all samples, including vanadium and empty cell. Although the temperature controller did not work on cooling, we were able to obtain 60 sets of data that allowed for a comprehensive comparison of the 3 polymorphs.

The figure shows the evolution of the normalized elastic intensity, S(q), for each sample. S(q) signal arises manly from the incoherent neutron scattering from hydrogen atoms, and is supposed to follow the expression $S(Q)=-\langle u_H^2 \rangle T$ From the figure we can clearly observe that up to 50K, the mean-square displacement $\langle u_H^2 \rangle$ increases steadily on cooling for α- and γ-polymorphs. In contrast for the β-polymorph, near 220K the line breaks indicating the excitation of new degrees of freedom. This observation agrees with adiabatic calorimetric studies where indication of a phase transition around 250K was observed [3]. Moreover anomalies were also noted in a Raman spectroscopy study [4]. However no manifestations of this transition could be followed by X-ray single-crystal diffraction, which agrees with the hypothesis of a second order phase transition [1,5].

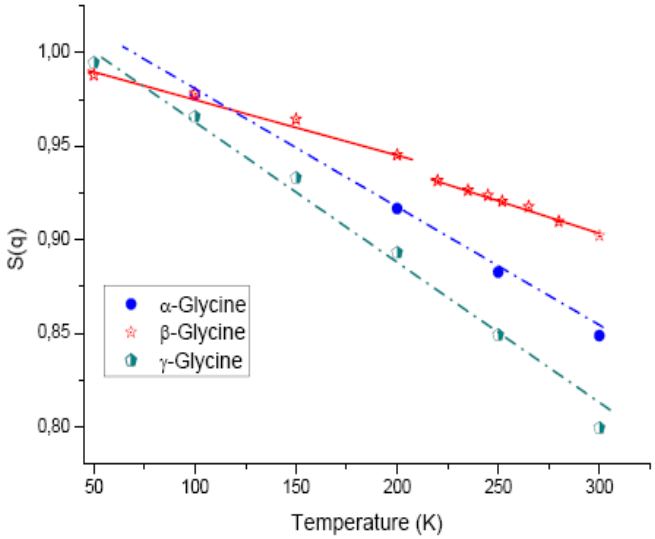

Furthermore in order to analyze the inelastic response of glycine we also obtained the generalized density of states (GDOS), within the framework of the "incoherent approximation" [6]. The data is not shown.

References:

[1]. V. Drebushchak et al., J. Thermal Analysis and Calorimetry, **74** (2003) 109-120.
[2]. V. Drebushchak et al. Journal of Crystal Growth, 2002, **241,** 266-268.
[3]. V.A. Drebushchak, et al J. of Thermal Analysis and Calorimetry, **79** (2005) .6336-6341.
[4]. E. Boldyreva private communication
[5]. E. Boldyreva, et al. Z. Krist. **218** (2003) 366-376.
[6]. J. Carpenter, C. Pelizarri, Phys. Rev. B 1975, **12**, 2391

	EXPERIMENTAL REPORT INS of cobalt hydroxy squarate	Proposal N° CHE-03-0427 Instrument **V3** Local Contact Margarita Russina
Principal Proposer: Experimental Team:	P. Wood – Univ. of Cambridge, UK R. Mole – Univ. of Cambridge, UK M. Russina – HMI, Berlin	Date(s) of Experiment 09.01. – 13.01.2006

Date of Report: 15.01.2007

Inelastic neutron scattering is an ideal probe to study both the single ion behaviour and the spin wave excitations within low dimensional materials. A preliminary experiment was performed using the multichopper time-of-flight inelastic neutron scattering instrument NEAT at the Hahn-Meitner-Institute on the compound cobalt hydroxy squarate $(Co_3(OD)_2(C_4O_4)_2.3D_2O$. Although the single ion effects and spin wave behaviour were expected to be of a similar order of magnitude, the exact energy of both is not known. To get a good overview of the effects, 3.6 Å neutrons were used - this allowed a large range of energies (0 to -6 meV) with good resolution at the elastic line. Data were collected at 2 K, 3.5 K and 7.5 K (Fig. 1); these temperatures are in line with the three ordered phases observed using neutron diffraction.

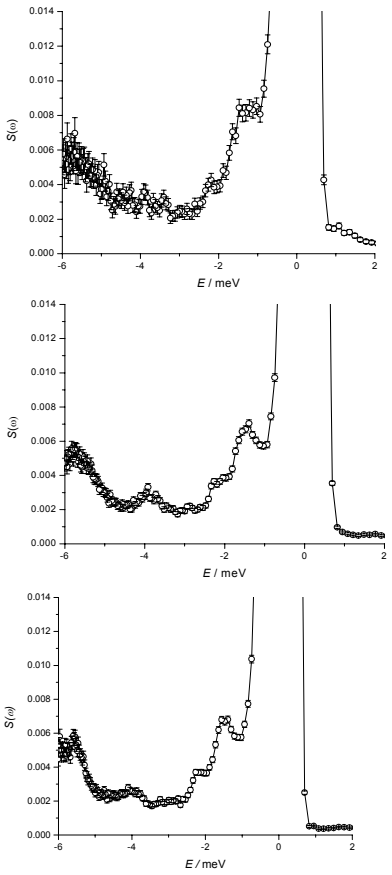

Fig. 1: *INS spectrum of $Co_3(OH)_2(C_4O_4)_2.3H_2O$ at 2 K, 3.5K and 7.5 K (right to left).*

The 2 K data shows two major features. Firstly there are two peaks very close to the elastic line at -1.35 meV and -2.09 meV. Secondly a broader peak at around -6 meV. The data at 3.5 K is almost identical to that at 2 K. At 7.5 K the high enerrgy feature is much broader no longer structured, while the excitations close to the elastic line now appear as a shoulder, as opposed to a separate peak.

On the basis of peak shape, energy and temperature dependence the feature at 6 meV has been assigned to spin wave excitations. Given the low resolution at this energy and the poor counting statistics no further analysis of this excitation has been carried out. The two excitations close to the elastic line have been assigned to single ion behaviour. The change in intensity of the -1.35 meV peak between 3.5 K and 7.5 K is in agreement with the structural analysis at these temperatures. During the phase transition at 6 K the symmetry of the structure becomes dependent on the single ion behaviour and thus zero field splitting of one of the two Co ions. This manifests itself in the INS spectrum by showing a change in population of the single ion energy levels of Co2. In comparison, the ordering transition for Co1, on going to the 2 K phase, is not dependent in a change in symmetry, consequently we would not expect to see a similar shift in population of the energy levels. To assign these transitions correctly we need to know the exact nature of the zero-field splitting (ZFS). For a cobalt ion in a perfect octahedral environment this splitting is well known. In the case of $(Co_3(OD)_2(C_4O_4)_2.3D_2O$, the distortion results in a reduction in symmetry. The complete description of the ZFS would have to assume C_s symmetry of the octahedral ion due to the asymmetric nature of the distortion. It is thought that symmetry can still be utilised to determine the ZFS, but more accurate and complementary data is needed to describe any electronic transitions.

To fully characterise all these excitations further data is required. In particular longer counting times are required to obtain better statistics, this would allow the *Q* dependence of all excitations to be determined - this is exceptionally important when distinguishing between single ion and spin wave effects. Further to this experimental work, more theoretical analysis is also required.

	EXPERIMENTAL REPORT **Analysis of microstrain in quartz regarding concrete stability**	Proposal N° GEO-01-1760 Instrument **E9** Local Contact Oleksandr Prokhnenko
Principal Proposer: Experimental Team:	G. Klöß – Uni, Leipzig S. Schorr, O. Prokhnenko – HMI, Berlin G. Klöß – Uni, Leipzig J. Stark, E. Freyburg – BHU, Weimar	Date(s) of Experiment 16.01. – 19.01.2006

Date of Report: 18.01.2007

Alkali-aggregate reaction (AAR) is a common cause of concrete cracking that result in significant damage to concrete structures worldwide. Until now the mechanism of this alkali-silica reaction was not really well understood [1,2].

Quartz is the most important additive in concrete. The AAR reactivity of quartz crystals may vary in wide limits. In particular the reactivity depends on the metamorphic exposure of quartz-rich rocks. The crystallographic background of the quartz reactivity can be found in a different real structure of the individual crystals (e.g. dislocation density).

One of the critical points of experimental microstrain measurements may be the considerable correlation between sample preparation and linewidth in the X-ray diffractogram. The detachment of grinding and natural induced peak broadening is not really practicable. Therefore a strong grinding of the samples should be evaded in order to avoid this problem.

Thus we used 1 mm coarse-grained "powder" samples of different stressed quartz-rich gravel. For comparison powder of rock crystals (1 mm and 63 µm grained) and a Sahara Desert fulgurite (10 x 1 cm^2) was used for the experiments at the E9 high resolution powder diffractometer. The large sample volume of about 4 cm^3 measured in the neutron diffraction experiment preserves the statistics.

The results given in figures 1 and 2 show a line fit of the measured FWHM values of 23 diffraction peaks of quartz (100, 011, 110, 102, 111, 021, 112, 202, 210, 121, 113, 300, 104, 032, 220, 131, 204, 132, 105, 214, 223, 320, 231). The fit of the instrumental standard coincides with the most perfect 1-mm-grained rock crystal virtually. The small differences and some lower values of rock crystal demonstrate the experimental reproducibility, whereas the difference between the two rock crystal samples at small tanθ indicates an effect of grain size (fig. 1). Fig. 2 gives the increased line width of quartz samples due to microstrain increasing from quartz_1 to quartz_3. These results were confirmed by undulatory extinction observed with crossed polars. The FWHM differences at higher tan between the 63-µm-fine-grained rock crystal and all metamorphic quartz samples show that the influence of grinding exists but is only small. Otherwise the anomalous thermal history of the fulgurite results in a huge line broadening.

Detailed results using Rietveld refinements will be reported in a related paper.

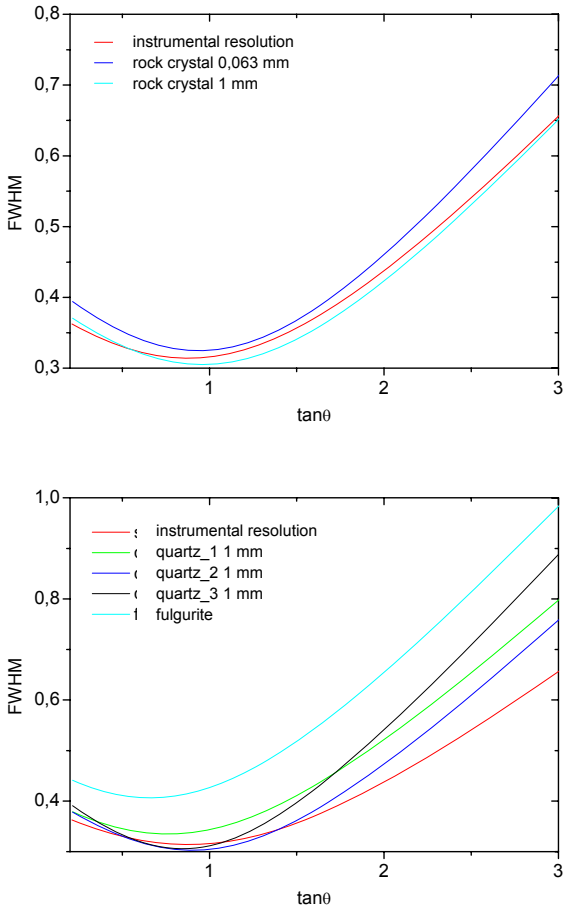

Fig.1 and 2: *Peak broadening of SiO_2-samples due to different microstrain.*

References:

[1]. Freyburg, E., Berninger, A.M.: IBAUSIL **2** (2003) 719-734

[2]. Chatterji, S. et. al. : Cement Concr. Res. **19** (1989) 177-183

BENSC	**EXPERIMENTAL REPORT** **Structure Refinement of Mn-Brownmillerite Phases**	Proposal N° GEO-01-1860 Instrument **E9** Local Contact Oleksandr Prokhnenko
Principal Proposer: Experimental Team:	S. Stöber – MLU Halle S. Schorr – Uni Leipzig O. Prokhnenko – HMI, Berlin	Date(s) of Experiment 29.03. – 03.04.2006

Date of Report: 26.04.2006

Brownmillerite phases with the chemical composition $Ca_2Fe_{2-x}Al_xO_5$ 0<x<1.66 are important clinker phases in Ordinary Portland Cements (OPC) and Calcium Aluminate Cements (CAC). These phases contribute in the hydration process by forming phases like Ettringite (OPC) or $2CaO{\cdot}Al_2O_3{\cdot}8H_2O$ (CAC), important for the strength of cement stone. It was proved that the addition of Mn-wastes materials to cement raw material optimized the properties like early strength and reduced the sinter temperature, however the possible fixation of Mn in clinker phases has not been studied.

The synthesis of $Ca_2(Fe,Al,Mn)_2O_5$ was performed in several steps. Stoichiometric amounts of CaO Al_2O_3, MnO_2 and Fe_2O_3 were ground in a disk mill pressed to disks and subsequently sintered at 1300°C in air for 2 days. After four sinter and grinding cycles and finally annealing for 2 weeks at 1300°C, the samples were quenched in ice water. Neutron powder diffraction experiments (table 1) were carried out at the diffractometer E9 at room temperatures and for sample 18 at 1.5K and 100K each. The wavelength was 1.79713 Å.

Phase	Number
$Ca_2Al_{0.16}Mn_{0.92}Fe_{0.92}O_5$	9
$Ca_2Al_{0.50}Mn_{0.75}Fe_{0.75}O_5$	18
$Ca_2Al_{0.84}Mn_{0.58}Fe_{0.58}O_5$	19
$Ca_2Al_{1.16}Mn_{0.42}Fe_{0.42}O_5$	20
$Ca_2Al_{1.50}Mn_{0.25}Fe_{0.2}5O_5$	21

Table 1: *Chemical composition of the samples*

As a first step the metric parameters and the space group for each sample was determined (Table 2). In opposition to the starting models of Fe – Al - Brownmillerites $Ca_2Fe_{2-x}Al_xO_5$ 0<x<1.66 (Redhammer 2004), the reflexions in the diffractometer plots of sample 9 and 18 could only be indexed and lattice parameters refined if the c - dimension was doubled. The LeBail – Method was used to refine unit cell parameters for sample 19, 20 and 21. Different orthorhombic Brownmillerite cells according Redhammer et al (2004) were chosen as initial parameters.

In Fe – Al - Brownmillerites the space group change at approximately x = 0.5 – 0.55 from Pnma to Ibm2, due to an increase of the Al_2O_3 concentration. However, the space group of sample 18 and 19 is Pnma (Table 2). The structure refinement of sample 19 showed that RB increased if Ibm2 was chosen ($R_{B\ Ibm2}$ = 5.508 $R_{B\ Pnma}$ = 2.511) and the discrepancy between calculated and observed pattern are clearly indicated.

Nr.	ao [Å]	bo [Å]	co [Å]	S.G.
9	5.3409	14.9158	11.0363	Pnma
18	5.3178	14.8918	11.0214	Pnma
19	5.3021	14.7892	5.5128	Pnma
20	5.2891	14.6632	5.5095	Ibm2
21	5.2724	14.5701	5.4829	Ibm2

Table 2: *Metric parameters of $Ca_2(Fe,Al,Mn)_2O_5$ Brownmillerites*

Rietveld refinements of the crystal structures of 19, 20 and 21 revealed that Mn occupies exclusively the octahedral position 4a (0,0,0) with Pnma and 4a (x,0,0) in the structure with Ibm2. Together with Mn, Fe and Al occupy octahedral sites too, whereas Al occupies preferentially tetrahedral sites, shared with Fe – ions.

The crystal structures of $Ca_2Al_{0.16}Mn_{0.92}Fe_{0.92}O_5$ and $Ca_2Al_{0.50}Mn_{0.75}Fe_{0.75}O_5$ were not recently refined because the starting models applied for the refinement of samples 9 and 18 were not close enough.

With the refinement of the oxygen occupancies in the structures 19, 20 and 21 the calculated oxygen concentrations are in the range 4.8…5 mole Oxygen per formula unit, indicating that Mn or Fe were slightly oxidized (Table 3). These results will be proofed immediately by different titration methods.

Phase	Number
$Ca_2Al_{0.84}Mn_{0.58}Fe_{0.58}O_{4.83}$	19
$Ca_2Al_{1.17}Mn_{0.42}Fe_{0.42}O_{4.87}$	20
$Ca_2Al_{1.50}Mn_{0.25}Fe_{0.25}O_{4.98}$	21

Table 3: *Calculated composition of Mn - Brownmillerites*

Work in progress:

- Crystal structure refinement of of $Ca_2Al_{0.16}Mn_{0.92}Fe_{0.92}O_5$ and $Ca_2Al_{0.50}Mn_{0.75}Fe_{0.75}O_5$
- Determination of oxygen concentration by Iodometric titration
- magnetic structure refinement of $Ca_2Al_{0.50}Mn_{0.75}Fe_{0.75}O_5$ at taken at 1,5 K and 100 K.

	EXPERIMENTAL REPORT **Preferred orientation in volcanic rocks from Kamchatka (Russia)**	Proposal N° PHY-01-1912-EF Instrument **E9** Local Contact Michael Tovar
Principal Proposer: Experimental Team:	J. Peters – HMI, Berlin M. and A. Belousov – IVS, Petropavlovsk, RU R. Naumann – GFZ, Potsdam M. Tovar – HMI, Berlin	Date(s) of Experiment June 2006

Date of Report: 16.12.2006

We studied two volcanic samples from Kamchatka (Russia), one of the most volcanically active regions of the world. The first sample comes from a lava flow of the Kluchevsky in 1994, the second sample from the lava flow of Avachinsky's crater in 2003. In a first step we performed a phase analysis from X-ray diffraction at the GFZ Potsdam to determine the main phases. For this purpose we produced homogeneous powders (< 30 μm) of small parts of the rocks. For both samples the main phases were analyzed to be the mineral andesine (a feldspar belonging to the plagioclase group albite ($NaAlSi_3O_8$) and anortite ($CaAl_2Si_2O_8$) with 30-50 Mol% anorthite; triclinic crystal symmetry, occurs in alkaline and acid rocks) and small amounts of chromite ($FeCr_2O_4$, a mineral of the spinel group, cubic crystal symmetry).

To study preferred orientation (with respect to the flow direction of the erupted magma) neutron diffraction was applied using fine resolution neutron powder diffraction technique. Since neutrons can penetrate the bulk sample one receives information not only from the surface but also from the interior of the sample.

For the **Kluchevsky sample** measurements were carried out applying omega rotation angles of 0°, 45°, 90°, 135° and 180°. To investigate the orientation of the individual phases whole powder pattern fitting was applied for the main phases andesine and chromite using starting parameters from the powder diffraction database ICDD-PDF2, cards 79-1149 and 34-0140, respectively. The profile fitting procedure did not result in a satisfying difference plot from the point of view of the best fit criteria. However, our interest was to distinguish both main phases in the neutron diffractogram to show the variations of the intensity as function of the rotation angle omega.

Fig. 1 shows a typical section of the collected neutron diffraction patterns. Diagrams at different omega angles are plotted with different colours to analyze the omega dependence of the reflection intensity. While the chromite 111-reflection remains nearly constant over all observed patterns, strong differences occur in the intensity of the 201, 040- and 202-reflections of the andesine sample component.

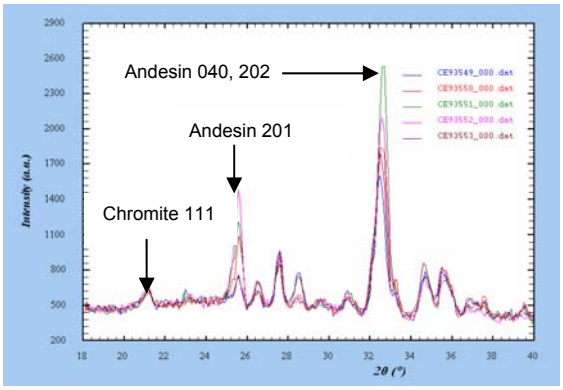

Fig. 1: *Diffraction patterns for the Kluchesky sample as function of 2θ for various omega angles.*

Sample Avachinsky: The same procedure was applied to investigate the reflection intensity as function of the rotation angle omega for the Avachinsky sample. In this case omega was changed in steps of 10° in 2θ which gives an improved resolved overview. For better comparison the zoom window of the staggered neutron powder patterns of the Avachinsky sample was chosen to be 18-40° 2θ as before for the Kluchevsky sample (Fig.2).

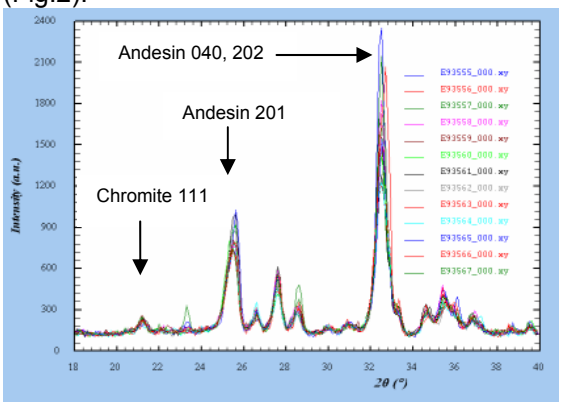

Fig. 2: *Diffraction patterns for the Avachinsky sample as function of 2θ for various omega angles.*

Again one can see strong differences in the intensity of the reflections, however the 201 reflection of the andesine phase does not show as strong changings as in the Kluchevsky patterns. The 111 reflection of the chromite phase again remains stable.
Next aim should be to combine the experimental data with the theoretical background given by the local volcanological research team.

	EXPERIMENTAL REPORT **Neutron tomography investigations of cracks in hard rock**	Proposal N° GEO-04-1220 Instrument **V7** Local Contact Nikolay Kardjilov
Principal Proposer: Experimental Team:	J. Tiedenmann – TU Berlin N. Kardjilov – HMI, Berlin A. Hilger – HMI, Berlin I. Manke – TU Berlin	Date(s) of Experiment 06.04. – 13.04.2006

Date of Report: December 2006

Introduction:
The investigation of the microstructure of hard rock as granite, limestone and sandstone is of special interest for basic research in applied geosciences. First of all, the influence exerted by the cavities as well as the closed and opened micro-cracks on the technical relevant parameters is a subject of research. In this context a method being essential is needed which enables to quantify the proportion and the pattern of both opened and closed micro-cracks of rock.
Neutron tomography allows for a detailed three dimensional analysis of cavities and cracks in the order of some hundred micrometers to centimetres.

Experiment:
The experiments were performed at the high-resolution measuring position of the V7 (CONRAD) instrument providing a spatial resolution of 250 µm. The number of the collected tomography projections in a 180° angular interval was 300 with exposure time of 15 s per projection.

Results:
Five different cylindrical rock samples (unloaded) with a diameter of 30 mm and height of 90 mm were investigated. The histograms for all of the samples were calculated and presented in Fig. 1.

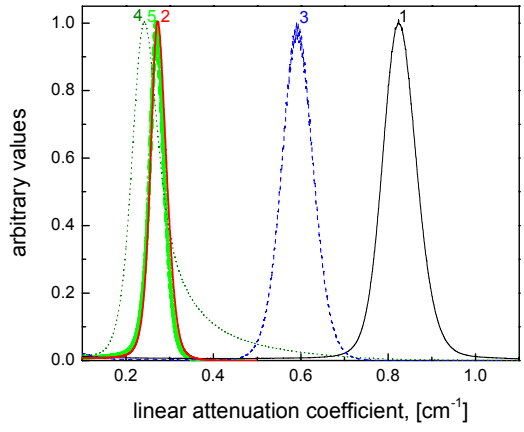

Fig. 1: *Histogram plots of five rock samples investigated by neutron tomographic method*

The samples cover a broad range of rock types with their particular composition of minerals, basalt as a volcanic igneous rock (sample 1), granite as a intrusive igneous rock (sample 4), greywacke as a clastic sedimentary rock (sample 3) and limestone as a chemical sedimentary rock (sample 2 and 5), which is also represented in the histogram of the attenuation coefficient.
The porosity of the samples was calculated qualitatively from the corresponding tomographic volumes using the rendering software VGStudioMax [1]. The results are shown in Table 1.

Table 1:

Sample	1	2	3	4	5
Porosity vol. %	0.0	0.8	1.5	0.1	1.5

The distribution of the cavities in the volume was visualised. Example of this is shown in Fig. 2.

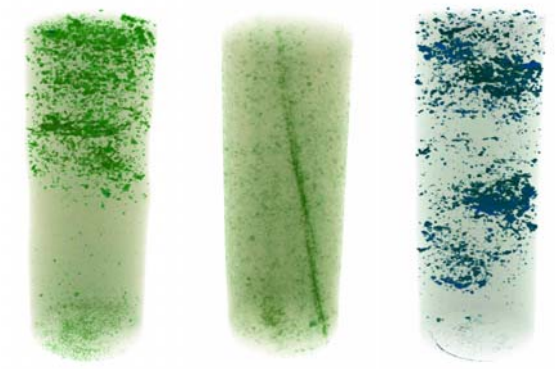

Fig. 2: *Tomographic reconstructed volumes of limestone (left), greywacke (middle) and another limestone sample (right). The cavities in the volume are emphasized.*

As it can be seen the cavities in greywacke form a crack which is not the case observed in limestone where the cavities are grouped in clusters.

References:
[1]. http://www.volumegraphics.com/

	EXPERIMENTAL REPORT REM and neutron tomography on five volcanic rocks from Kamchatka	Proposal N° PHY-04-1254-EF Instrument **V7** Local Contact Nikolay Kardjilov
Principal Proposer: Experimental Team:	J. Peters – HMI, Berlin J. Peters – HMI, Berlin M. and A. Belousov – IVS, Petropavlovsk, RU M. Wollgarten, N. Kardjilov – HMI, Berlin	Date(s) of Experiment March 2006

Date of Report: 15.12.2006

REM and neutron tomography investigations were performed on volcanic rocks from Kamchatka/Russia. The purpose of the study was to characterize the morphological structure of the rocks and to determine quantitative information about the rock composition as well as the void fraction in the rock material.

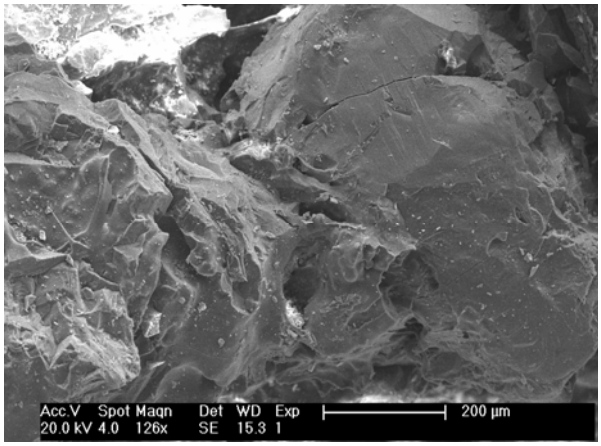

Fig. 1: *REM image of Bezymianny volcanic rock (eruption in 2004)*

First we did REM imaging on a sample (Fig. 1): The image consists of two main parts: left half - mostly vesiculated volcanic glass, containing several large irregular vesicles. In the middle part of the left border of the picture - a 50-micron-long pointed needle of glass, which are common inside large vesicles of Bezymianny pyroclistic flows. In the right part of the image - a big fractured crystal of Plagioclase surrounded by large vesicles. This is also common that during vesiculation of magma vesicles tend to grow on boundaries of phenocrystals, sometimes completely surrounding them. This process causes fracturing of the crystal.

The tomography experiments were performed at the neutron radiography station CONRAD at HMI with 300 projections in each tomography experiment for a sample rotation of 180°. The reconstructed volume data of two rocks from different vulcans are shown in Fig. 2.

The tomographic data were quantified by converting the voxel values in linear attenuation coefficients. For each sample the histogram plot was calculated – number of voxels vs. attenuation coefficient in the tomographic volume. The plots are shown in Fig. 3.

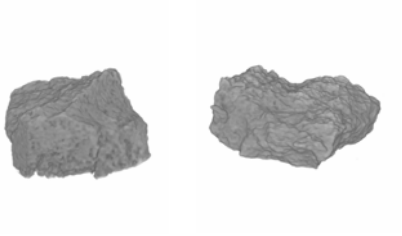

Kluchevsky *Avachinsky*

Fig. 2: *Tomographic reconstruction of two samples*

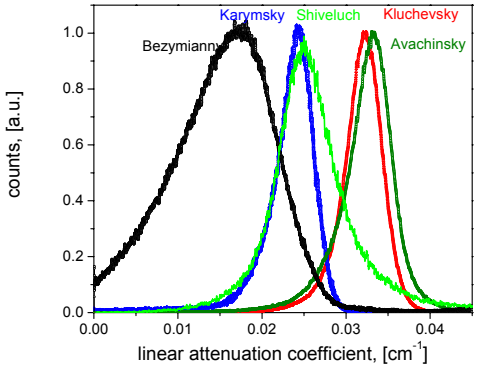

Fig. 3: *Number of voxels vs. attenuation coefficient*

The histogram plots show that the rocks can be separated into three groups – Group I (Bezymianny), Group II (Karymsky, Shiveluch) and Group III (Kluchevsky, Avachinsky). All samples have similar rock composition but different densities and solidities. The values of the attenuation coefficients shown in Fig. 3 are relatively low which means that the rock material is based on a composition consisting of low absorbing elements like Ca, Si, Al and O. The volume fraction of the voids in the samples was calculated using the 3D-rendering software VGStudioMax (results in Table 1). The errors were estimated by taking into account the uncertainty of the histograms.

Table 1: Void fraction, volume %, for all samples

sample	Bezymianny	Karymsky	Shyveluch	Kluchevsky	Avachinsky
void fraction	20.0±2	2.0±0.2	1.1±0.2	0.6±0.1	1.7±0.2

Biology & Soft Matter

	EXPERIMENTAL REPORT **Anomalous temperature behaviour of the thermal diffuse scattering in Alanine**	Proposal N° BIO-01-1696-EF Instrument **E2** Local Contact Jens-Uwe Hoffmann
Principal Proposer: Experimental Team:	D.N. Argyriou – HMI, Berlin H.N. Bordallo – HMI, Berlin J.-U. Hoffmann – HMI, Berlin	Date(s) of Experiment 19.07. – 25.07.206

Date of Report: 07.05.2006

Close inspection of the single crystal diffraction data obtained using E2 (λ =1.21Å), reveals a considerable amount of diffuse scattering (DS) around Bragg reflections along the [00ξ] direction in alanine. This is clearly seen in Fig. 1(a) where the 3D diffraction data vs temperature is shown. Moreover, as shown in Fig. 1(b), we find that for the (002) reflection this DS is temperature dependent, and therefore may originate from a dynamical response.

It is well known that the existence of some dynamical disorder in a crystal structure is revealed either by the presence of a QE signal in Raman spectroscopy or in IN neutron scattering, as found in ferroelectric systems [1], or by DS around a Bragg peak, as found in colossal magnetoresistance materials [2]. The origin of the thermal diffuse scattering (TDS) lies in the $1/\omega_j^2(\mathbf{q})$ dependence of the first-order scattering by lattice vibrations. Since the frequency, $\omega_j(\mathbf{q})$, of the acoustic modes is proportional to q for small q, (where q is a point in the first Brillouin zone away from a reciprocal lattice vector H), the TDS near the Bragg peak arising from these modes varies approximately as $1/q^2$ .. The TDS from optic modes will tend to remain roughly constant across the Bragg peak [3]. Assuming that only the acoustic modes of vibration are responsible for TDS and that these modes propagate with the same velocity vs v_s (v_j(q/=q) in all directions, close to a Bragg reflection q→0, the intensity distribution I_H(j**q**) in the first Brillouin zone is given by [3]:

$$I_H(j\mathbf{q}) = \frac{k_B T}{\rho v_s^2 q^2} Q^2 |G_H(j\mathbf{q}^2)|,$$

Where ρ is the density of the crystal, v_s is the velocity of sound in the material, Q is the magnitude of the scattering vector, and G_H (*j*q) is the structure factor for first-order scattering that includes the structure factor for Bragg scattering [*F*(H)], the Debye-Waller factor, and a phonon term. As shown in Fig. 1(b), the evolution of the TDS intensity as a function of temperature is quite unusual, showing the expected linear behaviour above 200K, and an abrupt decrease below 200K. This is in contrast to Eq. 1, evoking the presence of a dynamic response as opposed to less temperature-dependent diffuse scattering caused by defects in the crystal lattice.

Furthermore, the anomaly seen in the temperature dependence of the TDS intensity correlates well with the devil staircase-like behaviour of the c-lattice parameter [4].

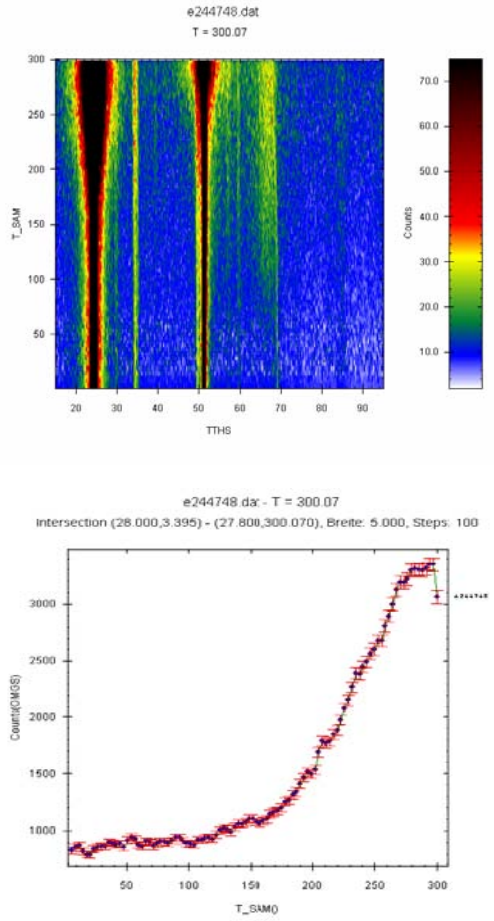

Fig. 1: *(a) E2 results along the [0 0 ξ] direction on L-$C_3D_7NO_2$ single crystal vs T. The integration along the the [002] refection was performed between 27.8° and 28°. (b) Dependence of the TDS intensity as a function of T. Note the abrupt decrease below 200K.*

References:

[1]. R. Almairac, H. N. Bordallo, A. Bulou, J. Nouet, R. Currat, Phys. Rev. B **55** (1997) 8249.

[2]. D. N. Argyriou, H. N. Bordallo, J. F. Mitchell, J. D. Jorgensen and G. F. Strouse, Phys. Rev. B **60** (1999) 6200.

[3]. B. T. M. Willis and A. W. Pryor, In Thermal Vibrations in Crystallography:Cambridge University Press, 1975.

[4]. M. Barthes, H. N.Bordallo, F. Denoyer, J.-E. Lorenzo, J. Zaccaro, A. Robert and F. Zontone, Eur. Phys. J. B **37** (2004) 375.

	EXPERIMENTAL REPORT D-alanine: Are enantiomers really identical?	Proposal N° BIO-01-1704-EF Instrument **E9** Local Contact Dimitri Argyriou
Principal Proposer: Experimental Team:	H. N. Bordallo – HMI, Berlin C. Fehr – HMI, Berlin D. N. Argyriou – HMI, Berlin	Date(s) of Experiment 07.02. – 15.02.2005

Date of Report: 23.11.2006

For the most part, enantiomers have identical physical and chemical properties. However, the difference between 2 enantiomers can have enormous impact, particularly in biological systems. Alanine ($C_2H_4(NH_2)COOH$) is one of the 20 protein amino acids serving as building blocks for proteins. Interestingly, a slightly different melting point, 314°C for L-alanine and between 291-295°C for D-alanine is observed. Further motivation for this particular system is related to unusual properties observed in this building block for proteins and model system for a large range of processes in biochemistry [1-6]. Recent birefringence and light depolarisation measurements indicate either some subtle symmetry breaking around 220 K [7], which is inconsistent with previous structural data [1,2], or a deformation of the molecule. Moreover new results on L-alanine, obtained using the ID10A beam line at ESRF together with X-rays and neutron structure determination indicate a progressive conformational change of the NH^{3+} group of the zwitter ionic molecule. Recent studies [10] showed indications that D- alanine crystal undergoes a reversible second-order phase transition at 247 K.

These findings may point to the possibility predicted by the Nobel Laureate A. Salam, that a phase transition in alanine could be related to a break of the as C_α-H bond where the H atom becomes a superconductive-like atom [11].

Considering that the peak shapes from neutron powder diffractometers are relatively simpler to model than that from synchrotrons, allowing for relatively straightforward and very accurate refinements of structural parameters, we carried out the study of fully deuterated D-alanine powder sample using E9.

In agreement with the earlier picture presented by Destro et al. [1], a subtle molecular deformation, clearly revealed by changes in specific bond lengths (Fig. 2), is observed. One notes that the $O^2...H^2$ bond distance diverges below 200K, while the average NH_3 bond angle as a function of temperature is almost constant. The comparison of L and D-alanine results demonstrate differences in the geometric changes between enantiomers as a function of temperature [12]. This result can be correlated to the fact that in other amino acids the response of the crystal structures of enantiomers is amazingly different to changes of temperature or pressure[13],[14],[15].

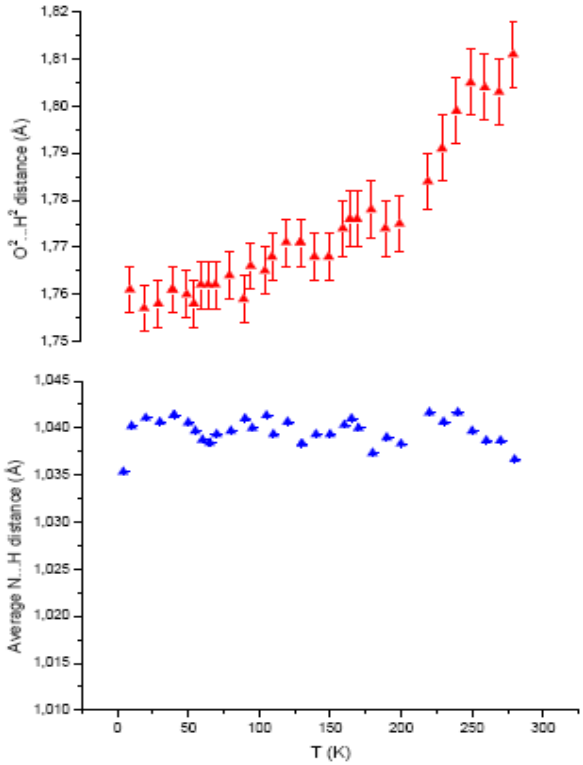

Fig. 1: *(TOP) Temperature dependence of the O2…H2 and (BOTTOM) N…H3 bond distances in D- Alanine.*

References:

[1]. R. Destroet al J. Phys. Chem. **92**, 966, (1988).
[2]. M. S. Lehmanet al J. A. Chem. Soc. **94,** 2657 (1972).
[3]. J. Bandekaret al, Spectrochimica Acta **39A**, 357 (1983).
[4]. C. H. Wang and R. D. Storms, J. Chem. Phys. **55**, 3291 (1971); K. Machidaet al, Spectrochim Acta **34**A 909 (1978).
[5]. A. Micu, et al, J. Phys. Chem. **99**, 5645 (1995).
[6]. R. S. Kwok et al, Sol. St. Comm. **74**, 1193 (1990).
[7]. M. Barthes et al, J. Phys. Chem. **A 106**, 5230-5241, (2002).
[8]. M. Barthes, H.N. Bordallo et al European Phys. J. B **37**, 375 (2004)
[9]. H. N. Bordallo, D.N. Argyriou and M. Barthes, BENSC experimental reports 2003
[10]. W. Wang et al, Phys. Chem. Chem. Phys., **5**, 4000 (2003)
[11]. A. Salam, Phys. Lett. B **288,** 153 (1992); H. Zepik et al.,Science 295, 1266 (2002)
[12]. H. N. Bordallo et al, submitted to J. Phys Chem B
[13]. E .V. Boldyreva et al., Z. Kristallogr. **220**, 50 (2005)
[14]. E. V. Boldyreva et al., Z. Kristallogr. **221**, 150 (2006)
[15]. S. A. Moggach et al. Acta. Cryst.B **61** (2005) 58. 2, 2391

	EXPERIMENTAL REPORT **Investigation of deuterium labelled stratum corneum lipid model membranes**	Proposal N° BIO-01-1796 Instrument **V1** Local Contact Thomas Haußß
Principal Proposer: Experimental Team:	D. Kessner – MLU, Halle. M. Kiselev – JINR Dubna, RU A. Rüttinger, R.Neubert – MLU, Halle S. Dante, T. Hauß – HMI, Berlin.	Date(s) of Experiment 23.11. - 03.12.2006

Date of Report: 30.12.2006

The outermost layer of mammalian skin, the stratum corneum (SC), consisting of corneocytes embedded in a lipid matrix, exhibits the main barrier, i.e. for drug penetration. The objective of the experiments *BIO-01-1796* was to give evidence of the role of CER[EOS] and CER[NS] in SC lipid model membranes.

All CER[NS]-derivatives were synthesized by ourselves at MLU, Halle (chemical structures are shown in **Fig.1**). Diffraction pattern from 4 different binary systems composed of *DPPC/ CER[NS], DPPC/ CER[NS]-D2, DPPC/ CER[NS]-D3* and *DPPC/ CER[NS]-D47* were recorded at molar ratio of CER[NS] 0.32. **Fig.2** presents 5 diffraction order recorded from *DPPC/ CER[NS]-D3* multilamellar membrane. Obtained results will be used for the Fourier synthesis of the neutron scattering length density profiles. We were interested in using the positive neutron scattering length of deuterium atoms in prominent positions of the CER[NS] molecules. We planned to get information about the possible conformation of the CER[NS] molecules in the membrane and about the best position of deuterium labeling for future chemical synthesizes. First calculation revealed a fully extended conformation of CER[NS], in which the polar head group obviously are shifted towards the center of the membrane. All experimental data, either from protonated or deuterated CER[NS] underline this controversial finding. More in-depth studies will follow.

Another focus was put on SC lipid model membranes as a continuation of the CER[EOS]- based model membrane. The article presenting results from neutron diffraction on CER[EOS]/ CER[AP]/ CHOL model system will be submitted soon to CPL.)

In *BIO-01-1796*, mixed SC lipid model systems composed of

CER[EOS]/ CER[NS]-D2/ CER[AP]/ CHOL and *CER[EOS]/ CER[NS]-D3/ CER[AP]/ CHOL* were measured.

In all experiments, the often-described long periodicity phase (LPP- 130Å), whose formation should be induced by CER[EOS] could not be detected.

Next to investigating the role of CER[EOS], we tried to elucidate the influence of the most prominent CER in SC lipid matrix, CER[NS]. First interpretation of the collected neutron diffraction pattern revealed the fully extended conformation of CER[NS] in the membrane. This is in accordance to the results taken from the binary systems. But because of the very small water layer in SC lipid model matrices, the polar head groups are at regular position. More intensive studies will be carry out at first part of 2007 (proposal BIO-01-2062).

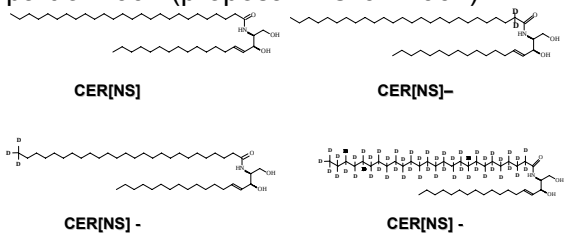

Fig1: *Chemical structures of CER[NS]-derivatives*

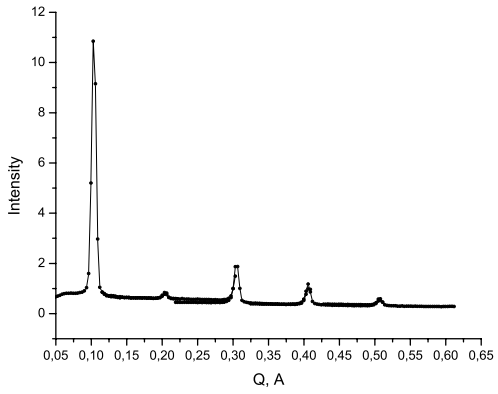

Fig2*: Diffraction pattern from mixed DPPC/ CER[NS]-D3 multilamellar film on a quartz slide at 32% of molar CER[NS]-D3 concentration. Humidity 60%, 8% D_2O, T=20°C. Repeat distance d=61.6 Å.*

Reference:

[1]. M.A. Kiselev, N.Yu. Ryabova, A.M. Balagurov, S. Dante, T. Hauss, J. Zbytovska, S. Wartewig, R.H.H. Neubert, 2005. New insights into structure and hydration of SC lipid model membranes by neutron diffraction. European Biophysical Journal. **34**: 1030-1040.

	EXPERIMENTAL REPORT **Investigation of ceramide 6 conformations in the multilamellar lipid membranes**	Proposal N° BIO-01-1800 Instrument **V1** Local Contact Thomas Hauß
Principal Proposer: Experimental Team:	M. Kiselev – JINR Dubna, RU N. Ryabova – JINR Dubna, RU S. Dante, T. Hauß – HMI, Berlin	Date(s) of Experiment 17.08 - 27.08.2006

Date of Report: 28.11.2006

Mixed binary membranes composed of dipalmitoylphosphatidylcholine (DPPC) and ceramide 6 (Cer6) were characterized by neutron diffraction as function of ceramide 6 mole concentration: 0%, 20%, 40%, 50%. Diffraction pattern was collected as rocking curves measured at appropriate scattering angles 2θ. Samples were equilibrated at 60% humidity of water with 8%, 20%, and 50% D_2O. Diffraction pattern in Fig. 1 demonstrates one lamellar phases, that proves the full mixing of Cer6 and DPPC at 40% Cer6 mole concentration. Five diffraction orders allows one to calculate the fourier profiles and determine the internal structure of the membrane as shown in Table 1. Only two diffraction order were detected for the case of 50% Cer6

As was reported in our previous study [1], the Cer6 molecules increase the thickness of the hydrophobic region of the membrane and decrease of the water layer thickness. The similar results presented in Table 1. The important founding of the present study is sufficient decrease in the membrane repeat distance at 50% Cer6. The repeat distance decreases on the value of 3 Å relative to the pure DPPC membrane, whereas the membrane thickness increases. This experimental fact supports the increase of the intermembrane interaction due to the fully extended (FE) conformation of the cer6 molecules [2]. Our results demonstrate that probability of the FE conformation is small enough in the mixed DPPC/Cer6 membranes.

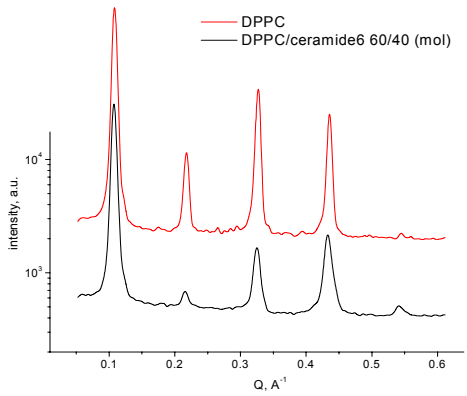

Fig. 1: *Diffraction pattern from mixed 60% DPPC/ 40% Cer6 membrane. 57% humidity, 8% D_2O, T=20 °C.*

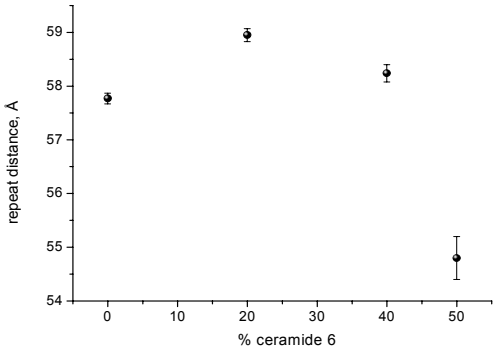

Fig. 2: *Dependence of the membrane repeat distance on the mole concentration of ceramide 6, 57% humidity, T=20 °C.*

Table 1: *Membrane structure. d- repeat distance, d_B – bilayer thickness, d_c – thickness of the hydrocarbon chain region, d_w – thickness of the water layer.*

Cer6	d, A	d_B, A	d_C, A	d_W, A
0%	57.8	49.2	37.7	8.5
20%	59.0	50.7	39.3	8.2
40%	58.2	51.3	40.8	7.0
50%	54.8			

References:

[1]. M.A. Kiselev, N.Yu. Ryabova, A.M. Balagurov, D. Otto, S. Dante, Th. Hauβ, S. Wartewig, R.H.H. Neubert. *Surface, X-ray, synchrotron and neutron research.* 6 (2006) 30-37 (in Russian).

[2]. M.A. Kiselev, N. Yu. Ryabova, A.M. Balagurov, S. Dante, T. Hauss, J. Zbytovska, S. Wartewig, R. H. H. Neubert. *European Biophys. J.* 34 (2005) 1030–1040.

	EXPERIMENTAL REPORT **Membrane interaction of annexin A1**	Proposal N° BIO-01-1982 Instrument **V1** Local Contact Thomas Haußß
Principal Proposer: Experimental Team:	J. Bradshaw – Univ. Edinburgh, UK N. J. Hu – Univ. Edinburgh, UK F. Sa'adedin – Univ. Edinburgh, UK T. Haußß – HMI, Berlin	Date(s) of Experiment 25.10. – 01.11.2006

Date of Report: 01.12.2006

Annexin A1 (AnxA1) is a protein with anti-inflammatory properties that shares the hallmark feature of calcium-dependent membrane binding with other members of the annexin family. In contrast to other annexins, AnxA1 possesses a second, calcium-independent membrane binding site at its N-terminal domain (Fig. 1). Furthermore, AnxA1 belongs to the subgroup of annexins that promote membrane 200 aggregations and fusion. It is believed that these unique properties play a central role in the protein's anti-inflammatory actions. In order to characterise the membrane-bound aggregating/fusogenic state of AnxA1, we are using neutron diffraction to study the structural interactions of AnxA1 N-terminal domain with lipid bilayer using N-terminal peptides and full-length protein.

Difference neutron scattering profiles of DMPC/DMPS (mol/mol 3:1) in the presence and absence of AnxA1 N-terminal peptides reveal that the N-terminal peptides are positioned at the interface of phospholipid headgroup and alkyl chain, indicating a direct interaction between the peptides and membrane (Fig. 2). The results correspond with previous knowledge about the structure of the N-terminal domain from X-ray crystallographic data suggesting the domain forms an amphipathic conformation and might interact with membrane in the absence of Ca^{2+}. Full-length AnxA1 was also prepared by mixing protein and unilamellar vesicles in aqueous buffer. Bragg analysis shows the d-repeat of the multilamellar bilayer in the presence of AnxA1 is 70 Å , which is much wider than the d-repeat of sample containing peptides (54 Å) suggesting AnxA1 expands the thickness of bilayer. However, rocking curve indicates the conformation of the multilamellar bilayer is powder-like, in which the lamellar structure might be disturbed by the full-length protein and thus enhances the mosaicity. The neutron scattering profile of protein-containing sample is difficult determine due to the poor diffraction at higher orders. Deuterated phospholipid can be used for next experiment to pinpoint the position of lipid.

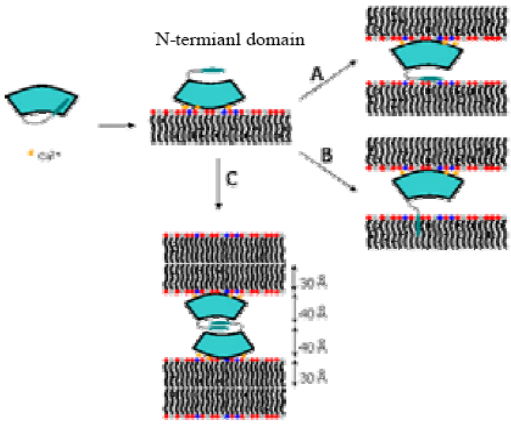

Fig. 1: *Models of AnxA1-mediated membrane aggregation.*

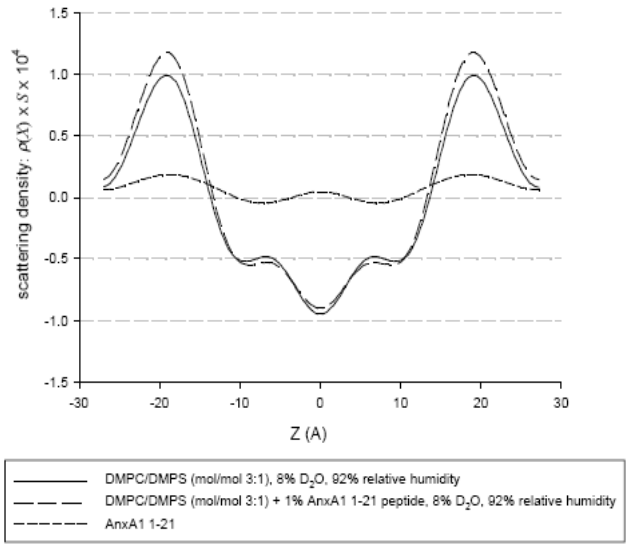

Fig. 2: *Neutron scattering length density profile in the presence and absence of AnxA1 N-terminal peptide 2-21.*

	EXPERIMENTAL REPORT **Localization of the antibacterial peptide C7**	Proposal N° BIO-01-1887 BIO-01-1980 Instrument **V1** Local Contact T. Hauß, S. Dante
Principal Proposer: Experimental Team:	S. Linser – GKSS Geesthacht R. Willumeit – GKSS Geesthacht S. Linser, B. Angelov – GKSS Geesthacht T. Hauß, S. Dante – HMI, Berlin	Date(s) of Experiment 12.03. – 19.03.2006 10.07. – 24.07.2006

Date of Report: 18.12.2006

The peptide-membrane interaction has been investigated by means of small angle neutron diffraction using supported lipid bilayers as a model system. Our study was focused on the peptide antibiotic C7 which is homologue to the third and fourth alpha helices of NK-lysin from porcine NK cells (pdb ID: 1NKL). This peptide is supposed to change biomembrane properties which results in cell death by membrane disruption. The details of this process are so far not understood. In order to investigate the structural details of the interaction of the C7 peptide with model membranes, we performed measurements on bilayers composed of POPC, POPG and POPE and four different mixtures of partially deuterated peptide C7. The oriented supported lipid bilayers were prepared by micropipeting the liquid mixtures on thin quartz slides, subsequent removal of the solvent under mild vacuum for at least 12h and final rehydration for 24h at room temperature at 98% relative humidity that was achieved by addition of K_2SO_4 salt into the water. The contrast was varied by changing the H_2O to D_2O ratio of vapours in the sample chamber to 30%, 8% and 0% D_2O. Diffraction intensities were detected within the wave vector range from 0.07 to 0.7 A^{-1}. Fig.1 shows the diffraction patterns of pure POPC, and two mixtures of POPC with antibiotic peptide C7 that is deuterated at different positions on its amino acid chain. These samples were hydrated in 8% D_2O. The measured lamellar spacing of pure POPC was 5.61 nm. The shown diffraction intensities, up to the 5th order, differ noticeably while the peak positions are essentially unchanged for the samples with and without peptide.

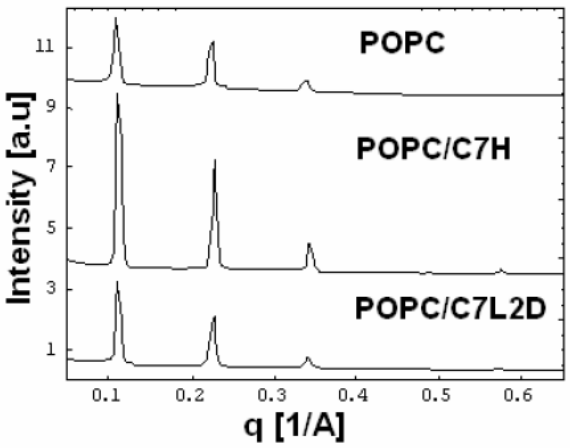

Fig.1

Fig.1: *Such results suggest that the peptide interacts with the model membranes. Further analysis has been initiated to reconstruct the scattering length density profile across the lipid bilayer.*

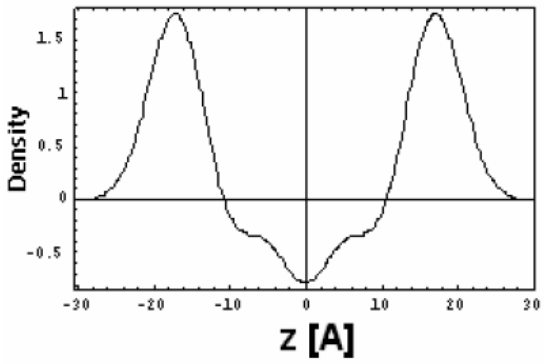

Fig.2

Fig. 2: *shows the POPC density profile. The lipid bilayer thickness was calculated to be near 4.2 nm and the thickness of the water layer to be 1.41 nm. Further analysis will be performed with the data from the peptide containing samples to get more details on the peptide localisation within the lipid membrane by a comparison of the different density profiles.*

	EXPERIMENTAL REPORT **Influence of the fatty acid chain length to the structure of a stratum corneum model membrane**	Proposal N° BIO-01-1888 Instrument **V1** Local Contact Thomas Hauß
Principal Proposer: Experimental Team:	A. Ruettinger – MLU, Halle M. Kiselev – JINR, Dubna D. Otto, B. Dobner, R. Neubert – MLU, Halle T. Hauß – HMI, Berlin	Date(s) of Experiment 01.02 - 14.02.2006

Date of Report: 14.09.2006

A composition of the quaternary system consisting of Ceramide 6/ Cholesterol/ free fatty acid (Stearic (C18), Docosanoic (C22), Tetracosanoic (C24) or Hexacosanoic acid (C26))/ Cholesterol sulfate with component ratio of 55/ 25/ 15/ 5 (w/w) was used to investigate the influence of the chain length of the free fatty acid to the stratum corneum lipid model membrane with neutron diffraction [1].

Samples were prepared as an oriented multilamellar film of lipids on quartz substrate. After equilibration for 12 hours in a chamber, samples studied at 20°C and at 58%humidity in mixtures of water and 8, 20 or 50% D_2O.

Diffraction patterns were recorded as sample rocking curves measured at appropriate scattering angles 2θ. The low mosaicity allowed to collect five diffraction orders.

Fig. 1 displays the repeat distance of the model membrane in dependence on the fatty acid chain length. With increasing chain length of the fatty acid incorporated into the bilayer, the repeat distance decreases due to an interdigitation of the chains of the fatty acids.

Another result obtained from the experiment is that the longer chained fatty acids, such as Tetracosanoic and Hexacosanoic acid create a new phase, which is due to the decreased solubility of the longer chained fatty acids within this Cer6 based model membrane. Fig. 2 shows such a diffraction pattern of the sample containing Hexacosanoic acid (C26). It demonstrates two lamellar phases: the main phase (phase b d=44.62 ± 0.43 Å) and a fatty acid rich phase (phase a, d=56.15 ± 0.36 Å).

The calculations of the neutron scattering density profiles provide more information about the bilayer structure and its hydration. The increase of the chain length of the fatty acid from Stearic (C18) to Cerotic (C26) has no proportional influence to the membrane thickness and structure of the bilayer is similar to the Palmitic acid based membrane [1].

More systematic study of the decrease of the membrane thickness due to the longer chained fatty is planed to be carried out at first part of 2007.

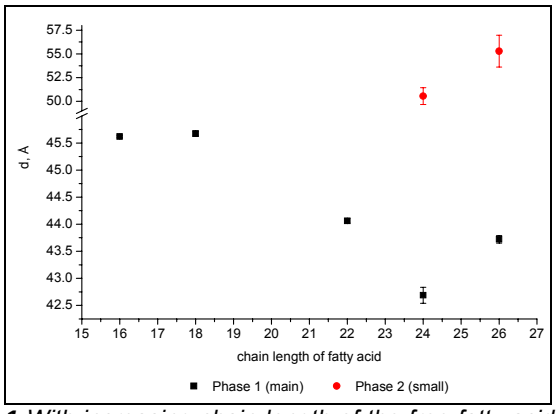

Fig. 1 *With increasing chain length of the free fatty acids inside the model system the membrane repeat distance decreases, while a new phase appears at a chain length of 24 C-atoms.*

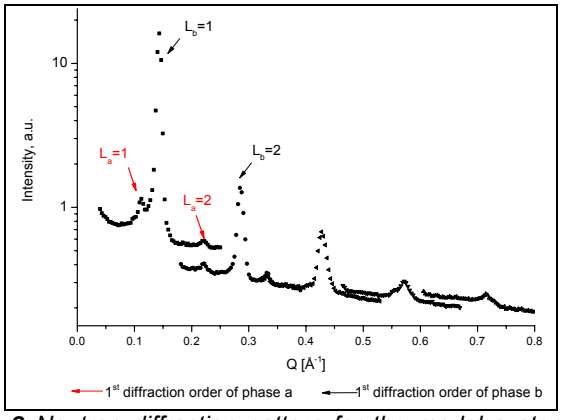

Fig. 2 *Neutron diffraction pattern for the model system with Hexacosanoic acid measured at five different detector angles at 58% humidity, 8% D_2O and T= 20°C*

References:

[1]. M. A. Kiselev, N. Y, Ryabova, A. M. Balagurov, S. Dante, T. Hauss, J. Zbytovska, S. Wartewig, R. H. H Neubert. *New insights into structure and hydration of stratum corneum lipid model membrane by neutron diffraction.* Eur. Biophys. J. **34**, 1030-1040 (2005).

	EXPERIMENTAL REPORT **Surfactant Protein B – interaction with lipid multilayers**	Proposal N° BIO-01-1889 Instrument **V1** Local Contact Thomas Hauß
Principal Proposer: Experimental Team:	F. Bringezu – Uni of Leipzig S. Wen – Uni of Leipzig S. Dante, T. Hauß – HMI, Berlin	Date(s) of Experiment 12.06. – 26.06.2006

Date of Report: 13.12.2006

Appropriate lung function requires a stable lipid film at the alveolar inner surface during breathing cycles. On inspiration, the surfactant protein B (SP-B) provides fast insertion of the lipids stored in multilamellar reservoirs. Moreover, SP-B is believed to attach the multilamellar structure close to the interface. Recent studies on potential surfactant replacements included SP-B and shorter peptide fragments in different lipid mixtures. The N-terminal segment SP-B_{1-25} of human SP-B_{1-79} was shown to recover most of the function of the native protein and using engineered mini-B peptides, optimal surfactant activity was attributed to the saposin folding pattern observed in both, the engineered and the native sequences.

Here we report diffraction studies performed on a model lipid membrane and subsequent mixtures of the model system containing either the truncated N-terminal SP-B_{1-25}, or the engineered mini-B that combines structural features of the C- and the N-term of the native human SP-B_{1-79}. The peptides were synthesized using deuterated amino acids to give partially deuterated sequences, which were used for the experiments.

Oriented samples were obtained by slightly dropping the aqueous lipid dispersion or respective mixtures on quartz slides (65 x 15 x 3 mm), removing the solvent using a vacuum desiccators (12 h) and final rehydration for 24 h at room temperature at 98 % humidity maintained by K_2SO_4 solution. The diffraction intensities were measured up the 5th order of the lamellar spacing at 20 °C. The sample quality was proofed by measuring the mosaicity using rocking scans.

The pure lipid depicts a mosaicity of 0.36° indicating an excellent sample quality. Fig. 1 compares the diffraction patterns obtained for the samples investigated. The SLD's were calculated from the phased structure factors obtained from Gaussian fits to the diffraction data, taking the phase information from isomorphous replacement into account (see Fig. 2).

From the diffraction pattern, a lamellar spacing of about 55 Å can be calculated. The peptide adsorption changes the scattered intensities, however, the d-spacing remains almost constant. Comparing the SLD profiles (Fig. 2) one could conclude that all peptides perturb the lipid chain ordering. Increased intensities in the hydrophobic part suggest the presence of the partially deuterated peptide in this region. The mini-B sequences contain larger amounts of ^2H, thus the intensity enhancement also points to partial insertion of the peptide into the layer. Larger mini-B concentration yields a preferential shift in the water layer suggesting the saturation of the peptide insertion.

Insertion of the peptide into the lipid bilayer could facilitate the attachment of multilamellar reservoirs at the interface, thus being essential for *in vivo* peptides function. The large insertion capability found for the mini-B could thus explain the superior response of the peptide in the replacement therapy.

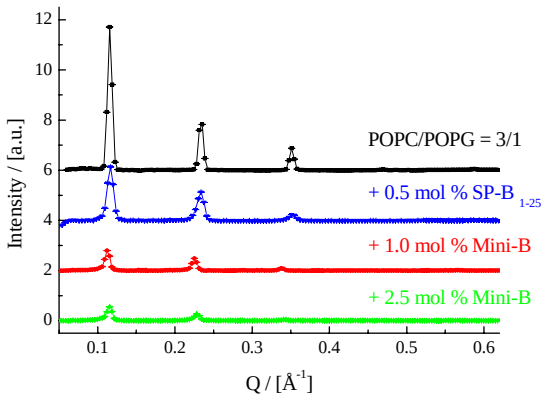

Fig. 1. *Diffraction patterns observed for pure lipid multilayers and subsequent mixtures with deuterated SP-B sequences as indicated at 8 % D_2O and 20 °C.*

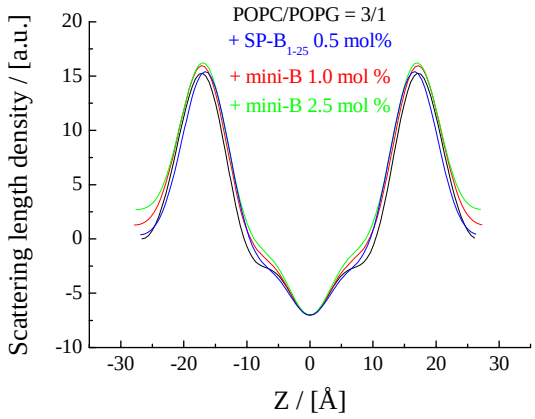

Fig. 2: *Scattering length density profiles as calculated from the structure factors obtained from the diffraction patterns.*

	EXPERIMENTAL REPORT **Structural Organization of Photosystem II Membranes of Green Plants**	Proposal N° BIO-01-1929-LT Instrument **V1** Local Contact Thomas Hauß
Principal Proposer: Experimental Team:	T. Hauß – TU, Darmstadt J. Pieper – TU, Berlin T. Hauß – TU, Darmstadt M. Weß, G. Renger – TU, Berlin	Date(s) of Experiment 17.01. – 19.01.2006

Date of Report: 19.01.2007

The photosynthetic water splitting (for a review see e.g. G. Renger [1]) takes place in a multimeric membrane-bound protein complex referred to as Photosystem II (PS II).

A number of studies have already indicated that certain PS II redox reactions exhibit a pronounced dependence on temperature (see e.g. [2]) as well as on the relative humidity of the sample (see e.g. [3]). Recently, we have investigated the protein flexibility in PS II membrane fragments as a function of temperature and hydration degree. A preliminary analysis of the data showed that a significant quasielastic contribution is present only for T > 240 K and for r.h. > 45 %, i.e. exactly the values where the PS II redox reactions are activated (4). These findings suggest that the functionality of PS II is strongly correlated with the protein flexibility in PS II membrane fragments.

A deeper understanding of these effects requires information on the structural organization of PS II membrane fragments and the location of hydration water molecules.

To address this point, we carried out neutron diffraction measurements for PS II membrane fragments using the membrane diffractometer V1 (see Fig. 1). The samples were hydrated using D_2O vapors of well-defined relative humidities (r.h.) from 45 - 90 %. In addition, a vacuum dried sample was studied. The sample preparation protocol was identical to that used for the preceding QENS studies. The results show a complex structure with peak positions depending on the hydration degree of the sample. The observed structure is qualitatively similar to that reported for intact thylakoids (5). A more detailed analysis is in progress (6).

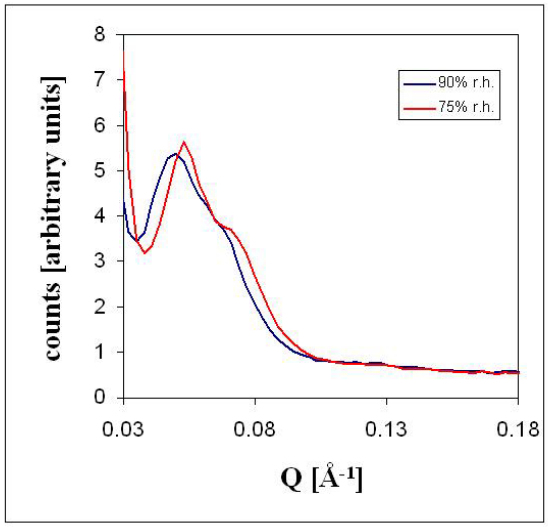

Fig. 1: *TOF-diffraction using the NEAT multi detector for PSII membrane fragments (full line) hydrated with D2O at 57 % r.h..fit. The dashed line gives the incoherent background.*

References:

[1]. G. Renger, Biochim. Biophys. Acta **1503** (2001) 210-228

[2]. O. Kaminskaya, G. Renger, V. A. Shuvalov, Biochemistry **42** (2003) 8119-8132

[3]. Garbers, F. Reifarth, J. Kurreck, G. Renger, F. Parak, Biochemistry 37 (1998) 11399-11404

[4]. P. Kühn, J. Pieper, O. Kaminskaya, H.-J. Eckert, R. Lechner, V. Shuvalov, G. Renger,. Photosyn. Res., **84** (2005) 317.

[5]. Posselt et al., in preparation

[6]. J. Pieper, T. Hauß, A. Buchsteiner, R. E. Lechner, and G. Renger, in preparation

BENSC	**EXPERIMENTAL REPORT** **Interactions between Oligonucleotides and phospholipid membranes: a neutron diffraction investigation**	Proposal N° BIO-01-1983 Instrument **V1** Local Contact T. Hauß, S. Dante
Principal Proposer: Experimental Team:	D. Berti – Univ. Firenze, I S. Milani – Univ. Firenze, I F. Baldelli Bombelli – Univ. Firenze, I T. Hauß, S. Dante – HMI, Berlin	Date(s) of Experiment 17.10. – 25.10.2006

Date of Report: 04.01.2007

We are interested self-assemblies composed of amphiphilic molecules with a nucleic base functionalization. These nucleolipids show, hen self-assembled, molecular recognition capabilities with the same selectivity pattern as in nucleic acids. Lamellar phases of 1-palmitoyl-2-oleoylphosphatidyl- adenosine, POPA, were investigated with neutron diffraction in the presence of polyuridylic acid, polyU, at 50 %w/w hydration (TRIS buffer, full hydration conditions). The main goal of the experiment was to extend SAXS experiments showing major structural modifications when polyU is in the buffer hydrating POPA bilayers. The structure of the adduct is reminiscent of the lipoplexes L_α^c, observed for complexation of DNA with cationic membranes. The relevance of this experiment lies in the fact that DNA complexation is produced by anionic lamellar phases with polymeric chains that spontaneously order in between the bilayers. The presence of PolyU causes the appeareance of a second lamellar phase with higher smectic period (Fig 1) and a third phase ascribable to the oligonucleotide ordering. However the precursor lamellar phase, ascribable to POPA is always present. The same preparation and annealing procedure used for reproducible SAXS experiments could not yield the same results in the same time window, as equilibration increases considerably. We are not currently able to explain this discrepancy. In summary the long equilibration, the time consuming annealing procedure (T cycles) and the necessity to control water content and isotopic ratio did not permit to observe the previous structures. Only a partial modification (prodromal of the final structure) with respect to POPA membrane was observed.

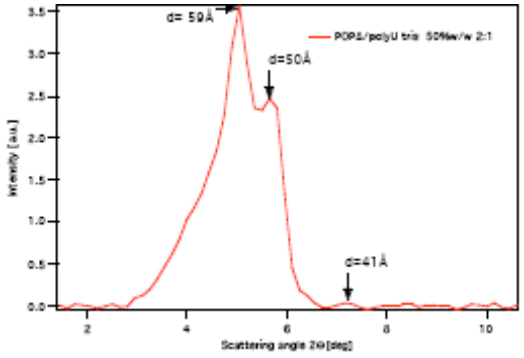

However, important information was obtained from this experiment for POPA/polyU samples at different contrast conditions, that is the POPA membrane mosaicity increases when the polar headgroups interact with complementary bases of polyU.

To further highlight molecular recognition properties of these assemblies, membrane formed mixing complementary lipid were studied by neutron diffraction. Ternary lamellar phases composed of POPA and POPU (1:1 and 1:2 ratios) of (20% and full hydration with TRIS buffer) were prepared and compared to the binary phases collected in the same conditions. The formation of a single lamellar phase, with structural properties ascribable neither to POPA nor to POPU nor to their linear combination, was observed. Figure 2 and 3 shows a summary of the data obtained for the mixture, and an analysis of the membrane profile obtained for 8%D_2O/92%H_2O contrast conditions.

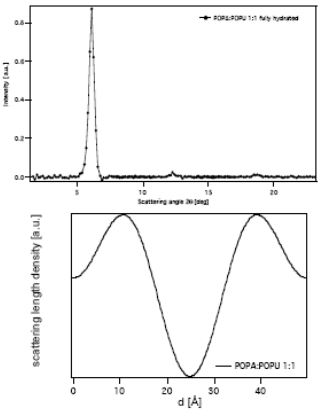

The following table reports the smectic periods sobtained for the measured samples.

Lipid/water	POPU	POPA	MIX 1:1	MIX 1:2
	d [Å]	d [Å]	d [Å]	d [Å]
20%	49.5 Å	49 Å	48.2 Å	48 Å
full	50 Å	50.5 Å	49.4 Å	50 Å

Only three Bragg reflections were found for POPA and mixtures, with respect to the five orders found for POPU. Since we have measured POPA starting from different methods of preparation and using several techniques, we can conclude that the lower number of reflections is due to POPA structure and not to poor orientation induced by preparation method. This difference is due to the nucleolipid headgroup hindrance and stacking constants.

	EXPERIMENTAL REPORT **Interaction of Aβ(1-42) with hydrogenated and deuterated lipid membranes**	Proposal N° BIO-01-2017-EF Instrument **V1** Local Contact Silvia Dante
Principal Proposer: Experimental Team:	S. Dante – HMI, Berlin S. Dante – HMI, Berlin T. Hauß – HMI, Berlin + TU, Darmstadt	Date(s) of Experiment 15.05. – 04.06.2006 24.07. – 16.07.2006

Date of Report: 31.10.2006

The role of amyloid-beta (Aβ) peptide in the neurodegenerative process of Alzheimer's disease has been widely investigated. The interaction of this 42 residue long peptide with the neural membrane may play a crucial role in the neurodegeneration. In our previous investigations [1,2,3] we have studied the effect of the neurotoxic fragment Aβ(25-35) on the structure of phospholipid stacked bilayers. We found that the monomeric Aβ(25.35) intercalates in the hydrophobic core region of the lipid bilayer, in a manner dependent of the membrane composition. In the present experiment we have studied the interaction of the full length peptide Aβ(1-42) with phospholipid membranes in the Lα phase.
Unilamellar vesicles of DMPC/DMPS 90:10 mol/mol, either in hydrogenated or in deuterated form, were dissolved in $CHCl_3$ and sprayed with the air-brush technique (1). The peptide, pretreated with trifluoroacetic acid was added to the lipid solution (lipid/peptide 1:50 mol/mol). The sample was dried under vacuum and rehydrated in a 98% relative humidity. Samples of pure DMPC/DMPS (protonated and deuterated) were investigated as reference.
The diffraction was performed by rocking the samples around the expected Bragg positions. The temperature was kept at 35°C, above the main transition of the lipids Five diffraction peaks were recorded and the membrane profiles were reconstructed *via* Fourier synthesis. All the samples were scanned at a 8% D_2O/H_2O contrast.
The presence of the Aβ(1-42) causes an increase in the lamellar repeat distance of bilayers.

The obtained profiles are shown in the figures.
Fig.1: *Refers to the samples containing protonated lipids. The solid line is the membrane without peptide, the dotted line is the membrane containing Aβ (1-42). The water region is at the boundary of the graph; the maxima are the lipid head group regions, and the dwell represents the terminal methyl groups of the lipid chains. The presence of the peptide increases the distance between the head groups and perturbs the inner region of the membrane profile.*
A similar effect is seen in the profiles of the membranes formed by deuterated lipids, reported in ***Fig.2.***

Further data analysis and modelling of the bilayer is expected to provide more quantitative information about the perturbation of the membrane induced by the toxic peptide.

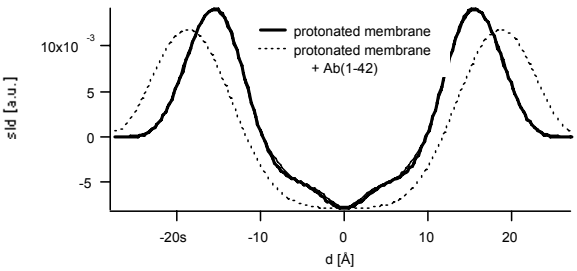

Fig. 1

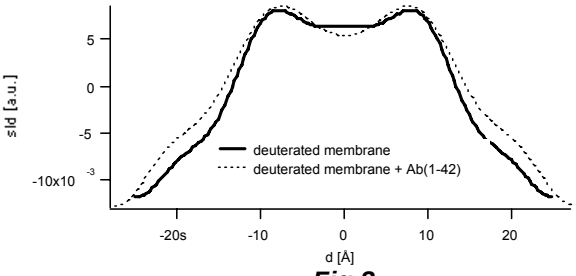

Fig.2

References:

[1]. S. Dante, T. Hauß, N. Dencher Biophys. J. 2002, **83**, 2610-2616
[2]. S. Dante, T. Hauß, N. Dencher Biochemistry 2003, **42**, 13667-13672
[3]. S. Dante, T. Hauss, N. Dencher European Biophys. J. 2006, **35**, 523-531

	EXPERIMENTAL REPORT **Thermo-optical rearrangements in the thylakoid membrane of green plants**	Proposal N° BIO-03-0401 BIO-01-1799 Instrument **V1, V3** Local Contact T.Hauß, A.Buchsteiner
Principal Proposer: Experimental Team:	G. Garab – HAS BRC Szeged, H G. Garab – HAS BRC Szeged, H A. Buchsteiner, T. Hauß – HMI, Berlin J. Pieper – TU, Berlin	Date(s) of Experiment 28.07. – 30.07.2006

Date of Report: 19.01.2007

Structural flexibility of the thylakoid membrane is essential in the temperature and light adaptation mechanisms of plants. There are light-induced structural reorganizations within the thylakoid membrane leading to changes in the long-range chiral order and to a monomerization of the trimeric light harvesting complex of photosystem II (LHC II) [1,2].

The aim of the current project was to extend the recently conducted quasielastic neutron scattering experiments at BENSC on randomly oriented thylakoid membranes (BIO-03-0372), to magnetically aligned membranes in order to separate in-plane and out-of-plane motions in PS II membrane fragments prepared from intact thylakoids.

For alignment, PS II membrane fragments in D_2O solution were exposed to the horizontal magnetic field of the HM-5 magnet (BENSC sample environment) at 2T and dried in an inert gas (N_2) atmosphere before the actual QENS experiment. The dried samples were rehydrated at a relative humidity of 75 % and sealed in a vacuum-tight sample container. Buffer samples were prepared following the same protocol for control purposes.

A characterization of the magnetically aligned samples at the membrane diffractometer V1 revealed a preferential orientation with a residual mosaicity of about 20°.

QENS spectra were recorded using an incident neutron wavelength of 5.1 Å and an elastic resolution of ΔE = 0.093 meV. Two sample orientations were studied so that for a scattering angle of 90°, the Q-vector was perpendicular and parallel to the membrane plane, respectively. A high reproducibility of the respective sample orientations was ensured by using a motor-driven sample stick with software control. Comparison of angle spectra for the different runs showed that the positioning was accurate within the detection limit of */-1°. QENS spectra obtained at the two respective membrane orientations for a scattering angle of 90° are shown in Figs. 1 and 2. A detailed analysis is currently in progress.

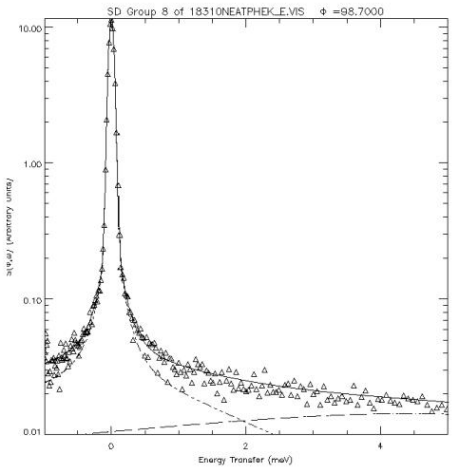

Fig. 1: *QENS spectrum of magnetically oriented PS II membrane fragments obtained at an orientation of 45°, i.e. with Q perpendicular to the membrane plane.*

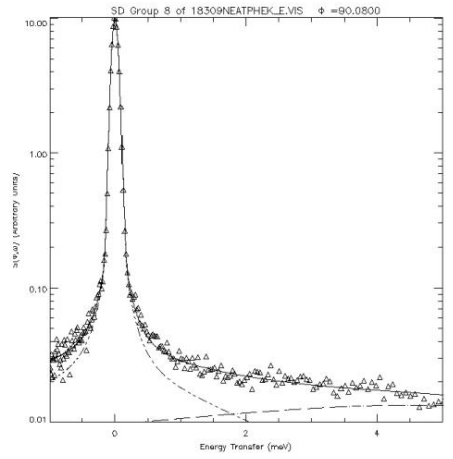

Fig. 2: *QENS spectrum of magnetically oriented PS II membrane fragments obtained at an orientation of 135°, i.e. with Q parallel to the membrane plane.*

References:

[1]. Garab et al. 1988, Biochemistry **27**, 2430
[2]. Dobrikova et al. 2003, Biochemistry **42**, 11272

	EXPERIMENTAL REPORT **Light-Induced Protein Dynamics in Photosystem II of Green Plants**	Proposal N° BIO-03-0412-EF Instrument **V3** Local Contact Jörg Pieper
Principal Proposer: Experimental Team:	J. Pieper – HMI, Berlin A. Buchsteiner – HMI, Berlin R. E. Lechner, T. Hauß – TU, Darmstadt M. Weß, G. Renger – TU, Berlin	Date(s) of Experiment 15.08. – 22.08.2005

Date of Report: 19.01.2007

The transformation of light energy into storable chemical energy by photosynthesis is a fundamental physiological process in nature. This photochemical process comprises the light-induced water oxidation and fixation of carbon by formation of a carbohydrate $(CH_2O)_n$ under release of oxygen. The key steps of photosynthetic water splitting take place in a multimeric membrane-bound protein complex referred to as Photosystem II (PS II) (for a review see G. Renger [1]).

The reaction pattern of PS II is characterized by a high degree of specific coupling between structural dynamics and function. A number of studies indicate that certain PS II redox reactions exhibit a pronounced dependence on temperature (see e.g. [2]) as well as on the relative humidity of the sample (see e.g. [3]). Just recently, it was shown by QENS [4] that the onset of the reoxidation of Q_A^- by Q_B is strictly correlated with the dynamical transition in PS II membrane fragments (Fig. 1).

In the present experiment, the protein dynamics in PSII membrane fragments was investigate on the timescale of the Q_A^- reoxidation by Q_B in a real-time QENS experiment. A special optical setup and electronics allowing for time-resolved data acquisition and synchronized laser excitation had been developed by us. The proper function of the setup was demonstrated in a previous experiment [5].

PS II membrane fragments were hydrated with D_2O and equilibrated using D_2O vapors of a relative humidity of 90 %. Real-time quasielastic neutron scattering (QENS) experiments were carried out using an incident neutron wavelength of 5.1 Å (~3.2 meV) with an elastic energy resolution of 93 µeV.

The protein dynamics of PS II membrane fragments was studied before and after laser excitation on the timescale of the Q_A^- reoxidation by Q_B by real-time QENS measurements. The results indicate an altered protein dynamics induced by laser excitation, which is perfectly reversible. A more detailed analysis is in progress [6].

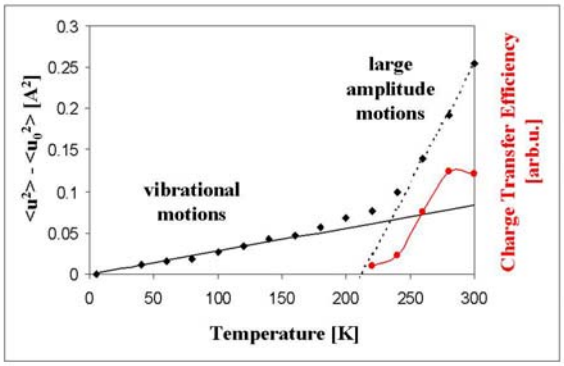

Fig. 1: *Mean square displacement of PSII membrane fragments as a function of temperature (diamonds) according to ref. [4]. The electron transfer efficiency is shown in red (2).*

References:

[1]. G. Renger, Biochim. Biophys. Acta **1503** (2001) 210-228

[2]. A. Garbers, F. Reifarth, J. Kurreck, G. Renger, F. Parak, Biochemistry **37** (1998) 11399-11404

[3]. O. Kaminskaya, G. Renger, V. A. Shuvalov, Biochemistry,**37** (2003) 8119 – 8132.

[4]. J. Pieper, T. Hauß, A. Buchsteiner, K. Baczyński, K. Adamiak, R. E. Lechner, and G. Renger, submitted

[5]. J. Pieper, T. Hauß, A. Buchsteiner, N.A. Dencher, R.E. Lechner, BENSC experimental report ° BIO-03-341-EF 2004.

[6]. J. Pieper, T. Hauß, A. Buchsteiner, R. E. Lechner, and G. Renger, in preparation

	EXPERIMENTAL REPORT **Light-Induced Protein Dynamics in Bacteriorhodopsin**	Proposal N° BIO-03-0414-EF BIO-03-0386-EF Instrument **V3** Local Contact Jörg Pieper
Principal Proposer: Experimental Team:	J. Pieper – TU, Berlin A. Buchsteiner – HMI, Berlin R. E. Lechner, T. Hauß – TU, Darmstadt N. Dencher – TU, Darmstadt	Date(s) of Experiment 08.08. – 15.08.2005 10.03. – 18.03.2005

Date of Report: 19.01.2007

The dynamics of Bacteriorhodopsin (BR) has been studied by laser-excited quasielastic neutron scattering (QENS) in real time.

BR is a light-driven proton pump embedded into the purple membrane of *halobacterium salinarum* [1]. Absorption of a light quantum by BR initiates a photocycle corresponding to a well-defined sequence of protein-chromophore states (intermediates). The intermediates of BR are characterized by specific absorption maxima and decay times ranging from 500 fs to 15 ms. One proton is pumped through the membrane during the photocycle creating a net transport from the cytoplasmic to the extracellular side of the membrane. This vectorial proton transport requires a structural change in the M-intermediate [2].

The internal protein dynamics of BR in its dark state has already been thoroughly studied by QENS (see e.g. ref 3 and references therein). However, information on the effect of the structural changes on protein dynamics during the photocycle is scarce and difficult to obtain. To selectively probe the protein dynamics in different intermediates in real time, the pulsed QENS-measurement has to be synchronized with repetitive light excitation.

A special optical setup and electronics allowing for time-resolved data acquisition and synchronized laser excitation had been developed by us (see Fig. 1). The proper function of the setup was demonstrated in a previous experiment [4]. Excitation conditions and time-course of the photocycle have been thoroughly characterized before the QENS experiment.

The protein dynamics of BR was studied in the dark state as well as with laser excitation in the ground state (BR_{568}) and in the M-intermediate by QENS experiments with an incident neutron wavelength of 5.1 Å and an energy resolution of 93 µeV. The results indicate a higher protein flexibility in the M-intermediate, a more detailed analysis is in progress [5]. To the best of our knowledge, this is the first successful experiment of its kind.

Fig. 1: *Optical setup for NEAT, which was developed by us for time-resolved laser-induced experiments.*

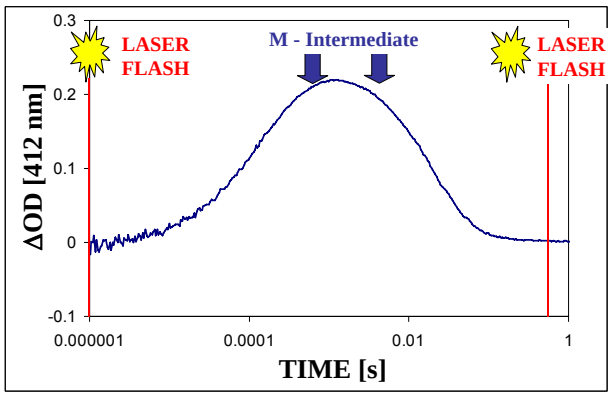

Fig. 2: *Accumulation of the M-intermediate following laser excitation of BR at 532 nm. The location of the neutron pulses within the M-intermediate is indicated by blue arrows.*

References:

[1]. J. K. Lanyi J. Phys. Chem. B **104** (2000) 11441.

[2]. N. A. Dencher, D. Dresselhaus, G. Zaccai, G. Büldt, Proc. Nat. Acad. Sci. USA **90** (1989) 9669.

[3]. J. Fitter, R. E. Lechner, N. A. Dencher, J. Phys. Chem. **103** (1999) 8036.

[4]. J. Pieper, T. Hauß, A. Buchsteiner, N.A. Dencher, R.E. Lechner, BENSC report BIO-03-341-EF 2004.

[5]. J. Pieper, T. Hauß, A. Buchsteiner, N.A. Dencher, R.E. Lechner, in preparation.

	EXPERIMENTAL REPORT **Solvent effects in the relationship between conformations and dynamics of a β-lactoglobulin protein**	Proposal N° BIO-03-0454 Instrument **V3** Local Contact Margarita Russina
Principal Proposer: Experimental Team:	M.-C. Bellissent-Funel – LLB-CEA/CNRS Saclay,F K. Yoshida – Univ. Fukuoka, JP M. Russina – HMI, Berlin	Date(s) of Experiment 06.11. – 12.11.2006

Date of Report: 06.01.2007

Solvent plays an important role in the protein folding. So far, the secondary structure of a-helix forming peptide and protein (Melittin and β-lactoglobulin (BLG)) was investigated in aliphatic and fluorinated alcohols [1]. So far, we measured quasi-elastic neutron scattering (QENS) of water and ethanol adsorbed BLG with the backscattering spectrometer in IFF (Juelich). A relatively slow relaxation was found with alcohol, implying the existence of a slow dynamics of both protein and surface solvents. Dynamics of water adsorbed BLG is faster than ethanol adsorbed BLG. It is consistent with MD simulation results that a small peptide (melittin) in pure water takes more various conformations than in alcohol-water mixture [2].

The BLG, the structure of which is β-sheet in water, is transformed into α-helical structure with increasing alcohol amount. The configurations and the local site dynamics of the protein obtained from the present results will help to better understand the mechanism of alcohol denaturation of the protein.

In order to reveal the role of solvent in protein folding, the dynamics of a β-lactoglobulin (BLG) protein in water and in alcohols-water mixtures have investigated using the time-of-flight spectrometer (NEAT). QENS measured on BLG solutions at room temperature. To get rid of the protein exchangeable hydrogen atoms, BLG powder was dissolved in D_2O and then was lyophilized. The dried BLG powder obtained was dissolved in D_2O, and ethanol-water and TFE-water mixtures. Concentrations of BLG solutions were 40 mg ml^{-1} for each solvent. Samples were kept in a cylindrical aluminium container under helium atmosphere. The sample path length was 2 mm. An accumulated time was over 12 h per sample. Measurements were also made for solvents and a sheet of vanadium. The *Q* range was from 0.5 to 2.0 $Å^{-1}$.

Figure 1 and 2 show dynamic structure factor $S(Q,\omega)$ of BLG in water and ethanol-water mixture (x_E = 0.4) at Q=1.4 $Å^{-1}$. The line width of the quasielastic line in water is wider than that in ethanol-water mixture indicating that proton in BLG is more mobile in water than in the mixture. It is consistent with the results of BSS. We will discuss the correlation of dynamics with three-dimensional structure obtained from SANS.

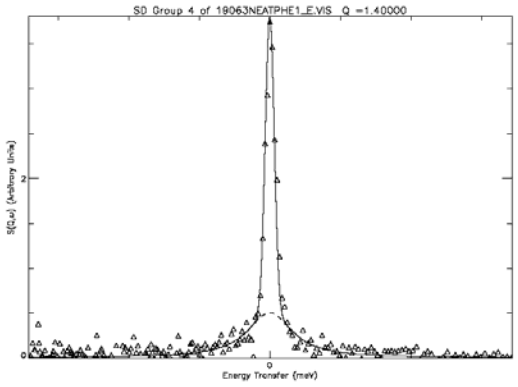

Fig. 1: *Dynamic structure factor S(Q,ω) of BLG in water at Q=1.4 Å^{-1}.*

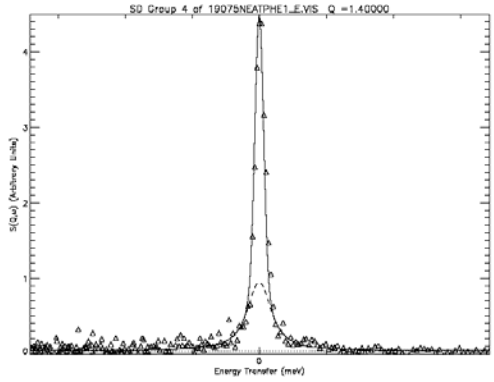

Fig. 2: *Dynamic structure factor S(Q,ω) of BLG in ethanol-water mixture (x_E= 0.4) at Q=1.4 Å^{-1}.*

References:

[1]. D. Hong, M. Hoshino, R. Kuboi, and Y. Goto, J. Am. Chem. Soc. **121**, 8427 (1999).

[2]. M. Fioroni, K. Burger, A. E. Mark, D. Roccatano, J. Phys. Chem. B **105**, 10967 (2001).

	EXPERIMENTAL REPORT **Dynamics function relationship in trehalose coated bacterial photosynthetic reaction centers from Rb. sphaeroides**	Proposal N° BIO-03-0457 Instrument **V3** Local Contact Alexander Schnegg
Principal Proposer: Experimental Team:	G. Venturoli – Univ. Bologna, I G. Palazzo – Univ. Bari, I A. Schnegg – HMI, Berlin	Date(s) of Experiment 11.09. – 18.09.2006

Date of Report: 05.01.2007

The photosynthetic reaction centre (RC) is a pigment-protein complex, located in specialized membranes of green plants and certain bacteria, which, via light induced electron transfer, catalyzes the primary events of photosynthesis. Insight into the dynamic-structure-function relationship of the RC protein, which determines the rate of electron transfer, can greatly help to understand these highly optimized processes. According to the energy landscape model, of special interest are fast librations (10^{-12}-10^{-9} s), which, acting as a lubricant, enable the protein to sample different conformational substates. These fast anharmonic motions are strongly coupled with the dynamics of the surrounding medium [1]. A very drastic effect on the electron transfer properties can be observed for RCs incorporated into dehydrated trehalose glasses where the kinetics of light-induced electron transfer at room temperature mimic those observable in water-glycerol systems at cryogenic temperatures [2]. In the present study we investigated photosynthetic RCs purified from the bacterium *Rhodobacter (Rb.) sphaeroides* R 26, to address the following points:

a) Determine the mobility of the detergent molecules (*n*-octyl-β-D-glucopyranoside (βOG)) in the micelles surrounding the RCs in liquid solution.

b) Compare the internal motion in RCs suspended in liquid solution (D_20 + *β*OG + buffer) and when incorporated into a dehydrated trehalose glass (trehalose + D_20 + *β*OG + buffer).

c) Evaluate the possibility of studying RCs in liquid solution and in trehalose matrices by laser light induced transient Qens measurements.

To examine the impact of the matrix on the protein mobility we performed Qens measurements on RCs dissolved in liquid detergent solution and on RCs embedded in a trehalose matrix. Deuterated or partly deuterated equivalents for water, βOG, buffer and trehalose were used to discriminate between the scattering contribution of protons from the protein and from the surrounding matrix [3]. We investigated separately solubilized RCs and the corresponding buffer solution as well as RCs embedded in trehalose and the trehalose matrix, in order to subtract the solvent contribution. Qens experiments were carried out using an incident neutron wavelength of 5.1 Å and an elastic resolution of 93 μeV on the NEAT spectrometer at 140 K and 300 K.

a) The mobility of the detergent molecules was determined by subtracting room temperature data obtained from RCs surrounded by deuterated and protonated βOG, respectively. The width of the remaining line shows a linear dependence upon Q^2 from which a diffusion coefficient close to that of water could be determined.

b) For RCs embedded in the trehalose matrix the contribution of the protein to the quasi-elastic onset on the Qens spectrum could be well separated from that of the trehalose matrix. At 300 K a Q dependent quasi-elastic broadening can be observed, which disappears at 140 K. Numerical fits of the data are in progress. Since we lost the reference for the liquid solution sample, the solvent background in the Qens spectra couldn't be precisely determined in this case. Further experiments are necessary for an accurate comparison between trehalose-coated and solution RCs.

c) Already from a qualitative data treatment it appears that the quasi-elastic contribution of the RC can be discriminated from that of the solvent (a precondition for studies of the internal protein dynamics). However, in the evaluation of laser induced mobility changes possibly accompanying conformational changes only a small fraction of neutron pulses probes the excited state of the protein after the laser flash, resulting in a reduced signal to noise ratio. We conclude that, to achieve the maximum laser-induced protein signal, additional measurements on dark adapted RCs are necessary.

References:

[1]. Frauenfelder, PNAS 2003, **100**, 8615
[2]. Palazzo et al. Biophys. J. 2002, **82**, 558
[3]. Gall et al. J. Phys. Chem. B 2002, **106**, 6303

Acknowledgements:

This research project has been supported by the European Commission under the 6th Framework Programme through the Key Action: Strengthening the European Research Infrastructures. Contract n: RII3-CT-2003-505925 (NMI 3).

	EXPERIMENTAL REPORT **Interaction of beta-amyloid (1-42) with unilamellar lipid vesicles by SANS**	Proposal N° BIO-04-1241-EF Instrument **V4** Local Contact Astrid Brandt
Principal Proposer: Experimental Team:	S. Dante – HMI, Berlin T. Hauß – HMI, Berlin A. Brandt – HMI, Berlin	Date(s) of Experiment 12.08. – 16.08.2006

Date of Report: 05.01.2007

The so-called Alzheimer's protein, beta-amyloid (1-42) is known to interact with lipid bilayers and to perturb the membrane structure. Our group investigated in the past the interaction of Aβ with stacked bilayers by neutron diffraction and we were able to ascertain the intercalation of the short fragment Aβ(25-35) into the membrane core as a function of the membrane surface charge and of the membrane composition [1-3]. In the present investigation we look at the interaction between unilamellar vesicles with the long native form of the Alzheimer's peptide, Aβ(1-42) by small angle scattering.

Unilamellar vesicles were prepared by extrusion of large multilamellar vesicles through a polycarbonate filter. We used a lipid mixture of POPC/POPS 90:10 mol/mol.The lipid concentration was 10 mg/ml. The size of the extrusion pores was 500 Å.

The peptide was pre treated with trifluoroacetic acid,in order to preserve it in a monomer form.

Aβ(1-42) was administered to the vesicle suspension in different amounts, i.e., 1:1000, 1:500, 1:100 and 1:50 peptide/lipid molecules and the samples were measured right after administration.

Two series of measurements were performed, at pH=6 and pH=7, since it is known that the pH influences the peptide structure.

The scattering curves obtained at pH=7 shown in Fig.1 and demonstrate the effect of the Aβ peptide on the vesicles as its concentration increases.

The radius of the vesicles as a function of the peptide concentration is reported in Fig.2.

The scattering curves have been fitted in the range of 0.03 Å-1<q<0.15 Å-1 with a step model, to evaluate the structure parameters of the POPC/POPS membrane under the influence of Aβ(1-42).

At the highest peptide/lipid ratio of 1:50, the vesicle radius is 330 Å, while the membrane thickness is not remarkably influenced by the peptide, thus indicating a fusogenic activity of Aβ(1-42).

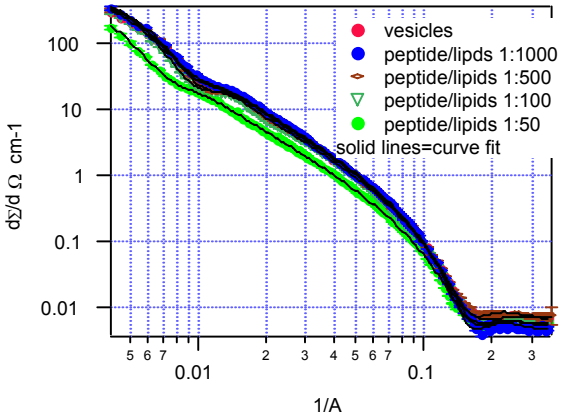

Fig.1

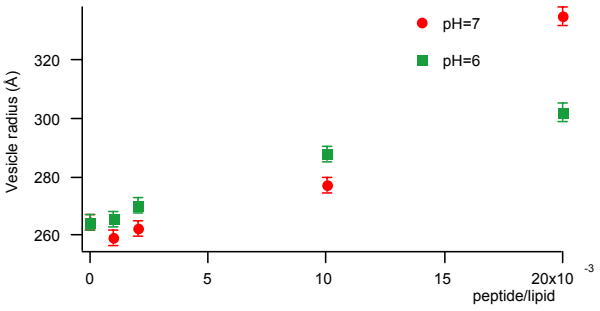

Fig.2

Reference:

[1]. S. Dante, T. Hauß, N.A. Dencher □*-amyloid 25 to 35 is intercalated in Anionic and Zwitterionic Lipid Membrane sto Different Extents*, Biophysical Journal, 2610-2616 (2002) **83**.

[2]. S. Dante, T. Hauß, N.A. Dencher *Externall administered amyloid β peptide 25-35 and perturbation of lipid bilayers* Biochemistry, 13667-72 (2003) **42**

[3]. S. Dante, T. Hauß, N.A. Dencher *Cholesterol inhibits the insertion of β-amyloid (25-35) into phospholipids membranes* accepted in European Biophysics Journal 523-531 (2006) **3**

	EXPERIMENTAL REPORT **SANS contrast variation study on the role of amelogenins in enamel mineralization**	Proposal N° BIO-04-1265 Instrument **V4** Local Contact Albrecht Wiedenmann
Principal Proposer: Experimental Team:	B. Aichmayer – MPI KGF Golm P. Fratzl – MPI KGF Golm H. Margolis – Forsyth Inst. Boston, USA F. Bidlack, E. Beniash - Forsyth Inst. Boston,USA S. Prévost, U. Keiderling – HMI, Berlin A. Wiedenmann – HMI, Berlin	Date(s) of Experiment 22.06. – 25.06.2006 06.11. – 09.11.2006

Date of Report: 11.01.2007

Amelogenin proteins play a crucial role in the formation of the highly organized structure of enamel, which consists of interwoven bundles of elongated hydroxyapatite (HAP) crystals. By means of SAXS and DLS, it was already shown that the protein forms so-called “nanospheres”, which can either exist as isolated particles or aggregate into assemblies of multiple nanospheres, depending on the pH value and temperature [1].

The SANS experiments at BENSC were performed to study the structure of the protein in the presence of *in vitro* grown HAP crystals. Our aim was to find possible correlations between the assembly of the protein and the arrangement of the mineral crystals. Therefore we prepared aqueous (H_2O/D_2O) protein suspensions as well as mineralized samples containing protein and HAP crystals. The *in vitro* mineralization was carried out as described in [2]. In order to separate the different scattering contributions we matched either the scattering length density of the protein or that of the mineral (corresponding to solvents of 42% and 69% D_2O, respectively). Due to the low solubility of the protein, the concentration was limited to 2 mg/ml. We chose a rather broad wavelength distribution (6 Å ± 18%) to increase the neutron flux. Furthermore, quartz glass cells with a magnetic stirrer were used to avoid sedimentation of the mineral. We used very long acquisition times (up to 10 hours at the maximum distance of 12 m) and carefully performed calibration as well as background measurements.

Nevertheless, it turned out, that it was not possible to get data of sufficient quality for all of our samples. Especially for the mineralized samples, the signal to noise ratio was too low to get reliable results. One of the reasons therefore was that the stirrer could only prevent part of the protein/mineral agglomerates from sedimentation.

In contrast thereto, for the samples which only contained protein (which is not prone to sedimentation), the statistics were much better (see the example given in Fig.1). The low Q data have to be interpreted with caution, since the (already subtracted) background arising from the empty cell was very high as compared to this signal.

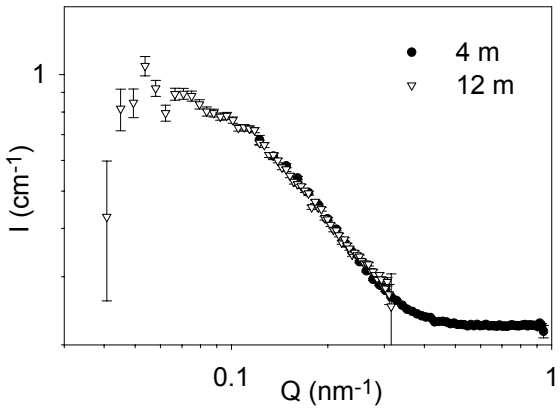

Fig.1: *SANS profile (Intensity vs. scattering vector Q) for the recombinant amelogenin rP172 (2mg/ml, pH 7.4, 25°C) in 69% D_2O, measured at two different distances.*

The measured scattering curves for the non-mineralized samples will be combined with SAXS data in order to model the shape of the protein agglomerates, which in fact strongly differ from spheres. However, the initial aim of studying the behaviour of the protein in the presence of mineral crystals by means of varying the contrast, can only be achieved by improving experimental conditions such as higher concentrations of the samples, higher neutron flux and sample containers with a lower background. A possible solution to the problems arising from the sedimentation, will be to use rotating cylindrical cells instead of the cuboid cells with magnetic stirrers.

References:

[1]. Aichmayer, B., Margolis, H.C., Sigel, R., Yamakoshi, Y., Simmer, J.P., Fratzl, P.: J. Struct. Biol. **151** (2005), 239-249.

[2]. Beniash, E., Simmer, J.P., Margolis, H.C.: J. Struct. Biol. **149** (2005), 182-190.

	EXPERIMENTAL REPORT **Structural modulation of lecithin reverse micelles operated by nucleolipids**	Proposal N° BIO-04-1283 Instrument **V4** Local Contact Astrid Brandt
Principal Proposer: Experimental Team:	D. Berti – Univ. Firenze, I F. Betti – Univ. Firenze, I F. Baldelli Bombelli – Univ. Firenze, I A. Brandt – HMI, Berlin	Date(s) of Experiment 27.11. – 01.12.2006

Date of Report: 29.12.2006

We are interested in the structural changes which occur in reverse microemulsions when oligonucleotides of different length are solubilized in the water pool. The amphiphiles are phospatidylnucleosides, synthetic molecules obtained from a phospholipid precursor whose polar head is substituted with a nucleic base through a transphosphatidylation reaction. The derivatives used in this study are Palmitoyl-Oleoyl-Phosphatidyl-Adenosine (POPA), Palmitoyl-Oleoyl-Phosphatidyl-Uridine (POPU), and their 1:1 mixture, POPMix. At a concentration of $5x10^{-2}$M, they form in cyclohexane ellipsoidal micelles, which undergo a transition to disk-like aggregates near the emulsification failure boundary (W_0=[water]/[POPN]=5) as shown by previous SANS and SAXS experiments (Figure 1.).

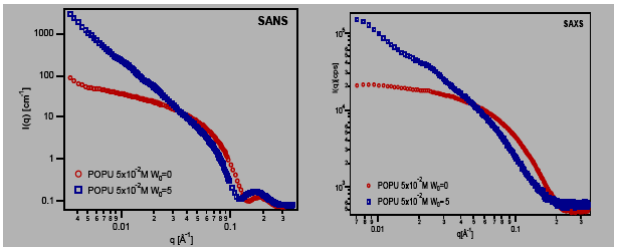

In order to extend the L2 of the ternary systems, and hence to make easier oligonucleotide inclusion, the amphiphile concentration has been increased up to $7.5x10^{-2}$M; experimentally in fact, W_{0max}=9. For each ternary system, small angle neutron scattering experiments have been performed as a function of the water content for the "empty" microemulsions, and as a function of the oligonucleotides concentration and length for the "filled" ones (Figure 2.).

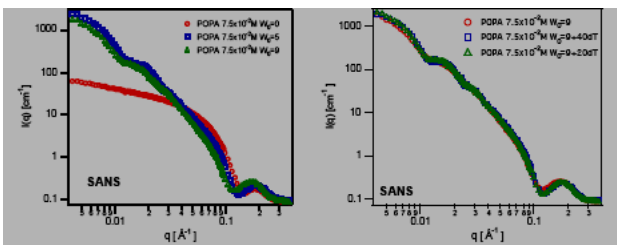

The amphiphile concentration increase has a minor effect on the structure of the aggregates; except for the binary systems in which polydispersed globular aggregates are formed instead of ellipsoid, the qualitative analysis of the data in the Guinier region shows, in fact, that locally disk-shape structures are formed, when water is added. Even if the overall shape of the aggregates does not change anymore with water amount, the thickness of the disk increases progressively (in the POPA system for example, t=40.6Å for W0=5 and t=46.5Å for W_0=9). The polar head nature influences only the size of the structures as it is shown in the figure below (Figure 3.); anyway it is interesting to notice the behaviour of the POPMix system, that is very similar to that of POPA and not intermediate between POPA and POPU.

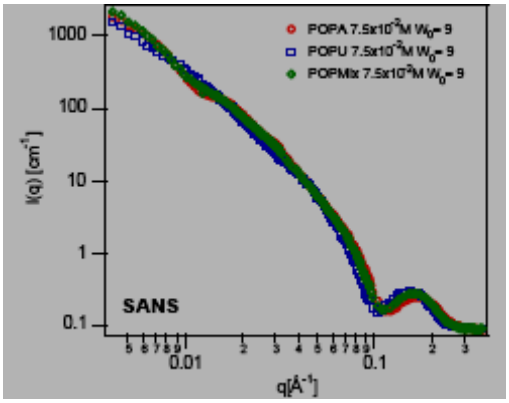

Contrary to what is reported about the solubilization of macromolecules in reverse micelles, the addition of oligonucleotides (40dA, 20dA, 40dT and 20dT) to the samples with W_0=9 does not affect the structure and the thickness of the aggregates. Information obtained from different techniques (SAXS, DLS, FT-IR and Circular Dichroism) will be useful to draw some conclusive remarks about the structural properties, and about the effects of the molecular recognition pattern. A more detailed data analysis is in progress.

	EXPERIMENTAL REPORT SANS on alpha-helical peptide fibrils	Proposal N° CHE-04-1260 Instrument **V4** Local Contact Uwe Keiderling
Principal Proposer: Experimental Team:	H. v. Berlepsch – FU, Berlin H. v. Berlepsch – FU, Berlin S. Wagner – FU, Berlin U. Keiderling – HMI, Berlin	Date(s) of Experiment 16.08. – 18.08.2006

Date of Report: 02.01.2007

Amyloid-forming proteins undergo a conformational transition from the native, mainly α-helical structure into an isoform with high β-sheet content. Those β-sheet rich intermediates are supposed to be the immediate precursors for the formation of amyloid fibers and were shown to be the toxic component in many neurodegenerative deseases. To unravel the molecular interactions that occur during the transformation from α-helix to β-sheet and the formation of amyloids is still a challenge. Therefore, the development of small model peptide that can serve as tools for such studies is of paramount importance. Recently we designed three model peptides (VW01, VW19, RR01) that contain structural elements for both, stable α-helical folding as well as β-sheet formation, as competing subunits.

At pH=7.4 (pH=4.0) and for concentrations above ~ 0.075 % the peptides VW19 (VW01, RR01) aggregate in the α-helical conformation. Cryo-TEM revealed fibrils of micrometer lengths and a diameter of ~ 2.5 nm for VW19[1] and RR01 or nanoscopic oligomers in case of VW01. The number of single α-helical strands forming the fibrils or the oligomers remained unknown.

To determine the mass per unit length of the VW19 fibrils from the low momentum transfer limit (cross-section Guinier plot) we carried out an external contrast variation (D_2O/H_2O-buffer mixtures containing 0, 40, 60 ,80, 100 % D_2O) SANS experiment. In case of the peptides RR01 and VW01 SANS has been measured in 100 % D_2O-buffer only. The peptide concentration was chosen to be only 0.3 % in each case to reduce interparticular interferences. Smaller values were not taken into account because of the suspected low scattering contrast.

Fig. 1 shows the SANS data for VW19. The scattered intensity does not reveal the expected cross-section Guinier regime ($\log(QI(Q)) \sim Q^2$) but instead decayed as $I(Q) \sim Q^{-2}$ almost over the whole Q-range (cf. the back-ground corrected SANS profiles in Fig. 2). Thus the local cylindrical structure of the fibrils is invisible whereas the gel properties obviously dominate.[2] This surprising result for a 0.3 % solution prevents the estimation of the fibrils mass per unit length. The peptide RR01 behaves similar. In contrast, for the peptide VW01 a Guinier analysis is possible (Fig. 3) providing a particle size (radius of gyration) of about 1.25 nm.

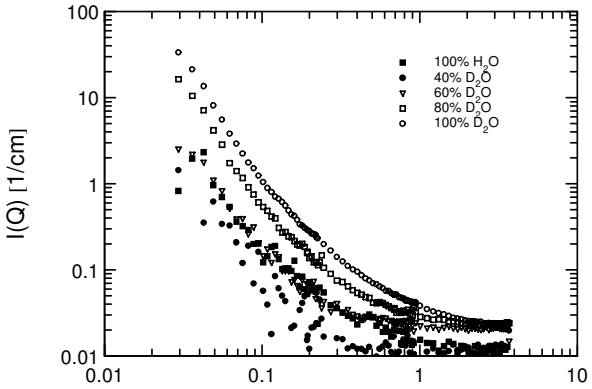

Fig. 1: *VW19, effect of external contrast variation*

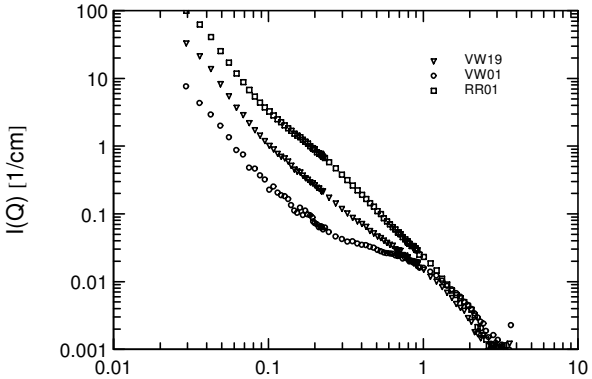

Fig. 2: *SANS data for samples in 100% D_2O-buffer*

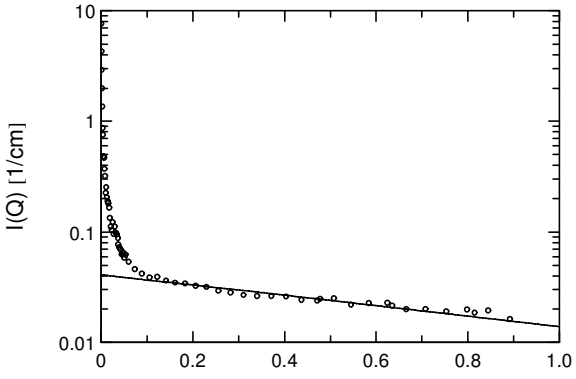

Fig. 3: *Guinier plot of intensity for VW01*

References:

[1]. [1] K. Pagel et al., JACS, **128**(2006)2196
[2]. [2] S. Koizumi et al., J. Chem. Phys. **121**(2004)12721

	EXPERIMENTAL REPORT **Neutron reflectivity study of PEG-like radiofrequency glow discharge (rfgd) plasma polymer (PEGpp) films**	Proposal N° CHE-04-1334 Instrument **V6** Local Contact Roland Steitz
Principal Proposer: Experimental Team:	C. Fong – CSIRO, Australia T.R. Gengengbach – CSIRO, Australia B.W. Muir – CSIRO, Australia R. Steitz – HMI, Berlin	Date(s) of Experiment 18.10. - 23.10.2006

Date of Report: *22.12.2006

The control of non-specific protein adsorption is crucial for determining the success of engineered surfaces and devices for biomedical implants. Uncontrolled exposure of such materials to a biological environment can trigger immunogenic responses leading to the ultimate rejection and failure of the device.

Poly(ethylene glycol) (PEG) modified surfaces are widely accepted as having excellent protein repellancy. The non-fouling nature of PEGs is often attributed to steric/entropic effects or alternatively, as a result of PEG-water hydrogen bonding interactions forming a 'water barrier' against protein adhesion. The application of radiofrequency glow discharge (RFGD) plasma polymerisation (pp) techniques to produce PEG-like coatings is a recent development. PEG-like pp films have several advantages over traditional wet chemistry methods such as the ability to easily vary the thickness, cross-link density and ether (EO) content of the films over a wide range in the dry state.

In the current study we are interested in the in-situ protein adsorption and swelling behaviour of deuterated PEG-like pp films of diethyleneglycol dimethylether (DDG-pp) with variable cross link density and EO content conferred by variation of the plasma deposition time. Two films of variable EO content and cross link density were examined in this study namely, DDG-30s (high EO and density) and a multilayer 3x3s film (low), DDG-3x3s. Deuteration confers greater contrast in the neutron experiment however, the effect upon the physico-chemical properties of these films is unknown.

Using the V6 reflectometer, we have initiated studies of these diglyme films with the aim of elucidating the interpenetration of protein (if any) into the PEG-like layers, protein orientation and water structuring at the film-aqueous interface. The chemical composition and film thickness as determined by XPS and AFM are detailed in Table 1. Figure 1 illustrates a comparision of the dry, wet and films exposed to protein for the DDG-30s film. Interestingly, XPS showed that the EO content of these films were similar and exposure to BSA (1 mg/ml in PBS buffer at pH 7.4) demonstrated a small but detectable nitrogen contribution indicative of protein adhesion. This suggests that these films are low fouling rather than non-fouling. However, neutron reflectometry (NRR) of this film suggests that the DDG-30s film is resistant to fouling in the presence of BSA (1 mg/ml and 7 mg/ml PBS/pH 7.4 buffer) as well as fibrinogen (2.5 mg/ml PBS/pH 7.4). This raises the question of the sensitivity of the reflectivity technique *cf* XPS for the detection of low levels of protein adhesion. The DDG-3x3s film is considerably less cross linked and the effect of swelling/loss of loosely bound material of the film *vs* protein adsorption/interpenetration was difficult to deconvolute using NRR alone. Interestingly, neither of these films exhibited significant H-D exchange over a three hour period. Currently, analyses of these data are continuing with further verification of the observed behaviour ongoing at CSIRO.

Table 1: Chemical Composition and Film Thickness

Sample	d (nm)	Chemical Composition (atom%)			
		C	O	N	N/C
DDG 30s	22.4	72.7	27.7	-	-
DDG 30s+BSA	-	73.4	26.1	0.3	0.004
DDG 3x3s	7.1	69.4	29.7	-	-
DDG 3x3s+BSA	-	70.3	28.9	0.1	0.002

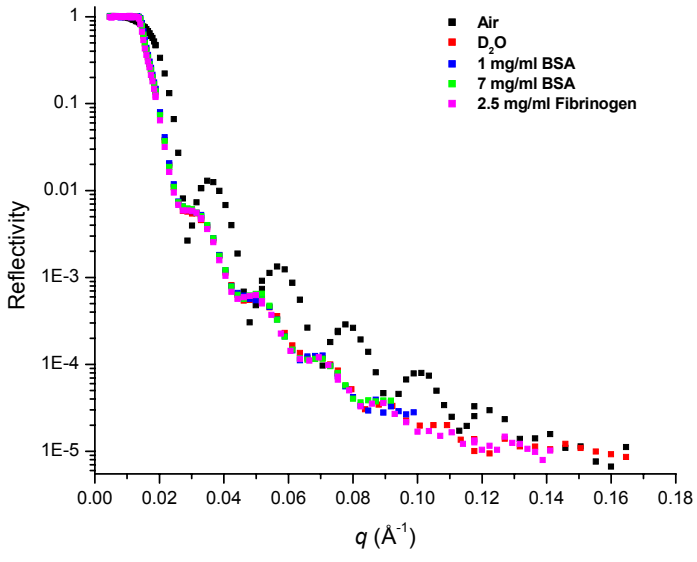

Fig. 2: *Reflectivity profiles of the D-DG pp 30s film*

	EXPERIMENTAL REPORT **Development of D_2O Tracer Method for Water Flow in Plants**	Proposal N° BIO-04-1224 Instrument **V7** Local Contact Nikolay Kardjilov
Principal Proposer: Experimental Team:	U. Matsushima – Iwate Univ., JP N. Kardjilov – HMI, Berlin W. Herppich – ATB Potsdam A. Hilger – HMI, Berlin	Date(s) of Experiment 08.06. – 19.09.2006

Date of Report: 19.01.2007

Background

Water uptake in tomato seedlings was successfully observed using cold neutron radiography and D_2O tracer. However, the time-lag of liquid exchange gave water shortage for the roots that can be drought stress of samples. The unstable environment in the irradiation hall also would be affected the sample condition, because water uptake is highly related to the stomata opening, and it is quite sensitive to temperature and humidity. Thus, the liquid tracer exchange system of this method was improved and a temperature and humidity control system was installed.

Materials and Methods

Figure 1 shows a schematic diagram of a syringe injection system that was employed to exchange liquid tracers, D_2O and H_2O, one after the other. An electric actuator controlled injection movement of two syringes. Liquid flow from both syringe switched over by controlling electric valves. First, an aspirator (1) removed a tracer liquid from the sample vase (7), then a syringe (1) injected the other tracer liquid to the sample.

Figure 2 shows a schematic diagram of temperature and humidity control system. To control the temperature, a peltier unit was set up on the sample container wall (2). Humidity in the sample container was modified using saturated water vapour pressure at a water tank (5) that temperature was lower than that of the sample container (1). Aerated air flow at the water tank flowed in the sample container (arrow in Figure 2). The temperature at water was controlled by a peltier unit (3). Both peltier units were controlled by a PID controller each other (6, 7).

Results and Discussion

By installing the syringe injection system, exchanging time of liquid tracer became stable and controllable. The exchanging time of 13 ml of liquid tracer was about 45 seconds. To remove old tracer for certain, injection was performed twice.

Temperature in the container became stable using the control method. However the peltier unit on the container wall condensed dew from circulation air. The condense would affect humidity controlling. When humidity was set up to around 60 %RH, it was changed from 30 %RH to 65 %RH.

Resistance of air flow by the thin tubings also disturbed the control of the humidity. Humidity controlling system is quite important for stable measurement and it should be improved for the next experiment.

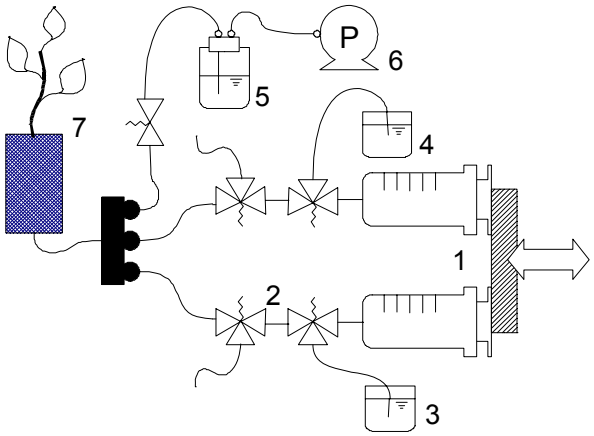

1 Two syringes manipulated by an actuator. 2 Electric valves 3, 4 D_2O and H_2O bottles 5 Aspirator 6 Pump 7 Sample

Fig. 1: *Syringe injection system*

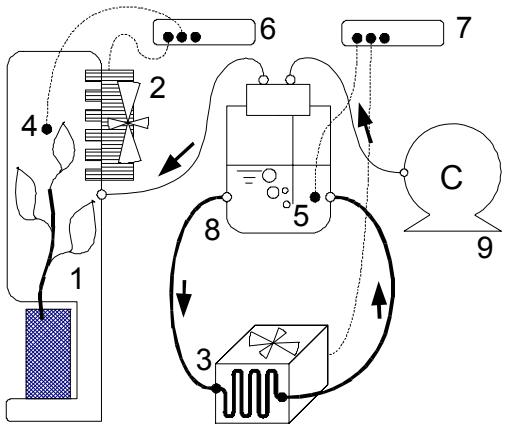

1 Sample container 2, 3 Peltier units
4, 5 Thermocouples 6, 7 Controllers 8 Water tank
10 Air compressor

Fig. 2: *Temperature and humidity control system*

	EXPERIMENTAL REPORT **Efficient Photosynthesis and Auto-exhaust Resistance in Street Trees**	Proposal N° BIO-04-1310 Instrument **V7** Local Contact Nikolay Kardjilov
Principal Proposer: Experimental Team:	U. Matsushima – Iwate Univ., JP N. Kardjilov – HMI, Berlin W. Herppich – ATB Postdam A. Hilger – HMI, Berlin	Date(s) of Experiment 17.09. – 27.09.2006

Date of Report: 19.01.2007

Background

The CO_2 emission from auto mobile is one of main causes of the greenhouse effect. The main idea of this research is to develop a CO_2 absorbing cycle using photosynthesis of street trees. The first step was to evaluate efficient photosynthesis and auto-exhaust resistance of street trees.

Materials and Methods

Cold neutron radiography with D_2O tracer and chlorophyll fluorescence imaging obtained information on water usage and photosynthetic activity of plants, respectively. Each data set is able to evaluate exhaust resistance of plants. Hibiscus, which is a popular street tree in Okinawa, Japan, was used for experiments. Branches of hibiscus trees were cut at the length of 10 cm from the tops. The branches were placed into a tub filled with water that was aerated. The branches were used as samples after they produced roots. A sample was transplanted in a glass tube filled with glass beads, then the top was covered by a sample cuvette.

Air containing approximately 2ppm of SO_2 gas was employed as simulated toxic auto-exhaust. This SO_2 concentration was obtained by diluting premixed SO_2 gas from the gas bottle with air. The dilution ratio was controlled by mass flowmeters. Gas mixture was given to the sample container through plastic tube. Air temperature and relative humidity at in the container cuvette was set to at 23 °C and 60 %.

The chlorophyll fluorescence imaging system was vertically placed to the neutron beam line to avoid direct irradiation. The sample was also vertically placed in the beam line to take neutron images. Therefore, the sample cuvette was rotated by an automatic rotation table to face to the fluorescence imaging camera. A fluorescence image was taken before giving simulated auto-exhaust gas. Afterwards, the gas was supplied for one hour while. Fluorescence images were taken every 20 min. Then, the cuvette was again flushed with normal air finishing giving the gas,and the imaging was continued for one hour.

During the experiment Cold cold neutron radiography images were taken every 15 seconds Twith an irradiation time of 10 seconds. The liquid tracers, which were D_2O and H_2O, were exchanged every 30 min.

Results and Discussion

Chlorophyll fluorescence imaging was suitable method to observe the effects of toxic auto exhaust to on plants. F_v/F_m , that is an parameter sensitive indicator of the efficiency and integrity photosynthetic efficiency of plants' photosynthesis, was immediately dropped from the initial value 0.6 to 0.4by 30% after supplying the simulated the auto-exhaust gas. Figure 1 shows the movement of D_2O tracer in the hibiscus stem. D_2O tracer successfully indicated water movement in the sample stem. However signal from became week when it spread into the leaf veins. A 5.5 Å monochromatic neutron beam was used to detect the week signal from D_2O. Small changes of contrast by D_2O can be observed by the low energy beam.

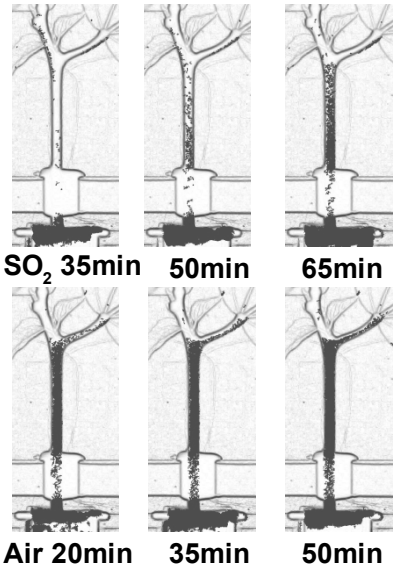

Fig. 1: *Movement of D_2O tracer in the hibiscus stem.*

	EXPERIMENTAL REPORT **Characterisation of bone substitutes of a bimodal size distribution of pores.**	Proposal N° BIO-04-1216 Instrument **V12a** Local Contact Markus Strobl
Principal Proposer: Experimental Team:	C. Panayiotou – AU Thessaloniki, GR C. Ritzoulis – AU Thessaloniki, GR M. Strobl – HMI, Berlin + TFH, Berlin	Date(s) of Experiment 15.05. – 26.05.2006

Date of Report: December 2007

Microporous biomaterials of bimodal pore size distribution intended for utilization as bone regeneration scaffolds have been prepared by means of emulsion droplet templating [1,2]. This project is a follow-up of BIO-04-1119, where composite microporous biomaterials of monomodal pore size distribution were successfully prepared and characterized by means of ultra small angle scattering (USANS) using the V12a double crystal diffractometer (DCD) at the Hahn-Meitner Institute in Berlin [3].

In the current project, bimodal pore size distribution of pore sizes ca. 5 μm and 100 μm (a condition essential for the development of bone tissue in the microporous bone scaffold) has been achieved by means of templating droplets from emulsions of bimodal droplet size distributions into solid protein-ceramic bone substitutes. The aim of the project is to study the correlation between template droplet sizes, as obtained from light scattering, and templated micropores, as obtained by means of ultra small angle scattering (USANS) using the V12a double crystal diffractometer (DCD) at the Hahn-Meitner Institute in Berlin.

The pore size distribution of a typical sample in comparison to due to the rendering expected sizes is presented in Fig. 1.

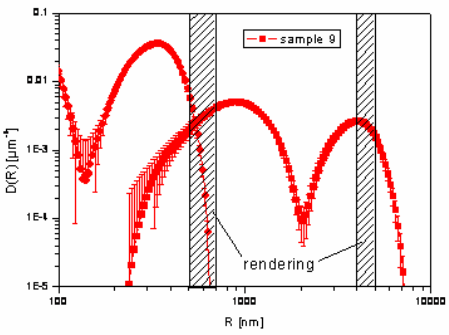

Fig. 1: *Pore size distribution for a typical porous sample..*

Of interest concerning the USANS measurements are the smaller pore size distributions. Such pores are essential for the successful growth of bone cells upon insertion as a bone substitute. The V12a data are now correlated to SEM and light scattering results aiming towards the optimization of our artificial bone manufacturing process. The pore size distribution of pores beyond the resolution of USANS, i.e. pores with diameters of around 100 μm, which are also essential for the biological function, will be examined by synchrotron tomography.

References :

[1]. C. Ritzoulis et al. Food Hydrocolloids (2004) **19** 575-581.
[2]. C. Ritzoulis et al. J Biomed Mat Res A (2004) **71A** 675-684.
[3]. M. Strobl et al. Journal of Applied Crystallography, in press

	EXPERIMENTAL REPORT **USANS study of shape changes of actively metabolising red blood cells**	Proposal N° BIO-04-1302 Instrument **V12a** Local Contact Markus Strobl
Principal Proposer: Experimental Team:	C. J. Garvey – ANSTO, Australia P. W. Kuchel – Univ. Sydney, Aus M. Strobl – HMI, Berlin	Date(s) of Experiment 04.09. – 11.09.2006

Date of Report: 05.01.2007

Mammalian red blood cells (RBC's) are highly specialized cells, and are quite simple in their construction. RBC's do not contain organelles, but rather the cytoplasmic solution is an extremely concentrated solution of protein (~30% volume fraction) hemoglobin (Hb_4). These concentrated solutions of protein are surrounded by a cell membrane. The cell membrane although important in a structural sense, does not contribute a measurable intensity to the scattering signal. The porous nature of the RBC membrane means that a suspension of red blood cells can easily prepared with D_2O as the "aqueous" environment. Previously experiments on S18 (ILL, Grenoble, France) obtained USANS data from RBC's in different equilibrium shapes. While there were clear differences in the scattering from different equilibrium shapes, the point detector and step scan of the q-range was less than optimal for good time-resolution. We used of the linear detector and the low qrange of the V12a instrument to investigate the changes in the scattering from suspensions of actively metabolising red blood cells at much higher time resolution than possible on S18. In comparison to measurements made with an optical microscope technique (Figure 1), neutron scattering data is more useful for cell volume fractions (Φ) close to that found in the blood, Φ >0.50, and rather than relying on reconstructing sample statistics from a two-dimensional representation, statistics are inherent in the sample volume sampled by the neutron beam. Data was collected on a path of 1cm of cells in differing concentrations of glucose with a time resolution approaching 10's of minutes. While the q-range of the instrument is not optimal to be sensitive to the shape an initial analysis has considered the total scattered intensity over the q-range measured, and the nature of the contrast factor for whole cells. In this q-range we consider contrast due to the difference in the Hb4 concentration difference between inside and outside the red-blood cell. Since the bulk hemoglobin concentration remains the same, changes in contrast will be due to:

1. Volume changes in the cell.
2. Lysis or rupture of the cell membrane and release of hemoglobin into the extra-cellular solution.

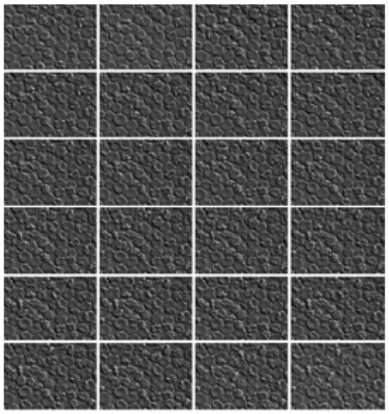

Fig. 1: *Optical micrograph of time series shape transitions of whole red blood suspension showing the the transition from normal discocytes (~ 8μm diameter) to spiked echinocytes.*

Figure 2 indicates the change in the integral scattered intensity from a suspension of whole cells at 85% volume fraction cells in the absence of glucose. The baseline descrease in scattered intensity has been attributed to the steady lysis of cells. This measurement has been made independently using hematological techniques. After approximately 10 hours there is an increase in the scattered intensity. We suggest that this is due to the rbc volume decrease, and increase in Hb4 concentration/increase in scattering contrast due to the discoyte to echinocyte transition.

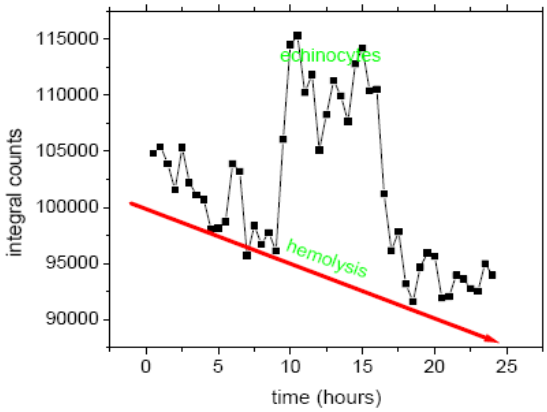

Fig. 2: *Change in integral scattered intensity for a solution of rbc's in 154 mM NaCl in D_2O.*

	EXPERIMENTAL REPORT **Role of collective fluctuations in model membranes with respect to two competing theoretical scenarios for the main phase transition**	Proposal N° PHY-02-0531 Instrument **V2** Local Contact Klaus Habicht
Principal Proposer: Experimental Team:	B. Brüning – ILL Grenoble + Uni Göttingen, F M. Rheinstädter – Univ. Missouri, USA T. Salditt – Uni Göttingen K. Habicht – HMI, Berlin	Date(s) of Experiment 28.03. – 07.04.2006

Date of Report: 02.07.2006

We proposed to investigate the collective short wavelength density fluctuations in the model membrane system DSPC-d70 using the cold triple axis spectrometer V2 (FLEX). We were able to measure the corresponding dispersion relations in the gel and the fluid phase of the bilayers by combining constant energy and constant q-scans. The temperature of the main phase transition in deuterated DSPC lies around 55°C. We have taken inelastic data at 50°C, in the gel phase and at 65°C in the fluid phase of the model membrane at 5 q-values between 1.0 and 2.3 $Å^{-1}$. We were able to resolve a minimum in the dispersion relation around Qr= 1.5 Å in both the gel and the fluid phase. Additionally scans at several temperatures between 50 and 65°C have also been taken in the minimum of the dispersion. The sample was kept in a dedicated humidity chamber supplied by T. Hauss and S. Dante which worked extremely well throughout the experiment. Elastic scans of the acyl chain correlation peak were repeatedly taken while changing the temperature with a temperature resolution of 0.3K. In contrast to DMPC the peak position does not change continuously, but abruptly (see Fig. 1). For DSPC, the data point to a coexistence of gel- and fluid domains indicated by the existence of two peaks in the range of the phase transition. The results from this experiment and previous experiments in DMPC [1] thus point to a coexistence of gel- and fluid domains in the range of the phase transition with distinctly different sizes for the two lipids. While the DMPC domains must be distinctly smaller than the coherence length of the neutrons ξ(about 500 Å) to average over the different nearest neighbour distances, the mismatch of the two phases seems to be larger for larger chain length and the systems tries to avoid domain boundaries by larger domain sizes (>ξ) in DSPC. The inelastic scans are currently being analyzed and show pronounced excitations and allow to determine the corresponding dispersion relations in the gel and fluid phase of the DSPC membrane.

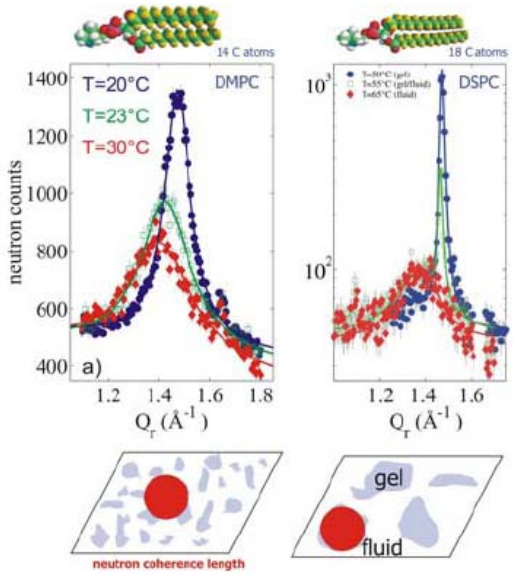

Fig. 1: *acyl chain correlation peak for DMPC and DSPC well in respective phases and at phase transition: coexistence of phases*

Refernece:

[1]. M. C. Rheinstadter, C. Ollinger, G. Fragneto, F. Demmel, T. Salditt; Phys. Rev. Lett. **93**: 108107 (2004)

BENSC	**EXPERIMENTAL REPORT** **Dynamics of field-induced ordering in magnetic colloids (II): TISANE**	Proposal N° EF Instrument **V3** Local Contact Magarita Russina
Principal Proposer: Experimental Team:	A. Wiedenmann – HMI, Berlin R. Gähler – ILL Grenoble, F A. Wiedenmann, U. Keiderling – HMI, Berlin K. Habicht, M. Russina – HMI, Berlin K. Thillosen – Gonit, St. Egreve, F	Date(s) of Experiment 21.09. – 25.09.2005

Date of Report: 29.12.2006

The onset of the field-induced local hexagonal ordering in concentrated Co ferrofluids has been studied by time-resolved SANS by applying a periodic sine-wave modulation of the magnetic field [1-4] In the low frequency range up to 500 Hz the reorientation of the magnetic particle moments could be analysed. At higher frequencies no reliable information on the dynamics was obtained from the continuous stroboscopic technique due to large damping factors $D(\Delta\lambda,\nu_s)$ which accounts for the smearing of the oscillations due to a spread of t_{TOF} times. In the TISANE technique [4,5], however, the time resolution is independent of the oscillation frequency and much weaker than in the continuous SANS mode, i.e. $\Delta t_R/T_S \approx 3.5\%$ (bars in Fig.1). Intensities $I(Q_{\alpha=0})$ and $I(Q_{\alpha=90})$ integrated over full angle sectors of 30° width, corresponding to an average value of $Q_B=0.4\pm0.3$ nm^{-1} are presented in Fig. 1. This shows impressively how the pulsed TISANE technique largely extends the frequency range of the continuous mode. Up to about 1300 Hz, the intensities oscillated again with a frequency twice of the B-field while at 1420 Hz and 2800 Hz no intensity modulation remained. The frequency dependence of the intensity was analysed as before in terms of Eq. (1) of report (I) using $B_{st}=0$ and a frequency independent damping $D(\Delta\lambda,\nu_s)$ which corresponds to the actual value of $\Delta t_R/T_S \approx 3.5\%$. The simultaneous fit of the oscillations measured between 300Hz and 1099Hz at two values of B_{max} according to Eq. (I-1) confirmed that the amount of freely oscillating moments f_e really decreases from 55 % at 300 Hz and 50% at 600Hz to 30% at 1099 Hz and drops to 0 at 1424 Hz. It has to be emphasized that the time independent 2D pattern at 1424 Hz was fully isotropic and no gap appeared between $I(Q_{\alpha=0})$ and $I(Q_{\alpha=90})$ showing the random moment orientation in the fully frozen state.

The data combined from the continuous and TISANE techniques indicate a two-step relaxation process. For about 40 % of the particles, moment rotation is blocked already below 100 Hz while between 600 and 1300 Hz the remaining particle moments continuously freeze out in a random orientation. The second step around $\nu = (2\pi\,\tau_B)^{-1} \approx$ 1000-1300 Hz corresponds closely to the characteristic time $\tau_B=160$ µs expected for Brownian rotational diffusion of individual core-shell particles of radius $R_p=R_c+D_s=6.4$ nm and a viscosity $\eta=0.2$Pas for the liquid "L9", according to $\tau_B = 4\pi\eta R_p^{\,3}/(k_B T)$. The field-induced ordering process must be governed by the fast particle rotation causing the magnetic moments to align along the direction of the magnetic field. Then the moments get stuck into locally ordered domains of about 100 nm in size. Magnetic relaxation takes place either by Brownian rotation of the whole domain or by rotation of magnetic moment inside the particle against the anisotropy energy barrier K_A according to the Néel mechanism given by $\tau_N = f_o \exp(K_A V_c / k_B T)$. The characteristic time of both mechanisms is expected to be 1-50 s, which corresponds closely to the values observed previously when the field was switched off allowing for full relaxation into equilibrium [2]. This slow relaxation of large ordered domains is at the origin of low frequency step. The incomplete relaxation gives rise to frozen random orientation of particle moments observed in an oscillating magnetic field. The sticking of particles must be induced by the strong dipolar interactions energy which amounts to $E_{dd}/(k_B T)=3$ for a pair in closest contact $\sigma=2(R_c+D_s)$.

In summary, the new time-resolved stroboscopic SANS techniques present a real breakthrough for dynamical studies of nanoscaled inhomogeneities. The observed threshold frequency around 1300 Hz is a real physical quantity since this value is still far below the instrumental time resolution and corresponds to Brownian rotation of core-shell particles.

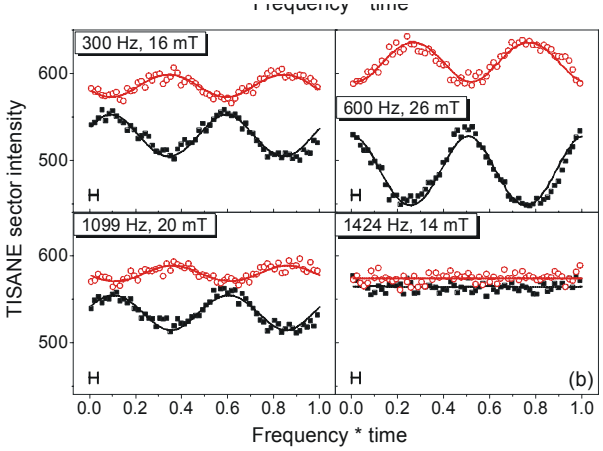

Fig. 1: *Frequency dependence of TISANE scattering intensities. Symbols: 0° (closed), 90° (open). Solid lines: fits to Eq. (3).Bars indicate expewrimental resolution.*

References:

[1]. A. Wiedenmann, A. Hoell, M. Kammel, and P. Boesecke, Phys. Rev. **E 68**, 031203 (2003).

[2]. A. Wiedenmann, U. Keiderling, R. May, and C. Dewhurst, Physica B **385-386**(2006)453-456

[3]. A.Wiedenmann, U. Keiderling, K. Habicht, M.Russina, R. Gähler. Physical Review Letters **97**, 057202 (2006)

[4]. A. Wiedenmann et al BENSC Report 2005, 2006

BENSC	**EXPERIMENTAL REPORT** **Extraction of radial and longitudinal dynamics of nano-alumina confined polymer**	Proposal N° PHY-03-0424 Instrument **V3** Local Contact Margarita Russina
Principal Proposer: Experimental Team:	J.-M. Zanotti – LLB-CEA/CNRS Saclay, F K. Lagrené – LLB-CEA/CNRS Saclay, F M. Russina – HMI, Berlin	Date(s) of Experiment 13.02. – 19.02.2006

Date of Report: 25.03.2006

We have used NEAT to check on the influence of confinement on poly(ethylene oxide) (^{h}PEO) melt dynamics.
The novelty of the experiment was to take advantage of the macroscopic orientation of Anodic Aluminum Oxide membranes (AAO) pores, to check about a possible orientational dynamical effect, namely radial or longitudinal by respect to the pore, induced by the highly anisotropic pore geometry.
AAO are made by fairly monodisperse oriented parallel cylindrical pores.
The membrane we used had pore radius, RP=130 Å. No striking confinement effect is expected if the polymer radius of gyration RG is not significantly larger the pore radius. We therefore used high molecular weight PEO (Mw=600000) with RG= 220 Å. The sample was studied at a single temperature of 373 K i.e. above the melting point (Tm=358 K).
Orientation dependant confinement effects are expected to be more striking at large scale (small Q) and long times (high resolution). In order to meet these length-scale and resolution requirements NEAT was used in large incident wavelength, high resolution mode: λ0=12 Å, R=35 µeV. In order to extract radial and longitudinal dynamics (by respect to AAO pores), all samples and calibrations have been measured with two orientations (45° and 135°) by respect to the beam.
Theoretically, the intensity measured at 90° is then related to the polymer dynamics:

i. parallel to the pores when the membrane is oriented at 45°.
ii. (ii) perpendicular to the pores when the membrane is oriented at 135°.

As shown on Fig.1, for the confined polymer, the elastic intensity scattered at 90° is significantly higher in (i) than in (ii) suggesting a faster dynamics in the longitudinal than in the radial direction. Since in bulk the polymer adopts an isotropic dynamics, the intensity at 90° is supposed to be independent of the sample orientation. Unfortunately, we also measure a slight but detectable effect of the orientation even in the case of the bulk polymer, leading to the conclusion that self absorption effects are not negligible and could lead to systematic errors in the measurement. If intensities of bulk and confined PEO are normalised by the mass of polymer in the beam, the orientation effect observed on the confined seems nevertheless more important than in the bulk.

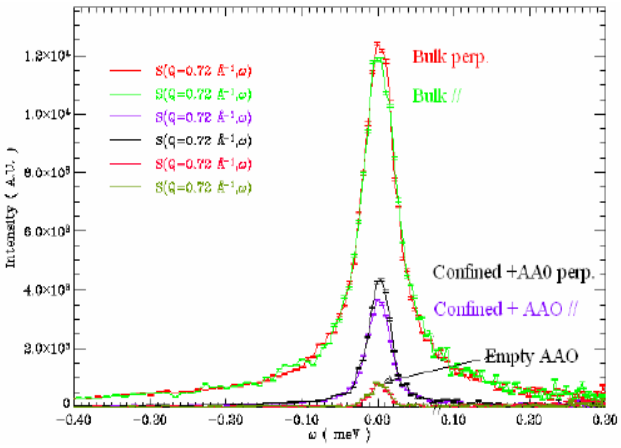

Fig. 1: *Intensity in the quasi-elastic region at Q=0.72 Å^{-1}, ^{h}PEO, confined PEO (pore diameter 50 nm), empty AAO membranes. Three detectors columns oriented at (2θ ≃ 90°) have been grouped to increase the signal to noise ratio. In each case, the direction of the vector **Q** by respect to the pores axe (perpendicular or parallel) is indicated.*

So, from this experiment, keeping in mind possible non physical orientation effects, we nevertheless feel that we were able to observe a slight signature that, under 1D confinement, the radial and longitudinal polymer dynamics are different.

	EXPERIMENTAL REPORT **Aggregate structure in the pores of SBA-15 silica studied by SANS with asymmetric collimation**	Proposal N° CHE-04-1140 Instrument **V4** Local Contact Astrid Brandt
Principal Proposer: Experimental Team:	G. H. Findenegg – TU Berlin G. H. Findenegg – TU Berlin T. Shin – TU Berlin A. Brandt – HMI, Berlin	Date(s) of Experiment 06.02. – 10.02.2006

Date of Report: 23.01.2007

We are studying the structure of surfactant aggregates adsorbed in the pores of SBA-15, a periodic mesoporous silica with two-dimensionally (2D) hexagonal arrangement of cylindrical pores of uniform size (pore radius 4 nm). The SANS spectra are analyzed in terms of a model which combines the structure factor S(q) of a 2D hexagonal lattice with the form factor F(q) of a core-shell cylinder representing the pores (radius R) with an adsorbed uniform surfactant film (thickness d). The model involves three SLD levels, corresponding to the core liquid (ρ_1), adsorbed film (ρ_2 =1.65x10^{10}cm^{-2}) and matrix (ρ_3 =3.7x10^{10}cm^{-2}).

In our earlier experiments at Instrument V4 [1-3] it was found that the (10) Bragg reflection and a combined peak arising from the (11) and (20) reflections of the SBA-15 matrix are resolved, and that the intensities of these two peaks are strongly affected by the adsorbed surfactant layer in the pores. Supplementary to these experiments, we have now studied some of the surfactant/silica systems at a better instrumental resolution. For this purpose we employed the asymmetric collimation option, with the collimator position fixed at 12 m for all detector positions.

Self-assembly of different types of surfactants in the pores of SBA-15 silica was investigated: Two nonionic surfactants of the alkyl ethoxylate (C_nE_m) and alkyl glucoside (C_nG_m) type, resp., and two cationic surfactants, dodecyl pyridinium chloride (DPC) and hexadecyl pyridinium chloride (CPC) were studied at two well-defined surfactant loadings in the pores. Samples were prepared in water of three scattering length densities (SLD), viz., pure D_2O (SLD = 6.34x10^{10}cm^{-2}), a H_2O/D_2O mixture of SLD = 5.0x10^{10}cm^{-2}, and contrast-matching H_2O/ D_2O (SLD = 3.7x10^{10}cm^{-2}). Measurements were made over a q range from 0.04 to 5 nm^{-1} (detector positions 1 m and 3.5 m).

Scattering curves exhibit Bragg peaks from the 2D-hexagonal lattice of the matrix (q_{10} = 0.68 nm^{-1} for the present SBA-15 sample). The scattering intensities at the positions of the prominent Bragg peaks (*10*, *11+20*, and *21*) which are strongly affected by the adsorption of the surfactant into the pores have been studied as a function of following experimental parameters:

(a) surfactant type ($C_{10}E_5$, $C_{10}G_2$, DPC and CPC)
(b) surfactant loading (maximum adsorption and 1/3 of this value)
(c) SLD of water (3.7, 5.0, or D_2O)
(d) salt concentrations (10^{-3} M or 10^{-1} M KCl) in the case of cationic surfactants

With the collimator positioned at 12 m distance the peak broadening effect could be reduced noticeably but not enough to resolve the combined peak of the (11) and (20) reflections. Fig. 1 shows scattering curves obtained with the new and old collimator positions. The major findings of our earlier investigations were reproduced, but a quantitative analysis of the data was not possible due to an artifact causing a distortion of the (10) peak shape, as shown in Fig. 1a.

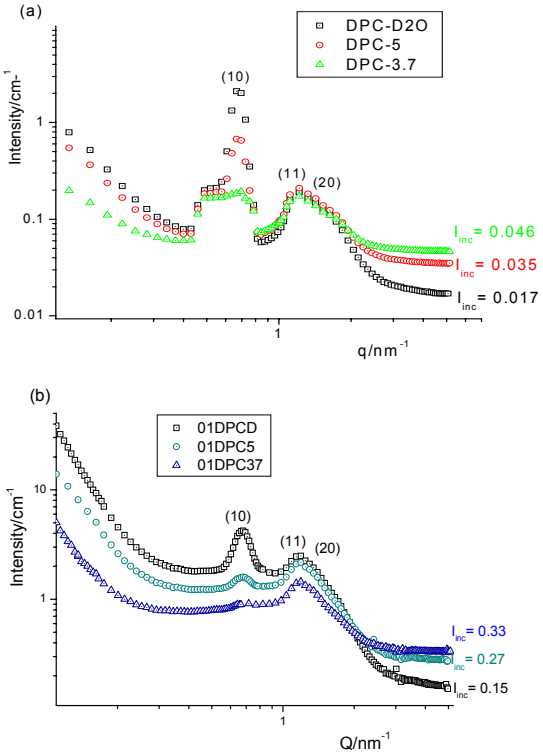

Fig. 1: *Scattering curves for DPC in SBA-15 at 0.1 M KCl and three SLD scenarios: (a) present experiment (CHE-04-1140); (b) previous experiment (CHE-04-1091)*

References:

[1]. BENSC Experimental Rep. CHE-04-0935 (2004)
[2]. BENSC Experimental Rep. CHE-04-1011 (2004)
[3]. BENSC Experimental Rep. CHE-04-1091 (2005)
[4]. Progr. Colloid Polym. Sci. **133**, 116-122 (2006) DOI 10.1007/2882_069

	EXPERIMENTAL REPORT **Solubilisation of chlorinated oils in triblock copolymers-surfactant mixed aggregates**	Proposal N° CHE-04-1152 Instrument **V4** Local Contact Sylvain Prévost
Principal Proposer: Experimental Team:	S. Miloto – Univ. Palermo, I M. Gradzielski – TU Berlin G. Lazzara, N. Muratore - Univ. Palermo, I S. Prévost – HMI, Berlin	Date(s) of Experiment 13.03. – 16.03.2006

Date of Report: 20.12.2006

Within the topic of surfactant enhanced solubilization of additives sparingly soluble in water, volumetric, solubility, conductivity and small-angle neutron scattering (SANS) experiments on mixtures composed of 1,2-dichloroethane, surfactant, copolymer and water were carried out at 298 K. The tri-block copolymer (ethylene oxide)$_{76}$(propylene oxide)$_{29}$(ethylene oxide)$_{76}$ (F68) was chosen. The selected surfactants are sodium decanoate (NaDec) and decyltrimethylammonium bromide (DeTAB) with comparable hydrophobicity and different charged heads. The 1,2-dichloroethane was chosen as a contaminant prototype. In the case of F68+D_2O solution both the volumetric and the SANS data reveal that the 1,2-dichloroethane 80 mmol kg^{-1} does not alter the copolymer unimeric state. By increasing the oil concentration, a strong increment in the absolute scattered intensity is observed in agreement with the copolymer aggregates formation induced by the oil (Figure 1). For the water+surfactant+copolymer mixtures, both the thermodynamic[1,2] and the SANS results[2] straightforwardly evidenced that: 1) monomers of NaDec and copolymer unimers generate small mixed aggregates; 2) monomers of DeTAB combined with copolymer unimers do not form aggregates and 3) unimeric copolymer is solubilized into the NaDec and DeTAB micelles. Moreover, they show that for the aqueous DeTAB-F68 system the additive trapping in both the copolymer-micelle aggregate and the pure micelles takes place being enhanced in the former aggregate in agreement with solubility experiments. For the NaDec-F68 mixtures, an additional solubilization process in the pre-micellar copolymer-surfactant microstructures occurs. SANS and conductivity data show that the additive incorporation into the mixed and the pure micelles does not essentially influence the structural properties of the aggregates.

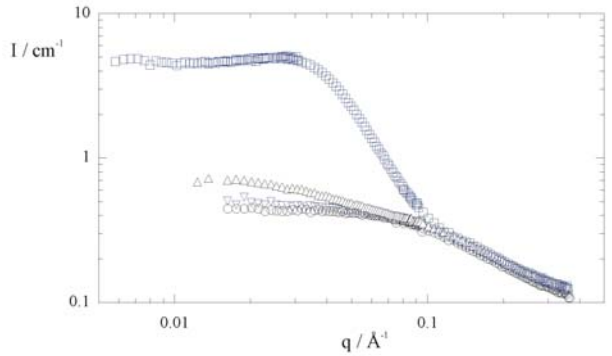

Fig. 1: *Scattering function of D_2O+F68 in the absence (o) and in the presence of $Cl_2(CH_2)_2$ at different concentration: 80 mmol kg^{-1} (▽); 150 mmol kg^{-1} (△) and 250 mmol kg^{-1} (□).*

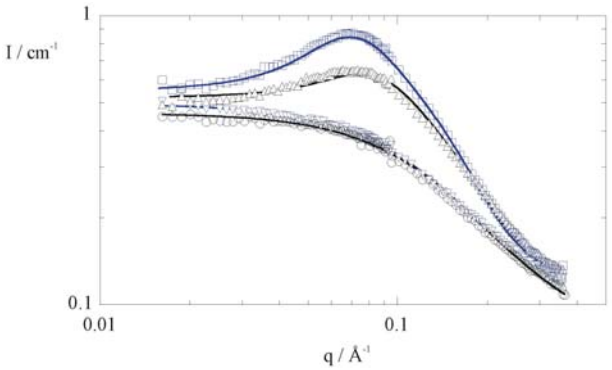

Fig. 2: *Scattering function of D_2O+F68 (○), D_2O+F68+$Cl_2(CH_2)_2$ (▽), D_2O+F68+NaDec (△) and D_2O+F68+NaDec+$Cl_2(CH_2)_2$ (□). NaDec, 66 mmol kg^{-1}; F68, 15 mmol kg^{-1} and 1,2-dichloroethane 80 mmol kg^{-1}. Lines are the best fits.*[2]

References:

[1]. R. De Lisi; G. Lazzara; S. Milioto; N. Muratore, *J. Phys. Chem. B* 2004, **108**, 1189

[2]. R. De Lisi; M. Gradzielski; G. Lazzara; S. Milioto; N. Muratore; S. Prevost *J. Phys. Chem. B* 2006, **110**, 25883

Acknowledgements:

This research project has been supported by the European Commission under the 6th Framework Programme through the Key Action: Strengthening the European Research Area, Research Infrastructures. Contract n°: RII3-CT-2003-505925 (NMI3)

	EXPERIMENTAL REPORT	Proposal N° CHE-04-1187-EF
BENSC	**Determination if inner structure and dimensions of surpramolecular fiber-like nanostructures obtainable- via self-assembly of peptide-polymer-building blocks.**	Instrument **V4** Local Contact Astrid Brandt
Principal Proposer: H. Börner – MPI, Golm Experimental Team: B. Smarsly, J. Hentschel – HMI, Berlin A. Brandt – HMI, Berlin T. Hellweg – TU, Berlin		Date(s) of Experiment 10.02. – 13.02.2006

Date of Report: 20.12.2006

Numerous native materials exhibit well-adapted, high performance properties due to their optimized structural design. Frequently, the structure formation processes within these biomaterials are guided via self-organization of polypeptides or proteins. Transferring these organization principles towards structuring of synthetic materials-would be of great interest. In particular fibrils or fibers are important structural elements in native materials. Diverse properties like anisotropic strength, structural stability or directed transport can be realized with these structures. In material science, nanofibers are important as high-strength components in composite materials, nanowires and fibers for medical applications. Recently, we utilized conjugates of poly(ethylene oxide) (PEO) and peptide segments, to access soluble, nano structured fibers in a controlled self-assembly process.**[1]** These anisometric core-shell fibers could be visualized by atomic force microscopy (AFM) and transmission electron microscopy (TEM) **(Fig. 1).** They exhibit a number average height of about 1.4 nm, a maximum length up to 2 µm and widths of about 13-17 nm.

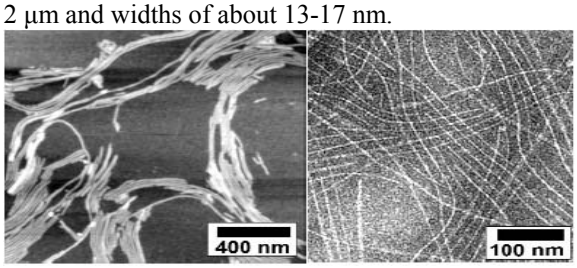

Fig. 1: *PEO fiber aggregates. AFM micrograph (0.08 mg/mL aq. solution), spin coated on Mica, tapping mode, z = 8 nm height) (left) and TEM image (20 mg/mL aq. solution, negatively stained) (right).*

Based on the observed dimensions and the literature describing the aggregation behavior of similar peptides without polymer block, a preliminary model was suggested. As outlined in figure 2, the fiber structure is most likely stabilized by the formation of an anti-parallel β-sheet of the peptide units. Thus the aggregate exhibits a core-shell structure, comprising a peptide β-sheet core and a PEO-shell. The latter contributes to solubility of the fiber and suppresses lateral aggregation. Probably the fiber structures are composed of double β-sheets denoted as ribbons **(Fig. 2, right).**

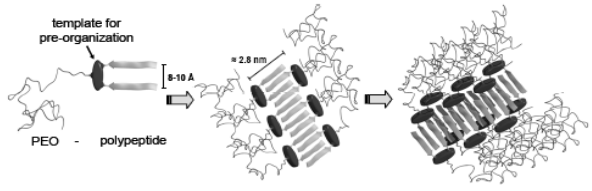

Fig. 2: *Idealized structure proposal for the aggregation of III into fiber like aggregates exhibiting peptide core and PEO shell.*

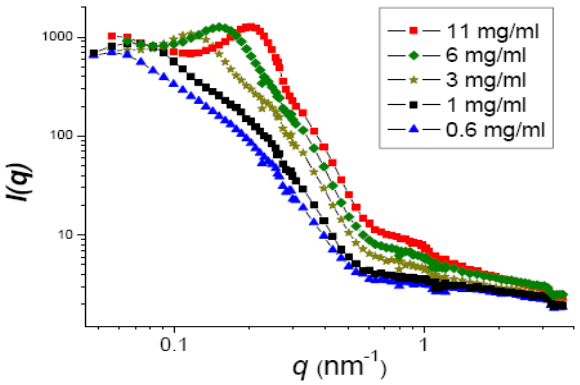

Fig. 3: *Radially averaged SANS data of aqueous solutions of the nano structured fibers acquired at the V4 beamline using different concentrations in D_2O.*

SAXS analysis of diluted, aqueous solutions suffered from the low scattering contrast, resulting in an inferior signal to noise ratio at larger q values. Hence, SANS experiments were performed using the V4 beamline in solution, addressing the accurate solution structure dimensions and information about the inner structure. In particular, the investigation (proposal 1187) addressed these issues by measuring D_2O solutions of nano structured fibers with different concentrations (11 mg/mL, 6 mg/mL, 3 mg/mL, 1 mg/mL, 0.6 mg/mL, 0.1 mg/mL) as well as solutions with different ratios of D_2O/H_2O using small angle neutron scattering. Already preliminary evaluation of the SANS data revealed interesting features **(Fig. 3)** and a good data quality. At higher concentrations the scattering curves showed a maximum, corresponding to the average distance of the fibers. Moreover, at ca. q = 0.3. 0.7 nm^{-1} damped oscillations can be observed, which can be interpreted as the form factor of the fibers, because the minimum at q = 0.6 nm^{-1} does not shift upon concentration changes. The SANS data thereby indicate a liquid crystalline nematic order in solution. This is consistent with the structure model shown above, describing stiff fiber-like mesogens. A straightforward evaluation of position of the minimum at q = 0.6 nm^{-1} provides an average radius of about 3 nm (cylinders), which corresponds well with the dimensions seen in TEM. Suitable theoretical scattering functions (e.g. fibers with a rectangular cross-section) will be developed to the fit the promising data to obtain structural parameters such as the diameter.

Reference:

[1]. Eckhardt, D., Groenewolt, M., Krause, E. & Borner, H. G. Rational design of oligopeptide organizers for the formation of poly(ethylene oxide) nanofibers. Chem. Commun., 2814-2816 (2005).

	EXPERIMENTAL REPORT SANS study of the gemini nonionic surfactant in micellar solutions	Proposal N° CHE-04-1205 Instrument **V4** Local Contact André Heinemann
Principal Proposer: Experimental Team:	A. Rajexska – IAE Otwock, PL D. Clemens – HMI, Berlin A. Heinemann – HMI, Berlin	Date(s) of Experiment 03.06. – 04.06.2006

Date of Report: 20.07.2006

Mixtures of surfactants: nonionic Gemini S-10 (α (α α'-[2,4,7,9-tetramethyl-5-decyne-4,7diyl]bis[ω hydroxyl- polyoxyethylene) and two classic cationic CTACl (cetyltrimethylammonium chloride), CTAB (cetyltrimethylammonium bromide) and two anionic classic SDS (sodium dodecyl sulfate), LiDS (lithium dodecyl sulfate) in D_2O (heavy water) were investigated with small angle neutron scattering method.
Samples were investigated in three series:

I series: 11 samples [S-10+D_2O ONLY (**6 samples**) for concentrations: 2.3%, 2.5%, 3.0%, 3.4%, 4.0%, and 5%; S-10+D_2O+CTACl (**5 samples**) for concentration S-10 with D_2O (**2.5%**) with add of cationic classic CTACl: 1. 0.005 mol/l, 2.0.01 mol/l, 3. 0.03 mol/l, 4. 0.05 mol/l **,** 5. 0.1 mol/l **]**

II series: 14 samples [S-10+D_2O (**6 samples**) for concentration S-10 with D_2O (**2.5%**) with add of anionic classic surfactant SDS:1. 0.005 mol/l, 2. 0.01 mol/l, 3. 0.03 mol/l, 4. 0.05 mol/l, 5. 0.1 mol/l, 6. 0.5mol/l; S-10+ D_2O (**5 samples**) for concentration S-10 with D_2O (**3.4%**) with add of anionic classic surfactant SDS:1. 0.005 mol/l, 2. 0.01 mol/l, 3. 0.03 mol/l, 4. 0.05 mol/l, 5. 0.1 mol/l; S-10+ D_2O (**3 samples**) for concentration S-10 with D_2O (**3.4%**) with add of cationic classic surfactant CTACl: 1. 0.01 mol/l, 2. 0.03 mol/l, 3. 0.05 mol/**]**

III series: 14 samples [S-10+ D_2O (**5 samples**) for concentration S-10 with D_2O (**2.5%**) with add of cationic classic surfactant CTAB:1. 0.005 mol/l, 2. 0.01 mol/l, 3. 0.03 mol/l, 4. 0.05 mol/l, 5. 0.1 mol/l; S-10+ D_2O (**2 samples**) for concentration S-10 with D_2O (**3.4%**) with add of cationic classic surfactant CTACl: 1. 0.005 mol/l, 2. 0.1 mol/l; S-10+ D_2O (**3 samples**) for concentration S-10 with D_2O (**5%**) with add of cationic classic surfactant CTACl: 1. 0.005 mol/l, 2. 0.03 mol/l, 3. 0.1 mol/l; S-10+ D_2O (**3 samples**) for concentration S-10 with D_2O (**5%**) with add of cationic classic surfactant SDS:1. 0.005 mol/l, 2. 0.03 mol/l, 3. 0.1 mol/l; S-10+ D_2O (**1 samples**) for concentration S-10 with D_2O (**5%**) with add of cationic classic surfactant LiDS: 1. 0.1 mol/l **]**

All of surfactants solutions were prepared using D_2O as a solvent (99.9% deuterated).
Our nonionic Gemini surfactant S-10 was obtained from Air Products & Chemicals, Inc., and used without further purification. Classic surfactants: CTAB, CTACl, SDS, LiDS were obtained from Fluka and were used without further purification, too.
All SANS measurements were performed on V-4 SANS spectrometer at BENSC, Berlin.
Neutrons were used in wavelength range of 0.05 – 5 $Å^{-1}$. For the measurements quartz cells of thickness 1 mm experiment. Up to 14 such cells were placed in a holder.
Part of our results, see Fig.1.

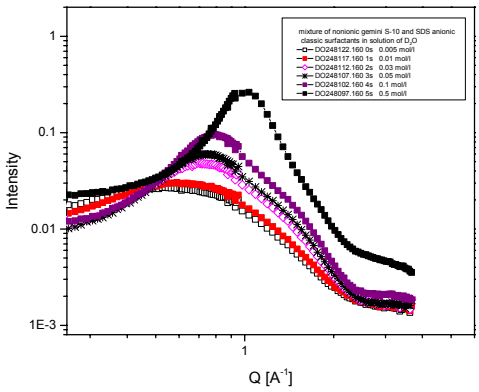

Fig. 1: *Intensity vs scattering vector Q for mixtures: solutions of S-10 nonionic Gemini and SDS (sodium dodecyl sulphate) anionic classic surfactants in D2O. Concentration of anionic surfactants SDS: 0.005 mol/l, 0.01 mol/l, 0.03 mol/l, 0.05 mol/l, 0.1 mol/l, 0.5 mol/l. (shift of max intensity of scattering neutrons to the big Q - average distance d - between micelles decrease with increase of anionic surfactant concentrations in such solutions).*

	EXPERIMENTAL REPORT **Micelles in room temperature ionic liquids**	Proposal N° CHE-04-1284 Instrument **V4** Local Contact Olivier Perroud
Principal Proposer: Experimental Team:	A. Triolo – CNR IPCF Messina, I A. Triolo – CNR IPCF Messina, I O. Perroud – HMI, Berlin	Date(s) of Experiment 14.12. – 17.12.2006

Date of Report: 16.01.2007

This experiment is the continuation of a previous one (PHY-04-1149) aiming to characterise the morphology of homo- and diblock- polymers dissolved in so called room temperature ionic liquids (RTILs). These are a novel class of materials which is attracting a great attention as an environmentally benign replacement for many toxic volatile organic solvents, such as benzene. In the previous and, in part, in the present experiment, we investigated the morphology of fully deuterated poly (ethylene oxide) (PEO) dissolved in 1-butyl-3-methyl imidazolium tetrafluoroborate (PHY-04-1149) and in 1-octyl-3-methyl imidazolium tetrafluoroborate (present experiment, Figure 1) at room temperature as a function of polymer concentration.

These studies highlighted the good solvent nature of RTILs towards PEO [1]. In this solvent, the polymer arranges in a random coil configuration, whose radius of gyration depends from the polymer concentration, following a power law.

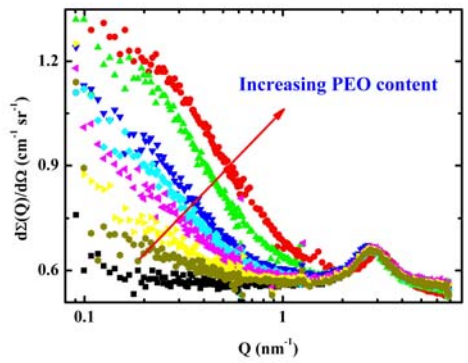

Fig. 1: *SANS data from a series of solutions of d-PEO dissolved in 1-octyl-3methyl imidazolium tetrafluoroborate, at 25°C.*

The affinity of RTILs towards PEO suggests that a block copolymers built up by the RTIL-philic PEO and a RTIL-phobic moieties would lead to the development of nanophase segregation, for example with a micellar morphology. Accordingly we investigated the SANS pattern from a series of PEO-block-poly (butadiene) (PEO-b-PB) solutions in 1-butyl-3-methyl imidazolium hexafluorophosphate (bmimPF6), as a function of polymer concentration.

The obtained data are reported in Figure 2.

These measurements are a complement to an analogous set of SAXS measurements.
Work is in progress in order to simultaneously model SANS and SAXS data with a micellar core+shell model.

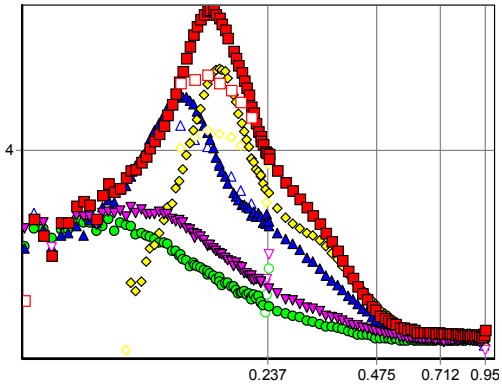

Fig. 2: *Selected SANS data from a series of solutions of PEO-b-PB dissolved in 1-butyl-3-methyl imidazolium hexafluorophosphate, at 25°C.*

References:

[1]. A. Triolo et al., Journal of Physical Chemistry B **110**, 1513 (2006)

BENSC	**EXPERIMENTAL REPORT** **Dynamics of field-induced ordering in magnetic colloids (I): Stroboscopic SANS**	Proposal N° MAT-04-1125-EF MAT-04-1182-EF Instrument **V4** Local Contact Albrecht Wiedenmann
Principal Proposer: Experimental Team:	A. Wiedenmann – HMI, Berlin A. Wiedenmann – HMI, Berlin U. Keiderling, K. Habicht – HMI, Berlin	Date(s) of Experiment 18.09 - 20.09.2005 01.11 - 06.11.2005

Date of Report: 27.12.2006

In concentrated Co-ferrofluids pseudo-crystalline hexagonal ordering of the nanosized magnetic particles is induced by an external magnetic field [1]. When the saturation magnetic field was switched off magnetic correlations between nanoparticles were found to decay exponentially within a characteristic time order of 1-5 s [2]. Here we report on a SANS study of the reversal and reordering of the particle moments in a concentrated Co-ferrofluid (MFT3) by applying a periodic sine-wave modulation of the magnetic field [3].

At low frequencies a periodic response to the oscillating magnetic field was clearly observed in the 2D scattering patterns. The scattering at B_{Max} = ±20mT is strongly anisotropic (Fig. 1a) for ν_s=100 Hz while for B=0 the patterns are almost isotropic. The SANS intensities averaged over a width of 20° in sectors at an angle α=30° and 90° between **Q** and **B** are plotted in Fig. 1b together with the corresponding curves for the static case. Fig. 1c and in Fig 2 show the time dependence of the intensities $I(Q_{i,\alpha})$, integrated in angle sectors α over the Q ranges shown in Fig.1b.. With increasing frequencies the intensity oscillations decrease in amplitude and fade away above about ν_s=600 Hz.

The SANS intensity is given by

$$I(\mathbf{Q},\alpha,B,T) = f_e \int \{(F_M^2 L^2(x)\sin^2\alpha + F_N^2)S(\mathbf{Q},\alpha) + F_M^2[2L(x)/x - \sin^2\alpha(L^2(x) - 1 + 3L(x)/x)]\}D(\Delta\lambda,\nu_s)d\Delta\lambda + (1-f_e)U(\mathbf{Q},\alpha,\nu_s) \quad (1)$$

F_N and F_M are the nuclear and magnetic form factors of the particles and $S(\mathbf{Q},\alpha)$ is an effective anisotropic structure factor [1-3]. $D(\Delta\lambda,\nu_s)$ accounts for the smearing of the oscillations due to a spread of t_{TOF} times. The dependence on the magnetic field enters in Eq. (1) via the Langevin function L(x), where $x = V_c m_0 B(t)/(k_B T)$. V_c is the core volume and m_0 is the spontaneous magnetisation of Co. As long as all particle moments follow the oscillating magnetic field, the SANS pattern should be described by Eq. (1) using

$$B(t) = B_{Max}\sin(2\pi\nu_s t) + B_{st}, \quad (2)$$

where B_{st} is a residual static field. $U(\mathbf{Q},\alpha,\nu_s)$ represents a time independent scattering contribution. Excellent agreement of all data was obtained by the model function of Eq. (1) as shown by the solid lines in Fig. 1c. and Fig. 2 when a unique set of parameters was used for all frequencies. While the decrease of the amplitudes between 100 and 600 Hz is explained by the damping factors $D(\Delta\lambda,\nu_s)$ alone, the amplitude at 100 Hz is only about half of the static case and much lower than expected from the factor $D(\Delta\lambda,\nu_s$=100)=0.93. Instead, it clearly indicates that at 100 Hz only a fraction f_e of the particle moments are still freely oscillating. The rest does not follow the external field but remains frozen more or less randomly, leading to the time-independent term in Eq.1.The fraction f_e of superparamagnetic moments which follows the field reversal was found to be of the order of 55% and nearly constant between 100Hz and 600Hz. At higher frequencies no reliable information on the dynamics can be derived from the continuous stroboscopic technique due to large damping factors $D(\Delta\lambda,\nu_s)$.

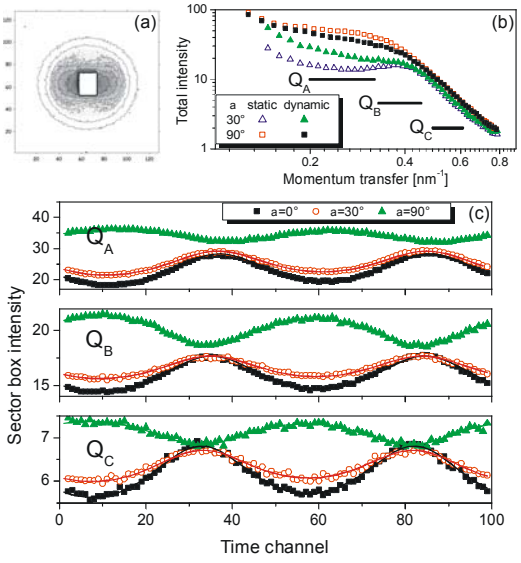

Fig. 1: *SANS intensities (a) in the 2D pattern and (b) after radial averaging in the static and dynamic (ν_s=100 Hz, B_{max}=±20mT) modes. (c) Time dependence at Q_A, Q_B and Q_C. Solid lines: fits to Eq. (3).*

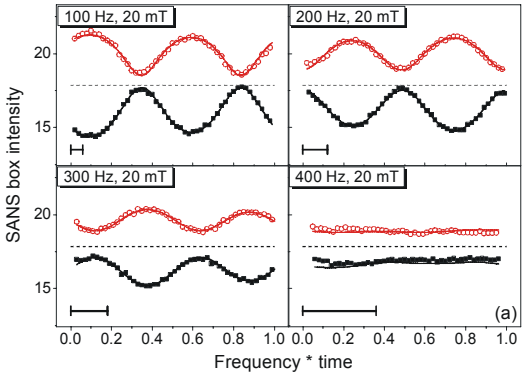

Fig. 2: *Frequency dependence of scattering intensities.Symbols: 0° (closed), 90° (open). Solid lines: fits to Eq. (3). Dashed lines: static SANS mode B=0.Bars indicate experimental resolution.*

References:

[1]. A. Wiedenmann, A. Hoell, M. Kammel, and P. Boesecke, Phys. Rev. E **68**, 031203 (2003).

[2]. A. Wiedenmann, U. Keiderling, R. May, and C. Dewhurst, Physica B **385-386**(2006)453-456

[3]. A.Wiedenmann, U. Keiderling, K. Habicht, M.Russina, R.Gähler. Physical Review Letters **97**, 057202 (2006)

	EXPERIMENTAL REPORT **Method to obtain well dispersed silica filled elastomers with weak interactions**	Proposal N° MAT-04-1197 Instrument **V4** Local Contact André Heinemann
Principal Proposer: Experimental Team:	H. Montes – UPMC - ESPCI, Paris, F T. Chaussee – UPMC - ESPCI, Paris, F A. Heinemann – HMI, Berlin	Date(s) of Experiment 06.03. – 09.03.2006

Date of Report: 30.03.2006

We have developed a new synthesis technique to perform some model filled elastomers with different interactions between the matrix and the elastomer. Our method is based on the Ford synthesis procedure, but we add a co-solvent during the polymerisation step to avoid depletion phenomenon. We perform SANS measurements to characterize the dispersion state of such filled elastomers. The grafts used are: n-Octyltriethoxysilane (C8TES), Hexamethyl-disilazane (HMDS) and Acetoxyethyldimethyl-chlorosilane (MCSNC). These three grafts lead to 2 different polymer/particle interactions at the interface: hydrogen bonding for MCSNC and low interacting system for HMDS and C8TES.

In this work we studied the influence of the concentration of the grafted-silica and the influence of two types of solvent (Methanol and Acetone) on the final particle dispersion state.

For the C8TES and HMDS grafts the scattered intensity shows that the addition of acetone lead to well dispersed filled elastomers even for high concentration using Acetone (see fig.1). With methanol, we observed bad dispersion state for HMDS grafted silica (see fig.2).

For the MCSNC grafts we do not obtain good dispersion state. We think that these bad results are due to a problem with the dialysis procedure during the synthesis. Unlike the two other grafts, we need to transfer the silica particles in propylene carbonate to graft the MCSNC molecules. The particles are then transferred to the ethylacrylate monomers and at least the monomers are polymerized. We think that the dialysis step could be not completely achieved: all the solvent (propylene carbonate) used for the chlorosilane grafting was not removed. This probably changes the particles/particles interaction and may lead to the aggregation of particles at high concentration (see fig.3). We need them to optimize this dialysis step for this graft.

However at low concentration (18 w%) in the presence of acetone we succeeded in obtaining well dispersed silica in the cross-linked poly(ethyl acrylate) matrix (see fig.3). This is a key point to understand now the influence of the matrix/particles interactions at the interface on the mechanical properties of these C8TES or HMDS filled systems. We also need to optimize the dialysis procedure in order to get well dispersed silica filled elastomer for the MCSNC graft at high silica concentration.

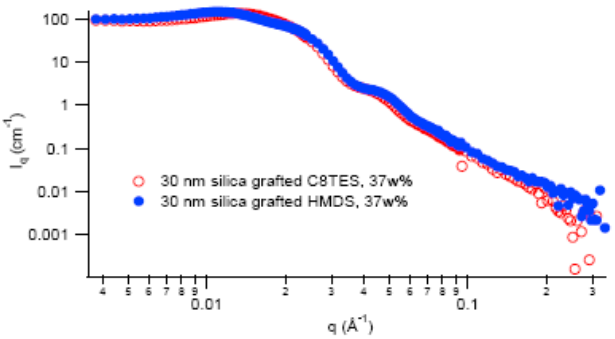

Fig.1: *30 nm silica grafted C8TES (red) and HMDS (blue) synthesised in the presence of acetone*

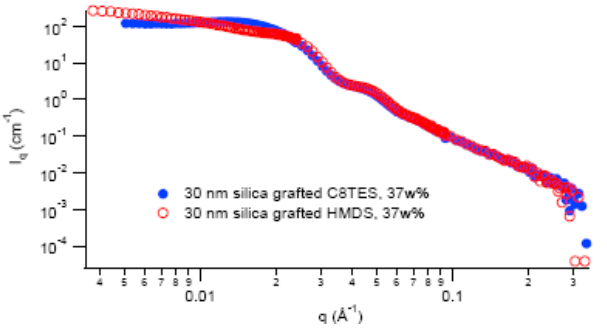

Fig.2: *30 nm silica grafted C8TES (blue) and HMDS (red) synthesised in the presence of methanol*

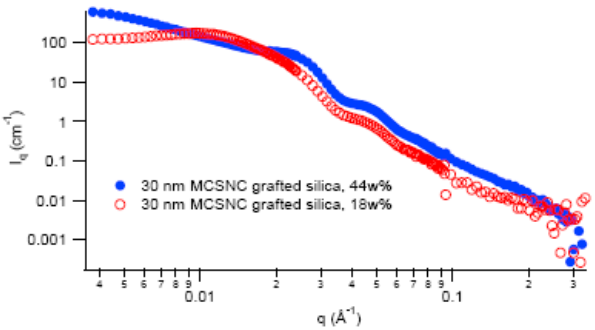

Fig.3: *30 nm silica grafted MCSNC at 18w% (red) and 44w% (blue) synthesised in the presence of acetone*

	EXPERIMENTAL REPORT **Tuning the aggregates in ferrofluids to control their properties**	Proposal N° MAT-04-1198 Instrument **V4** Local Contact Martin Kammel
Principal Proposer: Experimental Team:	R. Perzynski – UPMC LI2C, F J. de Andrade Gomes – UPMC LI2C, F E. Dubois, V. Dupuis – UPMC LI2C, F M. Kammel – HMI, Berlin	Date(s) of Experiment 22.05. – 25.05.2006

Date of Report: 17.01.2007

The knowledge and the control of the microstructure of magnetic liquids are essential in view of the numerous applications of these materials. In the purpose of understanding the microstructure of dilute and moderately concentrated magnetic liquids, a series of SANS experiments have been performed on V4 at BENSC – HMI in the q-range 2.8 10^{-3} Å^{-1} – 0.12 Å^{-1}. During the 4 allocated days (over the 7 which were asked) we have probed aqueous ferrofluids based on maghemite nanoparticles (γ-Fe_2O_3) with small particles (sample P) and large particles (sample G), chemically synthesized in our lab. Their magnetic size distribution (assumed to be log-normal) are (d_O = 7.6 nm, σ = 0.23) for sample P and (d_O = 10.5 nm, σ = 0.3) for sample G. The nanoparticles are dispersed in H_20, Φ equals 1.5 % or 5.1 %, the pH ranges between 2.3 and 3.7, and the ionic strength ranges between 10^{-3} mol/L and 0.13 mol/L.

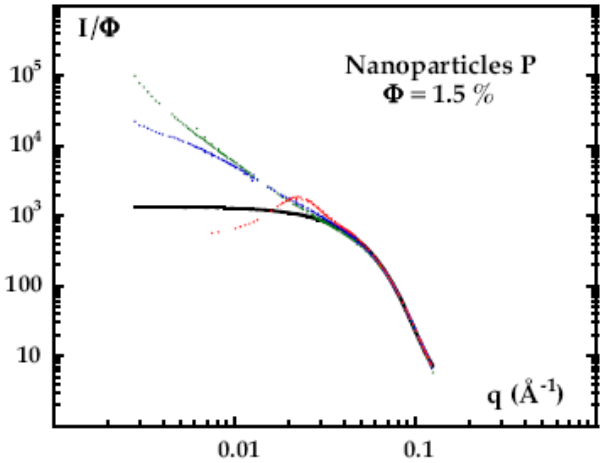

Fig. 1: *Reduced scattered intensity I/Φ for nanoparticles P at Φ = 1.5 % and various state of interaction (see text)*

Figure 1 shows the evolution of the intensity scattered by dispersions based on nanoparticles P at Φ = 1.5 % for various balances of interaction. The interparticle interaction is evolving from a marked repulsion (bottom curve at pH=3 and C_S = 10^{-3} mol/L) to a clear attraction (top curves respectively pH = 3.5, C_S = 0.065 mol/L and pH = 3.7, C_S = 0.13 mol/L). In the first situation the nanoparticles are individually dispersed, while in the two other ones an interparticle aggregation takes place. The full line is a best adjustment of the form factor of nanoparticles P supposed spherical with a log-normal distribution of diameter d_O = exp <lnd> = 67 Å and width σ = 0.24. Similar results are obtained with nanoparticles G, the best adjustment of their form factor being associated to a distribution d_O = exp <lnd> = 87 Å and width σ = 0.39. Figure 2 compares the structure factor of dispersions based on nanoparticles P and G, at the same volume fraction at Φ = 1.5 % and the same pH and C_S (repulsive bottom curves pH=3 and C_S = 10^{-3} mol/L; attractive top curves pH = 3.7 and C_S = 0.13 mol/L).

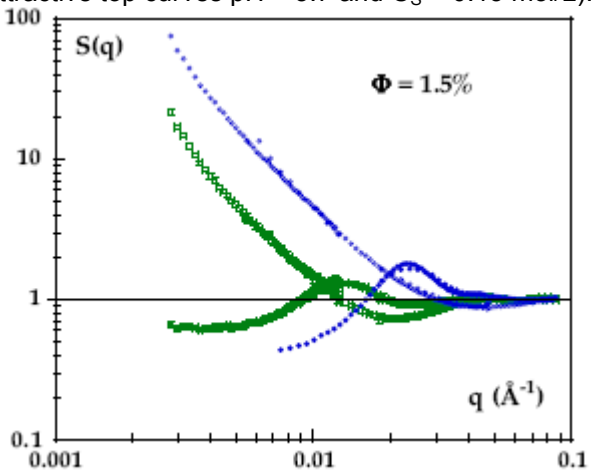

Fig. 2: *Structure factor of dispersions at Φ = 1.5 % based on nanoparticles P (full and open circles) and nanoparticles G (full and open squares). Full symbols: pH = 3 and C_S = 10^{-3} mol/L; Open symbols: pH = 3.7 and C_S = 0.13 mol/L*

Tests under a magnetic field of the order of 800 kA/m have shown anisotropic patterns for nanoparticles G of large parameter of dipolar interaction while the patterns are remaining totally isotropic for nanoparticles P of small dipolar interaction in agreement with [1].

We have thus demonstrated in this experiment, that it is possible to control the microstructure of the magnetic dispersion through various physico-chemical parameters such as nanoparticle size, pH and ionic strength. Further experiments with different ferrites are necessary together with a finer exploration of pH and C_S variations to be able to fully modelize the process.

Reference:

[1]. G. Mériguet, F. Cousin, E. Dubois, F. Boué, A. Cebers, B. Farago, R. Perzynski, *J. Phys. Chem. B* **110** (2006) 4378 – 4386

	EXPERIMENTAL REPORT **Influence of surfactants on the ordering phenomenon in ferrofluids**	Proposal N° MAT-04-1244-EF Instrument **V4** Local Contact Martin Kammel
Principal Proposer: Experimental Team:	A. Wiedenmann, M. Kammel – HMI, Berlin S. Prévost – HMI, Berlin + TU, Berlin M. Kammel – HMI, Berlin	Date(s) of Experiment 11.04. – 13.04.2006 13.06. – 15.06.2006

Date of Report: 16.01.2007

Previous studies on concentrated ferrofluids [1] have shown a complex structural ordering under the influence of external magnetic fields. The magnetic nanoparticles are forming oriented planes with a hexagonal ordering in plane as well as an orientation in chains along the magnetic field lines. The formation and breaking of these planes with hexagonal arrangement were already characterized by Small Angle Neutron Scattering (SANS) experiments with a dynamic field regime [2].
Molecular dynamic studies predict simple structures like chains. But what is the driving force for the formation of such a complex structure in planes with hexagonal ordering? Surfactants are used as stabilising agent for the magnetic particles to prevent their aggregation. It is known that surfactants themselves can create complex structures like cylinders and lamella. We performed SANS measurements with polarized neutrons on Ferrofluids to understand the role of the surfactant for the formation of structural ordering in Ferrofluids.
The magnetic particles were produced by the thermolysis of cobalt carbonyl in the presence of aluminium alkyls by the group of Prof. Bönnemann at the *Forschungszentrum Karlsruhe* [4]. The cobalt nanoparticles were stabilized with oleoylsakosine as surfactant and dispersed in L9 (technical oil) as solvent.
The ethanol-to-L9 partition coefficient of oleyolsarkosine is highly favourable to ethanol, and both solvents are immiscible. This property was used to reduce the amount of free surfactant in the samples by liquid-liquid extraction (further referred as “washed samples”). In a second preparation the Ferrofluid was diluted with propanol which is also a polar solvent but miscible with L9. This will influence the surfactant – solvent interaction (solubilisation of the surfactant in excess) and give us the possibility to study the influence of this interaction parameter to the magnetic induced structure.

All measurements were done on the instrument V4 of the BER II Reactor at the Hahn-Meitner-Institute. We used the powerful option of polarised neutrons at wavelength 0.6 nm^{-1}, allowing the distinction between nuclear and magnetic contributions of the scattering.
Figure 1 shows the resulting 2D scattering pictures of the original ferrofluid diluted with L9 (original solvent), and diluted with propanol (final concentration is identical). The scattering pattern is modified, meaning that the organisation of particles is changed depending on the solvent polarity. Unfortunately we were not able to measure the “washed sample” with a magnetic field due to hardware issues. Consequently, only part of the experiment was successfully achieved, making the analysis more difficult. The fine modelisation is in progress.
Work supported by DFG project Wi 1151/2-2 in the frame of priority program SPP1104.

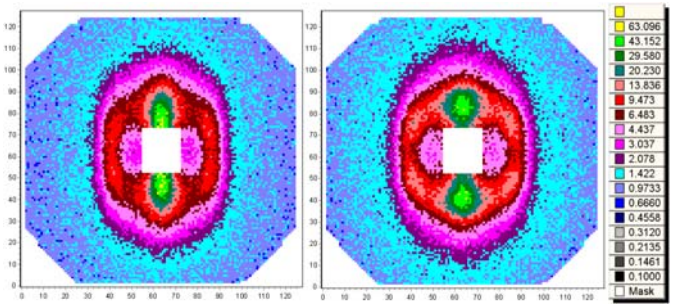

Fig. 1: *2D scattering pictures of original ferrofluid diluted by L9 (22) on left and the same ferrofluid diluted with propanol (14) on right with none polarised neutrons.*

References:

[1]. A. Wiedenmann, A. Hoell, M. Kammel, P. Boesecke, Physical Review E **68** (2003) 031203
[2]. A. Wiedenmann, U. Keiderling, K. Habicht, M. Russina, R. Gähler, Physical Review Letters **97** (2006), p. 057202/1-4
[3]. Z. Wang., C. Holm, Physical, Review E **68** (2003) 041401
[4]. H. Bönnemann, W. Brijoux, R. Brinkmann, N. Matussevitch, H. Modrow, N. Palina, N. Waldöfner, Inorganica Chimica Acta **350** (2003) 617-624.

	EXPERIMENTAL REPORT **Latex-confined cobalt iron oxide in aqueous solution**	Proposal N° MAT-04-1245-EF Instrument **V4** Local Contact Sylvain Prévost
Principal Proposer: Experimental Team:	A. Wiedenmann – HMI, Berlin B. Erné – Univ. Utrecht, NL S. Prévost – HMI, Berlin	Date(s) of Experiment 04.09. – 07.09.2006

Date of Report: 17.01.2007

With the help of polarized neutrons (SANSPOL), SANS is a key technique to study in detail the structure and the magnetic properties of ferrofluids, and their reciprocal effects.

A major step has to be overcome before the large scale application of ferrofluids, particularly in the biomedical domain: the stability in aqueous media of magnetic nanoparticles. Entrapping the magnetic particles in a water-soluble polymer has several advantages, as nowadays the functionalization of polymers is perfectly handled. In particular, a polymer capsule can be coated with bio-compatible compounds for biological tolerance as well as for vectorization with peptides. A polymer shell will prevent reactivity of the metallic surface and avoid aggregation via magnetic attractive interactions.

In collaboration with Ben Erné (Van't Hoff Laboratory, Utrecht University, The Netherlands), we studied by SANS and SANSPOL a water solution of $CoFe_2O_4$ nanoparticles embedded in latex.

On figure 1 are represented the 2D scattering pictures at 12 meters of the sample, when a 1T magnetic field is applied horizontally. When switching the polarization ($I^+ \rightarrow I^-$), the patterns are identical. The difference (I^+-I^-) only denoted the typical $\sin^2(\psi)$ shape, where ψ is the azimuthal angle, proving that particles still have a magnetic moment.

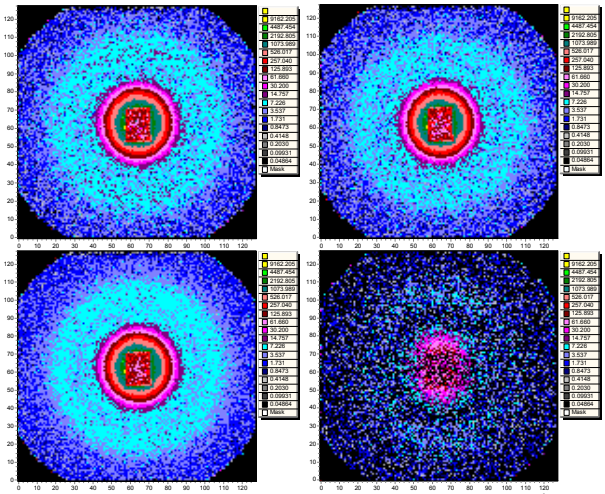

Fig. 1: *scattering picture with polarized neutrons I^+ (upper left) and I^- (upper right), sum (I^++I^-, bottom left) and difference (I^+-I^-, bottom right) of the scattering pictures for the sample in H_2O.*

A reasonable fit of the 1D spectrum has been achieved with a simple monodisperse-core – polydisperse-shell model (Figure 2). The total radius is 46 nm, the magnetic core having a radius of 11 nm. The volume fraction of the whole particle is 5%, the cobalt iron oxide core contributing to only 2% of the particle volume. No structure factor appears. This is in agreement with the very low concentration of magnetic material.

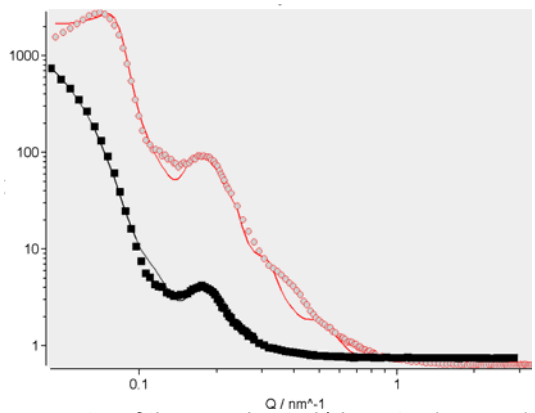

Fig. 2: *spectra of the sample at 5% in water (squares), and "dry" (open circles).*

We tried to increase the concentration by evaporation of the solvent. Unfortunately, this led to the formation of macroscopic aggregates.

The scattering curve of the "dry" aggregates (slightly humid) is represented on Fig 2. The model and the parameters used to fit the first curve are used to fit this new spectrum; only a hard sphere structure factor is added, and the contrast shell/solvent is adjusted together with the concentration. The model is able to reproduce most of the spectrum, which means for essence most of the structure in solution is retained. In particular, it seems there is no interpenetration of polymer chains (latex spheres are still disjointed).

Despite the retention of the latex sphere identity, this aggregation is not reversible in water. The reason for this remains unclear. The polymer should be modified, or the quality of the solvent toward the polymer should be increased.

	EXPERIMENTAL REPORT **In-Situ N_2 Adsorption in Hierachical Mesoporous KLE-IL-Silica Monitored by SANS**	Proposal N° PHY-04-1016 Instrument **V4** Local Contact Brandt, Wallacher
Principal Proposer: Experimental Team:	B. Smarsly – MPI Golm B. Smarsly, Ö. Sel – MPI Golm A. Brandt – HMI, Berlin D. Wallacher – HMI, Berlin	Date(s) of Experiment 09.09. - 12.09.2006

Date of Report: 09.10.2006

Bernd Smarsly and his group have developed methods to synthesize porous silica possessing a hierarchical pore structure with a well-defined pore size and morphology on different length scales. Such well-defined multimodal mesopore systems are needed for the elucidation of fundamental aspects of sorption theory such as diffusion and hysteresis. Recently, for the first time SiO_2 could be generated with spherical mesopores of 14 nm in diameter and with smaller wormlike mesopores (3 nm) connecting the larger spherical mesopores [1] (termed "KLE-IL-silica"). Furthermore, these model materials possess a few additional, non-defined micropores of ~ 1nm in size in the SiO_2 matrix. Using the new ADSE environment on V4 (see photograph and description below) the N_2 adsorption behaviour of KLE-IL-silica was studied at T=77K. The NpT-control of the new device is excellent, as can be seen in Figure 1.

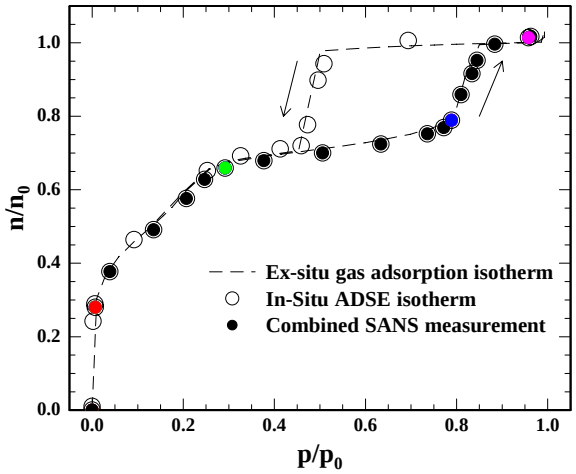

Fig. 1: *Comparison of the template isotherm obtained using a Micromeritics Tristar 3000 (- - -) with the points obtained by the ADSE set-up of HMI (○). For the points marked with a shaded circle the respective SANS spectra were measured. The coloured circles correspond to the data shown in figure 2.*

Due to the limited mount of beam time only the SANS data for the adsorption branch of the isotherm could be measured. In the case of Nitrogen adsorption on silica one is in the favorite situation that the scattering length density of liquid Nitrogen and silica are almost identical. Due to this contrast matching conditions it is quite straight forward to analyze the scattering data qualitatively. In the following we would like to discuss the scattering data for some selected points on the isotherm qualitatively (Figure 2). A detailed quantitative analysis is on the way.

▲: no Nitrogen adsorbed, empty silica matrix
The curve displays three distinct features: the oscillations of the form factor of polydisperse spheres of a diameter of 14nm, an additional scattering intensity around $q=2nm^{-1}$ which can be ascribed to the short-range ordering of the smaller mesopores confined between the larger mesopores and a contribution at $q=3nm^{-1}$ which can be attributed to the micropores in the silica matrix.

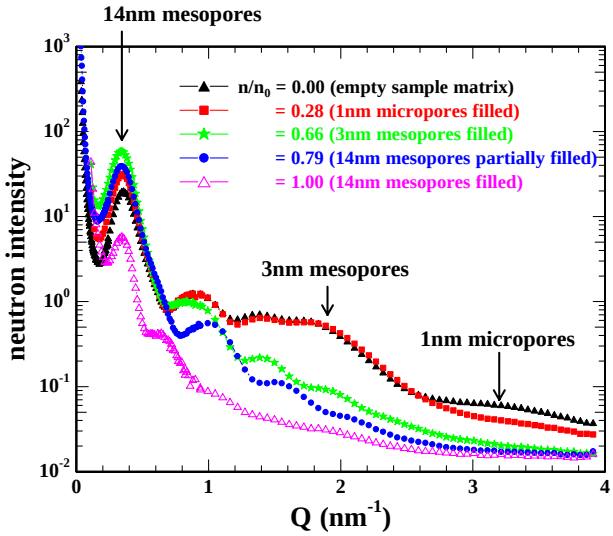

Fig. 2: *SANS curves for selected points on the isotherm corresponding to different relative amounts of adsorbed Nitrogen. The curves are background corrected.*

■: micropores filled
After introducing a small amount of Nitrogen into the system the scattering curve shows two distinct changes. The scattering intensity above $q=3nm^{-1}$ (which is attributed to the micropres) is vanished and the intensity of the first maximum of the form factor of the

polydisperse spheres is increased. Both features can be explained by the complete filling of the micropres in this first adsorption step. Due to the contrast matching between the filled micropores and the silica matrix the scattering intensity in the high q regime is vanishing. On the other hand the density of the matrix is increased by the filling of the micropres and this is resulting in an increase of the intensity of the first maximum of the form factor.

★: small mesopores filled
The filling of the small mesopores is clearly shown by the "loss" of the contribution from the short-range order around $q=2nm^{-1}$ and a further increase of the first maximum due to the increase of the silica matrix. No change in the position of the first minima of the form factor can be seen. This seems to be an indication that there are still no layers of liquid nitrogen inside the spherical mesopores.

●: partial filling of the spherical mesopores
For the first time during the adsorption experiment the intensity of the first maximum is decreasing. This decrease is caused by the loss of scattering contrast due to the partial filling of the spherical mesopores. In addition one observes a shift of the minima of the form factor to larger q, indicating that the radius of the spherical pores is decreasing with increasing amount of adsorbed Nitrogen. From the shift of the minima the layer thickness inside the spherical pores can be calculated (work in progress).
On the right wing of the first intensity maximum a new shoulder is developing. Its origin is not yet clear and must be studied further. At the moment we think of two possibilities: either we start to see the "peaks" of the fcc lattice which are lying underneath the form factor or there are even larger spherical pores in the silica matrix which are not fully accessible.

△: all pores are filled
The intensity has decreased even further and the features of the form factor of the 14nm polydispers spheres have diminished. What still can be seen is a well pronounced second maximum at the position of the above discussed shoulder. Discussion of this new feature is on the way.

A detailed study of the desorption branch of the isotherm is intended for the end of this year/beginning next year. In addition a detailed study of the filling procedure of the micropores is planned.

Experimental setup

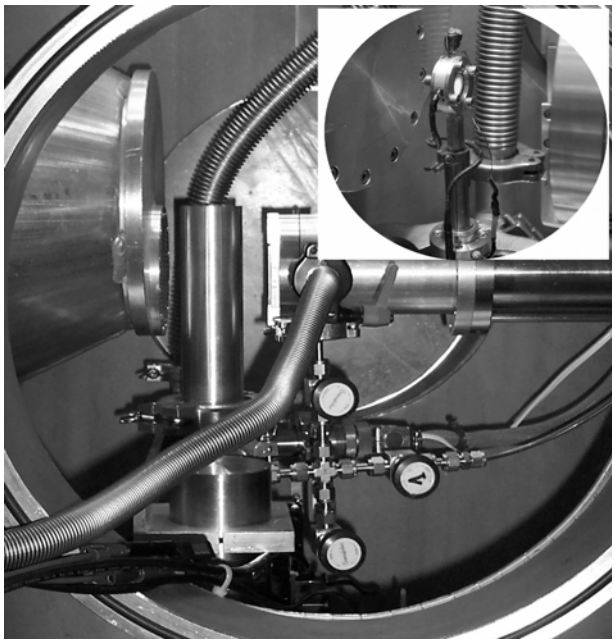

The photography shows the CGA-PTR sample environment at the SANS instrument (V4). The inset (top, right) shows the installation without the vacuum can. See "New Sample Environment for Experiments under Controlled Gas Atmospheres I: Low Temperatures, Low Pressures", in this report for further details.

The sample cell with Suprasil quartz windows of 10mm in diameter is mounted on the cold finger of a mini pulse tube refrigerator. The temperature was regulated at 77.000±0.010K. The cell is connected via a capillary to a gas manifold, which is equipped with several pressures gages and calibrated dosing volumes. From the manifold the sample can be exposed successively to small doses of Nitrogen. Thereby the gas uptake of the sample substrate at a given pressure is measured volumetrically.

Reference:
[1]. Ö. Sel; D.B. Kuang.; M. Thommes; B. Smarsly Langmuir 2006, **22**, 2311-2322

	EXPERIMENTAL REPORT **Hydration/dehydration of sugar solutions in confined geometry**	Proposal N° PHY-04-1176-EF Instrument **V4** Local Contact Astrid Brandt
Principal Proposer: Experimental Team:	A. Brandt – HMI, Berlin G. Lelong, D.L. Price – CNRS CRMD Orleans, F T. Steriotis, G.Charalambopoulou - NCSR Demokritos, GR M.-L. Saboungi – CNRS-CRMHT Orleans, F A. Wiedenmann – HMI, Berlin	Date(s) of Experiment 16.02. – 20.02.2006

Date of Report: 05.01.2006

Background:
Simple sugar molecules have been observed to possess important cryoprotective properties, and are produced in response to dessication or freezing by a number of living bodies adapted to survive extreme cold or drought.[1] Recently, we succeeded to confine sugar solutions into silica gels, with a size of pores mimicking the spaces between cellular membranes and with enough flexibility to allow shrinkage.[2] These gels are also an ideal candidate to probe the bioprotective effect of glucose molecules upon dehydration.

Results:
SANS measurements were performed on a series of as-produced as well as dehydrated SiO2-water-glucose gels. The dehydration process was simulated by evacuation i.e. by removing water from the system and thus increasing the sugar concentration. A special vacuum-tight system was used for this purpose, while samples containing different amounts of sugar were measured before and after dehydration.

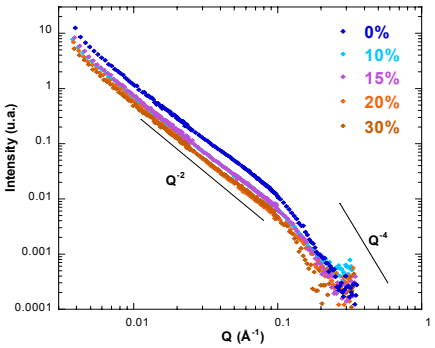

Fig. 1: *SANS spectra of the gels as a function of glucose concentration.*

The spectra of the as-produced different silica gels exhibit the same profile and a universal curve constituted of two regions has been obtained (Fig. 1). The fractal dimension of the gel aggregates has been calculated equal to 2, which is typical of a mass fractal. On the other hand the high Q region scales with a Porod (-4) power-law pointing to a smooth Euclidean surface with a surface dimension equal to 2.

Moreover, it was observed that the samples without sugar are not resistant to dehydration, in contrast to the gels containing glucose which appeared to be protected, as shown by the superposition of the spectra before and after dehydration (Fig. 2) (after dehydration, the effective sugar concentration is about 80%) The silica network of the gels is also protected from the loss of water by the sugar molecules. The active protection of the structure by the glucose molecules is thus clearly identified.

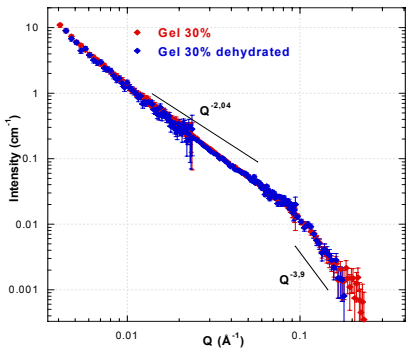

Fig. 2: *SANS spectra of the gel with initially 30% sugar concentration before and after dehydration.*

This study on the biopreservation of structures by sugar molecules under dehydration processes is the first one, and the in-situ dehydration set-up is an appropriate tool to probe the efficiency of different mono- and disaccharides.

References:
[1]. F. Franks, *Biophysics and Biochemistry at Low Temperatures*, Cambridge University Press (1985)
[2]. G. Lelong *et al.*, *J. Chem. Phys.* 2005, *122*, 164504.

	EXPERIMENTAL REPORT **Structure of oppositely charged polyelectrolyte complexes**	Proposal N° PHY-04-1196 Instrument **V4** Local Contact Daniel Clemens
Principal Proposer: Experimental Team:	M. Zeghal – Univ. Paris XI, F V. Mangarelli – Univ. Paris XI, F M. Gruber – WWU Münster L. Auvray – Univ. Evry, F D. Clemens – HMI, Berlin	Date(s) of Experiment 21.07. – 24.07.2006

Date of Report: 29.09.2006

Complexation of oppositely charged polyelectrolytes has been the subject of continuous and numerous researches due to the promising applications ranging from coatings and flocculants to systems mimicking biological systems like proteins and DNA vectors for gene therapy [1]. Unfortunately, despite the great number of studies, the mechanisms of electrostatic complexation together with the structure of the complexes remain poorly understood. For that reason, we started experimental studies of polyelectrolyte complexes (PEC) using several techniques such as NMR, Light Scattering and SANS. The structure of a PEC formed with linear (L-PEI) or branched (B-PEI) poly(ethylenimine) (M_w=25K) and a polyacid was investigated as a function of parameters such as the amount of added HCl or the [PEI]/[polyacid] ratio.

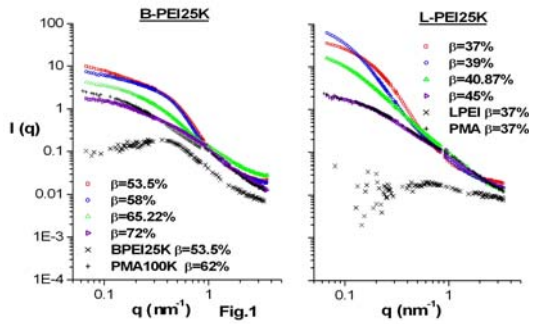

Fig.1

The formation of soluble and stable complex requires adding a strong acid to decrease the charge of the polyacid. We first focused our attention on the structure of the complex formed between a polymethacrylic acid (M_w=100k) and B-PEI or L-PEI (M_w=25k). The intensity scattered by B-PEI or L-PEI complexes ([PEI]/[PMA]=1) as a function of β=[HCl]/[PEI] ratio is shown on fig. 1 (coloured symbols). For the lower PMA charge (higher values of β) the intensity scattered by the mixture is roughly the sum of the intensities scattered by each polymer alone in water, showing that the polymers do not associate to form complexes. As β decreases, the intensity scattered by the PEI-PMA mixtures increases. For both linear and branched PEI, it appears that, as the polyacid charge increases, the electrostatic interactions lead to the formation of growing size aggregates. Below the lower β value, the entropic contributions that prevent aggregation are too weak to counterbalance the attractive Coulombian interaction, leading to the precipitation of the complex. It is also noticeable on the shape of the scattering functions that the structure of the aggregates changes drastically with the strength of the interaction. Furthermore, the structure and the size of the B-PEI and L-PEI complexes in the stability zone are very different.

We also started to observe the influence on the PEC structure of other parameters than the charge, such as the polyanion/polycation ratio and the polymer molecular weight.

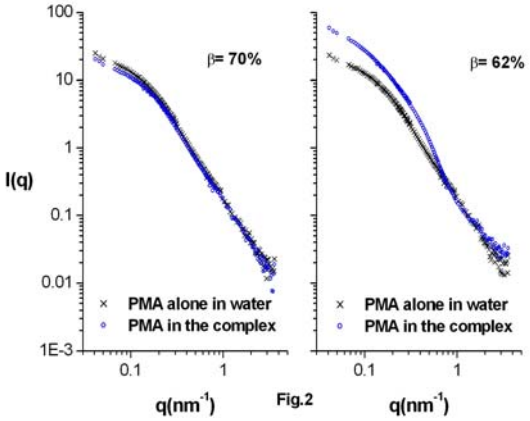

Fig.2

The contrast variation method [2] was used to measure the structure factor of each polymer in the complex and their interactions through the cross structure factor. For instance, when the B-PEI is contrast matched, one can observe directly the intensity scattered by the polyacid in the mixture (fig. 2). In the case of weak interactions (β=70%), the structure of the polyacid in the complex and in solution are the same, whereas for strong interactions (β=62%), the PMA form compact aggregates of about 4 chains. Further analysis is currently performed to obtain more accurate and quantitative descriptions of these complexes.

References:

[1]. A. F. Thünemann, M. Müller, H. Dautzenberg, J-F Joanny, H. Löwen, Adv. in Polym.Sci., **166**, 113 (2004).

[2]. M. Zeghal, L. Auvray, Eur. Phys.j. E **14,** 259-268 (2004).

	EXPERIMENTAL REPORT **Formation of rod like block copolymer micelles in aqueous salt solutions**	Proposal N° PHY-04-1210 Instrument **V4** Local Contact Martin Kammel
Principal Proposer: Experimental Team:	V.K. Aswal – BARC, India V.K. Aswal – BARC, India A. G. Wagh – BARC, India M. Kammel – HMI, Berlin	Date(s) of Experiment 30.05. – 03.06.2006

Date of Report: 13.09.2006

The formation of rod like micelles is of great interest in applications such as modifying the flow properties of a solution, nanocarriers for drug delivery, synthesis of nanorods and generating liquid crystals [1]. Most of the block copolymers form rod like micelles at higher temperatures and this as such can not be used in these applications. Herein, we show that selective salts can be used to induce the sphere-to-rod transition of block copolymer micelles at ambient temperature [2].

SANS measurements were performed on the water soluble PEO-PPO-PEO triblock copolymer P85 $[(EO)_{26}(PO)_{39}(EO)_{26}]$ in presence of salts KCl, KF and K_2CO_3 in aqueous solution. The measurements were made for 0.5 wt% of block copolymer with several concentrations of each salt till the phase separation (clouding) in these systems occurred. The concentrations of salts at which the clouding occurs are 3.8, 1.42 and 0.61 M for KCl, KF and K_2CO_3, respectively. The temperature was kept fixed at 30 ^oC for all the measurements in presence of salts. Temperature dependence of the rod like micelle formation was investigated with one of these samples and compared with its dependence on the salt concentration.

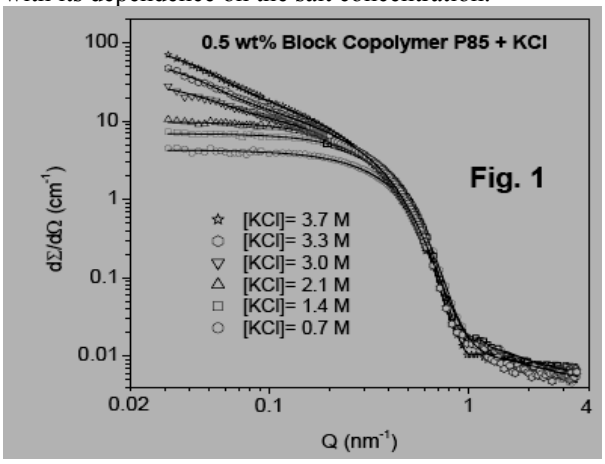

Fig. 1 shows the typical variation in SANS data from a block copolymer solution with increasing concentration of KCl. The scattering intensity in the low Q region at lower KCl concentrations increases with an increase in KCl concentration but remains flat. This is an indication of spherical micelles present in the system. At higher KCl concentrations, there is a dramatic change in the scattering intensity in the low Q region. The scattering intensity as a function of Q on log-log scale shows a straight line with the slope approaching –1 with increasing KCl concentration; this suggests the formation of rod like micelles at higher KCl concentrations [3].

Table 1 shows that at low KCl concentrations (up to 2.1 M) the block copolymer solution consist of spherical micelles. The data are fitted for spherical micelles coexisting with unimers. The core radius (R_m) and fraction of unimers converting into micelles (φ) increases with increasing KCl concentration. The block copolymer solution at and beyond the KCl concentration of 3.0 M consists of rod like micelles coexisting with spherical micelles. The rod like micelle fraction (φ_r) increases from 9 to 42 % on increasing the salt concentration from 3.0 to 3.7 M. On the other hand, the total volume fraction of micelles decreases as expected because hydrated water to micelles is reduced on the formation of rod like micelles. The length of the micelles (L) increases with an increase in the KCl concentration.

Table 1

[KCl] (M)	Structure	R_m (nm)	L (nm)	ϕ (%)	ϕ_r (%)
0.7	Spherical	3.44	-	0.94	0
1.4	Spherical	3.79	-	1.05	0
2.1	Spherical	3.90	-	1.22	0
3.0	Spherical + Rodlike	3.90	220	0.85	9
3.3	Spherical + Rodlike	3.90	350	0.72	20
3.7	Spherical + Rodlike	3.90	400	0.57	42

The effect of addition of salt has been found to be similar to that of increasing temperature. The hydration of salt ions is entropically favoured by the dehydration of the micelles [4]. The propensity of salt to induce micellization depends on the hydration properties of their ions. The fact that hydration of anions Cl^-, F^- and CO_3^{2-} follows the order $Cl^- < F^- < CO_3^{2-}$, the concentrations of corresponding salts needed to induce rod like micelles have also been observed in the same order. To the best of our knowledge this is the first report suggesting that rod like micelles coexist with spherical micelles even up to onset of the clouding in these systems.

References:

[1]. I.W. Hamely, Block Copolymers in Solution: Fundamentals & Applications, John Wiley & Sons, 2005.
[2]. V.K. Aswal et al. Chem. Phys. Lett. (Submitted).
[3]. M. Duval et al. Langmuir 21 (2005) 4904.
[4]. V.K. Aswal et al. Chem. Phys. Lett. 425 (2006) 118.

	EXPERIMENTAL REPORT **Freezing dynamics of magnetic colloids studied by time-resolved SANS**	Proposal N° PHY-04-1240-EF Instrument **V4** Local Contact Albrecht Wiedenmann
Principal Proposer: Experimental Team:	A. Wiedenmann – HMI, Berlin A. Wiedenmann, U. Keiderling – HMI, Berlin S. Prévost – HMI, Berlin + TU, Berlin D. Wallacher, M. Meißner – HMI, Berlin	Date(s) of Experiment 07.09. – 12.09.2006 19.10. – 21.10.2006

Date of Report: 17.01.2007

The new closed cycle refrigerator setup described in [1] was used for the first time to explore the temperature range between 300 K and 66 K to study the SANS scattering response to an applied magnetic ac-field up to 40 mT and between 50 and 500Hz, superimposed to a static field up to 20 mT. The sample was the same concentrated Co-ferrofluid (MFT3) as used in [2,3] which consisted of 6 vol. % Co-nanoparticles of R_c=4.4 nm radius coated with a shell of oleylsarcosin as surfactants with a thickness of D_s=1.9 nm and dispersed in a viscous oil "L9". Stroboscopic experiments with time-stamped list-mode data acquisition triggered by the frequency generator have been performed. Using a continuous neutron beam with a wavelength band of $\Delta\lambda/\lambda$=0.11 at λ=0.605 nm and a distance of L_2=4m between sample and detector allowed a frequency range up to 500 Hz to be explored reliably [3]. Data have been regrouped afterwards in histograms of 128*128 pixels of 0.5*0.5 cm^2 for position and n=100 time channels of widths $\Delta t = (n*\nu_s)^{-1}$. The Q range 0.2 nm^{-1} <Q<1.2 $nm^{-1}$and resolution of the order of $\Delta Q/Q$<0.1 allowed to properly resolve the characteristic correlation peaks of the local hexagonal ordering which appear for this sample at Q_1= 0.39 nm^{-1} and Q_3 = 0.29 nm^{-1} [3]. The reversibility of the reordering process in the dynamic mode has been checked by comparing the stroboscopic SANS results with those measured in the same coil device with a static magnetic field of the same amplitude.

The new experimental possibilities allow us

i. to check the validity of the Langevin statistics, for which the essential parameter is the ratio $x = V_c m_0 H(t)/(k_B T)$,
ii. to monitor the slowing down of the dynamics of moment rotation with decreasing temperature and to decide between the possible relaxation mechanisms (Néel and Brownian) and
iii. to study the effect of freezing of the solvent on the dynamics of the particle moments.

In Fig. 1 we present the scattering intensities of sector boxes corresponding to Q_1 perpendicular (upper curves) and and parallel to H (lower curves) measured at B_0=20mT and υ=100 Hz at different temperatures. Oscillating behaviour with decreasing amplitudes is clearly observed down to 200 K while at 100 K and 66 K (i.e. below the freezing temperature of the solvent) the system is fully static and shows no difference to the data obtained in a static magnetic field.

The first analysis in terms of eqn. 3 of ref [3] showed that down to 200 K the intensities can be simultaneously fitted using the same set of parameters. I.e. the dynamics can be fully described by the Langevin statistics. However, the amount of freely rotating particles following the oscillating field decreases from 60 % at 300 K to 12% at 250K and 5% at 200K. When the temperature decreases the phase of the oscillating response is increasingly shifted with respect to the inducing field the more pronounced the higher the frequency. The full analysis of the data including the effect of the dc-offset on the dynamical properties is in progress.

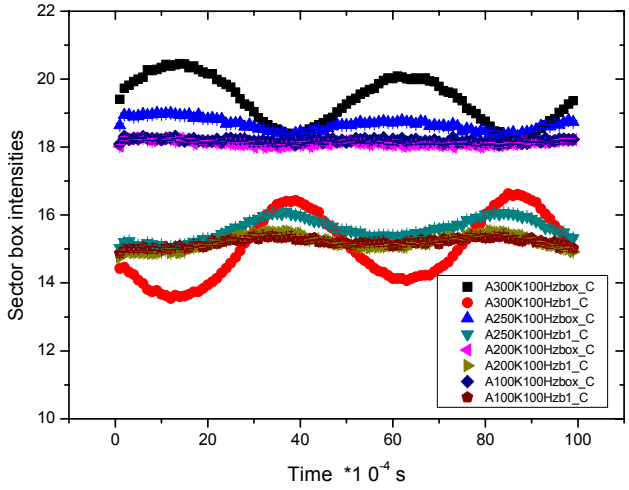

Fig. 1: *SANS intensities of a Co-ferrofluid sample MFT3N as a function of time in an oscillating magnetic field of 20 mT at f=100Hz. Upper curves- Q_1 perpendicular to B, lower curves - Q_1 // B*

References:

[1]. A. Wiedenmann, U. Keiderling, D.Wallacher, M. Meissner BENSC report 2006

[2]. A.Wiedenmann[1], U. Keiderling[1] , R. P. May[2],C. Dewhurst[2] Physica **B 385-386**(2006)453-456

[3]. A.Wiedenmann, U. Keiderling, K. Habicht, M.Russina, R. Gähler: Physical Review Letters **97**, 057202 (2006)

	EXPERIMENTAL REPORT **Relaxation of Co-ferrofluid at different magnetic fields**	Proposal N° PHY-04-1243-EF Instrument **V4** Local Contact Uwe Keiderling
Principal Proposer: Experimental Team:	U. Keiderling, A. Wiedenmann – HMI, Berlin U. Keiderling, A. Wiedenmann – HMI, Berlin	Date(s) of Experiment 07.04. – 11.04.2006

Date of Report: 19.01.2007

In an external magnetic field, concentrated Co-ferrofluid forms an inter-particle order revealing coexistence of a pseudo-crystalline hexagonal ordering of core-shell nanoparticles and segments of dipolar chains, which produce interference peaks in different Q-ranges. The decay of this order after switching off the field is characterized by time constants τ of a few seconds. This relaxation behaviour has been investigated using our newly developed stroboscopic Small Angle Neutron Scattering (SANS) technique based on listmode data acquisition. This technique utilizes the fact that the process of creation and decay of the inter-particle order is reversible, thus allowing to gain very good scattering statistics by stroboscopically repeating the process and superimposing the data from the individual cycles.

A concentrated Co-ferrofluid "MFT" contained in a Hellma quartz cell of 1 mm thickness was placed in the homogeneous horizontal field of an electromagnet, applied perpendicular to the incoming beam. Polarized measurements (SANSPOL) were performed at a sample-detector distance of 4 m, with various magnetic fields between 0.005 T and 1 T. For each field, scattering was measured with the incident beam polarization alternately parallel I(-) and antiparallel I(+) to the magnetic field. For each of these polarizations, listmode data were acquired with the field cycling between the two values "field on" (5s at 0.005 T...1 T, depending on the particular experiment) and "field off" (15 s at remanence < 0.005 T). For each measurement, 200 to 1200 cycles were recorded, with a trigger marker intricately merged with the listmode data stream. After the experiments, the listmode option of the "BerSANS" program was applied to superimpose the raw data from these cycles, regrouping the continuous stream of single detected neutrons into a set of two-dimensional histograms (time frames) with a spatial resolution of 128x128 cells and a time resolution of 100 ms. After regrouping, the time frames were corrected for sample transmission and background scattering, and normalized to water scattering, also using the "BerSANS" software. We then analyzed the difference between the parallel and antiparallel SANSPOL intensities I(-)-I(+).

The decay was generally characterized by an exponential course, assigned to Brownian rotation of locally ordered domains, although in the very beginning it appeared to take place faster, indicating a different decay mechanism. For the exponential parts, time constants τ for the decay of the inter-particle order were calculated in different regions of the two-dimensional histograms (Fig.1).

Fig.2 shows that at smaller fields up to approximately 0.1 T the field dependence of τ is weak. However at fields > 0.1 T τ significantly increases, indicating a stabilization of the structures. We attribute this stabilization to a larger size of the ordered domains which results from enhanced dipolar interactions.

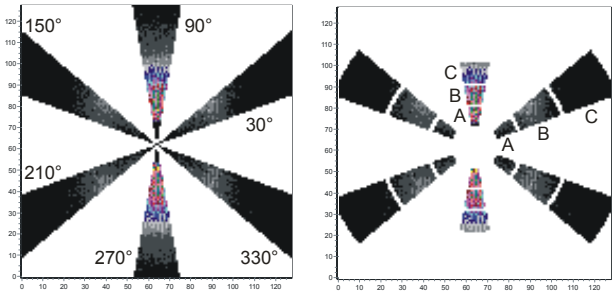

Fig. 1: *Regions used for calculation of peak intensities.*

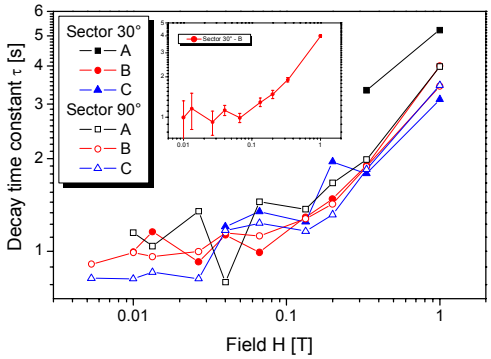

Fig.2: *Decay time constants calculated for different magnetic fields. Inset: one tyical course of error bar.*

References:

[1]. U.Keiderling, A.Wiedenmann, J.Haug, Physica B **385-386** (2006) 1183-1186.

[2]. U.Keiderling, A.Wiedenmann, accepted for J. Appl. Cryst (2007).

BENSC	**EXPERIMENTAL REPORT** **Vesicles-based systems: Templates-formation of a mesoporous material and Systematic investigation of Gemini-based catanionics**	Proposal N° PHY-04-1343-EF Instrument **V4** Local Contact Sylvain Prévost
Principal Proposer: Experimental Team:	M. Gradzielski – TU, Berlin S. Prévost – HMI, Berlin C. Oppel – TU, Berlin	Date(s) of Experiment 18.07. – 20.07.2006 04.12. – 11.12.2006

Date of Report: 17.01.2007

Vesicular systems are actively studied for there applications (encapsulation, material templating) as well as for fundamental issues (closed bilayer systems: models for biological membranes). The control of size, polydispersity and stability of vesicles is a key step for the use of such systems.
This beamtime was splitted with two objectives in mind: 1) to follow the structural changes of vesicles during the formation of a mesoporous material based on SiO_2 and 2) to get new insights in catanionics vesicles, via collaboration with Prof. André Laschewsky (Fraunhofer Institute, Potsdam). Most of these experiments being very recent, the analysis is still under heavy development.

1) Highly packed, unilamellar monodisperse vesicles are a domain of expertise for the Stranski Laboratorium. Such systems exhibiting high ordering can be obtained simply by adding octanol to an aqueous solution of a common surfactant, sodium oleate [1]. These systems have been successfully used in the lab as templates for the formation of mesoporous systems. The inorganic precursor $Si(OEt)_4$ is dissolve in the octanol; this oily solution is then mixed with the aqueous solution of sodium oleate. Hydrolysis of the precursor occurs, leading to the solid SiO_2. The mesoporous formation has been followed by SAXS. This technique being sensitive to electronic density, we could observe the final material, which is rather monodisperse, with size in agreement with those of initial vesicles. However, due to the low contrast between the solvent and the surfactants, this technique is not suitable to follow the structural changes of the amphiphilic compounds. Neutron scattering length densities of the inorganic material and of the surfactants are favourable to a clear distinction between both contributions by SANS. During the experiment, contrast matching was fruitfully used by adjusting the D_2O/H_2O ratio to follow either the formation of the silicate or the modification of the vesicles. We also modified the surfactant counter-ion (Na^+, NMe_4^+, NEt_4^+, NPr_4^+, NBu_4^+) to determinate its role in the characteristic size of the system. The experiment was successfully achieved. The first analysis shows a full retention of the vesicles structures. Varying the counter-ion induces a change in the size of micelles for the pure surfactant, as expected, but seems to have no effect on the size of the vesicles and silicate. Elaborate fitting models have to be determined for the full mastering of the samples analyzed, as structure factors and form factors of the solid and the bilayer lye in the same q-range and are interdependent. This will be done with the help of contrast matching experiments.

2) Mixtures of cationic and anionic surfactants form a variety of bilayers structures, including vesicles and other exotic shapes (icosahedra, flat disks…) [2]. Due to the high attraction between oppositely charged headgroups, catanionics are particularly interesting to understand the role of cohesion forces inside bilayers on the global phase diagram.
Designing catanionics to get tailored shape and size should be possible by tuning the interfacial rigidity of bilayers. To achieve this, we propose to impose partially the geometry between surfactants via a chemical binding. The ongoing study concerns the well-known anionic surfactant SDS and Gemini cationic surfactants based on DTAC (dodecyltrimethylammonium chloride), linked through their headgroups by various spacers (-CH_2-O-CH_2- = "EO-2", -CH_2-C_6H_6-CH_2- in *ortho*, *meta*, *para* positions, -CH_2-CH=CH-CH_2-) exhibiting different lengths and flexibilities [3].
The spectra obtained with SDS and Gemini EO-2 are represented Fig. 1. The size of the vesicles does not depend of the ratio cationic/anionic, which can be explained by a constant composition of the vesicles. This behaviour is different from what is observed with the classical catanionic mixture SDS/DTAB (counter-ion *Bromide*) [4], where vesicles sizes and compositions depend on the total composition. This first result is encouraging and, with the help of data for others Gemini, recently acquired, this systematic study should give us keys for catanionic vesicles size-control.

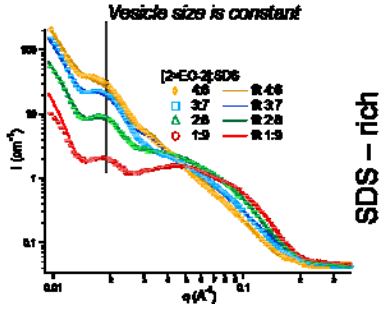

Fig. 1: *SANS spectra for various Gemini(EO-2):SDS ratios (relative to charges) at total concentration 1.25% v/v in D_2O. Fits include low-polydisp. vesicles (p=0,17) and ellipsoidal micelles.*

References:

[1]. M Gradzielski, J Phys Condens Matter **15** (2003) R655
[2]. C Tondre, C Caillet, Adv Colloid Interf Sci **93** (2001) 115
[3]. A Laschewsky et al., Colloid Polym Sci **283** (2001) 469
[4]. M Bergström, JS Pedersen, J Phys Chem B **103** (1999) 8502

	EXPERIMENTAL REPORT **Effect of temperature on the density profile of a PAA brush interacting with a protein**	Proposal N° CHE-04-1322 Instrument **V6** Local Contact Roland Steitz
Principal Proposer: Experimental Team:	C. Czeslik – Uni Dortmund O. Hollmann – Uni Dortmund R. Steitz – HMI, Berlin	Date(s) of Experiment 01.12. – 07.12.2006

Date of Report: 21.01.2007

Polyelectrolyte brushes made of poly(acrylic acid) (PAA) are known to have unique properties in binding proteins. At low ionic strength (about 10 mM) proteins are strongly adsorbed at a PAA brush, whereas an almost complete protein resistance of the PAA brush can be induced by adding a few 100 mM salt to the protein solution. Remarkably, this effect has turned out to be independent on the sign of the protein net charge.

In recent neutron reflectivity studies, the local distribution of protein molecules within a planar PAA brush was determined. Using BSA with a negative net charge as a model protein, a homogeneous filling of the PAA brush with protein molecules was found at low ionic strength [1,2].

In the present study, the effect of temperature on the structure of a PAA brush interacting with the protein α-lactalbumin was analyzed. α-Lactalbumin was chosen, because it has a negative net charge as BSA. Thus, one can show that the protein distribution found for BSA within a PAA brush [1,2] are not protein-specific. Neutron reflectivities were recorded at 20 and 40 °C in order to gain insight into the thermodynamics of adsorption: A possible increase of the degree of protein adsorption with temperature would indicate an entropic driving force for protein adsorption as predicted by a theoretical model [2].

Contrast variation was performed by choosing D_2O and a D_2O/H_2O mixture as the solvents. Thus, two neutron reflectivity curves have to be consistent with a single structure profile at a given temperature and solvent composition (with or without protein and salt).

A significant improvement in the preparation of the PAA brush could be realized in the present experiment by using the diblock copolymer d-PS-PAA where the poly(styrene) chain ends are perdeuterated (d-PS). The d-PS-PAA copolymer was deposited onto a thin film of d-PS. Thus, the d-PS chain ends of the copolymer and the d-PS film appear as a single layer in the density profile. In contrast, the non-deuterated PAA chain ends of the copolymer are clearly visible as the brush when using D_2O.

In Figure 1, some neutron reflectivity curves are shown that were measured in the present experiment. They illustrate the good quality of the data. All curves will be further analyzed by fitting layer models to them. From a simple inspection of the data shown in Figure 1, it can already be concluded that α-lactalbumin strongly adsorbs at the PAA brush at 40 °C and appears to desorb again, when 500 mM NaCl is added to the protein solution.

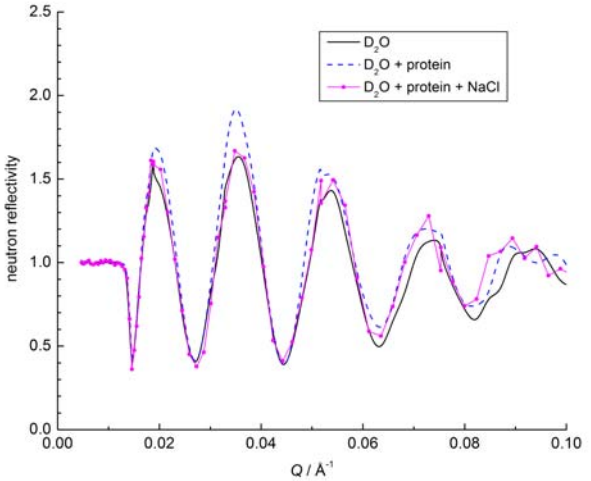

Fig. 1: *Neutron reflectivity curves of an Si/D_2O interface that has been modified with a poly(acrylic acid) brush. The curves were measured at 40 °C. For clarity, they are normalized to the reflectivity of an unmodified Si/D_2O interface. α-Lactalbumin was used as model protein that is interacting with the PAA brush under electrostatic repulsion.*

References:

[1]. O. Hollmann, T. Gutberlet, C. Czeslik, Langmuir (2006) in press.

[2]. C. Czeslik, G. Jackler, R. Steitz, H.-H. von Grünberg, J. Phys. Chem. B **108** (2004) 13395-13402.

	EXPERIMENTAL REPORT **Study of the water uptake of polyelectrolyte multilayers at solid/air interface**	Proposal N° CHE-04-1326 Instrument **V6** Local Contact Anke Teichert
Principal Proposer: Experimental Team:	C. Delajon, R. Krastev – MPI KGF Golm C. Delajon – MPI KGF Golm R. Krastev – MPI KGF Golm A. Teichert – HMI, Berlin	Date(s) of Experiment 24.07. – 30.07.2006

Date of Report: 16.01.2007

Polyelectrolyte (PE) multilayer (PEM) systems deposited on solid support gained increasing recognition. Their preparation is based on the Layer-by-Layer (LbL) deposition process [1]. The thickness and the density of PEM can be precisely tuned, by the number of adsorption cycles, salt concentration and pH of the PE solutions, temperature, etc. The response of PEM to external stimuli is important for practical applications such as controlled release or chemical sensing. The response of PEM to exterior conditions supplies basic information about their structure and properties. Neutron reflectometry (NR) studies have been performed with PEM to study their swelling in water vapours. Different water isotopes were used to assure high contrast between different parts of the films. The influence of the salt content in the PE solutions during the preparation of PEM on their thickness and density is well documented. Our previous studies characterised the water uptake in PEM prepared from poly(allylamine hydrochloride) (PAH) and fully deuterated poly(sodium 4-styrenesulfonate) (dPSS) in presence of 1 M NaCl. Here we report data on water uptake in PEM prepared from dPSS and PAH but from PE solutions which contained 0.5 M NaCl. The concentration of the PE in the solutions was always 10^{-2} monomol/L. Poly(ethylene imine) was used as a precursor layer deposited from salt free solution. One sample with a structure Si/PEI/$(dPSS/PAH)_6$/dPSS was studied. It was placed in a gas tight experimental cell. The NR scans were performed in θ/2θ geometry. Experiments were performed in dry N2 (reference state) and in H_2O or D_2O vapours at r.h. of around 98%. Always at least two consecutive runs were performed in order to prove that equilibrium conditions had been achieved. No differences were observed between the repeated reflectivity curves. This proves that the equilibrium water uptake/release occurs within hour after the exposure of the sample to the respective atmosphere. Fig. 1 summarises the equilibrium NR curves.

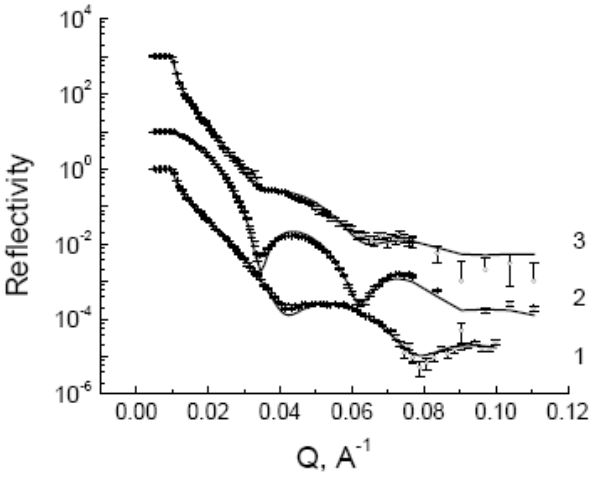

Fig. 1: *Reflectivity curves from a Si/PEI/$(dPSS/PAH)_6$/dPSS sample prepared from PE solutions with 0.5 M NaCl in: 1. dry N_2; 2. D_2O vapours; 3. H_2O vapours.*

The data were fitted with a single box model which represents the PEM sandwiched between two semi infinite phases. gas and Si support. The use of more complex models including more boxes or non equal distribution of the compounds in the PEM did not increase the precision of the fits. The parameters (thickness d, scattering length density ρ) which gave the best fit to the data are summarised in the Table. The data from previous studies for a sample with similar structure but prepared in presence of 1 M NaCl are shown also for comparison.

Table: *PEM thickness and SLD for a Si/PEI/$(dPSS/PAH)_6$/dPSS samples prepared in presence of a) 0.5 M NaCl and b) 1 M NaCl. a) 0.5 M NaCl b) 1 M NaCl*

	a) 0.5 M NaCl		b) 1 M NaCl	
	d, nm	ρ, 10^{-6}Å^{-2}	d, nm	ρ, 10^{-6}Å^{-2}
N_2	16.1	3.62	24.9	3.40
D_2O vap.	21.0	5.86	34.1	5.33
H_2O vap.	20.1	2.64	33.1	2.49

Reference:

[1]. G. Decher, Science 1997, **277**, 1232

[2]. G. Decher, J. D. Hong, J. Schmitt Thin Solid Films 1992, **210-211**, 831

	EXPERIMENTAL REPORT **Influence of PEI anchoring layer on the structure of polyelectrolyte multilayer films**	Proposal N° MAT-04-1234 Instrument **V6** Local Contact Elena Maltseva
Principal Proposer: Experimental Team:	M. Kolasińska – PAS Kraków, PL M. Kolasińska – PAS Kraków, PL R. Krastev – MPI KGF Golm P. Warszyński – PAS Kraków, PL E. Maltseva – HMI, Berlin	Date(s) of Experiment 01.03. – 06.03.2006

Date of Report: 10.01.2007

Due to possible applications of polyelectrolyte multilayers (PEMs) there was a need to study their stability at various conditions, at solid/liquid interface. In order to obtain information on behaviour of multilayers in various conditions, series of multilayer samples were chosen for neutron reflectometric studies. They were 13- and 14-layer films built up from PAH/PSS deposited directly on silicon blocks and films having the same number of layers but with PEI used as a first, precursor layer. Results of these experiments are presented in Tabs 1 and 2. Such choice of samples allowed to determine the effect of PEI and the charge of the outermost layer on the stability of selected PEMs. For that purpose multilayers were deposited on silicon blocks. Afterwards they were exposed to pH bath and straight after they were measured by NR in liquid D2O. When PAH/PSS structures are considered (see Tab. 1), one can observe that their density decreases (expressed as scattering length density) for treated films comparing to untreated ones. The difference in thickness between 'wet' and 'dry' samples (in dry state they were measured using XRR and results were presented in [1]) is bigger for both untreated and treated PSS terminated films comparing to analogically prepared but having PAH as a top layer. The difference is ranging ca. 40 % while for PAH terminated ones it is ca. 30%. In the presence of heavy water within multilayers, they demonstrate differences in thickness between treated and untreated films. These differences were negligible for dry samples [1]. Similarly to PAH/PSS multilayers, films with PEI are swollen comparing to dry samples. Difference in thickness between 'wet' and 'dry' samples is bigger for PSS terminated films comparing to those with PAH as a top layer (positively charged). The difference is ranging ca. 40 % whereas for PAH terminated treated films it is less than 20%. As far as density is concerned one can see the same effect of density decrease (expressed as scattering length density) for treated PAH terminated films as it was observed for PAH/PSS films. On the contrary, PSS terminated films built up on PEI seems to be most resistant of all studied PEMs, keeping the density more or less constant.

Roughness of both types of samples, e.g., terminated by polycations or polyanions, respectively is constant, varying only in the error range.

Tab. 1: *Parameters giving the best fit to the neutron reflectometric experimental results.*

	$Si/(PAH/PSS)_6PAH$		
	thickness /nm	ρ /nm^{-2} x10^8	roughness /nm
untreated	17.0±1.2	5.1±0.1	2.0±0.9
pH = 3	16.3±1.7	4.1±0.3	1.3±0.7
pH = 11	16.5±2.3	3.9±0.2	1.2±0.5
	$Si/(PAH/PSS)_7$		
	thickness /nm	ρ /nm^{-2} x10^8	roughness /nm
untreated	18.2±1.1	5.1±0.2	1.7±0.7
pH = 3	17.8±2.1	3.8±0.3	0.9±0.4
pH = 11	18.5±2.6	3.8±0.5	0.7±0.4

Tab. 2: *Parameters giving the best fit to the neutron reflectometric experimental results.*

	$Si/PEI/(PSS/PAH)_6$		
	thickness /nm	ρ /nm^{-2} x10^8	roughness /nm
untreated	21.5±1.5	5.1±0.2	1.3±0.4
pH = 3	18.5±1.6	4.1±0.3	1.2±0.6
pH = 11	18.5±1.7	4.0±0.5	0.9±0.6
	$Si/PEI/(PSS/PAH)_6PSS$		
	thickness /nm	ρ /nm^{-2} x10^8	roughness /nm
untreated	22.2±1.4	4.9±0.1	0.9±0.3
pH = 3	20.6±1.3	5.0±0.3	0.7±0.2
pH = 11	20.8±0.9	5.3±0.6	0.6±0.2

Reference:

[1]. M. Kolasinska et al., Experimental report, HMI (Berlin) 2005

	EXPERIMENTAL REPORT **Study of a Switchable Peptide Film at an Air- water Interface by Neutron Reflectivity**	Proposal N° MAT-04-1236 Instrument **V6** Local Contact Roland Steitz
Principal Proposer: Experimental Team:	L. He – Univ. Queensland, Australia R. Steitz – HMI, Berlin Y. Ding – Univ. Queensland, Australia L. He – Univ. Queensland, Australia	Date(s) of Experiment 21.11. – 30.11.2006

Date of Report: 15.01.2007

Similar to proteins, certain short (11-25 residue) peptides can form strong laterally bonded networks at fluid-fluid interfaces, with strengths only slightly lower than those of reference proteins (Jones and Middelberg, 2002). Furthermore, rationally designed peptides can form networks at least ten times stronger than the best available reference proteins. For example, a new designed synthetic peptide, AM1, has shown very interesting interfacial properties. It has a high interfacial elasticity modulus and maximum interfacial stress under conditions permitting network formation (Dexter et al., 2006). Remarkably, AM1 networks can be reversibly switched by adding and removing metal ions. AM1 can thus be used to alternately stabilize and destabilize emulsions and foams, thus offering unprecedented control over the behaviour of the interfacial layer in emulsion and foam systems.

One recent highlight of our study is the finding that addition of sodium dodecyl sulfate (SDS) can significantly enhance the performance of AM1 in stabilizing foams. At a suitable concentration of peptide and SDS, AM1 force transmission at an air-water interface can be doubled by adding SDS. In contrast, SDS alone is incapable of transmitting a force laterally in the plane of the interface. This behaviour clearly shows that there are cooperative interactions between SDS and AM1 at the interface.

In this reported work, we have investigated the interaction of AM1 and SDS at an air-water interface by neutron reflectivity. The composition of a mixed interfacial film of AM1 and SDS has been measured as a function of SDS concentration in the bulk solution while the AM1 concentration in the solution was held constant at 5 μM. A suitable concentration range for SDS was previously determined by combining interfacial force transmission and surface tension measurements In order to measure the surface excess of SDS and AM1 independently, we performed contrast variation using combinations of deuterated AM1/protonated SDS and protonated AM1/deuterated SDS. The neutron reflectivity measurements of the mixed system were carried out in null reflecting water (8.1% D_2O) and 100% D_2O, giving the adsorbed amount at the interface directly. As an example, Figure 1 shows typical reflectivity curves of the mixture of AM1 and SDS. We are currently analyzing these interesting data, and a manuscript is expected to be submitted in this year.

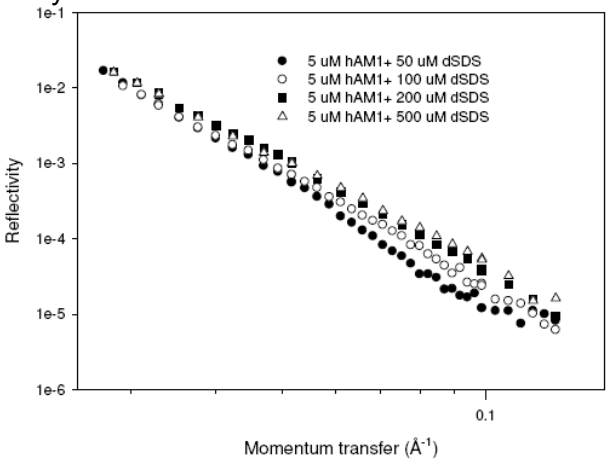

Fig. 1: *Reflectivity of a mixture of protonated AM1 and deuterated SDS at air-water interface (25 mM HEPES, pH 7.4, D_2O). The bulk concentration of AM1 was fixed at 5 μM while SDS concentration was varied from 50 μM to 500 μM.*

Reference:

[1]. Jones DB, Middelberg APJ. Langmuir. 2002, **18**:10357-10362.

[2]. Dexter AF, Malcolm AS, Middelberg APJ, Nat Mater. 2006, **5**:502-506.

	EXPERIMENTAL REPORT **Internal Order of Polyelectrolyte Multilayers**	Proposal N° PHY-04-1227 Instrument **V6** Local Contact Roland Steitz
Principal Proposer: Experimental Team:	C. A. Helm – EMAU Greifswald H. Ahrens, J.-U. Günther – EMAU Greifswald M. Gopinadhan – EMAU Greifswald O. Ivanova – EMAU Greifswald R. Steitz – HMI, Berlin	Date(s) of Experiment 14.02. – 19.02.2006 14.07. – 17.07.2006

Date of Report: 05.01.2007

Self-assembly processes of polyelectrolytes involving electrostatic interactions can be used to build-up multi- layered materials. The basic principle is the sequential adsorption of positively and negatively charged polyelectrolytes[1, 2]. With X-ray and neutron reflectivity the structure and composition of polyelectrolyte multilayers from poly (allylamine hydrochloride) (PAH) and poly (styrene sulfonate) (PSS) is studied as function of preparation conditions (salt concentration and solution temperature). The onset of a temperature effect occurs at 0.05 M NaCl (Debye length less than 1 nm) [3].

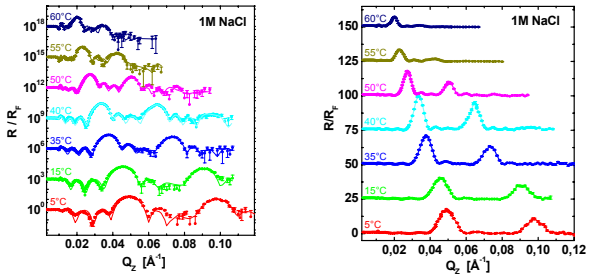

Fig. 1: *Neutron reflectivity curves of polyelectrolyte multilayers prepared from 1 M NaCl solution at temperatures indicated, both on a logarithmic (left) and on a linear scale (right). Always, r.h.=0 %. The polyelectrolyte multilayers consist of N=4 repeat units, (PAH/PSS)$_3$-PAH/PSS$_d$, and a substrate layer.*

Since the segmental distribution of one polyelectrolyte layer exceeds its thickness[1], the monomer density is constant along the surface normal for both PAH and PSS [1]. The interpenetration of consecutive layers is attributed to partial mixing during the adsorption process.
To calculate the reflected intensity the surface layer is described as a series of slabs (each with a density and a thickness, and a roughness parameter) [1, 3, 5]. The exact dynamic approach is used to fit the data. Approximate equations to calculate the reflectivity are provided by the kinematic approach, which have the advantage to provide intuitive insight.
With selectively deuterated polyelectrolyte layers a superstructure is formed. In the past, we investigated films exhibiting one superstructure peak [3]. The data show structure, thus four independent parameters can be extracted: the scattering length density of the (1) deuterated PSS$_d$-layer (from the height of the superstructure peak) and (2) of the nondeuterated layers (from the amplitude of the oscillations), (3) the thickness d_{bl} of a polyelectrolyte bilayer pair within a repeat unit (from the position of the superstructure peak) and (4) the thickness of the layer adjacent to the substrate (from the periodicity of the Kiessig oscillations). The internal roughness σ between adjacent slabs is not measured directly; it is set to half the thickness of the PSS$_d$-layer. This constraint was found to be valid for polyelectrolyte multilayers when only the salt concentration in the deposition solution is varied [1]. Then, the internal roughness is calculated from a molecular model, ie the monomer volumes and scattering lengths of PSS and PAH.
With two superstructure peaks, the internal roughness σ is measured directly from the ratio of the peak heights: $\frac{\sigma^2}{d_{rep.u.}^2} \approx \ln\left(4\frac{R/R_F(Q_{z1})}{R/R_F(Q_{z2})}\right)/12\pi^2$ with $d_{rep.u.}$ as the thickness of a repeat unit (assuming uniform water content in the film). Since σ is independent of film thickness, film/substrate and film/air roughness, the progressive damping of the peaks with their order for T≥50°C (cf. Fig. 1) indicates an increase in σ.
Roughly, the peak height yields the water content,

$$R/R_F(Q_{zm}) \approx \text{const} \cdot \left(N\frac{\rho_{d.bl}}{\rho_{sub}} m \frac{\sigma}{d_{rep.u.}}\right)^2 \cdot \exp\left(-(2\pi m \frac{\sigma}{d_{rep.u.}})^2\right),$$

(order of the peak is m, number of repeat units N, additional scattering length density of the PSS$_d$/PAH layer $\rho_{d.bl}$ and of the substrate $\rho_{sub.}$ $\rho_{d.bl}$ is derived from the volume V and the scattering length b of the water molecules, H_2O, and the monomeric segments PAH and PSS), since $\rho_{d.bl} = \frac{d_{rep.u.}}{4\sigma\sqrt{2\pi}} \cdot \frac{b_{PSSd} - b_{PSS}}{V_{PSS} + V_{PAH} + n_{H_2O} V_{H_2O}}$. →

Thus, an increase in water content decreases the peak height.

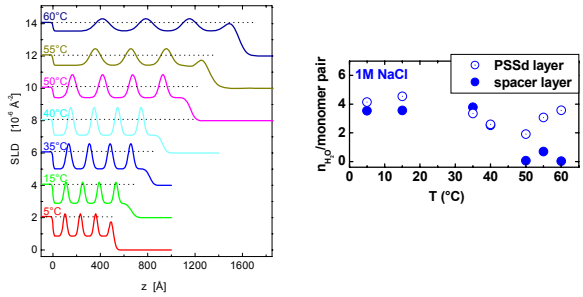

Fig. 2: *left: Scattering length density profiles obtained from the data shown in Fig.1. Right: number n of water molecules per deuterated (open spheres) and perprotonated (full spheres) monomer pairs.*

At 1 M NaCl, the film thickness increases by a factor of three on heating the deposition solution from 5 to 60°C (cf. Fig. 2). For films from T≤35°C, there are 3.4 water molecules per PAH/PSS monomer pair. At higher T the height of the 1st peak decreases (cf. Fig. 1), indicating water loss. However, fits according to the dynamic model (Fig. 1, left) reveal that the assumption of uniform water content fails for T≥50°. While there is no water in the perprotonated polyelectrolyte bilayers, about 2 water molecules per PSS_d/PAH pair remain.

References:

[1]. G. Decher, *Science*, 1997. **277**: 1232-1237
[2]. M. Schönhoff *Curr. Opin. Colloid Interface Sci.*, 2003. **8**:86-95
[3]. M. Gopinadhan, et al., subm
[4]. K. Büscher et al., *Langmuir*, 2002. **18**: 3585-3591
[5]. M. Gopinadhan et al., Macromolecules, 2005 **38** ; 5228-5235

	EXPERIMENTAL REPORT **Effect of geometrical confinement on the thermosensitivity of PNIPAM films**	Proposal N° PHY-04-1228 Instrument **V6** Local Contact Roland Steitz
Principal Proposer: Experimental Team:	R. von Klitzing – CAU, Kiel C. Ecker – CAU, Kiel R. von Klitzing – CAU, Kiel R. Steitz – HMI, Berlin	Date(s) of Experiment 13.03. – 19.03.2006

Date of Report: 19.01.2007

Thermosensitive microgel particles achieve large interest, in particular in the fields of drug release and sensing. For instance poly-(N-isopropylacryl-amide), PNIPAM, undergoes a temperature induced phase transition at ~32 °C which corresponds to a discontinuous shrinking with increasing sample temperature. Above the transition temperature solvent absorption becomes unfavourable and solvent is squeezed out of the polymer chains. As opposed to macrogels, PNIPAM microgel particles show a continuous phase transition due to finite size effects. Also that transition is reversible and leads to shrinking by a factor of 10 in bulk samples.

We utilized neutron reflectometry to study a potential geometrical confinement effect of PNIPAM microgel particles organized as ultrathin films (see Fig. 1) at the interface of silicon single crystal backings and liquid D_2O frontings. The microgel particles consisted of PNIPAM copolymerized with 5% acrylic acid. They were deposited by spin-coating from aqueous suspension on top of Silicon blocks (80 x 50 x 15 mm^3) that were pre-coated with polyethyleneimine.

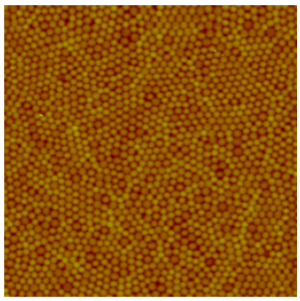

***Fig. 1**: AFM micrograph (20 x 20 μm^2) of a densely packed layer of P(NIPAM-co-AA) particles on Si.*

The coated silicon substrates served each as top of a flow cell filled with D_2O adjusted to pH 1.5. The incident neutron beam passed through the neutron-transparent silicon sub-strate and was reflected off the solid/liquid interface through the solid.

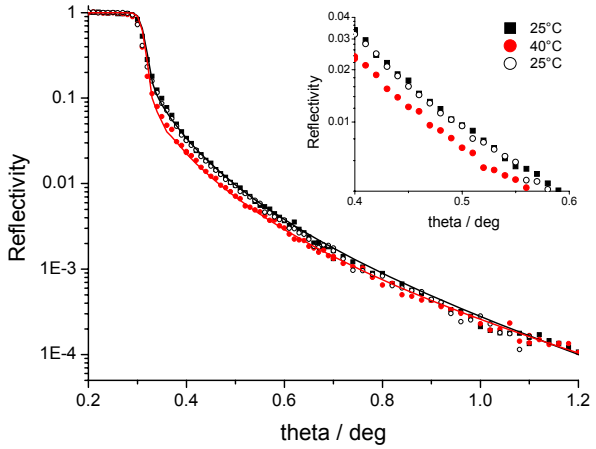

***Fig. 2**: Neutron reflectivities from sample w61 against liquid D_2O. Subsequent sample temperatures are indicated in the inset from top to bottom. Solid lines are best fits to the data. Note that the decay in reflectivity upon heating is fully reversible.*

Additional measurements were conducted on the dried films against air prior and after the measurements against the liquid phase. With a ratio of roughness over film thickness, σ/d, of 0.25-0.31, the dry films were found very rough, as expected from their morphology shown in Fig. 1.

Upon incubation with D_2O we observed a pronounced swelling of the PNIPAM layer by a factor of 12 at 25°C. The layer responded in a fully reversible manner to an increase in temperature both with a reduced thickness and a reduced scattering length density, Nb, (see table 1). In concordance with expectation the temperature-induced shrinking of the confined PNIPAM layer by a factor of 2 is less pronounced than in bulk samples.

***Tab.1:** Fit parameters for w61 against air and D_2O*

T / °C	d / Å	Nb / $Å^{-2}$	σ/d
air	344	$0.89 \cdot 10^{-6}$	0.25
25	3971	$5.84 \cdot 10^{-6}$	0.06
40	2012	$5.30 \cdot 10^{-6}$	0.11
25	3900	$5.82 \cdot 10^{-6}$	0.08
air	316	$0.82 \cdot 10^{-6}$	0.31

BENSC	**EXPERIMENTAL REPORT** **Switchable structure of block-copolymer brushes at interfaces**	Proposal N° PHY-04-1252-EF Instrument **V6** Local Contact Roland Steitz
Principal Proposer: Experimental Team:	R. Steitz – HMI, Berlin G.H. Findenegg, TU Berlin J.-U. Günther – EMAU Greifswald V. Papaefthimiou – TU, Berlin R. Steitz – HMI, Berlin	Date(s) of Experiment 13.06. – 20.06.2006

Date of Report: 19.01.2007

Modifying surface properties by ultrathin polymer coatings requires detailed understanding of the influences on the polymer chain conformation in those layers. Due to the interplay of long- and short-ranged electrostatic forces, charged polymers (polyelectrolytes) are an interesting item in that field of research [1].

In this work we studied the structural changes of polyelectrolyte brushes grafted to the solid-liquid interface of a silicon backing and a D_2O liquid fronting phase with varied sodium chloride content (c_{NaCl}). Brushes were prepared by Langmuir-Schäfer transfer of poly(ethyl ethylene)-b-poly(styrene sulfonate) ($PEE_{114}PSS_{83}$) films to the silicon substrates, pre-coated with a 30nm thin deuterated polystyrene layer (d-PS), at three different grafting densities (0.091, 0.125 and 0.154 molecules/nm^2).

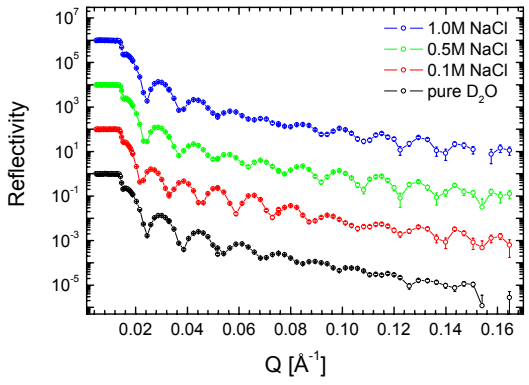

Fig. 1: *Neutron reflectivity curves from sample C, Si/d-PS/PEE-PSS against varied liquid subphases. Grafting density was 0.154 molecules / nm^2. Subphases were exchanged by rinsing with particular NaCl-D_2O solutions.*

The scattering length density profiles along the surface normal were studied by neutron reflectivity measurements (Fig. 1). The reflectivity curves show Kiessig oscillations with partially damped amplitude. With varied c_{NaCl} the onset of the amplitude damping shifts on the Q axis, a feature that is attributed to changes of polyelectrolyte brush lengths.

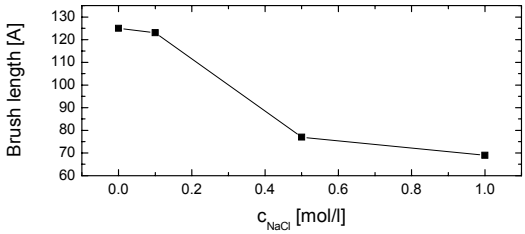

Fig. 2: *Variation of polyelectrolyte brush length as a function of NaCl concentration, i.e. ionic strength of the liquid subphase (same sample as in Fig. 1).*

For pure D_2O and 0.1M NaCl subphase the osmotic pressure of the incorporated counterions leads to strongly stretched polyelectrolyte chains (>50% of the contour length) [2]. With increasing c_{NaCl} the brush shrinks as predicted by the so called "salted brush regime" [1] (Fig. 2).

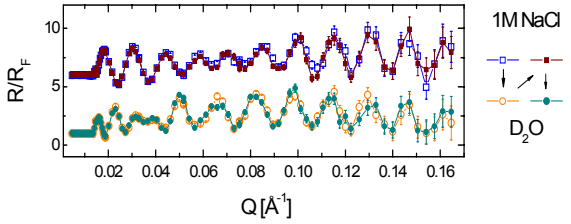

Fig. 3: *Reflectivity curves normalized to the Fresnel-reflectivity. Consecutive displacement of subphase: from 1M NaCl (open squares) to D_2O (open circles) back to 1M NaCl (closed squares) and again to D_2O (closed circles).*

Switching between two different subphases by alternate rinsing with 1M NaCl solution in D_2O and pure D_2O superimposes similar reflectivity curves (Fig. 3) – a sound proof of reversibility of the chain shrinking and stretching effect as triggered by the ion concentration in the polyelectrolyte's environment. The same observations were made for samples A and B prepared at grafting densities of 0.091 and 0.125 molecules/nm^2.

References :

[1]. N. A. Kumar, et al. Macromolecules; 2005, **38**, 9341.
[2]. H. Ahrens, et al. Phys. Rev. Lett., 1998, **81**, 4172.

	EXPERIMENTAL REPORT **Internal Order and Water Content of Polyelectrolyte Multilayers**	Proposal N° PHY-04-1324 Instrument **V6** Local Contact Roland Steitz
Principal Proposer: Experimental Team:	C.A. Helm – EMAU Greifswald M. Gopinadhan, O. Ivanova – EMAU Greifswald H. Ahrens, J.-U. Günther – EMAU Greifswald R. Steitz – HMI, Berlin	Date(s) of Experiment 15.09. – 18.09.2006 30.10. – 01.11.2006

Date of Report: 05.01.2007

The basic principle in the formation of polyelectrolyte multilayers is the sequential adsorption of positively and negatively charged polyelectrolytes[1, 2]. Polyelectrolyte adsorption onto an oppositely charged interface is determined by the interplay of electrostatic and secondary interactions.[4, 5] While the electrostatic contribution is rather well understood [2], little is known about the nature, the origin and the influence of the secondary forces[6, 7]. With neutral polymers, the solvent/solute interaction is controlled by varying the temperature. Similarly, we found that the thickness per polyelectrolyte layer pair increases on rise of the preparation temperature[6, 7], indicating a progressive deterioration of the solvent quality. To investigate the layer thickness, bound water and layer interpenetration, X-ray and neutron reflectivity measurements with selectively deuterated layers are performed [3]. Polyelectrolyte multilayers are prepared from poly (allylamine hydrochloride) (PAH) and poly (styrene sulfonate) (PSS).

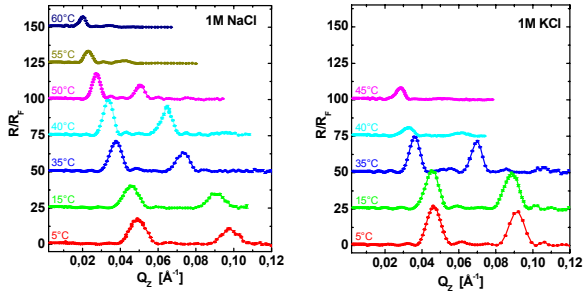

Fig. 1: *Neutron reflectivity curves of polyelectrolyte multilayers prepared from 1M NaCl (left) or 1M KCl (right) solution at temperatures indicated, both on a a linear scale. Always, r.h.=0 %. The polyelectrolyte multilayers consist of 4 repeat units, $(PAH/PSS)_3$-PAH/PSS_d, and a substrate layer.*

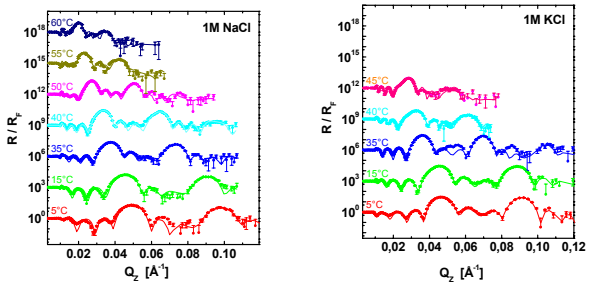

Fig. 2: *The same measurements as shown in Fig. 1, yet on a logarithmic scale. Lines are fits according to the dynamic model.*

While the PAH/PSS bilayer pair has the same thickness at the same preparation temperature (cf. Fig. 3, top left), at low temperature the superstructure peaks are smaller for films prepared from NaCl solutions (cf. Fig. 1). This is indicative for a larger water content: 3.4 compared to 2 water molecules per PAH/PSS monomer pair for films from KCl or NaCl solutions, respectively.

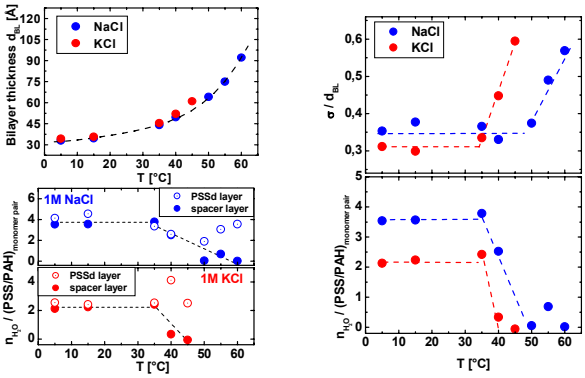

Fig. 3. *Comparison of parameters for films built from KCl or NaCl solution, respectively. Top, left: polyelectrolyte bilayer thickness as function of preparation temperature. Bottom, left: number n of water molecules per deuterated (open spheres) and perprotonated (full spheres) PAH/PSS monomer pairs. Right, top: internal roughness σ normalized by bilayer thickness d_{bl}. The increase of roughness is correlated with a loss of water molecules in the protonated layers (bottom)*

For films built from heated solutions containing 1M KCl (note that PSS precipitates from 1M KCl at about 60°C) or 1M NaCl, the qualitative features of the reflectivity measurements are the same (cf. Fig. 1): decreased amplitude of the 1st superstructure peak (40°C for KCl films and 50°C for NaCl films), accompanied by a pronounced damping of the 2nd peak. These effects get more prominent on further heating of the preparation solution.

This feature is indicative for an increased internal roughness, which seems to be correlated to a loss of water molecules in the protonated PAH/PSS bilayers. Note that in the deuterated bilayers about 2 water molecules per PAH/PSS monomer pair remain (cf. Fig. 3, bottom left), as is revealed by detailed data analysis according to the exact matrix formalism (cf. Fig. 2), and taking into account the high periodicity oscillations. We would like to emphasize that the different water content in the deuterated and protonated bilayers can only be resolved since there are Kiessig fringes as well as two superstructure peaks.

References :

[1]. G. Decher, *Science*, 1997. **277**: p. 1232-1237.
[2]. M. Schönhoff *Curr. Opin. Colloid Interface Sci.*, 2003. **8**:86-95.
[3]. M. Gopinadhan., O. Ivanova, H. Ahrens, J.-U. Günther, R Steitz, C.A. Helm subm.
[4]. R.R. Netz, J.-F. Joanny, *Macromolecules*, 1999. **32**: p. 9013-9025.
[5]. S.S. Shiratori, M.F. Rubner, *Macromolecules*, 2000. **33**: p. 4213-4219.
[6]. K. Büscher, et al., *Langmuir*, 2002. **18**: p. 3585-3591.
[7]. M. Gopinadhan., et al., *Macromolecules*, 2005. **38**: p. 5228-5235.

	EXPERIMENTAL REPORT **Development of D_2O Tracer Method for Water Flow in Plants - application for grafted tomato seedlings**	Proposal N° BIO-04-1318 Instrument **V7** Local Contact Nikolay Kardjilov
Principal Proposer: Experimental Team:	U. Matsushima – Iwate Univ., JP N. Kardjilov – HMI, Berlin W. Herppich – ATB Potsdam A. Hilger – HMI, Berlin	Date(s) of Experiment 17.09. – 27.09.2006

Date of Report: 19.01.2007

Background

A combination of cold neutron radiography with D_2O tracer is a powerful visualization tool of water movement in plants. However, it has not been cleared yet whether the application of D_2O tracer and irradiation with neutron negatively influence plants performance. In this experiment, we investigated the potential effects by using chlorophyll fluorescence analysis imaging, a tool that provides deep insight into photosynthetic efficiency and integrity of plants. Especially the parameter F_v/F_m, an indicator of the potential photosynthetic efficiency, is highly related to plant stress responses.

Materials and Methods

Tomato seedlings at the 3-real-leaves stage were used as samples. Each Sample was transplanted into a glass tubes with glass beads.

The experiments have 3 phases. The first initial phase was without any treatment. During the second phase, thee samples were given D_2O tracer and were irradiated with neutron. During phase three, the conditions were again the same as in phase one. Each phase lasted for one hour. Chlorophyll fluorescence imaging was performed every 15 minutes during the entire experiment. Four experiments were conducted using different sets of treatments and samples. The first treatment was to exchange of H_2O with H_2O. The 2nd treatment comprised the exchange of H_2O with D_2O tracer. During the 3rd treatment the samples were irradiate with neutrons. 4th treatment was to apply D_2O tracer and neutron irradiation at the same time.

Air temperature and relative air humidity were set to 23 °C and 60 %, respectively. To control temperature and humidity, fluorescence images were taken through the quartz glass window.

Results and Discussion

Before the experiment, the influence of the quartz glass window on fluorescence analysis was checked using a tomato seedling. There was no difference between images taken with the window and without the window. Figure 1 shows changes in F_v/F_m from the first phase to the 3rd phase. Irrespective of the treatment, there were no significant changes in F_v/F_m. Only one exception was observed at the beginning of the first phase of the H_2O exchange treatment. F_v/F_m was low due to increased sample temperature, because the temperature and humidity controller was not working before the experiment. The sample temperature was several degree higher than set up temperature at the beginning. However, it was controlled to the set up temperature immediately after start of the experiment. This result indicates that the effect of D_2O supply and/or neutron irradiation was smaller than the influence of increased temperature. Thus the influence of D_2O supply and/or neutron irradiation was negligible and the combination method was applicable to plant samples.

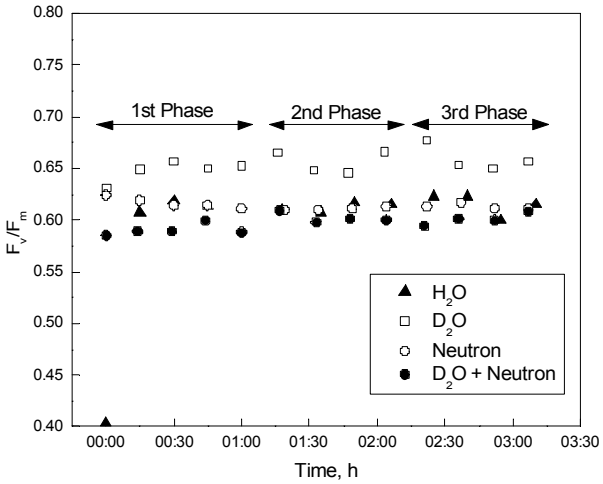

Fig. 1: *Changes in F_V/F_m from the 1st phase to the 3rd phase.*

	EXPERIMENTAL REPORT **Gel formulations through the modulation of structural properties**	Proposal N° MAT-04-1301 Instrument **V12a** Local Contact Markus Strobl
Principal Proposer: Experimental Team:	L. Paduano – Univ. Napoli, I L. Paduano – Univ. Napoli, I A. Molisso – Univ. Napoli, I M. Strobl – HMI, Berlin	Date(s) of Experiment 24.10. – 28.10.2006

Date of Report: 05.01.2007

Several drug delivery systems are currently developed or under development with the aim to increase the bioavailability and the amount of a drug in a required zone of the human body and to minimize its degradation and loss. Among drug carriers, hydrogels appear interesting because of their potential technological applications as delivery systems such as those required for transdermal patches or wound treatment.

There are many polymers used to form gel systems, among these, Poly(vinyl alcohol) PVA, because of its low cost and biocompatibility, is often used. A 10% wt PVA aqueous solution, if subjected to 3-4 freezing-thawing cycles, gives rise to physical gels with quite good mechanical properties. The introduction of another polymer able to change its conformation as a consequence of such modifications can lead to have a modulated release of the potential drug. In this contest, we have prepared a hydrogel formed by PVA 10% w/w, poly(acrylic acid) (HPA) 2% wt by 3-4 freezing-thawing cycles, with the aim to investigate the effect of HPA charge on its structural conformation in the gel system described above. The net charge of HPA can be changed acting on the pH: at high pH values the polymer backbone contains a high number of negative charges and, consequently, the expansion of the random coil HPA structure is inducted, whereas at low pH the random coil is more compact as shown by the lower value of the hydrodynamic radius.

Experiments were performed on six hydrogel samples and three solutions, all of them having the same amount of two gels investigated, but different neutralization degree.

In figure 1 two scattering spectra are shown. Black data correspond to a PVA/HPA/D_2O system where the poly(acrylic acid) has not been neutralized, whereas in the other system (red data) the 40% of the HPA has been neutralized with sodium hydroxide. Scattering data obtained in the USANS domain indicate a fractal behavior shown by the hydrogels analyzed. This is common to all the system investigated.

In the mesoscopic length scale, structures shown by the hydrogels are, at first glance, influenced by the pH values. At this aim SANS data become necessary in order to have information on the influence of pH in the microscopic length scale.

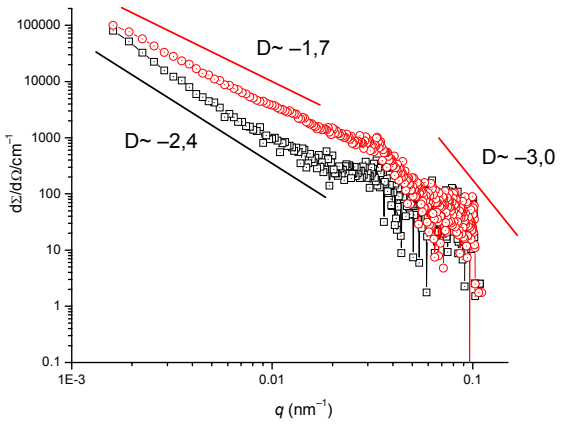

Fig. 1: *Scattering cross sections obtained at 25°C for the following systems*

- **PVA (10% wt) / HPA (2% wt) / D_2O**
- **PVA (10% wt) / HPA (2% wt, 40% neutralized) D_2O**

USANS collected data will be analyzed once the SANS data will be available using a mass fractal plus as reported in Journal of Applied Crystallography (1991), 24, 414.

Material Science

	EXPERIMENTAL REPORT **In situ study of the phase composition in the Na_3AlF_6-Al_2O_3 system within 900°C-1300°C**	Proposal N° MAT-01-1870 Instrument **E9** Local Contact Michael Tovar
Principal Proposer: Experimental Team:	L. Smrcok – SAS Bratislava, SK L. Smrcok, M. Kucharik – SAS Bratislava, SK O. Pritula – SAS Bratislava, SK M. Tovar – HMI, Berlin	Date(s) of Experiment 03.03. – 07.03.2006

Date of Report: 24.07.2006

Industrial production of primary aluminium is nowadays carried out only by the Hall-Héroult process. In this process alumina (Al_2O_3) is dissolved in electrolyte consisting mainly of liquid cryolite, Na_3AlF_6. The Hall-Héroult process belongs among the most energy demanding industrial productions and has considerable influence on environment. The molten cryolite completely dissociated into ionic entities, Na^+ as the only cation and into anions of AlF^{6-}, AlF^{5-}, AlF^{4-}, and F^- type. After an addition of alumina into molten cryolite so-called oxofluoroaluminate complex anions are expected to be formed.

The aim of the project was to find out the phase composition of crystalline matter in the Na_3AlF_6 – Al_2O_3 system at the temperatures within 930-1300°C in situ by high temperature neutron diffraction. The main goal was to find if oxofluoroaluminate compound was present in solid state. It was expected that oxofluoroaluminate compounds would appear just within the temperature interval 1000-1250°C. The existence of oxofluoroaluminate compound in solid state could support an assumption on their presence in liquid state.

Due to extreme chemical reactivity of fluorides the sample was encapsuled to a Pt tube closed by welding. The tube was put to Al_2O_3 holder preserving a slower heat transfer to avoid mechanical problems (breaking) which could be caused by thermal gradients. At all the temperatures a short diffraction pattern was collected for a check. Long time data collections were made at the four critical temperatures. It was realized, that the patterns were contaminated by a strong parasitic reflection (diffraction?) whose origin was not found. Preliminary data evaluation showed, that the pattern taken at 100°C contained cryolite, alumina and Pt peaks. After heating to 1150C diffractions of cryolite disappeared, but few weak diffraction of corundum indicated, that it was not completely dissolved.

It is assumed that the reason was in relatively large amount of Al_2O_3 presented in the sample (25 wt. %). The fact, that equilibrium between Al_2O_3 and melt was not yet reached means, that dissolving of such an amount is slower than it it could be expected just from indirect measurements. Presence of cryolite melt and amorphous Al_2O_3 was indicated by bumpy background between 55-75° . Later, at 1250°C, only diffraction of Pt were present, *i.e*. corundum was completely dissolved in cryolite. Upon cooling a pattern was taken again at 1150C. In that run only Pt peaks appeared indicating higher thermal inertia of the system. The next pattern measured at 1030°C showed traces of crystallizing corundum, but the broad peak remained. Finally, at 710°C corundum was unambiguously present. Preliminary results clearly show that no oxofluoroaluminate compounds appear at high temperatures in crystalline form. Our results are in accord with the results of the non-diffraction studies [1,2], which have, however, provided only indirect evidences.

It should be stressed that interpretation of diffraction patterns was hampered by absence of relevant high temperature diffraction data of cryolite and some extrapolation procedures must have been used. We are not aware of any neutron powder diffraction experiment reporting any crystallographic data of cryolite ah higher temperatures. High temperature single crystal study provides structural data only up to 900K [3]. Considering the technological importance of cryolite it is expected, that high temperature neutron diffraction will be used. It is therefore desirable to have available good reference data taken in a wider interval of temperatures.

References:

[1]. E. Skybakmoen, A. Solheim, A. Sterten Met. Mater. Trans.(1997) *B9*, 81

[2]. M. Kucharík, M. Boca, C. Bessada, H. Fuess, Eur. J. Inorg. Chem. (2005), 1781.

[3]. H. Yang, S. Ghose, D.M. Hatch. Phys. Chem Minerals (1993) 19, 528.

This research project has been supported by the European Commission under the 6th Framework Programme through the Key Action: Strengthening the European Research Area, Research Infrastructures. Contract n°: RII3-CT-2003-505925 (NMI3).

	EXPERIMENTAL REPORT **Determination of diffusion mechanism of nitrogen in Quaternary oxide hexaaluminate at temperatures up to 1200°K**	Proposal N° MAT-03-0421 Instrument **V3** Local Contact Margarita Russina
Principal Proposer: Experimental Team:	B. Saruhan-Brings – DLR Köln M. Stranzenbach – DLR Köln C. Mondragon Rodriguez – DLR Köln M. Russina – HMI, Berlin	Date(s) of Experiment 06.02. – 13.02.2006

Date of Report: 16.01.2007

The aim of the experiments on neutron scattering time of flight (TOF) at V3 was to determine the diffusion mechanisms of nitrogen chemisorbed on oxide catalysts. The neutron scattering experiment was focused on the analysis of nitrogen diffusion in $LaSrCrO_3$ catalyst. The adsorption of nitrogen oxide was carried out prior to the experiment by floating 1000 ppm NO in the carrier gas Argon over the $LaSrCrO_3$ powder with a flow rate of 20 ml/min. The temperature was then increased up to ~270°C during the nitrogen oxide chemisorption, then slowly cooled down to room temperature. Standard aluminium sample holders with a Viton ring, provided by HMI were used to support the ceramic powder. A vanadium plate was used as a standard reference. The corresponding scattering signal from the vanadium plate without the polymeric ring was also taken. This allowed us to evaluate the resolution function of the scattering contribution due only to the species adsorbed on our sample. The initial TOF neutron scattering experiment of the sample $LaSrCrO_3$ was carried out at 244K. The temperature was sequentially increased with 50K intervals up to the maximum temperature of 423K. The scattering neutron signal was measured over a period of 8 hours at each temperature. The conversion of the scattering signal to energy and the fitting of the results were made by using the software FITMO2.

The phenomenological analysis of the neutron scattering results showed a relative small quasielastic contribution, energy interval [-1.4meV, 1.4meV]. The variations observed in the quasielastic part of the scattering curves prove that at least two diffusion processes with different magnitude takes place. One molecule with a high contribution to one of the diffusion processes is the presence of co-adsorbed molecules like CO_2. Short exposure of the catalyst (after the NO chemisorption) to the air must be responsible for these observations. The co-adsorption (physisorption) of molecules like CO_2 on the catalyst surface can lead to a higher diffusion rate. The lower rate of nitrogen diffusion should be related to the nature of the chemical bond of NO with the surface. In general chemisorbed molecules on heterogeneous surfaces have higher activation energies. The interaction degree of NO and/or formation of different nitrate complexes on the surface sample, which would otherwise lead to a different diffusion rates, can not be completely excluded.

The elastic part of the energy spectra was in this case well fitted with the jump model. The jump model with two Lorenz bands describes the elastic contribution to the energy spectra. In contrast, the quasielastic contribution to the energy spectra was not well described with this model. The jump model with two Lorenz bands contributed to a better description of the quasielastic part of the spectra, but not good enough to describe the diffusion process. Similarly, the isotropic rotational model could not describe the diffusion process. The poor description of the quasielastic part of the spectra must be linked with the statistic deficiency obtained during the neutron scattering. The non-dependence of the energy with temperature and the corresponding structure factor are the evidence of a complicated diffusion mechanism. The behaviour observed in this case is the result of at least two diffusion processes as mentioned above. Unfortunately, neither the jump model nor the isotropic rotation model could fully describe the diffusion process detected during our neutron scattering experiments (TOF). The development of an alternative diffusion model of the chemisorbed gas species may contribute to an integral phenomenological description of the diffusion process. The quasielastic part of the energy spectra must also be well fitted with the new diffusion model in order to prove the nitrogen diffusion inside the catalyst.

	EXPERIMENTAL REPORT **Random copolymer association in solutions**	Proposal N° CHE-04-1274 Instrument **V4** Local Contact Uwe Keiderling
Principal Proposer: Experimental Team:	T. Cosgrove – Univ. Bristol, UK V. Rodin, D. Qui – Univ. Bristol, UK M. Murray – ICI, Wilton Centre, UK U. Keiderling – HMI, Berlin	Date(s) of Experiment 19.08. – 21.08.2006

Date of Report: 30.08.2006

Introduction: Aggregates and associates of random copolymers based on butyl methacrylate (BMA) and methacrylic acid (MAA) monomers can result in structured solutions. Small angle neutron scattering (SANS) is sensitive to these structures [1–3]. When the copolymers have been neutralised with an amine the rheology on the BMA–MAA isopropanol (IPA) solutions diluted with water showed a maximum in viscosity and SANS data gave a maximum in the scattering intensity at a momentum transfer Q* as a function of polymer concentration [3]. This work extends our previous NMR and SANS studies on these random copolymers in IPA [1, 2]. We have used SANS experiments at BENSC (Germany) to highlight the structural properties that give rise to the anomalous behaviour of BMA–MAA copolymers in mixed (water–IPA) solvents.

Objectives: The aim of this study was to investigate neutralized copolymers BMA–MAA (mole% BMA=70 and 80) in mixed solvents at 25 and 50^{o}C to clarify the structure of polymer aggregates.

Experimental: All the samples consist of a range of random copolymers of BMA and MAA (mole% BMA=80, 70) with nominal molecular weights of ~38K. The Tg for the copolymers was 90 ^{o}C (mole% BMA=80) and 101^{o}C (mole% BMA=70). All the samples have been measured in mixtures of deuterated water (D_2O) and D-isopropanol (DIPA). First the BMA/MAA 70/30 copolymers have been measured in mixtures of D_2O and DIPA in the range of 0.1–0.8% polymer concentration. The level of neutralization agent used in these samples (Triethanol amine (TEA)) was 1:1; 0.75:1 and 0.5:1 molar ratios of TEA to COOH in the polymer. All these measurements were carried out at 25°C. BMA/MAA 70/30 copolymers (0.8% polymer concentration) at neutralisation level 1:1 and 0.5:1 have been measured also at 25 and 50°C. A series of BMA/MAA 80/20 copolymers (30% polymer in DIPA/D_2O solutions at a 1:1 mole ratio of TEA to COOH in the polymer) with variable solvent ratio (D_2O:DIPA) (from 1:0 to 0.5:0.5) have been measured at 25°C. Additionally BMA/MAA 80/20 copolymer solutions (30% polymer) at solvent ratio (DIPA:D_2O) 0.6:0.4 and 0.7:0.3 have been measured also at 50°C. A series of different polymer concentrations (from 10% to 30%) of BMA/MAA 80/20 copolymers in DIPA/D_2O have been studied at fixed solvent ratio (DIPA:D_2O=0.52) at 25°C and 50°C.

Initial Results: Fig.1 shows the scattering functions of 30% BMA/MAA 80/20 copolymers in DIPA/D_2O as observed at 25°C and 50°C and two different solvent ratios. There are some important features: on increasing the fraction of D_2O the scattering intensity has increased significantly in the low and middle Q ranges (Fig.1 compares the 0.7:0.3 and 0.6:0.4 solvent ratios). This increase in intensity indicates a more collapsed structure (with increasing the fraction of D_2O in mixed solvent) and an interaction between polymer chains in comparison with copolymer in pure IPA or in mixed solvent with lower strong fraction of water. The increase in intensity with increasing the temperature indicates that a molecular interaction between polymers in solution becomes stronger. This supposes the formation of additional contacts between polymer scattering bodies. The increase in intensity is quite small for the copolymers with small fraction of water in mixed solvent. Fig.2 shows the scattering patterns from BMA/MAA 80/20 copolymers in mixed solutions at fixed solvent ratio DIPA:D_2O=0.52. Again there is an increase in intensity of scattering at low Q with increasing the temperature from 25 to 50^{o}C. The shape of structure peak observed at middle Q range changed significantly with decreasing the polymer concentration from 25 to 10%.

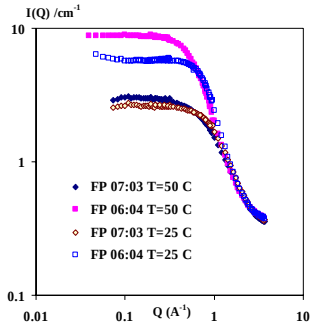

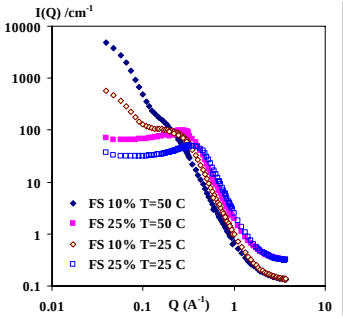

Fig.1 (left). *Scattering from BMA/MAA 80/20 copolymers (fixed polymer (FP) concentration =30%) at 25 and 50°C for solvent ratio DIPA:D_2O=0.7:0.3 and 0.6:0.4.*
Fig.2 (right). *SANS from BMA/MAA 80/20 solutions (polymer concentration 10 and 25%) in mixed solutions at fixed solvent (FS) ratio DIPA:D_2O=0.52. T=25 and 50°C.*

For the dilution experiments in DIPA/D_2O (0.1–0.8 % polymer) there is a clear indication of a peak in the data, similar to that obtained with other data [3] (Fig.3). Their intensity increases with decreasing the neutralisation level. An increase of a temperature doesn't change scattering function and the intensity of scattering at low polymer concentration (0.8%). Further analysis is still required.

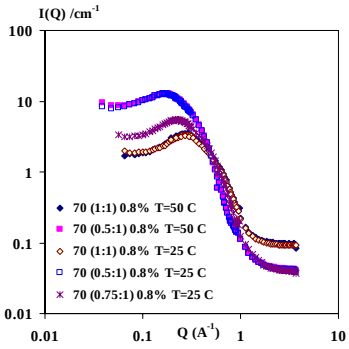

Fig.3. *Scattering from BMA/MAA 70/30 copolymer upon dilution with D_2O after neutralization by TEA in DIPA (1:1; 0.75:1; 0.5:1). Polymer concentration 0.8%. T=25 and 50°C.*

References:

[1]. V.Rodin, T.Cosgrove. *ISIS Experimental Report (Rutherford Appleton Laboratory).* RB No 20002 (2005)
[2]. T.Cosgrove, V.Rodin, D.Qiu, T.Geue. *SINQ Experimental Report.* II/04 S-50 (2005);
[3]. V.Rodin, T.Cosgrove, C.Flood, M.Murray *ILL Experimental Report.* N 9-11-1186 (2006);

	EXPERIMENTAL REPORT **Effect of Ni on the formation of defect-solute clusters in neutron irradiated iron alloys**	Proposal N° MAT-04-1191 Instrument **V4** Local Contact Martin Kammel
Principal Proposer: Experimental Team:	F. Bergner – FZ Rossendorf F. Bergner – FZ Rossendorf A. Ulbricht – FZ Rossendorf M. Kammel – HMI, Berlin	Date(s) of Experiment 14.07. - 17.07.2006

Date of Report: 13.09.2006

Irradiation of reactor pressure vessel (RPV) steels induces a degradation of the mechanical properties caused by the formation of nano-scale defect-solute clusters. Impurity Cu plays the major role in cluster formation, whereas the effect of the alloying element Ni depends on the Cu level and is not yet well understood.

The present experiment was devoted to the Ni effect. The SANS results for a Fe-3%Ni alloy and pure Fe are shown in Fig. 1 (lines). A significant but small irradiation-induced increase of the magnetic cross section is observed for pure Fe at $Q > 0.5\ nm^{-1}$. The same effect is only marginally larger in the case of Fe-3%Ni.

The increased cross section observed for model alloys A, D and F (symbols) are due to impurity and solute elements added to Fe in order to simulate RPV steels. It is of minor interest here. The effect of irradiation is more pronounced as in the case of the Cu-free pure systems even at a four times less value of neutron dose. This finding unequivocally shows the dominant effect of Cu and the inefficacy of Ni, if no Cu is present. The ranking A → D → F follows our expectation according to increasing Cu and Ni.

The calculated volume-related size distribution of irradiation-induced clusters is shown in Fig. 2. An RPV steel of similar Cu and Ni as alloy D is included for comparison. Of particular interest is the effect of Cu and Ni on the mean size of clusters. The basic finding from the present experiment and a previous one [1] is that Cu tends to raise mean size whereas Ni tends to reduce mean size. The RPV steel roughly fits this trend.

In a more detailed analysis, a comparison of the measured values of the ratio of magnetic and nuclear scattering (A-ratio) and the A-ratio deduced from composition obtained from both rate theory calculations and APFIM measurements will be included.

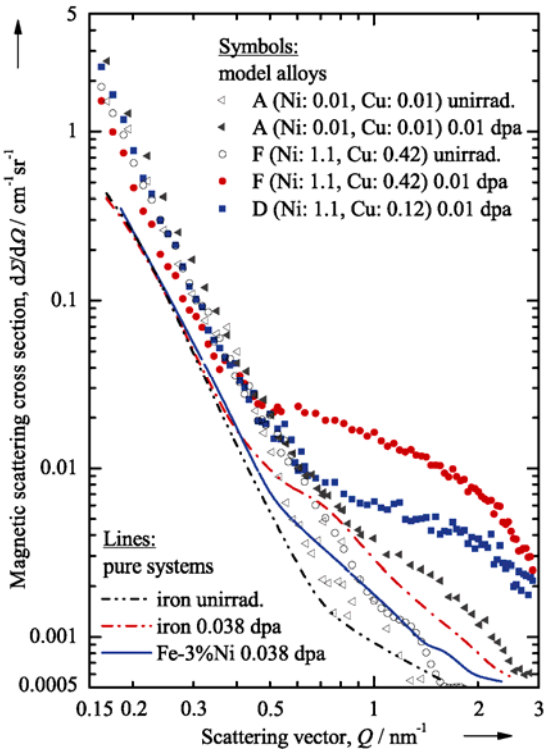

Fig. 1: *Magnetic scattering cross sections of neutron irradiated iron alloys and the unirradiated reference conditions.*

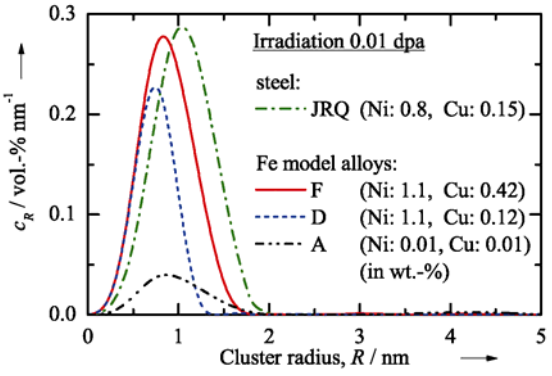

Fig. 2: *Size distribution functions of defect/solute clusters in neutron irradiated iron alloys and steel.*

Reference:

[1]. A. Ulbricht, J. Böhmert, M. Grosse, P. Strunz, Physica B **276-278** (2000) 936-938.

	EXPERIMENTAL REPORT **SANS investigation of the kinetics of rafting in a MCNG single crystal Ni base superalloy**	Proposal N° MAT-04-1199 Instrument **V4** Local Contact Uwe Keiderling
Principal Proposer: Experimental Team:	P. Bastie – CNRS St. Martin d'Heres, F N. Ratel – ILL Grenoble, F U. Keiderling – HMI, Berlin	Date(s) of Experiment 03.03. – 06.03.2006

Date of Report: 13.04.2006

Introduction and aim of the experiment:
Single crystal Ni base superalloys find their application in turbine blades for aerospace industry. The peculiar properties of these alloys arise from the presence of γ' precipitates embedded in a γ matrix. After a standard heat treatment, these γ' particles usually adopt a cuboidal shape (about 350nm edge) and are almost periodically distributed in the γ matrix along the <100> crystallographic directions [1]. After dynamically straining a sample at 850ºC in the plastic regime, internal stresses may relax during subsequent annealing at high temperature (around 1100ºC), thus inducing the directional coarsening (or rafting) of the γ' particles [2]. Recently, the addition of rhenium and ruthenium in the MCNG alloy has led to the observation of an improved high temperature creep behaviour, which is closely related to microstructure evolution and rafted morphologies. This experiment consists in the investigation by small angle neutron scattering (SANS) of the kinetics of rafting in this alloy. Systematic comparison with an alloy from a previous generation (AM1 [3]) will cast light on the role played by Re and Ru on the diffusion processes that control rafting of the γ' particles.

Experimental procedure:
Two MCNG samples were dynamically strained along the (001) direction at 850ºC prior to the SANS experiment. The plastic strain rates introduced in these samples were 0.2% and 0.6% for samples 1 and 2 respectively. Each sample was then oriented by Laue X-ray scattering in order to identify the <100> crystallographic axes. In order to avoid multiple scattering, thin slices (1.5mm) were cut in each specimen by spark erosion.
Each sample was then mounted in a Boron nitride diaphragm (0.4cm^2) and placed in a high temperature furnace that was available on the beamline. During annealing at 1100ºC and 1050ºC for samples 1 and 2 respectively, successive SANS patterns were recorded. The neutron wavelength was 6Å and the sample to detector distance was 16m so as to explore the smallest q range attainable without loosing too much neutron flux. The microstructure evolution occurring during each annealing can then be deduced from these measurements. After annealing, SANS patterns with λ=19Å were recorded so as to increase the investigated q range for the final microstructure. The coarsening of the precipitates results in an increased size of the particles, whose visibility becomes clearer in the small q range attainable at this wavelength. In these conditions, after sufficient ageing time, γ' platelets (or rafts) are formed perpendicularly to the tensile axis [001]. The SANS signal is therefore expected to decrease in the low q range along the [100] or [010] direction.

Experimental results:
Data was treated and reduced using BerSANS software developed at HMI [4]. Corrections for background, solid angle viewed by a pixel on the PSD, sample and cell transmissions were taken into account.

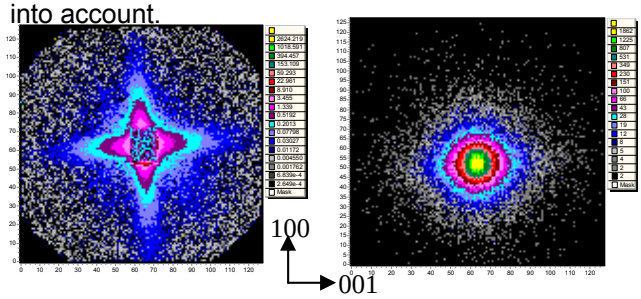

Fig. 1: *SANS patterns obtained before annealing at room temperature (left, λ=6Å) and after annealing at 1100ºC (right, λ=19Å).*

The fourfold symmetry observed on the SANS pattern that was obtained at room temperature prior to annealing is representative of the cuboidal shape and spatial arrangement of the γ' precipitates obtained after standard heat treatment. This fourfold symmetry becomes twofold during the annealing. As expected, the SANS intensity decreases along the [100] or [010] crystallographic direction during the annealing.

Conclusion:
The origin of the SANS pattern morphology change observed during the annealing is believed to be the rafting of γ' particles. However, this result needs to be confirmed by SEM observations.

References:
[1]. M. Durand Charre, "The microstructure of superalloys" ISBN: 90-5699-097-7 Gordon & Breach Science Publishers (1997)
[2]. N. Ratel, G. Bruno, P. Bastie, T. Mori, submitted to Acta Mater.
[3]. M. Véron, P. Bastie, Acta Mater., Vol.45, No. 8, 3277-3282 (1997)
[4]. U. Keiderling, Appl. Phys. A74 [Suppl.], S1455-S1457 (2002)

	EXPERIMENTAL REPORT **Influence of the load-axis direction on γ' morphology in creep-exposed single-crystal Ni-base superalloy CMSX-4**	Proposal N° MAT-04-1206 Instrument **V4** Local Contact Albrecht Wiedenmann
Principal Proposer: Experimental Team:	J. Zrník – TU Kosice, SK P. Strunz – ASCR NPI Rez, CZ J. Zrník – TU Kosice, SK A. Wiedenmann – HMI, Berlin	Date(s) of Experiment 26.07. – 30.07.2006

Date of Report: 08.01.2006

In nickel-base superalloys, the morphology of the originally cuboidal γ' precipitates is considerably altered by application of an uniaxial external stress at high temperatures. This phenomenon (rafting), corresponds to a formation of large plates perpendicular to the stress direction. Specimens of the single-crystal superalloy CMSX4 were loaded under tensile stress at various temperatures and they exhibited different deformation behaviour (strain to ruprure and time to fracture) for load-axis orientations <001> and <111>. The bulk-sensitive SANS method was used for the assessment of the morphological changes corresponding to the observed dependence on mutual crystallographic- and load direction.

CMSX4 was investigated by SANS after various loadings (temperature, stress - see Table) and at two orientations of load axis. Euler cradle was used to set the samples to special orientations.

Sample	Load axis	Temp. (°C)	Nominal stress (MPa)	Time to rupture (h)	Creep strain to rupture
C397h	<001>	---	---	---	---
C397	<001>	750	780	1000	15
D431	<001>	900	500	100	21
E430	<001>	900	300	2000	27
E415	<001>	950	250	500	30
B398h	<111>	---	---	---	---
B398	<111>	750	780	500	22
C404	<111>	900	500	50	22
E451	<111>	900	300	4000	20
A396	<111>	950	250	2000	20

The measurements were evaluated by NOC program for anisotropic SANS data treatment [1]. As a model, ordered cuboidal or rafted precipitates were used. The resulting scattering curves and models for samples C397 and E430 are displayed in Fig. 1. Scattering curves are displayed for two orientations out of the nine measured (ω-rotation and sample tilt).

Among the samples with the load axis <001>, the sample exposed at 750°C with 780MPa (time to rupture 1000h) showed no rafting indication (as the scattering pattern has fourfold symmetry when <100> as well as <001> are perpendicular to the beam), whereas the sample exposed at 900°C with 500MPa (100h) showed partial rafting. The other two samples exposed at 900°C with 300MPa (2000h) and at 950°C (250MPa, 500h) exhibited full rafting (practically no depedence of the SANS pattern on the rotation around the load axis).

The estimation of the morphology of the precipitates for samples with load axis <111> is more difficult as the raft microstructure is expected to be more complicated. Nevertheless, preliminary evaluation shows that the sample exposed at 750°C with 780 MPa (500h) exhibits no rafting and the same is highly probably valid for the sample exposed at 900°C with 500 MPa (50h). The other two samples (900°C, 300 MPa, 4000h and 950°C, 250 MPa, 2000h) exhibited nearly full rafting.

It can be deduced that the diffusion effects do not last long enough to form rafts for the samples exposed at lower temperatures and higher stresses. A quantitative comparison of <001> and <111> loaded samples in view of raft-formation-begin shows that there is not a striking difference, although some variations exist. Detailed evaluation of the more complex morphology for <111> orientation is beeing carried out.

[1] P. Strunz , R. Gilles, D. Mukherji and A. Wiedenmann: J.Appl.Cryst. **36** (2003) 854-859

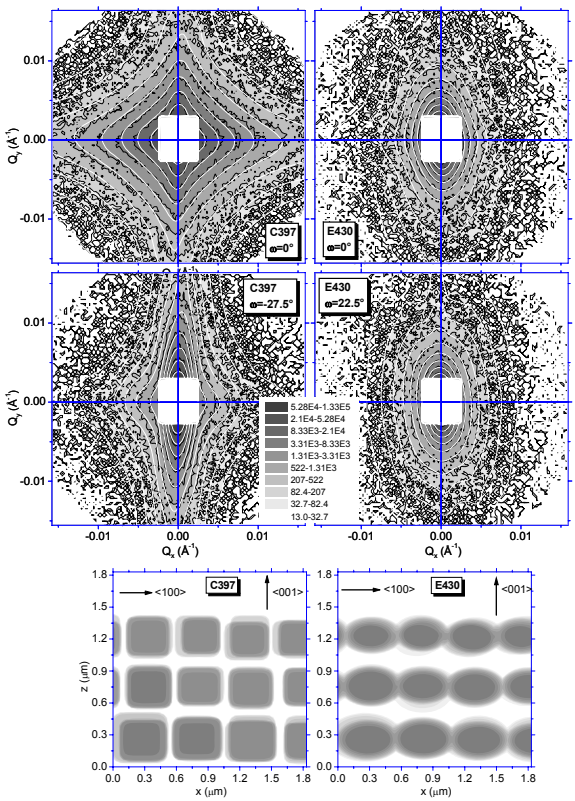

Fig: *Measured (gray scale) and fitted (white equiintensity lines) 2D scattering curves in logaritmic scale and the projections of the models corresponding to the fit.*

	EXPERIMENTAL REPORT SANS studies of Nd Fe Co Al alloys	Proposal N° MAT-04-1249-EF Instrument **V4** Local Contact Albrecht Wiedenmann
Principal Proposer: Experimental Team:	O. Perroud, E. Garcíca-Matres – HMI, Berlin A. Wiedenmann – HMI, Berlin O. Perroud, E. Garcíca-Matres – HMI, Berlin A. Wiedenmann – HMI, Berlin	Date(s) of Experiment 26.05. – 02.06.2004

Date of Report: 17.01.2007

In previous work and reports [1,2,3], we present the experiments realised on the hard magnetic Nd-Fe-Co-Al alloys. This report will now give some information about the results found by this experiment. The aim of the small angle neutron scattering investigation was to analyse the nanostructure of the $Nd_{60}Fe_xCo_{30-x}Al_{10}$ alloys as a function of temperature and magnetic field. We intended to explore the magnetic structure of the alloy containing 7.5% iron.

Small-angle neutron scattering were carried out at the instrument V4 with the help of a cryo-magnet that allows to measure between 5 K and 300 K and with a magnetic field on the sample up to 6 T.

$Nd_{60}Fe_{7.5}Co_{22.5}Al_{10}$ ingots were prepared by melting 99.9% pure Nd, Fe, Co and Al in an arc-melting furnace under argon atmosphere. The bulk cylinder of 3 mm diameter was obtained by ejecting the melt into a copper mould. The sample was cut in small pellets of 1 mm thickness.

The radially averaged scattering intensity plotted in Fig. 1 show the evolution of the intensity depending on the temperature. Fig. 2 is the interference term I- - I+ from the measurement with polarized neutrons.

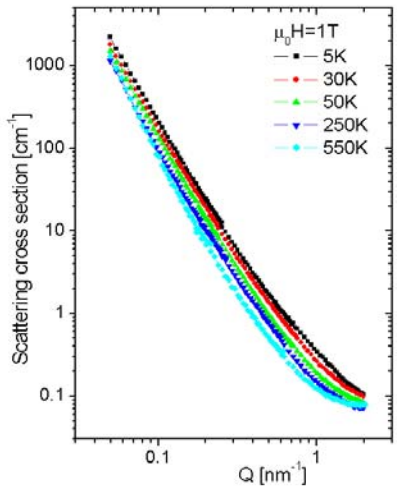

Fig. 1: *Sample $Nd_{60}Fe_{7.5}Co_{22.5}Al_{10}$ measured by $_0H$ = 1 T. Influence of the temperature of the sum (I- + I+)/2.*

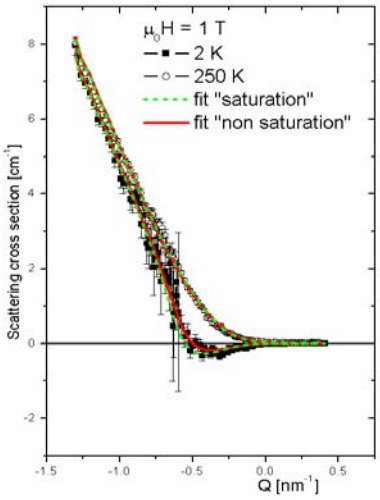

Fig. 2: *Sample $Nd_{60}Fe_{7.5}Co_{22.5}Al_{10}$ measured by $_0H$ = 1 T. Interference term I- - I+. The lines corresponds to the fit of a model in the case of a saturated sample (dash line) and random orientated magnetic domains (continuous line).*

The magnetic field dependence (not shown here) give only a small effect of the intensity. The reason is probably that the sample is very hard to saturate. Fig. 2 show two types of fit for the interference term. The first one considers a saturation of the sample (dash line) and the other that the sample assumes random orientated magnetic domains (continuous line). Both models can fit reasonably the intensity I- - I+ but only the second one is consistent with the sum ((I- + I+)/2 in fig. 1). Therefore can be conclude the presence of randomly orientated magnetic domains in the sample (see also [4]). The size of this domain is a few nanometers. This size corresponds also to the calculation in [5] for 4f-based alloys with a random local anisotropy.

This work is supported by DFG-Wi-1153/3-1

References :

[1]. MAT-04-800, MAT-04-1067-EF
[2]. E. García-Matres et al, Physica. B **350** e315-e318 (2004)
[3]. Perroud et al., Mat. sc. and eng. A (2006)
[4]. G. Kumar et al, J. of Alloys and Compounds **248** 309 (2003)
[5]. O'Handley, J. Appl. Phys. **62** R15-R49 (1987)

BENSC	**EXPERIMENTAL REPORT** **Dynamics of field-induced dipolar bands in colloidal dispersions of magnetite (preliminary session)**	Proposal N° PHY-04-1387 Instrument **V4** Local Contact Albrecht Wiedenmann
Principal Proposer: Experimental Team:	B. Erné – Univ. Utrecht, NL M. Klokkenburg – Univ. Utrecht, NL S. Prévost – HMI, Berlin A. Wiedenmann – HMI, Berlin	Date(s) of Experiment 23.10. – 26.10.2006

Date of Report: 04.01.2007

In our last SANS(POL) experiments,[1] we discovered field-induced hexagonal bands in colloidal dispersions of nearly monodisperse magnetite (Fe_3O_4) nanoparticles (Figure 1), structures whose presence was subsequently confirmed by cryogenic electron microscopy (Figure 2), leading to a first joint publication.[2] A manuscript describing the SANS(POL) results will soon be submitted. The dipolar bands are due to attraction between dipolar chains of nanoparticles, and theory predicts that one reason why the chains attract each other is thermal fluctuation of particle positions in the chains.[3] To test the theory, it was proposed to perform time-resolved stroboscopic SANS, a technique recently introduced at BENSC/HMI.[4] The key evidence that would support the theory is if on the length scale of individual particles, motion were slower along the field direction than perpendicular to it.

The present report relates to preliminary experiments that were carried out in the beam time of Dr. Wiedenmann. A close cycle refrigerator was installed inside the ac-field coil allowing to cool down the ferrofluid samples to 66 K. Additionally to the ac field (100-500Hz) with an amplitude up to 20 mT, a dc field up to 40 mT could be superimposed. The data is presently being analyzed and this will still require much more work. New software needs to be written to take into account time-dependent structure factors. Qualitatively, it was seen that the previously investigated structures [1] respond to an alternating magnetic field and that the characteristic time scales indeed appear to be dependent on the spatial orientation. A more extensive stroboscopic SANS session has been granted by BENSC/HMI with beam time from January 5-10, 2007. We look forward to those results.

This research has been supported by the European Commision under the 6th Framework through the Key Action: Strengthening the European Research Infrastructures. Contact nº: RII3-CT-2003-505925(NMI 3).

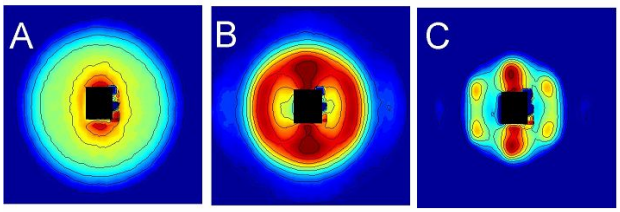

Fig. 1: *2D SANS intensity patterns of Fe_3O_4 nanoparticle dispersions with diameters of 12, 16, and 21 nm at room temperature at 1 Tesla (field perpendicular to the incoming neutrons).[1]*

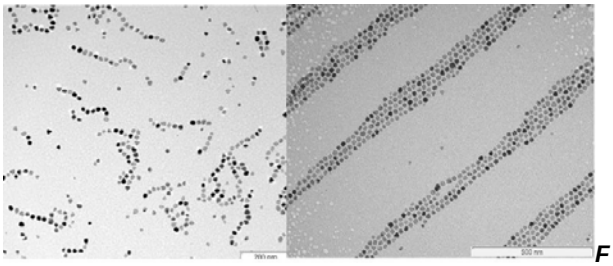

Fig. 2: *Cryogenic transmission electron microscopy (left) without field and (right) with field.[2] The origin of the hexagonal SANS patterns (Figure 1) is now obvious.*

References:

[1]. B. Erné, M. Klokkenburg, A. Wiedenmann, Experimental report "Nanostructures in Colloidal Dispersions of Nearly Monodisperse Magnetite", BENSC experiment PHY-04-1154 (V4 instrument: 07 Sept-16 Sept, 2006).

[2]. M. Klokkenburg, B.H. Erné, J.D. Meeldijk, A. Wiedenmann, A. Petukhov, R.P.A. Dullens, and A.P. Philipse, "In situ imaging of field-induced hexagonal columns in magnetite ferrofluids", *Phys. Rev. Lett.* 97, 185702 (2006). – identified as a "Research Highlight" by *Nature Nanotechnology*, 17 Nov. 2006.

[3]. E.M. Furst and A.P. Gast, "Dynamics and lateral interactions of dipolar chains", *Phys. Rev. E* **62**, 6916 (2000).

[4]. A. Wiedenmann, U. Keiderling, K. Habicht, M. Russina, and R. Gähler, "Dynamics of field-induced ordering in magnetic colloids studied by new time-resolved small-angle neutron-scattering techniques", *Phys. Rev. Lett.* **97**, 057202 (2006).

	EXPERIMENTAL REPORT **Liquid water formation in fuel cells - component optimization by means of neutron radiography**	Proposal N° MAT-04-1221 Instrument **V7** Local Contact Nikolay Kardjilov
Principal Proposer: Experimental Team:	C. Hartnig – ZSW, Ulm I. Manke – HMI, Berlin J. Kaczeroski – ZSW, Ulm N. Kardjilov, A. Hilger – HMI, Berlin	Date(s) of Experiment 16.01. – 22.01.2006 19.06. – 25.06.2006

Date of Report: 17.01.2007

Neutron radiography was used to study the influence of the degree of hydrophobization of the gas diffusion layers (GDLs) on the liquid water development and storage in operating Polymer Electrolyte Membrane Fuel Cells (PEMFCs). In previous projects neutron radiography at the neutron facility CONRAD has been proved as suitable tool to study the water management in single fuel cells as well as multi-cell stacks [1,2].

PEMFCs are developed for a wide range of mobile, portable and stationary applications. A well-balanced water management is a critical point in state-of-the-art PEM fuel cells. The product water stemming from the fuel cell reacition as well as the water originating from the humidification of the reactant gases are crucial in several ways for operating the fuel cell as a minimum humidifaction has to be ensured for a proper performance whereas excess water leads to flooding effects in the cell. Thereby, the GDL is the key component in a fuel cell that has to be optimised in order to ensure an optimal humidification and to prevent at the same time flooding of the catalyst layer and the porous structures.

In this work materials with varying content of PTFE and attached microporous layer (MPL) for gas diffusion layers (GDL) were investigated. In order to compare directly the different properties a segmented setup for the GDL was employed. In the first approach, a hydrophobic GDL with 5% PTFE on the left part of the cell and an untreated ('raw') GDL with prevalent hydrophilic properties were combined as this represents a considerable difference in terms of hydrophobicity. A neutron radiography image of these experiments is shown in Fig. 1 (top). From a first qualitative consideration it turns out that the left, hydrophobic side contains more liquid water than the hydrophilic GDL. The water content for the respective areas was quantified and the dependency of the water content on the current density analyzed. Figure 1 (bottom) shows that a significant difference in the water amount is found for low as well as for medium and high current densities. This introductory experiment proves the ability of neutron radiography to study properties of GDL materials.

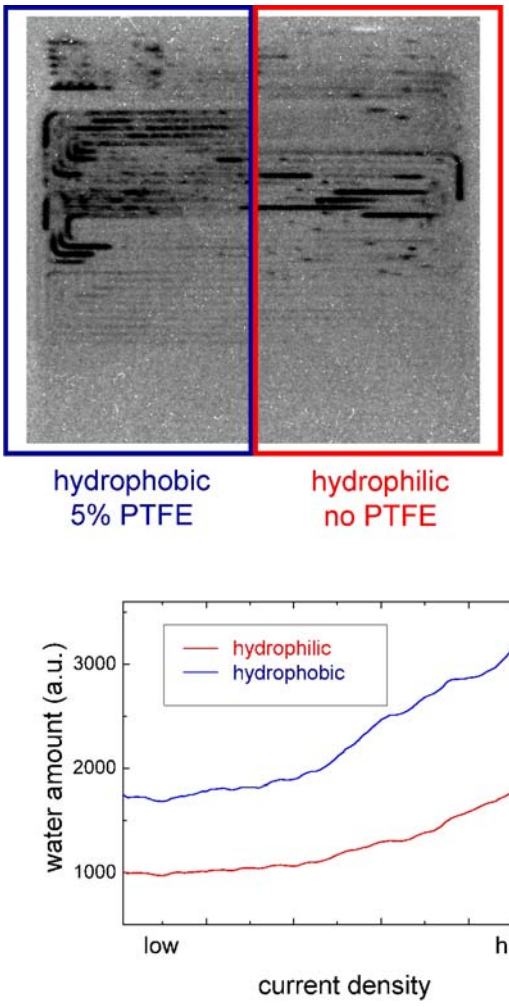

Fig. 1: *top: Neutron radiography image of an operating PEM fuel cell with a hydrophobic (left) and hydrophilic (right) GDL. bottom: Liquid water content of each segment as displayed in the upper image as function of current density.*

A more detailed study of the influence of material properties on the liquid water content is shown in Figure 2. Here the segmented GDL consists of three parts with different properties;

the PTFE content is varied within very narrow limits to determine the sensitivity of the method:

A 5% PTFE
B 3% PTFE
C 5% PTFE, no microporous layer (MPL)

On A and B the same hydrophobic MPL is attached.

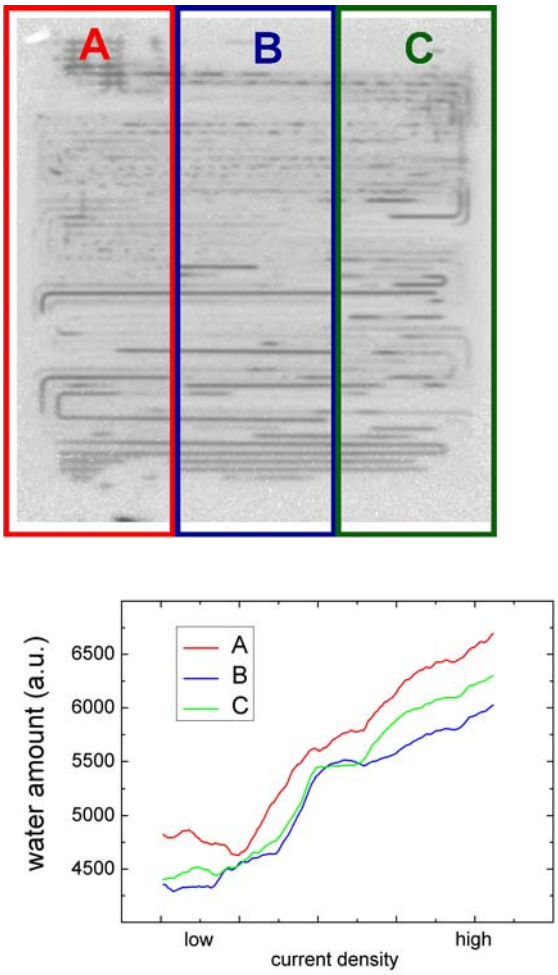

Fig. 2: *top: Neutron radiography image of an operating PEM fuel cell with three different GDLs. bottom: Liquid water content of each segment as displayed in the upper image as function of current density.*

In Figure 2 (bottom) the water content of each segment is quantified. Even for slight variations a significant difference in the amount of accumulated water can be observed.As already observed in the first example, the material B with the lowest PTFE content contains the lowest amount of liquid water. Special attention has hereby paid to the relative differences detected by neutron radiography compared from samples 1 to samples 2.

The results underline that the application of segmented GDLs is a very promising method for a fast screening of different materials to study the effects of varying hydrophobicity and other material parameters on the water management.

References:

[1]. [1]Ch. Hartnig, I. Manke , N. Kardjilov, A. Hilger, M. Grünerbel, J. Kaczerowski, J. Banhart, W. Lehnert, *Combined neutron radiography and locally resolved current density measurements of operating PEM fuel cells*, submitted to Journal of Power Sources

[2]. [2]I. Manke, Ch. Hartnig, N. Kardjilov, M. Grünerbel, A. Hilger, J. Kaczerowski, W. Treimer, M. Strobl, W. Lehnert, J. Banhart, *Quasi-in situ neutron tomography on polymer electrolyte membrane fuel cell stacks*, submitted to Applied Physics Letters

	EXPERIMENTAL REPORT **Liquid water formation in gas diffusion layers of fuel cells**	Proposal N° MAT-04-1214 Instrument **V12a** Local Contact M. Strobl, W. Treimer
Principal Proposer: Experimental Team:	C. Hartnig – ZSW, Ulm M. Strobl – TFH Berlin + HMI, Berlin I. Manke – TU Berlin N. Kardjilov, W. Treimer – HMI, Berlin	Date(s) of Experiment Feb. 2006

Date of Report: 17.01.2007

Ex-situ measurements investigating possible liquid water agglomerations in small pores of the gas diffusion layers (GDL) used in polymer electrolyte fuel cells (PEMFC) have been performed as a test for eventual in-situ measurements. For that purpose Al sample holders with round chambers for 2 – 3 layers of GDLs surrounded by an O-ring have been constructed including a channel in order to press in water through a drain tube. H_2O has been replaced by D_2O to avoid excessive incoherent scattering and because D_2O matches the scattering contrast of the GDL material (Toray paper) quite well. D_2O allows also for various cross fitting procedures of scattering curves achieved from the empty cell, the dry GDLs and the partially water filled GDLs. Unfortunately, the provided sample cells for these test measurements were not completely tight and so the exact amount of water inserted into the chamber could not be determined. In the measurements, the amount of D_2O inserted into the sample chamber has been increased from the measurements GDL1 to GDL3. The measurements of the dry and the wet GDLs have been fitted with the curves from the empty cell using monodisperse structural models. These fits provide pore size distributions of the GDLs and in the 'empty' case of the dry pores only. A third fit of the dry GDL measurements fitted with the corresponding wet GDL measurements should under certain circumstances be able to provide the size distribution of pores filled with D_2O. This method seems to work (at least qualitatively) in the cases GDL1 and GDL2. In the case of GDL3 (the highest amount of D_2O) the interpretation of the results is more difficult but seems to indicate that some neighboring pores of completely filled pores are only partially filled. Therefore pores smaller than originally present can be found while heavy water droplets larger than pores originally present can be detected as well (One might be aware that pores and GDL material can not be distinguished in the wet case).

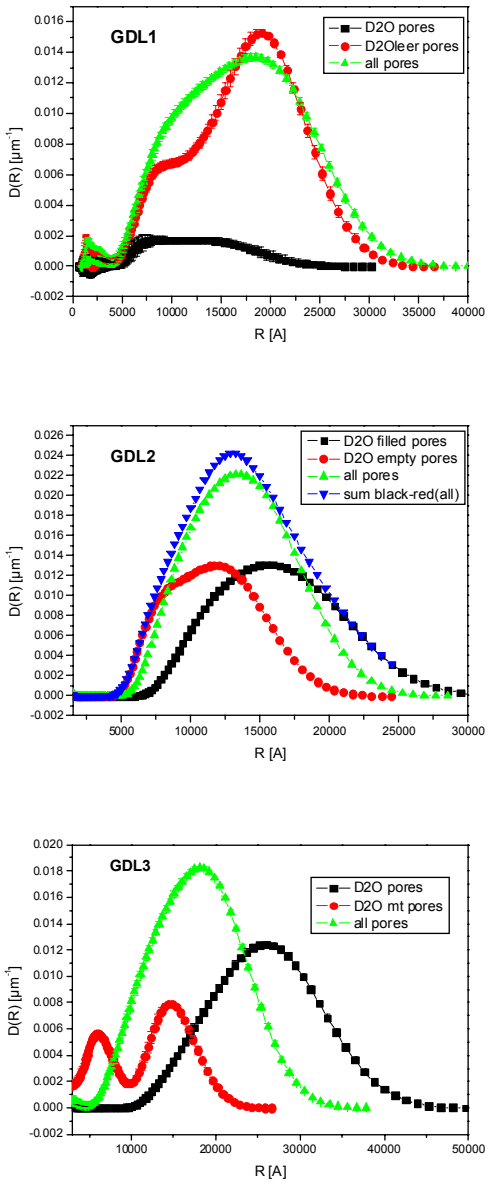

Fig. *Dry pores, wet pores and total pore size distributions for 3 GDL measurements*

	EXPERIMENTAL REPORT **Phase transitions and properties of nanostructured (x)KNO_2-(1-x)$NaNO_2$ solid solutions**	Proposal N° MAT-01-1774 Instrument **E9** Local Contact Michael Tovar
Principal Proposer: Experimental Team:	A. Naberezhnov – RAS Ioffe PTI St. Petersbg. M. Tovar – HMI, Berlin	Date(s) of Experiment 01.02. – 09.02.2006

Date of Report: 29.10.2006

The principal goal of this experiment was to study the peculiarities of the ferroelectric phase transitions of nanostructured (x)KNO_2-(1-x)$NaNO_2$ solid solutions produced by intrusion of melted solid solutions into porous glasses with average pore diameter 7±0.5 nm. The pores in these glasses form the dendrite random interconnected net. The volume amount of embedded materials achieved 20-22%. It is shown that finite-size effect results in the drastic changes of the phase transition (PT) features, and these anomalies become especially significant if the characteristic size is comparable with correlation length of the order parameter critical fluctuation. In particular the confined $NaNO_2$ shows the giant dielectric permittivity ε in the paraelectric phase above 420 K [1], but the temperature region, where the giant ε exists, is essentially above room temperature where this property has practical importance. One of the methods to decrease the T_C is dilution of the ferroelectric material by pure dielectric admixture. KNO_2 is dielectric and has no ferroelectric PT.

Neutron diffraction measurements were performed on E9 in the temperature region RT<T<447K, i.e. below and above the bulk PT temperature. The diffraction patterns at 350 K for x = 0, 0.05 and 0.1 are presented in Fig. 1. The arrows indicate the positions of Bragg peaks depending on order parameter.

Principle results are:

- Average sizes of nanoclusters for confined solid solutions are about 40 nm at all temperatures for both materials and coincide with size of nanoparticles in a case of embedded sodium nitrite.
- Structures of solid solutions correspond to the bulk $NaNO_2$ orthorhombic structure.
- At x=0.05 the Bragg peaks depending on order parameter are suppressed and this is not texture effect. At x=0.1 the ratios of reflection intensities differ essentially from analogous ones in confined $NaNO_2$ especially at small Q. The nature of these phenomena is not clear at present time, <u>but they did not observed in the bulk materials</u> [2].
- Unfortunately T_C (~ 425 K) for both solid solutions corresponds practically to the value observed in confined $NaNO_2$ within 7 nm pores [3] and this result is confirmed by measurements of dielectric permittivity ε. At the same time both confined materials demonstrate the giant growth of real and imaginary parts of ε in vicinity and above T_C [2]. Temperature dependence of order parameter follow a power law $(1-T/T_C)^{\beta}$ with β = 0.31±0.03 corresponding to 3D Ising model.

The results were presented on 9th International Conference Dielectric and Related Phenomena IDS&DRP 2006 Poznan, Poland 3-7 September 2006

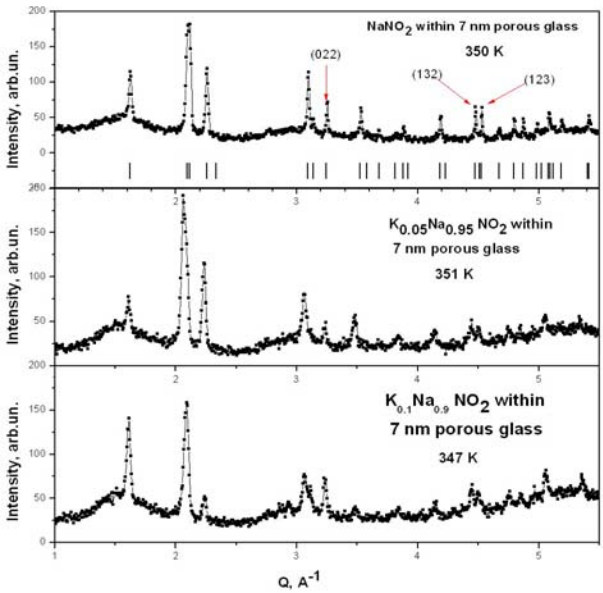

Fig.1: *Diffraction patterns for nanostructured (x)KNO2-(1-x)NaNO2 solid solutions at x= 0, 0.05 and 0.1*

References:

[1]. S.V.Pan`kova et al., J. Phys.: Condens. Matter, **8**, L203 (1996).

[2]. A. Filimonov, A. Naberezhnov, M. Tovar et al., Abstracts of 4th Conference International Dielectric Society and 9th International Conference Dielectric and Related Phenomena IDS&DRP 2006 Poznan, Poland 3-7 September 2006 pp. 209-210

[3]. A. Naberezhnov et al., Eur. Phys. J. E **12**, (2003), s21-s24

	EXPERIMENTAL REPORT **Residual Orientation in Injection Molded Polymer Samples**	Proposal N° MAT-04-1157 Instrument **V4** Local Contact Uwe Keiderlling
Principal Proposer: Experimental Team:	J. Healy – Monash Univ, Aus G. H. Edward – Monash Univ., Aus U. Keiderling – HMI, Berlin	Date(s) of Experiment 10.03. – 13.03.2006

Date of Report: 27.09.2006

Injection moulding is a common processing technique applied to thermoplastic materials. The injection moulding process is known to result in residual orientation in the finished part that manifests as anisotropic physical and optical properties.

Most studies on injection-moulded parts examine the overall local orientation through techniques such as Optical Birefringence or Infrared-dichroism. Small-Angle Neutron Scattering (SANS) is an excellent tool for measuring the overall molecular dimensions (monomer-monomer interactions at large length scales) in the bulk of a polymer sample. Unlike other techniques SANS provides information about the overall chain size, shape, and orientation and provides a unique tool for directly measuring the overall chain orientation rather than inferring the chain orientation from the average orientation of monomer segments. SANS is very sensitive to molecular orientation and has been applied to a number of such systems [1,2]. This study is an expansion of work published previously [3] to examine the orientation of chains of different length within a polydisperse matrix.

Partially deuterated Polystyrene blends of a single matrix with various narrow molecular weight distribution deuterated chains (4%w/w) were injection micro-molded into small rectangular plaques. Molecular weights for the deuterated chains included chains shorter than the critical entanglement length to chains just above the weight average molecular weight of the matrix.

The chain-scale orientation of the deuterated chains in each blend was measured using the V4 instrument at BENSC. A single orientation parameter was calculated by making an elliptical fit to isointensity contours of the fully reduced SANS data and extrapolating the eccentricity to the Guinier limit (I(q)xq=1). This technique compares well with a traditional approach of applying a Guinier approximation fit to data extracted using narrow sector averages along the orthogonal axes of the SANS data. The orientation was converted into a molecular draw ratio in each case assuming that the chain deformation was uniaxial and affine at long length scales.

The resultant orientation measured for a given thermal and shear history is shown in Chart 1. As expected, the orientation was seen to increase with increasing chain length with no observable orientation for chains below the critical entanglement length of polystyrene (~13kg/mole).

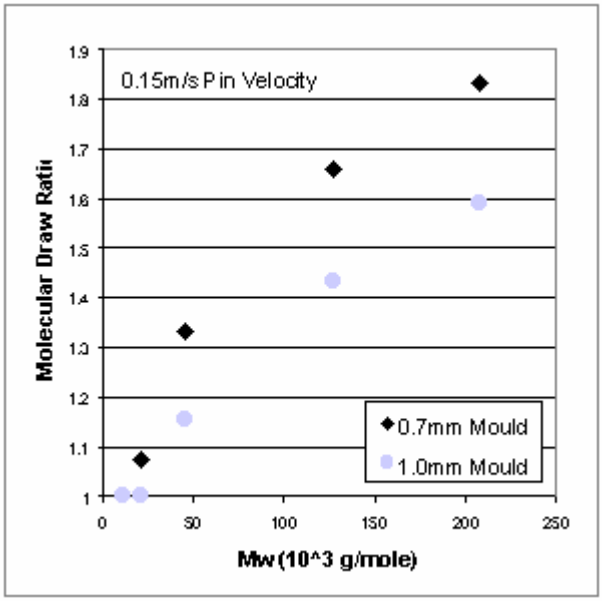

***Chart 1**: Molecular Draw Ratio vs deuterated chain weight*

References:

[1]. J. R. Schroeder, B. Hammouda, R. A. Bubeck, J. W. Chang, Journal of Polymer Science: Part B: Polymer Physics, **29**, 1607-1612, 1991.

[2]. G. Hadziioannou, L.-H. Wang, R. S. Stein, R. S. Porter, Macromolecules, **15**, 880-882, 1982.

[3]. J. Healy, G. H. Edward, R. B. Knott, Physica B, in press.

BENSC	**EXPERIMENTAL REPORT** **Structural Evolution of organic/inorganic nanohybrids incorporating titanium (IV) oxoalkoxyacylate nanoclusters**	Proposal N° MAT-04-1208 Instrument **V4** Local Contact André Heinemann
Principal Proposer: Experimental Team:	V. Hartley – Flinders Univ., Australia R. Knott – ANSTO, Australia A. Heinemann – HMI, Berlin	Date(s) of Experiment 06.03. – 19.03.2006

Date of Report: 24.03.2006

Objectives (limit 100 words)
One area of advanced materials development includes the fusion of organic with inorganic systems; one such system involves the incorporation of metal-oxide clusters into an established network polymer, poly methyl methacrylate – also known as Plexiglass in its commercial polymerised form.
An established Titanium (IV) oxide based cluster with methacrylate ligands is synthesised by the functionalisation of the metal alkoxide with organic ligands in a sol-gel process. The methacrylate ligands in this complex act as organic linkers on the 'surface' on the Ti_6O_4 core and these can then be polymerised into the compatible organic network polymer, PMMA. The role of the covalent link in modulating materials structure is the focus of this study.

Achievements/Difficulties (limit 250 words)
Two different types of Ti cluster were incorporated into a PMMA matix by free radical polymerisation. The PMMA matrix contrast was varied by the combination of different ratios of methyl methacylate and its perdeuterated analogue. Cluster 1 is $[Ti_6O_4(OEt)_8(OMc)_8]$ where Et = CH_2CH_3 and OMc is $O_2CC{=}CH_2CH_3$ and it polymerised into PMMA through its methacryl functionalities. Cluster 2 is $[Ti_6O_4(OEt)_8(OAc)_8]$ where OAc is O_2CCH_3 and is blended into PMMA during polymerisation of the matrix. To cover a broad range of particle sizes possible due to various degrees of particle agglomeration the following conditions were used with a wavelength of 6Å:
SD = 16m with COLL = 16; SD = 4m with COLL = 8; and SD = 1m with COLL = 8.
The scattering data of the poly(methyl methacrylate) (PMMA) matrices without either cluster 1 or 2 plotted as log(I) (cm_{-1}) vs log(q) (nm_{-1}) at high q (SD =1 m) are nice and flat, as we might expect for a "solvent-like" material (see Figure 1). In comparison, we have a q(-n) dependence in the samples containing either cluster 1 or 2 (see Figure 2); it's very clear that the presence of both clusters is modulating the structure.
The acetate and methacrylate cluster data are different, as we might expect. However, the acetate cluster does appear to be modifying the structure of the polymer matrix as well, even though it is not covalently bound to the matrix (compare scattering data for S1/S6; and S1/S12).
Further study involves modelling the scattering from the polymer matrices and in addition, subtracting scattering from the polymer to examine and model fit the scattering data from the clusters only. The model for the clusters at this point is core-shell with the Ti_6O_4 being the core and the acetate or methacryl ligands comprising the shell.

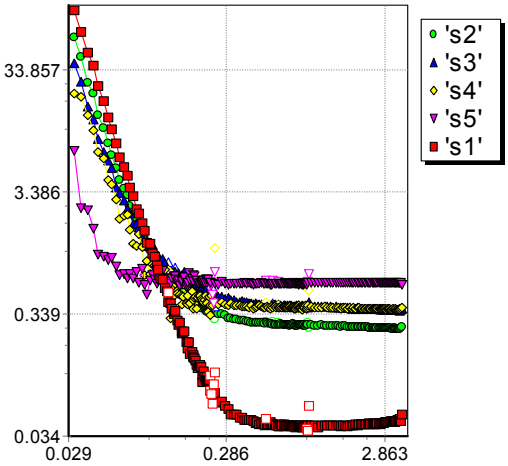

Fig. 1: log(I)(cm^{-1}) vs log(g)(nm^{-1}) of matrices

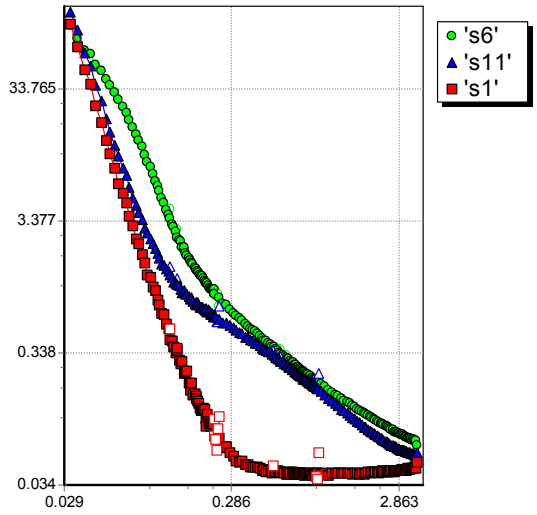

Fig. 2: log(I)(cm^{-1}) vs log(q)(nm^{-1}) of cluster doped samples

Sample #	d-MMA %	Loading level	Cluster Type
1	100	none	none
2	75	none	none
3	50	none	none
4	25	none	none
5	0	none	none
6	100	0.3mol%	$Ti_6O_4(OEt)_8(OMc)_8$
11	100	0.3mol%	$Ti_6O_4(OEt)_8(OAc)_8$

Table 1: *Selected samples from sample regime of 22 samples*

	EXPERIMENTAL REPORT **SANS investigation of 3Y-TZP superplastically deformed ceramics**	Proposal N° MAT-04-1266 Instrument **V4** Local Contact Martin Kammel
Principal Proposer: Experimental Team:	V. Ryukhtin – ASCR NPI Rez, CZ J. Šaroun – ASCR NPI Rez, CZ M. Kammel – HMI, Berlin Y. Motohashi – Ibaraki Univ., JP	Date(s) of Experiment 21.09. – 24.09.2006

Date of Report: 15.12.2006

Discovering of superplasticity effect in yttria-stabilised tetragonal zirconia polycrystals (Y-TZP) has triggered an extensive international research on ceramics superplasticity in last fifteen years. This phenomenon makes such ceramics very attractive from industrial point of view. Cavitation is closely connected with important mechanisms of superplastic deformation (SPD) in ceramics. Generally, cavities and/or cracks in conventional ceramics propagate in a direction perpendicular to the axis of an applied tensile stress. In contrast to conventional ceramics, the cavitation mode in 3Y-TZP (with 3 mol% of yttria) is similar to that in metallic systems where cavities grow and align in parallel to applied stress.

Our recent SANS experiments have detected the formation of new type of cavitation – flat cavities during high strain-rate superplastic deformation in 3Y-TZP [2]. These perpendicular to applied stress cavities have been found by means of SANS for the first time ever even at very early stage of SPD, *i.e.*, just in the yielding period of the tensile deformation. If so, the actual yield stress must have been higher than the observed one. This fact may affect the discussion of the mechanism of SPD in ceramics.

In this SANS experiment we studied *ex-situ* 3Y-TZP samples deformed under different SP deformation regimes up to true strain of e=10...30 % and up to yield point (e=0%). SPD of the specimens were carried out under constant strain rate at temperature T=1450 ^{0}C.

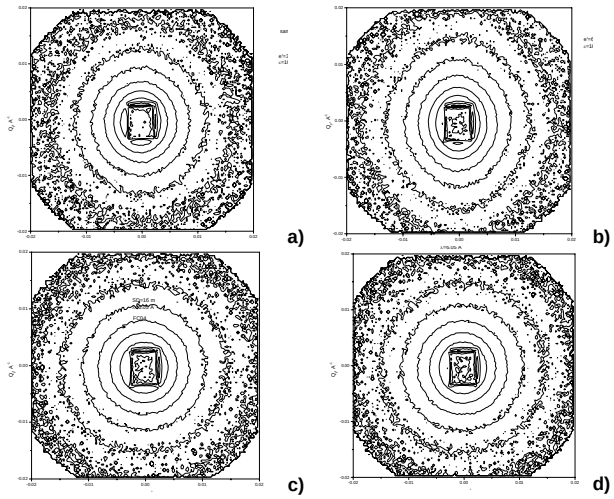

Fig. 1. *Scattering from the Y-TZP specimens deformed at (a) e'= 3.33x10^{-3} s^{-1} and (b) e'= 6.67x10^{-3} s^{-1} up to true strain of e=10% with (c) e'= 3.33x10^{-3} s^{-1} and (d) e'= 6.67x10^{-3} s^{-1} up to e=0% (at yield point) at temperature T=1450 ^{0}C.*

The specimens were installed vertically during the SANS experiment, *i.e.* strain direction is vertical as well. Incident beam was defined by rectangular cadmium aperture of size 2x10 mm^2 in order to avoid of refractions from sides of samples.

2D SANS scattering patterns are shown in Fig. 1. Slight anisotropy can be observed for the both samples even at very small deformations (e=10%, see Fig 1 a, b). Anisotropy is oriented vertically in the both cases but aspect ratio is slightly higher for material deformed at deformation rate e'= 6.67x10^{-3} s^{-1} (see Fig. 1 b) than for that deformed at two times lower deformation rate e'= 3.33x10^{-3} s^{-1}. Such orientation says about domination presence of cavities and fine cracks oriented perpendicular to applied stress and formation of prolate cavities with longer axis parallel to applied stress was not detected at such stages. Scattering for samples deformed just up to yield point are fully isotropic (see Fig. 1 c, d). Obviously, there are no the transversal cracks, the scattering arises due to residual porosity which randomly oriented in bulk of the samples.

However, the limited resolution on pin-hole instrument doesn't permit us to cover whole size range of cavities and pores in such materials; typically it is between 0.1 μm and 1 μm. The measured scattering functions obey the Porod's law, *i.e.* it is proportional to Q^{-4} in whole covered Q-range of the used facility (V4 SANS). Size information of the cavitation in studied materials could be obtained by means of ultra small-angle neutron scattering (USANS) techniques – DBC-SANS and/or DC-SANS. Nevertheless pin-hole measurements is important for such investigations because it extends Q-range toward bigger values and the pin-hole SANS permits to measure directly anisotropic scattering patterns in contrast to DC-SANS instruments. Simultaneous analysis of the data from both SANS techniques would provide unique information about behaviour of the caviataion in bulk of the studied material at early stages of SPD.

The research was partially support by grant agency of the Czech Republic 202/06/P198.

References:

[1]. V. Ryukhtin, J. Šaroun, S. Harjo, Y. Motohashi, M. Baron and R. Loidl, J. Appl. Cryst. **36** (2003) 478-483.

[2]. V. Ryukhtin, J. Šaroun, S. Harjo, Y. Motohashi, A. Wiedenmann, P. Strunz, Physica B, **350**, 1019-1022 (2004).

	EXPERIMENTAL REPORT **In-situ observation of the γ' microstructure in pre-deformed single crystal superalloys**	Proposal N° MAT-04-1267 Instrument **V4** Local Contact Albrecht Wiedenmann
Principal Proposer: Experimental Team:	P. Strunz – ASCR NPI Rez, CZ P. Strunz – ASCR NPI Rez, CZ H. Klingenhöffer – BAM, Berlin U. Keiderling, G. Schumacher – HMI, Berlin A. Wiedenmann – HMI, Berlin	Date(s) of Experiment 08.11. – 13.11.2006

Date of Report: 05.01.2007

Single-crystal Ni-base superalloys exhibit directional coarsening of γ' precipitates (rafting) during high-temperature creep. Recently, rafting was observed also at purely thermal treatment without the simultaneous presence of an external load when the superalloy was pre-deformed at relatively low temperatures. The observations of γ'-rafting in absence of external strain does hardly fit in the present models of raft formation. To study the precipitate-morphology evolution of pre-deformed superalloy in detail, in-situ SANS and X-ray investigation of single-crystal superalloy at high temperature was performed.

For the experiment, specimens from SCA425 superalloy were prepared. The bars were deformed at room temperature to strains 0.1% and 0.5% in compression along <001> crystallographic direction. Then, the plate-like SANS samples were cut out with the normal parallel to <010>. SANS measurements at elevated temperatures were performed at 940, 1050 and 1100°C, always with a hold lasting from 6 to 16 hours.

The measurements were evaluated by NOC program for anisotropic SANS data treatment [1]. As a model, ordered cuboidal particles were used.It was observed that the increase of the temperature and also hold at the temperature causes that originally nearly cubic precipitates become more rounded and finally nearly spherical. The resulting dependence for sample No. 2 (strain 0.5%) is displayed in Fig. 1. {Parameter β defines the rounding [1]: the object is a sphere for β=1 and it becomes more cuboidal when β decreases towards zero. In the limit (β -> 0), the object is the exact cube.}

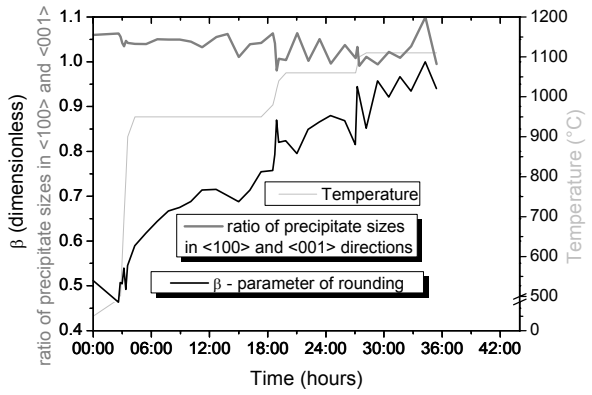

Fig. 1: *Time and temperature dependence of parameter β and $D_{<100>}/D_{<001>}$ ratio.*

Although certain morphological changes were visible, the rafting itself was not observed. The model, having independent size parameters of the precipitates in directions <100> and <010> on one side and <001> on the other, was fit to the data (the respective sizes are denoted $D_{<100>}$, $D_{<010>}$, $D_{<001>}$), so that generally $D_{<100>}=D_{<010>}\neq D_{<001>}$. The dependence of the ratio $D_{<100>}/D_{<001>}$ on thermal history is depicted in Fig. 1 as well. The ratio is always nearly equal to 1. Although there is no clear tendency of its evolution during the heat treatment, there might be a small decrease of the ratio and thus a very small elongation in <001> with time. This effect can be, however, also ascribed to the errors of measurement and evaluation. In any case, directional coarsening of the precipitates was not observed.

The causes why the used SCA425 samples did not show rafting (which is the opposite result with respect to the former observations in AM1 superalloy [2]) can be the following:

(i) insufficient straining, (ii) the orientation of the load (tensile stress used for AM1), (iii) compositional difference of the presently used superalloy (for example lower precipitate volume fraction at high temperatures in SCA425 which can hinder rafting, or different misfit dependence on temperature), (iv) different temperature of pre-deformation.

References:

[1]. P. Strunz, R. Gilles, D. Mukherji and A. Wiedenmann: J.Appl.Cryst. **36** (2003) 854-859

[2]. M. Veron, P. Bastie, Acta Mater. **45** (1997), 3277-3282

	EXPERIMENTAL REPORT **SANSPOL experiments on self-ordered arrays of electrodeposited Fe(x)Ni(1-x) nanowire materials**	Proposal N° PHY-04-1145 Instrument **V4** Local Contact André Heinemann
Principal Proposer: Experimental Team:	V. De La Prida – Univ. Oviedo, E J. Campo – Univ. Zaragoza, ICMA, E A. Heinemann – HMI, Berlin	Date(s) of Experiment 12.01. – 15.01.2006

Date of Report: 19.01.2007

Magnetic nanowires are among the most attractive nanometer-sized materials because of their unique properties that may lead to a huge variety of applications, including interconnections in magneto-optoelectronic and spintronic based devices [1]. Depending on the nanowires dimensions, two kind of electronic transport properties can be distinguished: classical conductance when the wires are much longer than the electron mean-free path and much thicker than the electron Fermi wavelength or quantum conductance when the wire is shorter than the electron mean-free path and its diameter is comparable to the electron wavelength. In this case, the quantum size confinement becomes relevant in the transverse direction of the wire and the electron transport becomes mainly ballistic, without collisions along the wire. In particular, magnetic nanowires are interesting systems in which carriers are confined in the radial dimension; even transport is only possible along the axial dimension of the nanowire. In some magnetic memory technology devices, the information is transmitted along ferromagnetic wires with submicrometer width by domain wall (DW) motion, being the device speed linked to the DW velocity. This peculiarity allows us fabricating regular arrays of magnetic elements with deep sub-micron feature sizes, each of which having uniaxial magnetic anisotropy and their easy axis oriented parallel or perpendicular to the substrate [1]. As a consequence of the nanometric size of the ferromagnetic nanowires, each single-domain nanowire could represent one bit, depending on its magnetization state. Motivated by the huge relevance this phenomenon plays, we planned to study by small angle neutron scattering (SANS) technique arrays of magnetic nanowires embedded into the self-ordered nanoporous alumina, in order to extract their local magnetic structure and correlations over a range of length scales. This experiment is a continuation of the previous one: PHY-04-1019.

In this experiment, we have performed a polarized neutrons SANS experience in the instrument V4, at BENSC in HMI, on arrays of ferromagnetic nanowires with nominal compositions of Fe(x)Ni(1-x), (x = 27, 78), and Co, with d = 35-40 nm in diameter, L = 5 microns in length and D = 105 nm of hexagonal lattice parameter. 2D SANSPOL diffraction patterns were collected at room temperature for the FeNi and Co samples, for detector distances of 12, 4 and 1 m, using the neutron wavelength of 6.07 Å, in the Q range 10-3 $Å^{-1}$ < Q < 2 $Å^{-1}$, and in the following configurations: without applied magnetic field, at the saturating magnetic field of 1 Tesla, at zero applied field again for the remanence state, and finally, at the coercive field value of each sample, so describing the different magnetic states of the hysteresis loop for this sample. The arrays of the ferromagnetic nanowires were perpendicularly aligned to the horizontally applied static magnetic field H in each case, and with rotating the sample respect to its vertical axis at low angles, in order to allow the separation of nuclear and magnetic scattering, as can be seen in the preliminary data treatment shown in the figure.

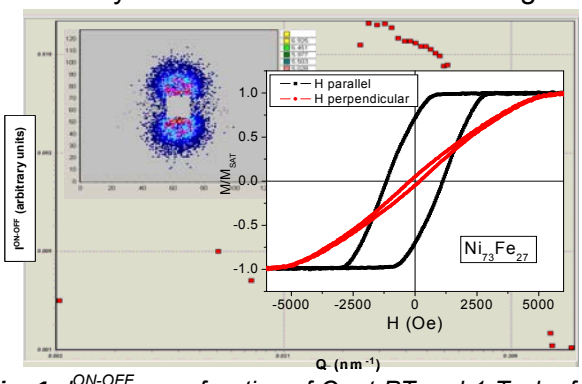

Fig. 1: *I^{ON-OFF} as a function of Q, at RT and 1 Tesla, for an array of $Fe_{27}Ni_{73}$ nanowires.*

Reference:

[1]. V.M. Prida et al, J. Nanosci. Nanotechnol, **7**, (2007) 272–285.

	EXPERIMENTAL REPORT **Structural and Magnetic Properties of Ordered Co Nanoparticles**	Proposal N° PHY-04-1200 Instrument **V4** Local Contact André Heinemann
Principal Proposer: Experimental Team:	S. Lee – Univ. Liverpool, UK S. Lee – Univ. Liverpool, UK R. Fan, J. P. Goff – Univ. Liverpool, UK A. Heinemann – HMI, Berlin	Date(s) of Experiment 06.01. - 14.01.2006

Date of Report: 09.03.2006

The magnetic and structural properties of Co nanoparticles were studied using SANSPOL. Thermal decomposition of Cobalt Octacarbonyl [1] enabled the fabrication of 6.5nm diameter spherical nanoparticles with a narrow size distribution. Slow evaporation of the particle-containing solvent on single-crystal Si substrates allowed the production of hexagonally ordered 2-D (single-layer) and 3-D (~ 5 layers) nanoparticle arrays, confirmed with TEM.

Studies of 2-D and 3-D samples were performed on instrument V4 using incident beam polarisation. Initial measurements were performed above the blocking temperature, T_B, at T=300K. The zero-field case is shown in figure 1. This has allowed the structural (isotropic) part of the scattering to be isolated.

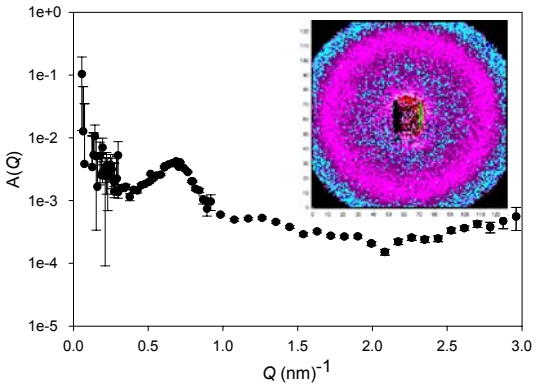

Fig. 1: *The isotropic component of intensity for a Co 3D array. A(Q) is defined [2] within the expression for SANS intensity: $I(Q)=A(Q) + B(Q)\sin^2\alpha$*

Application of *H*=1.1T at *T*=300K was sufficient to align the nanoparticle moments with the magnetic field. The saturated field case is shown in Figure 2.

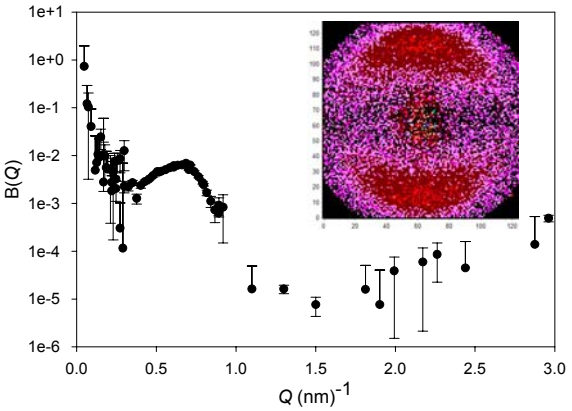

Fig. 2: *The anisotropic component, B(Q), with a saturating field.*

A preliminary analysis of the neutron data in a saturating-field and zero-field, when combined with TEM data, suggest that an oxide shell needs to be taken into account. SQUID measurements at *T*=100K reveal a strong exchange-bias in these samples, indicated by a field-shift in the hysteresis curve when the sample is cooled below T_B in a magnetic field. POLSANS measurements in zero-field performed under these conditions show that there are no magnetic correlations, indicating that the exchange-bias freezes the high-temperature configuration. This novel exchange-bias from the CoO shell provides a source of anisotropy that stabilises the magnetic moment of the Co cores, potentially helping to "beat the superparamagnetic limit" for high-density magnetic recording media. It is reminiscent of the behaviour for $Co_{core}CoO_{shell}$ particles in a CoO matrix[3], but more striking since this phenomena is observed with a non-magnetic matrix.

References:

[1]. C. Petit *et al. J. Phys. Chem. B* **103**, 1805-1810 (1999)
[2]. M. Bonini *et al. J. Phys. Chem B* **108**, 14901-14906 (2004)
[3]. V. Skumryev *et al. Nature* **323**, 850 (2003)

	EXPERIMENTAL REPORT SANSPOL Study of Solvent-Free Magnetic Fluid	Proposal N° PHY-04-1202 Instrument **V4** Local Contact Albrecht Wiedenmann
Principal Proposer: Experimental Team:	P. Baglioni – Univ. Firenze, I M. Bonini – Univ. Firenze, I E. Falletta – Univ. Firenze, I A. Wiedenmann – HMI, Berlin	Date(s) of Experiment 25.05. – 30.05.2006

Date of Report: 18.01.2007

Magnetic nanoparticles represents at the same time key components in modern technologies and useful model systems in fundamental research on dipolar fluids. In particular, highly concentrated ferrofluids are of outmost interest because of their peculiar properties, especially when they are exposed to an external magnetic field: in fact, by increasing the magnetic content in the ferrofluid it is possible to observe dramatic effects, such as partial or long-range ordering.

In this experiment we have prepared solvent-free magnetic fluids. This new class of colloidal systems consists of magnetic nanoparticles whose surface is covered by an appropriate cationic molecule. The charge balance is ensured by the presence of a counterion that provides the magnetic particles with the fluid-like behaviour when they are heated up to the counterion melting transition (see figure 1).

In details, fluids consist of $CoFe_2O_4$ magnetic nanoparticles (about 4 nm in radius) which were coated with an organosilane moiety terminating with a quaternary ammonium group. The counter ion of such a system consists of an organic molecule including a carboxylate group at the end of the alkylic chain (typically, a fatty acid). Namely, the counter-ions investigated in this study are laurate, stearate, poly(ethylene glycol) 4-nonylphenyl 3-sulfopropyl ether (herewith referred to as Aryl) and poly(ethylene glycol) n-alkyl 3-sulfopropyl ether (referred to as Ralufon). Samples were investigated at 50ºC, 70ºC and 100ºC, as well as at room temperature. In figure 2 the results obtained for the laurate, aryl and ralufon counterions at room temperatures are shown. The effect of the different counterions size is evident from the SANSPOL results, highlighting that it is possible the tuning of the nanoparticle distance within the ferrofluid.

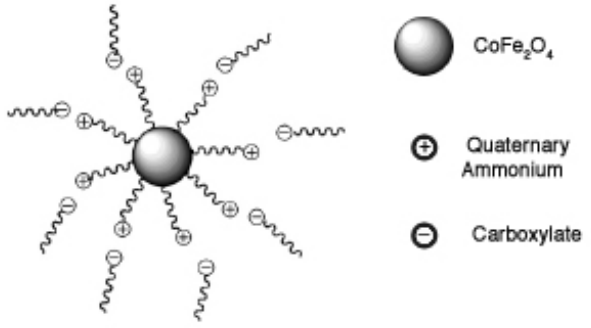

Fig. 1: *Sketch of the structure of the solvent-free magnetic fluids.*

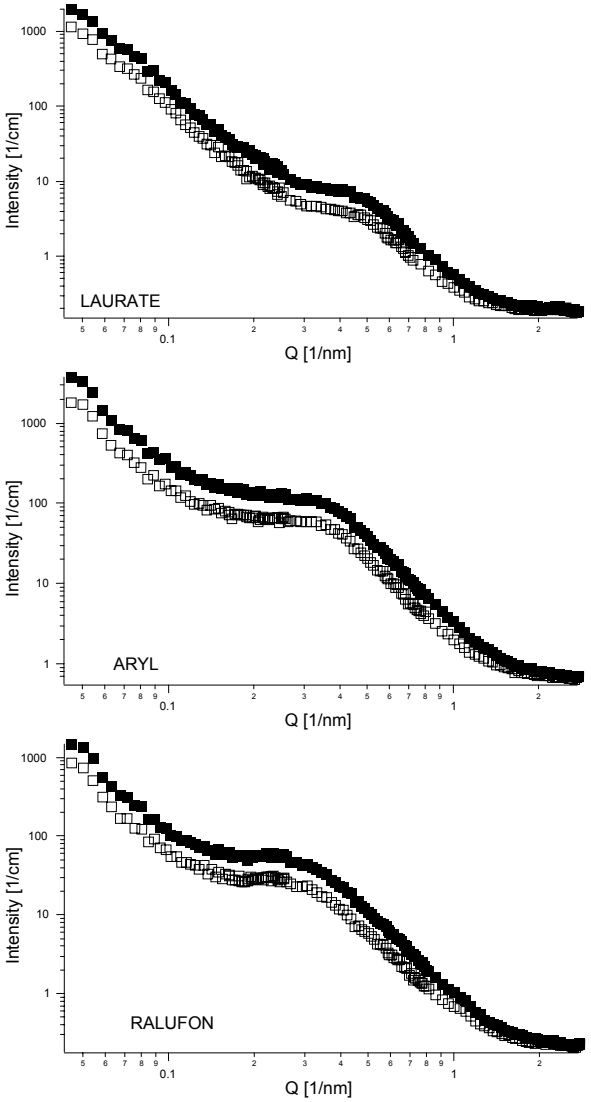

Fig. 2: *SANSPOL intensities perpendicular to the applied field for the samples with laurate, aryl and ralufon counterions at room temperature.*

	EXPERIMENTAL REPORT **Synthesis of magnetic cobalt nanoparticles: toward multilayer bimetallic process**	Proposal N° PHY-04-1344-EF Instrument **V4** Local Contact Sylvain Prévost
Principal Proposer: Experimental Team:	A. Wiedenmann – HMI, Berlin C. Giordano – Univ. Palermo, I S. Prévost – HMI, Berlin	Date(s) of Experiment 21.08. – 23.08.2006

Date of Report: 17.01.2007

Among the various applications suggested for magnetic nanoparticles, catalysis is of industrial interest. Catalytic magnetic particles would give the capacity to manipulate easily the catalytic agent with a magnetic field.

To achieve this result, a synthesis process has to be developed, to control the surface of the particle in several ways: control of the size, of the surface composition/state, and of the stabilizing coating.

A new collaboration with Cristina Giordano (Prof. Vincenzo Turco Liveri team, University of Palermo) is starting to obtain such a material. The precursor is a surfactant whose counter-ion has been exchange by Co^{2+}. These surfactants forms reversed micelles in apolar solvents. Hydrazine is then added to reduce the cobalt. Gold nanoparticles were already successfully synthesized by this team with this method [1].

The basic idea is to obtain a small Co core, with only a few surfactants as coating, to allow further step-by-step growing of the particles either with more Co-layers or with other metals, exhibiting catalytic properties (Rh, Ru, Yb…)

The first experiment was devoted to the analysis of the micellar structure when the coating agent is changed (no coating, short-chain carboxylic acid, long-chain carboxylic acid, or tetramethylammonium salt), to explore the effect of the chain length and of the surfactant/particle interaction. Interactions were also studied using either heptane (short chain, low viscosity) or dodecane (long chain, viscosity increased) as a solvent.

Two issues emerged with those samples: a fast oxidation when in contact with air, and a precipitation when trying to increase the concentration.

The concentration was consequently very low for a fine analysis in a reasonable time, and the major contribution to scattered intensity was generally due to a q^{-4} law arising from the non-stability of particles. We also observed a decrease at highest q-values, which means that there is probably very small structures (<1 nm) outside of the experimental q-range (more than 3 nm^{-1}).

Nevertheless, the 2D pictures let us see that with the appropriate surfactant (short-chain acid), we could improve the stability to air (maximum anisotropy when using polarized neutrons and applying a field of 1 T).

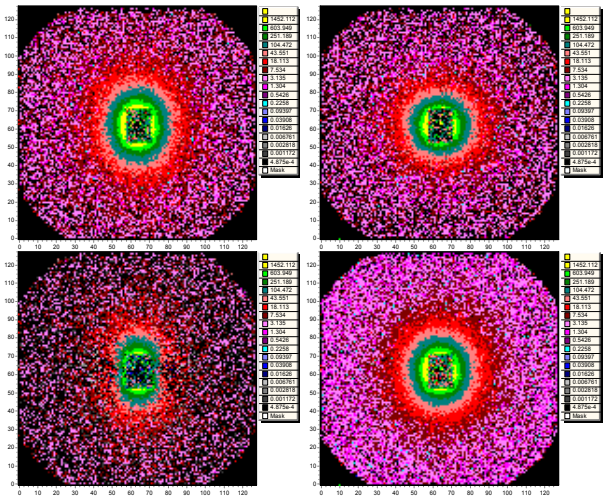

Fig. 1: *2D scattering picture obtained at 12 meters with polarized neutrons (I^+, upper left, Γ, upper right), difference I^+-Γ (down left), and sum I^++Γ (down right), for sample with short-chain surfactant and long-chain solvent. The difference of intensities shows a $\sin^2(\psi)$ dependence, where ψ is the azimuthal angle, denoting magnetic properties.*

This higher anisotropy with short-chain surfactant is correlated to the presence of a q^{-4}, which means that bigger aggregates are in formation. On the other hand, with long-chain surfactants, we observed a q^{-1} law, fitted as cylinders of very small diameters (less than 1nm). The fit cannot give accurate results, due to the limitation in q-range, and the fact that we do not know the concentration at the time the sample was scattering. Obtaining cylinders with long surfactants seems contradictory at first. Our opinion is that short-chains surfactants are efficiency covering the nanoparticles, protecting them from oxidation, but steric repulsions are not enough to prevent the formation of clusters. Whereas long-chains surfactants offer a poorer coverage of the particle surface due to steric effect and accordingly their shielding against oxidation is deficient.

The surfactant plays a key role in the protection of the particles against oxidation and precipitation. We have to tune the coating to balance nanoparticle growing and particle stabilization.

References:

[1]. Mater. chem. phys. **96** 1 (2006) 66

	EXPERIMENTAL REPORT **Nanoscale structure of silica from various biological sources**	Proposal N° BIO-04-1217 Instrument **V12a** Local Contact Markus Strobl
Principal Proposer: Experimental Team:	C. J. Garvey – ANSTO, Australia J. Ferris – ANSTO, Australia M Strobl – HMI, Berlin + TFH, Berlin	Date(s) of Experiment 03.04. – 10.04.2006

Date of Report: 05.01.2007

Previously we have used the V12a and V4 instruments, TEM and nitrogen adsorption to study the organisation of biosilica in samples of cell walls of phytoplankton called diatoms. The cell walls of diatoms show highly organised pore structures that is characteristic of the diatom species. Using bulk samples of cell walls obtained from cultures of three different species of diatoms scattering data was used to infer details of mechanisms of structural control of silica assembly in diatoms1,2. We are presently extending this knowledge of the assembly of biosilica to other groups of organisms.

The materials examined in this study were phytolith material extracted from the grass genus' Themeda and Heteropogon. Phytoliths are silicified replicas of plant cells. Another source of biolsilica was spicules extracted from an Antarctic glass sponge.

Other organisms are able to produce silica structures. In diatoms it appears that the control of silica morphology is via a templating mechanism where unitary building blocks of silica are laid down on a presumably proteinaceous framework. This research complements and extends continuing studies of biogenic and biomimetic silica where we aim to examine the length-scales of similarity with diatomaceous silica. These materials share the feature that the microscale features are highly specific to species of origin.

Using the methodology of the previous study we aim to compare the length scales of similarity of these samples and the samples in previous studies. We have obtained scattering data from samples of different path lengths of the materials with the aim of minimising the effects of multiple scattering. A typical scattering curve from Themeda is shown in Figure 1. The curves are typically featureless, with a lower slope of -3. This is equivalent to the Porod law for the slit-smeared geometry. It was found that the scattering curves for all grass samples were self-similar, i.e. were superimposable once scaled for the packing density of the sample.

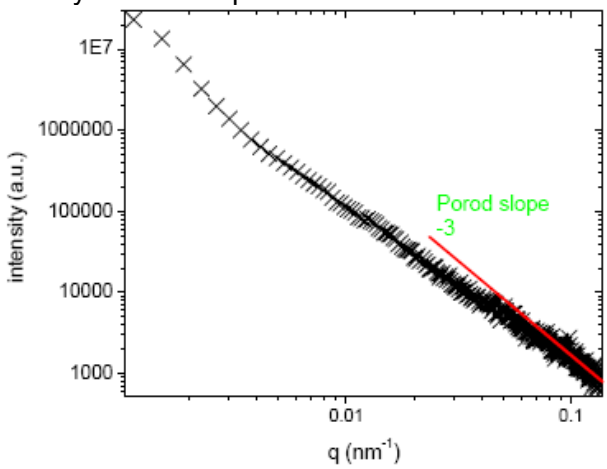

Fig. 1: *Slit smeared scattred intensity from a sample of Themeda phytoliths.*

We have also examined scattering from samples of fibres from a glass sponge. Unfortunately it was not possible to produce isotropic samples, nor was it possible to produce samples that were macroscopically oriented in a known fashion.

In conclusion it was not possible to complete the aims of this study, to compare the self-similarity of samples of biolsilica over a wide range of length scales, due to the limited qrange of the V12a instrument. Further works aims at completing this study and additionally investigating the size of unitary silica structures using x-ray diffraction.

References:

[1]. Garvey, C.J., and Ferris, J., "Fractal scaling andthe assembly of biosilica into diatom frustules.", Australian Society for Biophysics 28th Annual Scientific Meeting, Fremantle, p23 (2004).

[2]. Garvey, C.J. and Ferris, J.M. "Small angle neutron scattering studies on an absolute intensity scale of the structure of three cultured diatom frustules", Manuscript in preparation.

	EXPERIMENTAL REPORT **Characterization of metal-based homogeneous and graded porous biomaterials for bone tissue engineering by neutron tomography**.	Proposal N° MAT-04-1300 Instrument **V12b** Local Contact Markus Strobl
Principal Proposer: Experimental Team:	C. Renghini – UPM Ancona, I A. Manescu – UPM Ancona, I V. Calbucci – UPM Ancona, I M. Strobl – HMI, Berlin + TFH, Berlin	Date(s) of Experiment 20.09. – 23.09.2006

Date of Report: 19.01.2007

Homogeneous metal-based porous scaffolds (Ti+space-holder) with different porosities were investigated by Neutron tomography. These samples were fabricated by powder metallurgy combined with pressing, debinding and sintering at 1300°C for 2 hours in air (Fig. 1). They were analyzed after uniaxial testing to evaluate the mechanical properties arising from the treatment. The characteristics of the samples are summarized in Table 1.

Fig 1: *Homogeneous metal-based porous scaffolds (Ti+space-holder)*

Nr samples	***Geometry*** [mm]	***Mass*** [g]
IFAM2-1	Ø 5.01 x 10.02	0.40
IFAM2-2	Ø 5.01 x 9.96	0.39
IFAM2-3	Ø 4.99 x 10.01	0.38
IFAM2-4	Ø 5.01 x 10.01	0.36

Table 1: *Dimensions of samples*

In the present work neutron tomography measurements have been used to investigate in detail the original 3D-porous structure in terms of pore size, struts thickness and degree of pore interconnection. These results will be completed by triaxial mechanical tests in order to reveal microstructure-mechanical property relationships which will be used in transport and promechanical computer simulations of the scaffolds.
A 2 GHz Pentium with 1 Gb RAM and commercial software VGStudio MAX 1.1 was used to generate 3D images. In order to achieve optimal settings for the image quality, we used Scatter HQ algorithm with oversampling factor of 5.0 and activated color rendering.
Fig. 2 illustrates the reconstruction of IFAM2-2 sample.
Fig. 3 shows the scan obtained for IFAM2-3. A cross-sectional slice was obtained in the middle region of the cylinder in order to have a better view of the porosity and struts in the bulk of the specimen.

The pores appeared as dark spots on a gray background that represented the matrix.

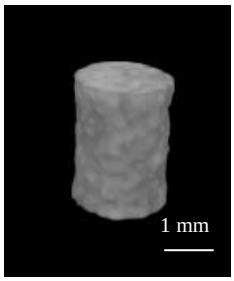

Fig 2: *3D reconstruction of the Ti+space holder scaffold*

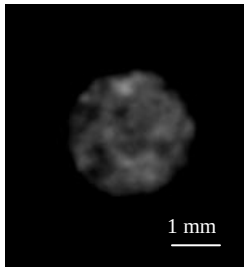

Fig 3: *2D slice of the Ti+space holder scaffold*

Unfortunately, the images are not extremely clear due to a not enough resolution offered by the instrument. Anyway, the level of porosity and the range of the pores dimensions in the bulk of the specimens was evaluated. A further analysis using X-ray tomography is foreseen for a better viewing of the pores and especially of the struts between the pores.

	EXPERIMENTAL REPORT **USANS Combined with In-situ Gas Adsorption Measurements on Porous Materials**	Proposal N° PHY-04-1250-EF Instrument **V12a** Local Contact Markus Strobl
Principal Proposer: Experimental Team:	A. Brandt – HMI, Berlin D. Wallacher – HMI, Berlin B. Smarsly – MPI KGF Golm I. Herrmann, M. Strobl – HMI, Berlin	Date(s) of Experiment 27.06. – 01.07.2006

Date of Report: 18.01.2007

Two sample substrates have been prepared for in-situ N_2-adsorption experiments at 77K combined with USANS at V12a: i) a porous SiO_2-matrix (S050 provided by the MPI Golm) with spherical mesopores of 20nm in diameter, which are arranged on a cubic lattice with inter-pore distances slightly larger than the pore size, see fig.1; ii) a commercial available Carbon molecular sieve (Ketjen Black 300) with disordered pores and a pore size distribution as shown in fig.3 (right), which was derived from ex-situ gas adsorption measurements performed in the SE-department with the commercial gas adsorption station "Autosorb" (Quanta-chrome).

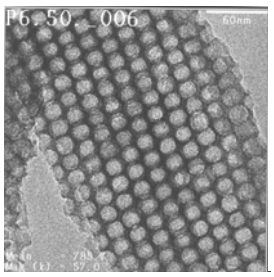

Fig.1: *TEM picture of the S050 silica sample with highly ordered spherical nanopores.*

The powders have been filled in the 2mm void of a vacuum sealed sample cell, which was mounted on the sample stick of the new CGA-OS sample environment (For details see: "New Sample Environment for Experiments under Controlled Gas Atmospheres I: Low Temperatures, Low Pressures", in this report).

The stick was inserted in the sample tube of a standard orange cryostat, which was suspended in a purpose-built frame for the double crystal USANS diffractometer. By the use of this setup the cryostat with the sample is mechanical decoupled from the spectrometer table, and allows the future use of HMI's standard sample environments at V12a. Each sample cell has been oriented in the beam by optimizing the maximum transmission intensity.

The sample substrates have been filled stepwise by condensing N_2 at 77K into the sample cell. For each fractional filling USANS-data have been recorded.

Somewhat unexpected the in-situ measured gas adsorption isotherm of sample i) showed up no adsorption-desorption-hysteresis which is typical for capillary condensation in mesoporous materials. Since the SiO_2-matrix and N_2 have nearly the same scattering length for neutrons, the scattering contrast should be matched by the cumulative filling of the pores. The expected changes in the scattering intensity could not be observed. In contrast to these findings, the TEM pictures of the sample material prove clearly the presence of spherical pores in an ordered arrangement. Therefore we have to conclude, that the pores of the investigated sample charge have been inaccessible to nitrogen gas. This means that the pores of this sample are not interconnected.

Because the q-range of V12a ($q<0.1nm^{-1}$) is not sensitive on structures smaller than 30nm the USANS results in fig.2 (left) show up identical diffraction patterns for the empty quartz cell and for the cell containing the sample powder.

In contrast to sample i) the ex-situ gas adsorption isotherm, and the out of it derived pore size distribution could be verified for sample ii) in the in-situ adsorption experiment at the USANS diffractometer.

A fit of the USANS-patterns of sample ii), see fig.3 (left), yields to a pore size distribution which is quite similar to the gas adsorption results. In fact the instrument is excellently suited for investigation in materials with pore-structures on the length scale of about 30nm to 100nm.

Changes in the diffraction patterns of the Carbon sample ii) due to the adsorption of nitrogen have not been observed, and are probably under the detection limit, because in contrast to quartz, carbon does not fulfil the matching conditions with the N_2 -adsorbate.

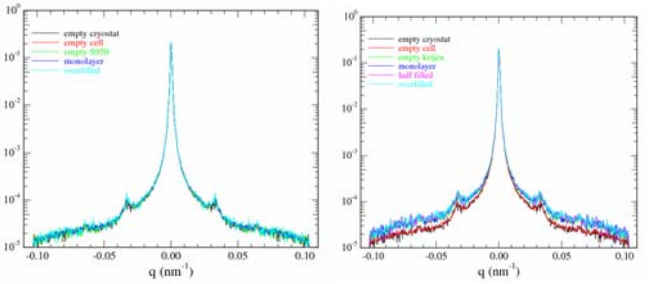

Fig.2: *USANS results for the porous samples at different N_2-filling levels of sample i) (left) and sample ii) (right).*

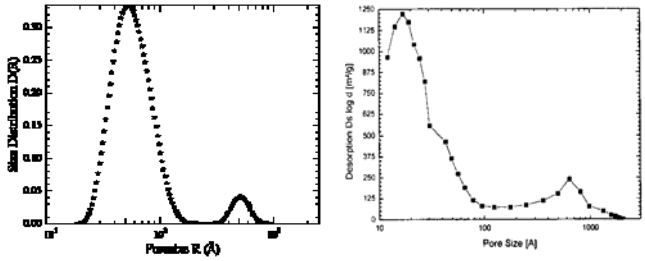

Fig.3: *Pore size distribution for sample ii) as derived from the USANS patterns (left) and from the gas adsorption isotherm of the sample (right).*

BENSC	**EXPERIMENTAL REPORT** **Near surface stress gradients**	Proposal N° EF Instrument **E3** Local Contact Poeste, Wimpory
Principal Proposer: Experimental Team:	F. Zilly – HMI, Berlin R. C. Wimpory – HMI, Berlin T. Poeste – HMI, Berlin R. Schneider – HMI, Berlin	Date(s) of Experiment 31.05. – 03.06.2006 02.02. – 06.02.2006

Date of Report: 11.01.2007

Two experiments were carried out using neutron diffraction on E3. In the first experiment a surface scan of a flat nickel specimen with very little strain in was measured in reflection geometry. This provided reference data for the computer simulations. The second experiment measured the wavelength gradient at the sample measuring position.

The gauge volume used a 2x2x2 mm3 cube. The specimen was measured in 0.5 mm steps. The Bragg reflection hkl 311 produced a 2theta angle of 80.536 degrees.

Figure 1 shows the scattering angle as a function of translator position. It can be seen that the peak shift resulting from the exit of the gauge volume from the surface can be approximated by a straight line. As soon as the gauge volume is completely filled the scattering angle stays constant. Figure 2 shows the relation of the scattering angle by scanning a ferritic iron pin through the beam in the second experiment. The pin was scanned perpendicular to the detector and so the change is completely related to the wavelength gradient. This information was essential for the first steps in the simulation of the E3 instrument using Mcstas in order to correct for the surface effect for the measurement of stress at the surface of a specimen.

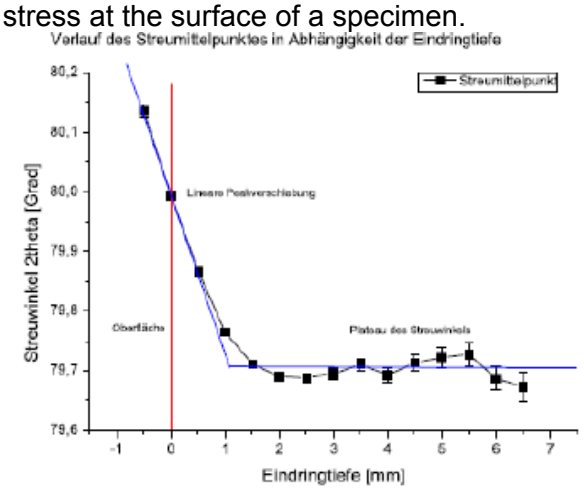

Fig. 1: *The scattering angle of the hkl 311 in the flat 'strain free' nickel sample as a function of translator position.*

Figure 3 shows two simulations using two different absorption coefficients. Simulation B was based on the experimentally determined value of the absorption coefficient whereas Simulation A shows the influence of using a smaller absorption coefficient.

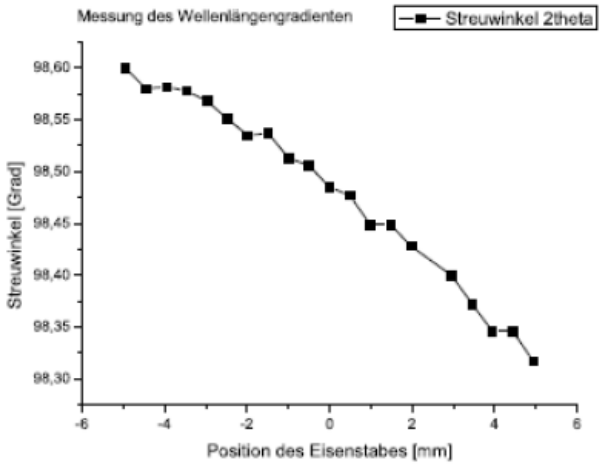

Fig. 2: *Scanning a ferritic iron pin through the beam (perpendicular to detector). The scattering angle changed is directly related to the wavelength.*

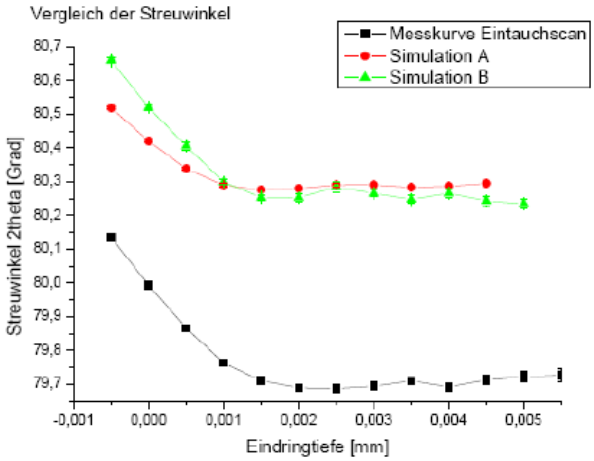

Fig. 3: *Comparison of simulation and measurement.*

BENSC	**EXPERIMENTAL REPORT** **Residual Stress in laser bent specimens**	Proposal N° EF Instrument **E3** Local Contact Robert C. Wimpory
Principal Proposer: Experimental Team:	R.C. Wimpory – HMI, Berlin A. Venter – NECSA Pretoria, ZA M. Van der Watt – NECSA Pretoria, ZA R.C. Wimpory, J. Li – HMI, Berlin	Date(s) of Experiment 16.09. – 23.09.2006 18.10. – 30.10.2006

Date of Report: 11.01.2007

The process of contactless laser bending using laser induced thermal stresses has been performed on ferritic steel. The influence of the number of passes of the laser beam on the residual stress has been investigated at various positions in the specimen. Figure 1 shows a schematic diagram of the specimen. Residual strain/stress measurements were made along a line transverse to the laser pass. The diagrams (fig 2 to 5) show a comparison of stresses between the front and centre of the specimen. A higher stress is seen with one pass compared to 3 passes showing an 'annealing effecting' in the longitudinal direction. The transverse and normal directions are essentially the same. The normal direction appears to be zero, as is expected normal to the surface.

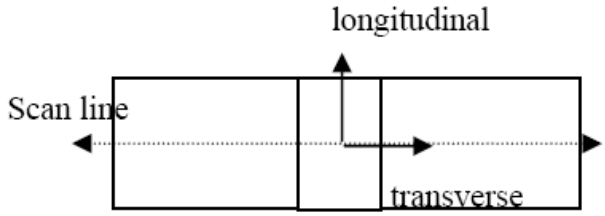

Fig. 1: *Schematic of laser bent specimen*

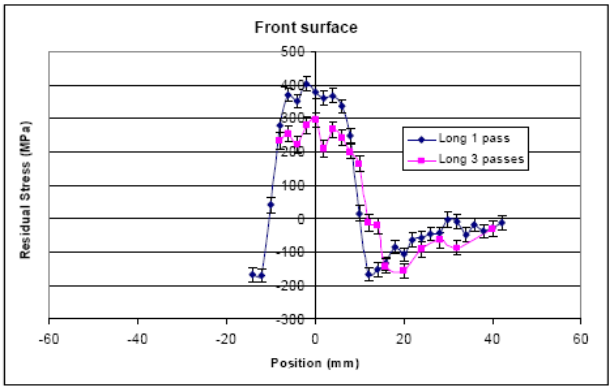

Fig. 2: *Stresses in the longitudinal direction at front surface.*

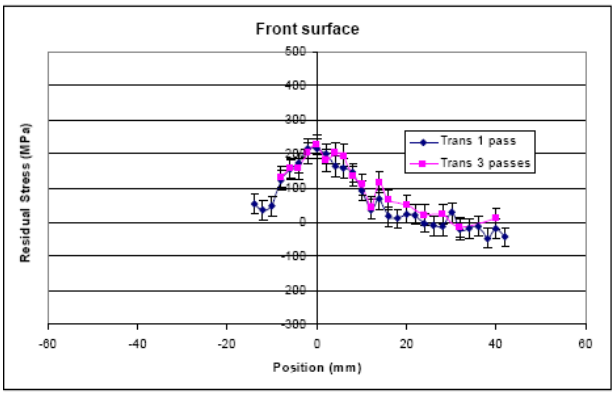

Fig. 3: *Stresses in the transverse direction at front surface.*

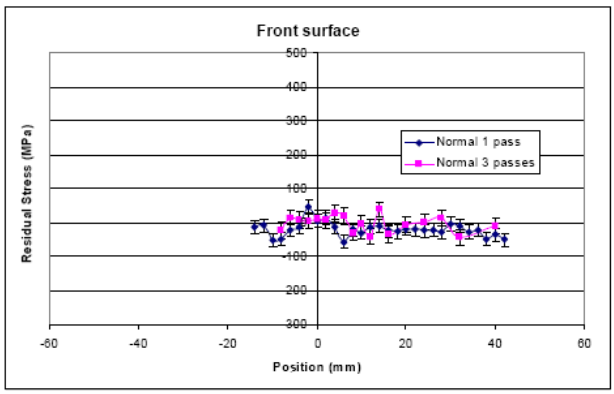

Fig. 4: *Stresses in the normal direction at front surface.*

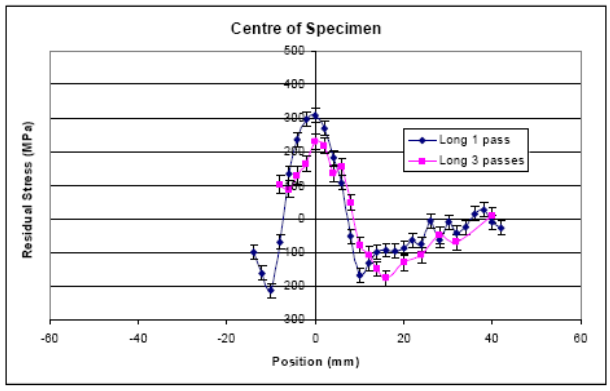

Fig. 5: *Stresses in the longitudinal direction at centre of specimen.*

BENSC	**EXPERIMENTAL REPORT** **Residual stress distribution in the vicinity of a sharp crack in a plastically deformed CT specimen**	Proposal N° MAT-01-1897 Instrument **E3** Local Contact Robert C Wimpory
Principal Proposer: Experimental Team:	K. Nikbin – ICL, UK K. Nikbin – ICL, UK R.C. Wimpory – HMI, Berlin	Date(s) of Experiment 28.02 – 07.03.2006

Date of Report: 05.05.2006

The goal of this work is to examine the effect of introducing a sharp crack, by electro-discharge machining (EDM), into a pre-existing residual stress field (see figure 1). The sharp crack represents the actual stress concentration experienced by a material containing a growing fatigue or creep crack in a material. The Compact Tension (CT) specimens have been taken from a stainless steel weld AISI Type 347 material.

The specimen presents a high hkl 200 texture, making this the only useable Bragg reflection. The hkl 200 reflection on E3 is at a scattering angle of 2θ = 45°, well away from the ideal 2θ = 90°. Before the specimen with the sharp crack was measured, an already measured [1] pre-compressed/heat-treated stress relaxed specimen (1000 h at 650 ^{o}C) of the same material was used as a 'reference' in order to confirm reproducibility with the E3 set-up. Figure 2 shows the excellent agreement between the ISIS measurement and E3 measurement.

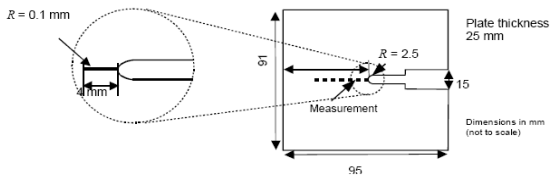

Fig. 1: *Geometry of the Compact specimen*

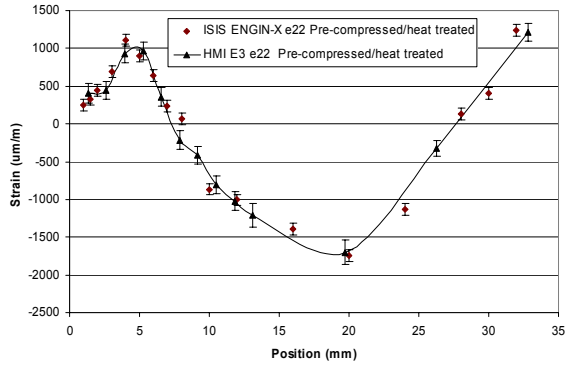

Fig. 2: *Comparison of e22 strain ISIS/HMI on pre-compressed heat-treated specimen.*

Measurements were subsequently made on the pre-compressed and EDM notched specimen (non-heated-treated) and compared to the strain before the introduction of the very sharp EDM notch (diameter 0.2 mm) [2] (see figures. 3 and 4). The results show the relaxation of the strain in the region of the notch (0mm to 4 mm).

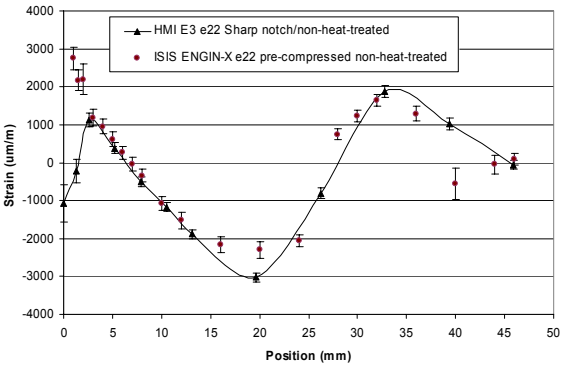

Fig. 3: *e22 strain before and after introduction sharp notch in plastically deformed (pre-compressed) CT specimen.*

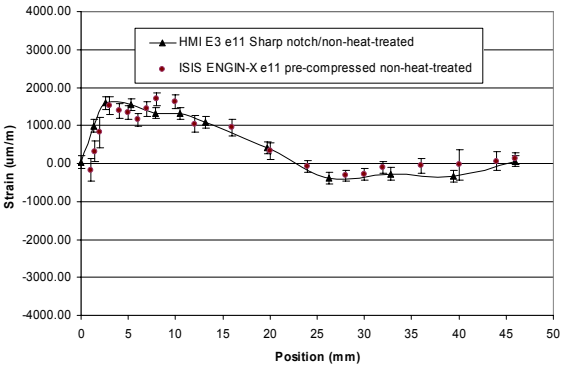

Fig. 4: *e11 strain before and after introduction sharp notch in plastically deformed (pre-compressed) CT specimen*.

These measurements will help to identify the role played by residual stresses in the premature failure of welded components. In conjunction with the neutron diffraction measurements finite element analysis will be carried out to estimate the residual stress generated during pre-straining and the subsequent redistribution of stress due to EDM notching. These tests are part of a Versailles agreement on Materials and standards VAMAS TWA31 Round Robin programme, on 'Crack growth in weldments containing residual stresses'.

References:

[1]. Experimental report RB 610129 ENGIN-X 2005
[2]. Experimental report RB 20300 ENGIN-X 200

	EXPERIMENTAL REPORT **Microstructure and plastic anisotropy effects on the stress free reference variation in a welded cladding**	Proposal N° MAT-01-1898 Instrument **E3** Local Contact Robert C. Wimpory
Principal Proposer: Experimental Team:	C. Ohms – EC-JRC-IE Petten, NL C. Ohms – EC-JRC-IE Petten, NL R. C. Wimpory – HMI, Berlin	Date(s) of Experiment 01.04. – 05.04.2006

Date of Report: 16.01.2007

Residual stress measurements by neutron diffraction in multi-pass welds are complicated because there is local variation in the material properties in the weld. As a consequence there is spatial variation of the stress free reference value. The aim of the proposed work is to make an assessment of such variations and to relate these to the visible microstructure of the welded test piece. For such experiments two slices cut from an austenitic cladding on a ferritic substrate have been prepared and the macroscopic stresses have been relieved.

The term “cladding” in the most general sense means covering of a material with another material exhibiting different properties. Joining dissimilar materials almost always leaves the user with potential problems arising from the mismatch of the thermo-mechanical properties. This leaves the component under a more or less significant residual stress in the as manufactured condition, and can lead to severe structural integrity problems, when the component is subjected to thermal and/or mechanical loads.

Variations of the free of stress reference lattice spacing in the welded cladding are normally addressed by using companion specimens cut from the same component for measuring the scattering angles corresponding to the free of stress lattice spacing, the reference scattering angle, test location by test location and per measurement direction.

The component under investigation in this case was a low alloy steel substrate covered by a stainless steel cladding, which has simply been welded onto the substrate. The two corresponding reference specimens (S2 and P2) that were prepared each 3 mm thick (see figure 1).

In order to mechanically relief the residual stresses in these specimens a grid of cuts was applied by EDM, such that the maximum length of uncut material was about 5 to 10 mm. It was assumed that no type I residual stresses could be sustained in the cut region of such a specimen. Figure 1. below depicts one of these specimens showing the substrate cladding interface and the grid of cuts applied.

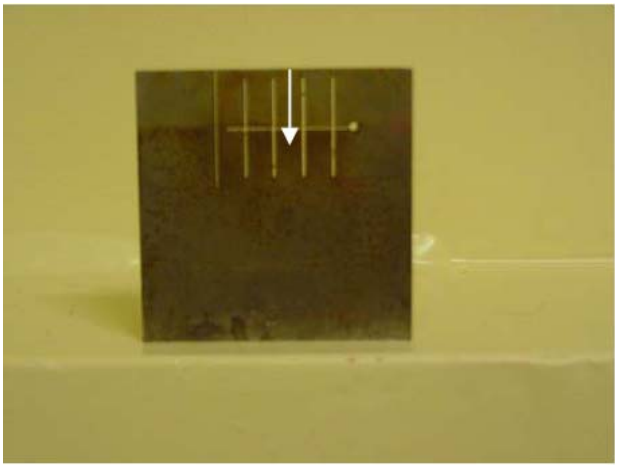

Fig. 1: *Reference specimen with macrostress relieving grid. Arrow indicates direction of scan.*

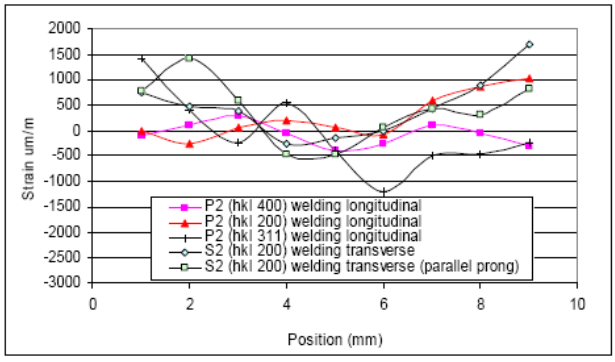

Fig. 2: *Microstrain in welding longitudinal direction.*

Figure 2 shows that the apparent microstrains in the austenitic part can be up to +/- 1000 microstrain. Part of the apparent strain is due to texture. This scatter can cause a large uncertainty in the calculation of the strain and hence stress within the austenite phase.

BENSC	**EXPERIMENTAL REPORT** **Residual stresses in welded CT specimens containing sharp cracks**	Proposal N° MAT-01-1988 Instrument **E3** Local Contact Robert C. Wimpory
Principal Proposer: Experimental Team:	K. Nikbin – ICL, UK K. Nikbin – ICL, UK R. C. Wimpory – HMI, Berlin	Date(s) of Experiment 20.07. – 26.07.2006

Date of Report: 11.01.2007

Modelling and measuring residual stresses in Weldments that contain sharp cracks is a Round Robin workpackage in the recently initiated Versailles agreement for Materials and Standards VAMAS TWA 31 "Creep/Fatigue Crack Growth of Welded Components" programme. The objectives are that the findings will lead to recommendations for a code of practice for measuring and analysing crack growth in welded specimens.

Failures in components are most likely to occur at or near weldments by fast fracture, creep or fatigue and these regions can exhibit microstructural inhomogeneity as well as the presence of micro-cracks and residual stresses. Cracking normally occurs in the heat affected zone (HAZ) of these welds and cracks can grow significantly under service loads.

Specimens have been machined directly from a non-stress relieved weldment. The creep crack growth tests showed anomalously short lives, with the crack path sometimes unexpectedly deviating away from the weld HAZ line at the centre of the specimen (Fig. 1). It is believed that this anomalous behaviour can be related to the presence of residual stresses resulting from the welding process, which may significantly influence the creep crack growth rate behaviour in the CT specimen.

Figure 2 shows the strain in the e22 direction which is perpendicular to the crack propagation direction. These results show low strain within the crack and a large strain ahead of the crack. Several measurements were made with a 2x2x2 mm3 gauge volume and 4x4x4 mm3 gauge volume on the hkl 200 reflection and along the centre and 5mm parallel to the centre as part of a sensitivity study. These measurements will help to identify the role played by residual strain/stresses in the premature failure of welded components. In conjunction with the neutron diffraction measurements finite element analysis will be carried out to estimate the residual stress generated during pre-straining and the subsequent redistribution of stress due to EDM notching. These tests are part of a Versailles agreement on Materials and standards VAMAS TWA31 Round Robin programme, on 'Crack growth in weldments containing residual stresses'.

Fig. 1: *CT specimen showing crack after heat treatment. Crack is approx 15mm long. Measurements made along the crack.*

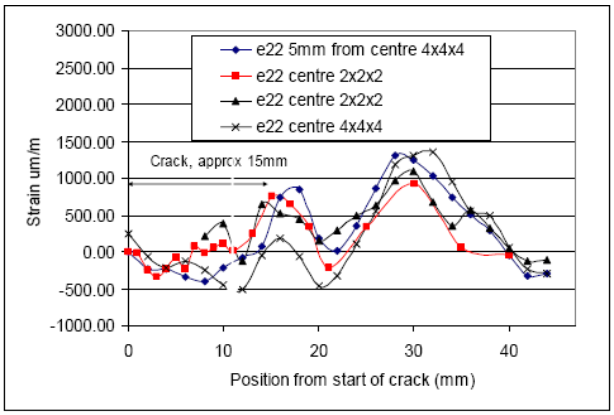

Fig. 2: *Strain perpendicular to crack propagation direction.*

BENSC	**EXPERIMENTAL REPORT** **Residual stresses in CFC-Cu joining brazed to CuCrZr alloy for nuclear fusion technology**	Proposal N° MAT-01-1989 Instrument **E3** Local Contact Robert C. Wimpory
Principal Proposer: Experimental Team:	A. Manescu – UPM Ancona, I A. Manescu – UPM Ancona, I V. Calbucci – UPM Ancona, I R. C. Wimpory – HMI, Berlin	Date(s) of Experiment 06.11. – 13.11.2006

Date of Report: 19.11.2006

With the aim to determine the residual stresses behaviour in CFC-Cu joining brazed to CuCrZr alloy, we have carried out diffraction measurements on the E3 instrument, analysing two different samples. Each of these two samples is constituted by two layers. The first one is graphite while the other layer is made of a Copper-Chromium-zirconium alloy. These two layers are connected by a pure copper interface (fig.1-2). The difference between these two samples is that one of them was submitted to thermal treatment.

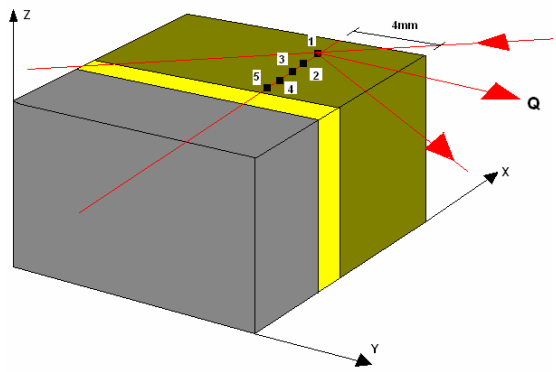

Fig. 1: *Geometry of the samples and measured points in the CuCrZr alloy. Example of transmission measurements for stress analysis in Y direction.*

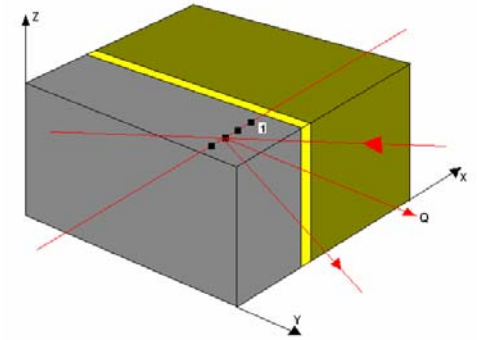

Fig. 2: *Geometry of the samples and measured points in the Graphite. Example of transmission measurement for stress analysis in Y direction*

All the measurements have been performed with a beam wavelength of 1.57 Å and a gauge volume of 2x2x2mm^3, selecting the primary and secondary slit of 2mm. Concerning the d0 value for the CuCrZr alloy we have carried out measurements in a CuCrZr reference sample while for the graphite we have considered the average value for the three analysed directions obtained in the point far from the interface.
The results obtained for the stresses in the CuCrZr alloy and graphite of the non-treated sample are reported in the following graphs. To obtain the values of the stresses, the following mechanical parameters have been utilized: E(CuCrZr)= 137000(MPa) and u(CuCrZr)=0,34; E(CFC)= 30000(MPa) and u(CuCrZr) = 0,4

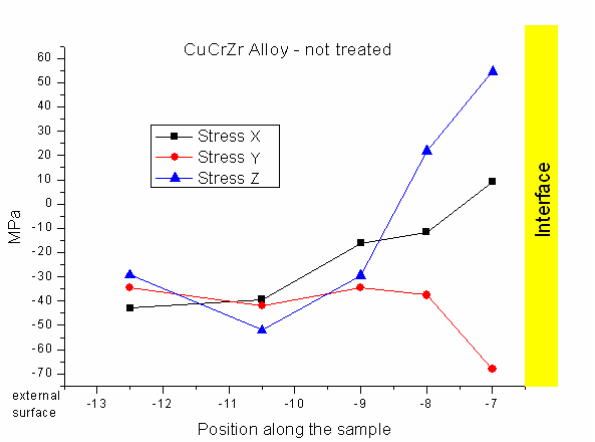

Fig. 3: *Stresses in the CuCrZr alloy in the non-treated sample.*

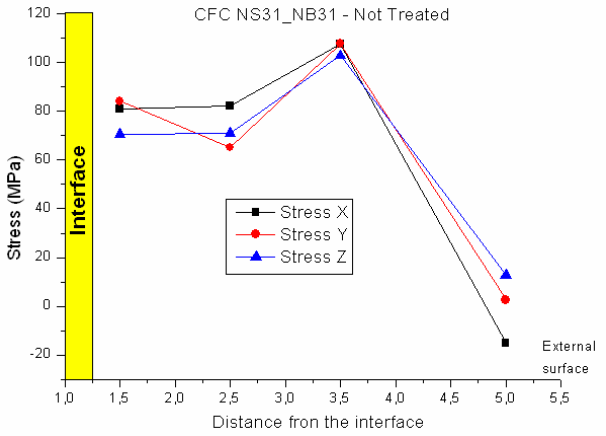

Fig. 4: *Stresses in the graphite zone of the non-treated sample*

	EXPERIMENTAL REPORT **Residual stress analysis in NiTi shape memory alloy**	Proposal N° MAT-01-1991 Instrument **E3** Local Contact Rainer Schneider
Principal Proposer: Experimental Team:	A. Giuliani – UPM Ancona, I A. Manescu – UPM Ancona, I R. Schneider – HMI, Berlin	Date(s) of Experiment 24.11. – 01.12.2006

Date of Report: 19.01.2007

It is unknown if any accumulation of residual stress occurs in NiTi shape memory alloys after the samples submission to the Impulse Electric Current Treatment (IECT).
For the first time, according to our revue, we applied a high-density impulse electric current treatment (IECT) to NiTi (50at.% Ni, 50at.% Ti) SMA samples for new and advanced applications – particularly those related to biomedical and transportation industries. The NiTi samples processing routes before the IECT treatment include: (1) Metal Injection moulding (MIM); (2) Combustion synthesis (CS); (3) Mechanical alloying and hot compaction (MA&HC). These developmental processing routes were selected because they offer potential advantages over currently employed routes such as reduced cost, easy alloying additions and refined microstructures.

Residual stress was evaluated in the parent phase, from the analysis of the same selected reflections before and after the IECT treatment.
The samples thickness was suitable to give a well detectable diffracted intensity in treated and not-treated MIM and CS samples, while in the MA&HC samples the nano-dimensions of the grains, verified with a preliminary 2theta scan, prevent the measurement to be carried out.
At the E3 Diffractometer, a 0.1373 nm wavelength was used for both the investigated types of sample (treated and not treated). Vertical and horizontal slits of 2mm defined a gauge volume of 2x2x2 mm^3.

The chosen 2theta angle for the (211) reflection of the NiTi cubic phase was 67°. We chose such reflection even if it is less intense than others because it was less affected by the presence of secondary overlapping phases.
The not-treated CS sample obtained lattice spacing was considered as d_0 for the CS treated samples (IMPER Nr.3 and Nr. 4), analysed in the same conditions.
The not-treated MIM sample obtained lattice spacing was considered as d_0 for the MIM treated sample, analysed in the same conditions.

It has to be underlined that the presence of big grains in both the types of samples (i.e. produced by metal Injection moulding (MIM) and combustion synthesis (CS)) implied the use of a continuous ω angle movement in the range of ω-5 to ω+5 degrees during the measurements in order to optimize the experimental conditions.

Data are still under analysis and the former conclusions will be formulated in the next months.

	EXPERIMENTAL REPORT **Hybrid organic/inorganic silica aerogels: "in situ" uniaxial compression test**[i]	Proposal N° MAT-04-1195 Instrument **V4** Local Contact Uwe Keiderling
Principal Proposer: Experimental Team:	V. Morales-Flórez – Univ. Cadiz, E N. de la Rosa-Fox – Univ. Cadiz, E U. Keiderling – HMI, Berlin	Date(s) of Experiment 19.06. – 22.06-2006

Date of Report: 15.01.2007

The complex structure of hybrid organic/inorganic aerogels is basically composed by an inorganic phase covalently bonded to an organic chain forming a copolymer. As a consequence the mechanical behaviour changes drastically, tuning from a brittle solid to an elastomer-like. After stress-strain experiments the Young's modulus decreases about three times whereas the rupture modulus increases giving the softer behaviour of these hybrids. As the polymer interlinks the silica clusters, the aerogel hardness and elastic modulus fall down drastically. These hybrid aerogels are viscoelastic regarding to the time dependence of the stress at fixed strain (relaxation) and of the strain at fixed stress (creep).

TEOS (tetraethoxysiloxane) a silicon alkoxide, easily polycondenses to form a 3D entangled network. We have modified the inorganic silica network with methyltriethoxysiloxane (MTES) an organosilicon compound and polydimethylsiloxane (PDMS) a hydroxyl terminated polymer. Some aerogels were doped with wollastonite ($CaSiO_3$) synthetic powders (350 nm average size) in order to study their mechanical behaviour as bioactive materials. Reactions were assisted by high power ultrasounds (0.6 kJ/cm^3). The resulting gels were dried under supercritical conditions of the solvent to obtain a monolithic aerogel. As a provision for the mechanical test, the samples were made as cylinders 18 mm long and 8 mm diameter approximately.

Figure 1

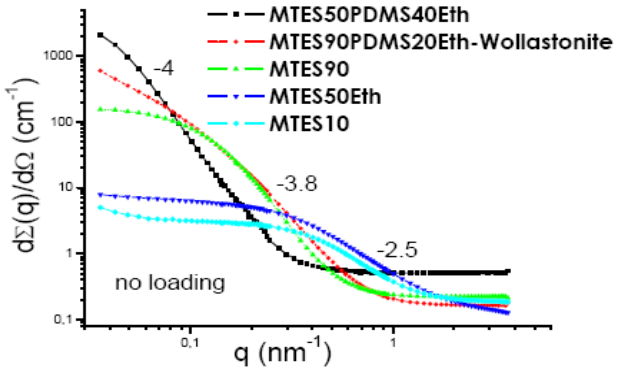

A specific sample-holder to measure the intensities under "in situ" uniaxial compression of the aerogel was made. Without load the intensities of several aerogels are depicted in Figure 1. Organic content and dilution in ethanol influence the contrast factor remarkably. Polymer content provokes an increase of the log-log slope (from 2.5 mass fractal to 3.8 surface fractal) becoming smoother interface between organic and inorganic phases.

On the contrary, under uniaxial compression the spectra were significantly anisotropic (butterfly pattern) indicating the rearrangement of the polymer along the perpendicular and parallel direction to load, as it is plotted on Figure 2.

Figure 2

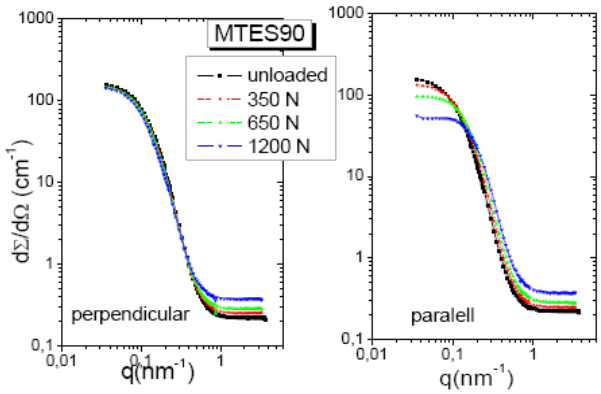

In this way, while the same features as the unloaded curve is maintained along the perpendicular direction, along the parallel direction to load there is an appreciable decrease of the intensity in the low q-side. As a matter of fact, a weak increase of the Guinier radius is produced along the perpendicular direcion ($R_G \perp$), but an important decrease along the parallel ($R_G \parallel$) one is apparent, as it is reported on the next Table:

MTES90	*ε (%)*	*$R_G \perp$ (nm)*	*$R_G \parallel$ (nm)*
unloaded	0	14.8	14.8
Load 350 N	7	15.0	13.0
Load 650 N	14	15.2	11.4
Load 1200 N	28	15.6	9.13

Eventually at high strain in the parallel curve (blue one) seems to develop a structure factor informing about the regular rearrangement of the organic phase. Form factor of these aerogels could be described by a two-correlation length based on the Debye and Gaussian random coil models. One first level corresponding to primary particles which are clustered into aggregates forming blobs. This second level is in equilibrium by the elastic constraints forming a secondary hierarchical level that is conducted by the porosity and determines the viscoelastic behaviour of these materials.

[i] Continuation of Proposal MAT-04-1098, BENSC Experimental Reports 2005

	EXPERIMENTAL REPORT **Evolution of morphology of gamma' precipitates during high-temperature deformations to very small strains in nickel-base superalloy**	Proposal N° MAT-04-1299 Instrument **V12a** Local Contact Markus Strobl
Principal Proposer: Experimental Team:	A. Manescu – UPM Ancona, I A. Manescu – UPM Ancona, I M. Zietara – AGH-UST Krakow, PL M. Strobl – HMI, Berlin	Date(s) of Experiment 14.07. – 221.07.2006

Date of Report: 19.01.2007

Ni-base single crystal superalloys have superior mechanical properties such as creep resistance and high temperature strength. Turbine blades operate at high temperature under a centrifugal force causing creep deformation of a material, which leads to so called rafting which is an essential factor determining creep strength of nickel-base single crystal superalloys at high temperature and influencing their applications.
This evolution of precipitate shape is sensitive to the sign and value of the precipitate misfit, and to the state of imposed stress. It is apparent that the superposition of a misfit and applied stresses has a pronounced influence on the microstructure evolution during creep.

The aim of the SANS experiment was to study the initial stages of the formation of rafted gamma' precipitate structure in the PWA 1484 single crystal Ni-superalloys after high temperature creep.

The samples were half of standard creep test specimens which were filed in order to bring their thickness to about 1mm in order to avoid a multiple scattering effect, the dimensions of the gauge volume being: 1mm (samples thickness) x 3mm (largeness of the slit) x 5mm (heigth of the slit). We analysed a number of 10 samples, each with different creep condition.

We observed important differencies between the specimens submited to different creep conditions corresponding to differencies in the structure present in the single crystal Ni-superalloys specimens – Fig. 1.

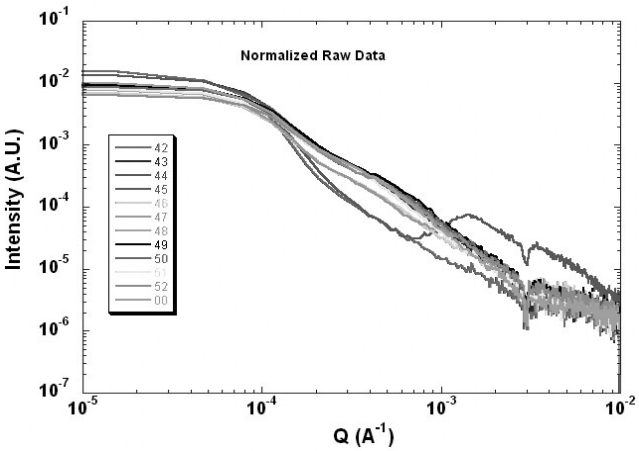

Fig. 1: *SANS curves for the analysed samples*

The evaluation procedure suited for anisotropic SANS was used for the detailed data treatment. The models that we used were either the cuboidal precipitates or the rafts or a combination of the two models.

One of the significant result which can be deduced from experiment is development of directional coarsening of γ' from a cuboidal to a plate – like morphology, which is oriented perpendicular to the applied stress axis. The γ' precipitates started to link together early during primary creep and continued to develop well into steady – state creep by their increased lateral extension. During the last stage, γ' rafts begin more "wavy" and they start to joining each other.

Cultural Heritage

	EXPERIMENTAL REPORT **Neutron tomography investigation of H content and distribution in ancient organ brass components**	Proposal N° ART-04-1311 Instrument **V7** Local Contact Nikolay Kardjilov
Principal Proposer: Experimental Team:	F. Fiori – UPM Ancona, I A. Manescu – UPM Ancona, I V. Calbucci – UPM Ancona, I N. Kardjilov – HMI, Berlin	Date(s) of Experiment 18.09. – 20.09.2006

Date of Report: 17.01.2007

A neutron tomography experiment was performed to investigate the H content and its bulk distribution in two brass components of a 17th century organ from St. Marienkirche in Stralsund (Germany), where an unexpectedly high hydrogen content was detected in a PGAA experiment recently carried out at BNC – Budapest. A neutron tomography experiment was proposed first because of the high sensitivity of neutrons to hydrogen content and then because of the capability of the technique to reconstruct the absorption properties of the different regions of the bulk materials, thus permitting the 3D reconstruction of the shallot volume and the determination of the distribution of hydrogen and other elements inside it. For the 3D reconstruction we used 300 projections covering a 180° angle (0.6° / projection).

The first result that we obtained was the absence of hydrogen in the shallots. It means that there was an error in the data analysing for the shallots at the experiment performed at BNC Budapest. Due to the large number of peaks involved in the PGAA analysis and due to their overlapping, one/some peaks we eronately assumed to belong to hydrogen. After having the neutron tomography results from HMI, a new analysis was performed on the results from BNC and we saw that some weak lead peaks overlap with the hydrogen peak, an explanation being obtained.

The second and the most important result that we obtained with the neutron tomography experiment was the presence of lead inclusions inside the brass, especially in the lower part (left side of Fig.1) of the shallots.

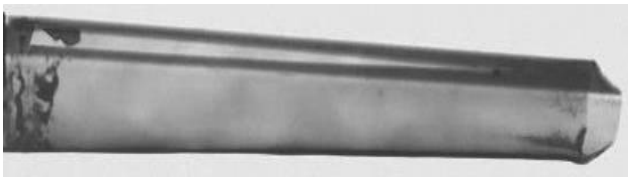

***Fig. 1**: Pb inclusions in the shallot.*

Another important aspect was the fact that these lead islands are inside the brass and not on surface. This was also proved by the neutron tomography; in Fig. 2 it is visualized a cross section in the shallot and one can see that the lead (darker spots) is surrounded by the brass (lighter material).

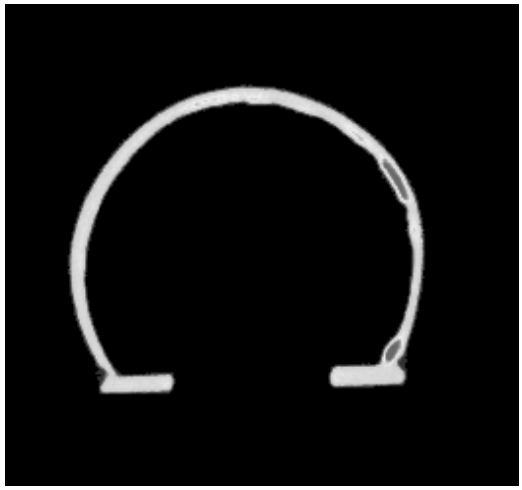

***Fig. 2:** Pb inclusions inside the brass*

In conclusion, the neutron tomography experiment gave us essential information for understanding of the manufacturing method and conditions of the historic brass shallots.

	EXPERIMENTAL REPORT **Identification of Hidden Objects of Archaeological interest**	Proposal N° ART-04-1317 Instrument **V7** Local Contact Nikolay Kardjilov
Principal Proposer: Experimental Team:	R. Triolo - CNR IPCF Messina, I I. Ruffo – Univ. Palermo, I V. Benfante – Univ. Palermo, I N. Kardjilov – HMI, Berlin	Date(s) of Experiment 16.05. – 18.05.2006 15.08. – 20.08.2006 30.10. – 07.11.2006

Date of Report: 11.01.2007

Combined Neutron Tomography and Diffraction have been applied to a variety of finds from ship wrecks in an area not far from Sicily southern coast characterized by a dangerous cliff (Scoglio della Bottazza). Both late Roman age finds (IV-V century A.D.) and "modern" finds (XVI century) have been studied. Indeed near Scoglio della Bottazza, in shallow waters, it has been possible to spot, during a preliminary investigation, part of the original sulphur load (sulphur bricks) and part of the artillery weapons and other arms used for self defense. Typical objects are swivel guns, long range cannons, various ammunitions and connection parts very well conserved, swords and simple parts. High resolution Neutron Tomography applied to ancient artillery and ship parts recovered from ship wrecks might help in dating the object and in determining best conditions for restoration and conservation treatment, whenever possible.
Figure 1 shows the tomographic reconstruction of a dagger with lime incrustations. The corrosion process fully removed the metal blade leaving only the calcareous matrix, as can be seen in figure 2. Figure 3 shows part of a sword whose Tomographic Reconstruction is shown in figure 4. Here we can see details that seem to indicate that the portion stuck to the hilt might possibly be a protective sheath, made out of wood, as shown in figure 5.

Figure 1

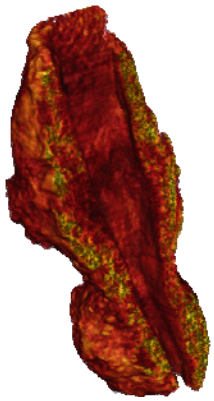

Figure 2

Figure 3

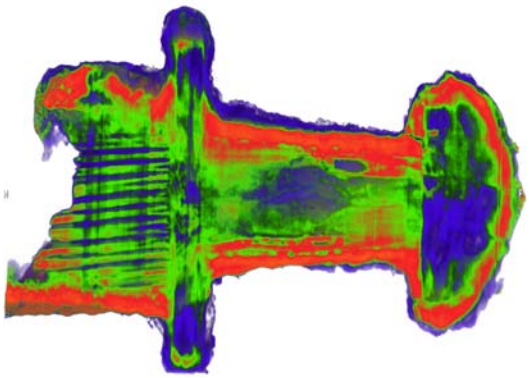

Figure 4

→

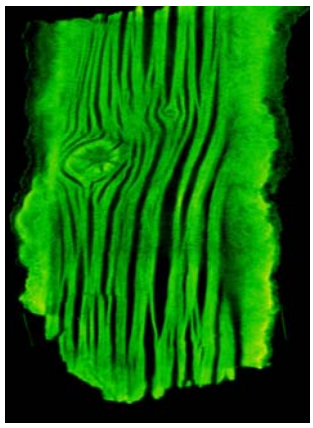

Figure 5

Figure 6 and 7 figure show the tomographic reconstruction of a bolt stuck in a wodden fragment (maybe a part of the ship's hull). The tomographic analysis gives the opportunity to highlight the corrosion process in which the bolt has been involved. The metallic phase diffused in the wood is clearly visible.
The Wide Angle Neutron Diffraction measurements (WAND) done on the same sample are shown in Table 1. WAND has been useful in obtaining information on the composition of the bolt that in this case is of bronze.

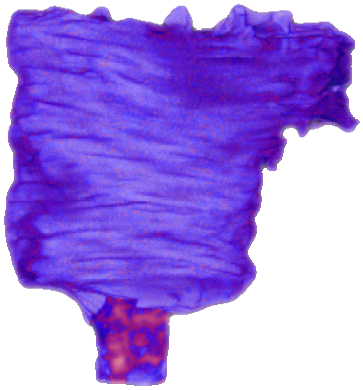

Figure 6

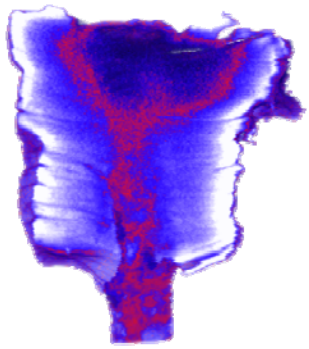

Figure 7

Table 1: *Chemical composition of the bolt*

Cu (w%)	Sn (w%)	Cu_2O (w%)
87.897(1)	12.103(1)	tracce

BENSC	**EXPERIMENTAL REPORT** **Morphological study of archaeological objects by neutron tomography**	Proposal N° OTH-04-1222 Instrument **V7** Local Contact Nikolay Kardjilov
Principal Proposer: Experimental Team:	F. Fiori – UPM Ancona, I F. Fiori – UPM Ancona, I A. Hilger, N. Kardjilov – HMI, Berlin	Date(s) of Experiment 06.03. – 08.03.2006

Date of Report: 13.03.2006

A neutron tomography experiment has been carried out on two bronze archaeological items, belonging to a private collection.

The first object examined is a small bronze statuette of solid cast bronze of the Ancient Egyptian civilization, presenting stylistic features distinctive of the Late Dynastic period (XXI-XXX Dynasties, c.1070-343 B.C.). The second artifact is a small statuette, also of solid cast bronze, of unknown provenance. Its origin is probably Etruscan, IV-III centuries B.C. The two objects are shown in fig.1.

Fig.1: *The two investigated items: Egyptian (left) and Etruscan (right).*

Both standard and phase-contrast tomography were performed. In the first case a 2 cm diameter diaphragm was used, with the object right in front of the detector, giving a resolution of about 200 μm. In the second case a 5 mm diameter pinhole was used, and the object to detector distance was set to 30 cm, with a resolution of about 100 μm. In both cases 300 projections were collected, covering 180° (0.6°/projection). The exposure time for each projection was set to 10 s for standard tomography and 120 s for phase-contrast tomography.

After background subtraction, the 3D structure was reconstructed using standard algorithms (phase-contrast).

Some pictures showing the internal structure of the two objects are shown in figs. 2 and 3.

Concerning the Etruscan statuette, several voids are detected inside it, with size roughly ranging from 0.5 to 7 mm. More absorbing elements (Fe?) than the bulk material are detected at the whole surface, that can be interpreted as the patina deposited through the ages due to environmental conditions of conservation, and whose presence was already determined by XRF. This patina is more concentrated in the left leg.

In the Egyptian item no bulk voids are found. More absorbing spots are detected in some surface regions, especially in the zone of right arm, maybe suggesting that the originally present patina was removed at some time, though not completely.

Further interpretation is presently in progress, also in the light of neutron and hard X-ray diffraction data [1].

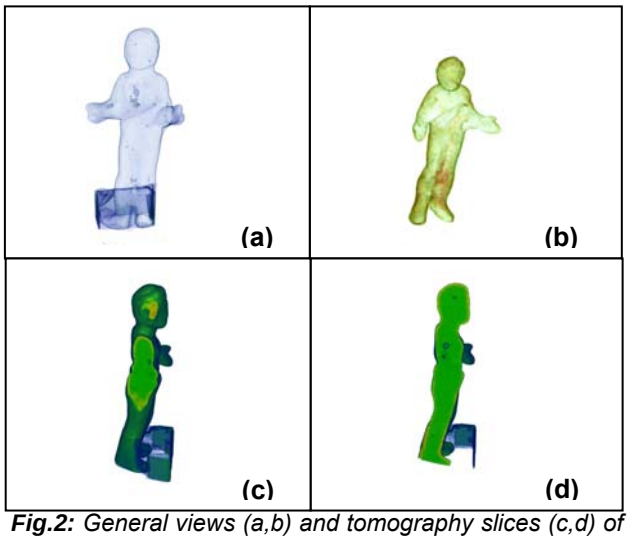

Fig.2: *General views (a,b) and tomography slices (c,d) of the Etruscam item, showing voids (dark spots in (a, (c) and (d)) and more absorbing elements (yellow/red spots in (b), (c) and (d)).*

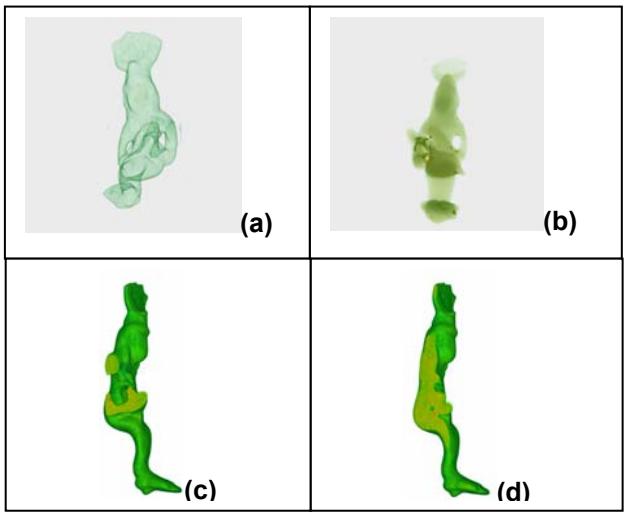

Fig3: *General views (a,b) and tomography slices (c,d) of the Egyptian item, showing the absence of voids (in (a)) and more absorbing elements (dark spots in (b) and yellow/red spots in (c) and (d)).*

Reference:

[1]. P. Bastie, B. Hamelin, F. Fiori, A. Giuliani, G. Giunta, F. Rustichelli, J. Gysens, A new method based on hard x-ray diffraction for the investigation of archaeological artefacts, Meas. Sci. Technol. **17** (2006) L1–L3.

Fundamental Physics and Others

	EXPERIMENTAL REPORT **Search for T-odd triple correlation in neutral component of ternary fission**	Proposal N° PHY-05-0018 Instrument **V13** Local Contact Margarita Russina
Principal Proposer: Experimental Team:	G. Danilyan – ITEP Moscow, RU V. Pavlov, V. Krakhotin – ITEP Moscow, RU P. Shatalov – ITEP Moscow, RU T. Wilpert, P. Granz, M. Russina – HMI, Berlin	Date(s) of Experiment January – June 2006

Date of Report: 02.10.2006

Our experimental setup consisted of low-pressure chamber and 6 neutron detectors outside it. In the chamber there are fission target which contains 48 mg of ^{235}U deposited on both side of the Zr (1 mm tick, 40 mm x 100 mm) plate and 2 low pressure multi-wire proportional counters to detect fission fragments. Six neutron detectors (plastic scintillators and photomultipliers) detect not only neutrons, but gamma-quanta too. To distinguish between them, time-of-flight technique was used. This setup has been used by us to search for the scission neutrons by measurement of P-odd correlation between prompt fission neutron momentum and spin of fissile nucleus, i.e., the correlation:

$$W(\theta) = \text{Const.}[\,1 + a(\mathbf{I},\mathbf{P}_n)] \rightarrow 1 + a\cos\theta \quad (1).$$

During previous reactor cycles we've found that $a = (2.2 \pm 0.6)\cdot 10^{-5}$. Because only scission neutrons can show such asymmetry, we concluded that the contribution of scission neutrons in total number of prompt fission neutrons equal (25±8)%. This amount is enough to search for the very interesting correlation between the momentum of scission neutron, the momentum of light fragment and the spin of fissile nucleus, i.e., the T-odd correlation:

$$W = \text{Const.}(1 + b\, P_n\,[I,P_{lf}]) \quad (2).$$

Such T-odd correlation has been found in ternary fission accompanied by long-range α-particle, origin of which is not understood yet. It can be the result of electromagnetic or strong interaction in final states of fission process. To distinguish between them we proposed to search for the same correlation for scission neutrons which are the neutral component of ternary fission.
To perform the measurement of correlation (2) we've modified our setup to determine the direction of light fragment emission from target. We have placed aluminium foils between target and each fragment detector. The range of light fragments in aluminium is 20% more than the range of heavy ones. We have calculated by MC simulation that the thickness of the foil needed to completely stop heavy fragment is about 12 μm. We have tested this calculation by measurement of P-odd correlation between light fission fragment and spin of fissile nucleus. We have found that the coefficient of this correlation conforms to the well-known value $8\cdot 10^{-5}$.

After this test experiment we began to measure the T-odd correlation (2). At the end of June we have obtained the value

$$b = (-1.9 \pm 1.5)\cdot 10^{-4}.$$

The T-odd correlation coefficient for α-particles in ternary fission of ^{235}U $b_\alpha = 8\cdot 10^{-4}$. So we expect that the magnitude of T-odd correlation coefficient for prompt fission neutrons can not be more than $2\cdot 10^{-4}$. This estimation and obtained result show that we have to achieve the accuracy about 3 times better than we have now.

	EXPERIMENTAL REPORT **Search for T-odd triple correlation in neutral component of ternary fission**	Proposal N° PHY-05-0020 Instrument **V13** Local Contact Margaritta Russina
Principal Proposer: Experimental Team:	G. Danilyan – ITEP Moscow, RU V. Pavlov, V. Krakhotin – ITEP Moscow, RU P. Shatalov – ITEP Moscow, RU T. Wilpert, P. Granz, M. Russina – HMI, Berlin	Date(s) of Experiment July – September 2006

Date of Report: 02.10.2006

Our experimental setup consists of low-pressure chamber and 6 neutron detectors outside it. In the chamber there are fission target which contains 48 mg of ^{235}U deposited on both side of the Zr (1 mm tick, 40 mm x 100 mm) plate and 2 low pressure multi-wire proportional counters to detect fission fragments. Six neutron detectors (plastic scintillators and photomultipliers) detect not only neutrons, but gamma-quanta too. To distinguish between them, time-of-flight technique was used. This setup has been used by us to search for the scission neutrons by measurement of P-odd correlation between prompt fission neutron momentum and spin of fissile nucleus, i.e. the correlation:

$$W(\theta) = \text{Const.}[\,1 + a(\mathbf{I},\mathbf{P}_n)] \rightarrow 1 + a\cos\theta \quad (1).$$

During previous reactor cycles we've found that $a = (2.2 \pm 0.6)\cdot 10^{-5}$. Because only scission neutrons can show such asymmetry, we concluded that the contribution of scission neutrons in total number of prompt fission neutrons equal (25±8)%. This amount is enough to search for the very interesting correlation between the momentum of scission neutron, the momentum of light fragment and the spin of fissile nucleus, i.e., the T-odd correlation:

$$W = \text{Const.}(1 + b\, P_n\,[I,P_{lf}]) \quad (2).$$

Such T-odd correlation has been found in ternary fission accompanied by long-range α-particle, origin of which is not understood yet. It can be the result of electromagnetic or strong interaction in final states of fission process. To distinguish between them we are searching for the same correlation for scission neutrons which are the neutral component of ternary fission.

To perform the measurement of correlation (2) we've modified our setup to determine the direction of light fragment emission from target. We have placed aluminium foils between target and each fragment detector. The range of light fragments in aluminium is 20% more than the range of heavy ones. So heavy fission fragments are completely stopped in the 12 μm foil, while part of light fragments pass the foil.

We are measuring the correlation (2) from the spring of 2006. At the end of September we have obtained the value

$$b = (0.3 \pm 1.1)\cdot 10^{-4}.$$

We are going to continue measurements and to reach the accuracy about $9\cdot 10^{-5}$ till the end of 2006. The T-odd correlation coefficient for α-particles in ternary fission of ^{235}U $b_\alpha = 8\cdot 10^{-4}$. So we expect that the magnitude of T-odd correlation coefficient for prompt fission neutrons can not be more than $2\cdot 10^{-4}$. This estimation shows that we have to achieve the accuracy about 2 times better than we have now.

	EXPERIMENTAL REPORT **Search for T-odd triple correlation in neutral component of ternary fission**	Proposal N° PHY-05-0022 Instrument **V13** Local Contact Margaritta Russina
Principal Proposer: Experimental Team:	G. Danilyan – ITEP Moscow, RU V. Pavlov, V. Krakhotin – ITEP Moscow, RU P. Shatalov – ITEP Moscow, RU T. Wilpert, P. Granz, M. Russina – HMI, Berlin	Date(s) of Experiment October–December 2006

Date of Report: 13.12.2006

During the second half of this year our setup was modified to measure simultaneously 2 effects: T-odd left-right asymmetry of prompt fission neutron (PFN) emission and so called ROT-effect in PFN emission. The ROT-effect in ternary fission of ^{235}U induced by cold polarized neutrons recently has been found at HFR of ILL [1].

Last 4 reactor cycles were used only to measure both effects. The accuracy achieved at the end of this year in T-odd asymmetry measurement is insufficient to make a definite conclusion:

More affecting results we achieved in investigation of ROT-effect.

T-odd correlation under our interest can be expressed by formula:

$$W = (1+D\,\mathbf{P}_{scn}[\mathbf{S}, \mathbf{P}_{lf}]), \qquad (1)$$

Where D_{scn} is the correlation coefficient, **S** – neutron beam polarization vector, $\mathbf{P}_{scn}$ and $\mathbf{P}_{lf}$ are moments of PFN and light fission fragments, correspondingly. The angular part of the expression (1) has maximum for orthogonal geometry.

To measure the ROT-effect in emission of PFN we used 4 additional detectors situated at average angles ($90^o \pm 15^o$) and ($270^o \pm 15^o$) relative to $\mathbf{P}_{lf}$. It must be mentioned that our detector detects prompt fission neutron as well as the prompt fission γ-quantum (PFG). The Time-of-flight technique allows us to distinguish between them.

We've found that for PFG the asymmetry of count rates under the neutron beam polarization reversal for angles 105^o and 285o is positive, but for angles 75o and 255^o is negative. It means that we measure another correlation instead of correlation (1). Such kind of asymmetry arises due to rotation of polarized fissile nuclei. The detected γ-quantum is a trigger and after its emission fissile nucleus polarized in definite direction turned at a small angle before rupture of the neck. Thus the angular distribution, (AD), of PFG is slightly shifted and the sign of this shifting depend on the direction of fissile nucleus spin direction relative to the direction on gamma-detector. The measured asymmetry of count rates is a difference between two shifted AD's divided on the sum of them. The magnitude of the measured asymmetry coefficient is equal: $R_\gamma = (5 \pm 1) \cdot 10^{-5}$, which is hundred times less then R_α in ternary fission. It's easy to explain it. The contribution of α-particles emission in ternary fission is 90%, while the probability of the prompt fission γ-quanta emission, which can trigger the fissile nucleus rotation, is unknown but should be less then a few percent. Finally the background of the γ-quanta emitted by excited fragments must suppress the measured asymmetry.

As it concerns the ROT effect in ScN emission the statistical accuracy is insufficient to make definite conclusion [$R_{PFN} = (8 \pm 7)\cdot 10^{-5}$], because the count rate under the gamma-peak is much larger then under the neutron-peak.

It's evidently that ROT-effect depends on the projection of fissile nuclei spin, *K*, on fission axis. Quantum number *K* defines the fission channel. If fission goes through channel with *K* = 0 the ROT-effect must be maximal while for channel with *K* = I (spin value of fissile nucleus) ROT-effect disappear. Therefore the ROT-effect can be used to search for fission channels. Of course, the magnitude of ROT-effect an order of 10^{-5} is too small to be practically used but if we'll know the spectrum of the ScG then we can exclude the fragments γ-rays background and increase the effect by hundred times.

BESSY

	EXPERIMENTAL REPORT **Exchange bias and uncompensated moments in fcc Co/FeMn/Cu(001)**	Proposal N° BESSY Instrument UE46-PGM **S1** Local Contact Detlef Schmitz
Principal Proposer: Experimental Team:	D. Schmitz – HMI, Berlin D.A. Tennant – HMI, Berlin M. Gruyters – HU, Berlin	Date(s) of Experiment 2006

Date of Report: Feb. 2007

Exchange bias occurs in systems where a ferromagnet (FM) and an antiferromagnet (AFM) are in contact [1, 2]. We studied epitaxially grown ferromagnetic Co (5 ML thick) on antiferromagnetic Fe_xMn_{1-x} (12 ML thick) on Cu(001), using the excellent results obtained in Ref. [3, 4] as a starting point, in order to elucidate the role of uncompensated Fe and Mn moments at the interface to Co. Epitaxially grown systems have the advantage to exhibit a much better defined interface as compared with polycrystalline systems prepared by sputtering. Per definition, spins of one antiferromagnetic sublattice are called "uncompensated" if moments of the other antiferromagnetic sublattice, oriented into the opposite direction and therefore usually compensating the moment from the first sublattice, are missing. If the magnetization direction of the FM is reversed, one part of the uncompensated moments of the AFM follows because the coupling to the FM dominates. Another part of the uncompensated moments does not reverse with the FM because the coupling to the AFM dominates. This is the so-called "pinned fraction" of uncompensated moments which has been supposed to be crucial for exchange bias [5].

The uncompensated moments can be detected and quantified by X-Ray Magnetic Circular Dichroism (XMCD) in absorption and X-Ray Resonant Magnetic Scattering (XRMS) in reflection. We performed XMCD and XRMS measurements by reversing the helicity of the synchrotron radiation in well defined magnetization states of the samples, *e.g.*, magnetized after deposition, after field cooling and after reversing magnetization after field cooling. Magnetizing after deposition creates a well defined state of the magnetization of the FM, field cooling activates the exchange bias, reversing the magnetization reverses rotatable uncompensated spins whereas the pinned fraction keeps the initial magnetization, and reversing the magnetization a second time serves to test whether the initial reversal behaviour is maintained. The sample was prepared and checked with XMCD at room temperature in the spectroscopy chamber at UE46-PGM, capped with 3 nm Pt, and transferred through air to the high-field end station at UE46-PGM where it was finally measured.

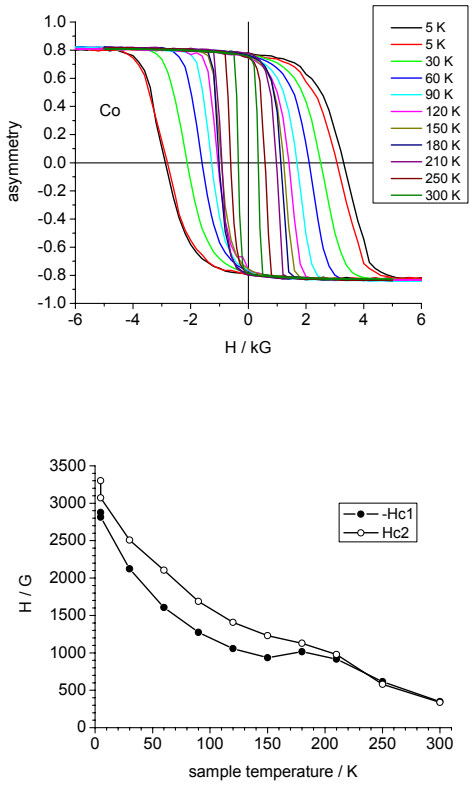

Fig.1: *Hysteresis loops (left) and coercive fields (right) of Co measured as a function of temperature after field cooling to 5 K in -5 kG.*

In Fig.1 the hysteresis loops (left) of Co measured in reflection as a function of temperature after field cooling to 5 K in -5 kG and the corresponding coercive fields $-H_{c1}>0$ and $H_{c2}>0$ (right) are shown. The exchange bias field is $H_{eb}=(H_{c1}+H_{c2})/2$. $H_c=(-H_{c1}+H_{c2})/2$ at 5 K is nine times larger than at 300 K, and between 50 K and 150 K H_c is seven times larger than H_{eb}. These observations indicate that the hysteresis loops are dominated by the anisotropy of the AFM. →

In detail, after field cooling to 5 K a coercive field H_c of about 3000 G and an exchange bias field H_{eb} of about 200 G are observed. After several hysteresis loops at 5 K H_{eb} decreases to 130 G, *i.e.*, there is a training effect. For increasing temperature H_{eb} first increases to 250 G at 60 K and then decreases to 0 G at about 230 K. At this blocking temperature a local maximum appears in $-H_{c1}$ and also but less pronounced in H_{c2}. This local maximum is usually explained by a decrease of the anisotropy of the AFM, so that more AFM moments rotate with the FM, resulting in an increase in H_c.

Hysteresis loops of the three elements Co, Fe and Mn are shown in Fig.2 for 5 K and 300 K after field cooling to 5 K in -5 kG. The saturation magnetization of Co at 5 K and 300 K is similar because both temperatures are far below the Curie temperature of the FM. Contrary, the saturation magnetization of uncompensated Fe and Mn is significantly lower at the higher temperature of 300 K. This might be the case because the higher temperature is close to the Néel temperature of the AFM which is 380 K for the present film thickness of 12 ML FeMn.

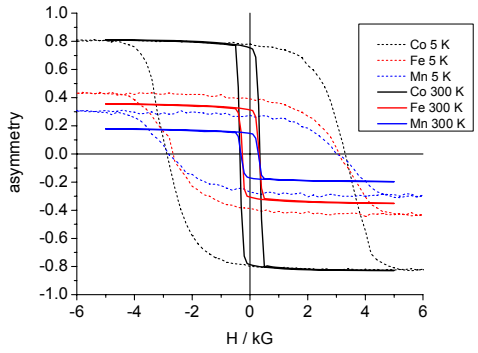

Fig.2: *Hysteresis loops of Co, Fe and Mn at 5 K and 300 K after field cooling to 5 K in -5 kG (left).*

Even at 5 K there is no significant vertical shift of the hysteresis loops, neither for Fe nor for Mn, indicating that the pinned fraction of uncompensated moments of the AFM is small, *i.e.*, at most 2%. This small fraction of uncompensated moments pinned to the AFM is in agreement with the relatively small exchange bias field of 200 G compared to the coercive field of 3000 G. In addition, the XMCD asymmetries measured at 5 K for Fe are tiny, i.e., at most 0.45% at the L_3 resonance. According to a simple estimate, this value of the asymmetry corresponds to a small number of uncompensated Fe moments of 0.05 ML.

References:

[1]. W.H. Meiklejohn, C.P. Bean, Phys. Rev. 102 (1956) 1413, Phys.Rev. **105** (1957) 904
[2]. W.H. Meiklejohn, J. Appl. Phys. **33** (1962) 1328
[3]. F. Offi, W. Kuch, J. Kirschner, Phys. Rev. B **66** (2002) 064419
[4]. F. Offi, W. Kuch, L.I. Chelaru, K. Fukumoto, M. Kotsugi, J. Kirschner, Phys. Rev. B **67** (2003) 094419
[5]. H. Ohldag, A. Scholl, F. Nolting, E. Arenholz, S. Maat, A.T. Young, M. Carey, J. Stöhr, Phys. Rev. Lett. **91** (2003) 017203

	EXPERIMENTAL REPORT **Sodium superlattice formation in Na_xCoO_2 (x = 0.8)**	Proposal N° BESSY Instrument MagS **S2** Local Contact Esther Dudzik
Principal Proposer: Experimental Team:	E. Dudzik – HMI, Berlin R. Feyerherm – HMI, Berlin D. A. Tennant – HMI, Berlin D. J. P. Morris – Univ. Liverpool, UK	Date(s) of Experiment 2006

Date of Report: Feb. 2007

The alkali cobaltate Na_xCoO_2 currently raises considerable interest as model compound for the doping of triangular transition metal oxide layers in comparison with the well-known square layered cuprate high-temperature superconductors. Extensive research efforts were initiated by the observation of superconductivity with T_C of up to 5 K in hydrated $Na_{0.35}CoO_2$ [1]. In Na_xCoO_2 the basic effect of a variation of the sodium concentration x is a simultaneous control of the magnetic and electronic degrees of freedom of the quasi two dimensional triangular CoO_2 sheets. For the stoichiometric $x = 1$ material, Co is in the Co^{3+} state with S = 0 in a low spin (LS) configuration. Compositions with $x < 1$ nominally are Co_x^{3+}/Co_{1-x}^{4+} mixed valence systems where Co^{4+} has a LS $S = 1/2$ configuration. This provides control for both the electronic and magnetic properties of these materials in a natural way, where the Na content x controls both the charge carrier concentration and the amount of magnetic ions. Consequently, the system Na_xCoO_2 exhibits a rich phase diagram as function of x with a wealth of interesting electronic and magnetic ground states [2].

In addition to providing a way of doping the CoO_2 sheets, variation of the Na content has been shown to result in various types of ordered Na superstructures, as demonstrated first by electron diffraction studies on a broad series of Na_xCoO_2 samples with x ranging from 0.15 to 0.75 [3]. Sodium ion ordering may affect the electronic and magnetic properties of these compounds considerably, because it may impose electronic constraints on the CoO_2 layer. Despite the importance of Na superstructure formation, the number of corresponding structure investigations is limited [3-6].

We therefore started a project with the aim of studying the sodium superlattice formation in the series Na_xCoO_2 (x = 0.3 - 1) by combined X-ray and neutron diffraction experiments. First X-ray diffraction results on a sample with x = 0.48 have been reported already in the BESSY Annual Report 2005, p. 295f. Here we report on results on a sample with nominal stoichiometry x = 0.75 obtained in January 2006 on the HMI operated 7 Tesla wiggler beamline MAGS, which is equipped with a six circle goniometer. The experiment was carried out using an X-ray energy of 12.4 keV. Since the sample was a relatively thin plate (0.15mm), this high energy allowed for X-ray diffraction experiments in transmission (Laue geometry). The sample was mounted to a closed-cycle cryostat.

In the diffraction experiment we focused on searching for superlattice reflections within the basal plane of the hexagonal structure, i.e., reflections of type (h k 0). The basic result of our study was the observation of various superlattice reflections related to sodium ordering below 285K belonging to two sets, namely a “commensurate” set, e.g., (0.4, 0.4, 0), and a seemingly “incommensurate” set, e.g., (0.065, 0.735, 0). The accurate determination of the position of the latter reflections was most important for the following analysis.

The temperature dependence of the intensities of these two types of reflection revealed that they vanished at exactly the same temperature, T_c = 285 K, suggesting that they may arise from a single complex superlattice. A detailed analysis showed that all observed reflections could be explained assuming a single supercell of $\boldsymbol{a'} = \boldsymbol{a} + 3\boldsymbol{b}$ and $\boldsymbol{b'} = 4\boldsymbol{a} - 3\boldsymbol{b}$, where $\boldsymbol{a}$ and $\boldsymbol{b}$ are the original hexagonal unit cell vectors in the basal plane. This experimental result was an important ingredient for the verification of similar experimental results from neutron diffraction on the same sample, which, however, did not give an accurate enough determination of the positions of the “incommensurate” reflections. It also was important for checking theoretical considerations concerning an organizational principle for understanding the sodium superlattice formation. In the theoretical studies, the screened Coulomb interaction among Na ions was identified as primary driving force for the Na ordering which appears to be governed by pure electrostatics. An organizational principle was derived that involves stabilization of charge droplets, namely di- and trivacancy clusters that order long range. Energetically the observed superstructure is within a few K of the most stable phase for the x = 0.80 tri-vacancy model. The deviation of the model value for x from the nominal value 0.75 points to a possible phase separation of the sample into regions with different x.

→

The complete work is published in Nature [7], where the present X-ray diffraction results entered as supplementary information.

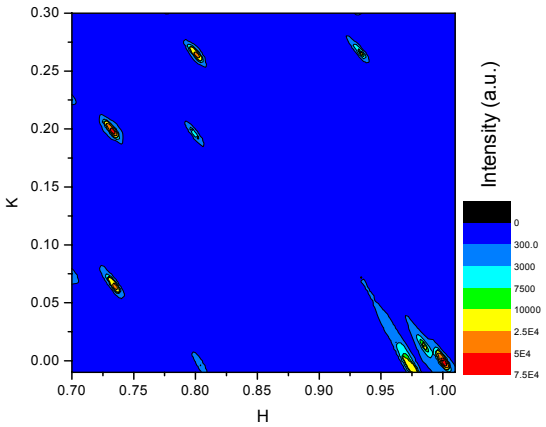

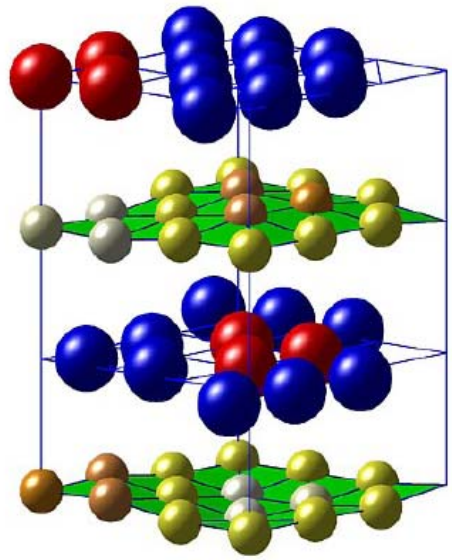

Fig. 1: *(left) section of reciprocal space showing strong superlattice reflections like (0.065,0.735,0) and (0.2,0.735,0) besides weak reflections like (0.8,0,0); (right) real space superstructure related to an x=0.80 tri-vacancy model fitting the experimental data. Blue are Na ions, red are Na vacancies clustered in triplets. Only Co ions are shown for CoO_2 sheets marked green.*

References:

[1]. K. Takada, H. Sakurai, E. Takayama-Muromachi, F. Izumi, R. A. Dilanian, and T. Sasaki, Nature (London) **422**, 53 (2003).

[2]. M. L. Foo et al., Phys. Rev. Lett. **92**, 247001 (2004).

[3]. H. W. Zandbergen, M. L. Foo, Q. Xu, V. Kumar, and R.J. Cava, Phys. Rev. B **70**, 024101 (2004).

[4]. Q. Huang, M. L. Foo, J. W. Lynn, H.W. Zandbergen, G. Lawes, Yayu Wang, B. H. Toby, A. P. Ramirez, N. P. Ong, R.J. Cava, J. Phys.: Condens. Matter **16**, 5803 (2004).

[5]. D. N. Argyriou, P. G. Radaelli, C. J. Milne, N. Aliouane, L. Chapon, A. Chemseddine, J. Veira, S. Cox, N. D. Mathur, P. A. Midgley, J. Phys.: Condens. Matter **17**, 3293 (2005).

[6]. J. Geck, M. v. Zimmermann, H. Berger, S. V. Borisenko, H. Eschrig, K. Koepernik, M. Knupfer, and B. Büchner, Phys. Rev. Lett. **97**, 106403 (2006)

[7]. M.Roger, D.J.P. Morris, D.A. Tennant, M.J.Gutmann, J.P. Goff, J.-U. Hoffmann, R. Feyerherm, E. Dudzik, D.Prabhakaran, N. Shannon, B. Lake and P.P. Deen, Nature (London) **445,** 631 (2007).

BENSC	**EXPERIMENTAL REPORT** **Charge order in a battery: electronic and ionic ordering in Na_xCoO_2**	Proposal N° BESSY Instrument MagS **S2** Local Contact Ralf Feyerherm
Principal Proposer: Experimental Team:	J. Geck – Univ. B. Columbia, C + EPF Lausanne, CH T. Kroll, L. Dunsch, – Univ. B. Columbia, C M. Knupfer, C. Malbrich – Univ. B.Columbia, C H. Berger – EPF Lausanne, CH B. Büchner – Univ. B. Columbia, C R. Feyerherm – HMI, Berlin	Date(s) of Experiment 2006

Date of Report: Feb. 2007

Introduction: The interactions among the electrons in condensed matter lead to a plenty of fascinating physical phenomena of high technological potential. Recently, the $NaxCoO_2$ cobalt oxides have garnered significant interest, thanks to their unusual physics. These materials consist of layers of covalent edge-sharing CoO_6-octahedra, which alternate along the perpendicular stacking direction with ionic Na-layers (Fig.1). The CoO_2-layers in these compounds constitute a realization of a correlated electron system based on a triangular lattice; a geometry which is known to be in favour of unconventional electronic ground states.

In addition to this, Na_xCoO_2 behaves very much like a rechargeable battery: sodium can be added or removed electrochemically, similar to the charging/discharging process of a battery. It is even possible to intercalate water molecules.

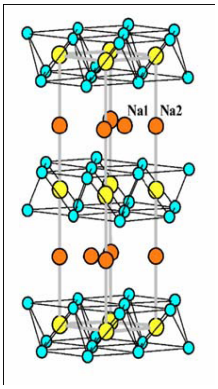

Fig. 1: Crystal structure of γ-NaxCoO2 [1]

Adding Na adds electrons to the CoO_2-layers, providing a convenient way to dope these correlated electron systems. Both changing x and water intercalation have dramatic effects on the electronic properties. Most notably, superconductivity emerges upon hydration and the non-hydrated compounds around x=0.7 display an anomalously high thermopower.

Aim: In this project we focus on the non-hydrated compounds Na_xCoO_2 with $0.5 \leq x \leq 0.9$. In these materials unconventional ordering phenomena associated with the CoO_2-layers as well as strong tendencies towards sodium order have been reported recently.

In order to unravel the complex physics of Na_xCoO_2, it is important to clarify whether or not the electronic ordering within the CoO_2-layers is coupled to, or even induced by, the ionic ordering in the Na-planes. This relation is currently largely unclear and it is the aim of this project to shed light on this issue.

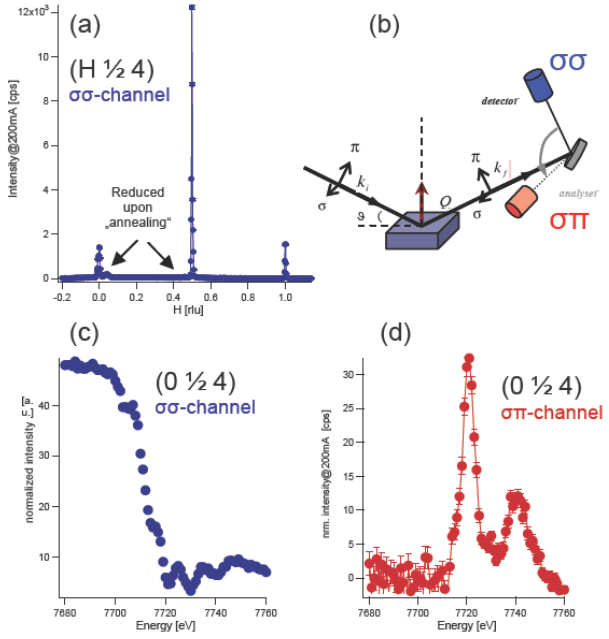

Fig. 2: Data collected at T=30 K. (a): (H ¼ 4)-scan taken off-resonance. Well defined superlattice peaks are observed. The weak peaks at incommensurate positions are reduced after "annealing" at 350 K. (b): Illustration of a typical RXS experiment. (c): Energy dependence of the (0 ½ 4) reflection in the σσ-channel (charge scattering). (d): Energy dependence of the (0 ½ 4) reflection in the σπ-channel. This intensity is largest, when the charge scattering is lowest.

Experimental techniques: The experimental technique employed for this purpose is resonant hard x-ray scattering (RXS) at the Co K-edge (7710eV). Since the resonant scattering process at this energy involves 1s→4p transition, RXS is highly sensitive to local distortions

→

around the Co-site. This means, however, that it does not provide a direct probe for Co-valence ordering. But since an ordering of Co-valences is connected to Co-sites with different local environments, RXS at the Co K-edge is very well suited to detect this type of charge ordering nonetheless. The advantage of this hard x-ray scattering experiment over the more direct resonant soft x-ray scattering is a larger region in reciprocal space that can be accessed and the possibility to perform an effective polarization analysis of the scattered beam.
The RXS experiments have been performed at the MAGS-beamline located at the 7T Wiggler of BESSY. Polarization analysis of the diffracted beam was performed using the (222) reflection of Al. Regarding the sample preparation the following approach was used: First, high-quality single crystals of Na_xCoO_2 with x=0.75 were prepared using chlorine flux methods. These crystals were then doped by electrochemical extraction or enrichment of Na in order to achieve different values of x.

Results: Here we will report the first RXS results obtained from an electrochemically doped $Na_{0.66}CoO_2$ single crystal. In Fig. 2, low-temperature RXS data for this crystal are shown. As demonstrated in Fig.2 (a) well defined superlattice peaks were observed off-resonance, which can be attributed to the ionic ordering within the Na-planes [2]. In addition, weak incommensurate reflections have also been observed. The intensity the incommensurate peaks could be considerably reduced upon “annealing” the sample at 350K. Most likely, the incommensurate peaks are related to Na inhomogeneities just after the electrochemical treatment.

In the following we focus on the (0 ½ 4) reflection. The energy dependence of this reflection in the σσ-channel (cf. Fig.2 (b)) is shown in Fig. 2 (c). Below the Co K-edge, a high intensity at the (0 ½ 4) position is observed, which is dramatically reduced due to absorption effects as the photon energy crosses the Co K-edge. The intensity in the σσ-channel is due to charge scattering caused by the ionic ordering of the Na-ions. In striking contrast to the behaviour of the σσ-intensity, we observe an enhancement around the Co K-edge in the σπ-channel. Up to our knowledge, this is the first time that this is observed for Na_xCoO_2.
The resonant enhancement of the (0 ½ 4) reflection at the Co K-edge implies that the Na-order generates inequivalent Co-sites. This is not unexpected. However, the charge scattering observed in the σσ-channel is constant below 250 K, i.e. the Na-order does not change in this temperature regime. The resonant scattering in the σπ-channel, on the other hand, is temperature dependent as shown in Fig. 3. In addition to this, the increase of the resonant scattering correlates with a cross-over behaviour observed in the electrical resistivity (Fig.3). This is strong evidence for charge correlations in the CoO_2-planes induced by the Na-order.
The experiment described above demonstrates that RXS at the Co K-edge is capable to study the interplay of ionic and charge ordering in Na_xCoO_2, which is important to develop a better understanding of these complex materials. In the future we plan to extend our studies to different doping levels. In particular, we want to study these effects for the commensurate doping x=0.5.

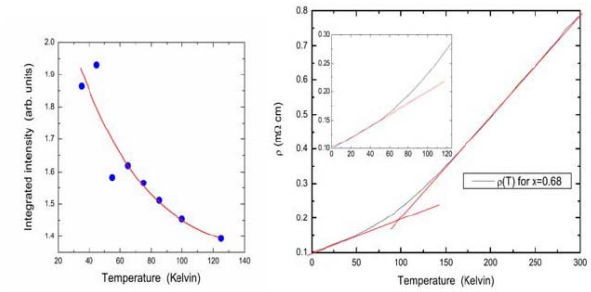

Fig. 3: *Comparison between the temperature dependences of the resonant σπ-scattering at the (0 ½ 4) position (x=0.66) and the electrical resistivity for x=0.68 (from Ref. 3)*

	EXPERIMENTAL REPORT First-order phase transition near 40°C in MnAs nanodisks	Proposal N° BESSY Instrument MagS **S2** Local Contact Ralf Feyerherm
Principal Proposer: Experimental Team:	B. Jenichen – PDI, Berlin Y. Takagaki, K.H. Ploog – PDI, Berlin N. Darowski, R. Feyerherm – HMI, Berlin I. Zizak – HMI, Berlin	Date(s) of Experiment 2006

Date of Report: Feb.2007

The phase transition near 40 °C of both as-grown thin epitaxial MnAs films prepared by molecular beam epitaxy on GaAs(001) and nanometer-scale disks fabricated from the same films is studied. The disks are found to exhibit a pronounced hysteresis in the temperature curve of the phase composition. In contrast, supercooling and overheating take place far less in the samples of continuous layers. Manganese arsenide on GaAs is a promising materials combination for spintronic applications based on spin injection [1]. MnAs is ferromagnetic at room temperature and has a large carrier spin polarization. It can serve as a source of spin polarized electrons. Furthermore MnAs may be applied for sensors and actuators thanks to its magnetoelastic response [2]. The room temperature ferromagnetic α-phase is metallic and crystallizes in the hexagonal NiAs(*B*81) structure. Near 40 °C MnAs transforms into the orthorhombic β-phase exhibiting the MnP(B31) structure. The temperature dependence of the magnetization near the transition was investigated in [2, 3], and a 20 K wide hysteresis loop was observed. At this first order structural phase transition a significant change in the lattice parameter α a is found, which amounts to ≈¼1.2% [4, 5].

During epitaxy [6, 7] the MnAs($1\bar{1}00$) film on GaAs(001) is attached by the side facet of the hexagonal unit cell) , so that the *c* lattice direction MnAs[0001] is parallel to GaAs[110]. The deformations in the layer lead to the phenomenon of phase coexistence, i.e. the phase content ξ does not change abruptly between zero and unity at a certain temperature as expected from the Gibbs phase rule. Two coexisting phases are found, on the contrary, in a wide temperature range [8]. Elastic domains of both phases form a periodic stripe pattern [9] in a self organized way. The domain period amounts to approximately five times the film thickness [10, 11]. Application of hydrostatic pressure [12, 13] or biaxial stress [14] has a considerable influence on the transition temperatures.

The phase transition can be affected further by imposing artificial constraints on the stripe pattern. Significant effects are expected from a lateral confinement when a film is patterned to small disks. Such disks with smaller sizes than the widths of the elastic domains enable elastic relaxation of the laterally periodic stresses accumulated inside the epitaxial layer. The tight restriction of the MnAs lattice along the interface is then released. As a consequence the formation of elastic domains in MnAs nanodisks seems to be no longer energetically favourable. The distribution of magnetic domains in such MnAs disks was investigated in [15].

The aim of the present work is to study in more detail the influence of such a lateral structuring on the phase coexistence of α and *β*MnAs. We investigate the temperature dependence of the phase composition in epitaxial MnAs films prior to and following the artificial modification using microfabrication technologies. The MnAs layers were grown by solid source molecular beam epitaxy (MBE) as described elsewhere [7, 16, 17]. The nanostructuring was carried out using electron beam lithography and Ar ion milling. The resulting disks were assembled in the form of a square array. In this sample, the diameter of the disks is smaller than 100 nm, i.e. well below the equilibrium size of the elastic domains in the original continuous MnAs layer. Temperature dependent synchrotron x-ray diffraction experiments were performed at the MAGS beamline at the BESSY storage ring using a Si(111) double crystal monochromator and 8 keV radiation. A six circle diffractometer equipped with a special cryostat was employed for the measurements. Preliminary experiments were performed at a similar diffractometer of the KMC 2 beamline at BESSY. In addition we performed laboratory experiments using a Panalytical X'Pert System with Ge (220) hybrid monochromator and Ge (220) analyzer crystal. The phase contents of the MnAs samples were obtained from the ratio of the integrated intensities of the corresponding *α*MnAs and *β*MnAs reflections measured in symmetrical ω/2*θ*-scans. The (3300) and (060) or the (1100) and (020) were analyzed [11, 18], and the layer reflections were fitted by Gaussian curves. The intensity ratio changes with temperature in the phase coexistence range [8]. The samples reached their equilibrium composition almost immediately after a certain temperature had been set, i.e. the relaxation times are significantly small. Samples consisting of MnAs disks having various diameters on the GaAs substrate were compared to their parent unstructured samples. The lateral period of the domain structure of the original MnAs epitaxial layer can be obtained from the distance between satellite maxima $\Delta\omega_S$ in the x-ray triple crystal ω-scan. The period Λd is calculated from the formula $\Lambda d=2\pi=(\Delta Q_x)=\lambda/(2\Delta\omega_S \sin\Theta_B)$, where ΔQ_x is the distance of the satellite maxima in reciprocal space, λ is the x-ray wavelength, and Θ_B is the Bragg angle [19]. The x-axis is defined to be perpendicular to the c-direction of MnAs and parallel to the interface. The angular distance of the satellite maxima measured at room temperature yields an average lateral period of the domain structure of 247 nm. The thickness of the original MnAs film was determined to be 38 nm using x-ray reflectivity measurements [11]. The equilibrium

domain period is thus estimated to be 190 nm [9]. As the diameters of the smallest disks are sufficiently small (≈80 nm) only one elastic phase domain exists in an individual disk, which was confirmed at room temperature using magnetic force microscopy [15]. The full triangles in Fig. 1 show the temperature dependence of the phase content ξ of αMnAs in the unpatterned continuous epitaxial layer. As reported in [8] the heating and cooling curves roughly coincide and hence the temperature hysteresis in the range of phase coexistence is negligible. In the present sample this range extends quite broad between 270 and 315 K. The overall phase coexistence range amounts to 45 K. In the vicinity of the transition temperature of 315 K the αMnAs content rises from zero almost linearly. When lowering the temperature further the rise of the phase content weakens, and the content gradually reaches the saturation level at unity. The temperature dependence of the phase content ξ in the small MnAs disks is also shown in Fig. 1 (hollow symbols). When cooling down the MnAs disks, αMnAs first emerges in the disks only at a temperature as low as 298 K. We observe a significant supercooling of the disks, i.e. all of them remain to be in the *β*-phase. Subsequently, the αMnAs content rises with further cooling until all the disks are transformed to the α-phase at 270 K. Once the β-phase had been realized entirely in all the disks, the sample was heated. Similar to the cooling case the temperature was as high as 285 K when the disks began transforming into the β-phase. Therefore, a significant extent of overheating takes place in the disks in contrast to the continuous MnAs layer. The behavior of the MnAs nanodisks at the first order phase transition is similar to that of bulk MnAs [2, 3]. The same widths of the hysteresis in the temperature dependencies of the magnetization in bulk MnAs [2] and of the phase content ξ(T) in the MnAs disk ensemble are found. Moreover no phase coexistence takes place in the individual disks [15]. Nevertheless, the phase transition in the disk ensemble does not occur abruptly at a certain temperature. The slope of the temperature curve dξ/dT has increased only by a factor of 2-3 compared to that of the layer curve. The fact that the experimental disks are not perfectly identical due to small fluctuations in their sizes and shapes and the random presence of defects may be responsible for the finite temperature window at the phase transition. The strong temperature hysteresis observed in the experiment (Fig. 1) manifests the supersaturation in individual disks.

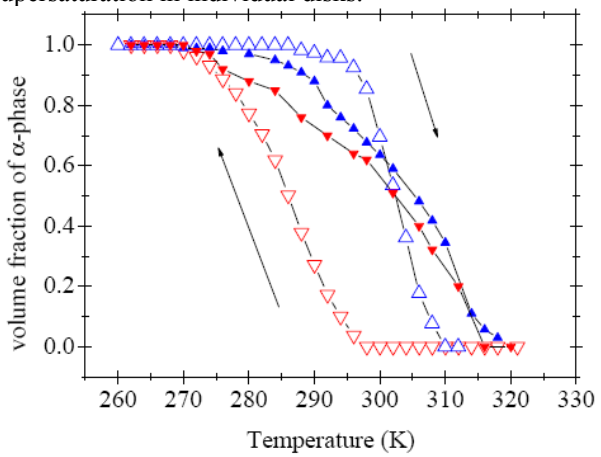

Fig. 1: Temperature dependence of the volume fraction ξ of the MnAs α-phase illustrating the coexistence of the two phases in the MnAs layer (full symbols) and the MnAs disk (hollow symbols) system. Upwards (downwards) directed triangles correspond to the heating (cooling) curve. The changes of the composition with temperature are steeper in the disk system than in the continuous layer system. The range of phase coexistence in the layer system is as large as 45 degrees and only a very small hysteresis is observed.The disk system changes from one phase to the other within 15 to 20 degrees and a strong hysteresis (width 20 ±5 K) of the temperature curve is found.

The authors thank E. Dudzik, E. Wiebecke, C. Herrmann, V. M. Kaganer, L. DÄaweritz, and A. Erko for their support and for helpful discussions.

References:

[1]. M. Ramsteiner, H. J. Hao, A. Kawahrazuka, H. J. Zhu, M. KÄastner, R. Hey, L. DÄaweritz, H. T. Grahn, and K. H. Ploog, Phys. Rev. B **66**, 081304 (2002).
[2]. V. A. Chernenko, L. Wee, P. G. McCormick, and R. Street, J. Appl. Phys. **85**, 7833 (1999).
[3]. G. A. Govor, J. of Magnetism and Magnetic Materials **54**, 1361 (1986).
[4]. B. T. Willis and H. P. Rooksby, Proc. Phys. Soc. London Sect. B **67**, 290 (1954).
[5]. R. H. Wilson and J. S. Kasper, Acta Cryst. **17**, 95 (1964).
[6]. M. Tanaka, J. Harbison, M. C. Park, Y. S. Park, T. Shin, and G. M. Rothberg, J. Appl. Phys. **76**, 6278 (1994).
[7]. F. Schippan, A. Trampert, L. DÄaweritz, and K. H. Ploog, J. Vac. Sci. Technol. B **17**, 1716 (1999).
[8]. V. M. Kaganer, B. Jenichen, F. Schippan, W. Braun, L. DÄaweritz, and K. H. Ploog, Phys. Rev. Lett. **85**, 341 (2000).
[9]. V. M. Kaganer, B. Jenichen, F. Schippan, W. Braun, L. DÄaweritz, and K. H. Ploog, Phys. Rev. B **66**, 045305 (2002).
[10]. T. Plake, M. Ramsteiner, V. M. Kaganer, B. Jenichen, M. KÄastner, , L. DÄaweritz, and K. H. Ploog, Appl. Phys. Lett. **80**, 2523 (2002).
[11]. B. Jenichen, V. M. Kaganer, C. Herrmann, L. Wan, L. DÄaweritz, and K. H. Ploog, Z. Kristallogr. **219**, 201 (2004).
[12]. C. P. Bean and D. S. Rodbell, Phys. Rev. **126**, 104 (1962).
[13]. N. Menyuk, J. A. Kafalas, K. Dwight, and J. B. Goodenough, Phys. Rev. **177**, 942 (1969).
[14]. F. Iikawa, M. J. S. Brasil, C. Adriano, O. D. D. Couto, C. Giles, P. V. Santos, L. DÄaweritz, I. Rungger, and S. Sanvito, Phys. Rev. Lett. **95**, 077203 (2005).
[15]. Y. Takagagi, B. Jenichen, C. Herrmann, E. Wiebecke, L. DÄaweritz, and K. H. Ploog, Phys. Rev. B **73**, 125324 (2006).
[16]. M. KÄastner, F. Schippan, P. SchÄutzendÄube, L. DÄaweritz, and K. H. Ploog, J. Vac. Sci. Technol. B **18**, 2052 (2000).
[17]. L. DÄaweritz, L. Wan, B. Jenichen, C. Herrmann, J. Mohanty, A. Trampert, and K. H. Ploog, J. Appl. Phys. **96**, 5056 (2004).
[18]. B. Jenichen, V. M. Kaganer, F. Schippan, W. Braun, L. Däweritz, and K. H. Ploog, Mat. Science and Eng. B **91**, 433 (2002).
[19]. B. Jenichen, O. Brandt, and K. H. Ploog, Appl. Phys. Lett. **63**, 156 (1993).

	EXPERIMENTAL REPORT **Doping dependence of the low-temperature order-disorder transition of the stripe phase in $La_{2-x}Sr_xNiO_4$**	Proposal N° BESSY Instrument MagS **S2** Local Contact Ralf Feyerherm
Principal Proposer: Experimental Team:	C. Schüßler-Langeheine – Univ. Köln R. Feyerherm, E. Dudzik – HMI, Berlin M. Benomar, M. Braden – Univ. Köln L.H. Tjeng – Univ. Köln	Date(s) of Experiment 2006

Date of Report: Feb. 2007

Sr doped La_2NiO_4 shows an intriguing ordering of spin and charge degrees of freedom at low temperature, the famous stripe phase, which is also found in isostructural high-temperature superconductors. The crystal structure (Fig. 1) consists of NiO_2 layers, which are separated by double layers of LaO. Replacing La by Sr introduces holes into the system. At low temperatures, the doped roles arrange themselves in parallel lines, which run diagonally through the NiO_2 planes and form antiphase domain walls for the antiferromagnetic order on the hole-poor Ni sites in between. This superstructure causes additional reflections in the diffraction pattern.

The hole concentration in the hole stripes is essentially constant so that different doping levels lead to different spacings between stripes. While the stripe order can be incommensurate, each stripe has to be in register with respect to the lattice. These two conflicting tendencies lead to frustration. Incommensurate order is realized by a statistical sequence of commensurate stripe spacings such that on average the stripe spacing matches the doping level. The situation is similar for the arrangement of stripes in neighbouring layers: Coulomb repulsion favours an antiphase arrangement, which can be readily, realized when the spacing in the NiO_2 layer is commensurate and an odd multiple of the lattice spacing. In all other cases the arrangement has to be partially disordered as well.

One particularly puzzling observation in these compounds is the different temperature dependence of the stripe order as found by neutron diffraction and x-ray diffraction respectively: While in neutron diffraction experiments the intensity of the stripe order peaks saturates at low temperatures resembling the *M(T)* curve of a conventional ferromagnet [1], x-ray diffraction finds a maximum intensity of the diffraction peak at intermediate temperatures and a decay of the peak when the sample is cooled further [2] (c.f. upper panel of Fig. 3). This decay towards lower temperatures is accompanied by a broadening of the diffraction features indicating a loss of spatial coherence. From a careful analysis of soft x-ray diffraction data from a sample with a Sr content (x) of 0.2, we found that the *integrated* intensity of the charge and spin order peak, which is a measure of the order parameter of the phase, essentially stays constant upon cooling; the decay of the peak height is mainly due to the broadening of the peak [3]. From this we conclude that upon cooling the phase breaks into smaller and smaller domains while the character of the order and its periodicity within each domain is conserved.

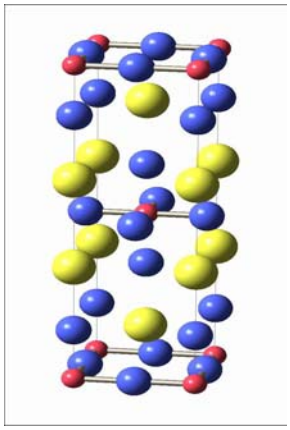

Fig. 1: *Crystal structure of the parent compound La_2NiO_4. Ni ions are red, O blue, La yellow. The NiO_2 planes are indicated by the Ni-O bonds.*

Such an order-disorder transition at low temperatures has been theoretically discussed for stripe phases, and two different mechanisms have been considered. One of them is a pinning of the stripes at low temperatures at the disorder potential created by the randomly distributed dopant ions [4]. The other mechanism is an intrinsic effect due to frustrations in the stripe phase that would lead to disorder at low temperatures even in a clean system [5].

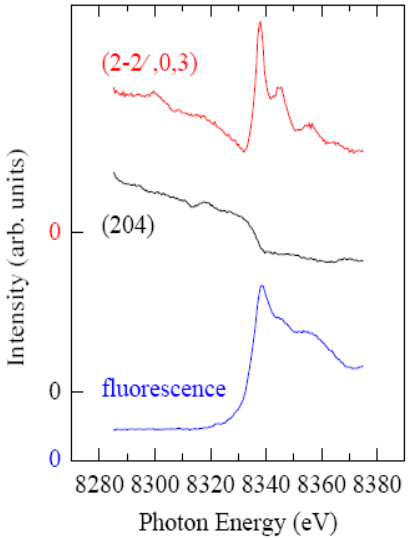

Fig. 2: *Ni-K Resonance of the (2-2ε,0,3) charge order peak in $La_{1.8}Sr_{0.2}NiO_4$ (red) compared to the energy dependence of the fundamental (204) Bragg peak (black) and the fluorescence signal (blue).*

In order to probe the relevance of both scenarios it is instructive to compare the order-disorder transition in

differently doped samples. We chose one sample with x ≈ ⅓, where the order is essentially commensurate and one sample with a lower doping level, x = 0.2, which shows incommensurate order. While the amount of intrinsic disorder is considerably different for the two samples, the influence of the dopant ions should be comparable.

The experiments were carried out at the MAGS-beamline of the Hahn-Meitner-Institute at BESSY at the Ni K-resonance around 8340 eV. The energy dependence of the (2-2ε,0,3) charge-order peak is presented in Fig. 2 (red line) together with that of the fundamental (204) Bragg peak (black) and the fluorescence signal (blue). The notation for the diffraction peaks is such that the H direction is along the modulation direction of the stripes in the NiO_2 plane, the K direction along the length of the stripes and the L direction perpendicular to the NiO_2 planes along c*.

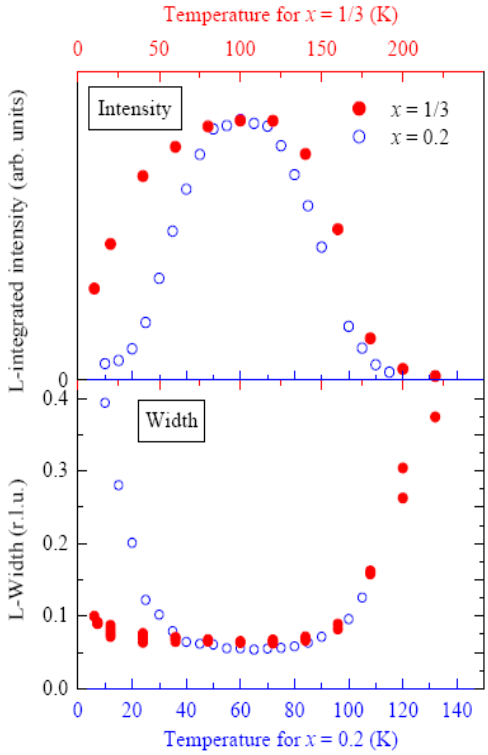

Fig. 3: *L-integrated intensity (upper panel) and width along L (lower panel) vs. temperature for the two studied samples.*

The charge-order spectrum shows a sharp resonance characteristic for an electronic modulation [6] with a moderate resonant enhancement of about 50 percent. In contrast to that, for the fundamental Bragg peak the loss of scattering volume caused by the reduced photon means free path above the resonance threshold is dominating and leads to an overall decreasing intensity.

At the Ni-K edge a wide part of the momentum space can be reached and the six-circle diffractometer at the MAGS beamline allows studying the peak width in all three directions of reciprocal space. The results along L are presented in the lower panel of Fig. 3. Two different temperature scales are used for the two samples to account for the doping dependence of the transition temperatures. Presented in this way the high- and intermediate-temperature behaviour of both samples are very similar. In the low-temperature region, however they curves look different. The incommensurate sample shows a dramatic loss of spatial coherence with the width at the lowest studied temperature being about 8 times larger than the minimum width around 60 K. Also the commensurate sample shows a loss of coherence, but the effect is much weaker, which is also reflected in the less prominent loss of peak height (upper panel). We can therefore assume that the influence of the disorder potential caused by the Sr ions is not the dominating because of the broadening and that the intrinsic disorder is more important here. It is interesting to consider, why the low-temperature order-disorder transition is not observed in neutron diffraction experiments. The intensity of a diffraction peak is distributed in a certain region of momentum space. A diffraction experiment integrates the intensity inside a volume given by the momentum resolution, i.e. by the detector acceptance and the beam divergence. If this probing volume is larger than the volume of the peak, a peak broadening will not affect the detected intensity as long as the peak is fully inside the probing volume. Usually, the resolution in neutron diffraction is worse than in synchrotron x-ray diffraction experiments. But the broadening, e.g. of the 0.2 sample is so strong that it should be visible even with very moderate resolution. The discrepancy between x-ray and neutron results must therefore have a different explanation and may be related to the different scattering cross sections and time scales probed in the respective experiments. In conclusion, we observed a striking difference in the low-temperature order-disorder transition in doped La_2NiO_4 between a sample with commensurate and one with incommensurate order. From this we conclude that the intrinsic disorder of the stripe phase is driving this transition rather than the disorder potential of the dopant ions. The change of the coherence length in the incommensurate sample is too strong to assign the fact, that neutron diffraction does not observe this transition, to the low momentum resolution in neutron experiments.

References:

[1]. J. M. Tranquada, D. J. Buttrey and V. Sachan, Phys. Rev. B **54**, 12318 (1996).
[2]. P. D. Spencer et al., Eur. Phys. J. B **46**, 27 (2005).
[3]. J. Schlappa et al., to be published.
[4]. S. Bogner and S. Scheidl, Phys. Rev. B **64**, 05417 (2001).
[5]. J. Schmalian and P. G. Wolynes, Phys. Rev. Lett. **85**, 836 (2000).
[6]. Y. Murakami et al., Phys. Rev. Lett. **80**, 1932 (1998).

BENSC	**EXPERIMENTAL REPORT** **Interplay between structural properties and electronic ground states in the organic superconductor κ-(BEDT-TTF)$_2$Cu[N(CN)$_2$]Br**	Proposal N° BESSY Instrument MagS **S2** Local Contact Ralf Feyerherm
Principal Proposer: Experimental Team:	A.U.B. Wolter – HMI, Berlin R. Feyerherm, E. Dudzik – HMI, Berlin S. Süllow – TU Braunschweig Ch. Strack, M. Lang – JWGU Frankfurt/M. D. Schweitzer – Univ. Stuttgart	Date(s) of Experiment 2006

Date of Report: Feb. 2007

Due to their exotic superconducting and normal-state properties, resembling those of the high-T_c cuprates, the organic charge-transfer salts κ-(BEDT-TTF)$_2$X, X = Cu(NCS)$_2$, Cu[N(CN)$_2$]Br and Cu[N(CN)$_2$]Cl have been intensively studied in recent years. Resulting from a layered crystal structure, consisting of alternating planes of conducting (BEDT-TTF)$_2^+$ cations and insulating anions X$^-$, the electronic properties of these materials are quasi two-dimensional. This leads to electronic ground state properties for the series of materials which are commonly summarized within a conceptual phase diagram, with the antiferromagnetic insulator X = Cu[N(CN)$_2$]Cl and the correlated metals X = Cu[N(CN)$_2$]Br, Cu(NCS)$_2$ on opposite sites of a bandwidth-controlled Mott transition [1].

In recent thermal expansion measurements on κ–(BEDT-TTF)$_2$Cu[N(CN)$_2$]Br (abbreviated κ-Br hereafter) three kinds of anomalies have been identified [2]: one associated to the superconducting transition at T_c = 11.6 K, a phase-transition-like anomaly at T^* ~ 40 K, and a kinetic glass-like transition at T_g = 77 K. The origin of the glass-like transition is still unclear and led to various hypotheses [2-4], from which the idea of a configurational freezing-out of the terminal ethylene groups (CH$_2$)$_2$ of the BEDT-TTF molecule taking place at T_g received most support. In this material, the terminal ethylene groups can adopt two possible configurations, with either an *eclipsed* or *staggered* relative orientation of the outer C-C bond. Then, the "glassy" state below T_g would be characterized by the level of frozen-in disorder of the two configurations, and which – by way of the history dependence of the freezing process – accounts for the pronounced cooling-rate dependencies of various bulk properties observed for this organic superconductor. These facts in combination with the striking sample-to-sample variations in the resistivity [5] above T_g, which have been linked to real structure effects (disorder, defects) [6], and the importance of information about the (local) structural properties for theoretical models to account for superconductivity in these compounds, lead to an increased interest in the local structure.

Therefore synchrotron x-ray diffraction experiments have been performed on two single crystals of κ-Br using the 7 T multipole wiggler beamline MAGS. To avoid sample heating as well as irradiation damages the power of the beam (full beam intensity 10^{12} photons/s at 10 keV) was reduced using appropriate absorber foils. The single crystals were grown by an electrochemical technique using different solvents for both syntheses

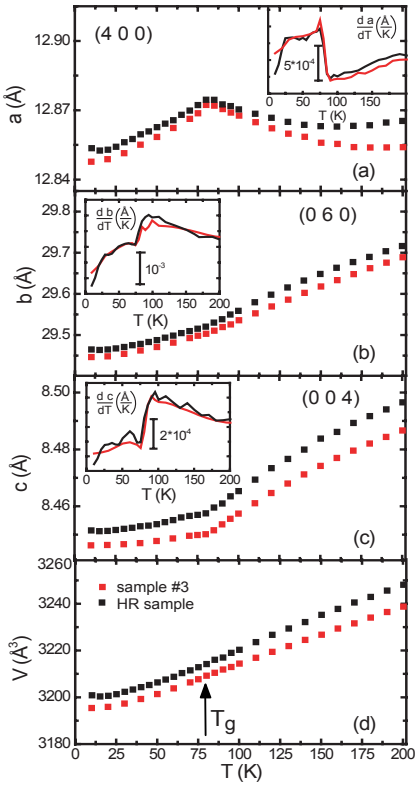

Fig. 1 (a)-(d): *The T dependence of the lattice parameters a, b, c and of the volume V for sample #3 and the HR sample of -Br. In the insets the derivative of the lattice parameters is shown, indicating a structural anomaly at ~ 80 K.*

routes, which may cause variations in the purity of the material and the structural perfection. They have been characterized in full detail including resistivity experiments [5] (sample #3 and sample labelled HR). Whereas the HR sample exhibits a braod maximum in the resistivity around 100 K, sample #3 has a lower resistivity and no maximum has been observed. Apart from this sample-dependent, extrinsic scattering contribution, however, the different variants behave almost identically with regard to the glass-like transition at T_g, abrupt changes in the resistivity data at T^* and the superconducting transition at T_c ~12 K.

In an attempt to search for possible structural differences of the two single crystals, the presence of local structural disorder and to establish if the structural parameters control the electronic ones in κ-Br, we have performed a detailed mapping of various Bragg peaks and measured the lattice parameters as function of temperature. All

temperature dependencies were measured on heating in order to avoid hysteresis effects, with cooling and subsequent heating rates of ~2 K/min for these investigations. From our data we do not observe any indication of splitting of Bragg reflections down to 10 K, excluding the possibility of a significant (monoclinic) distortion at the T^* or T_g transitions.

The temperature dependent results for the *a*, *b* and *c* parameters are depicted in Fig. 1. The data for the three principal axes show a highly anisotropic behaviour. Surprisingly, only the quantitative behaviour of the lattice parameters appears to be different, with the one from the HR sample being somewhat larger. For both samples, upon heating, for the *a* axis an upturn is observed. After reaching its maximum at T_g, the lattice constant abruptly decreases again up to ~200 K. In contrast, for the *b* and *c* directions we find a monotonic increase up to 200 K, with only a small kink at 80 K. However, as result of compensating lattice parameter anomalies, no anomaly in the unit cell volume *V(T)* is observed at T_g for both crystals. The anomalous behavior of the *a* lattice parameter suggests an anomalous change in the bond angle of --CN--Cu--NC-- in the polymeric chain in the temperature range well above T_g. This in turn might induce a change in the hydrogen bonding –CH···N—between terminal ethylene groups and nitrogen atoms on the polymer, thus affecting the electronic properties of κ-Br.

Another important question concerns the relationship between the ethylene ordering and a possible superstructure formation below T = 200 K [4,7]. In order to check for a superstructure formation we performed high-resolution synchrotron x-ray diffraction experiments at 28 K on sample #3. According to Ref [7], claiming that the wave vector of the displacive structural distortion doubles the lattice parameter along *c* and the reciprocal wave vector of all observed reflections has a sizeable a^* component, the following reflections have been examined in our work: (3 0 0.5), (5 0 0.5), (7 0 0.5), (6 0 3.5), (7 0 3.5), (8 0 3.5). We found no evidence for any superstructure formation for the crystal used in our work in contrast to former x-ray "monochromatic" Laue photographic studies claiming a commensurate lattice modulation with a propagation vector 0.5 c^*. This leads us to believe that these kinds of materials are extremely sensitive regarding their thermal history and handling in that sense that slow and rapid cooling through the glass-like transition may modify the local potential of the ethylene groups and thus the overall properties of the system.

Parts of the above results will be published in the near future [8].

References:

[1]. K. Kanoda, Hyperfine Interact. **104**, 235 (1997).
[2]. J. Müller *et al*., Phys. Rev. B **65**, 144521 (2002).
[3]. X. Su *et al*., Phys. Rev B **57**, R14056 (1998).
[4]. M. A. Tanatar, T. Ishiguro, T. Kondo, G. Saito, Phys. Rev. B **59**, 3841 (1999).
[5]. Ch. Strack *et al*., Phys. Rev. B **72**, 054511 (2005).
[6]. M. Lang *et al.*, ISCOM 2005 Conference: http://dx.doi.org/10.1007/s10909-006-9018-x
[7]. Y. Nogami *et al*., Solid State Comm. **89**, 113 (1994).
[8]. A. U. B. Wolter *et al*., Physical Review B in print (2007).

	EXPERIMENTAL REPORT **Formation of optically active nanoparticles in gold and silver doped silicate glasses: ASAXS studies of synchrotron activated growth.**	Proposal N° BESSY Instrument ASAXS **S3** Local Contact Armin Hoell
Principal Proposer: Experimental Team:	A. Hoell – HMI, Berlin K. Rademann, M. Eichelbaum – HU, Berlin D. Tatchev – BAS IPC Sofia, BG S. Haas – HMI, Berlin	Date(s) of Experiment 2006

Date of Report: Feb. 2007

Recently, we have developed a novel method to generate high concentrations of nearly monodisperse gold nanoparticles in soda lime silica glasses by irradiating samples with synchrotron light [1]. This way, gold and silver clusters even smaller than one nanometer become accessible and reveal extraordinary optical properties like high quantum yield photoluminescence. Gold and silver clusters were produced by local activation of a soda lime silica glass with synchrotron radiation provided by the dipole X-ray scanner DEX02 (Jenoptik MT GmbH) at the beamline of AZM in co-operation with Dr. Löchel.

The glass composition was $70SiO_2$-$20Na_2O$-10CaO (mol%). The gold or silver contents were 0.01 and 0.04 mol%, respectively. Gold containing samples for SAXS measurement were annealed at 550°C for 1, 3, 5, 10, 20, 30, 45, and 60 minutes. During these heat treatments, gold particles grow only in the activated glass areas. Significant SAXS scattering over the background is observed from 20 minutes of annealing on – Figure 1. The curves show both increase of the scattered intensity as well as growth of the size of the scattering objects. The intensity increase at high q values is the tail of the first WAXS peak of the glass matrix.

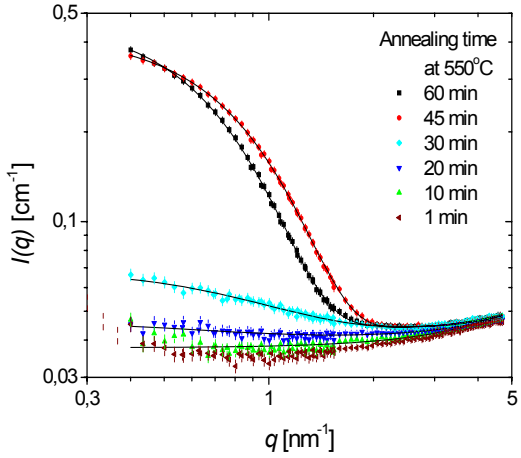

Fig. 1: Scattering curves obtained from gold containing glasses annealed for different time periods at 550°C.

The solid lines in Figure 1 represent fits obtained by a model of spherical particles with log-normal size distribution. The scattering of the glass matrix was approximated with an $A+Bq^2$ term [2]. The so obtained size distributions are shown in Figure 2, particle mean radii, particle numbers and volume fractions in Figure 3. These results show that the number of particles initially increases, but decreases for longer annealing times. This is in accordance with a two step growth process. Firstly, smaller clusters grow driven by diffusion of isolated atoms through the glass matrix, and secondly, after approximately 35 minutes larger particles start to grow at the expense of smaller ones (Ostwald ripening). This is accompanied by an increasing volume fraction of gold particles during the first stage, whereas this value nearly remains constant during the ripening process. It has to be noted that the volume fraction is rather low in the ripening regime. An estimate shows that maximum 7% of the added gold had precipitated.

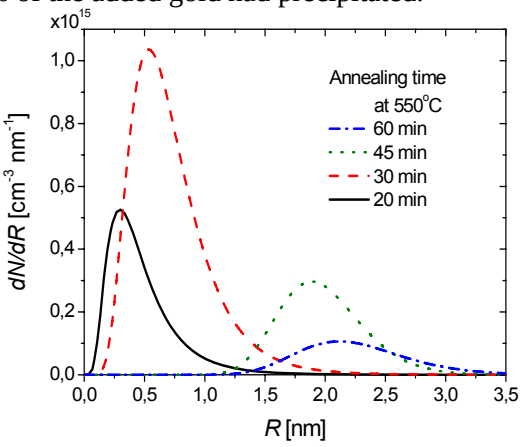

***F**ig. 2:* Size distributions of gold clusters in glass after different annealing times.

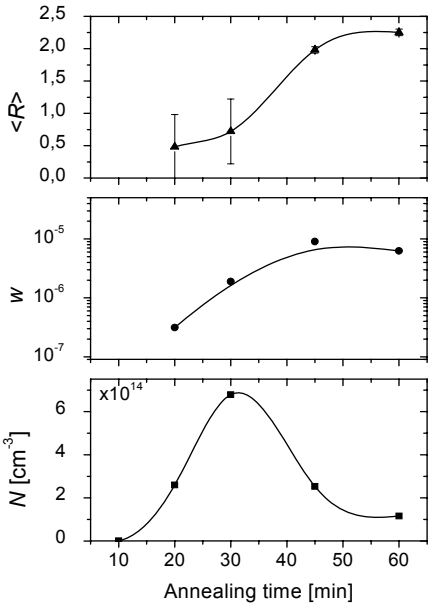

Fig. 3: Annealing time dependence at 550°C of gold clusters in glass; mean particle radius, <*R*>, volume fraction, *w*, and number of particles per unit volume, *N*.

The data were calculated under the assumption of pure gold particles. This is confirmed by ASAXS measurements, which were also accomplished during this beam time. Figure 4 shows a clear anomalous effect at the gold absorption edge. The sample was annealed for 45 minutes at 550°C. The magnitude of this effect will be further evaluated and compared to other annealing times, in order to learn more about the compositional aspects of the transformation.

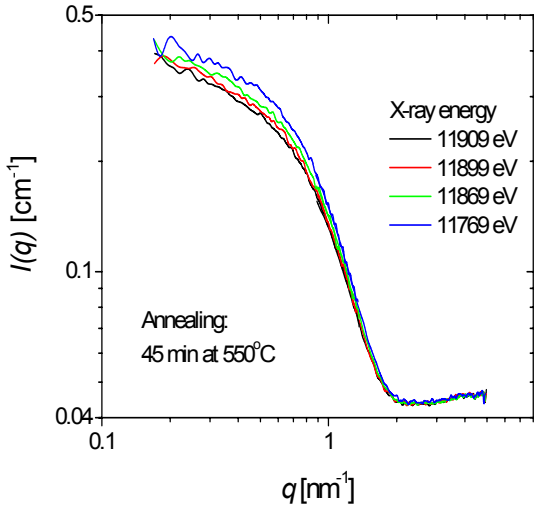

Fig. 4: Anomalous SAXS effect at the Au L_{III} absorption edge for a sample annealed at 550°C for 45 minutes.

Small angle scattering measurements were performed also on silver containing glasses. Selected size distributions, volume fractions, and numbers of particles per unit volume are shown in Figure 5. The determined particle radii range between 0.5 and 0.6 nm.

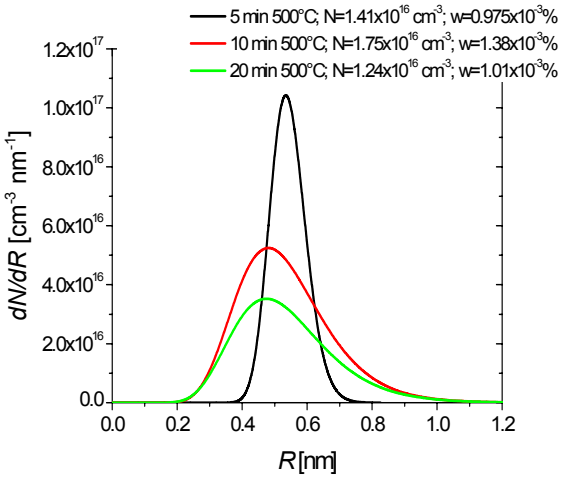

Fig. 5: Size distributions of silver particles in glasses formed after different thermal treatments.

Part of the reported data is already used in a paper submitted to Journal of the American Chemical Society.

References:

[1]. M. Eichelbaum, K .Rademann, R. Müller, M. Radtke, H. Riesemeier, W. Görner, Angew. Chem. Int. Ed. (2005) **44**, 7905-7909.

[2]. D. L. Weinberg, Phys. Lett. (1963) **7**, 324-325.

	EXPERIMENTAL REPORT Nano-structure of shed snake skins compared to human skin studied by SAXS	Proposal N° BESSY Instrument ASAXS **S3** Local Contact Armin Hoell
Principal Proposer: Experimental Team:	A. Hoell – HMI, Berlin M. Kumpugdee-Vollrath – TFH, Berlin T. Ngawhirunpat – TFH, Berlin I. Zizak – HMI, Berlin	Date(s) of Experiment 2006

Date of Report: Feb. 207

ABSTRACT

It is reported that shed snake skins can be used successfully as model membrane for in-vitro (outside human body) studies. There are many types (species) of snakes that can be used for this purpose and the skins can be received without killing and without any cost from the snake-farm or zoo. Therefore many species are used in this project in order to determine which skins have similarity to human skin. These skins can then be used as alternative model membranes in in-vitro test of medical products e.g. transdermal drug delivery systems (TDDs) as creams, ointment, gel, etc. to observe their pharmacological activities. Because of the high resolution of the small angle x-ray scattering (SAXS), this technique was mainly used in this project. The data from shed snake skins from different species and human skin were finally compared.

INTRODUCTION

Shed snake skin has been reported to have many advantages more than other natural skins [1]. The permeability profiles through the shed snake skin closely match that through human stratum corneum. There are many advantages in using the shed snake skin as a model membrane. It can be obtained without killing the animal. The variation in permeability was lower than that of cadaver and fresh human skin. It can be kept for months under refrigeration. It releases fewer interfering substances in analytical procedure. The behaviour of the shed snake skin is also very similar to that of human stratum corneum. There are two parallel permeation pathways: lipid and pore pathways in shed snake skin as in human stratum corneum. The lipid content of the shed snake skin is nearly equal to the human stratum corneum [2]. The lack of hair follicles and skin appendage, however, as well as the existence of scale in shed snake skin are the main differences between shed snake skins and human skin. There are some studies about shed snake skins, however, the basic permeation data of various drugs through the snake skin has been mainly performed by using shed snake skin of black rat snake Elaphae obsoleta [3] and found that it can be used as a model membrane for the invitro skin permeation studies of transdermal delivery systems (TDDs), especially lipophilic drugs. In Thailand are various species of Thai snakes such as Thai cobra (Naja kaouthia) and Thai python (Python molurus bivittatus), which were used in this present study compared to other skins. The small angle X-ray scattering (SAXS) can give details of the secondary structure up to nano-scale and was successfully used for characterizing the human stratum corneum [4]. Therefore SAXS was mainly used in this project.

MATERIALS AND METHODS

Materials

For this present study four species of shed snake skins i.e. Naja kaouthia (NK), Viper calloselasma (VC), Python molurus bivittatus (Pml) and E. obsoleta (EO) were obtained from Pata Department Store' Snake farm, Bangkok, Thailand. They were collected after the snake shed the skin from the body within 1 day. Human skin (human) was obtained from surgery department of a hospital. All the samples were stored at room temperature under dry conditions prior to use.

Method

Small Angle X-ray Scattering (SAXS) The experiments were performed at the new SAXS instrument of the Hahn-Meitner Institute (7T-MPW-SAXS) installed at the synchrotron source BESSY in Berlin, Germany. The scattering patterns were acquired using a 2D position sensitive gas detector with delay line read out (Molecular Metrology). About 5 mg of dry skins of both parts (hinge and scale area) were measured by SAXS, while increasing the temperatures of the samples in steps of 5 °C from 25 °C to 100 °C at X-ray energy of 8000 eV under vacuum. The effect of swelling was determined by soaking the skins in sterile water for at least 14 h. The samples were mounted then into the sample holder between two sealed capton foils and measured at temperatures between 25 °C to 100 °C in steps of 5 °C. The difference was that a wet sample was purged with helium gas during measurement in order to reduce air scattering background in the sample chamber.

RESULTS AND DISCUSSION

Figure 1 shows that the morphology of the skin from different snakes is different in diameter und a number of hinge and scale region. These differences may affect the secondary structure, which will be studied in the next project by using the setup that can focus on a particular region. Figure 2 shows that there are differences between SAXS-patterns on shed snake and human skins. This means that the repeat distance of components e.g. lipids and proteins have different thicknesses because the peak maxima are at different scattering vectors (q). The heating has an effect on the structure both for shed snake and human skins, which can be seen in the shifting of the peak maxima to the right with increasing temperature. This means that the repeat distance gets smaller because the peak maximum is shifting to larger scattering angles or larger magnitudes of scattering vectors. This may be

due to the fact that lipids are in both the skins which can be oriented in different forms e.g. gel-, crystalline-, hexagonalphase. This hypothesis may be proved in further experiments. If the SAXS technique is combined with other techniques e.g. calorimetry (DSC) and spectroscopy (FTIR) a deeper understanding about the structure of the skins can be deduced. The data from DSC and FTIR were formerly shown in another report [5].

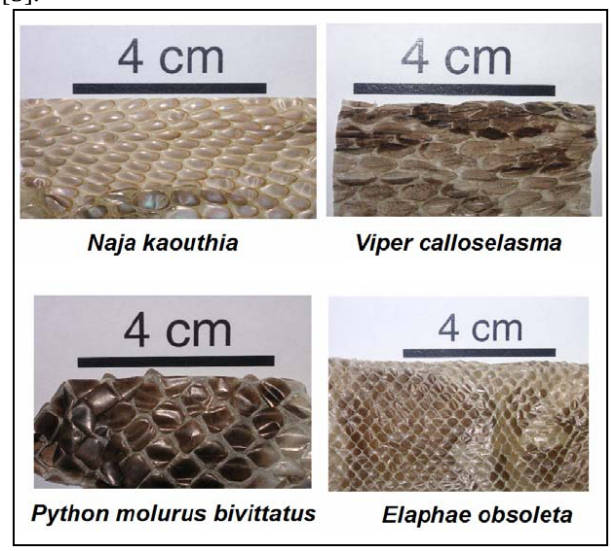

Fig. 1: *Photographs of different species of shed snake skins showing different diameters and a number of hinge and scale regions.*

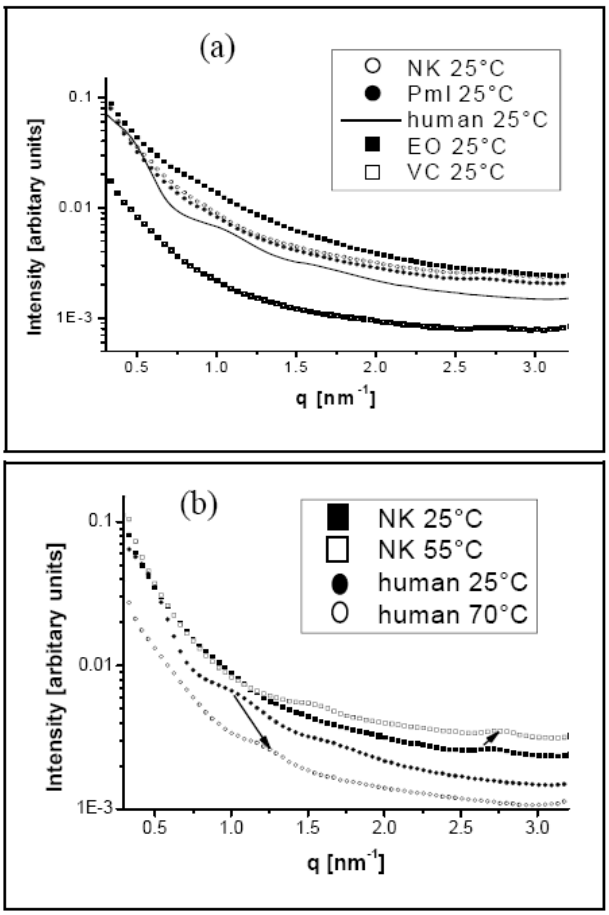

Fig. 2: ***(a)*** *SAXS curves show a significant difference of the shape of wet shed snake skins compared to human skin measured at 25°C,* ***(b)*** *SAXS curves of wet shed snake skins compared to human skin indicate a peak shifting to the right with increasing temperature.*

CONCLUSION/PROSPECTIVE PLAN

The next step will be the challenge to find out the phase of lipids or lipid-mixtures by using the mathematical model. The effect of different surroundings during measurement to simulate the conditions, which will be used in in-vitro-test, will be studied as well. The further type of model skins e.g. shed snake skin from snake types existing in Germany e.g. Kreuzotter (Vipera berus), etc. will be studied and compared with other commonly used skins e.g. pig skin, synthetic skin. The data from SAXS and eventually combined with that from other techniques can give deeper understanding why the in-vitro-test with a model membrane from shed snake skins is comparable or even better than that from other commonly used skin models. The number of in-vivo-tests or direct tests at the human bodies can therefore be reduced.

ACKNOWLEDGEMENTS

The authors would like to thank the German Synchrotron Source in Berlin (BESSY), Dr. Tatchev and Mr. Haas for their experimental support during SAXS experiments. Thanks are also given to the Master-students Ms. Gögebakan, Ms. Bilek, Mr. Heckötter, Mr. Delissen, Mr. Hanusch and Mr. Wlosnewski for experimental help.

References :

[1]. Takahashi, K., et al, 1993. Percutaneous absorption of basic compounds through shed snake skin as model membrane. J. Pharm. Pharmacol. 45, 882-886.

[2]. Ngawhirunpat, T., et al, 2006. Comparison of the percutaneous absorption of hydrophilic and lipophilic compounds in shed snake skin and human skin. Pharmazie **61** (4), 331-335.

[3]. Itoh, T., et al, 1990. Use of shed snake skin as a model membrane for in vitro percutaneous absorption studies: comparison with human skin. Pharm. Res. **7**, 1042-1047.

[4]. Gurny, R., Teubner, A., (Eds.) 1993. Dermal and Transdermal Drug Delivery. Wissenschaftliche Verlagsgesellschaft mbH, Stuttgart, Germany.

[5]. Kumpugdee-Vollrath, M., et al, Comparison of secondary structure of shed snake skins and human skin by small angle scattering (SAXS) technique, Proceeding 13th International Pharmaceutical Technology Symposium, 10-13/0972006, Antalya, Turkey.

	EXPERIMENTAL REPORT **Effect of MoO_3 on phase separation characteristics of a soda-lime-silica glass**	Proposal N° BESSY Instrument ASAXS **S3** Local Contact Armin Hoell
Principal Proposer: Experimental Team:	A. Hoell – HMI, Berlin R. Kranold – Uni Rostock D. Tatchev – BAS IPC Sofia, BG S. Haas – HMI, Berlin	Date(s) of Experiment 2006

Date of Report: Feb. 2007

1. Introduction

Glass-in-glass phase separation has been of interest, because it has an effect on numerous properties and the crystallization behaviour of glasses. The Na_2O-CaO-SiO_2 system, which is the basis of most commercial glasses, has a metastable miscibility gap in the high-silica corner of the ternary phase diagram. The glass investigated (NCS glass) with nominal composition 13 Na_2O-11CaO-76SiO_2 (mol%) separates via a binodal mechanism into dropletlike precipitates of nearly pure silica (Fig. 1) and a residual glass matrix [1]. The process has three stages which are nucleation, growth and Ostwald ripening. In previous small-angle Xray scattering (SAXS) studies, we investigated the effect of minor anionic additives, Cl^- [2] and OH^- [3], on the phase separation behaviour of the NCS glass. Here, the effect of small amounts of MoO_3 on the phase separation characteristics of the NCS glass is studied. In particular, the influence of MoO_3 on the two competitive parameters thermodynamic driving force, $\Delta\mu$, and interface tension between droplet phase and matrix, σ, controlling the phase separation process is investigated.

2. Glass samples

The glasses investigated were prepared from the same batch mixed to obtain the pure NCS glass with nominal composition 13Na_2O-11CaO-76SiO_2 (mol%). To one part of this batch, a certain amount of MoO_3 was added in order to obtain NCS glass doped with 0.5 mol% MoO_3. Details of the glass melting procedure are given elsewhere [3]. By wet chemical analysis, a Na_2O deficit of 1.4 mol% and a CaO excess of 0.6 mol% with regard to the nominal composition has been determined. Therefore, $\Delta\mu$ is a little increased for the NCS glass (Fig. 4 and Table) in comparison with a glass of nominal composition [1]. (The glasses were prepared and analyzed in the Jenaer Glaswerk GmbH.)

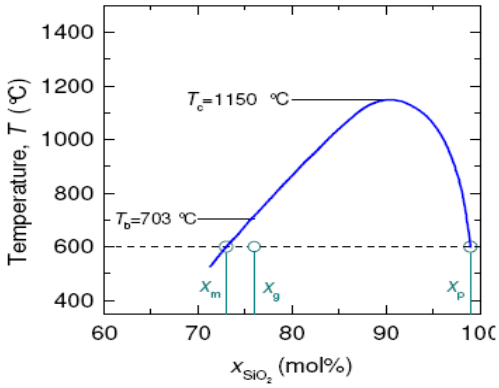

Fig. 1: *Miscibility gap according to the quasibinary tie line SiO_2-[(13/24)Na_2O- (11/24)CaO] given in Ref. [1]; T_c=critical temperature, T_b=binodal temperature. For T=600°C, the silica concentrations of the homogeneous glass, x_g=0.76, of the precipitates, x_p=0.99, and of the matrix, x_m=0.73, are marked.*

In order to obtain comparable SAXS results (Figs. 3 and 4) from the glasses with and without MoO3, the heat treatment of all glasses was performed simultaneously at 600 °C for each of the times indicated in Fig. 3.

3. Interface tension

The effect of MoO_3 on the interface tension, σ, was established by determining the wetting angle, α, at T=1200 °C of a drop of the liquid NCS melt, without and with 0.5 mol% MoO_3, on the flat surface of pure silica glass. It was estimated that the value of σ for the pure NCS glass at 600 °C amounts to about 0.08 N/m, that of the doped glass is nearly 40% higher.

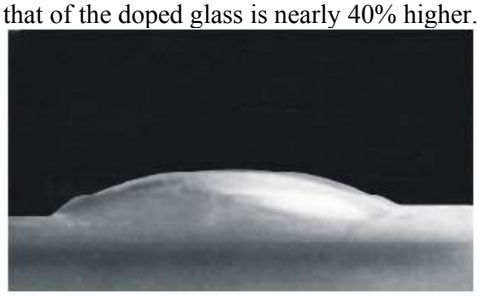

Fig. 2: a) *Drop of the pure NCS glass; α=30°*

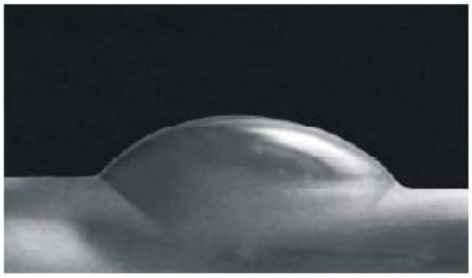

b) *Drop of the glass doped with 0.5 mol% MoO_3; α=37°*

4. Kinetics by SAXS

The kinetics of the phase separation process has been studied by conventional SAXS measurements using a Kratky instrument. A description of the SAXS experiment and of the analysis of the scattering data is given in [4].

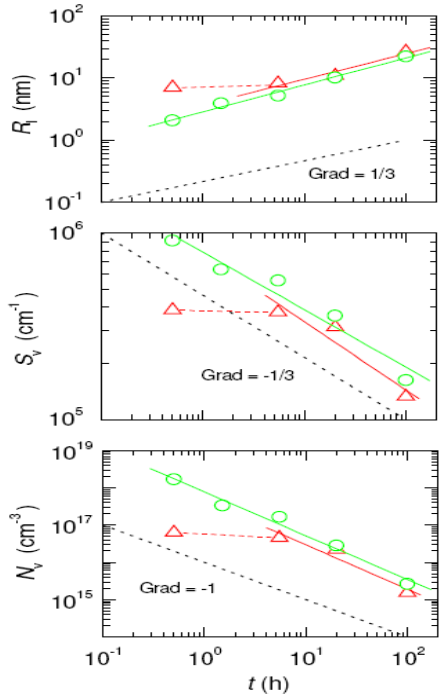

Fig. 3: *Average droplet radius, R_l, internal surface per unit volume, S_v, and particle number density, N_v, of the pure NCS glass (○) and NCS glass doped with 0.5 mol% MoO_3 (△) as a function of the time, t, of isothermal heat treatment at 600 °C. The black dotted lines correspond to the power laws of the classical theory [5] of diffusion controlled Ostwald ripening.*

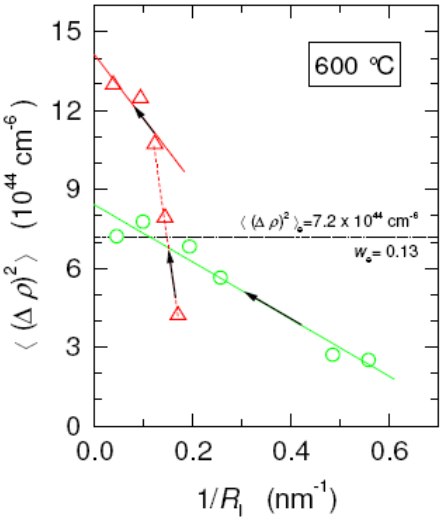

Fig. 4: *Mean square of electron density fluctuations, $\langle(\Delta\rho)^2\rangle$, versus reciprocal average radius of the droplets. Plotted data are obtained from samples of the pure NCS glass (○) and of NCS glass doped with 0.5 mol% MoO_3 (△) phase separated at 600 °C in the time interval 0 h ≤ t ≤ 100 h. The arrows illustrate the Directionn of increasing time of heat treatment. The equilibrium value of the volume fraction of the precipitates, we, and the corresponding value $\langle(\Delta\rho)^2\rangle_e$ for 600 °C calculated from the miscibility gap data (Fig. 1) is indicated by the dashed-dotted line.*

MoO_3 content (mol%)	$\langle(\Delta\rho)^2\rangle_e$ (10^{44}cm^{-6})	R^* (nm)
0	8.4	1.3
0.5	14.1	1.7

Fig. 3 demonstrates that during heat treatment both the pure and the doped NCS glass get to the stage of Ostwald ripening [5] but with varying kinetics. In Fig. 4, the SAXS parameters Rl and $\langle(\Delta\rho)^2\rangle$= w (1 - w) $(\Delta\rho)^2$are fitted with the expression $\langle(\Delta\rho)^2\rangle$= $\langle(\Delta\rho)^2\rangle_e$ -$\langle(\Delta\rho)^2\rangle_e$ R*/R|, developed for the first non-asymptotic stage of Ostwald ripening [2,6], where R*~σ/Δμ is the critical Gibbs-Thomson radius. It has been estimated that the scattering contrast, $\langle(\Delta\rho)^2\rangle$, cannot account for the largly increased value of $\langle(\Delta\rho)^2\rangle_e$ for the MoO_3 containing glass (Table). So, we have to conclude that the volume fraction, w, of the precipitated droplet phase is larger than that of the pure NCS glass.

5. Binodal temperature, Tb, by in situ high-temperature SAXS

In order to find out the cause of the increased precipitation of silica-rich droplets in the NCS glass doped with MoO_3, in situ high-temperature SAXS measurements were performed at the HMI SAXS beamline at BESSY, Berlin.

Fig. 5 shows that the silica precipitates in the pure NCS glass dissolve completely during a heat treatment at 710 °C, i.e. T_b< 710°C (compare Fig. 1). By contrast, during heat treatment of the NCS glass with 0.5 mol% MoO_3 at 770 °C, two processes can be observed. At first, the silica precipitates shrink in a reversion process until the silica concentration in the matrix reaches its new equilibrium value. Afterwards, the largest droplets grow again by slow ripening, i.e. T_b> 770°C. Obviously, the MoO_3 content of the glass gives rise to a shift of the miscibility gap to higher temperatures. Therefore, the increased value of $\langle(\Delta\rho)^2\rangle_e$ of the MoO_3 containing glass (Table) is caused by an increased precipitated volume fraction, w, resulting from a higher thermodynamic driving force, Δμ ~ (Tb-600 °C).

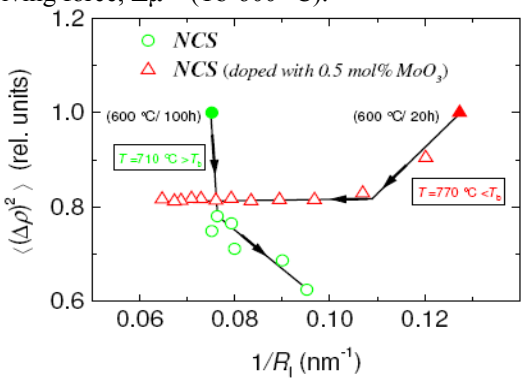

Fig. 5: Mean square of electron density fluctuations versus reciprocal average radius of the droplets. Plotted data points are obtained from glass samples, phase separated previously at 600 °C (filled symbols), in the course of in situ SAXS experiments at 710 °C and 770 °C, respectively, in vacuum. The arrows illustrate the direction of increasing time of heat treatment.

6. Conclusions

The presence of small amounts of MoO_3 in the NCS glass alters the kinetics as well as the equilibrium state of phase separation. Both the competitive parameters, thermodynamic driving force and interface tension, increase by an addition of MoO_3 to the base glass. The increased thermodynamic driving force results in a shift of the miscibility gap to higher temperatures and so to an increase of the precipitated volume fraction of the droplet phase.

References:

[1]. J.J. Hammel, J. Chem. Phys. **46**(1967)2234.
[2]. R. Kranold, M. Kammel, A. Hoell, J. Non-Cryst. Solids **293-295**(2001)642.
[3]. R. Kranold, M. Kammel, A. Hoell, Glass Technol. **43C**(2002)207.
[4]. A. Hoell, R. Kranold, U. Lembke, J. Aures, J. Non-Cryst. Solids **208**(1996)294.
[5]. J.M. Lifshitz, V.V.Slyozov, J. Phys. Chem. Solids **19**(1961)35.
[6]. J. Schmelzer, Phys. Status Solidi B **161**(1990)173.

BENSC	**EXPERIMENTAL REPORT** **Structural investigation of Carbon Supported Ru-Se Based Catalysts using Anomalous Small Angle X-Ray Scattering (ASAXS)**	Proposal N° BESSY Instrument ASAXS **S3** Local Contact Armin Hoell
Principal Proposer: Experimental Team:	A. Hoell – HMI, Berlin S. Haas – HMI, Berlin G. Zehl, I. Dorbandt – HMI, Berlin P. Bogdanoff, S. Fiechter – HMI, Berlin	Date(s) of Experiment 2006

Date of Report: Feb. 2007

Worldwide demand for energy is growing at an increasing rate. Currently, this demand is being met largely by fossil fuels, particularly crude oil. However, those reserves are diminishing and their exploration will become increasingly expensive. Hydrogen and methanol as energy carriers can be produced from both, fossil and renewable energy sources. By direct conversion into energy through an electrochemical reaction, fuel cells extract more power out of the same quantity of fuel when compared with traditional combustion. Due to their high activity, the use of platinum-based electrocatalyst in low temperature proton exchange membrane fuel cells (PEMFC) is present state of the art. However, the fact that commercial applicability of PEMFC technology is almost exclusively bound to this expensive and rare metal, may become a prohibitive factor for the successful adoption of fuel cells as mass-produced units.

As recently successfully demonstrated, Ruthenium based catalysts modified with Selenium also exhibit high catalytic activity for the oxygen reduction reaction [1]. One advantage of Ruthenium is that it is by a factor of 40 more common in the earth crust and its price presently amounts to only 17% of that of platinum. Furthermore, in direct methanol fuel cells (DMFC) the undesired crossover of methanol through the membrane from the anode space into the cathode compartment is still an unsolved issue. Therefore, platinum cathode catalysts suffer from activity losses due to methanol oxidation. As alternative, carbon supported Ruthenium nano-particles modified with Selenium feature absolute methanol tolerance. Although intense studies of these catalysts were performed during the last decade, no definite conclusion with respect to the nature of the catalytically active sites and the constitution of the RuSe nano-particles could be drawn. However, only a better understanding of the underlying principles is believed to pave the way towards higher active catalysts, thus making DMFCs more efficient and reliable.

Investigating RuSe electrocatalysts, data about the Selenium distribution over the catalyst's surface are particularly necessary, because catalytic efficiency depends strongly on the Selenium content of the catalysts. Anomalous Small Angle X-ray Scattering (ASAXS) represents a powerful tool for element sensitive analysis of nano-structured catalytic materials, whereas also useful data about the chemical composition in the sub-nanometer scale can be obtained. Using the ASAXS technique one takes advantage of the so-called anomalous or resonant behaviour of the atomic scattering amplitude of an element near its absorption edge to separate the scattering from different elements.

To clarify the structural features of these catalytically active Se-modified Ruthenium nano-particles, such materials were prepared by thermolysis of $Ru_3(CO)_{12}$ in an organic solvent with and without the presence of dissolved Selenium. The resultant Ruthenium nano-particles were supported on the commercial Black Pearls 2000® carbon black from Cabot.

We investigated with ASAXS a complete set of samples, including the final working RuSe catalyst supported on a commercial carbon black, and some intermediate preparation states such as non-modified (Selenium free) Ruthenium nano-particles or the bare carbon support. The scattering curves were taken in the vicinity below the Selenium and the Ruthenium K absorption edges, respectively.

Figure 1a shows that Ru and Se form nano-structures that alter the shape of the Black Pearls scattering curve dramatically. The sample which contains Selenium (Fig. 1 b) shows a small hump at Q ~ 7 nm^{-1} that is visible also at the Ru-K edge (Fig. 1 a). It was deduced that Selenium within the sample generates structural features clearly detectable and analysable by ASAXS (Fig. 1 c).

(a)

Ru + Se on Black Pearls and pure Black Pearls
Ru-K edge

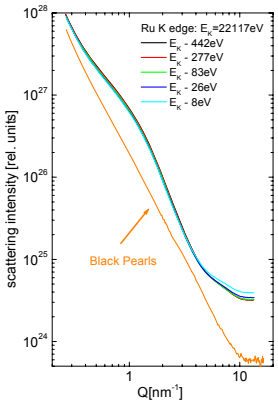

(b)

Ru + Se on Black Pearls
Se-K edge

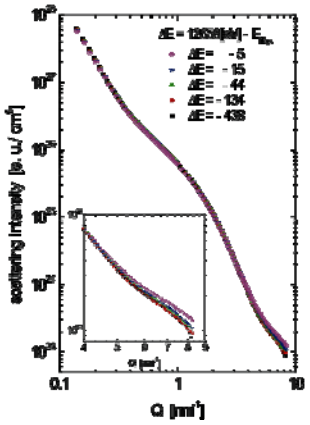

(c)

Comparision between scattering curves of Ru on Black Pearls with and without Se (sections)

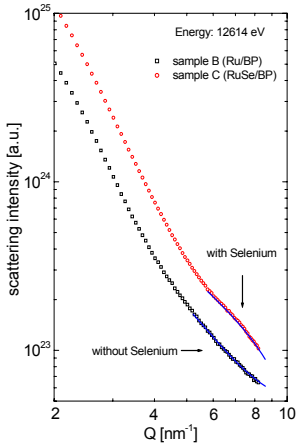

Fig. 1: *ASAXS scattering curves measured near below the K-absorption edges of Ruthenium (a) and Selenium (b and c).*

Taken into account the anomalous dispersion effect, in the vicinity of the Se- and the Ru-edge as well, of the scattering intensity of all measured samples, a structure model of the catalytically active metallic nano-particles has been deduced. That model suggests a nearly spherical Ru particle with a mean diameter of 2.3 nm decorated with Se aggregates. These structures onto the Ruthenium nano-crystallites feature a diameter around 0.5 nm. The results are supported by data from XRD, XPS, and EXAFS measurements, obtained from the same materials [2, 3]. Even so, the real shape of these small Selenium clusters is not yet finally clarified. However, free Selenium clusters of few atoms will form symmetric ring structures [4].

We also confirmed that the Selenium modified Ruthenium nano-particles are extremely resistant against agglomeration and particle growth. Even after annealing at 800°C the average particle size of the Ruthenium particles was found to remain below 2.5 nm in diameter.

Volume size distributions determined from ASAXS

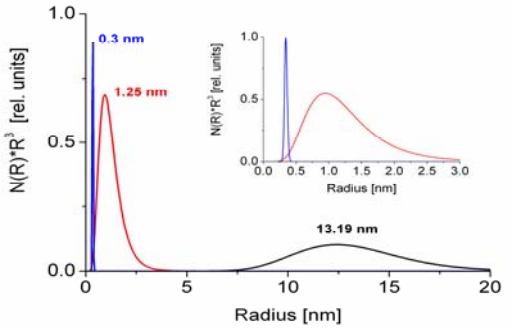

Suggested structure model

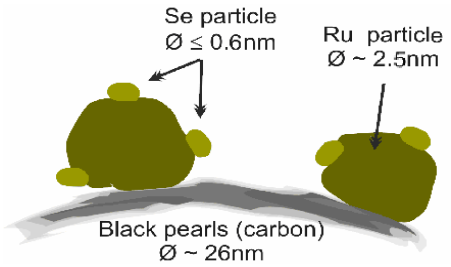

Fig. 2: *Structural model for Ruthenium based electrocatalysts supported on activated carbon and modified with Selenium at 800°C.*

Conclusions [5]

ASAXS revealed nano sized features of the samples that are hidden for SAXS or SANS methods alone. A structure model of the catalytically active metallic nano-particles has been deduced suggesting a Ruthenium core, with an average diameter of 2.3 nm, decorated with Selenium aggregates.

The Selenium structures onto these Ruthenium nano-crystallites feature a diameter less around 0.5 nm. Therefore, no closed Selenium coverage of the Ruthenium core particles could be affirmed.

Selenium modified Ruthenium nano-particles are extremely resistant against agglomeration and particle growth. Even after annealing at 800°C the average particle size was found to remain below 2.5 nm in diameter.

References:

[1]. Alonso-Vante, N.; Bogdanoff, P.; Tributsch, H.: On the Origin of the Selectivity of Oxygen Reduction of Ruthenium - Containing Electrocatalysts in Methanol - Containing Electrolyte; J. Catalysis **190** (2000) 240.

[2]. Fiechter, S.; Dorbandt, I.; Bogdanoff, P.; Zehl; G.; Schulenburg, H.; Tributsch, H.; Bron, M.; Radnik, J.; Fieber-Erdmann, M.: Surface modified Ruthenium nanoparticles: structural investigation and surface analysis of a novel catalyst for oxygen reduction; Journal of Physical Chemistry C, in press.

[3]. Zehl, G.; Dorbandt, I.; Fiechter, S.; Bogdanoff, P.: On the Influence of Preparation Parameters on the Catalytic Properties of Carbon Supported Ru-Se Electrocatalysts; Journal of New Materials for Electrochemical Systems, submitted.

[4]. Becker, J.; Rademann, K.; Hensel, F.: Ultraviolet photoelectron studies of the molecules Se5, Se6, Se7 and Se8 with relevance to their geometrical structure; Z. Phys. D. - Atoms, Molecules and Cluster **19** (1991) 229.

[5]. Haas, S; Hoell, A.; Zehl, G.; Dorbandt, I.; Bogdanoff P. and Fiechter S.: Structural investigation of Carbon Supported Ru-Se Based Catalysts using Anomalous Small Angle X-Ray Scattering; 211th ECS Meeting, Chicago, Illinois, May 6-11, 2007, accepted.

	EXPERIMENTAL REPORT **Ion-Beam Induced Nano-Sized Ag-Metal Clusters in Glass**	Proposal N° BESSY Instrument ASAXS **S3** Local Contact Armin Hoell
Principal Proposer: Experimental Team:	A. Hoell – HMI, Berlin H.-E. Mahnke, B. Schattat – HMI, Berlin P. Schubert-Bischoff, I. Zizak – HMI, Berlin N. Novakovic, V. Koteski – Vinca, Belgrad, Yu	Date(s) of Experiment 2006

Date of Report: Feb. 2007

Glasses containing metal clusters have attracted attention both in cluster research and in possible applications of such clusters for magnetic or optoelectronic purposes. Nanometer-sized clusters of noble metals in glasses exhibit strong absorption of visible light which, in addition, may be highly polarization dependant depending on size and shape with special alignment of the clusters [1, 2]. Various preparation methods are pursued to obtain control of the mechanisms to form such clusters. A promising approach is the irradiation of glasses containing the wanted metal as a metal oxide with heavy-ion beams at MeV/amu energies [3,4,5]. At such velocities the energy deposited along the ion path leads to track formation in the material. In the following, we show how synchrotron radiation techniques help to characterize ion-beam induced materials modifications.

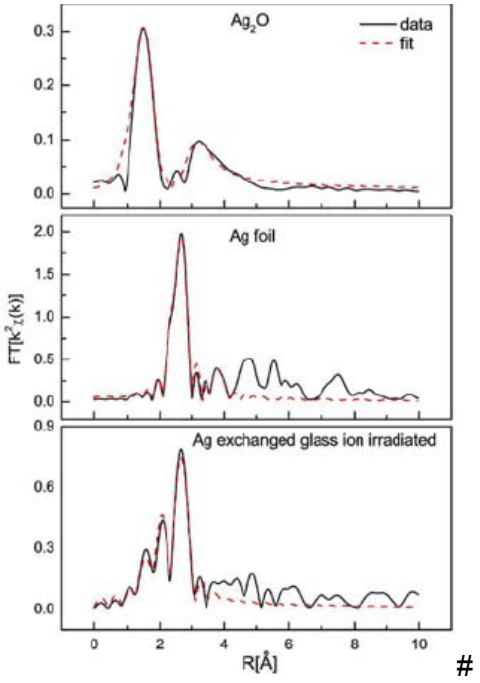

Fig. 1: *Fourier transformed EXAFS signal (k2-weighted): The irradiated glass sample (bottom) shows the ion beam induced formation of metallic Ag. The EXAFS signatures for Ag metal (middle) and for Ag2O (top) are given for comparison.*

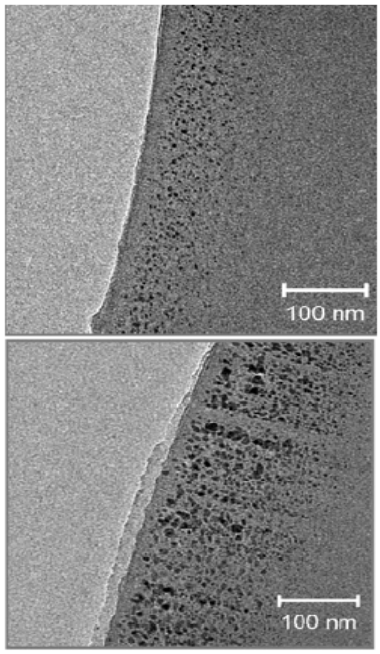

Fig. 2: *TEM picture of irradiated (bottom) and non-irradiated (top) glass samples: After irradiation with gold ions and subsequent annealing, clusters of metallic silver are visible arranged in chains along the direction of the ion beam. The TEM was operated at 120 kV.*

We have studied the formation of Ag-metal clusters in soda lime glass induced by heavy ion irradiation with x-ray absorption spectroscopy (XAS), while the shape of the formed clusters were studied both with transmission electron microscopy (TEM) and with small angle x-ray scattering (SAXS). Silver was introduced by ion exchange into 0.1-mm thick glass platelets (see [4]). We have irradiated these Ag-containing glass platelets kept at LN_2 temperature with 600-MeV Au ions with fluences around 10^{12} ions/cm^2 at the ion beam laboratory ISL. The ion flux was kept below 10^{10} ions/cm^{2}s.

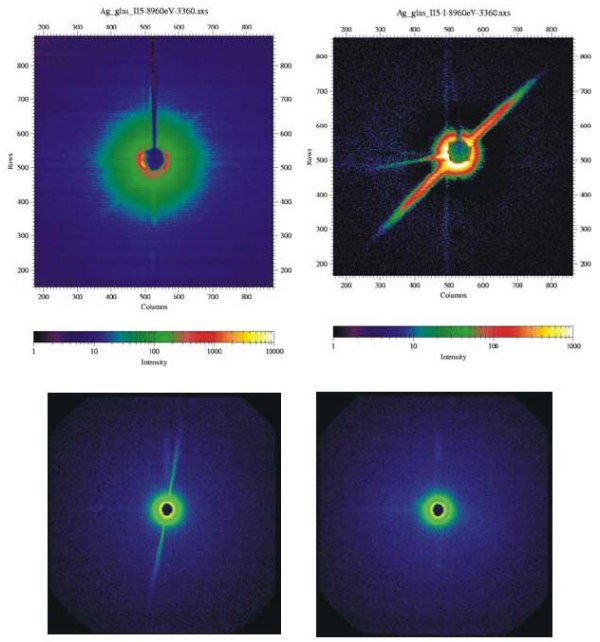

Fig. 3: *SAXS images of ion-irradiated (upper right) and non-irradiated (upper left) Ag containing glass samples revealing a column-like structure by the disc-like image. The dimensions in q space correspond to a diameter of the "columns", the arrangement of Ag droplets along chains in the ion direction, of around 7 nm. SAXS images on ion irradiated glass samples without Ag show ion tracks in glass (lower left) which disappear when annealed (lower right).*

Following the ion irradiation, the samples were investigated with X-ray absorption spectroscopy at the Ag K-edge. The EXAFS experiment, performed at the X1 beamline of HASYLAB, revealed the transformation of Ag from the oxidic type local structure after the ion-exchange process into the metallic form following the swift heavy ion irradiation and annealing (see Fig. 1, for details see ref. [6]).
First information on the shape of the formed clusters was obtained by transmission electron microscopy (TEM) on thin slices of some 10 nm cut out of the samples parallel to the ion impact and deposed onto a fine grid (see Fig. 2). For a more detailed study of the arrangement, the shape, and the formation process SAXS experiments including in-situ experiments at varying annealing temperatures are under way at the 7-T MPW beam line at BESSY.

While annealing under a reducing atmosphere of argon with a few % H2 alone already leads to the formation of metal clusters (we annealed for 30 minutes at 340°C), such clusters are not very uniform in size and are randomly distributed over the Ag-containing glass volume. The comparison presented in Fig.2 illustrates the significant influence of the ion irradiation: (i) the metal clusters have grown and their size distribution has become more uniform, but the most remarkable feature is that (ii) the clusters are arranged in chains parallel to the direction of the ion beam.

A more quantitative description of the arrangement seen in the TEM images can be achieved by SAXS measurements performed at the newly commissioned 7-T MPW beam-line of the HMI at BESSY. An illustration of the first experiment is given in Fig.3. The ion fluence in this case was $10^{11}cm^{-2}$, the sample was heat treated after the ion irradiation in the same way as the sample in Fig. 2. A glass platelet without Ag also shows ion tracks when ion irradiated at LN temperature. However, they disappear when the same annealing procedure is applied. Thus, the small angle scattering confirms the arrangement and shape of the Ag metal clusters as induced by the ion irradiation and proves to be a very valuable complementary way to study such ion induced structures.

Since some of the chains consist of clusters very similar in diameter and almost in contact, one is tempted to speculate that a totally columnar structure may be obtained by controlling the influencing parameters such as the ion fluence and the annealing parameters. First in-situ experiments to follow the subsequent annealing procedure are being analyzed.

The authors are grateful to the HASYLAB staff at DESY, in particular to J. Wienold and E. Welter. We very much appreciate P. Szimkowiak's help in sample preparation. Special thanks are expressed to the colleagues from the department SF3, A. Höll, S. Haas and D. Tachev, who helped as scientists at the SAXS 7-T MPW beam line.

References:

[1]. K. L. Kelly et al. , J. Phys. Chem. B **107** (2003) 668
[2]. A. Podlipensky et al., J. Phys. Chem. B **108** (2004) 17699
[3]. E. Valentin et al., Phys. Rev. Lett. **86** (2001) 99
[4]. G. Bataglin et al., Nucl. Instr. and Meth. in Phys. Res. B **200** (2003) 185
[5]. J.J. Penninkhof et al., Appl. Phys. Lett. **83** (2003) 4137
[6]. H.-E. Mahnke et al., Nucl. Instr. and Meth. in Phys. Res. B **245** (2006) 222

	EXPERIMENTAL REPORT **In-situ ASAXS study of sintering and corrosion of refractory ceramics**	Proposal N° BESSY Instrument ASAXS **S3** Local Contact Armin Hoell
Principal Proposer: Experimental Team:	A. Hoell – HMI, Berlin R. Winter, D. LeMessurier – Univ. Wales, UK S. Haas – HMI, Berlin	Date(s) of Experiment 2006

Date of Report: Feb. 2007

Refractories:
Refractories are used as linings in melting furnaces in the glass and metal producing industries. They are also used as coatings for sensors in hostile atmospheres and high-temperature environments as process control becomes more important to reduce waste and energy consumption. In some applications, clever nano-scale engineering can increase the mechanical strength of refractories as has been shown in the case of turbine blade coatings [1].
We are using a nano-scale analogue of an industrial alumina-zirconia-silicate refractory (cf. Fig. 1) as a physical model to understand the sintering and corrosion kinetics of this material class. The increased surface-to-volume ratio makes the model system ideally suited to kinetic investigations. We have studied this material by NMR [2] and SAXS [3], and we have recently published the first in-situ kinetic study of a heterogeneous material, silicate glass-forming batch, by NMR [4].

Refractory corrosion occurs when mobile ions from the glass melt penetrate into the amorphous binder phase of the refractory. We are looking into ways of increasing the viscosity of the refractory binder phase in order to reduce the penetration depth of the corrosives. One way to achieve this may be based on the mixed-alkali effect, the reduction of ionic conductivity when two mobile ions compete for conduction pathways in an amorphous structure [5] as ionic motion contributes to the flexibility of the network and hence decreases viscosity.

Fig. 1: *Nano-scale refractory analogue: Alumina and zirconia nanoparticles embedded in a sodium / potassium silicate glass matrix.*

Anomalous small-angle x-ray scattering: Anomalous scattering is the chemical contrast enhancement that occurs around the absorption edge of a probe element due to the resonance between scattering and absorption [6]. Near the edge, an energydependent complex correction $f' + if''$ is applied to the scattering factor to account for this resonance. As a consequence, the total scattering function splits into three parts, $I(q, E) = I_0(q) + f' I_{0r}(q, E) + (f'^2 + f''^2) I_r(q, E)$, i.e. the non-resonant, cross, and self terms.

There are only a small number of ASAXS studies reported in the literature so far, and even fewer attempt to monitor materials in situ while varying a process parameter. Systems that have been investigated by ASAXS so far are concerned with phase separation in alloys [7, 8], distribution of counter-ions in polymercoated core-shell particles [9], and porosity of catalyst supports [10]. The only in-situ studies so far are a kinetic study of an organometallic reaction leading to the formation of nano-particles [11], degradation of an electrocatalyst in operation [12] (both at room temperature) and phase separation kinetics in an alloy at moderate annealing temperatures [13].
Not all of the previous ASAXS studies make full use of the potential inherent in eq. (1) to separate the cross term, which contains the correlation between the probe and the remaining scatterers, from the self term, which relates to the autocorrelation of the probes themselves, i.e. the pattern that one might expect if the phase containing the probe was in an otherwise perfectly index-matched environment. In order to solve eq. (1), measurements at a great deal more than three energies are required, and in addition to the usual corrections, the data need to be corrected for fluorescence, the width of the beam spectrum, and any chemical shifts of the edge occurring during an in-situ experiment [14].

Experimental:
The in-situ experiments were designed to repeat cycles of four beam energies plus edge scan while heating a sample at a fixed temperature up to 1 000 °C (cf. Fig. 2). To study corrosion, the refractory analogue was mixed with another glass, with a higher content of mobile ions than the refractory's matrix. This glass is known as the corrosive. While the corrosive is the same sodium-based glass in all experiments, versions of the nano-scale refractory analogue with both sodium and potassium based binder phases were used. We therefore contrast the conventional case, where there is a concentration gradient of Na^+ ions from the melt into the refractory, with a situation where the total mobile ion concentration gradient is the same but Na^+ ions diffuse into a K^+-based structure.

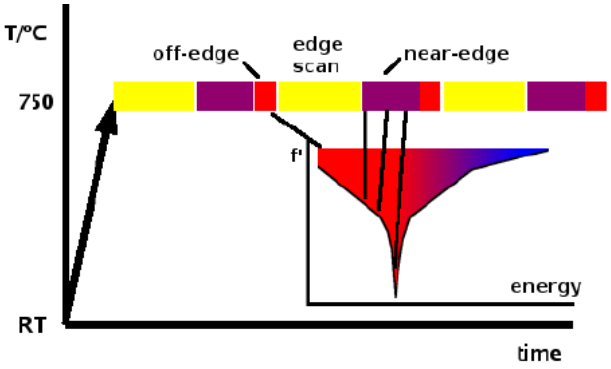

Fig. 2: *Experiment protocol for a typical in-situ ASAXS experiment using the Rostock furnace on the HMI SAXS beamline at Bessy.*

Results and Discussion:

We can see a difference in the energy dependence of the scattering pattern depending on whether a sodium or a potassium based corrosive is used. After the necessary corrections, radial averaging and absolute scaling of the scattering level by normalisation against an amorphous carbon sample, the straightforward difference is taken between runs near and well below the edge. A more detailed analysis is necessary but requires further software development, which is still work in progress. Figs. 3 and 4 show the difference plots for the sodium and the potassium based refractory, respectively, as three-dimensional data sets relating difference scattering intensity with momentum transfer (here shown as detector channel number) and time elapsed at a temperature of 820 °C. Each time slice corresponds to about 3 min. Positive differences mean that the normalised scattering is stronger well below the Zr K edge than in the resonant region just below the edge, i.e. that scattering from Zr is greater than average in these positive-difference regions of the pattern. While a conclusive interpretation will require a more detailed analysis once the required software is available, the fact that the potassium corrosive shows an effect on the zirconium signal while the sodium corrosive does not is a significant result. Sodium is the only mobile ion in the refractory's glassy binder phase. A sodium-based corrosive, although containing a significantly higher amount of sodium ions, does not seem to affect the zirconia phase in the refractory. However, the potassium corrosive does change the zirconia nanostructure right from the beginning of the experiment, although equilibrium is reached after about 15 min. The slight remnant curvature along the q axis suggests that the Guinier radius of the embedded zirconia particles is reduced during the initial reaction.

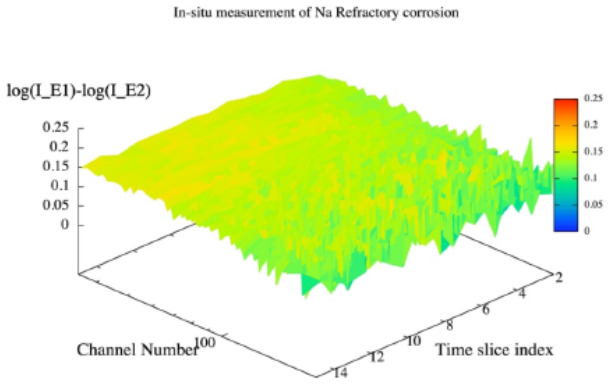

Fig. 3: *ASAXS difference patterns as a function of time for the sodium-based refractory.*

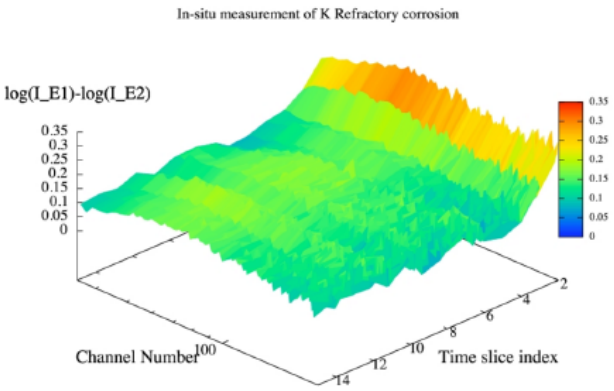

Fig. 4: *ASAXS difference patterns as a function of time for the potassium-based refractory.*

Conclusions and Outlook:

This first in-situ ASAXS experiment at the HMI SAXS beamline at Bessy has demonstrated that the beamline can provide the necessary time and energy resolution to enable us to study the kinetics of solid state reactions such as refractory corrosion. However, the temperatures available on the furnace used at the beamline at the time were not sufficient for the corrosion studies intended. Ways of improving and testing the furnace have been identified which will enable us to finish off this work in a follow-up experiment. These include operating the furnace with an inert gas atmosphere and placing the sample, which is a powder pellet, between two slivers of mica to improve mechanical stability.

Dissemination:

Preliminary results of this work have been presented at the European Society of Glass Science and Technology conference at Sunderland and at the Synchrotron Radiation User Meeting at Diamond, both in September 2006. A journal publication is underway but needs some further software development as indicated above. Follow-on beamtime at Bessy has been awarded and scheduled for March 2007, which will provide further in-situ ASAXS data on refractory's to complete the picture.

References:

[1]. JR Nicholls, RGWellman, MJ Deakin; Materials at High Temperatures 20 (2003) 207
[2]. DA Le Messurier, N Sissouno, AR Vearey-Roberts, S Evans, DA Evans, RWinter; Mater Sci Technol 20 (2004) 975
[3]. RWinter, DA Le Messurier; SRS Experimental Report (2004) RB 40 296
[4]. AR Jones, RWinter, P Florian, D Massiot; J Phys Chem B 109 (2005) 4 324
[5]. A Bunde, MD Ingram, S Russ; Phys Chem Chem Phys 6 (2004) 3 663
[6]. R Br ¨ uckner, U Lembke, R Kranold; Nucl Instr Meth Phys Res B 97 (1995) 190
[7]. WLiu, WL Johnson, S Schneider, U Geyer, P Thiyagarajan; Phys Rev B 59 (1999) 11 755
[8]. A Hoell, A Wiedenmann, F Bley, JP Simon, A Mazuelas, P Boesecke; Scripta Mater 44 (2001) 2 335
[9]. B Guilleaume, M Ballauff, G Goerigk, MWittemann, M Rehahn; Colloid Polym Sci 279 (2001) 829
[10]. A B´ ota, G Goerigk, T Drucker, HG Haubold, J Petr´ o; J Catal 205 (2000) 354
[11]. K Angermund et al.; J Phys Chem B 107 (2003) 7 507
[12]. HG Haubold, XHWang, G Goerigk,WSchilling; J Appl Cryst 30 (1997) 653
[13]. G Goerigk, HG Haubold,WSchilling; J Appl Cryst 30 (1997) 1 041
[14]. M Patel, S Rosenfeldt, M Ballauff, N Dingenouts, D Pontoni, T Narayanan; Phys Chem Chem Phys 6 (2004) 2 962

	EXPERIMENTAL REPORT **Nano-structure of different drug delivery systems studied by synchrotron radiation**	Proposal N° BESSY Instrument ASAXS **S3** Local Contact Armin Hoell
Principal Proposer: Experimental Team:	A. Hoell – HMI, Berlin M. Kumpugdee-Vollrath – TFH, Berlin P. Opanasopit – TFH, Berlin P. Guttmann – Uni Göttingen I. Zizak – HMI, Berlin	Date(s) of Experiment 2006

Date of Report: Feb. 2007

1. ABSTRACT

Nowadays several drug delivery systems are available e.g. liposomes, lipid emulsion, micellar solution, nanoparticles, etc. This present work is based on these systems in order to understand deeply their structures during formulations. Finally the most suitable system for being used as a site specific delivery system of the model drugs can be chosen. The determination of the structure in nanoscale was performed by using synchrotron radiation in different instruments e.g. SAXS and X-ray microscopy.

2. INTRODUCTION

Different nano-delivery systems e.g. liposomes, niosomes, lipid emulsion, micellar solution and nanoparticles are available as drug delivery systems in the pharmaceutical field. Advantages and disadvantages of these systems are discussed in the literature [1]. However, there are only few systems which work as an active site delivery system. Therefore the target of the project is to find out the most suitable system for delivery of model drugs (hydrophilic and hydrophobic drugs). Formerly researchers have mostly used the classical techniques e.g. light scattering, electron microscopy, etc. in order to characterize these delivery systems. The interpretation of the structure in nanoscale is mostly built up on the approximation base on theory. In this project the modern characterizing techniques such as small angle x-ray scattering (SAXS) and x-ray microscopy were used additionally to the classical one and the results can provide a better understanding in nanoscale of the structure of these delivery systems [2]. The modern synchrotron sources, like BESSY II, with their intense and highly collimated x-ray beams and the development of suitable lenses, i.e. Fresnel zone plates, have involved that x-ray microscopy is a powerful imaging method in different application fields. Nowadays, x-ray microscopy offers a lateral resolution of about 20 nm. Moreover the measurements can be performed with wet samples with only small volume (~ µl). The structure of the core and shell of the wet systems e.g. micelles or nanoparticles can be determined. On the other hand the SAXS technique can give information about the secondary structure (gel-, liquid crystalline-, hexagonal phase) as well as the phase transition temperatures.

3. MATERIALS

Different nano drug delivery systems e.g. polymer micelles, lipid emulsion and liposomes were investigated in this present work.

3.1 Polymer Micelles:

The synthetic polymer N-phthaloylchitosan-grafted poly (ethylene glycol) methyl ether was used to entrap different drugs (hydrophilic and hydrophobic) by a dialysis method [3].

3.2 Lipid Emulsion:

In order to prepare lipid emulsion the medium chain triglyceride, lecithin, surfactant, drug and water were mixed together by the emulsification method [4].

3.3 Liposomes:

The dry film method was used to prepare liposomes from different phospholipids. Different drugs were incorporated into the liposomes [5].

4. METHODS

4.1 Small Angle X-ray Scattering (SAXS)

The experiments were performed at the new SAXS instrument of the Hahn-Meitner Institute (7T-MPW-SAXS) installed at the synchrotron source BESSY in Berlin, Germany. The scattering patterns were acquired using a 2D position sensitive gas detector with delay line read out (Molecular Metrology). The samples (3.1-3.3) were measured at room temperature under vacuum conditions by using quartz capillaries of about 1 mm of thicknesses as sample holders (Fig. 2) at energy of 8000 eV. The resolution is about 1 nm.

4.2 X-ray Microscopy

The experiments were performed at the soft x-ray microscope (U41-TXM), BESSY, Berlin, Germany. About 5 µl of the sample (3.1) was laced in the sample holder (Fig. 4) and the thickness of the sample was adjusted to below 10 µm. The images were taken in amplitude contrast mode at the wavelength of 2.4 nm (~ 524 eV) at room temperature. The sample was placed vertically to the radiation with the dimension of maximum 3 mm. The lateral resolutions during the experiments were about 25 nm due to the objective in use.

5. RESULTS AND DISCUSSION

5.1 SAXS

The x-ray scattering curve (Fig. 2) of the liposomes loaded with the drug lidocaine HCl (water soluble) shows two peaks at different Q-values. The peak positions differ after addition of the drug to the liposomes which means that the structure of the

liposomes had changed. The similar result was shown with the SAXS data from the lipid emulsion (Fig 3). The scattering curve of the polymer micelles showed a broad spectrum which means that the micelles has an small unilamellar structure (data not shown).

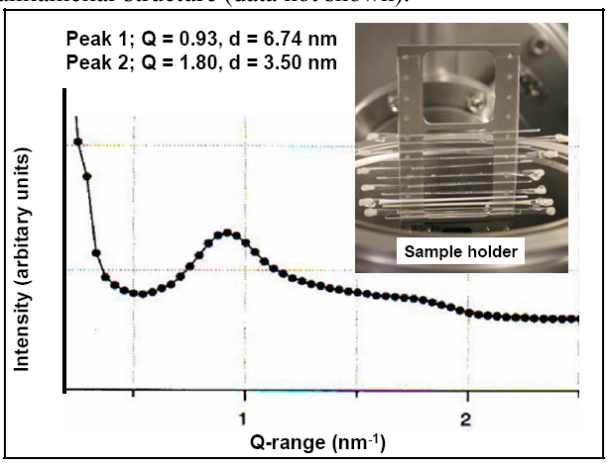

(a)

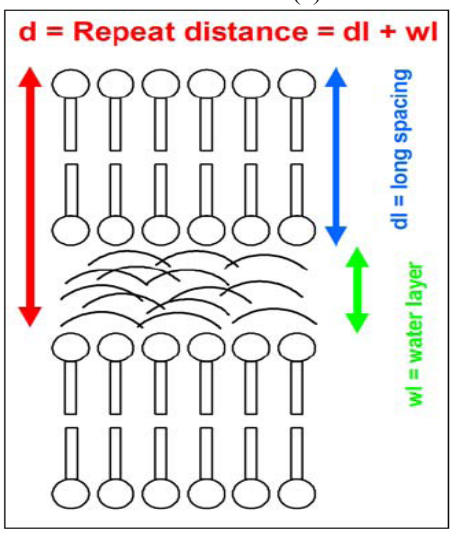

(b)

Fig. 1: (a) *SAXS data of liposomes loaded with the drug lidocaine HCl, the magnification of sample holders,* ***(b)*** *the repeat distance consists of lipid bilayer and water layer.*

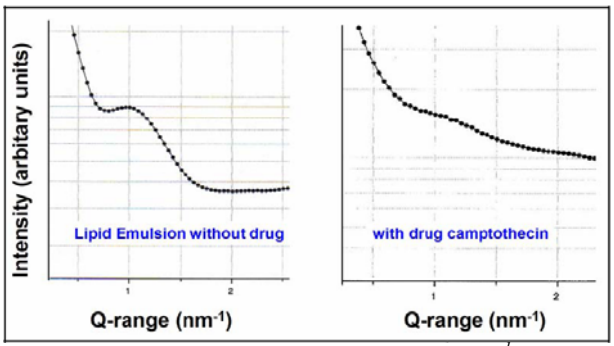

Fig. 2: *Lipid emulsion without drug (Q = 1.07 nm^{-1}, d = 5.89 nm) and with the drug camptothecin (Q = 1.20 nm^{-1}, d = 5.23 nm) studied by SAXS.*

5.2 X-ray Microscopy

The direct imaging can give information of the structures formed by polymer micelles from chitosan loaded with a drug (Fig. 4). For this, x-ray microscopy will give additional input for the models of nano-delivery systems.

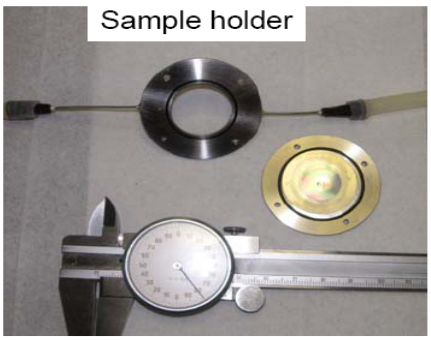

(a)

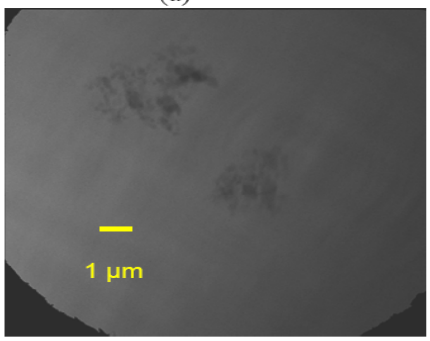

(b)

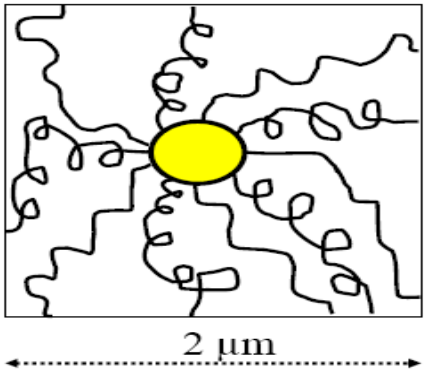

(c)

Fig. 3: (a) *a sample holder for x-ray microscopy,* ***(b)*** *x-ray micrograph and* ***(c)*** *scheme of the structure of polymer micelles from chitosan loaded with a drug. It can be seen that the structure of polymer micelles has a core with a diameter of about 0.5 µm and the shell with a thickness of about 1.0-1.5 µm.*

6. References:

[1]. Hillery, A.M., Lloyd, A.W. and Swarbrick, J. (Eds.), Drug Delivery and targeting for pharmacist and pharmaceutical scientists, Taylor&Francis, 2001

[2]. Lindner, P. and Zemb, T., Eds. Neutrons, x-rays and light scattering methods applied to soft condensed matter. Elsevier B.V., Amsterdam, Netherland. (2004)

[3]. Opanasopit, P., et al, European Journal of Pharmaceutics and Biopharmaceutics, **64**(3):269- 76. (2006)

[4]. Chinsriwongkul, A., et al, The 5th World Meeting on Pharmaceutics Biopharmaceutics and Pharmaceutical Technology, 27-30 March, Geneva, Switzerland. (2006)

[5]. .Kumpugdee, M., et al, Proceeding of the International Meeting on Pharmaceutics, Biopharmaceutics and Pharmaceutical Technology, **15-18** March, Nurnberg, Germany, 121-122. (2004)

BENSC	**EXPERIMENTAL REPORT** **In-situ study of microstructure changes at room temperature and elevated temperatures in nanocrystalline electrodeposits**	Proposal N° BESSY Instrument EDDI **S4** Local Contact Christoph Genzel
Principal Proposer: Experimental Team:	K. Pantleon – TU, Denmark K. Hansen – TU, Denmark C. Genzel – HMI, Berlin	Date(s) of Experiment 2006

Date of Report: Feb. 2007

Electrochemical deposition has become the method of choice for manufacturing functional thin copper films, because it provides excellent filling behaviour for small vias and trenches as required for the ongoing miniaturization of advanced microelectronic devices. The functionality and reliability of electrochemically deposited thin films depend on their microstructure. however, the thermodynamically non-equilibrium state of as-deposited films causes substantial changes of the microstructure and related properties with time already at room temperature and/or at elevated (operating) temperatures.

Copper, which has become the dominant material for interconnects in integrated circuits in microelectronics, is unstable even at room temperature; this phenomenon is called self-annealing. Recently, in-situ studies applying conventional X-ray diffraction with simultaneous measurements of the electrical resistivity have been carried out to investigate the evolution of the microstructure in electrodeposited copper layers [1]. It has been reported [1] that considerable growth of the as-deposited nanocrystalline grains and a drastic weakening of the crystallographic texture occur as function of time at room temperature and multiple twinning was suggested as the mechanism for self-annealing in copper electrodeposits [1,2].

In contrast, electrodeposited nickel, a promising material to realize movable structures for micro-electro-mechanical applications, is relatively stable at room temperature, but well-known for changes of the internal structure at elevated temperatures resulting in a dramatic deterioration of mechanical properties. Annealing the nickel layers in a conventional furnace or oil bath with subsequent microstructure characterization (ex-situ), as usually applied, allows just a comparison between as-deposited and annealed microstructures, but does not yield information on its time dependent evolution, which, however, is essential for understanding the mechanisms of (self-)annealing.

The factors controlling these processes in the nanocrystalline thin films and limiting their long-term applicability are at present largely unknown. In-situ experiments applying synchrotron diffraction were carried out in order to supplement current research work on electrochemically deposited copper, silver and nickel layers.

At BESSY at the beamline EDDI (part of ID 7T-MPW), the room temperature evolution of the microstructure was investigated for copper and silver layers. Great importance was attached to start the experiments before the onset of self-annealing; for this purpose, the as-deposited layers were frozen down to -20°C and first subjected to room temperature when the experiments were ready to start. For investigations of the self-annealing kinetics room temperature atmosphere was essential, i.e. radiation induced heat input into the sample had to be avoided. By inserting appropriate absorbers in the primary beam path, the temperature could be reduced down to about 25°C, whereas without absorbers the sample would have been subjected to a temperature of 85°C, which would have triggered self-annealing considerably. The kinetics of self-annealing was studied with energy dispersive diffraction by repeating measurements of the complete energy spectra both for copper and for silver layers with various thicknesses in the range of a few micrometers. Energy dispersive diffraction spectra were collected at a fixed diffraction angle of $2\Theta = 15°$, for which a multitude of reflections was expected in a wide energy range. As an example, Fig. 1 shows a part of an energy dispersive diffraction spectrum recorded within only 30s (i.e. information can be obtained extremely fast) for a 2.6 µm thick copper layer deposited onto a Si-wafer with a Au-film on top.

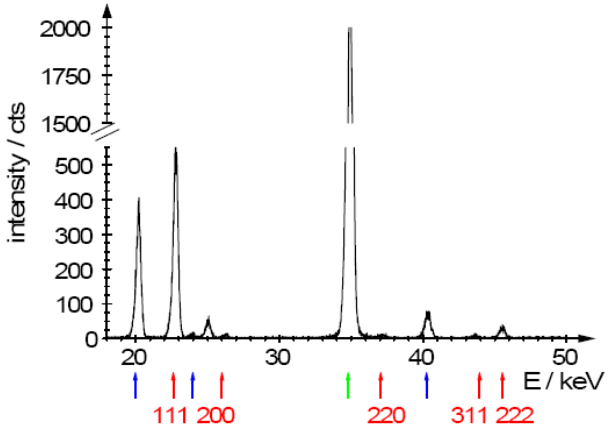

Fig. 1: *Energy dispersive diffraction spectrum measured for a copper layer with 2.6 µm thickness electrochemically deposited onto a Au covered Si-wafer. Various diffraction lines are marked: Cu (red), Au (blue), Si (green). Only part of the spectrum is shown, although lines can be identified up to about 100 keV.*

For the analysis of lattice strain (stress) the samples were tilted applying azimuth angles $0 \leq \psi \leq 89°$ with a step size of $\Delta\psi = 5°$, which allows to determine residual stresses according to the $\sin^2\psi$-method. The variety of information contained in the energy spectra (a multitude of reflections corresponding to different lattice planes is recorded simultaneously and each reflection originates

from a specific penetration depth) allows the determination of stress gradients perpendicular to the surface [3] and additionally, due to repeated measurements over the period of about one week, the evolution of stresses can be followed with time. Furthermore, the room temperature evolution of the microstructure can be followed with time by line profile analysis, i.e. separating the effects of grain size (size of coherently diffracting domains) and microstrain on the broadening of the measured diffraction lines. Evaluation of the diffraction spectra measured for the electrodeposits, however, indicated that diffraction line profile analysis for the interesting copper phase is not straightforward because of partly overlapping lines and weak intensities due to the very low layer thicknesses. Furthermore, line profile analysis for energy dispersive diffraction is not a standard technique yet and the relatively broad instrumental profile as measured on a standard Si-powder (NIST 640c) as well as the even broader lines of the samples requires careful profile fitting, which is still the subject of current work.

For nickel electrodeposits preliminary diffraction studies with conventional X-rays revealed that the microstructure of nickel layers is stable at room temperature, in contrast to the behaviour of copper and silver layers. At BESSY, the behaviour of nickel at elevated temperatures was investigated in-situ at the beamline MagS (part of ID 7T-MPW) applying a heating facility for temperatures up to 800 K. Measurements were carried out applying a monochromated beam with photon energies of 12.4 eV (wavelength λ = 0.1 nm). Different temperature regimes were applied: i) isothermal annealing at different times (3h…8h) at various temperatures (400K…600K) and ii) isochronal annealing between 300K and 750K with temperature intervals of 50K. During the isothermal experiments, line profiles were successively measured for the 111, 222, 200, 400 and 311 reflections of nickel and measurements were repeated until no further changes of the line profiles could be detected. For the isochronal experiments, one series of the various nickel reflections was measured at each temperature, i.e. the holding time at the individual temperatures amounted to a few minutes only. Line profile analysis was applied to separate the various contributions to line broadening: the size of coherently diffracting domains, which is interpreted as the grain size, and microstrains were determined as a function of time and/or temperature. Furthermore, the evolution of preferred grain orientations was evaluated based on the integrated intensities of the various reflections. Fig.2 shows some examples of observed changes of the measured diffraction lines.

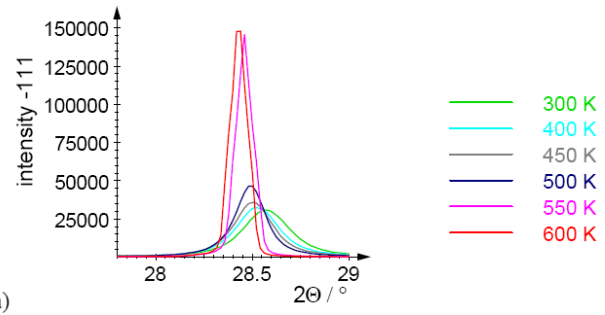

a)

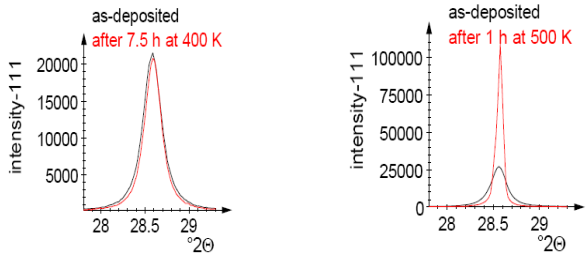

b) c)

Fig. 2: *Examples of diffraction lines measured for electrochemically deposited nickel layers as function of time and/or temperature: stepwise increase of the temperature from 300 K to 600 K (a) and isothermal annealing at 400 K (b) or 500 K (c).*

Fig.2a indicates that only temperatures above 400K yield considerable changes of the line profiles (similarly as shown here for the 111 diffraction line, it also was observed for the 222, 200, 400 and 311 lines), i.e. grain growth and crystallographic texture changes occurred more pronounced for higher temperatures. Figs.2b and c also emphasize the effect of the temperature: while during isothermal annealing at 400K no changes of the line profiles were observed even after several hours indicating a stable microstructure at that temperature, at 500K grain growth occurred immediately (actually, it started already during the heating phase) and was completed after isothermal holding of less than one hour. The as-deposited nanocrystalline grains with grain sizes of about 20 nm increased by grain growth during annealing to grain sizes of up to 180nm as obtained for the annealed microstructure. The kinetics of grain growth was found to be strongly affected by the applied temperature regime, while it was less dependent on both the electrochemical deposition parameters of the nickel layers and the applied substrate.

From the observed annealing behaviour of the nickel layers during isothermal and isochronal annealing the activation energy of grain growth was calculated based on the kinetics and the temperature dependence of the evolution of the line profiles, respectively. The obtained results will essentially contribute to a model description of (self-) annealing in electrochemically deposited films taking into account the effect of surface, interface and grain boundary energies on the driving force.

Refernces:

[1]. K. Pantleon, M.A.J. Somers, J. Appl. Phys. **100** (2006) 114319-1-7.

[2]. K. Pantleon, A. Gholinia, Proc. of the EBSD Users meeting 2006, Oxford Instruments HKL Technology, 47-49.

[3]. Ch. Genzel, I.A. Denks, M. Klaus, Mat. Sci. For. **524-525** (2006) 193-198.

We are grateful to Esther Dudzik and Ralf Feyerherm (HMI, Berlin) for experimental support at the beamline MagS and acknowledge Manuela Klaus and Ingwer Denks (HMI, Berlin) for experimental assistance at the beamline EDDI. The organisation of Danish users of hard X-ray synchrotron facilities (DANSYNC) is gratefully acknowledged for financial support.

	EXPERIMENTAL REPORT **Residual stresses in CrN/Fe structures at high temperature**	Proposal N° BESSY Instrument EDDI **S4** Local Contact Christoph Genzel
Principal Proposer: Experimental Team:	E. Eiper – ÖAW Leoben, A K.J. Martinschitz, J. Keckes – ÖAW Leoben,A M. Klaus, C. Genzel – HMI, Berlin	Date(s) of Experiment 2006

Date of Report: Feb. 2007

Hard coatings are routinely used to protect working tools from abrasion and corrosion. Residual stresses in the coatings as well as in the interface region of a working tool influence decisively the tool wear and thermal fatigue resistance, the coating adhesion and finally the lifetime of the component. Temperature cycling results usually in the annihilation of point defects in the coatings and relaxation of compressive stresses what negatively influences the lifetime. In order to design new coating/substrate systems with improved performance, it is of great importance to assess temperature-induced changes in the residual stresses occurring during temperature cycling.

In recent years especially hard coatings based on CrN have been used to increase wear and corrosion resistance of working tools. The optimization of thermal fatigue represents however still a challenging task and currently it is not known how CrN on steel behaves at high temperature and what kind of structural changes occur [1].

In this work, high-energy X-ray diffraction at EDDI beamline was used to characterize residual stresses in 3µm nanocrystalline CrN coatings deposited on shot-peened surfaces of steel in the temperature range of 25-800 C°. The CrN/Fe structures were thermally cycled using the heating stage DHS 900 [2] in N2 atmosphere and changes in the residual stresses in the coating and the substrate were characterized.

A temperature dependence of residual stresses in the CrN coating obtained collected two temperature cycles is presented in Fig. 1. The results indicate that the coating behaves predominantly thermo-elastically and there is surprisingly no significant relaxation of the stresses caused by point defect annihilation. The slope of the stress-temperature dependence corresponds to the mismatch of coefficients of thermal expansion of CrN and Fe. About 600 °C, the stress in the coating is tensile what represent a critical point in the temperature behaviour of the coating.

In the case of underlying Fe substrate, it was possible to evaluate the temperature dependence of stress gradient during the temperature cycling. In Fig. 2, the results from the first temperature cycle are presented. Since the substrate was shot peened before the coating deposition, a relatively large compressive stress of about -900 MPa was observed in the surface region at room-temperature. Upon heating up, the residual stress relaxes especially about 600 degrees. When cooled down, the stress does not change what documents that the coating has no significant influence on the substrate stress. In the future, the in-situ characterization of residual stresses will be devoted to multilayered hard coatings in order to assess the structural changes in distinct sublayers and an attempt will be made to evaluate residual stress depth gradients as a function of temperature.

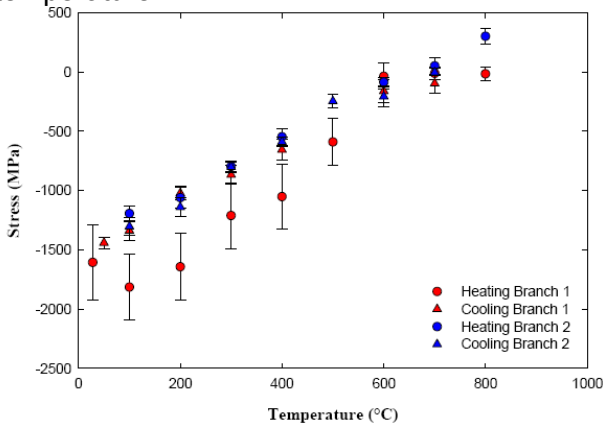

Fig. 1: *Temperature dependence of residual stresses in 3µm thick CrN coating on polycrystalline iron. The coating behaves during both temperature cycles thermo-elastically.*

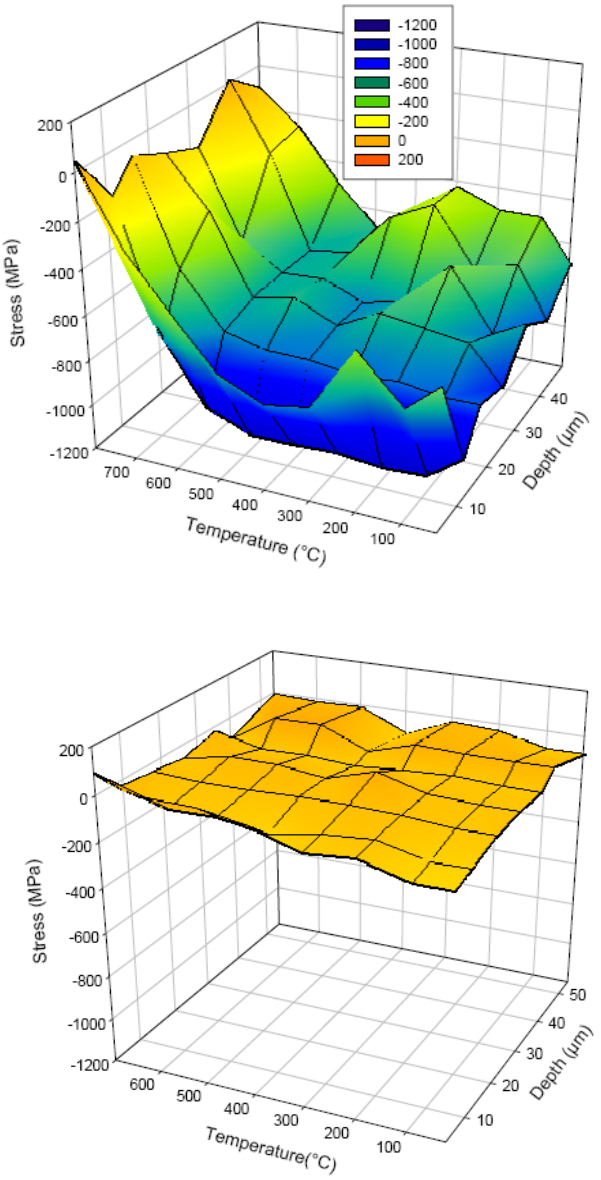

Fig. 2: *Temperature dependence of residual stress gradient in the surface region of a shot peened steel during first heating up (left) and cooling down (right). During the second cycle, the stresses in the substrate are below 100 MPa in the whole temperature range.*

Acknowledgments:

We gratefully acknowledge the European Community for a financial support grant through the Contract N° RII 3-CT-2004-506008. A part of this work was supported by the Austrian NANO Initiative via a grant from the Austrian Science Fund FWF within the project "StressDesign - Development of Fundamentals for Residual Stress Design in Coated Surfaces".

References :

[1]. J. Jagielski et al., Appl. Surf. Sci.**156** (2000) 47–64.

[2]. R. Resel, E. Tamas, B. Sonderegger, P. Hofbauer and J. Keckes, J. Appl. Cryst. **36** (2003) 80-85.

BENSC	**EXPERIMENTAL REPORT** **Energy dispersive x-ray diffraction for the in situ investigation on the rapid thermal processing of $CuInS_2$ for thin film solar cell fabrication**	Proposal N° BESSY Instrument EDDI **S4** Local Contact Christoph Genzel
Principal Proposer: Experimental Team:	C. Genzel – HMI, Berlin I.M. Kötschau, C. Streeck – HMI, Berlin H. Rodriguez-Alvarez – HMI, Berlin A. Weber, M. Klaus, I. A. Denks – HMI, Berlin J. Gibmeier, H.W. Schock – HMI, Berlin	Date(s) of Experiment 2006

Date of Report: Feb. 2007

Highly efficient thin film solar cells based on chalcopyrite materials such as $Cu(In,Ga)Se_2$ show record efficiencies of up to 19.5% on the laboratory scale [1]. Solar cells made of plain $CuInS_2$ have not reached these record efficiencies yet but are also of significant interest due to a number of advantages in comparison with the more widely investigated selenium containing chalcopyrites. The main advandtage lies in the much faster deposition process. $CuInS_2$ thin films are deposited by a rapid thermal process, whereby sputtered Cu/In precursors are completely sulphurized within a few minutes. Both, solar cells made of $Cu(In,Ga)Se_2$ as well as CuInS2, are on the verge to large scale industrial production. A detailed understanding of the deposition process is indispensable.

The high flux available at the recently commissioned EDDI beam line facilitates energy dispersive X-ray diffraction (EDXRD) experiments at fixed geometry with a rather short acquisition time of typical 10sec per spectrum. Thereby the in situ monitoring of the solid state reactions during the rapid thermal process (RTP) of metallic precursors (i.e.: Cu and In) with elemental sulphur or selenium is possible.

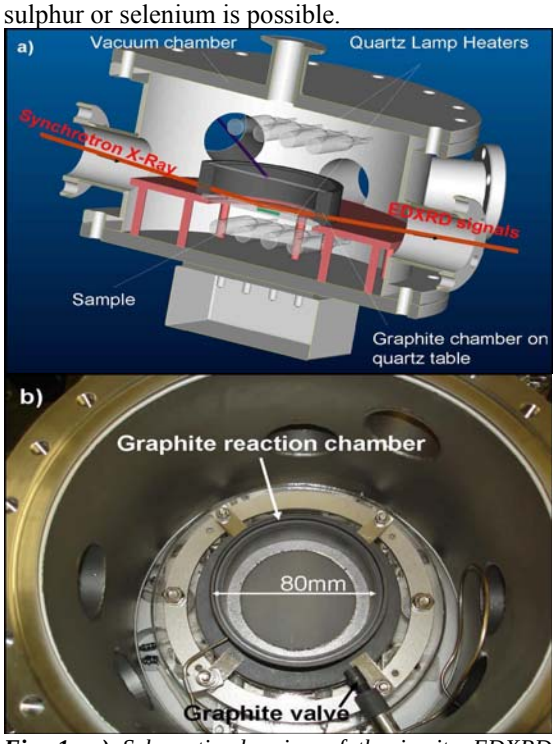

Fig. 1: a) *Schematic drawing of the in-situ EDXRD rapid thermal processing reaction chamber.* ***b)*** *View inside the vacuum chamber with the inner graphite reaction chamber.*

The analysis of a whole series of EDXRD spectra gives valuable information on the reaction pathway leading from the metallic precursors to the chalcopyrite thin films. The aim of the experiment is to investigate RTP type processes for the synthesis of chalcopyrite and chalcopyrite related thin films. Of particular interest is the influence of the maximum pressure of the chalcogen during the reaction.

A special reaction chamber was constructed, suitable for in situ EDXRD experiments at the EDDI beam line. Glass substrates with metallic precursors are placed in an evacuated graphite reactor which is enclosed itself in a vacuum chamber equipped with two banks of high performance quartz lamp heaters (Fig. 1). The graphite reactor has a quartz glass window at top and on the bottom and can be sealed with graphite valve. Maximum heating rates are up to 250K/ min. The temperature is monitored by two thermocouples placed close to the quartz lamp heaters and directly at the graphite reactor. Depending on the amount of elemental sulphur the maxi -mum pressure during the reaction can be adjusted. Metallic precursors where deposited by sequential sputtering of the elements on molybdenum coated soda lime glass according to the HMI baseline process for $CuInS_2$ solar cells [2]. Copper is supplied in excess (Cu/In=1.6) and segregates during the sulphurization as binary Cu-S phase on top of the $CuInS_2$ thin film. It can be removed after the process by etching in a suitable KCN solution. A well defined amount of elemental sulphur (40% excess) is placed on the bottom of the graphite reaction chamber next to the precursor substrate. The graphite reaction chamber is closed with a quartz glass window and the vacuum chamber is closed and evacuated to a pressure below $1x10^{-4}$ mbar. Subsequently the graphite valve is closed and the computer controlled RTP-process is started while simultaneously acquiring EDXRD spectra. The maximum pressure in the reaction chamber of about 1.5 mbar and corresponds to the state when all sulphur is completely evaporated but not consumed by the solid state reaction. The angle of the incident and emerging x-ray beam with the sample surface is the same (3.7°) and is kept fixed during the whole experiment (see Fig. 1a). The diffractometer setup at the EDDI beamline allows the arrangement of a nearly perfect parallel beam geometry. Thus, the sample position can be optimized easily for high count rates of the thin film and low background of the (amorphous) signal of soda-lime glass. This is important because small movements of the sample due to thermal expansion of the entire sample

stage (in the RTP zone) may be compensated during the experiment without loss of accuracy in the position of diffraction peaks (ΔE<10eV @ 40keV). Figure 2 shows two typical EDXRD spectra of the Cu/In precursor (Cu/In=1.8) before and after the sulphurization. The comparison shows that the metallic $CuIn_2$ phase disappears in favour of a single chalcopyrite $CuInS_2$ phase at the end of the process. The signal very high since the spectra where acquired for 240 sec prior to the start an after the end of the RTP process.

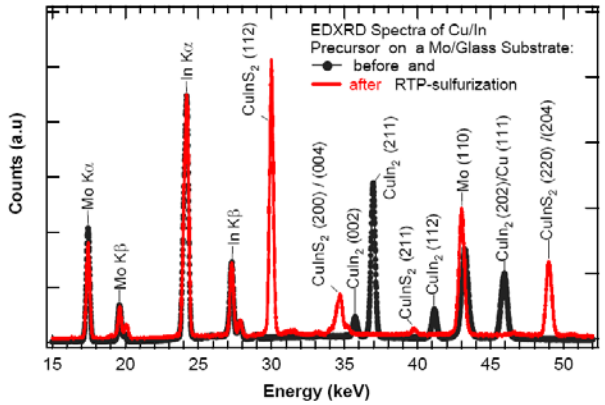

Fig. 2: *Typical in-situ EDXRD spectra before and after sulphurization of a sputtered Cu/In precursor on a Mo/Glass substrate. The metallic phases like $CuIn_2$ and Cu are completely consumed and single phase $CuInS_2$ is formed after the RTP process.*

So far the information can also be obtained by conventional laboratory based XRD experiments (not energy dispersive). However, the power of using the synchrotron lies in the high flux available and the short time necessary to acquire a spectrum which entails the qualitative information of all crystallographic phases present in the thin film at a particular time during the solid state reaction. Figure 3 shows a whole series of EDXRD spectra in a 2D representation which is obtained if the consecutively recorded spectra are plot ted next to each other as a line in a grey scale format.

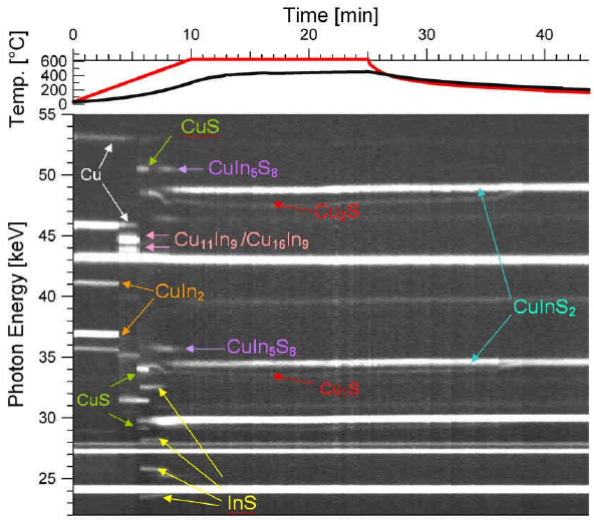

Fig. 3: *2D representation of a whole series of EDXRD patterns of the RTP processing of a metallic Cu/In precursor thin film under sulphur atmosphere. The plot shows directly the phase predominance in the thin film at a given time. Thereby the dominant reaction pathway of the solid state reaction can be identified. The temperature of the sample lies between the nominal temperature of the heaters (red) and the graphite reactor (black).*

The top axis shows the process time (? spectrum number) and the left axis identifies the photon energy. The intensity of the diffraction pattern is represented by the grey scale. Brighter areas signify diffraction peaks with higher intensity. On top the nominal temperatures of the heater (red) and the graphite box (black) are shown as a function of process time. The heating rate for this particular experiment was 63K/min with a subsequent annealing time of 15 min. at a top temperature of 630°C. The chosen representation as 2D image allows very quickly to discern the qualitative phase predominance at a given time and thereby to identify the various stages of the absorber formation. During the sulphurization of the Cu-rich Cu/In precursor different crystallographic phases can be identified: Cu, $CuIn_2$, $Cu_{11}In_9$, $Cu_{16}In_9$, CuS, Cu_2S, InS, $CuIn_5S_8$ and finally $CuInS_2$. In contrast to other experiments carried out at much lower sulphur partial pressure ($p_{max}< 10^{-3}$ mbar) [3] the reaction pathway follows the formation of the chalcopyrite from binary intermediate phases (CuS and InS) via a Cu-deficient defect phase ($CuIn_5S_8$) [4]. Other experiments with a much higher amount of elemental sulphur show a different behaviour in the onset of the chalcopyrite phase in comparison to the binary phases InS and CuS. The first results of this new experiment already confirm that the chalcogenide thin film formation is very sensitive to the vapour pressure in the gas phase during the solid state reaction. The experiment allows to systematically control this parameter and to study the absorber formation very close to the industrial process conditions. Therefore the optimization of the process conditions can be significantly accelerated and principle features of the growth mechanism can be identified. Preliminary experiments have shown that the time for the spectral acquisition can be further reduced to 3-5 seconds per spectrum. Real time experiments very similar to the HMI baseline RTP process with a much shorter the heat up phase of 2 min (instead of 10 min) will then be investigated by in situ EDXRD.

References:

[1]. M. A. Contreras, K. Ramanathan, J. AbuShama, F. Hasoon, D. L. Young, B. Egaas and R. Noufi, Prog. Photovolt: Res. Appl. **13** (2005); p. 209–216

[2]. K. Siemer, J. Klaer, I. Luck, J. Bruns, R. Klenk, D. Bräunig, Solar Energy Materials & Solar Cells, **67**, (2001), p. 159-166.

[3]. Ch. von Klopmann, J. Djordjevic, E. Rudigier, R. Scheer, Journal of Crystal Growth **289** (2006), p. 121-133

[4]. F.O. Adurodija, J. Song, S.D. Kim, S.K. Kim, K.H. Yoon, Jpn. J. Appl. Phys. Vol. **37** (1998) p. 4248-4253

Part II

LIST OF PUBLICATIONS

Thesis 2006
Examina

PhD thesis

2006

Kucharik, M. **Phase analysis of the system Na_3AiF_6-Ai_2O_3 (PhD thesis)** Slovak Institute of Technology, Bratislava, 2006	E9 NMI3: 1178 NMI3: 1113
Miliyanchuk, K. **Synthesis and study of new hydrides based on *f*-metals (PhD thesis)** Charles University, Prague, 2006	E2 NMI3: 1148
Prchal, J. **Study of magnetic properties of $RT^1_{1-x}T^2_xX$ compounds (PhD thesis)** Charles University, Prague, 2006	E4
Tereda, N. **Studies of Frustrated Heisenberg Triangular Magnet $CuFeO_2$ by Neutron Scattering and Synchrotron X-ray Diffraction (PhD thesis)** Tokyo University of Science, 2006	E4
Ulbricht, A. **Untersuchung an neutronenbestrahlten Reaktordruckbehälter-stählen mit Neutronen-Kleinwinkelstreuung (PhD thesis)** TU Freiberg, 2006	V4

Diploma

Chemnitzer, R. **Intercalation von Stickstoff und Wasserstoff in Sr_2N sowie ortsabhängige Feststoffcharakterisierung mit Laserablation (diploma)** TU Dresden, 2006	E9

Publications 2006
BENSC Experiments and BENSC Authors

2003 (supplement)

Bellmann, D.; Clemens, H.; Matijasevic, B.; Heinemann, A.; Banhart, J. **Investigation of early stages of metal foam formation by small-angle neutron scattering techniques** Cellular Metals and Metal Foaming Technology Eds: Banhart, J.; Fleck, N.A.; Mortensen, A. (2003), 113 - 118	V4
Prots, Y.; Auffermann, G.; Tovar, M.; Kniep, R. **Sr_4N_3: Ein bisher fehlendes Glied in der Stickstoff-Druck-Reaktionsreihe Sr_2N - Sr_4N_3 - SrN - SrN_2** Angew. Chem. **114** (2003), 2392 - 2394	E9
Prots, Y.; Auffermann, G.; Tovar, M.; Kniep, R. **Sr_4N_3: A hitherto missing member in the Nitrogen-Pressure-Reaction series Sr_2N - Sr_4N_3 - SrN - SrN_2** Angew. Chem. Int. Ed. Engl. **41** (2003), 2288 -	E9

2004 (supplement)

Anderson, C.; Holub-Krappe, E.; Konishi, T.; Karis, O.; Maletta, H.; Arvanitis, D. **Spin Reorientation in Au/Co: in-situ prepared ultra-thin films** MAX-Lab Activity report 2003 (2004), 330 - 331	
Rack, A.; Heibel, A.; Bütow, A.; Matijasevic, B.; Banhart, J. **Charcterization of Metal Foams with Synchrotron-Tomography and 3D Image Analysis** www.ndt.net/article/wcndt2004/pdf/materials_characterization/ (2004)	S5

2005 (supplement)

Garcia Moreno, F.; Kardjilov N. **Cellular Architecture - Overview of X-ray and Neutron Radioscopy and Tomographyin Metal Foams** Materials World internet journal **6** (2005)	V7
Link, T., Epishin, A., Klaus, M., Brückner, U., Recnizek, A. **<100> Dislocations in nickel-base superalloys: Formation and role in creep deformation** Materials Science and Engineering A **405** (2005), 254 - 265	S4
Schneider, R.P.; Poeste, T.; Freydank, H.; Hofmann, M. **The dedicated residual stress diffractometers E3/E7 at HMI Berlin ans Stress-Spec at FRM II** IAEA-TECDOC-1457 (2005), 61 - 70	E3
Ulbricht, A.; Böhmert, J.; Uhlemann, M.; Müller, G. **Small-angle neutron scattering study on the effect of hydrogen in irradiated reactor pressure vessel steels** Journal of Nuclear Materials **336** (2005), 90 - 96	V4

2006

Abbas, S.; Wagh, A.; Strobl, MK.; Treimer, W. **Observation of neutron forward diffraction by single crystal prisms** Solid State Physics (India) **51** (2006), 351 - 352	V12b
Aliouane, N. ; Argyriou, D.N. ; Strempfer, J. ; Zegkinoglou, I. ; Landsgesell, S. ; Zimmermann, M. v. **Field-induced linear magnetoelastic coupling in multiferroic $TbMnO_3$** Physical Review B: Condensed Matter **73** (2006), 020102/1 - 4	E9
Andersen, A.H.; Jensen, J.; Jensen, T.B.S.; Pinholt, R.; Zimmermann, M.V.; Noergaard Toft, K.; Abrahamsen, A.B.; Hedegard, P.; Vorderwisch, P.; Canfield, P. **Magnetic and quadrupolar ordering in $TmNi_2B_2C$** Physica B - condensed matter **385 - 386** (2006), 36 - 65	E1 IHP II:501
Baranov, N.V. ; Yermakov, A.A. ; Pirogov, A.N. ; Proshkin, A.V. ; Gvasaliya, S.N. ; Podlesnyak, A. **Irreversibility of the magnetic state of $Tm_{1-x}Tb_xCo_2$ revealed by specific heat, electrical resistivity, and neutron diffraction measurements** Physical Review B: Condensed Matter **73** (2006), 104445/1 - 11	E4
Bayrakci, S.P.; Keller, T.; Habicht, K.; Keimer, B. **Spin-wave lifetimes throughout the Brillouin zone** Science **312** (2006), 1926 - 1929	V2
Behrens, S.; Bönnemann, H.; Matoussevitch, N.; Dinjus, E.; Modrow, H.; Palina, N.; Frerichs, M.; Kempter, V.; Maus-Friedrichs, W.; Heinemann, A.; Kammel, M.; Wiedenmann, A.; Pop, L.; Odenbach, S.; Uhlmann, E.; Bayat, N.; Hesselbach, J.; Guldbakke, J.M. **Air-stable Co-, Fe-, and Fe/Co-nanoparticles and ferrofluids** Zeitschrift für Physikalische Chemie **220** (2006), 3 - 40	V4
Bentley, P.M. ; Kilcoyne, S.H. **Determination of hyperfine field distributions in amorphous magnets** Journal of Physics: Condensed Matter **18** (2006), 7751 - 7759	
Bentley, P.M. ; Pappas, C. ; Habicht, K. ; Lelievre-Berna, E. **Evolutionary programming for neutron instrument optimisation** Physica B - condensed matter **385 - 386** (2006), 1349 - 1351	V5
Boin, M. ; Haibel, A. **Compensation of ring artefacts in synchrotron tomographic images** Optics Express **14** (2006), 12071 - 12075	S5
Bordallo, H.N.; Aldridge, L.P.; Desmedt, A. **Water dynamics in hardened ordinary Portland cement paste or concrete: from quasielastic neutron scattering** Journal of Physical Chemistry B **110** (2006), 17966 - 17976	V3
Borzi, R.A.; Grigera, S.A.; Farrell, J.; Perry, R.S.; Lister, S.L.S.; Lee, S.L.; Tennant, D.A.; Maeno, Y.; MacKenzie A.P. **Formation of a Nematic Fluid at High Fields in $Sr_3Ru_2O_7$** ScienceDOI: 10.1126/science.1134796 (Nov 2006)	E1
Chatterji, T.; Koza, M.M.; Demmel, F.; Schmidt, W.; Hoffmann, J.-U.; Amann, U.; Schneider, R.; Dhalenne, G.; Suryanarayanan, R.; Revcolevschi, A. **Coexistence of ferromagnetic and antiferromagnetic spin correlations in $La_{1.2}Sr_{1.8}Mn_2O_7$** Physical Review B: Condensed Matter **73** (2006), 104449/ 1-6	E2
Conder, K. ; Stingaciu, M. ; Pomjakushina, E. ; Podlesnyak, A. **Structural, magnetic and transport properties of layered cobaltites $LnBaCo_2O_{5+x}$** Advances in Science and Technology **45** (2006), 2554 - 2559	E4

Danilyan, G.; Fedorov, A.; Krakhotin, V.; Pavlov, V.; Brakhman, E.; Karpikhin, I.; Korobkina, E.; Golub, R.; Wilpert, T.; Russina, M. **Search for Scission Neutrons Using Specific Angular Correlations in ^{235}U Fission Induced by Slow Polarized Neutrons** Physics of Atomic Nuclei **69** (2006), 1 - 3	V13
Dante, S.; Hauß, T.; Dencher, N.A. **Cholesterol inhibits the insertion of the Alzheimer's peptide A\beta(25-35) in lipid bilayers** European Biophysics Journal **35** (2006), 523 - 531	V1
De Lisi, R.; Gradzielski, M.; Lazzara, G.; Milioto, S.; Muratore, N.; Prevost, S. **Aqueous Block Copolymer-Surfactant Mixtures and Their Ability in Solubilizing Chlorinated Organic Compounds. A Thermodynamic and SANS Study** Journal of Physical Chemistry B **110** (2006), 25883 - 25894	V4 NMI3: 1135
Denks, I.A.; Klaus, M.; Genzel, Ch. **Determination of real space residual stress distributions $\sigma_{ij}(z)$ of surface treated materials with diffraction methods. Part II: Energy dispersive approach** Materials Science Forum **524 - 525** (2006), 37 - 42	S4
Dennison, S.R.; Haußß,T.; Dante, S.; Brandenburg, K.; Harris, F.; Phoenix, D.A. **Deuteration can affect the conformational behaviour of amphiphilic alpha-helical structures** Biophysical Chemistry **119** (2006), 115 - 120	V1 NMI3: 1035 IHP II: 581
Dudzik, E.; Feyerherm, R.; Diete, W.; Signorato, R.; Zilkens, C. **The new HMI beamline MAGS: an instrument for hard X-ray diffraction at BESSY** Journal of Synchrotron Radiation **13** (2006), 421 - 425	S2
Efimov, V.V.; Efimova, E.A.; Iakubovskii, K.; Karpinskii, D.V.; Khasanov, S.; Kochubey, D.I.; Kriventsov, V.V.; Kuzmin, A.; Sazonov, A.P.; Sikolenko, V.; Sakharov, M.; Shmakov, A.N.; Tiutiunnkov, S.I. **Effect of high-current pulsed electron beam irradiation on the structure of $La_{0.7}Sr_{0.3}CoO_3$ powder** Journal of Physics and Chemistry of Solids **67** (2006), 2001 - 2006	E9, E1 NMI3: 1170
Fåk, B.; Rüegg, Ch.; Niklowitz, P.G.; McMorrow, D.F.; Canfield, P.C.; Bud'ko, S.L.; Janssen, Y.; Habicht, K. **Magnetic phase diagram of heavy fermion YbAgGe** Physica B - condensed matter **378 -3 80** (2006), 669 - 670	V2 NMI3: 1056
Falus, P.; Vorobiev, A.; Krist, T. **Test of a two-dimensional neutron spin analyzer** Physica B **385 - 386** (2006), 1149 - 1151	V14
Feyerherm, R.; Dudzik, E.; Aliouane, N.; Argyriou, D.N. **Commensurate Dy magnetic ordering associated with incommensurate lattice distortion in multiferroic $DyMnO_3$** Physical Review B: Condensed Matter **73** (2006), 180401/1 - 4	S2
Fiori, F.; Giunta, G.; Hilger, A.; Kardjilov, N.; Rustichelli, F. **Non-destructive characterization of archaeological glasses by neutron tomography** Physica B - condensed matter **385 - 386** (2006), 1206 - 1208	V7
Fiori, F.; Hilger, A.; Kardjilov, N.; Albertini, G. **Crack detection in Al alloy using phase-contrast neutron radiography and tomography** Measurement Science and Technology **17** (2006), 2479 - 2484	V7 NMI3: 1061
Flores Renteria, A.; Saruhan, B.; Schulz, U.; Raetzer-Scheibe, H.-J.; Haug, J.; Wiedenmann, A. **Effect of morphology on thermal conductivity of EB-PVD PYSZ TBCs** Surface and Coatings Technology **201** (2006), 2611 - 2620	V4

Fujisawa, M.; Ono, T.; Fujiwara, H.; Tanaka, H.; Sikolenko, V.; Meissner, M.; Smeibidl, P.; Gerischer S.; Graf, H.A. **Impurity- and field-induced magnetic orderings in doped quantum antiferromagnet $TlCu_{1-x}Mg_xCl_3$** Journal of Magnetism and Magnetic Materialsdoi:10.1016/j.jmmm.2006.10.378	E1
Fujisawa, M; Ono, T; Fujiwara, H.; Tanaka, H.; Sikolenko, V.; Meissner, M.; Smeibidl, P.; Gerischer, S.; Graf, H. A. **Drastic Change of Magnetic Phase Diagram in Doped Quantum Antiferromagnet $TlCu_{1-x}Mg_xCl_3$** Journal of the Physical Society of Japan **75** (2006), 033702/ 1-4	E1
Furrer, A.; Rüegg, Ch. **Bose-Einstein Condensation in magnetic materials** Physica B - Condensed Matter **385 - 386** (2006), 295 - 300	V2 NMI3: 1006
Garlea, V.O.; Nagler, S.E.; Zarestky, J.L.; Stassis, C.; Vaknin, D.; Kögerler, P.; McMorrow, D.F.; Niedermayer, C.; Tennant, D.A.; Lake, B.; Qiu, Y.; Exler, M.; Schnack, J.; Luban, M. **Probing spin frustration in high-symmetry magnetic nanomolecules by inelastic neutron scattering** Physical Review B: Condensed Matter **73** (2006), 024414/1 - 5	
Gilles, R.; Mukherji, D.; Hoelzel, M.; Strunz, P. ; Toebbens, D.; Barbier, B. **Neutron and X-ray diffraction measurements on micro- and nano-sized precipitates embedded in a Ni-based superalloy and after their extraction from the alloy** Acta Materialia **54** (2006), 1307 - 1316	E9
Gilles, R.; Mukherji, D.; Hoelzel, M.; Strunz, P. ; Toebbens, D.; Barbier, B. **Neutron and X-ray diffraction measurements on micro- and nano-sized precipitates embedded in a Ni-based superalloy and after their extraction from the alloy** Acta Materialia **54** (2006), 1307 - 1316	E9
Glavatska N.; Dobrinskiy A.; Glavatskiy I.; Urubkov I.; Ge Y.; Soderberg O.; Hannula S.-P. **Effect of alloying on transformation temperatures and magnetoplasticity in Ni-Mn-Ga alloys** Functional Materials **13** (2006), 331 - 336	E2
Glavatskyy, I.; Glavatska, N.; Soderberg, O.; Hannula, S.-P.; Hoffmann, J.-U. **Transformation temperatures and magnetoplasticity of Ni-Mn-Ga alloyed with Si, In, Co or Fe** Scripta Materialia **54** (2006), 1891 - 1895	E2
Golosova, N.O.; Kozlenko, D.P.; Sikolenko, V.V.; Sazonov, A.P.; Troyanchuk, I.O.; Savenko, B.N.; Glazkov, V.P. **High pressure effects on the crystal and magnetic structure of the $Nd_{0.78}Ba_{0.22}CoO_3$ cobaltite.** Journal of Experimental and Theoretical Physics Letters **84** (2006), 16 - 20	
Golosovsky, I.; Dvornikov, V.; Hansen, T.; Fokin, A.; Koroleva, E.; Korotkov, L.; Naberezhnov, A.; Tovar, M. **Structure and Conductivity of Nanostructured Sodium Nitrite** Solid State Phenomena **115** (2006), 221 - 228	E9
Golub, R.; Gähler, R.; Habicht, K., Klimko, S. **Bunching of continous neutron beams** Physics Letters A **349** (2006), 59 - 66	V2
Haibel, A.; Rack, A; Banhart, J. **Why are metal foams stable?** Applied Physics Letters **89** (2006), 154102/ 1 - 3	S5

Hassanein, R.; de Beer, F.; Kardjilov, N.; Lehmann, E. **Scattering correction algorithm for neutron radiography and tomography tested at facilities with different beam characteristics** Physica B - condensed matter **385 - 386** (2006), 1194 - 1196	V7
Haug, J.; Wiedenmann, A.; Flores, A.; Saruhan-Brings, B.; Strunz, P. **Evolution of pore microstructure in thermal barrier coatings studied by SANS** Physica B - Condensed Matter **385 - 386** (2006), 617 - 619	V4
Heinemann, A.; Hoell, A.; Wiedenmann, A.; Popp, L.M. **Small-angle scattering of orientated magnetic structures and applications to magnetic colloids** Physica B - Condensed Matter **385 - 386** (2006), 461 - 464	V4
Henkel, F.; Hermeking-Goebel, U.; Lemke, P.; Wilpert, T.; Pietsch, C.; Schneider, R. **E7 - New starin scanner at HMI - high q-resolution for phase sensitive analysis of stress distributions** Materials Science Forum **524 - 525** (2006), 205 - 208	E7
Hilger, A.; Kardjilov, N.; Strobl, M.; Treimer, W.; Banhart, J. **The new cold neutron radiography and tomography instrument CONRAD at HMI Berlin** Physica B - Condensed Matter **385 - 386** (2006), 1213 - 1215	V7
Hoell, A.; Kranold, R.; Goerigk, G.; Tatchev, D.; Haas, S.; Müller, M. **The structure of silver free photochromic glasses studied by ASAXS** Hasylab Annual report 2005 (2006), 545 - 546	
Hoelzel, M.; Del Genovese, D.; Gilles, R.; Mukherji, D.; Toebbens, D.; Roesler, J. **Phase analysis and lattice mismatches in superalloys DT706 and Inconel 706** Physica B - Condensed Matter **385 - 386** (2006), 594 - 596	E9
Hofmann, M.; Schneider, R.; Seidl, G.A.; Rebelo-Kornmeier, J.; Wimpory, R.C.; Garbe, U.; Brokmeier, H.-G. **The new materials science diffractometer STRESS-SPEC at FRM-II** Physica B - Condensed Matter **385 - 386** (2006), 1035 - 1037	
Hofmann, M.; Seidl, G.A.; Rebelo-Kornmeier, J.; Garbe, U.; Schneider, R.; Wimpory, R.C.; Wasmuth, U.; Noster, U. **The new materials science diffractometer STRESS-SPEC at FRM-II** Materials Science Forum **524 - 525** (2006), 211 - 216	
Höhn, P.; Armbrüster, M.; Auffermann, G.; Burkhardt, U.; Haarmann, F.; Mehta, A.; Kniep, R. **$Sr_2[(NC)NiN]$: Ein Cyano-Nitrido-Nickelat(0)** Zeitschrift für Anorganische Allgemeine Chemie **632** (2006), 2129	E9
Höhn, P.; Auffermann, G.; Ramlau, R.; Rosner, H.; Schnelle, W.; Kniep,R. **$(Ca_7N_4)[M_x]$ (M=Ag, Ga, In, Tl): Linear Metal Chains as Guests in a Subnitride Host** Angew. Chem., Int. Ed. Engl. **45** (2006), 6881 - 6885	E9
Höhn, P.; Auffermann, G.; Ramlau, R.; Rosner, H.; Schnelle, W.; Kniep,R. **$(Ca_7N_4)[M_x]]$ (M=Ag, Ga, In, Tl): Linear Metal Chains as Guests in a Subnitride Host** Angew. Chem. **118** (2006), 6833 - 6837	E9
Hoinkis, E.; Röhl-Kuhn **In situ small angle neutron scattering study of nitrogen adsorption and condensation in mesoporous silica glass CPG-10-75** Journal of Colloid and Interface Science **296** (2006), 256 - 262	V4

Idzikowski, B.; Kudryavtsev, Y.V.; Hyun, Y.-H.; Lee, Y.-P.; Klenke, J. **Magnetic effects of structural disorder in the itinerant ferromagnet Ni3Al studied by magnetic and neutron methods on stoichiometric and off-stoichiometric samples** Journal of Alloys and Compounds **423** (2006), 267 - 273	E1 IHP II: 575
Jauch, W. ; Reehuis, M. **Electron density distribution in paramagnetic chromium: A gamma-ray diffraction study** Physical Review B **73** (2006), 085102/1 - 8	
Jenichen, B.; Takagaki, Y.; Ploog, K.H.; Darowski, N.; Feyerherm, R.; Zizak, I. **Nucleation at the phase transition near 40 C in MnAs nanodisks** Applied Physics Letters **89** (2006), 051915/1 - 3	S2
Kammel, M. ; Wiedenmann, A. ; Heinemann, A. ; Bönnemann, H. ; Matoussevitch, N. **Oxide coating of Co-ferrofluids studied by polarised SANS** Physica B - Condensed Matter **385 - 386** (2006), 457 - 460	V4
Kardjilov, N. ; Fiori, F. ; Giunta, G. ; Hilger, A. ; Rusticheli, F. ; Strobl, M. ; Banhart, J. ; Triolo, R. **Neutron tomography for archaeological investigations** Journal of Neutron Research **14** (2006), 29 - 36	V7 NMI3: 1214 V4, V12a, V7 NMI3: 1136
Kardjilov, N. ; Garcia-Moreno, F. **Overview of imaging with X-rays and neutrons** Notizario Neutroni e Luce di Sincrotrone **11** (2006), 15 - 23	V7
Karpinsky, D.V.; Troyanchuk, I.O.; Dobryansky, V.M.; Szymczak, R.; Tovar, M. **Crystal structure and magnetic properties of $LaCo_{0.5}Fe_{0.5}O_3$ perovskite** Chrystallography Reports **51** (2006), 596 - 600	E9
Karpinsky, D.V.; Troyanchuk, I.O.; Sikolenko, V.V. **Inhomogeneous magnetic states in Fe and Cr substituted LaMnO3** Journal of Physics: Condensed Matter doi:10.1088/0953-8984/19/3/036220 **19** (2006), 036220/ 1 - 9	E9
Kartini, E.; Arai, M.;Mezei,F.; Nakamura,M.; Russina, M. **Structure and Dynamics on Superionic Conducting Phosphate Glasses by Neutron Scattering** Physica B - Condensed Matter **385 - 386** (2006), 236 - 239	V3
Kavečanský, V.; Mihalik, M.; Mat'aš, S.; Mitróová, Z.; Lukáčová, M. **Crystal structure and magnetism of $Pr[Fe(CN)_6]\ 4D_2O$** Zeitschrift für Kristallographie **23** (2006), 543 - 548	E6 IHP II: 468 E9
Keiderling, U.; Wiedenmann, A.; Haug, J. **Stroboscopic time-resolved SANS technique for dynamical studies of slow relaxation processes** Physica B: Condensed Matter **385 - 386** (2006), 1183 - 1186	V4
Keller, T.; Aynajian, P.; Habicht, K.; Boeri, L.; Bose, S.K.; Keimer, B. **Momentum-resolved electron-phonon interaction in lead determined by neutron resonance spin-echo spectroscopy** Physical Review Letters **96** (2006), 225501/ 1 - 4	V2
Keppas, L.K.; Katsareas, D.E.; Wimpory, R.C.; Anifantis, N.K.; Youtsos, A.G. **Letterbox type repair weld finite element simulation and residual stress prediction** Materials Science Forum **524-525** (2006), 445 - 450	E3
Khalyavin, D.D.; Argyriou, D.N.; Amann, U.; Yaremchenko, A.A.; Kharton, V.V. **Spin-state ordering and magnetic structures in $YBaCo_2O_{5.5/5.44}$** Physical Review B: Condensed Matter http://arxiv.org/ftp/cond-mat/papers/0610/0610179.pdf (2006)	E2, E9 NMI3: 1177

Khomchenko, V.A.; Troyanchuk, I.O.; Sazonov, A.P.; Sikolenko, V.V. Szymczak, H.; Szymczak, R.. **Metamagnetic behaviour in $TbCo_{0.5}Mn_{0.5}O_{3.06}$ perovskite** Journal of Physics: Condensed Matter **18** (2006), 9541 - 9548	E9
Kiselev, M.; Ryabova, N.Yu., Balagurov, A.M., Otto, D., Dante, S., Hauß, Th., Wartewig, S., Neubert, R.H.H. **Ceramide 6 influence the structure and hydration of multilamellar dipalmitoylphosphatidylcholine membrane** Surface, X-ray, synchrotron and neutron research **6** (2006), 30 - 37	V1
Klokkenburg, M.; Erné, B.H.; Meeldijk, J.D.; Wiedenmann, A.; Petukhov, A.V.; Dullens, R.P.A; Philipse, A.P. **In situ imaging of field-induced hexagonal columns in magnetite ferrofluids** Physical Review Letters **97** (2006), 185702/ 1 - 4	V4 NMI3: 1140
Köbler, U.; Hoser, A.; Hoffmann, J.-U., Thomas, C. **One-dimensional bulk ferromagnetics: $NdAl_2$ und hcp cobalt** Solid State Communications **137** (2006), 301 - 305	E2
Krappe, H.J. **Bayesian methods in the evaluation of scattering data** International Journal of Modern Physics E **15** (2006), 354 - 361	
Laurenze-Landsberg, C.; Schmidt, C.; Schröder-Smeibidl, B.; Mertens, L.A. **BENSC neutrons for cultural heritage research: Neutron autoradiography of paintings** Notizario Neutroni e Luce di Sincrotrone **11** (2006), 24 - 27	B8
Lee, H.-Y. ; Biglari, F.R. ; Wimpory, R, ; Nikbin, K.M. **Treatment of residual stress in failure assessment procedure** Engineering Fracture Mechanics **73** (2006), 1755 - 1771	E3
Lenné, T.; Bryant, G.; Garvey, C. J.; Keiderling, U.; Koster, K. L. **Location of sugars in multilamellar membranes at low hydration** Physica B - Condensed Matter **385 - 386** (2006), 862 - 864	V4
Levchanovsky, F.V. ; Litvinenko, E.I. ; Nikiforov, A.S. ; Gebauer, B. ; Schulz, Ch. ; Wilpert, Th. **Software modules of DAQ PCI board (DeLiDAQ) for positive-sensitive MWPC detectors with delay line readout** Nuclear Instruments and Methods in Physics Research Section A **569** (2006), 900 - 904	
Lieutenant, K.; Peters, J.; Mezei, F. **Monte Carlo simulation of the new time-of-flight powder diffractometer EXED at the Hahn-Meitner-Institut** Journal of Neutron Research **14** (2006), 147 - 165	E9
Lieutenant, K.; Mezei, F. **Monte Carlo simulations of a powder diffractometer installed on a long pulse target station using wavelength frame multiplication** Journal of Neutron Research **14** (2006), 177 - 191	
Link, T.; Zabler, S.; Epishin, A.; Haibel, A.; Bansal, M.; Thibault, X. **Synchrotron tomography of porosity in single-crystal nickel-base superalloys** Materials Science and Engineering A **425** (2006), 47 - 54	S5
Lobanovsky, L.S.; Troyanchuk, I.O.; Szymczak, H.; Prokhnenko, O. **Structure and physical properties of layered double perovskite $NdBaCo_2O(5.5 + 0.25)$** Journal of Experimental and Theoretical Physics **103** (2006), 740 - 746	E9

Lumsden, M.D.; Nagler, S.E.; Sales, B.C.; Tennant, D.A.; McMorrow, D.F.; Lee, S.H. **Magnetic excitation spectrum of the square lattice S=1/2 Heisenberg antiferromagnet K2V3O8** Physical Review B: Condensed MatterPhys Rev B arxiv:cond-mat/0609775 (2006)	
McEwen, K. A.; Jensen, J.; Beirne, E. D.; Allen, J. P.; Habicht, K.; Adroja, D. T.; Bewley, R. I.; Fort, D. **Multiple magnetic singlet-singlet excitations in intermetallic PrNiSn** Physical Review B: Condensed Matter **73** (2006), 014402/ 1 - 7	V2 IHP II: 423
McLain, S.E.; Dolgos, M.R.; Tennant, D.A; Turner, J.F.C.; Barnes, T.; Proffen, Th.; Sales, B.C.; Bewley, R.I. **Magnetic behaviour of layered Ag(II) fluorides** Nature Materials **5** (2006), 561 - 566	
McLain, S.E.; Tennant, D.A.; Turner, J.F.C; Barnes, T.; Dolgos, M.R.; Proffen, T; Sales, B.C.; Bewley, R.I. **2D Ferromagnetism in the High-Tc Analogue Cs_2AgF_4** Nature Materials: arxiv:cond-mat/0509194 (2006)	
Mehta, A.; Höhn, P.; Schnelle, W.; Petzold, V.; Rosner, H.; Burkhardt, U.; Kniep, R. **$Ba_2[Ni_3N_2]$: A Low-Valent Nitridonickelate – Synthesis, Crystal Structure and Physical Proerties** Chem. Eur. J. **12** (2006), 1667 - 1676	E9
Mezei, F. **Accelerator requirements for next generation neutron sources** Nuclear Instruments and Methods in Physics Research Section A **562** (2006), 553 - 556	
Milani, S.; Baldelli Bombelli, F.; Berti, D.; Hauss, T.; Dante, S.; Baglioni, P. **Structural investigation of bilayers formed by 1-palmitoyl-2-oleoylphosphattidylnucleosides** Biophysical Journal **90** (2006), 1260 - 1269	V1 NMI3: 1063
Miliyanchuk, K; Havela,L; Pereira, L.C.J.; Gonçalves, A.P.; Prokeš, K. **Peculiarities of U_2T_2X hydrides** Journal of Magnetism and Magnetic Materials: doi:10.1016/j.jmmm.2006.10.157 (2006)	E2 NMI3: 1148
Nakamura, M; Iwase, H.;, Arai, M.; Kartini, E.; Russina, M.; Yokoo, T.; Taylor, J.W. **Low energy vibrational excitations characteristic of superionic glass** Physica B - Condensed Matter **385 - 386** (2006), 552 - 554	V3
Nakamura,M.; Arai, M; Kartini, E.; Taylor, J.W; Russina, M. **Unique vibrational excitations in superionic conducting glass** Flow dynamics: The second international conference on flow dynamics Eds.: Tokuyama, M.; Maruyama, S. (2006), 504 - 507	V3
Notbohm, S.; Ribeiro, P.; Lake, B.; Tennant, D.A.; Schmidt, K.P.; Uhrig, G.S.; Hess, C.; Klingeler, R.; Behr, G.; Büchner, B.; Reehuis, M.; Bewley, R.I.; Frost, C.D.; Manuel,P; Eccleston, R.S. **One- and Two-Triplon Spectra of a Cuprate Ladder** Physical Review Letters: arxiv:cond-mat/0608109 (2006)	
Notbohm, S.; Tennant, D.A.; Lake, B.; Canfield, P.C.; Fielden, J.; Kögerler, P.; Mikeska, H.-J.;Luckmann, C.; Telling, M.T.F. **Temperature effects on multi-particle scattering in a gapped quantum magnet** Journal of Magnetism and Magnetic Materialsdoi:10.1016/j.jmmm.2006.10.692	

Perroud, O.; Garcia-Matres, E.; Kumar, G; Eckert, J.; Wiedenmann, A. **Small Angle Neutron Scattering studies of hard magnetic $Nd_{60}Fe_{30-x}Co_xAl_{10}$ bulk amourphous alloys** Materials Science and Engineering Adoi:10.1016/j.msea.2006.02.361 (2006), web - release	V4
Peters, J.; Bleif, H.-J.; Kali, G.; Rosta, L.; Mezei, F. **Performance of TOF powder diffractometers on reactor sources** Physica B - Condensed Matter **385 - 386** (2006), 1019 - 1021	V15
Peters, J.; Champion, J.D.M.; Zsigmond, G.; Bordallo, H.N.; Mezei, F. **Using Fermi choppers to shape the neutron pulse** Nuclear Instruments and Methods in Physics Research Section A **557** (2006), 580 - 584	V15
Peters, J.; Lieutenant, K.; Clemens, D.; Peters, J. **EXED - the new Extreme Environment Diffractometer at the Hahn-Meitner-Institut Berlin** Zeitschrift für Kristallographie **23** (2006), 189 - 194	V15
Poeste, T.; Wimpory, R.C.; Schneider, R. **The new and upgraded neutron instruments for material science at HMI - current activities in cooperation with industry** Materials Science Forum **524 - 525** (2006), 223 - 228	E3
Prokhnenko, O.; Arnold, Z.; Kuchin, A.; Ritter, C.; Isnard, O.; Kamarad, J.; Iwasieczko, W.; Drulis, H. **Influence of lattice volume on magnetic states of $Ce_2Fe_{16}MnD_y$ compounds (y=0,1,2.3)** Journal of Applied Physics **100** (2006), 013903/ 1 - 9	
Prokhnenko, O.; R. Feyerherm, E. Dudzik, S. Landsgesell, N. Aliouane, L.C. Chapon, and D. N. Argyriou **Enhanced ferroelectric polarization by induced Dy spin-order in multiferroic $DyMnO_3$** Physical Review Lettersarxiv:cond-mat/0609024 (2006)	S2
Qureshi, N; Fuess, H; Ehrenberg, H; Hansen, T; Ritter, C; Prokeš, K; Podlesnyak, A; Schwabe, D **Magnetic properties of the Kagomé mixed compounds $(Co_xNi_{1-x})_3V_2O_8$** Physical Review B: Condensed Matter **74** (2006), 212407/ 1 - 4	E4
Rehfeldt, F.; Steitz, R.; Armes, S.P.; von Klitzing, R.; Gast, A.P.; Tanaka, M. **Reversible activation of diblock copolymer monolayers at the interface by pH modulation, 1: Lateral chain density and conformation** Journal of Physical Chemistry B **110** (2006), 9171 - 9176	V6
Ribeiro, P.A.; Steitz, R.; Lopis, I. E.; Haas, H.; Souza, N.C.; Oliveira, O.N.; Raposo, M. **Thermal stability of poly(o-methoxyaniline) layer-by-layer films investigated by neutron reflectivity and UV-vis spectroscopy** Journal of Nanoscience and Nanotechnology **6** (2006), 1396 - 1404	V6
Roger, M.; Morris, D.J.P.; Tennant, D.A.; Gutmann, M.J.; Goff, J.P.; Prabhakaran, D.; Shannon, N.; Lake, B.; Coldea, R.; Deen, P.P. **Formation of Vacancy Clusters and Electrochemical Control of Electrons in Na_xCoO_2** Sciencearxiv.org/ftp/cond-mat/papers/0507/0507040.pdf (2006), web - release	
Rosenthal, D.; Zizak, I.; Darowski, N.; Magkoev, T.T.; Christmann, K. **The growth and structure of titanium dioxide films on a Re(10-10) surface: Rutile (011)-(2x1)** Surface Science **600** (2006), 2830 - 2840	
Rossner, H.H.; Schmitz, D.; Imperia, P.; Krappe, H.J.; Rehr, J.J. **Bayes-Turchin analysis of X-ray absorption data above the Fe $L_{2,3}$-edges** Physical Review B: Condensed Matter **74** (2006), 134107/ 1 - 12	S1

Russina, M.; Kartini, E.; Nakamura, M.; Arai., M.; Mezei, F.; **Mobile cations motion in superionic glasses** Physica B - Condensed Matter **385 - 386** (2006), 240 - 242	V3
Šaroun, J.; Kočík, J.; Garcia-Matres, E.; Muraňský, O.; Strunz, P. **Characterisation of radiation-induced precipitates in reactor pressure vessel steels** Zeitschrift für Kristallographie **23** (2006), 393 - 398	V4 IHP II: 550
Sass, B.; Buschhorn, S.; Felsch W.; Schmitz, D.; Imperia, P. **Thin layers of Fe, Co, and Ni on V_2O_3(11-20) and V_2O_3(0001): a comparison of the interfacial magnetic interactions** Journal of Magnetism and Magnetic Materials **303** (2006), 167 - 177	S1
Saurel, D.; Brûlet, A.; Heinemann, A.; Simon, C.; Martin, C. **Magnetic field dependence of the nanometric magnetic phase separation in the $Pr_{1-x}Ca_xMnO_3$ manganite studied by Small-Angle Neutron Scattering** Physical Review B: Condensed Matter **73** (2006), 094438/ 1 - 9	V4 NMI3: 1017
Sazonov, A.P., I.O.Troyanchuk, D.P.Kozlenko, A.M.Balagurov, V.V.Sikolenko **Magnetic ordering in the $Nd_2CoMnO_{6+\delta}$ perovskite system** Journal of Magnetism and Magnetic Materials **302** (2006), 443 - 447	
Sazonov, A.P.; Troyanchuk, I.O.; Sikolenko, V.V. **Spin state of cobalt ions in $NdCoO_3$** Crystallography Reports **51** (2006), 11 - 15	E9 NMI3: 1075
Schorr, S.; Tovar, M.; Stuesser, N.; Sheptyakov, D.; Geandier, G. **Where the atoms are: cation disorder and anion displacement in $D^{II}X^{VI}$-$A^{I}B^{III}X^{VI}_2$ semiconductors** Physica B - Condensed Matter **385 - 386** (2006), 571 - 573	E6 E9
Schorr, S.; Wagner, G.; Tovar, M.; Sheptyakov, D. **Cation disorder and anion displacement in $D^{II}X^{VI}$ - $A^{I}B^{III}X^{VI}_2$ semiconductors** Physica Status Solidi (c) **3** (2006), 2614 - 2617	E6 E9
Schreiber, A.; I. Ketelsen, G. H. Findenegg, E. Hoinkis **Thickness of adsorbed nitrogen films in SBA-15 silica from small-angle neutron diffraction** Studies in Surface Science and Catalysis **160** (2007), 17 - 24	
Schreyer, A.; Reimers, W.; Wroblewski, T.; Haibel, A.; Pyzalla, A.; Clemens, H. **First autumn school on engineering materials science with neutrons and synchrotron radiation** Synchrotron Radiation News **19** (2006), 22 - 23	S5
Senff, D.; Link, P.; Hradil, K.; Hiess, A.; Regnault, L.P.; Sidis, Y.; Aliouane, N.; Argyriou, D.N.; Braden, M. **Magnetic excitations in multiferroic $TbMnO_3$** Physical Review Lettersarxiv:cond-mat/0610620 (2006)	
Shapiro, S.M.: Vorderwisch, P.; Habicht, K.; Hradil, K.; Schneider, H. **Observation of phasons in magnetic shape memory alloy Ni_2MnGa** Physical Review Lettersarxiv.org/ftp/cond-mat/0608/0608729.pdf (2006)	V2
Shin, T.; Findenegg, G.H.; Brandt, A. **Surfactant adsorption in ordered mesoporous silica studied by SANS** Progress in Colloid and Polymer Science **133** (2006), 116 - 122	V4
Sikolenko, V.; Sazonov, A. P.; Efimov, V.V.; Efimova, E.A.; Kriventsov, V.V.; Kochubej, D. I.; Zimmermann, U. **Phase separation in $La_{1-x}Sr_xCoO_3$ solid solutions with perovskite structure** Crystallography Reports **51** (2006), S67 - S75	E9 NMI3: 1168
Sikolenko, V.; Sazonov, A.; Efimov, V.; Krivencov, V.; Darowski, N.; Vyalikh, D. **Neutron diffraction and synchrotron radiation studies of $La_{1-x}Sr_xCoO_3$ magnetic properties** Journal of Magnetism and Magnetic Materialsdoi:10.1016/j.jmmm.2006.10.130 (2006)	E9

Stöber, S.; Prokhnenko, O.; Schorr, S.; Pöllmann, H. **Mangan modifizierte Perovskite in Tonerdezementsystemen** European Journal of Mineralogy **18** (2006), 137 - 137	E9
Stockert, O.; Deppe, M.; Faulhaber, E.; Jeevan, H.S.; Schneider, R.; Stußer, N.; Geibel, C.; Loewenhaupt, M.; Steglich, F. **Antiferromagnetism in $CeCu_2(Si_{1-x}Ge_x)_2$ nature of the A phase** Physica B: Condensed Matter **359 – 361** (2006), 349 - 356	E2/E6/E9
Stone, M.B.; Broholm, C.; Reich, D.H.; Vorderwisch, P.; Harrison, N. **Quantum criticality in an organic magnet** Physical Review Letters **96** (2006), 257203/ 1 - 4	V2
Strunz, P.; Schumacher, G.; Vaßen, R.; Wiedenmann A.; Ryukhtin, V. **In situ small-angle neutron scattering study of $La_2Zr_2O_7$ and $SrZrO_3$ ceramics for thermal barrier coatings** Scripta Materialia **55** (2006), 545 - 548	V4
Stüßer, N.; Sofin, M.; Bircher, R.; Güdel, H.-U.; Jansen, M. **Competing magnetic interactions in $Na_{10}Co_4O_{10}$ studied by neutron diffraction** Chemistry : A European Journal **12** (2006), 5452 - 5457	
Süllow, S.; Otop, A.; Klenke, J.; Feyerherm, R.; Hendrikx, R.W.A.; Mydosh, J.A. **Magnetic irreversibility in the antiferromagnetic state of UPt_2Si_2** Journal of Applied Physics **99** (2006), 08F704/1 - 3	E1/ E5
Süllow, S.; Wolter, A.U.B.; Feyerherm, R.; Rakoto, H.; Broto, J.M.; Glocke, S.; Klümper, A.; Honecker, A.; Brenig, W. **Magnetization of staggered *S = 1/2* antiferromagnetic Heisenberg chain systems** Journal of Physics: Conference Series **51** (2006), 183 - 186	S2
Sun, Z.; Y. -D. Chuang, A. V. Fedorov, J. F. Douglas, D. Reznik, F. Weber, N. Aliouane, D. N. Argyriou, H. Zheng, J. F. Mitchell, T. Kimura, Y. Tokura, A. Revcolevschi, D. S. Dessau **Quasiparticle-like peaks, kinks, and electron-phonon coupling at the (π,0) regions in the CMR oxide $La_{2-2x}Sr_{1+2x}Mn_2O_7$** Physical Review Letters **97** (2006), 056401/ 1 - 4	
Teichert, A, Krist, T., Mezei, F. **Stress dependence in $Fe_{89}Co_{11}$-Si multilayers on layer thicknesses** Physica B - Condensed Matter **385 - 386** (2006), 1262 - 1264	V14
Tovar, M.; Torabi, R.; Welker, C.; Fleischer, F. **Structural and magnetic properties of Cu-Ni-Cr spinel oxides** Physica B - Condensed Matter **385 - 386** (2006), 196 - 198	E9
Treimer, W. ; Strobl, M. ; Kardjilov, N. ; Hilger, A. ; Manke, I. **Wavelength tunable device for neutron radiography and tomography** Applied Physics Letters **89** (2006), 203504/ 1 - 3	V7
Triolo, A.; Russina, O.; Keiderling, U.; Kohlbrecher, J. **Morphology of Poly(ethylene oxide) Dissolved in a Room Temperature Ionic Liquid: A Small Angle Neutron Scattering Study** Journal of Physical Chemistry B **110** (2006), 1513 - 1515	V4 NMI3: 1134
Tripadus, V.; Radulescu, A.; Pieper, J.; Buchsteiner, A.; Podlesniak, A.; Janssen, S.; Serban, A. **Molecular Dynamics in Triglycine Sulphate by Cold Neutron Spectroscopy** Chemical Physics **322** (2006), 323 - 330	V3 NMI3: 1031 IHP II: 579
Troyanchuk, I. O.; D. V. Karpinsky, A. N. Chobot, D. G. Voytsekhovich, V. M. Dobryanskiy **Phase Transformations in $Pr_{1-x}Sr_xCoO_3$** Journal of Experimental and Theoretical Physics Letters **84** (2006), 151 - 155	E9
Troyanchuk, I. O.; M. V. Bushinsky, and D. V. Karpinsky **Magnetic Ordering in Manganites Substituted by Chromium Ions** Journal of Experimental and Theoretical Physics **103** (2006), 580 - 588	E6

Ulbricht, A.; Bergner, F.; Böhmert, J.; Valo, M.; Mathon, M.-H.; Heinemann, A. **SANS response of VVER440-type weld material after neutron irradiation, post-irradiation annealing and reirradiation** Philosophical Magazine A (2006), 1 - 16	V4
Ulbricht, A.; Bergner, F.; Dewhurst, C.; Heinemann, A. **Small-angle neutron scattering applied to post-irradiation annealed of neutron-irradiated pressure vessel steels** Journal of Nuclear Materials **353** (2006), 27 - 34	V4
Vasilovsky, S. G.; V. V. Sikolenko, A.I. Beskrovny, A.V. Belushkin, I. N. Flerov, A. Tressaud, A. M. Balagurov **Neutron diffraction studies of temperature induced phase transitions in Rb_2KFeF_6 Elpasolite** Zeitschrift für Kristallographie **23** (2006), 467 - 472	
Vokhmyanin, A.P.; Lee, S.; Jang, K.-H.; Podlesnyak, A.A.; Keller, L.; Prokes, K.; Sikolenko, V.V.; Park, J.-G.; Skryabin, Y.N.; Pirogov, A.N. **Commensurate-incommensurate phase transition in $TbNi_5$** Journal of Magnetism and Magnetic Materials **300** (2006), e411 - e414	E4
Vorderwisch, P.; Shapiro, S.M. **Phonon dispersion in the ferromagnetic shape-memory alloy Ni_2MnGa studied by neutron spectroscopy** Materials Science and Engineering A **438-440** (2006), 450 - 453	V2V2
Wiedenmann, A. **Magnetic and Crystalline Nanostructures in Ferrofluids as probed by Small Angle Neutron Scattering** Computer Simulations in Condensed Matter: From Materials to Chemical Biology, Vol. 2 **594** (2006), 33 - 58	V4
Wiedenmann, A.; Kammel, M.; Heinemann, A.; Keiderling, U. **Nanostructures and ordering phenomena in ferrofluids investigated using polarized small angle neutron scattering** Journal of Physics: Condensed Matter **18** (2006), S2713 - S2736	V4
Wiedenmann, A. ; Keiderling, U. ; Habicht, K. ; Russina, M. ; Gähler, R. **Dynamics of field-induced ordering in magnetic colloids studied by new time-resolved small-angle neutron-scattering techniques** Physical Review Letters **97** (2006), 057202/ 1 - 4	V3/ V4
Wiedenmann, A.; Keiderling, U.; May, R.P.; Dewhurst, C. **Dynamics of field-induced ordering processes in ferrofluids studied by polarised small-angle neutron scattering** Physica B - Condensed Matter **385 - 386** (2006), 453 - 456	V3/ V4
Wimpory, R.C.; Biglari, F.R.; Schneider, R.; Nikbin, K.M.; O'Dowd, N.P. **Effect of residual stress on high temperature deformation in a weld stainless steel** Materials Science Forum **524 - 525** (2006), 311 - 316	E3
Wimpory, R.C.; Ohms, C.; Hornak, P.; Neov, D.; Youtsos, A.G. **Residual strain measurement of C/C-SiC tubes at high temperature** Materials Science Forum **524 - 525** (2006), 665 - 670	
Wolska, E.; Darul, J.; Nowicki, W.; Piszora, P.; Tovar, M.; Prokhnenko, O.; Baehtz, C.; Knapp, M. **X-ray and neutron studies on cation distribution in the $LiMn_2O_4/LiFe_5O_8$ spinel solid solution** Acta Crystallographica Section A: Foundations of Crystallography **A62** (2006), 198	E9 NMI3: 1218
Wolska, E; Tovar, M; Andrzejewski, B; Nowicki, W; Darul, J; Piszora, P; Knapp M; **Structural and magnetic properties of the iron substituted lithium-manganese spinel oxide** Solid State Sciences **8** (2006), 31 - 36	E9 NMI3: 1143

Zabler, S.; Riesemeier, H.; Fratzl, P.; Zaslansky, P. **Fresnel-propagated imaging for the study of human tooth dentin by partially coherent x-ray tomography** Optics Express **14** (2006), 8584 - 8597	S5
Zvyagin, S.A.; Wosnitza, J.; Kolezhuk, A.K.; Krzystek, J.; Feyerherm, R. **Elementary excitations in S = 1/2 Heisenberg spin chains with alternating g-tensor and the Dzyaloshinskii-Moriya interaction** Journal of Physics: Conference Series **51** (2006), 39 - 42	S2

Seminars and Conference Contributions 2006

Invited Talks

2005 (supplement)

Danilyan, G.; Fedorov, A.; Krakhotin, V.; Pavlov, V.; Brakhman, E.; Karpikhin, I.; Korobkina, E.; Golub, R.; Wilpert, T. **Search for Scission in Neutrons Using Specific Angular Correlations in U-235 Fission Induced by Slow Polarized Neutrons** LV National Conference on Nuclear Physics “Frontiers in the Physics of Nucleus”, Saint-Petersburg, Russia, 28.06. - 01.07.2005	V13

2006

Argyriou, D. N. **Opening the devils flower: complex magnetism in multiferroic perovskites manganites** Theoretical and Experimental Magnetism Meeting, Abingdon, UK, 03.08. - 04.08.2006	
Argyriou, D. N. ; Prokhnenko, O. ; Kiefer, K.; Milne, C. J. **Evidence for weak charge ordering above TN in near half doped $Na_{0.46}CoO_2$** First International workshop on the physical properties of lamellar cobaltates, Orsay, France, 16.07. - 20.07.2006	
Argyriou, D.N. **Opening the Devils Flower: Complex Structure and Magnetism in Multiferroic Perovskite Manganites** Self-organized Strongly Correlated Electron Systems, Seillac, France, 29.05. - 31.05.2006	
Argyriou, D.N. **Jahn-Teller Correlations and Dynamics in Manganites** International Symposium on the Jahn-Teller Effects: Novel Aspects in Orbital Physics and Vibronic Dynamics of Molecules and Crystals, Trieste, Italy, 28.08. - 01.09.2006	
Bentley, P. M. **Evolution in the guide halls** Invited seminar, Hahn-Meitner Institut, 23.01. - 23.01.2006	
Bentley, P. M. **Evolution in the guide halls** Invited seminar, Institut Laue-Langevin, Grenoble, France, 06.02. - 06.02.2006	
Danilyan, G. **Search for Scission in Neutrons Using Specific Angular Correlations in U-235 Fission Induced by Slow Polarized Neutrons** XL PNPI Winter School on Nuclear and Particle Physics, Russia, St.Petersburg, Repino, 20.02. - 25.02.2006	V13
Darowski, N.; Dudzik, E.; Feyerherm, R. **Structural and magnetic transitions in MnAs/GaAs epitaxial films and perovskite manganite single crystals** Kolloquium des Laboratoriums für Neutronenstreuung des Paul-Scherrer-Instituts, Villingen, Schweiz, 15.03. - 15.03.2006	

Denks, I.A. **Diffraktometrische Eigenspannungsanalyse mit weißer Synchrotronstrahlung - Grundlagen, Anwendungen und Perspektiven** Werkstoffseminar, Kassel, 30.10. - 30.10.2006	
Genzel, C. **X-ray diffraction analysis of residual stress fields in thin films - basic aspects and applications** Frühjahrstagung der Deutschen Physikalischen Gesellschaft (DPG), Dresden, 27.03. - 31.03.2006	
Habicht, K. **Phonon and magnon linewidths measured with TAS / NRSE** ILL - College 4 Seminar, ILL, Grenoble, France, 10.03. - 10.03.2006	
Habicht, K. **Polarized Neutron Scattering at the Cold-Neutron Triple-Axis Spectrometer V2/FLEX at BENSC** Workshop on Inelastic Neutron Spectrometers 2006 (WINS2006), Berlin, 29.09. - 30.09.2006	
Hoell, A. **Zur Charakterisierung von Nanostrukturen mit Röntgen-Kleinwinkelstreuung** Kolloquiumsvortrag an der Universität Halle im Rahmen eines Sonderforschungsbereiches, Halle, Germany, 12.12. - 12.12.2006	
Holub-Krappe, E. **Soft X-Ray Studies of Spin Reorientation in Thin Au/Co/Au Films** Int. Workshop on Properties of Ultrathin Magnetic Films, Bialowieza, Poland, 07.09. - 09.09.2006	
Ivanova, O. **Temperature Dependence of the Structure of Polyelectrolyte Multilayer Films** IMPRS Graduate School, Greifswald, 22.06. - 22.06.2006	V6
Jauch, W.; Reehuis,M. **Charge density in paramagnetic chromium from gamma-ray diffraction** 4th European Charge Density Meeting, Brandenburg (Havel), 26.01. - 29.01.2006	
Jauch, W.; Reehuis,M. **Charge density in paramagnetic chromium from gamma-ray diffraction** Sagamore XV Conference on Electron Charge Spin and Momentum Densities, Market Bosworth, GB, 13.08. - 18.08.2006	
Krist, T. **Developments in neutron optics** American Conference on Neutron Scattering, Saint Charles, Ill, USA, 18.06. - 22.06.2006	
Peters, J.; Mezei, F. **General Time-of-Flight Technique for ultra-high Resolution Diffraction on a continuous Source** ESS-S workshop on long pulse instrumentation, Lund, Sweden, 20.04. - 21.04.2006	
Peters, J.; Mezei, F. **Le nouvel instrument EXED (Extreme Environment Diffractometer) au Hahn-Meitner-Institut de Berlin** 14èmes Journées de la Diffusion Neutronique, Murol (Puy de Dôme), 17.05. - 19.05.2006	

Peters, J.; Treimer, W.; Mezei, F. **Etude des domaines magnétiques et des parois de Bloch dans un monocristal de nickel par la diffusion de neutrons** 14èmes Journées de la Diffusion Neutronique, Murol (Puy de Dôme), 17.05. - 19.05.2006	
Prokhnenko, O. **Pressure induced helimagnetism in Fe-rich intermetallic compounds** 44th EHPRG Conference, Prague, Czech Republic, 03.09. - 08.09.2006	E4 NMI3: 1047 NMI3: 1085 NMI3: 1118
Prokhnenko, O.; Kamarad J.; Prokes, K.; Arnold, Z.; Andreev, A.V **Helimagnetism in Fe-rich intermetallic compounds** 44th European High Pressure Research Group International Conference, Prague, 04.09. - 08.09.2006	
Rüegg, Ch. **Quantum critical points in magnetic insulators** Condensed Matter and Material Physics Conference of the Institute of Physics, Exeter, UK,	V2 NMI3: 1127 NMI3: 1164
Rüegg, Ch. **Investigation and characterization of the excitation spectrum and of the field-, pressure-, and doping-induced quantum phase transitions in quantum spin systems** Annual Meeting of the Swiss Physical Society, Lausanne, Switzerland	V2 NMI3: 1006
Rüegg, Ch. **Quantum phase transitions in S=1/2 ladder and dimer spin systems** International Conference on Low Energy Electrodynamics in Solids, Tallinn, Estonia	V2 NMI3: 1127 NMI3: 1164
Rüegg, Ch. **The phase diagrams of gapped quantum spin systems studied by inelastic neutron scattering** International Conference on Magnetism, Kyoto, Japan	V2 NMI3: 1127 NMI3: 1164
Rüegg, Ch. **Finite-temperature effects on the excitation spectrum in quantum critical magnetic insulators** Computational Approach to Quantum Critical Phenomena, Kashiwa, Japan	V2 NMI3: 1127 NMI3: 1164
Rüegg, Ch. **Field-induced quantum phase transitions in low-dimensional magnetic insulators** Strongly Correlated Transition Metal Compounds II, Cologne, Germany	V2 NMI3: 1127 NMI3: 1164
Rupp, A., Klenke, J. **Assembling of the filling station and local refilling set-up for SANS** 6th NSF-JRA Committee meeting, Berlin, 28.09. - 28.09.2006	
Schneider, R. **Residual Stress and Texture Analysis using Neutron and Synchrotron Radiation** Materialwissenschaftliches Seminar, Universität Kassel, 26.05. - 26.05.2006	
Schneider, R.; Fähler, S. **Development of a Web-Database to Achieve Consistency in SPP 1239 Results** DFG Schwerpunkt 1239 Meeting, IFW Dresden, 19.09. - 20.09.2006	
Schneider, R.; Hofmann, M.; Genzel, C. **Ortsaufgelöste, zerstörungsfreie Ermittlung von Eigenspannungen im Innern von hochbelasteten industriellen Bauteilen** Härtereikolloquium, Wiesbaden, 11.10. - 13.10.2006	

Schneider, R.; Hofmann, M.; Genzel, C. **Ortsaufgelöste, zerstörungsfreie Ermittlung von Eigenspannungen im Innern von hochbelasteten industriellen Bauteilen** AWT Fachausschuss Qualitätssicherung, Hagen, 06.12. - 06.12.2006	
Schneider, R.; Hofmann, M.; Wimpory, R.; Poeste, T.; Rebelo-Kornmeier, J. **The new and refurbished materials science diffractometers at BER II and FRM II - standardization and automation** Workshop POLDI, PSI(CH), 27.10. - 27.10.2006	
Schneider, R.; Hofmann, M.; Wimpory, R.; Poeste, T.; Rebelo-Kornmeier, J. **The new and refurbished materials science diffractometers at BER II and FRM II - current projects in co-operation with industry** BBAA Workshop “Leightweight Aero Structures Design and Repair Technology”, Berlin, 22.11. - 22.11.2006	
Schneider, R.; Mecklenburg, A. **Development of Magnetic Shape Memory Actuators Based on the Standardization of Crystal Growth, Treatment, Training and Quality Assurance** DFG Schwerpunkt 1239, Stiftung Caesar, Bonn, 13.03. - 14.03.2006	
Schorr, S. **Structural aspects of adamantine like multinary chalcogenides** E-MRS Spring Meeting, Nizza, Frankreich, 29.05. - 02.06.2006	E6 E9
Steitz, R. **Neutron reflectivity in soft matter** ADAM Workshop, Bochum, 19.05. - 19.05.2006	
Vakhrushev, S.; Golosovsky, I.; Kumzerov, Yu.; Naberezhnov, A.; Fokin, A.; Hansen, T.; Tovar, M.; Kutnjak, Z.; Vodopivec, B.; Zalar, B.; Lebar, A.; Blinc, R. **Porous matrices based ferroelectric and magnetic materials** Fundamental Physics of Ferroelectrics 2006, Williamsburg, VA, USA, 12.02. - 15.02.2006	
Wimpory, R. C.; Ohms, C.; Hornak, P.; Neov, D.; Youtsos, A. G. **Residual Strain measurement of C/C-SiC tubes at high temperature** The 7th European Conference on Residual Stresses 13-15 September 2006 Berlin, Germany, Berlin, 13.09. - 15.09.2006	
Wimpory, R.C **Neutron measurements 2005-2006 For VAMAS TWA 31** VAMAS TWA 31 Meeting, Geesthacht (Hamburg), Germany., 18.12. - 18.12.2006	
Wimpory, R.C. **Residual stress measurements for SKF** SKF Engineering Research Centre, Nieuwegein The Netherlands, 12.01. - 12.01.2006	
Wimpory, R.C. **NET Task Group 1:** **Residual Stress Analysis for a Single Bead on Plate Weld** NET-European Network, 10th Steering Committee Meeting, JRC-Petten, Petten, Holland, 30.11. - 01.12.2006	
Wimpory, R.C. **The complimentary use of SANS and Diffraction in industry** **Part : 1** NET-10th Steering Committee Meeting, JRC-Petten, Petten, Holland, 30.12. - 01.12.2006	

Wimpory, R.C.; Biglari, F. R.; Schneider, R.; Nikbin, K. M.; O'Dowd, N. P. **Effect of residual stress on high temperature deformation and cracking in a weld stainless steel** The 7th European Conference on Residual Stresses, Berlin, 13.09. - 15.09.2006	
Wimpory, R.C.; Hofmann, M.; Poeste, T.; Rebelo-Kornmeier, J.; Garbe, U.; Schneider, R. **Neutron Instruments for Materials Research** Joint NET PECO workshop and 9th NET Steering Committee Meeting, Yeditepe University, Istanbul, 08.06. - 09.06.2006	
Wimpory, R.C.; Nikbin, K. **Assessment of residual stresses in cracked Fracture Mechanics CT specimens.** Deutsche Tagung für Forschung mit Synchrotronstrahlung, Neutronen und Ionenstrahlen an Großgeräten 2006, Hamburg, 04.10. - 06.10.2006	

Seminars and Conference Contributions 2006

Talks

2006

Aliouane, N.; Argyriou,D.N.; Strempfer, J.; Zegkinoglou, I.; Zimmerman, M. v. **Field induced linear magneto-elastic coupling in multiferroic $TbMnO_3$** 2006 American Physical Society March Meeting, Baltimore, USA, 13.03. - 17.03.2006	E9
Aliouane, N.; Argyriou,D.N.; Landsgesell, S. **Field induced incommensurate to commensurate magnetic transition in multiferroic $TbMnO_3$** DPG-Tagung, , 27.03. - 31.03.2006	
Aliouane, N.; Argyriou,D.N.; Strempfer, J.; Zegkinoglou, I.; Landsgesell, S.; Zimmermann, M. v. **Field induced magneto-structural transition in multiferroic $TbMnO_3$** German Conference for Research with Synchrotron Radiation, Neutrons and Ion Beams at Large Facilities 2006, Hamburg, 04.10. - 06.10.2006	
Andersson, C.; Konishi, T.; Holub-Krappe, E.; Karis, O.; Hunter Dunn, J.; Maletta, H.; Arvanitis, D. **Revising the spin-reorientation in in-situ prepared Au/Co/Au ultra-thin films by means of XAFS** 13th Int. Conf. on X-ray Absorption Fine Structure, Stanford, CA, USA, 09.07. - 15.07.2006	
Argyriou, D. **Charge Localization and near zero in-plane thermal expansion in layered $NaCoO_2x12$** 2006 American Physical Society March Meeting, Baltimore USA, 13.03. - 17.03.2006	

Argyriou, D.N.; Aliouane, N.; Strempfer, J.; Zegkinoglou, I.; Zimmermann, M. v. **Melting of magneto-electric state in $TbMnO_3$ with c-axis aligned magnetic field** German Conference for Research with Synchrotron Radiation, Neutrons and Ion Beams at Large Facilities 2006, Hamburg, 04.10. - 05.10.2006	
Argyriou, D.N.; Chapon, L.C.; Milne, C.; Prokhnenko, O.; Radaelli, P.G. **Structural and Electronic properties of the Layered Na_xCoO_2** DPG-Tagungen, Dresden, 27.03. - 31.03.2006	
Arvanitis, D.; Andersson, C.; Konishi, T.; Holub-Krappe, E.; Karis, O.; Maletta, H. **Magnetization reorientation in Au/Co: in-situ prepared ultrathin films** Frühjahrstagung Festkörperphysik der DPG, Dresden, Germany, 27.03. - 31.03.2006	
Barath, H.; Kim, M.; Cooper, S.L.; Mahns, I.; Ruebhausen, M.; Argyriou, D.N. **Investigation of coupling between antiferromagnetic and ferroelectric orders in $TbMnO_3$ using magnetic field dependent Raman scattering** 2006 American Physical Society March Meeting, Baltimore USA, 13.03. - 17.03.2006	
Berggold, K.; Lorenz, T.; Baier, J.; Meier, D.; Hemberger, J.; Argyriou, D.N.; Vasiliev, A.; Hemberger, J. **Thermal transport in multiferroics** DPG Tagung, Dresden, 27.03. - 31.03.2006	
Helm, C.A. **Effect of Deposition Temperature on Internal Order of Polyelectrolyte Multilayers** Polyelectrolytes 2006, Dresden, 04.09. - 08.09.2006	V6
Erné, B.H. **Microstructure and magnetism of monodisperse magnetite ferrofluids** EUROMECH Colloquium 470, Recent Development in Ferrofluid Research, Dresden, Germany, 27.02. - 01.03.2006	V4 NMI3: 1140
Garvey, C.J.; Strobl, M.; Loidl, R.; Kuchel, P. W. **Red Blood Cell Shape and Volume Changes Observed by SANS** AUSTRALIAN SOCIETY FOR BIOPHYSICS,30th Annual Scientific Meeting, ASB2006, University of Sydney, 11.12. - 13.12.2006	V12a
Garvey, C.J.; Strobl, M.; Loidl, R.; Kuchel, P. W. **Red Blood Cell Shape and Volume Changes Observed by SANS** 5th AINSE/ANBUG Neutron Scattering Symposium (AANSS 2006), Lucas Heights, Australia, 11.12. - 13.12.2006	V12a
Gondek, L.; Szytula, A.; Kaczorowski, D.; Szewczyk, A.; Gutowska, M.; Prokhnenko, O. **Complex magnetic properties of $Ho_3Cu_4Sn_4$** 15th International Conference on Solid Compounds of Transition Elements, Krakow, Poland, 15.07. - 20.07.2006	E9 NMI3: 1174
Habicht, K.; Aynajian, P.; Keller, T.; Mezei, F.; Keimer, B. **Effect of the Superconducting Transition on Phonon Lifetimes in Nb investigated with the Neutron Resonance Spin-Echo technique** Polarised Neutrons in Condensed Matter Investigations (PNCMI 2006), Berlin, Germany, Berlin,, 25.09. - 28.09.2006	
Haibel, A.; Scheuerlein, C.; Hoffmann, J.-U.; Schneider, R.; Banhart, J. **Phase analysis in multifilament Nb3Sn superconduction strands during in-situ heat treatments using neutron diffraction** European Powder Diffraction Conference,EPDiC-10, Geneva, 01.09. - 04.09.2006	

Haibel, A.; Scheuerlein, C.; Schneider, R.; Hoffmann, J.-U.; Wimpory, R.; Lake, B.; Banhart, J.; Tennant, A. **Investigation of the Nb_3Sn phase formation in multifilamentary superconductors using synchrotron tomography and neutron diffraction** SRMS-5, Chicago, USA, 30.07. - 02.08.2006	
Heinemann, A.; Wiedenmann, A.; Kammel, M. **SANS signatures of local magnetic colloid structure reordering under external magnetic field variation** SAS 2006, Kyoto, Japan, 09.07. - 13.07.2006	
Hoell, A.; Haug, J.; Tatchev, D.; Haas, S.; Boesecke, P.; Wollgarten, M.; Sahoo, K. L.; Banhart, J. **Element sensitive investigation of phase formation in $Al_{94-x}Ni_6La_x$ (x=5, 7) alloys by ASAXS** Small Angle Scattering 2006 (SAS 2006), Kyoto, Japan, 09.07. - 13.07.2006	
Hoell, A.; Zizak, J.; Haas, S.; Tatchev, D.; Banhart, J. **The A- and Gi-SAXS dedicated SAXS instrument at Bessy 7T wiggler** SNI2006, Hamburg, Germany, 04.10. - 06.10.2006	
Holub-Krappe,E.; Hahlin, A.; Maletta, H.; Andersson, C.; Karis, O.; Hunter Dunn, J.; Arvanitis, D. **On the temperature driven reorientation in Au/Co/Au: the influence of the structure** Frühjahrstagung Festkörperphysik der DPG, Dresden, Germany, 27.03. - 31.03.2006	
Kamarad, J.; Prokhnenko, O.; Prokes, K.; Arnold, Z. **Magnetic Moments and Structures in Fe-rich Intermetallics under Pressure** Novel Pressure-induced Phenomena in Condensed Matter Physics, Fukuoka, Japan, 26.08. - 29.08.2006	E4 NMI3: 1085 NMI3: 1047 NMI3: 1118
Kammel, M.; Wiedenmann, A.; Heinemann, A.; Pop, L.M. **Different types of ordering in Cobalt ferrofluids investigated by Small Angle Neutron Scattering** International Conference on Magnetism 2006, Kyoto, Japan, 20.08. - 25.08.2006	
Kardjilov, N.; Hilger, A.; Manke, I.; Strobl, M.; Treimer, W. **Specifics of the neutron tomography in NDT** 9th European Conference on Non-Destructive Testing, Berlin, Germany, 25.09. - 29.09.2006	
Kardjilov, N.; Hilger, A.; Manke, I.; Strobl, M.; Treimer, W.; Banhart, J. **Strain mapping by energy-selective neutron radiography** DPG Tagung 2006, Dresden, 27.03. - 31.03.2006	
Kardjilov, N.; Hilger, A.; Manke, I.; Strobl, M.; Treimer, W.; Banhart, J. **Multifunctional tomography instrument with cold neutrons at HMI** 8th World Conference on Neutron Radiograhy 2006, Gaithersburg, USA, 16.10. - 19.10.2006	
Kardjilov, N.; Hilger, A.; Manke, I.; Strobl, M.; Treimer, W.; Banhart, J. **Phase-contrast tomography with cold neutrons using the propagation technique** 8th World Conference on Neutron Radiography 2006, Gaithersburg, USA, 16.10. - 19.10.2006	
Kardjilov, N.; Hilger, A.; Manke, I.; Strobl, M.; Treimer, W.; Banhart, J. **The new cold neutron radiography and tomography instrument CONRAD at HMI Berlin** DPG-Frühjahrstagung 2006, Dresden, Germany, 27.03. - 31.03.2006	

Kardjilov, N.; Hilger, A.; Manke, I.; Strobl, M.; Treimer, W.; Banhart, J. **Strain mapping by energy-selective neutron radiography** DPG-Frühjahrstagung 2006, Dresden, Germany, 27.03. - 31.03.2006	
Kardjilov, N.; Hilger, A.; Manke, I.; Strobl, M.; Treimer, W.; Banhart, J. **Specifics of the neutron tomography in NDT** ECNDT 2006, Berlin, 25.09. - 29.09.2006	
Keiderling, U.; Wiedenmann, A. **Field-dependent relaxation behaviour of Co-ferrofluid investigated with stroboscopic time-resolved SANS** Polarised Neutrons in Condensed Matter Investigations, Berlin, Germany, 25.09. - 28.09.2006	
Klaus, M. **Energiedispersive Materialforschung an der Synchrotronbeamline EDDI bei BESSY - Rückblick auf ein Jahr Messbetrieb, Stand und Perspektiven** Sitzung des FA13 der AWT Eigenspannungen, , 30. - 31.05.2006., München, 30.05. - 31.05.2006	
Klaus, M. **X-Ray Diffraction Analysis of Nonuniform Residual Stress Fields sii(t) under Difficult Conditions** 7th European Conference on Residual Stresses (ECRS-7), Berlin, 13.09. - 15.09.2006	
Klaus, M.; Denks, I.; Genzel Ch. **Residual stress analysis in multilayer systems with synchrotron radiation - complementary investigations using angle and energy dispersive diffraction methods** DPG (Deutsche Physikalische Gesellschaft e.V.) - spring meeting of the Division of Condensed Matter, Dresden, 26.03. - 31.03.2006	
Mahns, I.; Bastjan, M.; Rauer, R.; Neuber, G.; Schulz, B.; Mueller, S.; Rusydi, A.; Ruebhausen, M.; Argyriou, D. N.; Kim, M.; Barath, H.; Cooper, S.L. **Temperature depending studies of multiferroic $TbMnO_3$ by spectral ellipsometry and Raman scattering** 2006 American Physical Society March Meeting, Balitmore, USA, 13.03. - 17.03.2006	
Mahns, I.; Bastjan, M.; Rauer, R.; Neuber, G.; Schulz, B.; Mueller, S.; Rusydi, A.; Ruebhausen, M.; Argyriou, D. N.; Kim, M.; Barath, H.; Cooper, S.L. **Resonant soft X-ray scattering from $LaMnO_3$ and $SmMnO_3$ Superlattices** 2006 American Physical Society March Meeting, Baltimore USA, 13.03. - 17.03.2006	
Mahns, I.; Bastjan, M.; Rauer, R.; Neuber, G.; Schulz, B.; Mueller, S.; Rusydi, A.; Ruebhausen, M.; Argyriou, D. N.; Kim, M.; Barath, H.; Cooper, S.L. **Resonant soft X-ray scattering from multiferroic $TbMnO_3$** 2006 American Physical Society March Meeting, Balitmore, USA, 13.03. - 17.03.2006	
Manke, I.; Haibel, A.; Rack, A.; Kardjilov, N.; Hilger, A.; Zabler, S.; Melzer, A.; Banhart, J. **In-situ investigation of discharge of alkaline batteries by means of tomography** ECNDT-9, Berlin, 25.09. - 29.09.2006	
Manke, I.; Kardjilov, N.; Hartnig, C.; Hilger, A.; Strobl, M.; Treimer, W.; Lehnert, W.; Banhart, J. **Neutron radiography and tomography on fuel cells** ECNDT-9 2006, Berlin, 25.09. - 29.09.2006	
Naberezhnov, A.; Fokin, A.; Vakhrushev, S.; Korotkov, L.; Dyadkin, V.; Tovar, M.; Kutnjak, Z.; Vodopivec, B.; Zalar, B.; Lebar, A.; Blinc, R.; Kinka, M.; Banys, J.	E2 E9

Ferroelectrics in confinement 4th Conference International Dielectric Society and 9th International Conference Dielectric and Related Phenomena IDS&DRP 2006, Poznan, Poland, 03.09. - 07.09.2006	
Perroud, O.; Wiedenmann, A.; Kumar, G.; Eckert, J.; Kohlbrecher, J. **Influence of Nd-nanoparticles on hard magnetic properties of bulk amorphous alloys studied by small-angle neutrons scattering** Nano 2006, Bangalore, Indien, 20.08. - 25.08.2006	
Peters, J.; Mezei, F. **First Results at the new Extreme Environment Diffractometer (EXED) at the Hahn-Meitner-Institut Berlin** EPDIC 10European Powder Diffraction Conference, Geneva, 01.09. - 04.09.2006	
Prokhnenko, O.; Feyerherm, R.; Dudzik, E.; Landsgesell, S.; Aliouane, N.; Chapon, L.C.; Argyriou, D.N. **Induced Dy spin-order enhancing the ferroelectric polarization in $DyMnO_3$** 5th Workshop on Orbital Physics and Novel Phenomena in Transition Metal Oxides, Berlin, 11.10. - 12.10.2006	
Schneider, R.; Hofmann, M.; Wimpory, R.; Poeste, T.; Rebelo-Kornmeier, J. **The new and refurbished materials science diffractometers at BER II and FRM II - current projects in co-operation with industry** AWT Fachausschuss Eigenspannungen, Garching, 31.05. - 31.05.2006	
Schorr, S. Tovar, M. Hoebler, H.-J. **Neutron diffraction structure investigation of the stannite-kesterite join** Workshop Neutrons for Geoscience, München, 14.07.2006	E9
Schorr, S.; Tovar, M.; Hoebler, H.-J. **The stannite-kesterite join studied by neutron diffraction** 19th general Meeting of the Interantional Mineralogical Association, Kobe, Japan, 24.07. - 28.07.2006	E9
Schorr, S.; Tovar, M.; Hoebler, H.-J. **Structure investiagtions of the solid solution series Cu_2FeSnS_4 Cu_2ZnSnS_4** 15th International conference on ternary and multinary compounds, Kyoto, Japan, 06.03. - 10.03.2006	E9
Schorr, S.; Tovar, M.; Hoebler, H.-J. **Neutron diffraction study of the multinary chalcogenides $CuFe_{1-x}Zn_xSnS_4$ a potential photovoltaic material** Deutsche Tagung für Forschung mit Synchrotronstrahlung, Neutronen und Ionenstrahlen an Großgeräten, Hamburg, 04.10. - 06.10.2006	E9
Sikolenko, V. **Neutron scattering studies of the Co-based perovskite-type systems** V workshop on investigation at IBR-2, Dubna, 06.06. - 14.06.2006	
Sikolenko, V.; Sazonov, A.; Efimov, V.; Krivencov, V.; Darowski, N.; Vyalikh, D. **Neutron diffraction and synchrotron radiation studies of $La_{1-x}Sr_xCoO_3$ magnetic properties** International Conference on Magnetism Kyoto, Japan, Kyoto, 20.08. - 25.08.2006	
Steitz, R.; Wong, J. E.; von Klitzing, R.; **Swelling kinetics and structural changes of polyelectrolyte multilayers in contact with aqueous solution and water vapor** SNI2006, Hamburg, 04.10. - 06.10.2006	
Steitz, R.; Wong, J.E.; v. Klitzing, R.; **Kinetics of water uptake and release of polyelectrolyte multilayers** 20th European Colloid and Interface Society Conference, Budapest, 17.09. - 22.09.2006	

Strempfer, J.; Aliouane, N.; Bohnenbuck, B.; Argyriou, D. N.; Zegkinoglou, I.; Zimmermann, M. v. **Magnetic field induced linear magneto-elastic coupling in multiferroic $TbMnO_3$** DPG-Tagung, Dresden, 27.03. - 31.03.2006	
Stüßer, N.; Sadykov, R.; Hoser, A. **Neutronenbeugungsuntersuchungen zur druckabhängigen magnetischen Struktur in $CsCuCl_3$** Deutsche Tagung für Forschung mit Synchrotronstrahlung, Neutronen und Ionenstrahlen an Großgeräten 2006SNI 2006, Hamburg, 04.10. - 06.10.2006	
Tatchev, D.; Goerigk, G.; Hoell, A.; Valova, E.; Kranold, R.; Armyanov, S.; Dille, J. **Composition of nanoprcipitates in Ni_{83} P_{17} amorphous alloy** NANOPHEN International Workshop, Sandanski, Bulgaria, 25.03. - 30.03.2006	
Wiedenmann, A.; Keiderling, U.; Habicht, K.; M. Russina,M.; Gähler,R. **Time-resolved SANS studies of field-induced ordering in ferrofluids** Deutsche Tagung für Forschung mit Synchrotronstrahlung, Neutronen und Ionenstrahlen an Großgeräten 2006 (SNI 2006), Hamburg, Germany, 04.10. - 06.10.2006	
Wiedenmann, A.; Keiderling, U.; Habicht, K.; Russina, M.; Gähler, R. **Time-resolved SANS studies (TISANE) of field induced ordering in Ferrofluids** SAS 2006, Kyoto, Japan, 09.07. - 13.07.2006	
Wiedenmann, A.; Keiderling, U.; Kammel, M.; Heinemann, A.; May, R.P.; Dewhurst, Ch. **Statics and dynamics of field induced ordering in Ferrofluids studied by Polarised Small Angle Neutron Scattering** Nanotech 2006, Boston, USA, 07.05. - 11.05.2006	
Zabler, S.; Zaslansky, P.; Thermann, K.; Riesemeier, H.; Kremmin, B. **The use of Fresnel propagation in 3D hard x-ray imaging of mineral matter** XTOP, Karlsruhe, Germany, 19.09. - 22.09.2006	

Seminars and Conference Contributions 2006

Poster

2005 (supplement)

Lenné, T.; Gary Bryant, G.; Garvey, C.J.; Keiderling U.; Koster, K.L. **Location of sugars in multilamellar membranes at low hydration** 2005 International Conference on Neutron Scattering, Sydney, Australia, 27.11.2005	V4

2006

Argyriou, D.N.; Prokhnenko, O.; Kiefer, K.; Milne, C. **Possible evidence for weak charge ordering near half doping in $Na_{0.46}CoO_2$** German Conference for Research with Synchrotron Radiation, Neutrons and Ion Beams at Large Facilities 2006, Hamburg, 03.10. - 04.10.2006	
Bastjan, M.; Rusydi, A.; Neuber, G.; Singer, S.; Ruebhausen, M.; Argyriou, D.N.; Aliouane, N.; Kim, M.; Barath, H.; Cooper, S.L. **Role of the orbital-lattice interaction in multiferroic behavior** German Conference for Research with Synchrotron Radiation, Neutrons and Ion Beams at Large Facilities 2006, Hamburg, 04.10. - 05.10.2006	
Bohnenbuck, B.; Strempfer, J.; Zegkinoglou, I.; Aliouane, N.; Argyriou, D.N.; Landsgesell, S.; Zimmermann, M.v. **Investigation of multiferroic $TbMnO_3$ and $DyMnO_3$ in high magnetic fields** German Conference for Research with Synchrotron Radiation, Neutrons and Ion Beams at Large Facilities 2006, Hamburg, 04.10. - 06.10.2006	
Bordallo, H. N. **Remarkable physical properties triggered by dynamical Jahn-Teller effect in the chiral amino-acid Alanine** International Symposium on the Jahn-Teller Effects: Novel Aspects in Orbital Physics and Vibronic Dynamics of Molecules and Crystals, Trieste, Italy, 28.08. - 31.08.2006	
Bordallo, H. N.; Aldridge, L.P.; Desmedt, A. **Water dynamics in hardened cement paste - from Inelastic Neutron Scattering** Deutsche Tagung für Forschung mit Synchrotronstrahlung, Neutronen und Ionenstrahlen an Großgeräten 2006, Hamburg, 04.10. - 06.10.2006	
Bordallo, H. N.; Jalarvo, N.; Aliouane, N.; Pieper, J.; Adams, M.A.; Argyriou, D.N. **Understanding the role of water in the superconductor $Na_{0.28}CoO_2$ $1.3H_2O$ using inelastic neutron scatering** Deutsche Tagung für Forschung mit Synchrotronstrahlung, Neutronen und Ionenstrahlen an Großgeräten 2006, Hamburg, 04.10. - 06.10.2006	
Bordallo, H.N.; Aldridge, L.P.; Desmedt, A. **Water dynamics in micro-pores & interlayer space in cement paste** Workshop 3rd International Workshop on Dynamics in Confinement, Grenoble, France, 23.03. - 26.03.2006	
Bordallo, H.N.; Argyriou, D.N.;Strempfer, J.; Barthès, M.; Dénoyer, F. **Negative thermal expansion and confomation changes in the smallest chiral amino acid, Alanine** DPG - German Physical Society, Dresden, 27.03. - 31.03.2006	

Bordallo, H.N.; Kalceff, W.; Argyriou, D.N.; Barthès, M.; Seydel, T.; Fehr, C.; Juranyi, F. **Hydrogen in N-Methylacetamide: Positions and dynamics of the hydrogen atoms using neutron scattering** Deutsche Tagung für Forschung mit Synchrotronstrahlung, Neutronen und Ionenstrahlen an Großgeräten 2006, Hamburg, 04.09. - 05.10.2006	
Clemens, D.; Peters, J.; Bleif, H.J.; Pappas, C.; Mezei, F. **Instrumentierung in der Neutronenleiterhalle-II bei BENSC** SNI2006, Hamburg, 04.10. - 06.10.2006	
Darowski, N., Zizak I.; Gupta A.; Erko, A.; Meneghini, C. **Depth profiling of marker layers with sub-nanometer spatial resolution using X-ray waveguide structures.** BESSY Users' Meeting 2006, Berlin, 07.12. - 08.12.2006	
Darowski, N., Zizak, I.; Gupta, A.; Erko, A.; Meneghini, C. **Tiefenaufgelöste Charaktersierung der ioneninduzierten Durchmischung von dünnen Marker-Schichten mittels Röntgenabsorption in Wellenleitergeometrie** Deutsche Tagung für Forschung mit Synchrotronstrahlung, Neutronen und Ionenstrahlen an Großgeräten 2006, Hamburg, 04.10. - 06.10.2006	
Darowski, N.; Zizak, I.; Gupta, A.; Erko, A.; Meneghini, C. **Depth profiling of marker layers using X-ray waveguide structures.** 4th International Workshop on Nanoscale Spectroscopy and Nanotechnology, Rathen, 17.09. - 21.09.2006	
Denks, I.A.; Genzel, Ch.; Dudzik, E.; Feyerherm, R.; Klaus, M.; Wagener, G. **The new HMI hard X-ray diffraction Beamlines at BESSY** 9th International Conference on Synchrotron Radiation, Daegu, Korea, 28.05. - 03.06.2006	
Denks, I.A; Klaus, M.; Gibmeier, J.; Genzel, Ch. **Application of white beam high energy X-ray diffraction to the analysis of near surface gradients** Frühjahrestagung des Arbeitskreises Festkörperphysik der DPG, Dresden, 27.03. - 31.03.2006	
Dudzik, E.; Feyerherm, R. **The new MAGS beamline: an instrument for hard x-ray diffraction at Bessy** SNI2006, Deutsche Tagung für Forschung mit Synchrotronstrahlung, Neutronen und Ionenstrahlen an Großgeräten 2006, Hamburg, 04.10. - 06.10.2006	
Feyerherm, R.; Dudzik, E.; Aliouane, N.; Argyriou, D.N.; Prokhnenko, O. **Multiferroic $DyMnO_3$ studied by x-ray resonant magnetic scattering** SNI2006, Deutsche Tagung für Forschung mit Synchrotronstrahlung, Neutronen und Ionenstrahlen an Großgeräten 2006, Hamburg, 04.10. - 06.10.2006	
Filimonov, A.; Fokin, A.; Koroleva, E.; Naberezhnov, A.; Tovar, M. **Structure and dielectric properties of confined solid solution $NaNO_2$-KNO_2** 4th Conference International Dielectric Society and 9th International Conference Dielectric and Related Phenomena IDS&DRP 2006, Poznan, Poland, 03.09. - 07.09.2006	E9
Freydank, H.; Poeste, T; Denks, I.A.; Genzel, Ch. **Investigation on the Residual Stress State in Steel Drawn Cups** BESSY User Meeting, Berlin, 07.12. - 08.12.2006	
Genzel, Ch.; Denks, I.A.; Klaus, M. **The Materials Science Beamline EDDI for Energy-Dispersive Analysis of Subsurface Residual Stress Gradients** 7th European Conference on Residual Stresses, Berlin, 13.09. - 15.09.2006	
Genzel, Ch.; Denks, I.A.; Klaus, M.; Gibmeier, J. **The Materials Science Beamline EDDI for Energy-Dispersive Diffraction Analysis of Subsurface Residual Stress Gradients** Bessy User Meeting, Berlin, 07.12. - 08.12.2006	

Glavatskyy, I.; Glavatska, N.; Urubkov, I.; Hoffmann, J.-U.; Bourdarot, F. **Crystal and magnetic structure temperature** 7th European Symposium on Martensitic Transformations and Shape Memory Alloys, Bochum, Germany, 10.09. - 15.09.2006	E1 E2
Gopinadhan, M.; Ivanova, O.; Ahrens, H.; Günther, J.-U.; Steitz, R.; Schönhoff, M.; Helm, C. A. **Chain Stratification in Polyelectrolyte Multilayers** Polyelectrolytes 2006, Dresden, 04.09. - 08.09.2006	V6
Gräber, H. G.; Apel, C.; Rack, A.; Manke, I.; Haibel, A.; Riesemeier, H.; Zabler, S.; Weidemann, G.; Goebbels, J.; Banhart, J. **Hochauflösende Synchrotron-Tomographie zur Darstellung kariöser Prozesse** Bessy-User-Meeting 2006, Berlin, Germany, 07.12. - 08.12.2006	S5
Haas, S.; Hoell, A.; Zehl, G.; Fichter, S. **Anomalous small-angle X-ray scattering investigation of Ru-Se catalysts supported on carbon** Deutsche Tagung für Forschung mit Synchrotronstrahlung, Neutronen und Ionenstrahlen an Großgeräten 2006, Universität Hamburg, 04.10. - 06.10.2006	
Hahlin, A.; Holub-Krappe, E.; Maletta, H.; Andersson, C.; Karis, O.; Hunter Dunn, J.; Arvanitis, D. **Novel findings on the temperature driven spin reorientation in Au/Co/Au** 13th Int. Conf. on X-ray Absorption Fine Structure, Stanford, CA, USA, 09.07. - 15.07.2006	
Haibel, A.; Scheuerlein, C.; Schneider, R.; Hoffmann, J.-U.; Wimpory, R.; Lake, B.; Banhart, J.; Tennant, A. **Untersuchung intermetallischer Phasenbildung in Nb_3 Sn Supraleitern mittels Synchrotron-Tomographie und Neutronendiffraktion** SNI 2006, Hamburg, Germany, 04.10. - 06.10.2006	
Hartnig, Ch.; Manke, I.; Kardjilov, N.; Haibel, A.; Schmidt, G.; Banhart, J.; Lehnert, W. **Investigation of water distribution in porous structures for fuel cell applications by means of synchrotron tomography** Bessy-User-Meeting 2006, Berlin, Germany, 07.12. - 08.12.2006	
Heinemann, A.; Wiedenmann, A.; Kammel, M.; Pop, L.M. **Separating different types of ordering in magnetic fluids with polarised small-angle neutron scattering** Polarised Neutrons in Condensed Matter Investigation - PNCMI 2006, Berlin, Germany, 25.09. - 28.09.2006	
Hoell, A.; Goerigk, G.; Kranold, R.; Tatchev, D.; Haas, S.; Müller, M.; Rademann, K.; Eichelbaum, M.; Banhart, J. **The formation of optically active nanoparticles in silicate glasses** HASYLAB Users Meeting, Hamburg, Germany, 27.01. - 27.01.2006	
Hoell, A.; Zizak, I.; Haas, S.; Tatchev, D.; Banhart, J. **The new A- and GI-SAXS dedicated SAXS instrument installed at the Berlin synchrotron BESSY** Small Angle Scattering 2006 (SAS 2006), Kyoto, Japan, 09.07. - 13.07.2006	
Holub-Krappe, E.; Andersson, C.; Konishi, T.; Karis, O.; Maletta, H.-J.; Arvanitis, D. **Spin Reorientation in Thin Au/Co/Au Films: in-situ XMCD and EXAFS Study** SOLEIL Users Meeting, Saint Aubin/ Gif-sur-Yvette, France, 18.01. - 19.01.2006	
Holub-Krappe, E.; Andersson, C.; Konishi, T.; Karis, O.; Maletta,H.; Arvanitis, D. **Magnetization reorientation in Au/Co: In-situ prepared ultra-thin films** International Workshop on Magnetism at SOLEIL, Saint Aubin/ Gif-sur-Yvette, France, 16.01. - 17.01.2006	

Kamarad, J.; Prokhnenko, O.; Prokeš, K.; Arnold, Z.; Andreev, A.V. **Pressure induced helimagnetism in Y_2Fe_{17} and Lu_2Fe_{17} intermetallic compounds** International Conference on Magnetism, Kyoto, Japan, 20.08. - 25.08.2006	E4 NMI3: 1118 NMI3: 1047 NMI3: 1085
Keiderling, U.; Wiedenmann, A. **Field-dependent relaxation behavior of Co-ferrofluid investigated with stroboscopic time-resolved SANS** SAS 2006, Kyoto, Japan, 09.07. - 13.07.2006	
Kumpugdee-Vollrath, M.; Ngawhirunpat, T.; Hoell, A.; Zizak, I. **Comparison of secondary structure of shed snake skins and human skin by Small Angle X-Ray Scattering (SAXS) Technique** 13th International Pharmaceutical Technology Symposium, Antalya, Turkey, 10.09. - 13.09.2006	
Landsgesell, S.; Prokhnenko, O.; Aliouane, N.; Argyriou, D.N. **Evolution of incommensurate magnetic order from A-type antiferromagnetism in $Nd_xY_xMnO_3$** German Conference for Research with Synchrotron Radiation, Neutrons and Ion Beams at Large Facilities 2006, Hamburg, 04.10. - 06.10.2006	
Manke, I. **Application Centre NIXE at HMI Berlin** Industrieforum (dt. Synchrotron Einrichtungen), Karlsruhe, Germany, 17.11. - 17.11.2006	
Manke, I.; Kardjilov, N.; Haibel, A.; Strobl, M.; Hilger, A.; Rack, A.; Zabler, S.; Treimer, W.; Banhart, J. **Industrial research at the Application Centre NIXE (Hahn-Meitner-Institut Berlin)** ECNDT-9, Berlin, 25.09. - 29.09.2006	
Miliyanchuk, K; Havela, L; Pereira, L.C.J.; Gonçalves, A.P.; Prokeš, K. **Peculiarities of U_2T_2X hydrides** International conference on magnetism, Kyoto, 20.08. - 25.08.2006	E2 NMI3: 1148
Notbohm, S.; Tennant, D.A.; Lake, B.; Canfield, P.C.; Fielden, J.; Kögerler, P.; Mikeska, H.-J.;Luckmann, C.; Telling, M.T.F **Temperature and Field Effects in the Gapped Quantum Magnet $Cu(NO_3)_{22.5}2O$** International Conference of Magnetism, Kyoto, Japan, 20.08. - 25.08.2006	
Perroud, O.; Wiedenmann, A.; Kumar, G.; Eckert, J. **Small-angle neutrons scattering study of magnetic domains in Nd-Fe-Co-Al alloys by use of polarized neutrons** Deutsche Tagung für Forschung mit Synchrotronstrahlung, Neutronen und Ionenstrahlen an Großgeräten 2006, Universität Hamburg, 04.10. - 06.10.2006	
Peters, J.; Mezei, F. **The new time-of-flight powder diffractometer for extreme sample environments at the Hahn-Meitner-Institut Berlin** ILL Millenium Symposium and European User's Meeting, Grenoble, 27.04. - 29.04.2006	
Prokhnenko, O.; Arnold Z.; Kuchin A.; Ritter C.; Isnard O.; Kamarad J.; Iwasieczko W.; Drulis, H. **Magnetostructural Properties of $Ce_2Fe_{16}MnDy$ (y = 0,1,2.3) Under Pressure** International Conference on Magnetism, Kyoto, 20.08. - 25.08.2006	
Prokhnenko, O.; S. Landsgesell , D. Argyriou , L.C. Chapon **Magnetic Ordering in Multiferroic $DyMnO_3$** German Conference for Research with Synchrotron Radiation, Neutrons and Ion Beams at Large Facilities 2006, Hamburg, 04.10. - 06.10.2006	

Ratel, Bruno, Bastie, Demé, Keiderling **Role de la plasticité dans la mise en radeaux des precipités gamma prime dans les superalliages de nickel monocristallins** Matériaux 2006, Dijon, 13.11. - 17.11.2006	V4 NMI3: 1158
Rodriguez-Alvarez, H., Kötschau, I., Streek, C., Weber, A., Klaus, M., Denks, I., Gibmeier, J., Genzel, Ch., Schock, H.W. **First Results from in-situ EDXRD Investigations on the Rapid Thermal Processing of $CuInS_2$ for Thin Solar Cells Fabrication** BESSY User Meeting, Berlin, 07.12. - 08.12.2006	
Rossner, H.H.; Schmitz, D.; Darowski, N. **EXAFS and MEXAFS at overlapping L-edges** BESSY Users' Meeting, Berlin-Adlershof, 07.12. - 08.12.2006	
Saensunon, B.; Stewart, G. A.; Gubbens, P. C. M.; Hutchison, W. D.; Buchsteiner, A. **Crystal field scheme for Er^{3+} in $ErNiAl_4$** Fifth AINSE/ANBUG Neutron Scattering Symposium (AANSS2006), Lucas Heights, 11.12. - 13.12.2006	V3
Schorr, S, Tovar, M. Sheptyakov, D. **Where the atoms are: cation disorder and anion displacement in $D^{II}X^{VI}$-$A^{I}B^{III}X^{VI}2$ semiconductors** International Conference on Neutron Scattering, Sydney, Australien,	E6 E9
Schorr, S.; Tovar, M.; Sheptyakov, D. **Electronic similar elements on different structural sites: a solution by neutron powder diffraction** 14th Annual meeting of the Germany Society of Crystallography, Freiburg, 03.04. - 06.04.2006	E6 E9
Steitz, R.; Wong, J. E.; von Klitzing, R.; **Swelling kinetics and structural changes of polyelectrolyte multilayers in contact with aqueous solution and water vapor** 6th International Symposium on Polyelectrolytes, Dresden, 04.09. - 08.09.2006	
Strunz, P.; Mukherji, D.; Rösler, J.; Gilles, R.; Näth, O.; Haug J.; Wiedenmann, A. **In-situ SANS investigation of solution treatment of single-crystal Ni-base superalloy containing rhenium ($CMSX_4$)** International Conference on Small-Angle Scattering, Kyoto, Japan, 09.07. - 13.06.2006	V4 NMI3: 1119
Veira, J.R.; Argyriou, D.N.; Kiefer, K.; Amann, U.; Hoffmann, J.-U.; Bordallo, H.N.; Almairac, R.; Hangleiter, Th. **Investigations on the coupling between multiferroic and structural properties of $BaMnF_4$** German Conference for Research with Synchrotron Radiation, Neutrons and Ion Beams at Large Facilities 2006, Hamburg, 04.10. - 06.10.2006	

AUTHOR INDEX

AUTHOR INDEX

AUTHOR INDEX

AUTHOR INDEX

AUTHOR INDEX